# Journal of
# lied Mechanics

*...ributions of the ASME Applied Mechanics Division)*


...s for an Inexpensive Supersonic Wind Tunnel—1. . . . . *Joseph Kaye, J. B. Keenan, G. A. Brown, and R. H. Shoolbred* 289
...s for an Inexpensive Supersonic Wind Tunnel—2. . . . . *Joseph Kaye and G. A. Brown* 297
...Distributions Within a Wide Curved Bar Subjected to Pure Bending . . . . . *Bernard W. Shaffer and Raymond N. House, Jr.* 305
...Symmetric Rotating Rays . . . . . *P. G. Hodge, Jr.* 311
...Under Explosive Attack . . . . . *K. B. Broberg* 317
...Cylinder Under Combined Compression, Torsion, and Bending Loads . . . . . *C. T. Wang, R. J. Vaccaro, and D. F. De Santo* 324
...Sessions . . . . . *N. J. Hoff* 329
...metrical Beams . . . . . *H. L. Langhaar* 335
...Swept Wing—A Problem of Plane Elasticity . . . . . *B. C. Hanks and J. R. M. Radok* 337
. . . . . *J. Zickel* 348
...Heliotropic Strips . . . . . *H. D. Conway* 353
...Rotor-Fuselage System Induced by the Main Rotor Blades in Flight . . . . . *M. Mordukhovich, S. W. Yuan, and H. Reissner* 355
...Flexibility . . . . . *J. E. Brock* 361
...Freezing Films . . . . . *R. S. Brand* 363
...Subjected to an Impulse . . . . . *E. G. Thomsen and R. Goodstein* 365
...Methods of Measuring and Simulating Vibration Environments . . . . . *C. T. Morrow and R. B. Machmer* 367
...of Waves in Plates . . . . . *H. G. Hopkins and W. Prager* 372
...Reflection of a Plastic Plate Under Blast Loading . . . . . *A. J. Wang* 375
...Theory of the Viscous Vibration Damper . . . . . *F. M. Lewis* 377
...Inhomogeneous Bending Theory and Its Application to the Sweep-Plate Problem . . . . . *H. J. Plass, Jr.* 383
...Boundary-Value Problems of the Thin-Walled Circular Cylinder . . . . . *Frederick V. Pohle and S. V. Nardo* 389
...Body on an Infinite Elastic Solid . . . . . *R. N. Arnold, G. N. Bycroft, and G. B. Warburton* 391
...Strips—II . . . . . *J. S. Born and G. Horvay* 401
...Trailer . . . . . *G. A. G. Pershing* 407
...With Fixed Principal Directions . . . . . *R. A. Davis* 411
...Solid Surface and the Assumption of Linearity in the Plastic Stress-... *P. M. Naghdi, J. C. Rowley, and C. W. Beadle* 416
...of Size and Shape Effects in Fatigue . . . . . *F. A. McClintock* 421
...Scatter in Fatigue Testing . . . . . *F. A. McClintock* 427
...Loading . . . . . *J. A. H. Hunt* 432
. . . . . *J. H. Huth* 432
...Beam With Restraining Restoring Force . . . . . *H. N. Abramson* 434
...Published papers by *J. T. Kenney, Jr.; I. Miklowitz and H. H. Uhlig; E. W. ... Yi-Yuan Yu; L. H. Long, Jr.; G. D. Galletly; G. Horvay and I. M. ...* 436
. . . . . 446



SEPTEMBER, 1955

VOL. 22, NO. 3

Published by The American Society of Mechanical Engineers

# Journal of Applied Mechanics

Papers Contributed and Presented Meetings by the ASME Applied Mechanics Division

[illegible]

R. D. Mindlin, *Secretary*

[illegible] *Technical Editor*

*Published Quarterly by*

The American Society of Mechanical Engineers

[illegible] 29th and Northampton Streets, Easton, Pa.

Editorial Department and Headquarters of the Society, 29 West Thirty-Ninth Street, New York 18, N. Y.

OFFICERS OF THE SOCIETY

[illegible], *President*

C. E. Davies, *Secretary*

[illegible], *Treasurer*

PUBLICATIONS COMMITTEE

[illegible], *Chairman*

Graham A. Stevens, *Editor*

K. W. Gunderson, *Mgr. Editor*

By-Laws: The Society shall not be responsible for statements or opinions advanced in papers or . . . printed in its publications (B13, Par. 4).

Published Quarterly by The A[illegible] Publication office at 20th and Northampton Streets, Easton, Pa. The editorial department is located at the Society headquarters, 29 West Thirty-Ninth Street, New York 18, N. Y. Cable address, "Dynamic," New York. Price $1.50 a copy, $5.00 a year; to members and students of the Society, $1.00 a copy, $4.00 a year. Add 25¢ for postage to all countries outside the United States, Canada, and Mexico. Remittances should be made payable to the order of the Society and sent by mail to the Society headquarters seven weeks before they are to be effective on the mailing list. Please send old as well as new address when notifying us of change of address. Allow one month for change to become effective. Entered as second-class matter March 14, 1952, at the Post Office at Easton, Pa., under the act of August 24, 1912. . . . Copyright, 1953, by The American Society of Mechanical Engineers. Reprints from this publication may be made on condition that full credit be given the JOURNAL OF APPLIED MECHANICS and the author, and that date of publication be stated.

# Heat-Transfer Measurements in an Inexpensive Supersonic Wind Tunnel

## 1 Apparatus and Results for a Laminar Boundary Layer Based on a Simple One-Dimensional Flow Model

By JOSEPH KAYE,[1] J. H. KEENAN,[2] G. A. BROWN,[3] AND R. H. SHOULBERG[4]

**Reliable experimental data, obtained at relatively low cost, are presented in the form of heat-transfer coefficients for air moving at supersonic speeds in a round tube. These data are analyzed, interpreted, and compared with available data in the literature. The experimental local heat-transfer coefficients are for laminar, transitional, and turbulent boundary layers. The data for a laminar boundary layer, comprising 17 runs, are discussed here for Mach numbers at tube inlet of 2.8 and 3.0. The range of values of diameter Reynolds number covered is from 20,000 to 100,000 for these laminar-flow tests, while the length Reynolds number extends to about 4,000,000. The computed quantities are obtained on the basis of a simple one-dimensional flow model, but a companion paper will analyze the same data in greater detail on the basis of a two-dimensional flow model.**

### Nomenclature

The following nomenclature is used in the paper:

$A$ = cross-sectional area, $\pi D^2/4$
$A'$ = heat-transfer area, $\pi D \Delta L$
$c_p$ = specific heat at constant pressure
$c_v$ = specific heat at constant volume
$c_w$ = discharge coefficient of nozzle
$D$ = inside diameter of pipe
$g$ = acceleration given to unit mass by unit force
$G$ = flow per unit area, $w/A$
$h$ = coefficient of heat transfer, $q/A'(t_w - t_{aw})$
$k$ = ratio of specific heats, $c_p/c_v$
$L$ = distance from end of curved contour of nozzle
$\mathsf{M}$ = Mach number, $V/\sqrt{gkRT}$
$p$ = static pressure
$q$ = rate of heat transfer
$R$ = perfect-gas constant
$\mathrm{Re}_D$ = diameter Reynolds number, $DG/\mu g$
$\mathrm{Re}_L$ = length Reynolds number, $LG/\mu g$
$t$ = temperature, deg F
$T$ = temperature, deg F abs
$V$ = velocity
$w$ = mass rate of flow
$\mu$ = viscosity
$\lambda$ = thermal conductivity

Superscript * refers to throat of supersonic nozzle where $\mathsf{M} = 1$

Subscripts:

0 = hypothetical entrance plane of tube, where boundary layer is of zero thickness
$oi$ = upstream stagnation conditions
$w$ = wall conditions
$\infty$ = free-stream conditions for flat-plate flow

### Introduction

A wind tunnel is usually considered to be a device in which models may be inserted and tested under controlled conditions. Wind tunnels also have been used, however, to study basic phenomena in fluid mechanics, such as boundary-layer mechanics, turbulence, stability of the laminar boundary layer, interaction of shock waves and boundary layers, and, in more recent years, heat-transfer phenomena in supersonic flow. Most steady-state and blowdown supersonic wind tunnels which are large enough to insert models of reasonable size are expensive to build and to operate, and also expensive when used to measure heat-transfer data. Steady supersonic flow established under controlled conditions in a small round tube, 1/2 in. diam, can be used to measure local heat-transfer coefficients. The corresponding apparatus, which is described herein, may be considered to be an example of an inexpensive supersonic wind tunnel, in that it is both relatively cheap to design and construct, and also, relatively low in operational costs.

A recent survey (1)[5] has shown the great need for reliable heat-transfer data for supersonic flow in view of the small amount of such data published during the years from 1948 to 1953. For this reason a fairly detailed account of the results obtained in an investigation of heat-transfer coefficients for supersonic flow of air in a round tube is to be presented in two papers. The first paper, which is the present one, consists of a brief description of the apparatus used, and the calculated results for a laminar boundary layer based on a simple one-dimensional flow model. The second

[1] Associate Professor of Mechanical Engineering, Massachusetts Institute of Technology, Cambridge, Mass. Mem. ASME.
[2] Professor of Mechanical Engineering, Massachusetts Institute of Technology. Fellow ASME.
[3] Shell Fellow in Mechanical Engineering, Massachusetts Institute of Technology. Assoc. Mem. ASME.
[4] Design Engineer, The M. W. Kellogg Company, New York, N. Y.

Contributed by the Applied Mechanics Division and presented at the Annual Meeting, New York, N. Y., November 28–December 3, 1954, of The American Society of Mechanical Engineers.
Discussion of this paper should be addressed to the Secretary, ASME, 29 West 39th Street, New York, N. Y., and will be accepted until October 10, 1955, for publication at a later date. Discussion received after the closing date will be returned.
Note: Statements and opinions advanced in papers are to be understood as individual expressions of their authors and not those of the Society. Manuscript received by ASME Applied Mechanics Division, June 15, 1954. This paper was not preprinted.

[5] Numbers in parentheses refer to the Bibliography at the end of the paper.

paper will present the calculated results for a laminar boundary layer based on a two-dimensional flow model for the entrance region of a tube.

The present investigation of heat-transfer coefficients for supersonic flow of air in a round tube was started some seven years ago under the sponsorship of the Office of Naval Research. Preliminary data and results were obtained several years ago with the first apparatus, described herein as test combination C. Similar results were not then available in the literature for comparison. The possibility of systematic errors in the data and the lack of knowledge of the type of boundary layer which existed in the supersonic flow of air in the tube were two main reasons for designing, building, and testing a new apparatus to get more reliable heat-transfer coefficients for supersonic flow.

In the past few years the results obtained for the steady supersonic flow of air in a round tube, with and without heat transfer to the air stream, have been placed on a firm foundation as indicated by the following evidence:

1 The experimental data obtained by different teams of observers working with different test combinations, for both adiabatic flow and diabatic flow, have shown the absence of significant systematic errors.

2 The nature of the boundary layer present in the tube flow has been demonstrated conclusively by means of accurately measured velocity profiles (2, 3).

3 The accurately measured velocity profiles for supersonic flow in the tube also have demonstrated the basic soundness of the two-dimensional flow model used to interpret the data.

4 Theoretical solutions (4) have been obtained for the system of partial differential equations of energy, momentum, and continuity for the case of supersonic flow of air in a tube in the entrance region. These solutions describe the behavior of supersonic flow in a tube with a laminar boundary layer developing from the entrance plane of the tube.

## Methods of Testing

The experimental program described here has consisted of two parts. In the first part, a well-insulated round tube was used to measure values of the local adiabatic wall temperature and local static pressure of a supersonic stream of air. The results of these tests, with a complete description of the apparatus, are given in references (5) and (6). In order to minimize the amount of repetition, the reader is referred to these two papers for many details not given in this paper. In the second part of the program, two different test combinations were used in which steam was condensed outside a round brass tube in order to measure the local coefficient of heat transfer to a supersonic stream of air flowing inside the tube.

The general preparation of the air flow and the method of drying the air stream are given in detail in reference (5). These are the same for both parts of the program. The schematic layout of the entire flow system is shown in Fig. 1. The purpose of the major changes made for the tests with diabatic flow was to insure that almost saturated or slightly superheated steam entered the outer steam chest of the apparatus and to minimize the heat losses from the apparatus to the surroundings.

A major difference between tests for adiabatic and diabatic flow was the length of time required to bring the large mass of heat-transfer apparatus up to a fixed temperature corresponding to that of the condensing steam. This transient heating process was observed and recorded carefully in the diabatic tests until a steady-state condition was obtained. Heat-transfer measurements were made only for the steady state. During the large time interval required for both the transient process and the measurements, the conditions in the steam main varied only slowly. Control devices were found necessary to superheat or desuperheat the steam only slightly in order to maintain constant the state of the steam fed to the steam chest of the apparatus. They are indicated in the schematic layout of Fig. 1. The measured superheat was found to be about 0.5 deg F on the average.

## Experimental Apparatus

Some salient features of the two test combinations of heat-transfer apparatus are described in Table 1. The length-diameter ratio in Table 1 is based on the distance from the end of the curved contour of the supersonic nozzle to the exit plane of the test section.

TABLE 1 TEST COMBINATION OF HEAT-TRANSFER APPARATUS

| Symbol | Nozzle | Test section | $L/D$ | $M_3$ |
|---|---|---|---|---|
| C | Brass | Brass | 31.8 | 3.0 |
| D | Stainless steel | Brass | 49.8 | 2.8 |

The nozzles used to produce supersonic flow in test combinations C and D were different in design and in final contour. Details of design and of construction of these two nozzles are shown in reference (5). In the brass nozzle of test combination C, no means of measuring the temperature gradient along the axial length was available, whereas two thermocouples were installed in the stainless-steel nozzle to determine the axial temperature gradients for test combination D.

*Design Considerations for Test Sections.* The first test section, used in test combination C, was designed to produce a small thermal resistance for radial heat flow through the tube wall in comparison with the thermal resistance being measured, namely, that from the wall to the air stream in the tube. Brass was therefore selected for the tube material. The temperature of the tube was maintained constant over its entire length by surrounding it with condensing steam.

The experience gained after operation of test combination C for about 2 years resulted in the following additional design requirements for test combination D:

1 The joint between the nozzle and collar, and that between the collar and test section should be made as nearly perfect as possible. A misfit in excess of 0.0002 in. in the diameter of 0.5 in. is undesirable.

2 The axial heat flow from the hot test section to the cooler nozzle should be reduced to a minimum. This objective was achieved in test section D by use of a nozzle and a collar made of stainless steel which has a considerably lower thermal conductivity than that of brass.

3 The no-load or blank-run condensation rate, which is determined by flow of steam into the steam chest for zero flow of air in the test section and which is an indication of the total amount of undesired heat flow from the steam to the surroundings, should be minimized, especially when a laminar boundary layer is established in the test section.

4 The state of the steam entering the steam chest must be controlled carefully to be slightly superheated, and the steam-flow distribution into and within the steam chest must be as nearly uniform as practicable.

The details and dimensions of test combinations C and D, the original data, the analysis and the calculated results are omitted from this paper but may be found in reference (7). Some details of test combination D are given in Fig. 2.

## Experimental Results

The number of runs made with test combinations C and D, the ranges of Reynolds numbers covered, and the prevailing type of

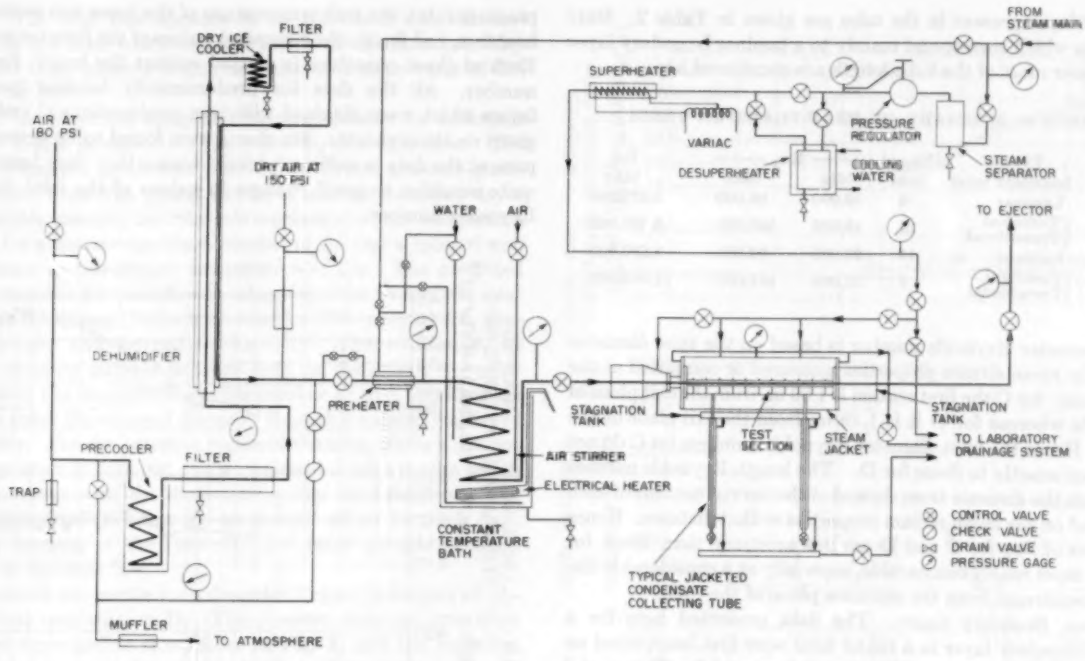


SCHEMATIC LAYOUT OF TEST COMBINATIONS C AND D

FIG. 1

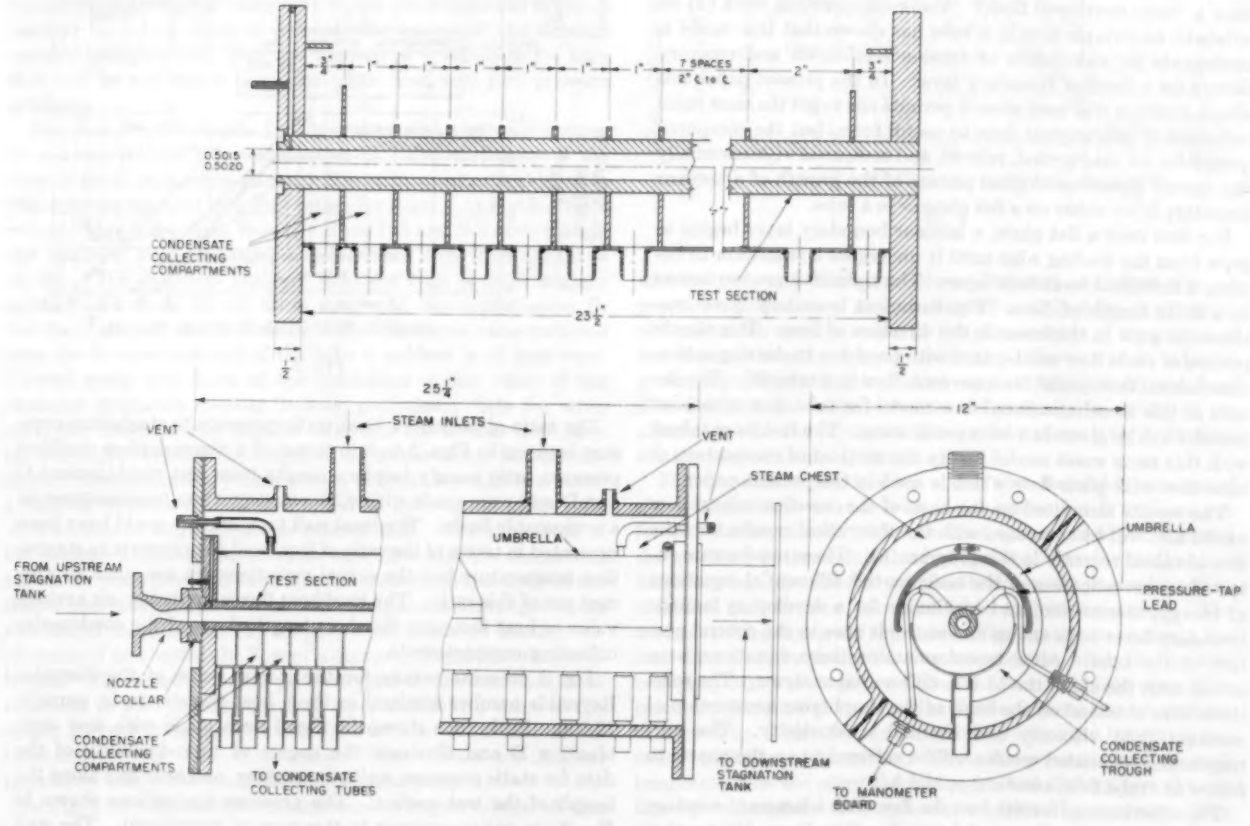


DETAILS OF TEST COMBINATION D

FIG. 2

boundary layer present in the tube are given in Table 2. Only those data which correspond mainly to a laminar boundary layer existing over most of the tube length are considered here.

TABLE 2 SUMMARY OF HEAT-TRANSFER TESTS

| Test combination | Type of boundary layer | No. of runs | $Re_D$ Min | $Re_D$ Max | $Re_L$ Max |
|---|---|---|---|---|---|
| C | Laminar | 4 | 52,000 | 96,000 | 2,270,000 |
| C | Turbulent / Transitional | 19 | 43,000 | 380,000 | 8,560,000 |
| D | Laminar | 13 | 22,000 | 92,000 | 3,590,000 |
| D | Turbulent / Transitional | 6 | 20,000 | 492,000 | 12,000,000 |

The diameter Reynolds number is based on the tube diameter and on the mean stream properties measured or computed at the first station; for C the first station is 1.66 in. from the exit plane of the nozzle whereas for D it is 1.19 in. from the exit plane of the nozzle. Hence the inlet diameter Reynolds numbers for C do not correspond exactly to those for D. The length Reynolds number is based on the distance from the end of the curved contour of each nozzle and on the mean stream properties at that distance. Hence the values of $Re_L$ for C and D are less arbitrary than those for $Re_D$ and more nearly comparable, especially at a considerable distance downstream from the entrance plane of the tube.

*Laminar Boundary Layer.* The data presented here for a laminar boundary layer in a round tube were first interpreted on the basis of a simple one-dimensional flow model. This model ignores completely the growth of the laminar boundary layer in the tube and also the fact that this type of supersonic flow is mainly one of "entrance flow" with insufficient flow length to produce a "fully developed flow." Moreover, previous work (5) on adiabatic supersonic flow in a tube has shown that this model is inadequate for calculation of friction coefficients and recovery factors for a laminar boundary layer. In the present paper this simple model is still used since it permits one to get the most rapid reduction of the original data to useful form, but the computed quantities are interpreted, related, and compared with essentially the correct phenomenological picture of the growth of a laminar boundary layer either on a flat plate or in a tube.

For flow over a flat plate, a laminar boundary layer begins to grow from the leading edge until it undergoes a transition to become a turbulent boundary layer. The transition process occurs in a finite length of flow. The turbulent boundary layer continues to grow in thickness in the direction of flow. This simple picture of plate flow can be used with precision to develop a two-dimensional flow model for supersonic flow in a tube (6). The details of this two-dimensional flow model for tube flow with heat transfer will be given in a later publication. The results obtained with this more exact model justify the method of comparison of tube flow with plate flow which is used in the present paper.

The results computed on the basis of the one-dimensional flow model also will be compared with the theoretical results for tube flow obtained recently in this program (8). These results were obtained by investigation of the basic partial differential equations of energy, momentum, and continuity for a developing laminar boundary layer adjacent to an isentropic core in the central portion of the tube. After transformations these equations were solved with the aid of the M.I.T. differential analyzer. The solutions were obtained on the basis of the simplifying assumption of constant fluid viscosity and thermal conductivity. The corresponding calculated results will be referred to on the charts to follow as "tube flow, constant $\mu$, and $\lambda$."

The experimental results for tube flow with a laminar boundary layer, covering the range of inlet diameter Reynolds number from about 20,000 to 100,000 are presented in six charts, Figs. 3 to 8. Each chart shows the measured values of the modified pressure ratio, the wall temperature of the brass test section, the heat flux, and finally the computed values of the Stanton number. Each of these quantities is plotted against the length Reynolds number. All the data for predominantly laminar boundary layers which were obtained with test combinations C and D are given on these charts. Six charts were found to be necessary to present the data in sufficient detail because they were found to be quite sensitive to small changes in values of the inlet diameter Reynolds number.

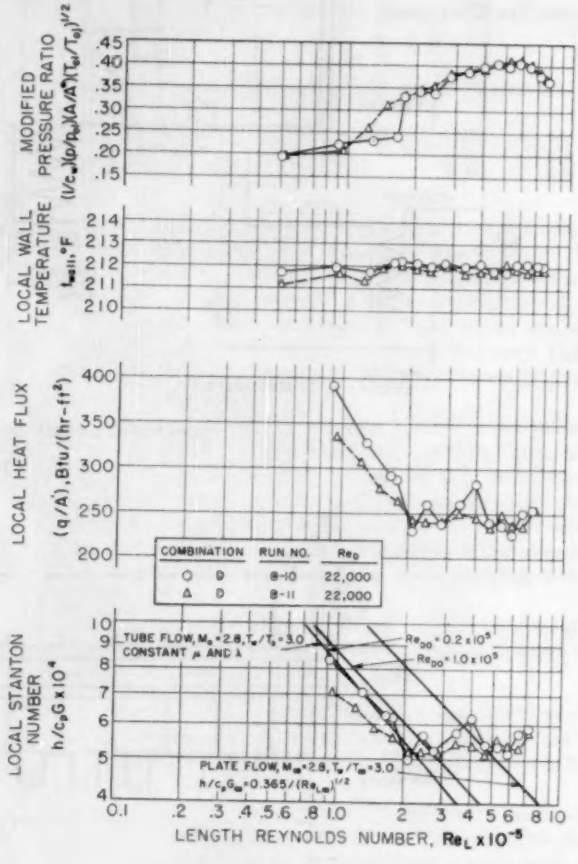
MODIFIED PRESSURE RATIO
LOCAL WALL TEMPERATURE
LOCAL HEAT FLUX
(q/A), Btu/(hr-ft²)
COMBINATION RUN NO. Re_D
C 8-10 22,000
D 8-11 22,000
LOCAL STANTON NUMBER
TUBE FLOW, M_e = 2.8, T_s/T_e = 3.0
CONSTANT μ AND λ
Re_DD = 0.2 x 10^5
Re_DD = 1.0 x 10^5
PLATE FLOW, M_e = 2.8, T_s/T_e = 3.0
LENGTH REYNOLDS NUMBER, Re_L x 10^-5

FIG. 3

The ratio of measured local static pressure to stagnation pressure is given in Figs. 3 to 8 in terms of a dimensionless modified pressure ratio mainly to place results from test combinations C and D and runs made with different stagnation temperatures on a comparable basis. The local wall temperature could have been presented in terms of the ratio of local wall temperature to stagnation temperature but the actual variations are too small to warrant use of this ratio. The local heat flux is, in reality, an average value of heat flux over the short length of one of the condensate-collecting compartments.

Fig. 3 presents results for the lowest value of the diameter Reynolds number attained in these heat-transfer tests, namely, 22,000. Both runs shown in Fig. 3 were made with test combination D and illustrate the degree of reproducibility of the data for static pressure, wall temperature, and heat flux along the length of the test section. The pressure fluctuations shown in Fig. 3 are not uncommon in this type of experiment. The wall temperature is remarkably constant along the length, with an average deviation from a mean value of less than a fraction of 1

deg F. The heat flux appears to be smooth in the entrance portion of the tube which corresponds to the laminar boundary layer, and then appears to fluctuate about a mean value of 235 Btu/(hr sq ft).

Fig. 3 compares the computed Stanton number for tube flow with the values predicted for plate flow and for tube flow. The predicted Stanton number for plate flow with zero pressure gradient is taken from Van Driest (9) for a laminar boundary layer with variable viscosity and thermal conductivity; the comparison is made for a free-stream Mach number of 2.8 and a ratio of wall temperature to free-stream temperature of 3.0. The predicted Stanton number for tube flow is taken from the theoretical solution given by Toong (8) for a laminar boundary layer with constant viscosity and thermal conductivity. This solution shows that the Stanton number depends both on the length Reynolds number and the diameter Reynolds number so that two lines are shown to cover the range of diameter Reynolds number employed in the tests. For the entrance region of the tube, where a laminar boundary layer is forming, the experimental tube results are in good agreement with the theoretical values for tube flow. The experimental data lie below the theoretical values for plate flow, probably because of the presence of a large adverse pressure gradient in the tube flow.

Fig. 4 shows the results for a diameter Reynolds number of 32,000 for test combination D. The pressure data are smoother and more reproducible than those in Fig. 3, and the heat-flux data cover a much larger range of values than those in Fig. 3. The heat-flux data and the Stanton numbers both indicate a sharp rise in value near the exit of the test section; this sharp rise is one of the first signs noted of transition from a laminar to a turbulent boundary layer in the tube. As in the previous case, where a laminar boundary layer is present, the values of the Stanton number compare well with the theoretical predictions for tube flow but lie well below those for plate flow with zero pressure gradient.

Fig. 5 shows the results for three runs with test combination D and one run for test combination C. The sensitivity of the data to small changes in diameter Reynolds number is evident in Fig. 5 where the local heat-flux values for Runs B-14 and K-20 are considerably larger than those for Runs B-2 and B-4 even though the diameter Reynolds number is increased only from 45,000 to 51,000. The modified pressure ratio for Run K-20 is slightly smaller than those for the three runs with test combination D, but the same slow rise in pressure with a maximum value attained near the downstream end of the tube is evident in all four runs. Careful study was made of the conditions at this value of the diameter Reynolds number because preliminary data for adiabatic flow had indicated that for this value the laminar boundary layer occupied most of the length of the test section. Substantiation of these preliminary data is seen in Runs B-2 and B-4 where a laminar boundary layer was found to exist up to station 17, with a value of length-diameter ratio of 45.3. The agreement of the measured Stanton numbers for tube flow with the theoretical values for plate flow and tube flow is excellent on the basis of the simple one-dimensional flow model. Similar excellent agreement was found in reference (5) for the local apparent friction coefficients of adiabatic tube flow at a diameter Reynolds number of 80,000. Fig. 5 also indicates that the start of the transition from a laminar to a turbulent boundary layer occurs at a value of the length Reynolds number of 900,000 for Run K-20 and about 1,300,000 for the other three runs. These values are in good agreement with those for transition on a flat plate.

In Fig. 3 the value of the Stanton number begins to level off at a length Reynolds number of 200,000, and fluctuations about a constant value extend to a Reynolds number of 800,000. In Fig. 4 a similar behavior is noted between Reynolds numbers of 300,000

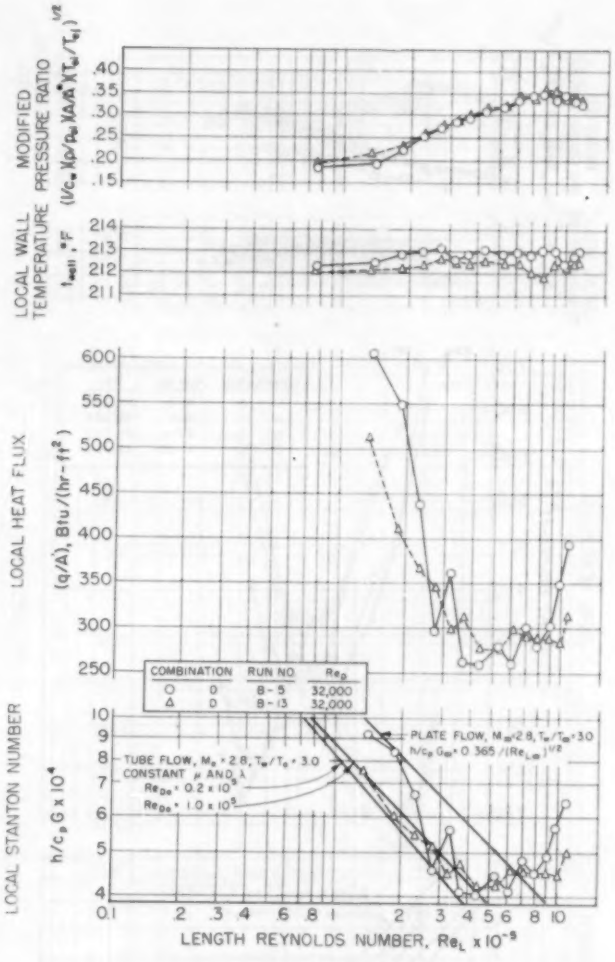
MODIFIED PRESSURE RATIO
LOCAL WALL TEMPERATURE
LOCAL HEAT FLUX
(q/A), Btu/(hr-ft²)
LOCAL STANTON NUMBER
h/c_p G x 10⁴
COMBINATION RUN NO. Re_D
○ D B-5 32,000
△ D B-13 32,000
TUBE FLOW, M_∞ = 2.8, T_w/T_0 = 3.0
CONSTANT μ AND λ
Re_D0 = 0.2 x 10⁵
Re_D0 = 1.0 x 10⁵
PLATE FLOW, M_∞=2.8, T_w/T_∞=3.0
LENGTH REYNOLDS NUMBER, Re_L x 10⁻⁵

FIG. 4

and 900,000, and in Fig. 5 between 500,000 and 1,000,000. A possible explanation of this leveling off and fluctuation of values of the Stanton number could be the phenomenon of separation of the laminar boundary layer under the influence of an adverse pressure gradient which is present over a long length of tube flow. The fluctuations could be explained partially in terms of reattachment of the separated laminar boundary layer. Further work is needed to test this explanation.

Fig. 6 presents the data for a diameter Reynolds number of about 70,000 for two runs with test combination D and one run for test combination C. The excellent agreement of the values of the modified pressure ratio and of the heat flux for the laminar boundary layer for the two completely different test combinations indicates the absence of appreciable systematic errors. The second striking feature of the data in Fig. 6 is the steep rise in the heat flux, and likewise in the Stanton number, when the laminar boundary layer undergoes a transition to a turbulent one. The older and shorter test combination C was not long enough to show this feature. The steep rise in heat flux observed here is an excellent indicator of transition. The static pressure, and the wall temperature on the other hand, changed but slightly over the entire eight diameters of length of this transition process. The values of the measured Stanton numbers in Fig. 6 are in excellent agreement with those predicted for plate flow, and are larger than those for tube flow with a laminar boundary layer. The better

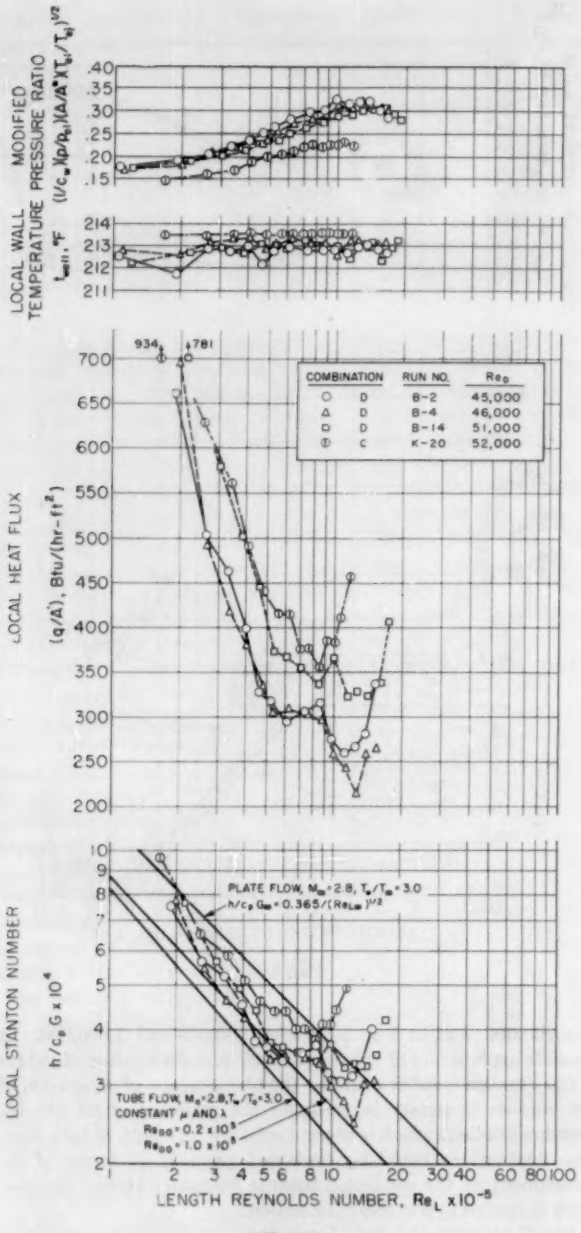
MODIFIED PRESSURE RATIO
LOCAL WALL TEMPERATURE
LOCAL HEAT FLUX
(q/A), Btu/(hr-ft²)
934
781
COMBINATION | RUN NO. | Re_D
D | B-2 | 45,000
D | B-4 | 46,000
D | B-14 | 51,000
C | K-20 | 52,000
LOCAL STANTON NUMBER
h/c_p G x 10⁴
PLATE FLOW, M_∞ = 2.8, T_w/T_∞ = 3.0
h/c_p G_∞ = 0.365/(Re_L∞)^1/2
TUBE FLOW, M_∞ = 2.8, T_w/T_0 = 3.0
CONSTANT μ AND λ
Re_DO = 0.2 x 10⁵
Re_DO = 1.0 x 10⁵
LENGTH REYNOLDS NUMBER, Re_L x 10⁻⁵

Fig. 5

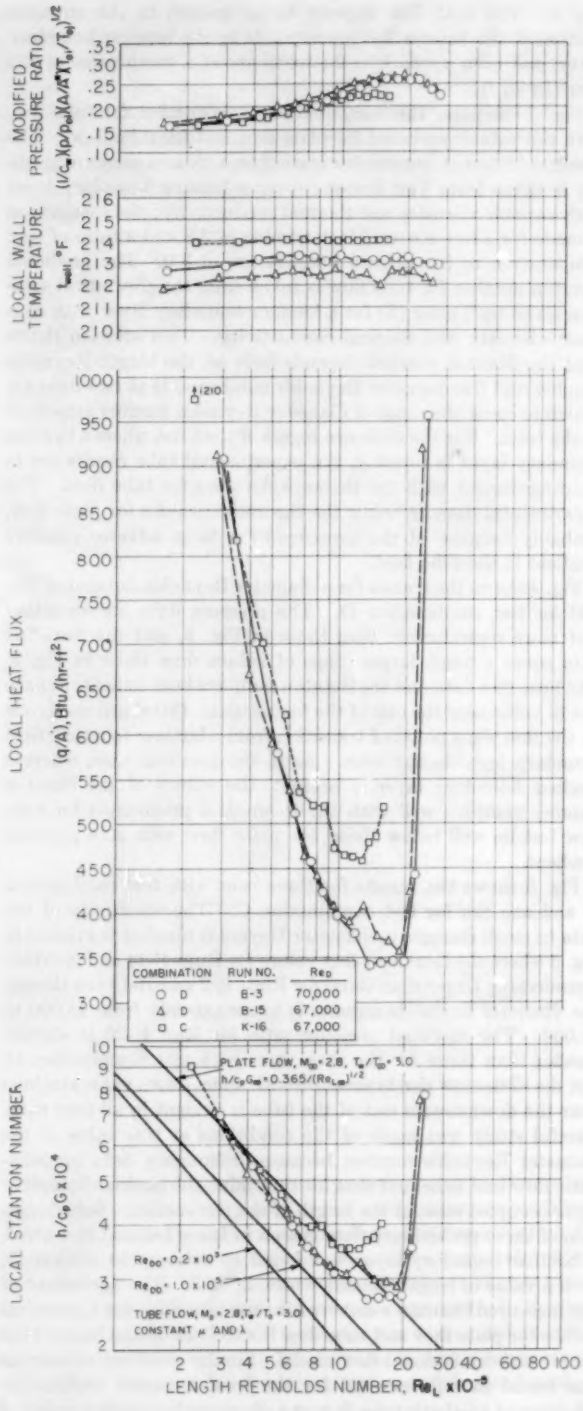
MODIFIED PRESSURE RATIO
LOCAL WALL TEMPERATURE
LOCAL HEAT FLUX
(q/A), Btu/(hr-ft²)
1210
COMBINATION | RUN NO. | Re_D
D | B-3 | 70,000
D | B-15 | 67,000
C | K-16 | 67,000
LOCAL STANTON NUMBER
h/c_p G x 10⁴
PLATE FLOW, M_∞ = 2.8, T_w/T_∞ = 3.0
h/c_p G_∞ = 0.365/(Re_L∞)^1/2
Re_DO = 0.2 x 10⁵
Re_DO = 1.0 x 10⁵
TUBE FLOW, M_∞ = 2.8, T_w/T_0 = 3.0
CONSTANT μ AND λ
LENGTH REYNOLDS NUMBER, Re_L x 10⁻⁵

Fig. 6

agreement with predicted values for plate flow also may be due to smaller pressure gradient present in the data in Fig. 6 than in Figs. 3, 4, and 5.

Fig. 7 shows the data for a diameter Reynolds number of about 80,000 for Runs B-1 and B-9. The results are similar to those noted for Fig. 6, especially with respect to the steep slope of the curve for heat flux during transition. It should be noted that as the value of the diameter Reynolds number is increased from Fig. 3 to Fig. 8, the value of the length Reynolds number at transition, computed on the basis of the one-dimensional flow model gradually increased from about 900,000 to about 2,200,000. The agreement between measured values of the Stanton number and those predicted for plate flow is excellent for this type of measurement in view of published data.

Fig. 8 shows the data for Runs B-7, B-16, K-19, and K-23 for the last and largest value of the diameter Reynolds number, 90,000, which was chosen to demonstrate the data for a predominantly laminar boundary layer. The agreement between the data for the two different test combinations is again excellent. The steep slopes of the curves for heat flux and for Stanton number are again emphasized in the data taken with the longer test

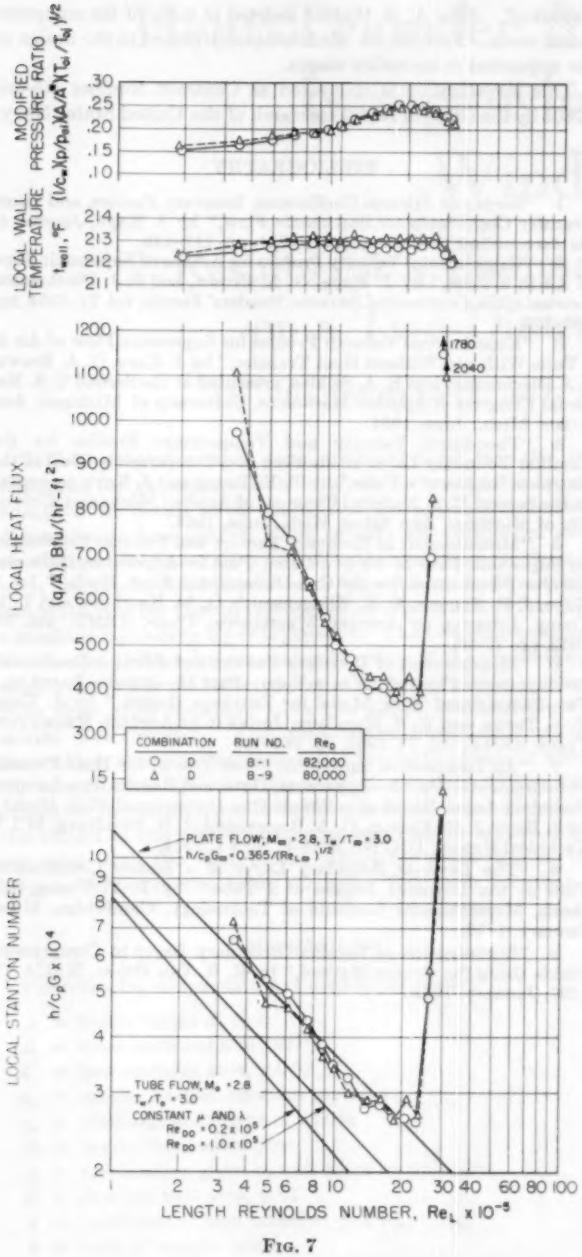


FIG. 7

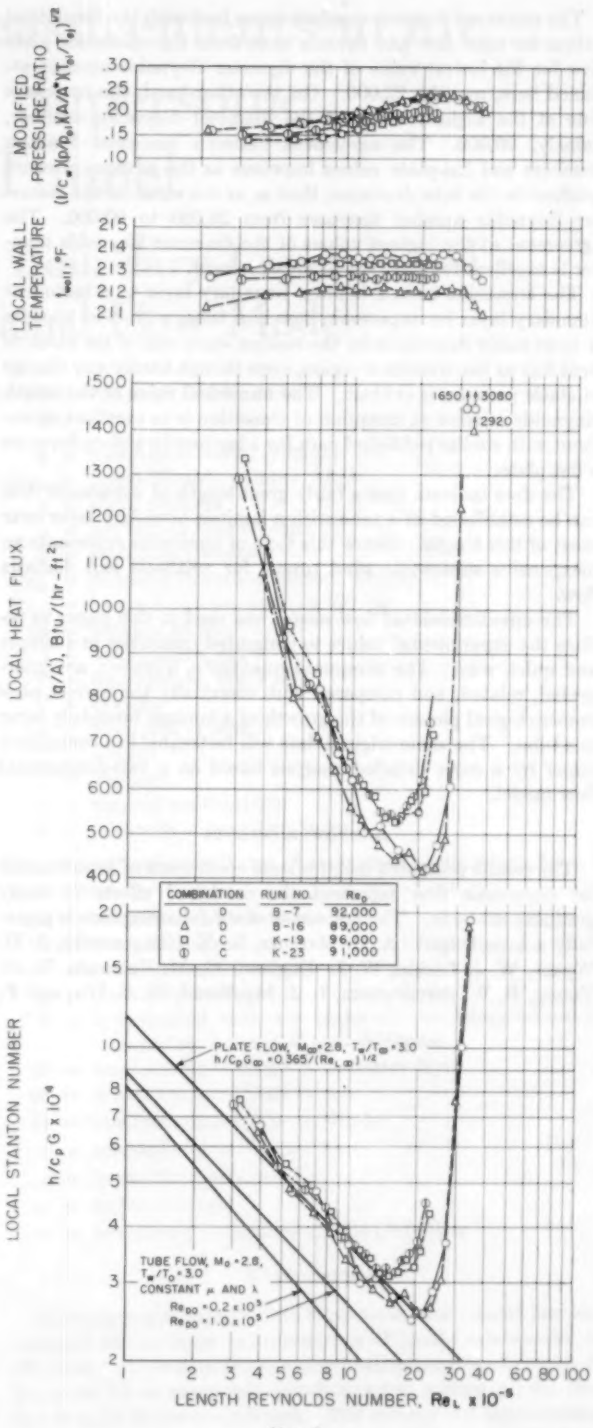


FIG. 8

combination D. Figs. 7 and 8 indicate smaller values of the adverse pressure gradient than do the preceding figures. For these four runs, the agreement between measured Stanton numbers and plate-flow values for zero pressure gradient is excellent.

## CONCLUSIONS

Reliable data on heat-transfer coefficients to air flowing at supersonic velocities in a round tube are presented here for the case of a laminar boundary layer. The agreement found between measurements made with completely independent test combinations by different groups of observers provides assurance that no significant systematic errors exist.

The data for tube flow were first treated in the usual fashion on the basis of a simple one-dimensional flow model. Since this model is not fully adequate to explain or interpret the heat-transfer data for supersonic tube flow, these data are interpreted in terms of a laminar boundary layer which begins to grow at tube entrance. The calculated values are compared with the theoretical predictions for a laminar boundary layer developing over a flat plate with zero pressure gradient and with the theoretical predictions for tube flow based on constant viscosity and constant thermal conductivity.

The measured Stanton numbers agree best with the theoretical values for tube flow and deviate most from the values for plate flow for the lowest value of the diameter Reynolds number attained here, namely, 22,000. On the other hand, the reverse is true at the highest value of the diameter Reynolds number, namely, 90,000. The agreement between measured Stanton numbers and flat-plate values improves as the adverse pressure gradient in the tube decreases, that is, as the value of the diameter Reynolds number increases from 20,000 to 90,000. The agreement at the highest values of the diameter Reynolds number is excellent for this type of measurement.

The transition from a laminar boundary layer to a turbulent boundary layer for supersonic flow in a tube, with heat transfer is most easily detectable by the sudden sharp rise of the value of heat flux at the transition region, even though hardly any change in static pressure is evident. The numerical value of the length Reynolds number at inception of transition is in excellent agreement with similar published data for a laminar boundary layer on a flat plate.

The data indicate that a fairly great length of supersonic flow can be established in a tube with a laminar boundary layer over most of this length. Hence this type of apparatus represents an inexpensive supersonic wind tunnel for adiabatic and diabatic flow.

The one-dimensional flow model was used in this paper to reduce the experimental values to computed quantities in a simple and quick way. The computed quantities, however, are interpreted, related, and compared with essentially the correct phenomenological picture of the growth of a laminar boundary layer in a tube. The same original data will be treated in a companion paper by a more detailed analysis based on a two-dimensional flow model.

## Acknowledgments

The results presented here for local coefficients of heat transfer for supersonic flow represent the combined efforts of many graduate students. The assistance of the following men is gratefully acknowledged: A. G. Marcuse, K. K. Klingensmith, J. D. Wyant, W. J. Larkin, W. L. England, G. M. Ketchum, W. O. Young, B. W. Birmingham, L. J. Ingolfsrud, W. S. Wu, and P. Ashurkoff. Mrs. A. B. Walker assisted in some of the computational work. Prof. W. H. McAdams contributed to the design of the apparatus in its earlier stages.

This investigation is sponsored as Contract Number N5-ori-07805 by the Office of Naval Research of the United States Navy.

## BIBLIOGRAPHY

1 "Survey of Friction Coefficients, Recovery Factors, and Heat-Transfer Coefficients for Supersonic Flow," by J. Kaye, *Journal of the Aeronautical Sciences*, vol. 21, 1954, pp. 117–129.

2 "Experimental Velocity Profiles for Adiabatic Supersonic Flow of Air in a Tube," by J. Kaye, G. A. Brown, and J. J. Dieckmann, *Journal of the Aeronautical Sciences*, Readers' Forum, vol. 21, 1954, pp. 203–205.

3 "Experimental Velocity Profiles for Supersonic Flow of Air in a Tube With and Without Heat Transfer," by J. Kaye, G. A. Brown, J. J. Dieckmann, and E. A. Sziklas, presented at the Second U. S. National Congress of Applied Mechanics, University of Michigan, Ann Arbor, Mich., June, 1954.

4 "Theoretical Velocity and Temperature Profiles for the Laminar Boundary Layer of the Flow of a Compressible Fluid in the Entrance Region of a Tube," by T. Y. Toong and J. Kaye, presented at the Second U. S. National Congress of Applied Mechanics, University of Michigan, Ann Arbor, Mich., June, 1954.

5 "Measurement of Recovery Factors and Friction Coefficients for Supersonic Flow of Air in a Tube; Part I—Apparatus, Data, and Results Based on a Simple One-Dimensional Flow Model," by J. Kaye, J. H. Keenan, K. K. Klingensmith, G. M. Ketchum, and T. Y. Toong, Journal of Applied Mechanics, Trans. ASME, vol. 74, 1952, pp. 77–96.

6 "Measurement of Recovery Factors and Friction Coefficients for Supersonic Flow of Air in a Tube; Part II—Results Based on a Two-Dimensional Flow Model for Entrance Region," by J. Kaye, T. Y. Toong, and R. H. Shoulberg, Journal of Applied Mechanics, Trans. ASME, vol. 74, 1952, pp. 185–194.

7 "An Inexpensive Supersonic Wind Tunnel for Heat-Transfer Measurements; Part I—Apparatus, Data, and Results for a Laminar Boundary Layer Based on a Simple One-Dimensional Flow Model," by J. Kaye, J. H. Keenan, G. A. Brown, and R. H. Shoulberg, M.I.T. Technical Report, DIC No. 6418-7, June 1, 1954.

8 "The Laminar Boundary Layer of a Steady Compressible Flow in the Entrance Region of a Tube," by T. Y. Toong, ScD thesis, Massachusetts Institute of Technology, Cambridge, Mass., January, 1952.

9 "Investigation of Laminar Boundary Layer in Compressible Fluids Using the Crocco Method," by E. R. Van Driest, NACA TN 2597, January, 1952.

# Heat-Transfer Measurements in an Inexpensive Supersonic Wind Tunnel

## 2 Results for a Laminar Boundary Layer Based on a Two-Dimensional Flow Model

By JOSEPH KAYE[1] and G. A. BROWN,[2] CAMBRIDGE, MASS.

**Reliable experimental data on local heat-transfer coefficients for supersonic flow of air in a round tube are reanalyzed in detail with the aid of an approximate two-dimensional flow model. The results are compared with similar results based on a one-dimensional flow model and with the theoretical predictions for supersonic flow over a flat plate and for flow in the entrance region of a tube when a laminar boundary layer is present. The two-dimensional flow model yields a better understanding of the phenomena which occur for diabatic supersonic flow of air in a round tube than that obtained with the aid of the one-dimensional flow model. The two-dimensional flow model shows that the core Mach number is nearly constant along the length of test section for a range of values of the inlet diameter Reynolds number. For a laminar boundary layer the values of the local Stanton number agree within a few per cent with the theoretical values for plate flow at the largest values of the inlet diameter Reynolds number.**

### Nomenclature

The following nomenclature is used in the paper:

$a$ = inside radius of pipe
$A$ = cross-sectional area, $\pi D^2/4$
$A'$ = heat-transfer area, $\pi D \Delta L$
$c_p$ = specific heat at constant pressure
$c_w$ = discharge coefficient of nozzle
$D$ = inside diameter of pipe
$g$ = acceleration given to unit mass by unit force
$G$ = flow per unit area, $w/A$
$h$ = coefficient of heat transfer, $q/A'(t_w - t_{aw})$
$k$ = ratio of specific heats
$L$ = distance from end of curved contour of nozzle
$\mathsf{M}$ = Mach number, $V/\sqrt{gkRT}$
$n$ = summation index, Equation [15]
$\mathrm{Nu}_L$ = length Nusselt number, $hL/\lambda$
$p$ = static pressure
$q$ = net rate of heat transfer
$R$ = perfect-gas constant
$\mathrm{Re}_D$ = diameter Reynolds number, $DG/\mu g$
$\mathrm{Re}_L$ = length Reynolds number, $LG/\mu g$
St = Stanton number, $h/c_p G$
$t$ = temperature, deg F
$T$ = temperature, deg F abs
$V$ = velocity
$w$ = mass rate of flow
$\rho$ = density
$\mu$ = viscosity
$\lambda$ = thermal conductivity
$\delta$ = thickness of boundary layer

Superscript * refers to throat of supersonic nozzle where $\mathsf{M} = 1$.

Subscripts:

$aw$ = adiabatic wall conditions
$b$ = boundary layer
$c$ = isentropic core
$j$ = station numbers
0 = hypothetical entrance plane of the tube, where the boundary layer is of zero thickness
$0b$ = stagnation conditions in boundary layer
$0c$ = stagnation conditions in core
$0i$ = upstream stagnation conditions
$r$ = atmospheric conditions
$s$ = isentropic conditions
$w$ = wall conditions
$\infty$ = free-stream conditions for flat-plate flow

### Introduction

An inexpensive steady-state supersonic wind tunnel has been designed for accurate measurements of local heat-transfer coefficients. It consists of a convergent-divergent nozzle which delivers dry air at supersonic speeds to a test section, 1/2 in. diam and 30 to 50 diameters in length. The various test apparatusand the measurements obtained therefrom have been described previously in detail (1).[3] Sufficient measurements have been made to demonstrate their reliability when a laminar boundary layer exists in the test section for adiabatic and diabatic supersonic flow. The heat-transfer data were first analyzed (1) with the aid of a simple one-dimensional flow model, abbreviated hereafter as

[1] Associate Professor of Mechanical Engineering, Massachusett Institute of Technology. Mem. ASME.

[2] Shell Fellow in Mechanical Engineering, Massachusetts Institute of Technology. Assoc. Mem. ASME.

Contributed by the Applied Mechanics Division and presented at the Annual Meeting, New York, N. Y., November 28–December 3, 1954, of The American Society of Mechanical Engineers.

Discussion of this paper should be addressed to the Secretary, ASME, 29 West 39th Street, New York, N. Y., and will be accepted until October 10, 1955, for publication at a later date. Discussion received after the closing date will be returned.

Note: Statements and opinions advanced in papers are to be understood as individual expressions of their authors and not those of the Society. Manuscript received by ASME Applied Mechanics Division, June 15, 1954. This paper was not preprinted.

[3] Numbers in parentheses refer to the Bibliography at the end of the paper.

1-DFM, but it was shown that this model is not fully adequate to explain, interpret, and correlate these measurements.

The value of these measurements of local heat-transfer coefficients would be considerably enhanced if they could be compared with similar measurements for other types of supersonic flow with a laminar boundary layer, such as plate flow, cone flow, etc. One reason for subjecting the data given in (1) to further analysis and computation is to lay the foundation for such comparisons. A second reason is that accurately measured values of local heat-transfer coefficients for supersonic flow with a laminar boundary layer are practically nonexistent so that further analysis of tube-flow data might produce information useful to the designer of devices moving at supersonic speeds. A third reason for using a more complicated flow model to reanalyze the same data is to provide the experimenter with a better phenomenological explanation of the processes which occur in supersonic flow in the entrance region of a tube. The two-dimensional flow model, abbreviated hereafter as 2-DFM, will be used in this paper to analyze and interpret some selected values of the data given in (1).

The analysis of supersonic flow in the inlet region of a tube can be accomplished, on the one hand, in an extremely simple fashion, such as with the aid of the 1-DFM, and on the other hand, in an extremely difficult fashion, such as by investigation of the partial differential equations of energy, momentum, and continuity. Although both of these methods of analysis have been used in the present research program, an intermediate type of analysis is used here to obtain results close to those based on the most exact analysis. This 2-DFM should be considered to represent closely the actual supersonic flow phenomena in the tube.

The 2-DFM is used here only for supersonic flowin the entrance region of a tube with a laminar boundary layer originating at tube inlet. Experimentally it has been found possible to maintain a laminar boundary layer over the entire length of test section by careful control of the inlet conditions. Independent measurements of the velocity and temperature profiles of the tube flow for these inlet conditions have confirmed the existence of this laminar boundary layer. In the previous paper (1) certain values of the tube inlet conditions were selected to present the data for a laminar boundary layer. In the present paper the same values of these inlet conditions are selected to present the results of computation based on the 2-DFM. Comparisons of the results based on the 1-DFM and on the 2-DFM, for the same original data, will be given here. The results based on the 2-DFM also will be compared with theoretical solutions for plate flow and for tube flow.

## Assumptions for Two-Dimensional Flow Model With Heat Transfer

The 2-DFM arbitrarily divides the supersonic flow in the entrance region of a tube into two parts, a laminar boundary layer and a central core of fluid, as shown in Fig. 1. The laminar boundary layer originates near the tube inlet and grows in thickness by transference of mass from the central core. This 2-DFM is consistent with Prandtl's concept of the boundary layer since it is assumed that both the viscous and thermal effects are concentrated in the boundary layer, and that both are negligible in the core region; i.e., the fluid remaining in the central core undergoes an isentropic process. The basic soundness of this 2-DFM has been demonstrated conclusively by means of accurately measured velocity profiles at various positions along the test section of Fig. 1, for both adiabatic and diabatic flow (2, 3), and also by means of unpublished recently measured temperature profiles.

The present paper deals with a simplified version of the actual 2-DFM in that the actual velocity and temperature profiles are represented by simple approximations for both the laminar

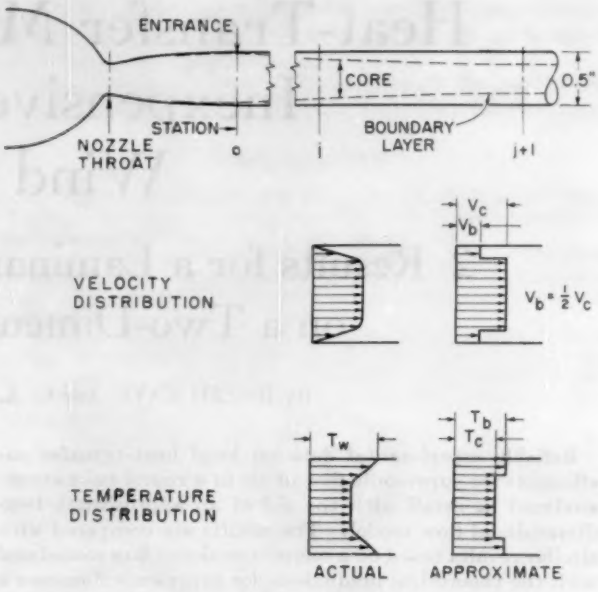


Fig. 1

boundary layer and the core. The boundary-layer thickness is assumed to be the same for both the velocity and thermal boundary layers. This thickness is arbitrarily taken to correspond to that thickness at which the local velocity in the boundary layer equals 99 per cent of the mean velocity in the core. These simplifications are shown in Fig. 1. They were introduced mainly to reduce the computational time since it was found, after considerable study, that the use of these simplified velocity and temperature profiles yielded results nearly identical to those obtained using a nonlinear velocity profile but requiring considerably greater computational time.

The following assumptions are made in the analysis of the 2-DFM:

1 A laminar boundary layer, in which both the viscous and thermal effects are predominant, exists for supersonic flow in the entrance region.

2 The air which remains in the central core undergoes an isentropic change of state from an upstream stagnation state to the static pressure measured at a given section.

3 The properties in the central core of fluid are assumed to be uniform at a given section.

4 The static pressure is assumed to be uniform across each section of the tube.

5 Air is a perfect gas with a constant value of the ratio of specific heats ($k = 1.40$) over the range of temperature under consideration.

6 The laminar boundary layer has a linear distribution of velocity which is further approximated by an average velocity in the boundary layer equal to one half the core velocity, as shown in Fig. 1.

7 The stagnation temperature of the central core is assumed to be constant at all sections, equal to $T_{oc}$, whereas the stagnation temperature of the boundary layer is assumed to be uniform at a given section but variable from section to section.

8 The flow is adiabatic up to the tube inlet where the heat transfer originates.

### Analysis of Simplified Two-Dimensional Flow Model With Heat Transfer

The following relations hold at each section of the flow in the tube shown in Fig. 1:

| | | |
|---|---|---|
| Continuity: | $w = w_b + w_c$ | [1] |
| Continuity: | $w_c = \rho_c V_c A_c$ | [2] |
| Continuity: | $w_b = \rho_b V_b A_b = \rho_b V_b (A - A_c)$ | [3] |
| Geometry: | $A_c = \pi[(D/2) - \delta]^2$ | [4] |
| Geometry: | $A = A_b + A_c$ | [5] |
| Equation of state: | $p = \rho_c R T_c$ | [6] |
| Equation of state: | $p = \rho_b R T_b$ | [7] |
| Definition: | $\mathsf{M}_c^2 \equiv V_c^2/gkRT_c$ | [8] |
| Assumption: | $V_b = V_c/2$ | [9] |

The following relations hold between the upstream stagnation state and a state in the core at any tube section:

| | | |
|---|---|---|
| Isentropic: | $p_{0i}/p = (\rho_{0i}/\rho_c)^k$ | [10] |
| Isentropic: | $T_{0i}/T_c = (p_{0i}/p)^{(k-1)/k}$ | [11] |
| Isentropic: | $T_{0i} = T_{0c}$ | [12] |
| Isentropic: | $c_p T_{0c} = c_p T_c + V_c^2/2g$ | [13] |
| Definition: | $c_p T_{0b} \equiv c_p T_b + V_b^2/2g$ | [14] |

Application of the energy equation for steady flow to a control volume which encloses the fluid between the upstream stagnation region and any tube section $j$ yields

$$(1/2)q_j + \sum_{n=1}^{n=j-1} q_n = w_{cj}(c_p T_{cj} + V_c^2/2g) + w_{bj}(c_p T_{bj} + V_b^2/2g) - w c_p T_{0i} \quad [15]$$

The summation in Equation [15] starts at the first station at which heat-transfer data were measured. This first station for test combinations C and D is described in reference (1).

*Method of Computation.* A sample calculation and the computed results, omitted from this paper for lack of space, can be found in reference (6).

### Results

*General.* The original measurements of heat-transfer coefficients for supersonic flow obtained with test combinations C and D, comprising four runs with the former and thirteen runs with the latter, are given in detail in (1). These data have been selected for those stagnation conditions where a laminar boundary layer is present over most of the test section. Hence the method of computation outlined in the foregoing for the simplified 2-DFM should be applicable for these seventeen runs. In view of the large amount of calculation involved, however, only seven runs have been studied in detail by means of the simplified 2-DFM, namely, one and six from test combinations C and D, respectively.

The results for six runs made with test combination D are given in Figs. 2 to 7, inclusive. Six charts were found necessary to present these results in sufficient detail because they are sensitive to small changes in the value of the inlet diameter Reynolds number. The results for one run made with test combination C are given in Fig. 8. One run was selected here mainly to reduce the total computational time and to show the effect of a shorter test section on the data. On each of these seven charts the calculated quantities based on one flow model are plotted without reference to the quantities calculated from the other flow model. Thus, in the curve of Mach number versus length Reynolds number, the

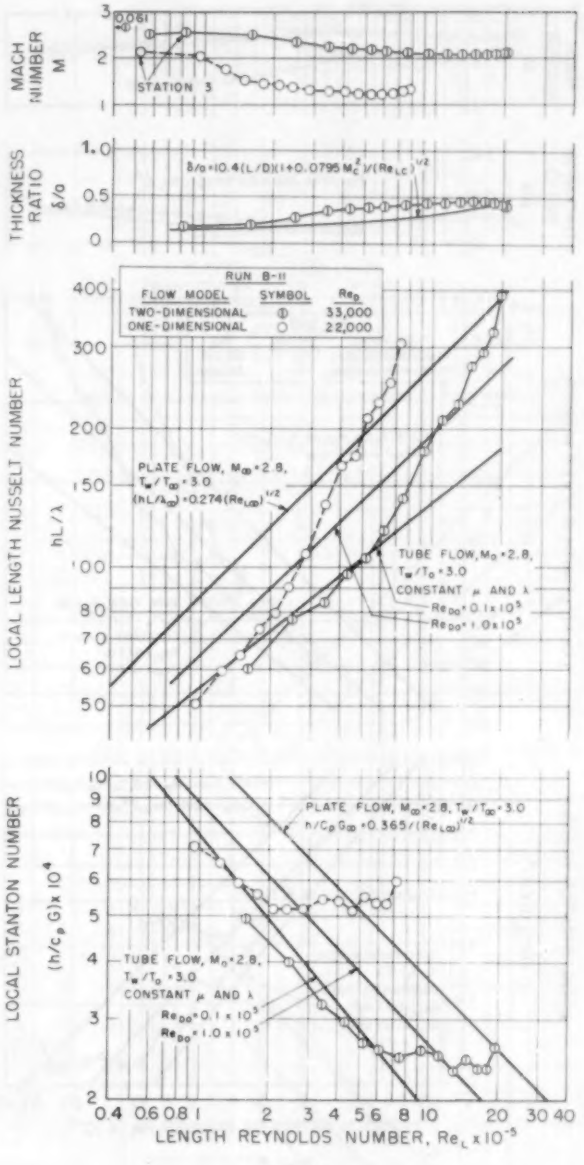


Fig. 2

values of Mach number and Reynolds number are taken from either the 1-DFM or from the 2-DFM.

Each of the seven charts presents the Mach number, boundary-layer thickness ratio, local length Nusselt number, and local Stanton number. For the 2-DFM, the Mach number, Nusselt number, and Stanton number are based on properties of the central core of fluid. The local Nusselt and Stanton numbers are, in reality, average values over the short length of flow of 2 or 4 pipe diameters. In the discussion of these seven charts, the value of the inlet diameter Reynolds number chosen for identification corresponds to that computed by means of the 2-DFM.

Each of the seven charts contains a comparison of the results based on the 2-DFM with the theoretical predictions of supersonic flow with a laminar boundary layer on a flat plate and with the theoretical predictions for tube flow for constant values of the viscosity and thermal conductivity. The former predictions are taken from Van Driest (4) and the latter from Toong (5). This

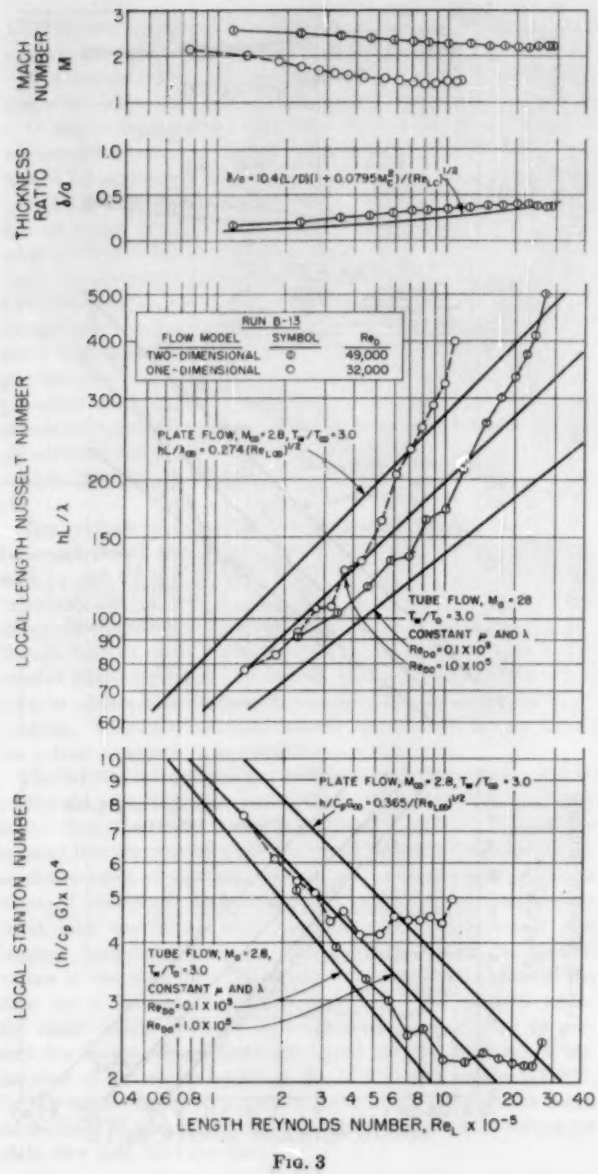
MACH NUMBER M
THICKNESS RATIO δ/a
δ/a = 10.4(L/D)(1 + 0.0795M_C^2)/(Re_LC)^1/2
LOCAL LENGTH NUSSELT NUMBER hL/λ
RUN B-13
FLOW MODEL SYMBOL Re_D
TWO-DIMENSIONAL ⊙ 49,000
ONE-DIMENSIONAL ○ 32,000
PLATE FLOW, M_∞ = 2.8, T_w/T_∞ = 3.0
hL/k_∞ = 0.274(Re_L∞)^1/2
TUBE FLOW, M_0 = 2.8
T_w/T_0 = 3.0
CONSTANT μ AND λ
Re_D0 = 0.1 X 10^5
Re_D0 = 1.0 X 10^5
LOCAL STANTON NUMBER (h/c_p G)x 10^4
PLATE FLOW, M_∞ = 2.8, T_w/T_∞ = 3.0
h/c_p G_∞ = 0.365/(Re_L∞)^1/2
TUBE FLOW, M_0 = 2.8,
T_w/T_0 = 3.0
CONSTANT μ AND λ
Re_D0 = 0.1 X 10^5
Re_D0 = 1.0 X 10^5
LENGTH REYNOLDS NUMBER, Re_L x 10^-5

FIG. 3

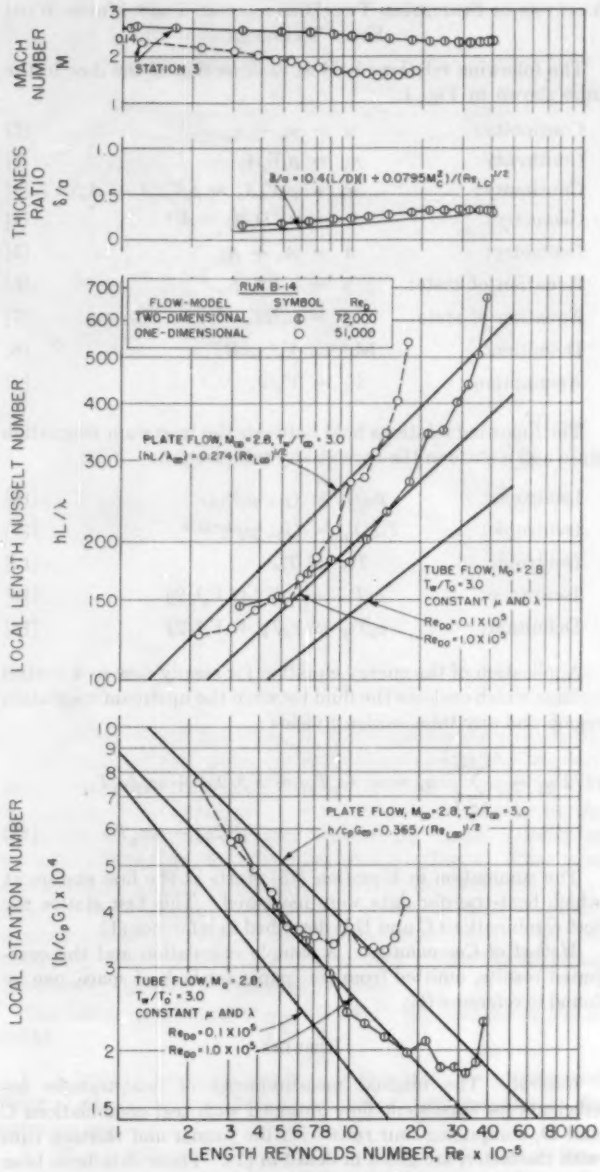
MACH NUMBER M
STATION 3
THICKNESS RATIO δ/a
δ/a = 10.4(L/D)(1 + 0.0795M_C^2)/(Re_LC)^1/2
LOCAL LENGTH NUSSELT NUMBER hL/λ
RUN B-14
FLOW MODEL SYMBOL Re_D
TWO-DIMENSIONAL ⊙ 72,000
ONE-DIMENSIONAL ○ 51,000
PLATE FLOW, M_∞ = 2.8, T_w/T_∞ = 3.0
(hL/k_∞) = 0.274(Re_L∞)^1/2
TUBE FLOW, M_0 = 2.8
T_w/T_0 = 3.0
CONSTANT μ AND λ
Re_D0 = 0.1 X 10^5
Re_D0 = 1.0 X 10^5
LOCAL STANTON NUMBER (h/c_p G)x 10^4
PLATE FLOW, M_∞ = 2.8, T_w/T_∞ = 3.0
h/c_p G_∞ = 0.365/(Re_L∞)^1/2
TUBE FLOW, M_0 = 2.8,
T_w/T_0 = 3.0
CONSTANT μ AND λ
Re_D0 = 0.1 X 10^5
Re_D0 = 1.0 X 10^5
LENGTH REYNOLDS NUMBER, Re x 10^-5

FIG. 4

type of comparison of results based on the 2-DFM with predictions for plate flow and for tube flow should be regarded as a temporary expedient until exact solutions for tube flow and accurate experimental data for plate flow with adverse pressure gradients are available.

*Results for Test Combination D—Mach Number.* Fig. 2 presents the results based on the simplified 2-DFM for the lowest value of the inlet diameter Reynolds number, namely, 33,000. The Mach number based on the 2-DFM decreased only from 2.7 to 2.1 along the length of the test section whereas that for the 1-DFM decreases from 2.1 to about 1.2. This same type of behavior of the Mach numbers for the two flow models is found also in Figs. 3 to 7. In Fig. 7 the Mach number based on the 2-DFM decreased only from 2.65 to 2.50 over 50 diameters of length of flow. This constancy of the Mach number based on the 2-DFM supports the contention that this type of test section is, in reality, a useful and inexpensive type of steady-state supersonic wind tunnel. The 2-DFM shows that the core Mach number does not vary as much as that indicated by the 1-DFM and that the value of the core Mach number is significantly greater than the corresponding value based on the 1-DFM. Independent measurements of velocity and temperature profiles at several stations near the tube exit lead to calculated values of the core Mach number which agree, within 1 per cent, with the values of the core Mach number based on the 2-DFM.

*Boundary-Layer Thickness.* The boundary-layer thickness at any section in the tube is defined by Equation [4] for the 2-DFM. It should be noted that this thickness is taken arbitrarily as zero in the 1-DFM. For the smaller values of the inlet diameter Reynolds number, namely, from 33,000 to 72,000 in Figs. 2, 3, and 4, this ratio increased from about 20 per cent at tube inlet to about 40 to 50 per cent at tube exit. For the larger values of Reynolds number, namely, from 88,000 to 115,000 in Figs. 5, 6, and 7, this ratio increases from about 10 per cent at tube inlet to about 25 per cent at tube exit. Such behavior of the thickness

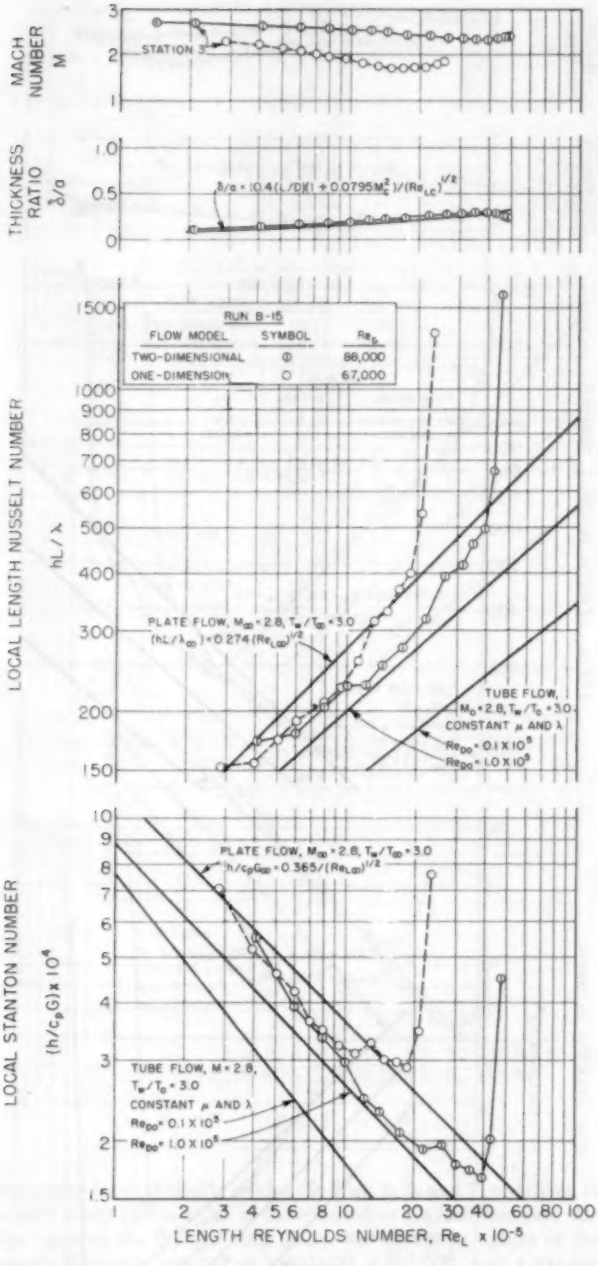
MACH NUMBER M
STATION 3
THICKNESS RATIO δ/a
δ/a = 10.4(L/D)(1 + 0.0795M_c²)/(Re_Lc)^1/2
RUN B-15
FLOW MODEL | SYMBOL | Re_D
TWO-DIMENSIONAL | ⊕ | 88,000
ONE-DIMENSION | ○ | 67,000
LOCAL LENGTH NUSSELT NUMBER hL/λ
PLATE FLOW, M_∞ = 2.8, T_w/T_∞ = 3.0
(hL/λ_∞) = 0.274(Re_L∞)^1/2
TUBE FLOW, M_o = 2.8, T_w/T_o = 3.0
CONSTANT μ AND λ
Re_Do = 0.1 X 10^5
Re_Do = 1.0 X 10^5
LOCAL STANTON NUMBER (h/c_pG) x 10^4
PLATE FLOW, M_∞ = 2.8, T_w/T_∞ = 3.0
h/c_pG_∞ = 0.365/(Re_L∞)^1/2
TUBE FLOW, M = 2.8,
T_w/T_o = 3.0
CONSTANT μ AND λ
Re_Do = 0.1 X 10^5
Re_Do = 1.0 X 10^5
LENGTH REYNOLDS NUMBER, Re_L x 10^-5

FIG. 5

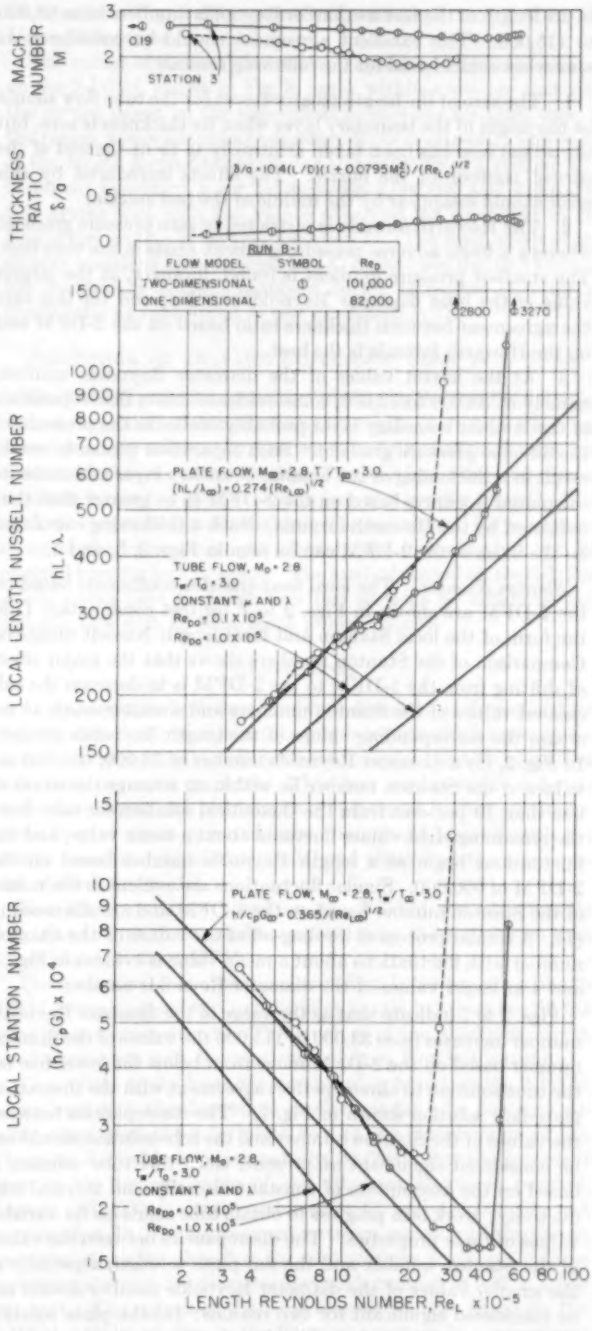
MACH NUMBER M
0.19
STATION 3
THICKNESS RATIO δ/a
δ/a = 10.4(L/D)(1 + 0.0795M_c²)/(Re_Lc)^1/2
RUN B-1
FLOW MODEL | SYMBOL | Re_D
TWO-DIMENSIONAL | ⊕ | 101,000
ONE-DIMENSIONAL | ○ | 82,000
0.2800
0.3270
LOCAL LENGTH NUSSELT NUMBER hL/λ
PLATE FLOW, M_∞ = 2.8, T_w/T_∞ = 3.0
(hL/λ_∞) = 0.274(Re_L∞)^1/2
TUBE FLOW, M_o = 2.8
T_w/T_o = 3.0
CONSTANT μ AND λ
Re_Do = 0.1 X 10^5
Re_Do = 1.0 X 10^5
LOCAL STANTON NUMBER (h/c_pG) x 10^4
PLATE FLOW, M_∞ = 2.8, T_w/T_∞ = 3.0
h/c_pG_∞ = 0.365/(Re_L∞)^1/2
TUBE FLOW, M_o = 2.8,
T_w/T_o = 3.0
CONSTANT μ AND λ
Re_Do = 0.1 X 10^5
Re_Do = 1.0 X 10^5
LENGTH REYNOLDS NUMBER, Re_L x 10^-5

FIG. 6

ratio could be interpreted in two ways. Either the laminar boundary layer does not fill the tube at exit and a fully developed flow pattern is not attained for this entrance type of flow, or for the flow length of 50 diameters the supersonic flow is, in reality, one corresponding to a fully developed flow but with a velocity profile which is quite different than that for fully developed incompressible flow in a round tube. Additional experimental data on velocity profiles for several stations near the tube exit are needed before these views can be resolved.

The thickness ratio for tube flow based on the 2-DFM can be compared with a similar ratio derived for the thickness of a laminar boundary layer of a compressible fluid flowing on a flat plate for zero pressure gradient. The theoretical results of Howarth (7) lead to the following equation for the thickness ratio

$$(\delta/a) = 10.4(L/D)(1 + 0.0795\,M_e^2)/(\mathrm{Re}_{Le})^{1/2} \quad \ldots\ldots [16]$$

Here the thickness corresponds to that value at which the local velocity in the boundary layer on the flat plate is 99 per cent of the free-stream value. The values of the thickness ratio based on the 2-DFM are slightly larger than those based on Equation [16] for values of the diameter Reynolds number from 33,000 to 72,000, but both sets of values are in excellent agreement over the

entire length of the test section for Reynolds numbers from 88,000 to 115,000. This excellent agreement should be considered as somewhat coincidental for the following reasons:

1 The zero of the length measurement for the tube flow should be the origin of the boundary layer when its thickness is zero, but the actual zero has been taken arbitrarily to be at the end of the curved contour of the nozzle. The effects introduced by this error should disappear by the middle of the test section.

2 The Howarth formula is restricted to zero pressure gradient whereas a finite adverse pressure gradient exists in the tube flow. The smallest pressure gradient is found, however, at the largest value of the inlet diameter Reynolds number, and for this case the agreement between thickness ratio based on the 2-DFM and on the Howarth formula is the best.

3 At the lowest values of the diameter Reynolds number, namely at 33,000 to 72,000, some evidence exists that separation of the laminar boundary layer probably occurs in the presence of the adverse pressure gradient. Such separation probably would result in a thickening of the laminar boundary layer and cause its calculated thickness based on the 2-DFM to be greater than that indicated by the Howarth formula. Such a thickening calculated on the basis of the 2-DFM can be seen in Figs. 2, 3, and 4.

*Stanton Number.* The local heat-transfer coefficients based on the 2-DFM are shown in Figs. 2 to 7 for test combination D in the form of the local Stanton and local length Nusselt numbers. Comparison of the Stanton numbers shows that the major effect of shifting from the 1-DFM to the 2-DFM is to decrease the calculated values of the Stanton numbers and simultaneously to increase the corresponding values of the length Reynolds number. In Fig. 2, for a diameter Reynolds number of 33,000, the first six values of the Stanton number lie within an average deviation of less than 10 per cent from the theoretical solution for tube flow, the remaining eight values fluctuate about a mean value, and the fluctuations begin at a length Reynolds number based on the 2-DFM of 600,000. Similar fluctuations are evident in the values of the Stanton number based on the 1-DFM and are discussed in (1). A similar process of leveling-off of the values of the Stanton number with fluctuations about a mean value is evident in Figs. 3 and 4 at larger values of the diameter Reynolds number.

Figs. 2 to 7 indicate that as the value of the diameter Reynolds number increases from 33,000 to 115,000 the values of the Stanton number based on the 2-DFM move from below the lower line for the tube solution to almost perfect agreement with the theoretical plate-flow solution shown in Fig. 7. The discrepancies between the values of the Stanton number and the tube solution should not be considered significant at present, since this tube solution is based on the assumption of constant viscosity and thermal conductivity; work is in progress to obtain tube solutions for variable values of these properties. The discrepancies between the values of the Stanton number and the flat-plate solution, especially at the smaller values of the diameter Reynolds number should not be considered significant for two reasons: (*a*) the plate solution is based on zero pressure gradient but the data were taken with an adverse pressure gradient in the tube; note that the best agreement between the tube-flow data and the flat-plate solution occurs for the smallest value of the adverse pressure gradient in the tube. (*b*) At the smallest values of the diameter Reynolds number, there is some evidence of separation of the laminar boundary layer so that one would expect some deviations from the theoretical solution for plate flow in which separation effects were neglected.

*Nusselt Number.* The values of the local length Nusselt number based on the 2-DFM and on the 1-DFM are also shown in Figs. 2 to 7. The main reason for including the Nusselt number is to compare the value of plotting the calculations in different

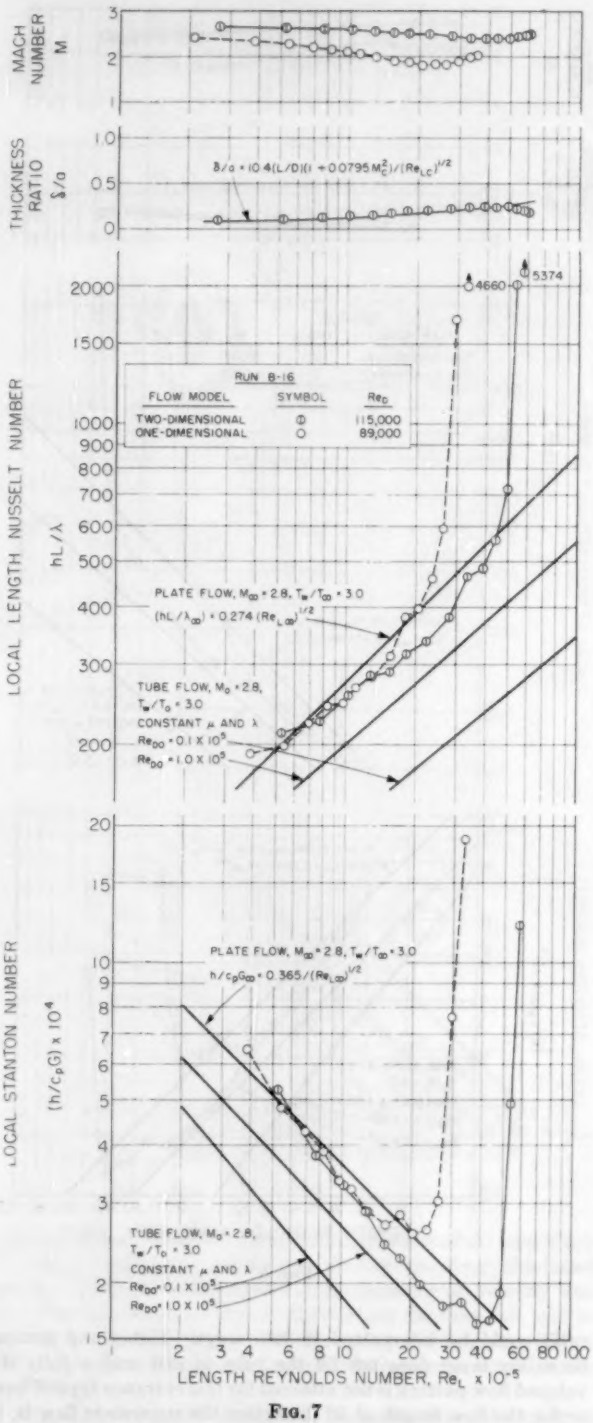


FIG. 7

ways. All the conclusions reached so far with the aid of the curves of Stanton number are also evident from examination of curves for the Nusselt number, except that the leveling-off of the Stanton numbers in Figs. 2, 3, and 4 is almost completely masked in the sharply rising values of the Nusselt number at the same length Reynolds number. This masking is a result of using the tube length as a multiplicative factor in the Nusselt number.

*Transition.* The transition from a laminar to a turbulent

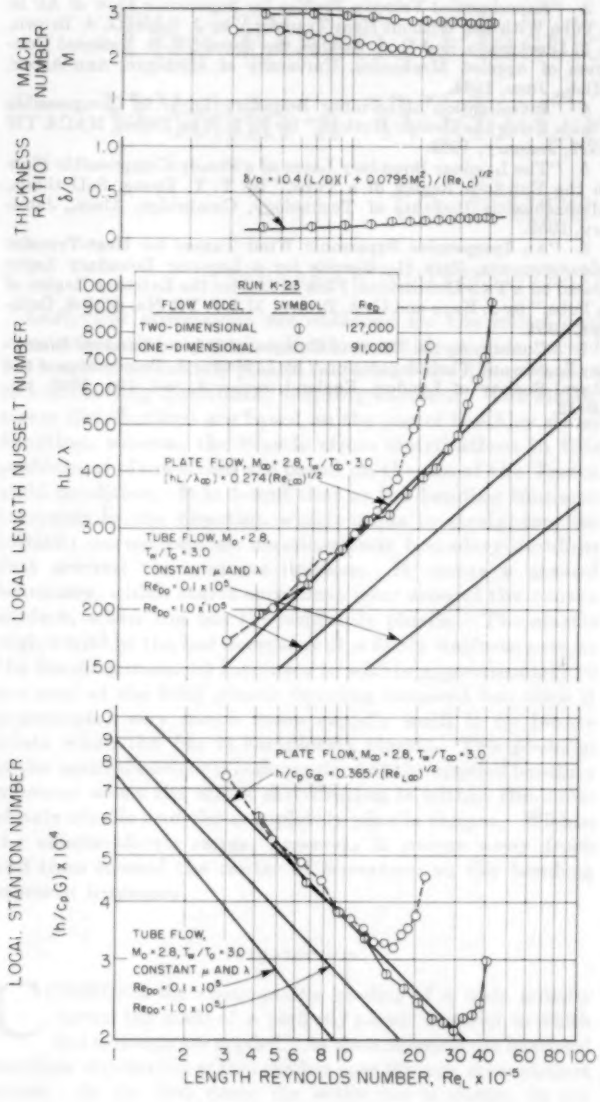
MACH NUMBER M
THICKNESS RATIO δ/a
δ/a = 10.4 (L/DX1 + 0.0795 M_C^2)/(Re_LC)^1/2
LOCAL LENGTH NUSSELT NUMBER hL/λ
RUN K-23
FLOW MODEL
SYMBOL
Re_D
TWO-DIMENSIONAL
127,000
ONE-DIMENSIONAL
91,000
PLATE FLOW, M∞ = 2.8, Tw/T∞ = 3.0
(hL/λ∞) = 0.274 (Re_L∞)^1/2
TUBE FLOW, M0 = 2.8, Tw/T0 = 3.0
CONSTANT μ AND λ
Re_D∞ = 0.1 x 10^5
Re_D∞ = 1.0 x 10^5
LOCAL STANTON NUMBER (h/cpG) x 10^4
PLATE FLOW, M∞ = 2.8, Tw/T∞ = 3.0
h/cp G∞ = 0.365/(Re_L∞)^1/2
TUBE FLOW, M0 = 2.8, Tw/T0 = 3.0
CONSTANT μ AND λ
Re_D∞ = 0.1 x 10^5
Re_D∞ = 1.0 x 10^5
LENGTH REYNOLDS NUMBER, Re_L x 10^-5

FIG. 8

boundary layer is clearly evident in Figs. 5, 6, and 7, occurring as a very sharp rise in value of the Stanton or Nusselt number. On the basis of the 2-DFM, this sharp rise occurs at values of the length Reynolds number of 4,000,000, 4,500,000, and 4,500,000 in Figs. 5, 6, and 7, respectively. These values of the length Reynolds number at the start of transition are in good accord with values given in the literature for transition of a laminar boundary layer on a flat plate with zero pressure gradient.

*Results for Test Combination C—Effect of Shorter Test Section.* The results of using the 2-DFM for calculation of one run with test combination C are shown in Fig. 8. The value of the inlet diameter Reynolds number is 127,000, which corresponds to the highest value for test combination D shown in Fig. 7. Hence the effect of a shorter length of test section may be obtained by comparison of these two figures. Fig. 8 shows that the value of the Mach number, based on the 2-DFM, remains nearly constant. The boundary-layer thickness ratio increases from 10 per cent at inlet to about 20 per cent at exit, thus duplicating the behavior of the boundary-layer thickness ratio of test combination D in Fig. 7. This ratio in Fig. 8 also agrees well with that computed by the Howarth formula.

The values of the local Stanton and local Nusselt numbers based on the 2-DFM, shown in Fig. 8, agree within a few per cent with the values based on the theoretical predictions for plate flow, in the region where a laminar boundary layer is present. The value of the length Reynolds number at transition from a laminar to a turbulent boundary layer lies between 3,000,000 and 4,000,000; this agrees well with the values observed for transition in the longer test section of test combination D. The main effect of the shorter length of test combination C is that the rise in values of the Stanton or Nusselt numbers during transition is never as spectacular as that found in test combination D.

## Prediction of Diabatic Supersonic Flow in a Tube

The 2-DFM provides a means of predicting the flow behavior for diabatic supersonic flow in the entrance region of a tube if a laminar boundary layer exists. In essence, this method of prediction was confirmed when test combination D was designed to be 50 diameters long instead of 30 for the previous test combination C. The analysis for prediction for diabatic flow is obtained by rearrangement of the basic equations given in the foregoing but will be omitted here for lack of space. The analysis based on the 2-DFM is also being used to design new test sections for adiabatic and diabatic flow with an inlet Mach number near 5.

## Conclusions

An approximate and simplified two-dimensional flow model for the entrance flow region of a tube yields results which are in agreement with theoretical predictions for tube flow and for plate flow with zero pressure gradient. This flow model yields a better understanding of the phenomena which occur in diabatic supersonic flow of air in a round tube than that obtained with the simple one-dimensional flow model and eliminates the inadequacies of the latter model.

The Mach numbers based on the 2-DFM are significantly larger and much more nearly constant along the test section than those based on the 1-DFM.

The thickness of the laminar boundary layer based on the 2-DFM increases slowly from tube inlet to exit but does not fill the tube cross section at exit. These values of the thickness are in good agreement with those calculated from Howarth's results.

The values of the local Stanton number based on the 2-DFM agree best with the theoretical predictions for tube flow and deviate most from those for plate flow at the lowest value of the diameter Reynolds number, namely, 33,000. But the reverse is true at the highest value of the diameter Reynolds number, namely, 127,000 for test combination C, and 115,000 for test combination D. The agreement between measured tube values and predictions for plate flow for zero pressure gradient for these last two values of the diameter Reynolds number is within a few per cent. The values of the local Nusselt number based on the 2-DFM behave similar to the Stanton numbers in comparisons with the theoretical predictions for tube flow and plate flow but are of less value in understanding and interpreting the phenomena.

The effect of varying the length of test section from 30 to 50 diameters on the results based on the 2-DFM is negligible, except that the shorter length does not delineate transition as clearly.

The transition from a laminar to a turbulent boundary layer for diabatic supersonic flow in a tube is clearly evident in the sudden and very sharp rise of the values of the local Stanton number. The values of the length Reynolds number at the start of the transition are in excellent agreement with similar data for a laminar boundary layer on a flat plate.

### Acknowledgments

The assistance of W. S. Wu, P. Ashurkoff, D. M. Coleman, and Mrs. A. B. Walker in the computations is gratefully acknowledged.

This investigation is sponsored as Contract Number N5-ori-07805 by the Office of Naval Research of the United States Navy.

### BIBLIOGRAPHY

1 "An Inexpensive Supersonic Wind Tunnel for Heat-Transfer Measurements, Part I—Apparatus, Data, and Calculated Results for a Laminar Boundary Layer Based on a Simple One-Dimensional Flow Model," by J. Kaye, J. H. Keenan, G. A. Brown, and R. H. Shoulberg, M.I.T. TR No. 6418-7, June 1, 1954. A condensation of this report is published in this issue, pp. 289–296.

2 "Experimental Velocity Profiles for Adiabatic Supersonic Flow of Air in a Tube," by J. Kaye, G. A. Brown, and J. J. Dieckmann, *Journal of the Aeronautical Sciences*, Readers' Forum, vol. 21, 1954, pp. 203–205.

3 "Experimental Velocity Profiles for Supersonic Flow of Air in a Tube With and Without Heat Transfer," by J. Kaye, G. A. Brown, J. J. Dieckmann, and E. A. Sziklas, the Second U. S. National Congress of Applied Mechanics, University of Michigan, Ann Arbor, Mich., June, 1954.

4 "Investigation of Laminar Boundary Layer in Compressible Fluids Using the Crocco Method," by E. R. Van Driest, NACA TN 2597, January, 1952.

5 "The Laminar Boundary Layer of a Steady Compressible Flow in the Entrance Region of a Tube," by T. Y. Toong, ScD thesis, Massachusetts Institute of Technology, Cambridge, Mass., January, 1952.

6 "An Inexpensive Supersonic Wind Tunnel for Heat-Transfer Measurements, Part II—Results for a Laminar Boundary Layer Based on a Two-Dimensional Flow Model for the Entrance Region of a Tube," by J. Kaye and G. A. Brown, M.I.T. TR No. 6418-8, October, 1954.

7 "Concerning the Effect of Compressibility on Laminar Boundary Layers and Their Separation," by L. Howarth, Proceedings of the Royal Society of London, England, series A, vol. 194, 1948, pp. 16–42.

# The Elastic-Plastic Stress Distribution Within a Wide Curved Bar Subjected to Pure Bending[1]

By BERNARD W. SHAFFER[2] and RAYMOND N. HOUSE, JR.,[3] NEW YORK, N. Y.

**Analytical expressions are obtained for the radial and circumferential stress distributions within a wide curved bar made of a perfectly plastic material when it is subjected to a uniformly distributed bending moment. The elastic stress distributions are based on the use of the Airy stress function, whereas the plastic stress distributions in this problem of plane strain are based on the use of the Tresca yield condition. It is found that as the bending moment increases in the direction which tends to straighten the initially curved bar, an elastic-plastic boundary develops first around the concave surface. It meets a second boundary, which starts sometime later around the convex surface, when the bar is completely plastic. The elastic region within the bar decreases at a fairly uniform rate as the bending moment increases to within approximately 90 per cent of the fully plastic bending moment but then it degenerates very much more rapidly until it no longer exists when the bar is completely plastic. The position of the neutral surface is independent of the applied bending moment when the stress distribution is within the completely elastic and the completely plastic ranges. Within the elastic-plastic range, however, it moves away from and then toward the center of curvature as the bending moment increases.**

## Introduction

CONSIDER the elastic-plastic bending of a wide initially curved bar made of a perfectly plastic material to which end moments are applied. As these moments are increased the stress distribution within the bar goes through three distinct phases. In the first phase the entire bar is elastic; in the second a portion of the bar is plastic whereas the remainder is elastic; in the third phase the entire bar is plastic. It is our intention to present a solution for the stress distribution within the bar during each of these phases. Even though the completely elastic[4] and the completely plastic[5,6] solutions to this problem have been previously reported, these solutions will be repeated here because they will serve as the limiting case to the problem with which we are primarily concerned.

A typical section of the curved bar, which is of uniform cross section and whose dimension perpendicular to the plane of curvature is very large, is shown in Fig. 1(*a*). The bending moment is uniformly distributed along the length of the bar. Aside from end sections, therefore, we may calculate the stress distribution at any radial section as a problem in plane strain.

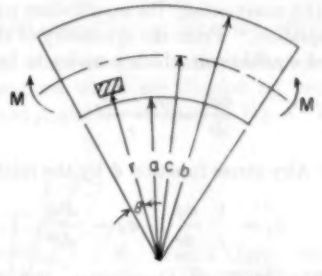


Fig. 1(*a*) Geometry of the Curved Bar

Let $a$ and $b$ denote the inner and outer radii of the curved bar, respectively, and $M$ the bending moment per unit length perpendicular to the plane of the paper. The stresses on a typical element within the bar, shown shaded in Fig. 1(*a*), are shown in Fig. 1(*b*) where $\sigma_r$ denotes the radial stress and $\sigma_\theta$ the circumferential stress. These stresses do not depend on $\theta$ but only on $r$, because the bending moment is the same in all radial cross sections. We will obtain, in this paper, expressions for the stresses $\sigma_\theta$ and $\sigma_r$ for each of the three phases of the problem.

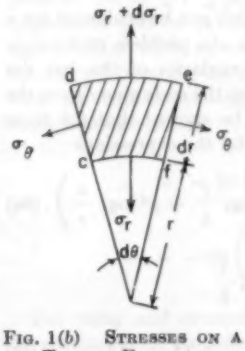


Fig. 1(*b*) Stresses on a Typical Element

The strains in the elastic-plastic problem are of the order of magnitude of elastic strains. We may assume, therefore, as we do in an elastic solution, that the physical dimensions of the bar do not change significantly during loading.

A perfectly plastic material obeys Hooke's law within the elastic range and does not work-harden within the plastic range. Plastic flow occurs whenever the stress

---

[1] The results presented in this paper were obtained in the course of research sponsored by the Office of Ordnance Research, Department of the Army (Ordnance Corps) under Contract No. DA-30-069-ORD-1135, with New York University.

[2] Associate Professor of Mechanical Engineering, New York University. Assoc. Mem. ASME.

[3] Instructor of Mechanical Engineering, New York University. Assoc. Mem. ASME.

Contributed by the Applied Mechanics Division and presented at the Annual Meeting, New York, N. Y., November 28–December 3, 1954, of The American Society of Mechanical Engineers.

Discussion of this paper should be addressed to the Secretary, ASME, 29 West 39th Street, New York, N. Y., and will be accepted until October 10, 1955, for publication at a later date. Discussion received after the closing date will be returned.

Note: Statements and opinions advanced in papers are to be understood as individual expressions of their authors and not those of the Society. Manuscript received by ASME Applied Mechanics Division, March 26, 1954. Paper No. 54—A-94.

[4] "Theory of Elasticity," by S. Timoshenko and J. N. Goodier, McGraw-Hill Book Company, Inc., New York, N. Y., second edition, 1951, pp. 61–65.

[5] "The Mathematical Theory of Plasticity," by R. Hill, Oxford University Press, London, England, 1950, pp. 287–289.

[6] "Bending of an Ideal Plastic Metal," by J. D. Lubahn and G. Sachs, Trans. ASME, vol. 72, 1950, pp. 201–208.

components satisfy the Tresca yield condition,[7] namely

$$\sigma_{max} - \sigma_{min} = 2k \quad [1]$$

where $k$ is the maximum shear stress of the material equal to one half the tensile yield stress. For plane strain

$$\sigma_r \leq \sigma_z \leq \sigma_\theta, \quad \text{or } \sigma_\theta \leq \sigma_z \leq \sigma_r \quad [2]$$

where $\sigma_z$ is the stress in the longitudinal direction, perpendicular to the plane of curvature.

For the problem of pure bending there are no shear stresses acting on the element $c$-$d$-$e$-$f$ which is shown in Fig. 1($b$). The stresses $\sigma_r$, $\sigma_\theta$, and $\sigma_z$ are, therefore, the principal stresses and the Tresca yield condition may be written in the form

$$\sigma_\theta - \sigma_r = 2k \quad [3a]$$

or

$$\sigma_r - \sigma_\theta = 2k \quad [3b]$$

whichever is applicable.

## The Elastic Solution

The stresses on a typical element within the elastic range, shown in Fig. 1($b$), must satisfy the equilibrium equation and the compatibility equation.[4] From the symmetry of the problem, the only equation of equilibrium which remains to be satisfied is

$$\frac{d\sigma_r}{dr} = \frac{\sigma_\theta - \sigma_r}{r} \quad [4]$$

If we define the Airy stress function $\phi$ by the relationships

$$\sigma_r = \frac{1}{r}\frac{d\phi}{dr}, \quad \sigma_\theta = \frac{d^2\phi}{dr^2} \quad [5]$$

the equation of equilibrium is identically satisfied, and the compatibility equation reduces to

$$\frac{d^4\phi}{dr^4} + \frac{2}{r}\frac{d^3\phi}{dr^3} - \frac{1}{r^2}\frac{d^2\phi}{dr^2} + \frac{1}{r^3}\frac{d\phi}{dr} = 0 \quad [6]$$

Its solution is

$$\phi = A \log_e r + Br^2 \log_e r + Cr^2 + D \quad [7]$$

where $A$, $B$, $C$, and $D$ are constants which can be evaluated for a given set of boundary conditions. For the problem under consideration the concave and convex boundaries of the bar are stress-free whereas the normal stresses at the ends give rise to the applied bending moment $M$. It can be shown[4] that for these conditions the elastic solution is given by the expressions

$$\sigma_r = -\frac{4M}{N}\left(\frac{a^2b^2}{r^2}\log_e\frac{b}{a} + b^2\log_e\frac{r}{b} + a^2\log_e\frac{a}{r}\right) \quad [8a]$$

$$\sigma_\theta = -\frac{4M}{N}\left(-\frac{a^2b^2}{r^2}\log_e\frac{b}{a} + b^2\log_e\frac{r}{b} + a^2\log_e\frac{a}{r} + b^2 - a^2\right) \quad [8b]$$

where

$$N = (b^2 - a^2)^2 - 4a^2b^2\left(\log_e\frac{b}{a}\right)^2 \quad [8c]$$

Whenever bending is in the direction shown in Fig. 1($a$), the radial stress $\sigma_r$ is always tensile whereas the circumferential stress $\sigma_\theta$ is compressive near the outer surface but tensile near the inner surface. At a particular radius $r = c$, the radius of the neutral surface, the circumferential stress is zero. We can see from Equation [8$b$] that the position of the neutral surface depends only on the geometry of the problem, not on the applied load.

As the bending moment increases, $\sigma_\theta$ and $\sigma_r$ increase, and so does the difference in their numerical value. This difference is greatest at the inner surface of the curved bar and it is this surface, therefore, at which yielding will begin. The corresponding bending-moment expression may be obtained by substituting the expressions for $\sigma_r$ and $\sigma_\theta$ at $r = a$ (see Equations [8]) into the yield condition, Equation [3$a$], to find

$$M = \frac{k\left[(b^2 - a^2)^2 - 4a^2b^2\left(\log_e\frac{b}{a}\right)^2\right]}{2\left(a^2 - b^2 + 2b^2\log_e\frac{b}{a}\right)} \quad [9]$$

With an increase in bending moment exceeding the numerical value given in Equation [9], a plastic zone forms around the lower fibers of the cross section and we enter upon what we will call the first stage of the elastic-plastic solution.

## The Elastic-Plastic Solution—Stage 1

In view of the symmetry of the problem, the stress distribution at each radial cross section is identical, and should the elastic-plastic boundary be at $r = \rho_i$ in one section, it will be in the same place in every other section. For this problem, therefore, unlike most elastic-plastic problems, it is possible to predict the shape of the elastic-plastic boundary. Its position, of course, would depend on the applied moment.

Fig. 2 First Stage of the Elastic-Plastic Solution

The position of the elastic-plastic boundary for Stage 1 is shown in Fig. 2. The plastic zone is contained within the region $a \leq r \leq \rho_i$ whereas the elastic zone is contained within the region $\rho_i \leq r \leq b$.

Every element within the plastic zone satisfies the equation of equilibrium, Equation [4], and the yield condition. Equation [3$a$] is the appropriate yield condition for this region because the circumferential stresses below the neutral surface are tensile and greater than the radial stresses. Upon substituting Equation [3$a$] into Equation [4] and reintroducing the results into Equation [3$a$], we find that the stresses within the plastic zone are

$$\sigma_r = 2k\log_e\frac{r}{a}, \quad a \leq r \leq \rho_i \quad [10]$$

$$\sigma_\theta = 2k\left(1 + \log_e\frac{r}{a}\right), \quad a \leq r \leq \rho_i \quad [11]$$

Within the elastic zone, the stresses from Equations [5] and [7] are

[7] "Theory of Perfectly Plastic Solids," by W. Prager and P. G. Hodge, Jr., John Wiley & Sons, Inc., New York, N. Y., 1951, p. 23.

$$\sigma_r = \frac{A}{r^2} + B(1 + 2\log_e r) + 2C \quad \ldots\ldots [12a]$$

$$\sigma_\theta = -\frac{A}{r^2} + B(3 + 2\log_e r) + 2C \quad \ldots\ldots [12b]$$

At the convex surface of the elastic zone, $r = b$, the radial stress $\sigma_r$ is equal to zero. At the concave surface, the boundary between the elastic and plastic regions, the radial and circumferential stresses are continuous. In view of Equations [10] and [11], the stresses within the elastic region, $\rho_i \leq r \leq b$, described in Equations [12] are given, therefore, by the expressions

$$\sigma_r = \frac{2k}{N_1\rho_i^2b^2r^2}\left\{\rho_i^2b^2\log_e\frac{b}{a} - r^2\left[\rho_i^2\log_e\frac{r}{a} + b^2\left(1 + 2\log_e\frac{\rho_i}{a}\right)\log_e\frac{b}{r}\right]\right\} \quad \ldots\ldots [13]$$

$$\sigma_\theta = \frac{2k}{N_1\rho_i^2b^2r^2}\left\{r^2\left[b^2\left(1 + 2\log_e\frac{\rho_i}{a}\right)\left(1 - \log_e\frac{b}{r}\right) - \rho_i^2\left(1 + \log_e\frac{r}{a}\right)\right] - \rho_i^2b^2\log_e\frac{b}{a}\right\} \quad \ldots\ldots [14]$$

where

$$N_1 = \frac{b^2 - \rho_i^2 - 2b^2\log_e\dfrac{b}{\rho_i}}{\rho_i^2b^2}$$

The position of the neutral surface $r = c$, corresponding to $\sigma_\theta$ equal to zero, is then given by the expression

$$\left(1 + 2\log_e\frac{\rho_i}{a}\right)\left(1 - \log_e\frac{b}{c}\right) - \frac{\rho_i^2}{b^2}\left(1 + \log_e\frac{c}{a}\right) = \frac{\rho_i^2}{c^2}\log_e\frac{b}{a} \quad \ldots\ldots [15]$$

The bending moment per unit width of cross section during the

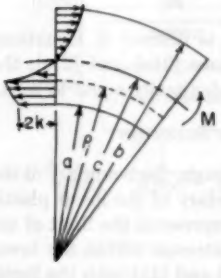


FIG. 3 (*Left*) CIRCUMFERENTIAL STRESS DISTRIBUTION ON A SECTOR OF THE BAR DURING THE FIRST STAGE OF THE ELASTIC-PLASTIC SOLUTION

first stage of the elastic-plastic solution is obtained by considering the equilibrium of the section shown in Fig. 3

$$-M = \int_a^{\rho_i}\sigma_\theta r dr + \int_{\rho_i}^{b}\sigma_\theta r dr \quad \ldots\ldots [16]$$

If we substitute the expressions for $\sigma_\theta$ found in Equations [11] and [14] into the first and second integrals on the right-hand side of Equation [16], respectively, the resulting expression is

$$\left(\frac{2M}{k} - a^2\right)\left(1 - \frac{\rho_i^2}{b^2} - 2\log_e\frac{b}{\rho_i}\right) = \rho_i^2\left[1 + 2\left(1 + 2\log_e\frac{b}{\rho_i}\right)\log_e\frac{b}{a}\right] - b^2\left(1 + 2\log_e\frac{\rho_i}{a}\right) \quad \ldots\ldots [17]$$

Equation [17] also may be used to establish the position of the elastic-plastic boundary $\rho_i$ for a given bending moment. Its numerical value is needed to evaluate the stress components as well as the position of the neutral axis.

A check on the stress distribution computed in this section shows that the resultant force vanishes across an arbitrary radial cross section.

As the applied moment increases so do the stress components in the elastic region. When the moment is large enough, yielding will begin at the convex surface of the bar. The stress components at this surface, given by Equations [13] and [14] for $r = b$, satisfy the yield condition, Equation [3*b*], whenever

$$b^2\left(1 - \log_e\frac{ab}{\rho_i^2}\right) = \rho_i^2\left(1 + \log_e\frac{b}{a}\right) \quad \ldots\ldots [18]$$

The corresponding bending moment may be found by substituting the numerical value of $\rho_i$, specified in Equation [18], into Equation [17]. Bending moments greater than that obtained from the simultaneous solution of these equations will cause the appearance of an upper plastic zone which together with the existing lower plastic zone will advance toward the neutral surface. Thus we enter the second stage of the elastic-plastic solution.

## THE ELASTIC-PLASTIC SOLUTION—STAGE 2

In the second stage of the elastic-plastic solution there are three distinct regions which are divided by two elastic-plastic boundaries, one at $\rho_i$ and the other at $\rho_0$, Fig. 4. For $a \leq r \leq \rho_i$,

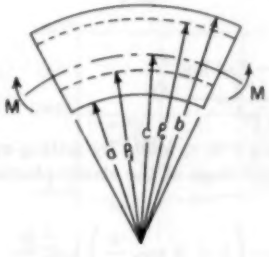


FIG. 4 (*Left*) SECOND STAGE OF ELASTIC-PLASTIC SOLUTION

the plastic solution given by Equations [10] and [11] is still applicable; for $\rho_i \leq r \leq \rho_0$, the elastic solution, Equations [12], is applicable; and for $\rho_0 \leq r \leq b$, a different plastic solution will apply. Since $\sigma_r > \sigma_\theta$ within this region, this latter solution is determined by using the yield condition, Equation [3*b*], together with the equilibrium equation, Equation [4]. Therefore the stresses are given by

$$\sigma_r = 2k\log_e\frac{b}{r}, \quad \rho_0 \leq r \leq b \quad \ldots\ldots [19]$$

$$\sigma_\theta = -2k\left(1 - \log_e\frac{b}{r}\right), \rho_0 \leq r \leq b \quad \ldots\ldots [20]$$

The radial and circumferential stresses are continuous across the elastic-plastic boundaries, $r = \rho_i$ and $r = \rho_0$. Hence in view of Equations [10], [11], [12], [19], and [20] we may write

$$\frac{A}{\rho_i^2} + B(1 + 2\log_e\rho_i) + 2C = 2k\log_e\frac{\rho_i}{a} \quad \ldots\ldots [21a]$$

$$-\frac{A}{\rho_i^2} + B(3 + 2\log_e\rho_i) + 2C = 2k\left(1 + \log_e\frac{\rho_i}{a}\right). \quad [21b]$$

$$\frac{A}{\rho_0^2} + B(1 + 2\log_e\rho_0) + 2C = 2k\log_e\frac{b}{\rho_0} \quad \ldots\ldots [21c]$$

$$-\frac{A}{\rho_0^2} + B(3 + 2\log_e \rho_0) + 2C = -2k\left(1 - \log_e \frac{b}{\rho_0}\right) \quad [21d]$$

From the first three Equations [21a–c] we may evaluate the constants $A$, $B$, $C$, which, upon substitution into Equation [21d], yields

$$\rho_0^2\left(1 - \log_e \frac{ab}{\rho_i^2}\right) = \rho_i^2\left(1 + \log_e \frac{\rho_0^2}{ab}\right) \quad [22]$$

a relationship between the positions of the elastic-plastic boundaries.

The stresses in the elastic region $\rho_i \leq r \leq \rho_0$, given by Equations [12], are now given as

$$\sigma_r = \frac{2k}{N_2\rho_i^2\rho_0^2r^2}\left\{\rho_i^2\rho_0^2\log_e\frac{\rho_0^2}{ab} - r^2\left[\rho_i^2\log_e\frac{r}{a} + \rho_0^2\left(1 + 2\log_e\frac{\rho_i}{a}\right)\log_e\frac{\rho_0}{r} - \rho_0^2\left(1 - 2\log_e\frac{r}{\rho_i}\right)\log_e\frac{b}{\rho_0}\right]\right\} \quad [23]$$

$$\sigma_\theta = \frac{2k}{N_2\rho_i^2\rho_0^2r^2}\left\{r^2\left[\rho_0^2\left(1 + 2\log_e\frac{\rho_i}{a}\right)\left(1 - \log_e\frac{\rho_0}{r}\right) - \rho_0^2\left(1 + 2\log_e\frac{r}{\rho_i}\right)\log_e\frac{b}{\rho_0} - \rho_i^2\left(1 + \log_e\frac{r}{a}\right)\right] - \rho_i^2\rho_0^2\log_e\frac{\rho_0^2}{ab}\right\} \quad [24]$$

where

$$N_2 = \frac{\rho_0^2 - \rho_i^2 - 2\rho_0^2\log_e\dfrac{\rho_0}{\rho_i}}{\rho_i^2\rho_0^2}$$

The position of the neutral surface $r = c$, found by setting $\sigma_\theta$ equal to zero, is given for the second stage of the elastic-plastic solution by the expression

$$\left(1 + 2\log_e\frac{\rho_i}{a}\right)\left(1 - \log_e\frac{\rho_0}{c}\right) - \left(1 + 2\log_e\frac{c}{\rho_i}\right)\log_e\frac{b}{\rho_0} - \frac{\rho_i^2}{\rho_0^2}\left(1 + \log_e\frac{c}{a}\right) = \frac{\rho_i^2}{c^2}\log_e\frac{\rho_0^2}{ab} \quad [25]$$

The radii $\rho_i$ and $\rho_0$, which appear in Equations [23], [24], and [25] are related to each other by Equation [22]. They are uniquely prescribed for a given bending moment $M$.

To find the relationship between $M$ and these radii let us consider the equilibrium of the sector shown in Fig. 5, subject to the

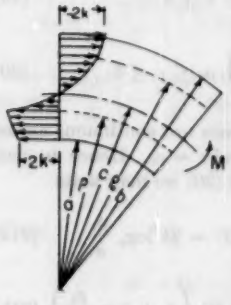


FIG. 5 (*Left*) CIRCUMFERENTIAL STRESS DISTRIBUTION ON A SECTOR OF THE BAR DURING THE SECOND STAGE OF THE ELASTIC-PLASTIC SOLUTION

applied bending moment $M$ and the circumferential stress distribution just computed

$$-M = \int_a^{\rho_i}\sigma_\theta r\,dr + \int_{\rho_i}^{\rho_0}\sigma_\theta r\,dr + \int_{\rho_0}^{b}\sigma_\theta r\,dr \quad [26]$$

If we substitute the expressions for $\sigma_\theta$ found in Equations [11], [5], and [20], respectively, then in view of Equations [21a] and [21c], it may be written[8]

$$M = k\left[\rho_i^2\log_e\frac{\rho_i}{a} - \rho_0^2\log_e\frac{b}{\rho_0} + \frac{1}{2}(b^2 - \rho_0^2 - \rho_i^2 + a^2)\right] + A\log_e\frac{\rho_0}{\rho_i} + B(\rho_0^2\log_e\rho_0 - \rho_i^2\log_e\rho_i) + C(\rho_0^2 - \rho_i^2) \quad [27]$$

After substituting the constants $A$, $B$, and $C$, obtained from Equations [21a–c], the expression for bending moment may be rewritten to read

$$\left(\frac{2M}{k} - a^2 - b^2\right)\left(1 - \frac{\rho_i^2}{\rho_0^2} - 2\log_e\frac{\rho_0}{\rho_i}\right) = 2\rho_i^2\left[1 + \left(1 + 2\log_e\frac{\rho_0}{\rho_i}\right)\log_e\frac{\rho_0^2}{ab}\right] - 2\rho_0^2\left(1 - \log_e\frac{ab}{\rho_i^2}\right) \quad [28]$$

The numerical values of the radii $\rho_i$ and $\rho_0$ needed to evaluate the stress components and the position of the neutral surface may be computed for a prescribed bending moment from Equations [22] and [28].

The resultant force over an arbitrary radial cross section, given as

$$F = \int_a^{\rho_i}\sigma_\theta dr + \int_{\rho_i}^{\rho_0}\sigma_\theta dr + \int_{\rho_0}^{b}\sigma_\theta dr \quad [29]$$

leads to the expression[9]

$$F = \rho_0\left[\frac{A}{\rho_0^2} + B(1 + 2\log_e\rho_0) + 2C\right] - \rho_i\left[\frac{A}{\rho_i^2} + B(1 + 2\log_e\rho_i) + 2C\right] + 2k\rho_i\log_e\frac{\rho_i}{a} - 2k\rho_0\log_e\frac{b}{\rho_0} = 0 \quad [30]$$

when the substitution is made for $\sigma_\theta$, as defined in Equations [11], [5], and [20]. In view of Equations [21a] and [21c], the resultant force is, as we would expect, identically equal to zero.

## THE COMPLETELY PLASTIC SOLUTION

When the bending moment is large enough, the boundary of the upper plastic zone $r = \rho_0$ and the boundary of the lower plastic zone $r = \rho_i$ meet at the surface which represents the limit of the degenerating elastic zone $r = c$. The stresses within the lower plastic zone are given by Equations [10] and [11] with the limits $a \leq r \leq c$. For the upper plastic zone, now contained within the region $c \leq r \leq b$, the stresses are given by Equations [19] and [20]. For the completely plastic case, $\rho_i = \rho_0 = c$, Equation [30] reduces to

$$2k\log_e\frac{c}{a} = 2k\log_e\frac{b}{c} \quad [31]$$

which shows, according to Equations [10] and [19] for $r = c$, that the radial stresses are still continuous across the neutral surface.

---

[8] $\int_{\rho_i}^{\rho_0}\frac{d^2\phi}{dr^2}\,r\,dr = r\frac{d\phi}{dr}\Big]_{\rho_i}^{\rho_0} - \int_{\rho_i}^{\rho_0}\frac{d\phi}{dr}\,dr = r\frac{d\phi}{dr}\Big]_{\rho_i}^{\rho_0} - \phi\Big]_{\rho_i}^{\rho_0}$

$\phi$ is defined in Equation [7].

[9] $\int_{\rho_i}^{\rho_0}\frac{d^2\phi}{dr^2}\,dr = \frac{d\phi}{dr}\Big]_{\rho_i}^{\rho_0}$. $\phi$ is defined in Equation [7].

It immediately follows from Equation [31] that the radius of the neutral surface for the fully plastic case is

$$c = \sqrt{ab} \quad [32]$$

Finally, when $\rho_i = \rho_0 = c$, Equation [27] reduces to

$$M = k\left[c^2 \log_e \frac{c^2}{ab} + \frac{1}{2}(b^2 - 2c^2 + a^2)\right] \quad [33]$$

and, in view of Equation [32], the bending moment per unit width of cross section for the fully plastic state $M_p$ is given by the expression

$$M_p = \frac{k}{2}(b - a)^2 \quad [34]$$

## Discussion of Results

We have seen in the previous sections that as the bending moment on an initially curved bar increases, the bar passes through three distinct phases, i.e., the completely elastic, the elastic-plastic, and the fully plastic phase. Mathematical expressions have been derived which describe for each phase the stress distribution, the position of the elastic-plastic boundary, and the position of the neutral axis as a function of the bending moment and the physical dimensions of the problem.

In order that we may better understand the interrelationship between some of the parameters, numerical calculations were made and their results indicated in Figs. 6 through 9. In preparing some of these calculations it was found convenient, because of the form of the equations presented in the previous sections, to choose $\rho_i$ as the independent variable. According to Equation [32], $\rho_i$ lies between the limits $a$ and $\sqrt{ab}$. Whenever $\rho_i$ was greater than $a$, but less than the value obtained from Equation [18], its numerical value was substituted into Equations [17], [15], [14], and [13] as needed. Whenever $\rho_i$ was greater than the value prescribed in Equation [18] but less than $\sqrt{ab}$, the bar was within the second stage of the elastic-plastic solution and $\rho_i$ as well as $\rho_0$, obtained from Equation [22], were substituted as needed into Equations [28], [25], [24], and [23].

The stress distribution within the lower plastic zone, Equations [10] and [11], and within the upper plastic zone, Equations [19] and [20], are independent of the numerical value of $\rho_i$ and $\rho_0$, although the limits of the equations do depend on the position of the elastic-plastic boundaries.

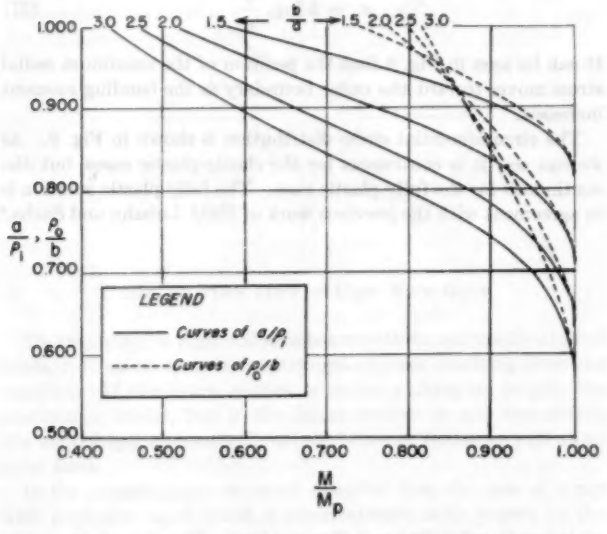


Fig. 6 Relative Position of the Elastic-Plastic Boundaries

Fig. 6 was prepared from the computed results just described in order to show the relative positions of the elastic-plastic boundaries $a/\rho_i$ and $\rho_0/b$ as a function of the bending moment ratio $M/M_p$ for several values of $b/a$. $M_p$, as the reader will recall, is the bending moment for the fully plastic case, whereas $M$ is the bending moment at a given instant.

It can be seen that for a constant ratio of $b/a$, the radius to the inner elastic-plastic boundary $\rho_i$ increases, whereas the radius to the outer elastic-plastic boundary $\rho_0$ decreases as $M/M_p$ increases until they meet for the fully plastic case when $M/M_p$ is equal to unity. It also can be seen that the elastic-plastic boundaries advance almost linearly as the bending moment increases to within 90 per cent of the completely plastic case whereas small increases in bending moment within the last 10 per cent cause a rapid degeneration of the elastic zone. This trend is even more pronounced as the ratio $b/a$ increases.

In the previous sections we saw that the position of the neutral surface is independent of the bending moment when the stresses are completely elastic or completely plastic. Within the elastic-plastic range, however, its position is a function of the bending moment. This effect may be seen in Fig. 7 where the dimensionless ratio, $c-a/b-a$, the relative position of the neutral surface, is shown to be a function of $M/M_p$ for several representative values of $b/a$.

We can see in Fig. 7 that as the bending-moment ratio increases, the neutral surface moves away from, then toward, the center of curvature. It is interesting to see that the range in which

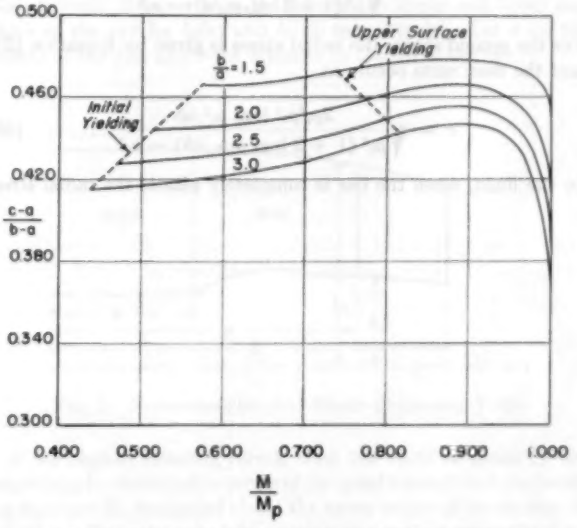


Fig. 7 Relative Position of the Neutral Surface

we observe the movement toward the concave surface approximately coincides with the range in which we previously saw the rapid degeneration of the elastic region. The relative movement is more prominent as the ratio $b/a$ increases.

It also may be seen that after initial yielding has taken place, the increase in $M/M_p$ required to cause the initiation of upper surface yielding is greatest for large $b/a$ ratios. Thus an increase in material for a constant numerical value of $a$ not only increases the bending moment required for the fully plastic case, but increases the range for which we would have but one plastic zone.

In Figs. 8 and 9 the radial and circumferential stress distribution for a $b/a$ ratio of 2.0 is shown for a series of loading conditions between $M/M_p$ of 0.516, at which initial yielding occurs, and

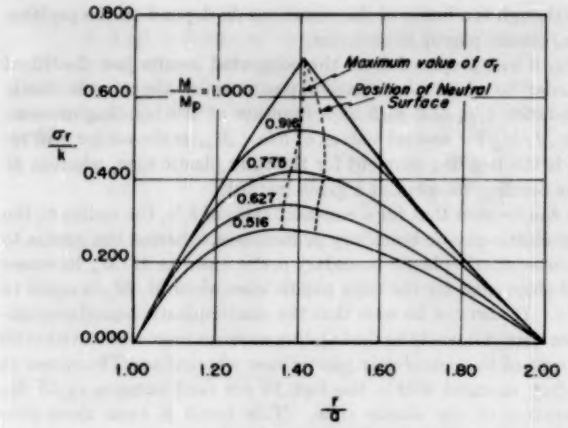


FIG. 8 RADIAL STRESS DISTRIBUTION FOR $b/a = 2.0$

1.000, the fully plastic case. Yielding begins at the upper surface when $M/M_p$ equals 0.775.

The points of maximum radial stress for each of the loading conditions are connected by a dotted line in Fig. 8. The radius at which the maximum occurs may be found by differentiating the appropriate solution described in the previous sections. For the first stage of the elastic-plastic solution, the radial stress is given by Equation [13] and attains its maximum value at

$$r = \sqrt{\frac{2\rho_i^2 b^2 \log_e b/a}{b^2(1 + 2\log_e \rho_i/a) - \rho_i^2}} \quad \ldots\ldots [35]$$

For the second stage, the radial stress is given by Equation [23] and the maximum occurs at

$$r = \sqrt{\frac{2\rho_i^2 \rho_0^2 \log_e \rho_0^2/ab}{\rho_0^2(1 + 2\log_e \rho_i\rho_0/ab) - \rho_i^2}} \quad \ldots\ldots [36]$$

In the limit, when the bar is completely plastic the radial stress

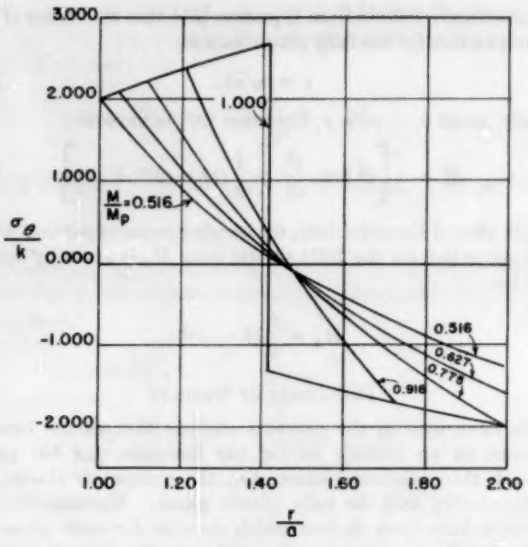


FIG. 9 CIRCUMFERENTIAL STRESS DISTRIBUTION FOR $b/a = 2.0$

reaches its maximum value at the neutral surface described in Equation [32]. Its magnitude, obtained by combining Equations [32] and [19] for $r = c$, is given as

$$\sigma_r = k \log_e \frac{b}{a} \quad \ldots\ldots [37]$$

It can be seen in Fig. 8 that the position of the maximum radial stress moves toward the outer boundary as the bending moment increases.

The circumferential stress distribution is shown in Fig. 9. As we can see, it is continuous for the elastic-plastic cases, but discontinuous for the fully plastic case. The fully plastic solution is in agreement with the previous work of Hill,[5] Lubahn and Sachs.[6]

# Stress Distributions in Nonsymmetric Rotating Rays

By P. G. HODGE, JR.,[1] BROOKLYN, N. Y.

**The centrifugal forces acting upon a rotating ray will produce longitudinal stresses along the ray. If the ray is not symmetric, these stresses will result not only in a longitudinal force, but also in a bending moment. A technique for finding the stress distribution in this case is developed and illustrated by means of simple examples. The limiting elastic speed and the maximum speed before large-scale plastic deformation commences are computed. An indication is given of how similar methods may be used to analyze a rotating disk with no plane of symmetry perpendicular to the axis.**

## 1 Introduction

LET us consider a rotating disk with several protruding rays, as indicated in Fig. 1. We assume that the disk is sufficiently strong to be considered rigid, and we wish to determine the stresses in a typical ray.

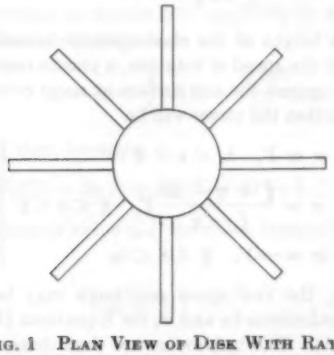

Fig. 1 Plan View of Disk With Rays

The ray may be regarded as a beam with no externally applied loads, but acted upon by centrifugal stresses resulting from the rotation. If the beam section is uniform along its length, the problem is trivial, but if the beam section is not symmetric, the centrifugal stresses will induce bending forces as well as an axial force.

In the present paper we shall consider first the case of a ray with moderate taper which is nonsymmetric with respect to the plane of rotation. The problem will be analyzed under certain simplifying assumptions. The "axis" of the ray is defined as some convenient radial line of the ray. Observe that this axis can coincide with the line of centroids only in the case where the ray is symmetric. We then assume that plane sections normal to the axis of the ray remain plane and normal to the (deformed) axis. As mentioned previously, we assume that the disk is rigid. We also assume that the radius of the disk is sufficiently large compared to the cross-sectional dimensions of the ray so that the curvature of the junction may be ignored. This junction also is assumed rigid, so that the ray may be regarded as a nonuniform cantilever beam acted upon by a centrifugal force.

In Section 2 we shall find the elastic stresses in such a ray which is of moderate taper, of constant thickness, symmetric with respect to a plane through the axis of rotation, but nonsymmetric with variable depth with respect to the plane of rotation. The results will be illustrated by a triangular beam with one side parallel to the plane of rotation. In Section 3 the same problem will be solved for a ray of a perfectly plastic material. Next, we shall indicate how the approach used for rays may be extended to rotating disks. Finally, Section 5 will summarize the conclusions and limitations of the theory.

## 2 Nonsymmetric Ray, Elastic Solution

Consider a ray of uniform width $t$, but with variable depth, Fig. 2. Let $r$ be the co-ordinate along the axis of the ray, and denote the algebraic distance from the axis to the upper and lower surfaces of the ray by $h_2(r)$ and $h_1(r)$, respectively. Let $a$ be the radius of the disk and $b$ the distance to the tip of the ray.

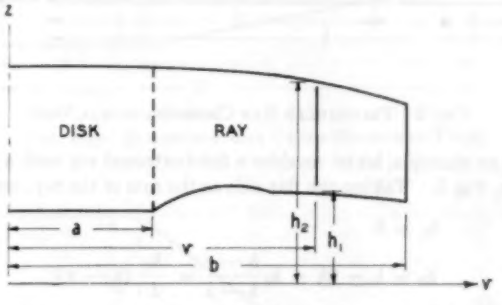


Fig. 2 Nonsymmetric Ray Cross-Sectional View

If we neglect shearing forces, then the state of stress in the beam may be described in terms of the axial force $N$ and the bending moment $M$, computed about the mean height of the section in question. Since the only forces acting on a section are induced by the centrifugal force due to the material beyond that section, the stress resultants are given by

$$\left.\begin{aligned} N(r) &= \rho\omega^2 t \int_r^b sh(s)ds \\ M(r) &= \rho\omega^2 t \int_r^b s[\bar{h}(r) - \bar{h}(s)]h(s)ds \\ &= \bar{h}(r)N(r) - \rho\omega^2 t \int_r^b sh(s)\bar{h}(s)ds, \end{aligned}\right\} \quad \ldots\ldots [1]$$

where the depth $h$ and mean height $\bar{h}$ are defined by

$$h = h_2 - h_1, \bar{h} = \frac{h_1 + h_2}{2} \quad \ldots\ldots [2]$$

[1] Associate Professor of Applied Mechanics, Polytechnic Institute of Brooklyn. Mem. ASME.

Contributed by the Applied Mechanics Division and presented at the Annual Meeting, New York, N. Y., November 28–December 3, 1954, of The American Society of Mechanical Engineers.

Discussion of this paper should be addressed to the Secretary, ASME, 29 West 39th Street, New York, N. Y., and will be accepted until October 10, 1955, for publication at a later date. Discussion received after the closing date will be returned.

Note: Statements and opinions advanced in papers are to be understood as individual expressions of their authors and not those of the Society. Manuscript received by ASME Applied Mechanics Division, March 17, 1954. Paper No. 54—A-96.

As long as the material remains everywhere elastic, the assumption that plane sections remain plane is equivalent to assuming that the stress is linear across each vertical section. Therefore, if $\sigma_1$ and $\sigma_2$ are the values of the stress at the bottom and top surfaces, respectively

$$\sigma = \sigma_1 + \frac{z - h_1}{h_2 - h_1}(\sigma_2 - \sigma_1) \quad [3]$$

where $z$ is the height above the axis. The stress resultants $N$ and $M$ may now be expressed in terms of $\sigma_1$ and $\sigma_2$

$$\left.\begin{aligned} N &= \int_{h_1}^{h_2} t\sigma dz = th\,\frac{\sigma_1 + \sigma_2}{2} \\ M &= \int_{h_1}^{h_2} t\sigma(\bar{h} - z)dz = \frac{th^2}{12}(\sigma_1 - \sigma_2) \end{aligned}\right\} \quad [4]$$

Solving Equations [4] for $\sigma_1$ and $\sigma_2$, and using the values of the resultants from Equations [1] we finally obtain the surface stress in the form

$$\left.\begin{matrix}\sigma_1 \\ \sigma_2\end{matrix}\right\} = \frac{\rho\omega^2}{h^2}\int_r^b s[h(r) \pm 6\bar{h}(r) - 6\bar{h}(s)]h(s)ds \quad [5]$$

The stress at any interior point may now be found from Equation [3].

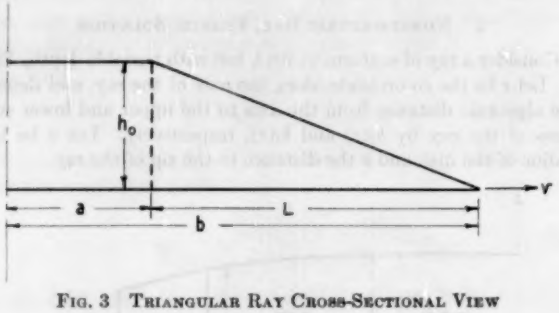


FIG. 3 TRIANGULAR RAY CROSS-SECTIONAL VIEW

As an example, let us consider a flat-bottomed ray with a linear taper, Fig. 3. Taking the flat side as the axis of the ray, we have

$$h_1 = 0$$

$$h_2 = h = 2\bar{h} = h_0\frac{b - r}{b - a} = \frac{h_0}{L}(b - r) \quad [6]$$

Substituting Equations [6] into [5], we obtain, after some computation

$$\left.\begin{aligned} \sigma_1 &= \frac{\rho\omega^2}{12}(b - r)(5b + 7r) \\ \sigma_2 &= -\frac{\rho\omega^2}{12}(b - r)^2 \end{aligned}\right\} \quad [7]$$

The negative sign preceding $\sigma_2$ indicates that the top surface is in a state of compression.

Obviously, the numerically largest stress occurs at the lower surface. If the ray is to remain entirely elastic, this stress must everywhere be less than the yield stress $Y$ in tension. It is readily computed that if $b$ is less than $7a$, the maximum value of $\sigma_1$ occurs at the junction of the hub with the disk and hence is given by

$$\sigma_m = \frac{\rho\omega^2}{12}(b - a)(5b + 7a) \quad [8]$$

On the other hand, if $b$ is greater than $7a$, the maximum value occurs at $r = b/7$ and is given by

$$\sigma_m = \frac{3}{7}\rho\omega^2 b^2 \quad [8b]$$

Since the maximum stress must be less than the yield stress, the condition on the speed for fully elastic behavior is

$$\left.\begin{aligned} \rho\omega^2 &\leq \frac{12Y}{(b - a)(5b + 7a)}, \quad b < 7a \\ \rho\omega^2 &\leq \frac{7Y}{3b^2}, \quad b > 7a \end{aligned}\right\} \quad [9]$$

## 3 NONSYMMETRIC BEAM, PLASTIC SOLUTION

If the speed of rotation is greater than the values given by Equations [9] the ray will be partially plastic and the preceding solution no longer will be valid, since the stress is no longer linear. Instead, there will be certain cross sections of the ray which will be partially plastic, and, for a perfectly plastic material, the stress in the plastic regions will be equal to the yield stress. For values of the speed slightly above the maximum elastic speed, the plastic regions will be next to the bottom surface (assuming, for definiteness, that the shape of the ray is such that $\sigma_1$ is greater than $\sigma_2$). In this case, Equation [3] will be replaced by

$$\left.\begin{aligned} \sigma &= Y, \quad h_1 < z < \eta \\ \sigma &= Y + \frac{z - \eta}{h_2 - \eta}(\sigma_2 - Y), \quad \eta < z < h_2 \end{aligned}\right\} \quad [10]$$

where $\eta$ is the height of the elastic-plastic boundary. For still larger values of the speed of rotation, a plastic region in compression will form against the top surface at some cross sections. At such a cross section the stress will be

$$\left.\begin{aligned} \sigma &= Y, \quad h_1 < z < \eta \\ \sigma &= \frac{\xi + \eta - 2z}{\xi - \eta}Y, \quad \eta < z < \xi \\ \sigma &= -Y, \quad \xi < z < h_2 \end{aligned}\right\} \quad [11]$$

In either case, the two stress resultants may be computed in terms of two unknowns ($\eta$ and $\sigma_2$ for Equations [10], $\eta$ and $\xi$ for Equations [11]). The unknowns are then determined from the externally computed moment and force.

The details of the foregoing computation become quite laborious, even for simple ray shapes, and cannot be completed in closed form. Rather than carry out a numerical solution, let us seek to determine directly the speed at which some section of the ray first becomes fully plastic. This speed is critical, since once any section becomes fully plastic large-scale plastic deformation becomes possible and the ray becomes unserviceable.

At a fully plastic section then, the stress is

$$\left.\begin{aligned} \sigma &= Y, \quad h_1 < z < \eta \\ \sigma &= -Y, \quad \eta < z < h_2 \end{aligned}\right\} \quad [12]$$

where $\eta$ represents the height of the neutral axis. The stress resultants in this case are

$$N = 2tY(\eta - \bar{h}), \quad M = tY\left[\frac{h^2}{4} - (\eta - \bar{h})^2\right] \quad [13]$$

Let us define $M_0$ as the moment at a section which is fully plastic in pure bending ($\eta = \bar{h}$), and $N_0$ as the force at a section which is fully plastic in simple tension ($\eta = h_2$)

$$M_0 = \frac{th^2Y}{4}, \quad N_0 = thY \quad [14]$$

Eliminating $\eta$ between Equations [13], and using [14], we find

that at a fully plastic section the stress resultants must be related by

$$\frac{M}{M_0} + \left(\frac{N}{N_0}\right)^2 = 1 \quad \ldots\ldots [15]$$

Since a perfectly plastic section cannot carry stresses greater than the yield stress, at all sections of the ray the resultants must satisfy the "yield inequality"

$$\frac{M}{M_0} + \left(\frac{N}{N_0}\right)^2 \leq 1 \quad \ldots\ldots [16]$$

To determine the maximum plastic speed, then, we substitute Equations [1] into the yield Inequality [16] to obtain an inequality involving the speed and the co-ordinate $r$. We then seek the maximum value of $\omega$ for which this inequality is valid for all $a \leq r \leq b$.

As an example, consider the ray whose elastic solution was found in the previous section. In view of Equations [6], [1], and [14] the yield Inequality [16] for this case may be written

$$\left(\frac{\rho\omega^2 b^2}{6Y}\right)^2 \left(1 - \frac{r}{b}\right)^2 \left(1 + 2\frac{r}{b}\right)^2 + \frac{\rho\omega^2 b^2}{6Y}\left(1 - \frac{r}{b}\right)\left(1 + \frac{r}{b}\right) - 1 \leq 0 \quad \ldots\ldots [17]$$

It will be convenient to discuss this inequality in terms of dimensionless quantities defined by

$$u = 1 - \frac{r}{b}, \quad P = \frac{\rho\omega^2 b^2}{6Y} \quad \ldots\ldots [18]$$

Inequality [17] then becomes

$$P^2u^2(3 - 2u)^2 + Pu(2 - u) - 1 \leq 0 \quad \ldots\ldots [19]$$

We seek the largest value of $P$ for which Inequality [19] is valid for all

$$0 \leq u \leq 1 - \frac{a}{b} \quad \ldots\ldots [20]$$

For any fixed value of $u$, the left side of Inequality [19], considered as a function of $P$, is a parabola concave upward. Since it is negative at $P = 0$, there are two real values of $P$ for which it is equal to zero, and all admissible $P$ must lie between these values. Physically, $P$ must be greater than zero, so that $P$ must be less than the positive root of Inequality [19], considered as an equality. Thus, at all sections, we must have

$$P \leq \frac{\sqrt{\left(\frac{2-u}{3-2u}\right)^2 + 4} - \frac{2-u}{|3-2u|}}{2u\,|3-2u|} \quad \ldots\ldots [21]$$

Since Inequality [21] must be valid for all $u$ satisfying [20], we seek that value of $u$ which will make the right-hand side of Inequality [21] a minimum. In the Appendix it is shown that this value is the root of the equation

$$-34u^3 + 104u^2 - 99u + 30 = 0 \quad \ldots\ldots [22]$$

or

$$u \simeq 0.818 \quad \ldots\ldots [23]$$

Substituting Equation [23] into Inequality [21] we obtain

$$P \leq 0.59$$

Finally, in view of the second Equation [18], the maximum plastic speed is

$$\omega_p = 1.88\sqrt{\frac{Y}{\rho b^2}} \quad \ldots\ldots [24]$$

Equation [24] is correct only if the value of $u$ given by Equation [23] actually lies on the ray. This will be the case provided $b > 6.5a$. For $b < 6.5a$, the minimum value of Inequality [21] occurs at $r = a$ and hence is obtained by substituting $u = 1 - a/b$ into [21].

By way of comparison, it is interesting to observe the effect of the lack of symmetry on the critical speeds. For simplicity we consider only the case where the ray is sufficiently long so that the critical section is away from the disk. For a symmetric ray of the same depth, Fig. 4($a$), the critical section becomes plastic all at once, so that the critical elastic and plastic speeds coincide. This value readily is computed to be

$$\omega_e = \sqrt{\frac{16Y}{3\rho b^2}} = 2.32\sqrt{\frac{Y}{\rho b^2}} \quad \ldots\ldots [25]$$

The analysis also has been carried out for an undercut ray of the same depth, Fig. 4($b$). The results are summarized in Table 1.

TABLE 1 CRITICAL SPEEDS

| Type of beam | Critical section | | Critical speed $\left(\omega\sqrt{\frac{\rho b^2}{Y}}\right)$ | |
|---|---|---|---|---|
| | Elastic | Plastic | Elastic | Plastic |
| Symmetric, Fig. 4(a) | 0.25 | 0.25 | 2.32 | 2.32 |
| Flat bottom, Fig. 3 | 0.14 | 0.18 | 1.53 | 1.88 |
| Undercut, Fig. 4(b) | 0.08 | 0.07 | 1.04 | 1.34 |

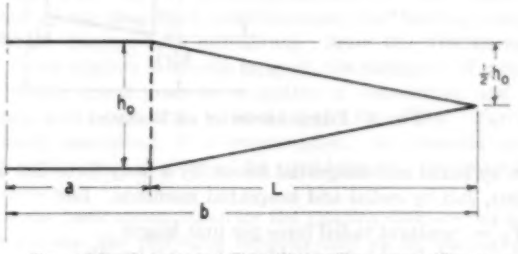


FIG. 4($a$) SYMMETRIC RAY CROSS-SECTIONAL VIEW

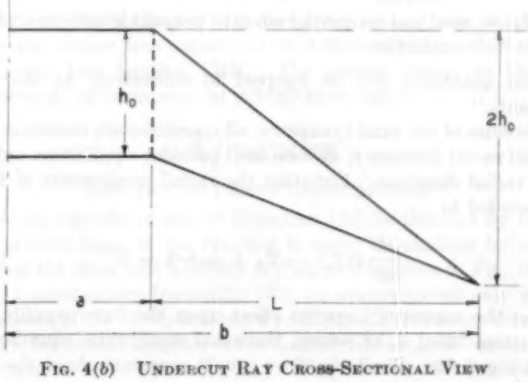


FIG. 4($b$) UNDERCUT RAY CROSS-SECTIONAL VIEW

## 4 ROTATING DISK

The general approach used for a rotating ray also can be used to derive the differential equations for a rotating elastic disk with no plane of symmetry perpendicular to the axis. To this end we replace the usual assumption for symmetric disks, that the stresses are uniform across a section, by the assumption that linear elements parallel to the axis of rotation remain linear. In the elastic case, this is equivalent to assuming that the stress distribution is linear across the thickness of the disk. Shearing and axial stresses

will still be neglected although the former at least may exert some significant effect in the nonsymmetric case.

We use the same notations for the disk as for the ray, so that Fig. 2 may now be regarded as a cross section of the disk. The inner radius $a$ may be zero, indicating a solid disk. To obtain the equilibrium equations, we consider an element of the disk bounded by the planes $\theta$ and $\theta + \Delta\theta$, the cylinders $r$ and $r + \Delta r$, and the surfaces of the disk, Fig. 5. This element will be acted

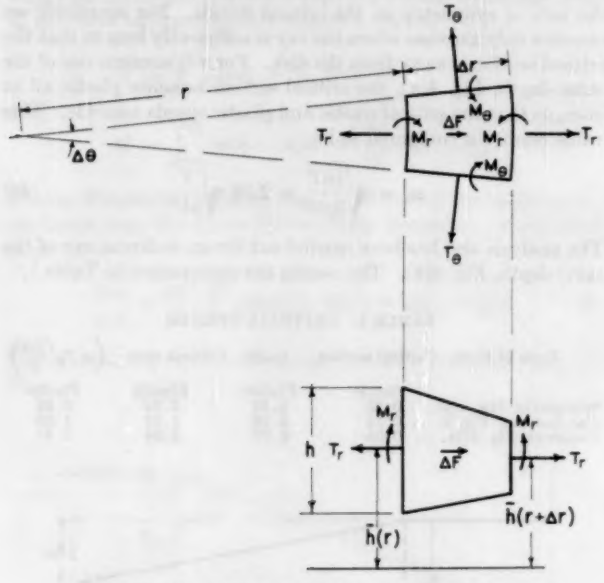


FIG. 5 EQUILIBRIUM OF AN ELEMENT

upon by radial and tangential forces, by a body force due to the motion, and by radial and tangential moments. Let

$T_r$ = resultant radial force per unit length
$T_\theta$ = resultant tangential force per unit length
$M_r$ = resultant radial moment per unit length about local centroid
$M_\theta$ = resultant tangential moment per unit length about local centroid

These quantities will be referred to collectively as the "resultants."

Because of the axial symmetry, all quantities are functions only of the radial distance $r$, and we need consider equilibrium only in the radial direction. Equating the radial components of force we are led to

$$\frac{d}{dr}(rT_r) - T_\theta + \rho\omega^2 r^2 h = 0 \quad \ldots\ldots\ldots [26a]$$

Since the moments have no effect upon the force equilibrium, Equation [26a] is, of course, the usual equilibrium equation for rotating disks. Similarly, if we equate moments about the centroid at $r$, we obtain

$$\frac{d}{dr}(rM_r) - M_\theta - rT_r\frac{d\bar{h}}{dr} = 0 \quad \ldots\ldots\ldots [26b]$$

Equations [26] represent two equations in the four unknowns $T_r$, $T_\theta$, $M_r$, and $M_\theta$. To obtain further equations we must consider the displacement of a linear element which was initially parallel to the $z$-axis. Because of the centrifugal force acting on the element it will be displaced radially, while owing to the bending moments it will be rotated. Let $u(r)$ be the radial displacement of the centroid, and let $\phi(r)$ be the angle through which it is rotated. The angle $\phi$ will be considered positive when it corresponds to greater tension on the bottom surface, Fig. 6. The

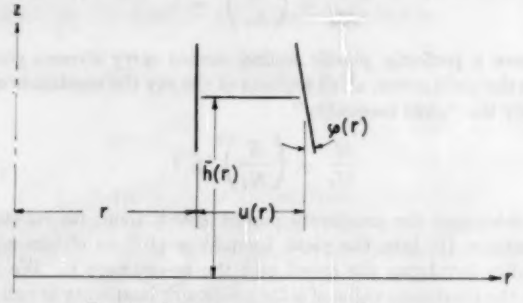


FIG. 6 DISPLACEMENT OF AN ELEMENT

total radial displacement of the particle initially at $r$, $z$ is then given by

$$u_r(r, z) = u(r) - [z - \bar{h}(r)]\phi(r)$$

Since this is the only displacement component, the radial and tangential strains are

$$\left.\begin{aligned} \epsilon_r &= \frac{\partial u_r}{\partial r} = \frac{du}{dr} - (z - \bar{h})\frac{d\phi}{dr} + \phi\frac{d\bar{h}}{dr} \\ \epsilon_\theta &= \frac{u_r}{r} = \frac{u}{r} - (z - \bar{h})\frac{\phi}{r} \end{aligned}\right\} \quad \ldots [27]$$

If the axial stress is equal to zero, the remaining stresses and strains are related by Hooke's law in the form

$$\sigma_r = \frac{E}{1-\nu^2}(\epsilon_r + \nu\epsilon_\theta),\ \sigma_\theta = \frac{E}{1-\nu^2}(\epsilon_\theta + \nu\epsilon_r) \quad \ldots [28]$$

Using Equations [27] and [28], we can easily express the resultants in terms of $u$ and $\phi$

$$\left.\begin{aligned} T_r &= \int_{\bar{h}-h/2}^{\bar{h}+h/2}\sigma_r(r, z)\,dz = \frac{Eh}{1-\nu^2}\left[\frac{du}{dr} + \nu\frac{u}{r} + \phi\frac{d\bar{h}}{dr}\right] \\ T_\theta &= \int_{\bar{h}-h/2}^{\bar{h}+h/2}\sigma_\theta(r, z)dz = \frac{Eh}{1-\nu^2}\left[\nu\frac{du}{dr} + \frac{u}{r} + \nu\phi\frac{d\bar{h}}{dr}\right] \end{aligned}\right\} \quad [29a]$$

$$\left.\begin{aligned} M_r &= \int_{\bar{h}-h/2}^{\bar{h}+h/2}(\bar{h} - z)\sigma_r(r, z)dz = \frac{Eh^3}{12(1-\nu^2)}\left[\frac{d\phi}{dr} + \nu\frac{\phi}{r}\right] \\ M_\theta &= \int_{\bar{h}-h/2}^{\bar{h}+h/2}(\bar{h} - z)\sigma_\theta(r, z)dz = \frac{Eh^3}{12(1-\nu^2)}\left[\nu\frac{d\phi}{dr} + \frac{\phi}{r}\right] \end{aligned}\right\} \quad [29b]$$

Equations [26] and [29] represent six equations in the six unknowns $T_r$, $T_\theta$, $M_r$, $M_\theta$, $u$, $\phi$. Together with suitable boundary conditions they provide a determinate problem for the resultants, displacement, and rotation. They may be reduced to a set of two second-order equations by either of the same techniques which are useful in symmetric disk problems. Obviously, the substitution

of Equations [29] into Equations [26] yields two second-order equations for $u$ and $\phi$. However, since the boundary conditions are usually not given in terms of displacements, the resulting equations are generally not so useful as stress equations would be. A method for obtaining these latter equations is to introduce a pair of stress functions defined by

$$\left.\begin{aligned} T_r &= \psi/r, \quad T_\theta = \psi' + \rho\omega^2 r^2 h \\ M_r &= \chi/r, \quad M_\theta = \chi' - \psi\bar{h}' \end{aligned}\right\} \quad \ldots\ldots\ldots [30]$$

to satisfy the equilibrium Equations [26] identically. Substituting these stress functions into Equations [29] and eliminating the displacements $u$ and $\phi$ we obtain finally

$$\psi'' + \left(1 - \frac{rh'}{h}\right)\frac{\psi'}{r} - \left[1 - \nu\frac{rh'}{h} + 12\left(\frac{r\bar{h}'}{h}\right)^2\right]\frac{\psi}{r^2} + \frac{12}{h}\left(\frac{r\bar{h}'}{h}\frac{\chi'}{r} - \nu\frac{\chi}{r^2}\right) + (3+\nu)\rho\omega^2 rh = 0 \ldots [31a]$$

$$\chi'' + \left(1 - 3\frac{rh'}{h}\right)\frac{\chi'}{r} - \left(1 - 3\nu\frac{rh'}{h}\right)\frac{\chi}{r^2} - r\bar{h}'\left[\frac{\psi}{r} + \left(1 + \nu - 3\frac{rh'}{h} + \frac{r\bar{h}}{h'}\right)\frac{\psi}{r^2}\right] = 0 \ldots [31b]$$

Equations [31] are generally similar to the defining equation

$$\psi'' + \left(1 - \frac{rh'}{h}\right)\frac{\psi'}{r} - \left(1 - \nu\frac{rh'}{h}\right)\frac{\psi}{r^2} + (3+\nu)\rho\omega^2 rh = 0 \quad \ldots\ldots\ldots [32]$$

encountered in the theory of symmetric rotating disks, and to a similar equation in the theory of bending of plates. Therefore it is reasonable to hope that many of the techniques used in these connections will be useful here. The results of some investigations into this problem will be reported on elsewhere.

## 5 Conclusions and Limitations

The present paper has solved the problem of nonsymmetric rotating rays on the basis of certain simplifying assumptions. Without doubt the most questionable of these assumptions is that sections normal to the axis of symmetry in the plane of rotation remain plane and normal to the deformed axis. This is not the same as the usual assumption of beam theory concerning sections normal to the axis of centroids. If the gradient of the mean height is large, then this assumption could introduce a considerable error.

A second assumption is the neglect of shear. Here again we have departed from the usual beam-theory approach and the approximation would become less valid as the gradient of the mean height increased.

A final source of error is the effect of the bending displacement on the centrifugal bending moments. For sufficiently small speeds this effect will be negligible, but for larger speeds a nonlinear effect will be observed, since the correct line of action of the centrifugal force should be computed from the deformed ray position. For a very long ray this effect might become important at speeds well below the maximum elastic speed. In such an elastic analysis the magnitude of the effect could always be estimated by computing the transverse displacement at the end from the predicted stresses. If this is large then an iteration technique could be devised using the predicted final shape of the first approximation as a basis for a second approximation. In any event, the effect of such a displacement is always to lower the maximum stress, so that the analysis given here is conservative in this respect.

The problem of the end displacements in relation to the plastic analysis is somewhat more complex. In order to gain an understanding of the principles involved, let us consider first a rigid-plastic material with an infinite elastic modulus but a finite yield stress. A ray made of such a material will remain perfectly rigid until the critical plastic speed is reached at which one section is fully plastic. A rotation about the neutral axis is now permissible. If the load were independent of the deformation, this rotation could become indefinitely large and the ray would fail by any criterion. However, in this problem the load is dependent upon the rotation and the effect will be to reduce the moment. Thus, after infinitesimal rotation, the section will remain plastic only if the speed is further increased.

For the ideal plastic-rigid material we now have a choice of two definitions of "limiting plastic speed." If we choose to define it as the lowest speed at which any deformation becomes possible, the present analysis is correct. On the other hand, if we define it as the speed at which an indefinitely large deformation becomes possible, an analysis must be made taking account of the deformations.

The application of these ideas to an elastic-plastic material is qualitatively the same. As the speed is slowly increased, small transverse displacements will be observed, increasing approximately linearly with the square of the speed. Assuming that deformation effects can be neglected in the elastic range, this will continue until the maximum elastic speed is reached. Further increases in $\omega^2$ will produce relatively larger increases in the displacement, but these will be of the same order of magnitude as the elastic ones until the speed approaches $\omega_p$. Now the effect becomes sharply magnified, small increases in $\omega^2$ leading to larger and larger displacement increments. Since the displacement-speed curve exhibits a smooth tangent, the definition of a maximum plastic speed must be a matter of convention, and the approach used here has the merit of relative simplicity. Further, as already mentioned, it is conservative. An absolute upper bound on the speed is obtained by considering the corresponding symmetric ray.

Since the basic assumptions for the rotating disk are the same as for the ray, the preceding remarks may all be qualitatively applied to the results of Section 4.

### Acknowledgment

The research leading to the foregoing results was obtained while the author was consultant to AiResearch Manufacturing Company, Los Angeles, Calif. The author wishes to thank AiResearch for permission to publish these results.

# Appendix

### Location of First Plastic Section

Let the right-hand side of Equation [21] be denoted by $f(u)$. The general shape of the function is easily determined by considering the zeros and infinities of $f(u)$, and is given in Fig. 7(*a*). Since $u$ must satisfy Inequality [20], we are concerned only with the branch of the curve between 0 and 3/2. In this range there is a single horizontal tangent, so the desired minimum will be at the point where

$$f'(u) = 0, \qquad 0 < u < 3/2 \ldots\ldots\ldots\ldots [33]$$

Computing this derivative, setting it equal to zero, and simplifying, we obtain

$$\frac{2-u}{3-2u} + \frac{2(3-2u)(3-4u)}{3-6u+2u^2} = \sqrt{\left(\frac{2-u}{3-2u}\right)^2 + 4} \ldots [34]$$

Since we are considering only the range between 0 and 3/2, the absolute value signs are no longer necessary. Next we square both sides of Equation [34], simplify, and divide by the nonvanishing factor $3 - 2u$ to obtain finally Equation [22]

$$g(u) = -34u^3 + 104u^2 - 99u + 30 = 0 \quad \ldots\ldots [35]$$

The function $g(u)$ is sketched in Fig. 7($b$). It is seen that there are three real positive roots, of which one is greater than 3/2 and hence of no concern in the present analysis. However, the other two are both between zero and 1 and are approximately given by

$$u_1 \simeq 0.70, \qquad u_2 \simeq 0.82$$

Since the preliminary analysis of $f(u)$ showed only one root of $'(u)$ in $0 < u < 3/2$, an extraneous root must have been introduced

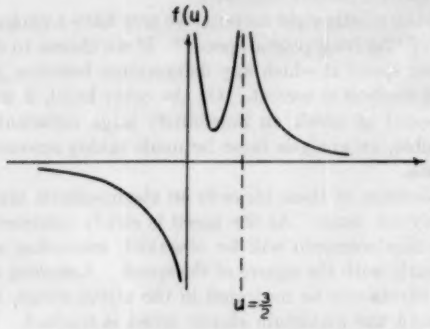


FIG. 7($a$) QUALITATIVE PICTURE OF $f(u)$

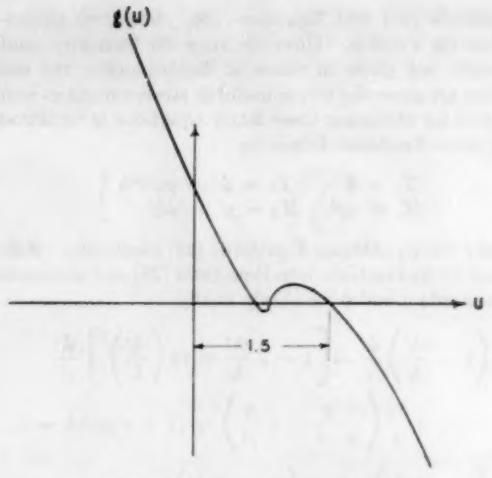


FIG. 7($b$) QUALITATIVE PICTURE OF $g(u)$

by the squaring of Equation [34]. It can be seen readily which root is extraneous by observing that a necessary condition for Equation [34] to be valid is that the left-hand side be positive. Since this condition is satisfied by $u_2$ but not by $u_1$, the desired root is given by Equation [23].

# Studies on Scabbing of Solids Under Explosive Attack

By K. B. BROBERG,[1] STOCKHOLM, SWEDEN

**The purpose of this paper is to analyze the mechanism of the scabbing phenomenon that occurs when an intense shock wave in a solid is reflected against a free surface. Only plane shock waves with normal incidence to the free surface are discussed. The shock wave is assumed to be initiated by the detonation of an explosive (especially TNT with a loading density of 1.5 g/cm³). The calculations are based upon values given by H. Jones and A. R. Miller (for the detonation pressure), D. J. McAdam (for the strength of the material at combined stresses), P. W. Bridgman (for the quantitative behavior of the material at very high pressures) and, finally, upon results from the author's own experiments regarding the impulse and the pressure-time curve at detonation in contact with a metal surface. It is shown that fracture sometimes is likely to occur in several parallel layers of the material. Experiments have been performed which support the theoretical analysis. The research was carried out at the Royal Swedish Fortification and Works Administrative Service, Stockholm.**

## The Behavior of Material at Uniaxial Deformation and High Pressures

The deformation is assumed to be uniaxial

$$\epsilon_1 \neq 0$$

$$\epsilon_2 = \epsilon_3 = 0$$

where $\epsilon_1$, $\epsilon_2$, and $\epsilon_3$ denote strains along three orthogonal directions. In the elastic region

$$\sigma_2 = \sigma_3 = \frac{\nu}{1-\nu}\sigma_1 \quad \ldots\ldots\ldots\ldots\ldots\ldots [1]$$

where $\sigma$ denotes stress and $\nu$ Poisson's ratio.

As the stress combination is cylindrical it is possible to represent the limits for yielding and fracturing on a two-dimensional diagram (1).[2] Fig. 1 shows such a diagram schematically. It applies to uniaxial straining when the stress history is such as described later. The curve $Y$ represents the elastic limit and the curve $L$ the locus of fractures. For negative values of $\sigma_2$ the curve $Y$—according to reasonable yield theories and experimental researches (2)—is approximately represented by the straight lines $\sigma_1 = \sigma_2 \pm \sigma_Y$. The diagram is valid for a certain temperature and a certain rate of strain; moreover, the ductility influences the locus of fractures (1, 3, 4).

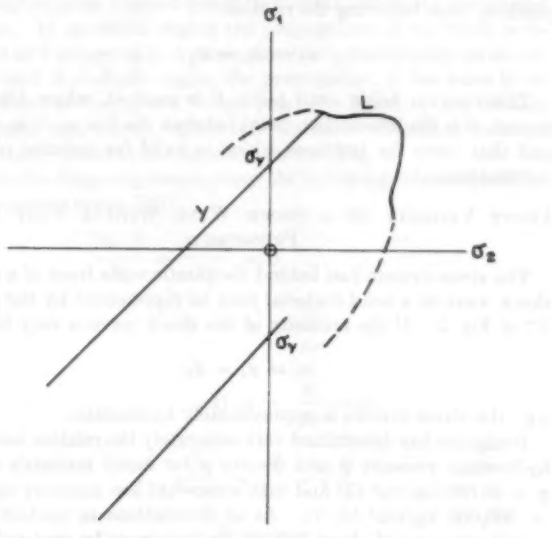


Fig. 1 Two-Dimensional Diagram for Yielding and Fracturing

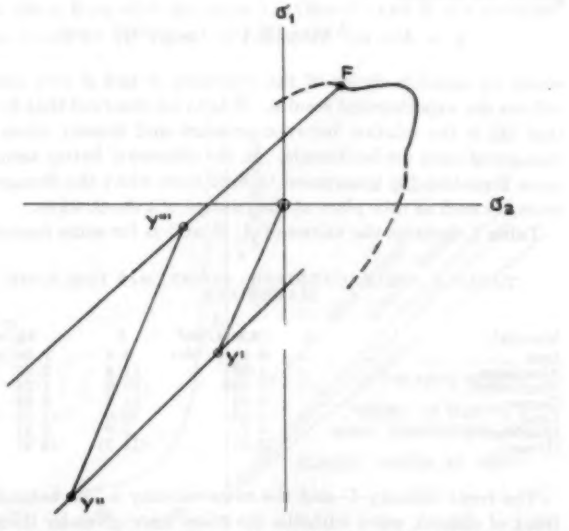


Fig. 2 Stress Composition at Uniaxial Deformation

Let us start with a virgin material and load it with successively increasing $|\sigma_1|$ (compressive). At first the material behaves elastically, the stress system following Equations [1] as indicated by the line $OY'$ in Fig. 2. Then the yield point is reached and the material yields under a stress system approximately given by the relation

$$\sigma_1 - \sigma_2 = -\sigma_Y \quad \ldots\ldots\ldots\ldots\ldots\ldots [2]$$

e.g., the stress system is represented by the line $Y'Y''$, Fig. 2.

[1] The Royal Swedish Fortifications and Works Administrative Service.

[2] Numbers in parentheses refer to the Bibliography at the end of the paper.

Contributed by the Applied Mechanics Division and presented at the Annual Meeting, New York, N. Y., November 28–December 3, 1954, of The American Society of Mechanical Engineers.

Discussion of this paper should be addressed to the Secretary, ASME, 29 West 39th Street, New York, N. Y., and will be accepted until October 10, 1955, for publication at a later date. Discussion received after the closing date will be returned.

Note: Statements and opinions advanced in papers are to be understood as individual expressions of their authors and not those of the Society. Manuscript received by ASME Applied Mechanics Division, June 8, 1953. Paper No. 54—A-95.

If $|\sigma_1|$ is decreased after the point $Y''$ is reached, the material again behaves elastically following the relation

$$\sigma_2 - \sigma_{2Y} = \frac{\nu}{1-\nu}(\sigma_1 - \sigma_{1Y})$$

where $\nu$ varies so little with the mean pressure $-\frac{1}{3}(\sigma_1 + \sigma_2 + \sigma_3)$ that the relation is very accurately represented by a straight line until the point $Y'''$ is reached when the material again starts yielding, then following the relation

$$\sigma_1 - \sigma_2 = \sigma_Y$$

This relation holds until point $F$ is reached, where fracture occurs. $F$ is the intersection point between the line $\sigma_1 - \sigma_2 = \sigma_Y$ and that locus for fractures which is valid for uniaxial plastic deformation.

### Front Velocity of a Shock Wave With a Very High Pressure

The stress system just behind the plastic wave front of a plane shock wave in a solid material may be represented by the point $Y''$ of Fig. 2. If the intensity of the shock wave is very high

$$\sigma_1 \approx \sigma_2 = \sigma_3$$

e.g., the stress system is approximately hydrostatic.

Bridgman has determined very accurately the relation between hydrostatic pressure $p$ and density $\rho$ for many materials up to $p = 30{,}000$ kg/cm² (5) and with somewhat less accuracy up to $p = 100{,}000$ kg/cm² (6, 7). As at detonations in contact with metals pressures of about 300,000 kg/cm² are to be expected, it is necessary for quantitative calculations to extrapolate Bridgman's experimental results. Pack, Evans, and James (8) have suggested the relation

$$p = A(\rho/\rho_0)^{3/2}[\exp\{\beta[1 - (\rho_0/\rho)^{1/2}]\} - 1] \quad [3]$$

which by suitable choice of the constants $A$ and $\beta$ very closely follows the experimental results. It is to be observed that Equation [3] is the relation between pressure and density when the changes of state are isothermic. In the absence of better assumptions Equation [3] is assumed to hold even when the changes of state are such as take place at the passage of a shock wave.

Table 1 contains the values of $A$, $\beta$, and $\rho_0$ for some materials.

TABLE 1 CHARACTERISTIC CONSTANTS FOR SOME MATERIALS

| Material | $A$ dynes/cm² | $\beta$ | $\rho_0$ kg/m³ |
|---|---|---|---|
| Iron | $6.01 \times 10^{11}$ | 8.4 | $7.86 \times 10^3$ |
| Aluminum | 1.90 | 11.4 | 2.72 |
| Magnesium | 0.639 | 15.6 | 1.74 |
| Copper | 3.52 | 11.7 | 8.93 |
| Lead | 1.32 | 10.0 | 11.34 |
| Quartz glass | 4.7 | 2.0 | 2.21 |
| (Brass) | (3.0) | (11.7) | (8.3) |

The front velocity $U$ and the mass velocity $u$ just behind the front of a shock wave with the direction 1 are given by the relations

$$U^2 = -\frac{\rho}{\rho_0}\frac{\sigma_1}{\rho - \rho_0} \quad [4]$$

$$u = -\frac{\sigma_1}{\rho_0 U} \quad [5]$$

Calculations of $U$ and $u$ as functions of $\sigma_1$ have been performed with the aid of Equations [3], [4], and [5] for iron, aluminum, magnesium, copper, lead, quartz glass, and brass. The relations obtained are represented graphically in Fig. 3. To give an idea of

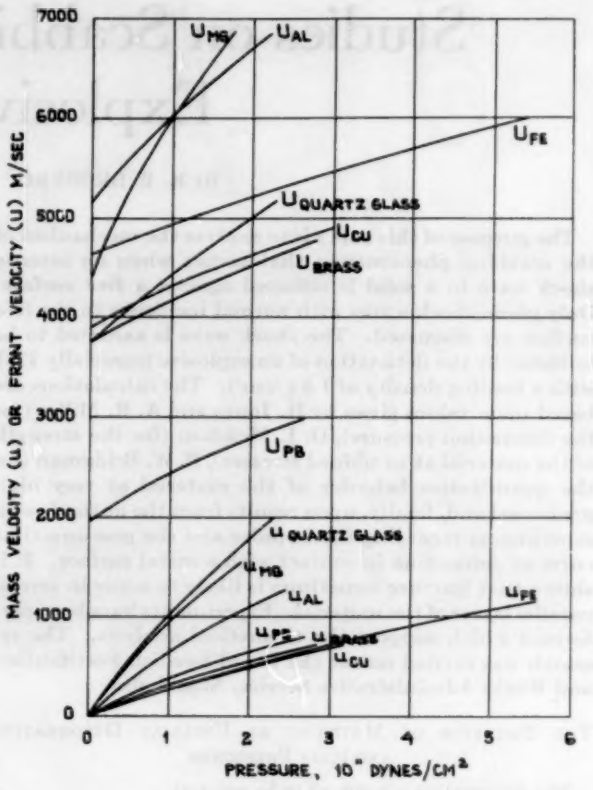


Fig. 3 Front and Mass Velocity as Functions of Front Pressure

the pressure that is necessary to make the velocity of the plastic wave front higher than that of elastic waves, the results obtained by Bridgman are extrapolated to 530,000 kg/cm² for steel.

A calculation of the pressure at a detonation in contact with a metal surface implies knowledge of the following:

(*a*) The gas relationships at reflection against a moving wall (pressure as a function of the velocity of the wall).

(*b*) The velocity of the wall (mass velocity as a function of pressure).

The latter relation—$u$ as a function of $\sigma_1$—is already worked out for several different materials, Fig. 3. However, rather little is known about the gas relationships at the high pressures that are to be expected at a detonation in contact with a solid. Jones and Miller (9) have assumed an empirical equation

$$pv'/N' = RT + bp + cp^2 + dp^3 \quad [6]$$

where $v'$ denotes the volume of the gaseous products from detonation of one mole of TNT and $N'$ the number of moles. The constants $b$, $c$, and $d$ were chosen so as to give agreement between calculated and measured values of the detonation velocities of TNT with different low loading densities. Complete agreement also for high loading densities was impossible to obtain with Equation [6]; thus an extrapolation to the considerably higher pressures that are reached at detonation in contact with metals is somewhat doubtful but is used here to give an idea of the pressures that are to be expected.

When the detonation wave reaches the surface of the solid, a shock wave[3] emerges from that surface into the detonation gases. The mass velocity just behind the front of that shock wave has

[3] In some cases a rarefaction wave emerges.

initially the same value as the velocity given to the surface. Thus it is possible to calculate the pressure initially reached at the moving surface as a function of the velocity of that surface by means of the Hugoniot-Rankine equations, Equation [6], and the expression given by Jones and Miller (9) of the internal energy of the detonation gases. The "ambient" pressure, viz., the pressure at the detonation wave front, is 160,000 kg/cm² for TNT with a loading density of 1.5 g/cm³ (9).

Then the following relation is obtained

$$10^{-6}(1580 - u)^2 = (10^{-11}p - 1.60)^2(10^{-11}p + 0.33)(3.03 - 10^{-11}p)/1.60(10^{-11}p + 0.10)$$

where $u$ (m/sec) is the velocity of the wall and $p$ (dynes/cm²) the pressure at the intermediate surface just after the arrival of the detonation wave. The relation is graphically represented in Fig. 4 together with relations between mass velocity and front pressure of shock waves in various media. The relation obtained is assumed to hold approximately even on the rarefaction side. In the case of air accurate experimental results agree with the values shown in Fig. 4.

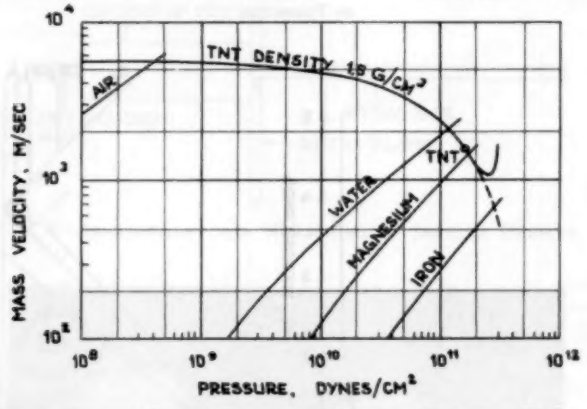


FIG. 4 GRAPHIC DETERMINATION OF MAXIMUM PRESSURE WHEN A CHARGE OF TNT WITH A LOADING DENSITY OF 1.5 G/CM³ IS DETONATED IN CONTACT WITH VARIOUS MEDIA

However, the gas equation does not seem to hold for the very high pressures that are supposed to be reached when the velocity of the intermediate surface is low. The results for high velocities of the surface are therefore extrapolated graphically to give a physically possible relation between pressure and velocity in the low-velocity range. It is to be emphasized that the values thus obtained tend to be mere guesses for the materials toward the bottom of Table 2.

TABLE 2 CALCULATED MAXIMUM PRESSURES

| Material | Pressure at detonation in contact with the material (TNT, 1.5 g/cm³) dynes/cm² |
|---|---|
| (Air) | $0.45 \times 10^{9}$ |
| (Water) | $1.20 \times 10^{11}$ |
| Quartz glass | 1.65 |
| Magnesium | 1.7 |
| Aluminum | 2.1 |
| Lead | 2.6 |
| Brass | 2.7 |
| Iron | 2.8 |
| Copper | 2.8 |

## APPROXIMATE TREATMENT OF PLANE PROPAGATION OF A SHOCK WAVE IN A SOLID MATERIAL

A hypothetical case is to be studied, where the following approximations will be used:

1 The propagation velocity of plane elastic waves in relation to ambient material is independent of the pressure. This velocity is called $c_e$.

2 The propagation velocity of plane plastic waves in relation to ambient material is independent of the pressure. This velocity is called $c_p (c_p < c_e)$.

3 The mass velocity $u$ is small compared with $c_e$ or $c_p$.

4 Influence of the temperature is unimportant.

If the propagation of the shock wave were represented on an $x$-$t$-diagram, that diagram would be divided into elastic and plastic regions. In an elastic region the propagation of the wave is regarded as if occurring in a virgin elastic region (without an elastic limit) and in a plastic region the propagation of the wave is regarded as if occurring in a "virgin plastic" region. As the division into elastic and plastic regions is not predetermined a correlation is necessary between the $x$-$t$-diagram and Fig. 2.

With the foregoing assumptions the following relations hold in each separate region (10)

$$\frac{D_+ P}{Dt} = \frac{D_- Q}{Dt} = 0$$

$$P = -\frac{\sigma_1}{\rho_0 c} + u$$

$$Q = -\frac{\sigma_1}{\rho_0 c} - u$$

$$\frac{D_+}{Dt} = \frac{\partial}{\partial t} + c\frac{\partial}{\partial x}$$

$$\frac{D_-}{Dt} = \frac{\partial}{\partial t} - c\frac{\partial}{\partial x}$$

where $c$ is either $c_e$ or $c_p$. The equations express that $P$ is a constant along lines with the slope $1/c$ (line $P$) and $Q$ is a constant along lines with the slope $-1/c$ (line $Q$).

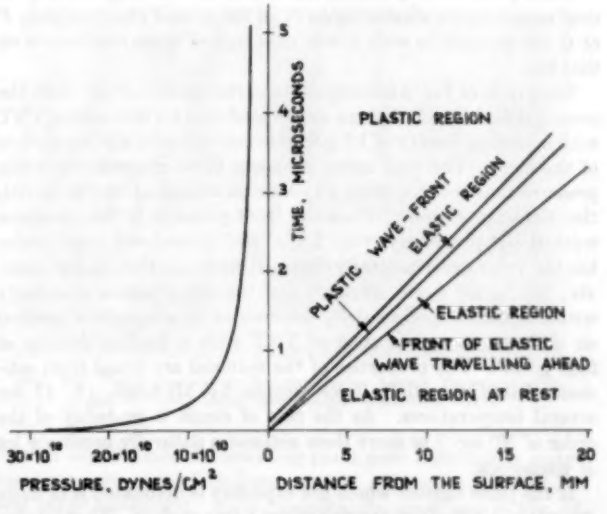


FIG. 5 PROPAGATION OF PRESSURE PULSE INTO STEEL PLATE OF INFINITE THICKNESS

Assuming the load on the material surface to be of the form $p = p(t)$ that is graphically shown to the left of the $x$-$t$-diagram in Fig. 5, it is obvious that the $x$-$t$-diagram is divided into two plastic regions (one of which degenerates into a straight line of finite length) and two elastic regions (which are not separated completely). An elastic wave with the constant stress

$$\sigma_1 = -\frac{1-\nu}{1-2\nu}\sigma_Y$$

precedes the plastic wave front. Immediately behind the plastic wave front at the co-ordinate $x_C$ (the point $C$ of Fig. 6) the value of $P$ is

$$P = -\frac{1-\nu}{1-2\nu}\frac{\sigma_Y}{\rho_0}\alpha - \frac{\sigma_{1C}(x_C)}{\rho_0}\gamma$$

where

$$\frac{1}{c_p} - \frac{1}{c_e} = \alpha$$

$$\frac{1}{c_p} + \frac{1}{c_e} = \gamma$$

The line $P$ through the point $C$ emerged from the point $B$. There the line $P$ intersects the line $Q$ that emerged from the point $A$. On the latter line

$$Q = \frac{1-\nu}{1-2\nu}\frac{\sigma_Y}{\rho_0}\alpha + \frac{\sigma_{1A}(\theta x_C)}{\rho_0}\alpha$$

where $\theta = \alpha/\gamma$.

Thus at the point $B$

$$\frac{P+Q}{2} = \frac{P(\alpha x_C)}{\rho_0 c_e} = -\frac{\sigma_{1C}(x_C)}{2\rho_0}\gamma + \frac{\sigma_{1A}(\theta x_C)}{2\rho_0}\alpha$$

By recursion the following expression is obtained

$$-\sigma_{1C}(x) = \frac{2}{\gamma c_e}[p(\alpha x) + \theta p(\theta\alpha x) + \theta^2 p(\theta^2\alpha x) + \ldots .]$$

where the index $C$ of $x$ is dropped. That expression holds along the line $OC'$.

When a line $P$ or $Q$ crosses the line of the $x$-$t$-diagram, Fig. 5, that separates the elastic region from the second plastic region, $P$ or $Q$ are changed in such a way that $\sigma_1$ and $u$ are continuous on that line.

The graph of Fig. 5 is designed to agree quantitatively with the propagation in steel of plane waves produced by detonating TNT with a loading density of 1.5 g/cm³ in contact with a plane surface of the steel. The load curve is chosen to be approximately the pressure-time relation from a cylindrical charge of 50 grams with the diameter 24 mm. Thus the front pressure is that pressure worked out previously, viz., $2.8 \times 10^{11}$ dynes/cm², the impulse has the value experimentally obtained on detonation against steel, viz., $3.5 \times 10^5$ dynes sec/cm², and the shape agrees essentially with the shape experimentally determined by a capacitive method on detonation against steel of TNT with a loading density of 0.80 g/cm³. The properties of the material are found from estimates based essentially upon graphs by McAdam (1, 4) for several temperatures. As the rate of strain is probably of the order of $10^6$ sec$^{-1}$ or more these estimates naturally involve a lot of guesswork.

If the plate against which the explosive is detonated is of finite thickness, a reflection occurs against a free surface. That implies that lines $Q$ emerge from that surface on which

$$Q = -P$$

A graphic design for a steel plate of 20 mm thickness with one surface exposed to direct detonation with a charge of the kind mentioned is shown in Fig. 7. Through correlation with Fig. 2 the point $S_1$ of the $x$-$t$-diagram is found which is the earliest point of the diagram that corresponds to the point $F$ of Fig. 2. Thus

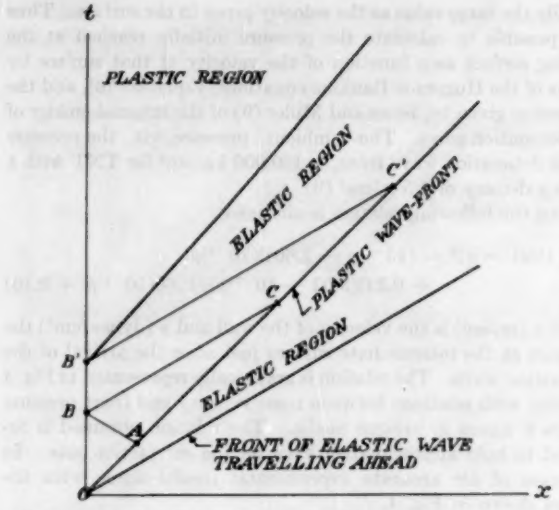


FIG. 6 PROPAGATION OF PRESSURE PULSE NEAR SURFACE SUBJECT TO PRESSURE

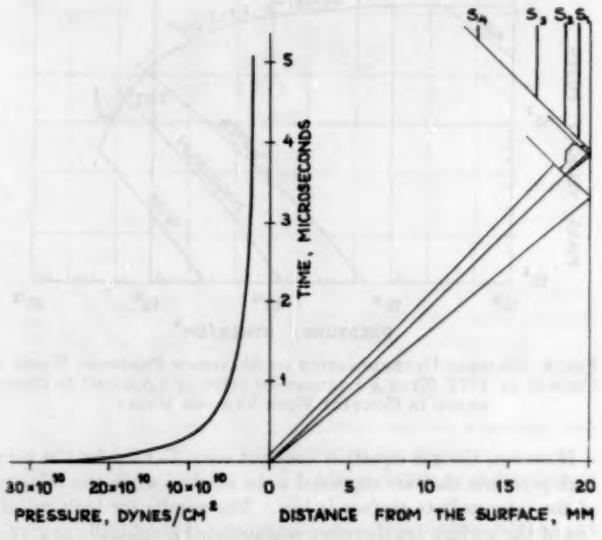


FIG. 7 PROPAGATION OF PRESSURE PULSE INTO STEEL PLATE OF FINITE THICKNESS; GRAPHIC DETERMINATION OF SCABBING

scabbing occurs from the surface $x = x(S_1)$ which thereupon offers another free surface. Thus the process can be repeated and several fractures are likely to occur ($S_2$, $S_3$, . . .).

## EXPERIMENTAL INVESTIGATIONS

*Determination of the Pressure-Time Curve.* A simple method to determine the impulse density on detonation in contact with a metal surface presents itself. At one end of a cylindrical bar of the metal a plate of the same metal was fastened as shown in Fig. 8.

The charge was then detonated in contact with the end of the bar and the plate. The velocity of the bar after the detonation was measured in a simple way and the impulse is easily calculated. With the charge described previously (50 grams) the impulse density was found to be $3.5 \times 10^5$ dynes sec/cm² against steel and copper. Experiments with other materials than high-quality steel and copper failed because the bar fractured.

Some measurements of the movement of the right end of a steel bar, according to Fig. 8, have been made with a capacitive method when detonating 50 grams of TNT with a loading density of 0.80 g/cm³. The pressure seems to fall off from the maximum value (14,000 kg/cm²) very rapidly (down to 5000 kg/cm² in about 7 μsec) but the decrease is slower than for the exponential curve with the same initial decrease. Thus the impulse density has reached only half its final value at 7 μsec. As the pressure decrease after the first few microseconds is essentially regulated by the expansion of the gas sphere, the correspondence in that interval between the pressure-time curves for TNT with a loading density of 1.5 g/cm³ and 0.80 g/cm³ is obvious. These considerations together with the experimental value of the total impulse density and the calculated values of the maximum pressure form the basis for the choice of the pressure-time curve of Fig. 5.

*Experimental Method to Obtain Plane Spallings.* When detonating an explosive in contact with a plate the scab generally has the shape shown in Fig. 9. The fracture first occurs on the central

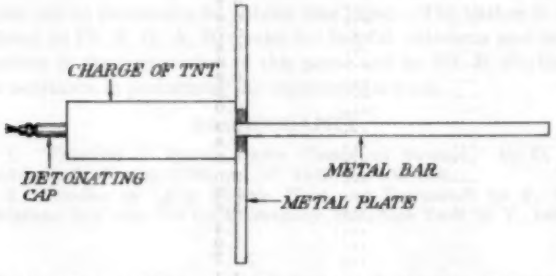


FIG. 8 ARRANGEMENT FOR MEASURING OF IMPULSE DENSITY

FIG. 9 GENERAL SHAPE OF SCAB FROM PLATE
(Note spheroidal form. The scab is cut into two equal pieces.)

parts as a cleavage parallel to the free surface; then the velocity of the portion between that cleavage and the free surface causes a spheroidal deformation of that portion and then another fracture that separates it completely from the plate. If two or more cleavages occur, they generally flow together during the spheroidal deformation. To avoid that spheroidal deformation the method used was to bore a hole 6 mm diam through a steel plate, then to push a bar in that hole and place the charge upon the bar as shown in Fig. 10. The deviations from the plane case are then very small for strong materials like steel, but for lead, brass, etc., they are still very great depending on the fact that the plastic flow (especially on the charge side) has a large component normal to the cylindrical surface of the bar. To minimize that flow a cylinder of the bar material with a diameter of 18 mm was inserted into a hole in a steel plate. The bar of 6 mm diam was then placed in a hole axially into the cylinder as shown in Fig. 11. Thus the deformations were essentially uniaxial and no important disturbances from the steel affected the bar.

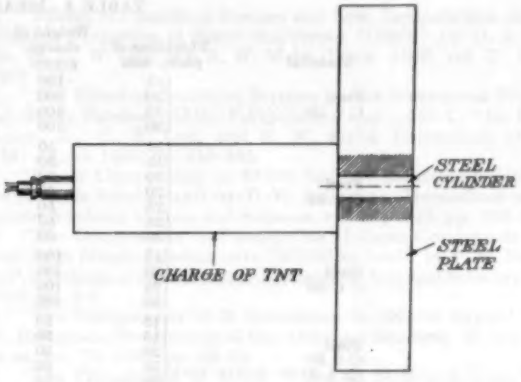


FIG. 10 ARRANGEMENT TO OBTAIN PLANE SCABS IN STEEL

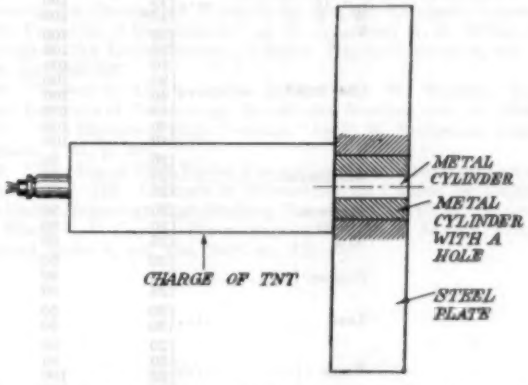


FIG. 11 ARRANGEMENT TO OBTAIN PLANE SCABS IN METALS OTHER THAN STEEL

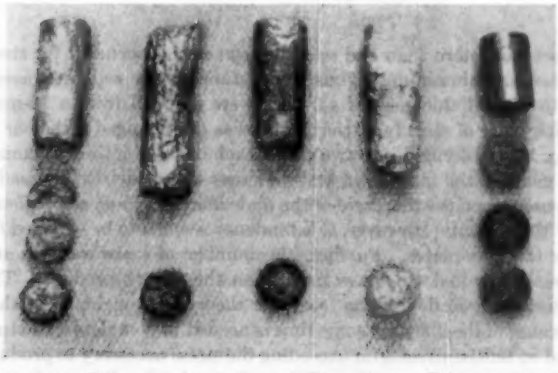

FIG. 12 PHOTOGRAPH OF SCABS; BARS AFTER DETONATIONS
(*Left to right:* Brass, lead, copper, aluminum, steel.)

In all experiments the scabbing parts were collected in water, thus preventing secondary deformations. The scabs from the bar were easily recognized. Some typical scabs are shown in Fig. 12. The thicknesses of the separate scabs were determined by weighing.

The charges used were all of TNT with a loading density of 1.5 g/cm³ and were cylindrical with their length three times their diameter. Some of the charges weighed 100 grams, and others 50 grams.

The thickness of the plate varied from 15 mm to 30 mm.

The results from the experiments are given in Table 3.

The predictions from the theory proved to be correct in the re-

TABLE 3 MEASUREMENTS ON SCABS

| Material | Thickness of plate, mm | Weight of charge, grams | Thickness of scab 1st scab, mm | 2nd scab, mm | 3rd scab, mm | Total thickness of scabs, mm |
|---|---|---|---|---|---|---|
| Steel C 0.20 | 15 | 100 | 6.4 | ... | ... | 6.4 |
| | 20 | 100 | 5.6 | 4.2 | ... | 9.8 |
| | 25 | 100 | 12.0 | 3.6 | ... | 15.6 |
| | 30 | 100 | 17.0 | 3.1 | ... | 20.1 |
| Steel C 0.35 | 15 | 50 | 3.7 | 2.4 | 1.5 | 7.4 |
| | 15 | 50 | 3.6 | 2.6 | ... | 6.2 |
| | 20 | 50 | 2.5 | 10.0 | ... | 12.5 |
| | 20 | 50 | 2.7 | 9.9 | ... | 12.6 |
| | 25 | 50 | 2.2 | 1.6 | ... | 3.8 |
| | 25 | 50 | 2.2 | 16.0 | ... | 18.2 |
| | 30 | 50 | 6.9 | ... | ... | 6.9 |
| Steel C 0.50 | 15 | 100 | 6.5 | ... | ... | 6.5 |
| | 20 | 100 | 1.2 | 0.8 | 6.5 | 8.5 |
| | 25 | 100 | 11.4 | 1.6 | 1.6 | 14.5 |
| | 30 | 100 | 16.7 | 0.8 | 2.9 | 20.3 |
| Steel C 0.30 Cr 1.3 Ni 4.25 | 15 | 50 | 3.2 | ... | ... | 3.2 |
| | 15 | 50 | 1.6 | 1.6 | ... | 3.2 |
| | 20 | 50 | 2.3 | 1.4 | ... | 3.7 |
| | 20 | 50 | 2.6 | 10.7 | ... | 13.3 |
| | 25 | 50 | 2.2 | 15.7 | ... | 17.9 |
| | 25 | 50 | 2.1 | ... | ... | 2.1 |
| | 30 | 50 | ... | ... | ... | 0.0 |
| Steel C 1.15 W 0.5 V ... | 15 | 100 | 1.3 | 1.2 | 2.0 | 4.5 |
| | 15 | 100 | 1.3 | 1.2 | 2.0 | 4.5 |
| | 15[a] | 100 | 1.3 | 1.2 | 2.0 | 4.5 |
| Cast iron[b] | 30 | 100 | 0.7 | ... | ... | 0.7 |
| | 30 | 100 | 0.9 | ... | ... | 0.9 |
| | 30 | 100 | 0.7 | ... | ... | 0.7 |
| | 30 | 100 | 0.8 | ... | ... | 0.8 |
| | 40 | 100 | 1.3 | ... | ... | 1.3 |
| | 40 | 100 | 0.9 | ... | ... | 0.9 |
| | 40 | 100 | 1.5 | ... | ... | 1.5 |
| | 40 | 100 | ... | ... | ... | 0.0 |
| Aluminum | 20 | 50 | 2.6 | ... | ... | 2.9 |
| | 20 | 50 | 3.5 | ... | ... | 3.8 |
| | 25 | 50 | 3.9 | ... | ... | 4.0 |
| Electron Mg 93 Al 7 | 20 | 50 | ... | ... | ... | 3.0 |
| | 20 | 50 | ... | ... | ... | 3.3 |
| | 25 | 50 | ... | ... | ... | 5.6 |
| Copper | 20 | 50 | 1.3 | ... | ... | 1.4 |
| | 20 | 50 | 1.8 | ... | ... | 1.9 |
| | 25 | 50 | 1.7 | ... | ... | >1.7 |
| Lead | 30 | 50 | 1.1 | ... | ... | 1.1 |
| | 30 | 50 | 1.4 | ... | ... | 1.4 |
| Brass | 20 | 50 | 1.4 | 0.6 | 0.2 | 2.1 |
| | 20 | 50 | 1.1 | 0.6 | 0.2 | 1.9 |
| | 25 | 100 | 1.2 | 0.5 | 0.5 | 2.2 |
| | 30 | 100 | 1.3 | 0.8 | ... | 2.1 |
| Quartz glass | 30 | 50 | (1) | ... | ... | ... |

[a] The bar divided into two parts, each of the length of 7.5 mm.
[b] 20 mm diameter of the bar.

spect that more than one scabbing sometimes occurred for steel, brass, and aluminum. Thus, for instance, three separate pieces, with a total thickness of 4.5 mm, were scabbed from a 15-mm-thick plate of steel (and that result was not changed if the bar in Fig. 10 was divided into two parts, each of the length of 7.5 mm). In general, the number of scabs decreased and their thickness increased when the thickness of the plate increased, just as predicted by the theory. However, this tendency seemed to be changed for the thinnest plates. Further, the number of scabs was less and their individual thickness more than the theory predicts. The cause of these deviations from the theory is thought to be that because of the ductility some time is needed to complete a fracture and so tensile stresses far exceeding the stress necessary to produce a fracture under normal conditions may exist simultaneously on a rather thick layer near the bottom of the plate. When fracture is completed at one surface, it is possible that fractures started at other surfaces may be prevented from being completed, because reloading waves emerge from the completed fracture. Some of the scabs from thin steel plates also show signs of started but not completed fractures. It is to be noted that the time between separate completed fractures is of the order of some tenths of a microsecond and that the theory presupposes the fracture to occur instantaneously, thus providing complete reflections against free surfaces.

If the material were completely brittle, fracture would occur instantaneously and the two free surfaces on each side of the fracture would separate at a velocity which immediately will reach a rather high value because of reflections of the waves traveling toward the fracture surfaces. For instance, the surfaces at fracture $S_1$ of Fig. 7 separate at an initial velocity of 90 m/sec.

In a ductile material, fracture is not completed instantaneously and thus the two portions on each side of a partial fracture tend to separate with a rather low velocity because the waves traveling toward the "fracture" surface are not reflected completely. Suppose the velocity difference between two parallel layers at a distance of 0.5 mm at fracture $S_1$ of Fig. 7 to be 50 m/sec; then this portion elongates 0.005 mm during 0.1 microsec, which means an average strain of 1 per cent. But in 0.1 microsec a reloading wave from fracture $S_2$ has arrived thus preventing completed fracture.

As regards quartz glass, no results were obtained because the whole glass plate disintegrated completely into extremely small grains. Thus the result was disappointing because quartz glass was expected to behave as the foregoing theory predicts because of its brittleness. Yet in the quartz sand some fragments from the bar were found, having the size of about 1 mm.

## Discussion

The theory developed in the foregoing explains qualitatively some scabbing phenomena though the quantitative agreement between theory and experiments is not good.

The differences between the theoretical and the experimental results are thought to be caused by the following imperfections of the theory:

1 The bar material is not completely brittle and therefore fracture does not occur instantaneously.

2 The strength properties of the bar material are not known accurately at very high pressures and very high rates of strain.

3 The elastic constants of the bar material are not known accurately at very high pressures. Thus Poisson's ratio has been assumed to be constant, an assumption which obviously is not fulfilled (11).

4 The temperature changes and their effects on the strength properties and elastic constants have not been considered. The maximum temperature is believed to reach the melting point in the case of aluminum, magnesium, lead, and quartz glass. Temperatures above the melting point, caused by suddenly applied very high stresses, sometimes can be reached even in the case of steel (12). A rough estimate shows that the "residual" temperature increase in the metal just below the charge is about 50 deg C for steel and 20 deg C for copper.

### Acknowledgments

The author wishes to express his appreciation to the Royal Swedish Fortifications and Works Administrative Service, Stockholm, for its permission to publish this paper. The author is indebted to Dr. S. G. A. Bergman for helpful criticisms and suggestions in the preparation of this paper and to Mr. B. Skylling for assistance in performing the experimental work.

### BIBLIOGRAPHY

1 "Fracture of Metals Under Combined Stresses," by D. J. McAdam, Jr., Trans. ASM, vol. 37, 1946, pp. 538–566.

2 "Studies in Large Plastic Flow and Fracture," by P. W. Bridgman, McGraw-Hill Book Company, Inc., New York, N. Y., 1952.

3 "Effects of Combined Stresses and Low Temperatures on the Mechanical Properties of Some Nonferrous Metals," by D. J. McAdam, Jr., G. W. Geil, and R. W. Mebs, Trans. ASM, vol. 37, 1946, pp. 495–537.

4 "The Effect of Combined Stresses on the Mechanical Properties of Steels Between Room Temperature and —188 C," by D. J. McAdam, Jr., G. W. Geil, and R. W. Mebs, Proceedings of the ASTM, vol. 45, 1945, pp. 448–485.

5 "Linear Compression to 30,000 kg/cm², Including Relatively Incompressible Substances," by P. W. Bridgman, Proceedings of the American Academy of Arts and Sciences, vol. 77, 1949, pp. 189–234.

6 "The Compression of Twenty-One Halogen Compounds and Eleven Other Simple Substances to 100,000 kg/cm²," by P. W. Bridgman, Proceedings of the American Academy of Arts and Sciences, vol. 76, 1945, pp. 1–7.

7 "The Compression of 39 Substances to 100,000 kg/cm²," by P. W. Bridgman, Proceedings of the American Academy of Arts and Sciences, vol. 76, 1948, pp. 55–70.

8 "The Propagation of Shock Waves in Steel and Lead," by D. C. Pack, W. M. Evans, and H. J. James, Proceedings of the Physical Society, vol. 60, 1948, pp. 1–8.

9 "The Detonation of Solid Explosives: The Equilibrium Conditions in the Detonation Wave-Front and the Adiabatic Expansion of the Products of Detonation," by H. Jones and A. R. Miller, Proceedings of the Royal Society, London, England, series A, vol. 194, 1948, pp. 489–507.

10 "Waves in Compressible Media," by W. Weibull, Trans. Royal Institute of Technology, Stockholm, Sweden, vol. 18, 1948.

11 "The Physics of High Pressure," by P. W. Bridgman, London, England, 1931, p. 386.

12 "The Use of Flat-Ended Projectiles for Determining Dynamic Yield Stress. III. Changes in Microstructure Caused by Deformation Under Impact at High-Striking Velocities," by W. E. Carrington and Marie L. V. Gayler, Proceedings of the Royal Society, London, England, series A, vol. 194, 1948, pp. 323–331.

# Buckling of Sandwich Cylinders Under Combined Compression, Torsion, and Bending Loads[1]

By C. T. WANG,[2] R. J. VACCARO,[3] AND D. F. DE SANTO,[4] NEW YORK, N. Y.

**A theoretical investigation is carried out on the buckling of sandwich cylinders under combined compression, torsion, and bending loads. The governing differential equation is solved by using Galerkin's method. The interrelationship obtained between the critical loads is plotted in the form of nondimensional interaction curves. In the limiting cases of axial compression alone, torsion alone, bending alone, and combined bending and axial compression, the results agree with those obtained previously (1-3).[5]**

## Nomenclature

The following nomenclature is used in the paper:

$a$ = radius of cylinder to mid-plane, in.
$C$ = $hG$, lb per in.
$D$ = flexural stiffness of isotropic sandwich cylinder, in-lb
$D$ = $Eth^2/2(1-\nu^2)$
$E$ = Young's modulus for the face material, lb per sq in.
$F$ = $2tE/a^2$
$G$ = shear modulus of the core material, psi
$h$ = depth of isotropic sandwich plate measured between middle planes of faces, in.
$I$ = moment of inertia of sandwich cylinder about its diameter
$l$ = length of cylinder, in.
$M$ = bending moment, in-lb
$m$ = number of half-waves longitudinally
$N_x$, $N_y$ = resultant normal forces in $x$ and $y$-directions, lb per in.
$N_{xy}$ = resultant shearing force, lb per in.
$N_1$ = applied normal force in axial direction, lb per in.
$n$ = number of full waves circumferentially
$T$ = torsional moment, in-lb
$t$ = thickness of the faces, in.
$u$, $v$, $w$ = displacements in $x$, $y$, $z$-directions, respectively, of a point in middle surface of cylinder, in.
$x$, $y$, $z$ = rectangular co-ordinates (Fig. 1)
$\nu$ = Poisson's ratio for the face material
$\theta$ = circumferential co-ordinate
$\nabla^4$ = operator, $\left(\frac{\partial^2}{\partial x^2}+\frac{\partial^2}{\partial y^2}\right)^2 = \left(\frac{\partial^4}{\partial x^4}+2\frac{\partial^4}{\partial x^2\partial y^2}+\frac{\partial^4}{\partial y^4}\right) = \left(\frac{\partial^2}{\partial x^2}+\frac{\partial^2}{a^2\partial\theta^2}\right)^2$
$\nabla^8$ = operator, $\left(\frac{\partial^2}{\partial x^2}+\frac{\partial^2}{\partial y^2}\right)^4 = \left(\frac{\partial^2}{\partial x^2}+\frac{\partial^2}{a^2\partial\theta^2}\right)^4$
$\lambda$ = $m\pi a/l$

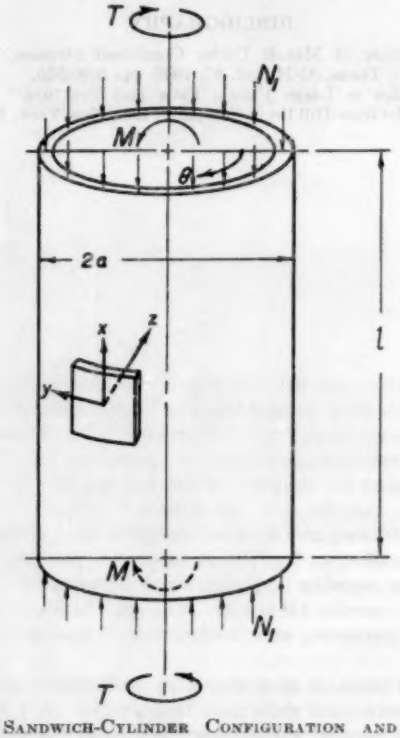


Fig. 1 Sandwich-Cylinder Configuration and Loading

## Introduction

In previous papers (1 to 5), the senior author and his associates have investigated the buckling behavior of sandwich cylinders under axial compression, torsion, bending, and combined bending and axial compression. The investigation is now extended to the buckling of sandwich cylinders under combined compression, torsion, and bending loads. By solving Donnell's equation modified to include the effects of transverse shear for sandwich curved plates and shells using Galerkin's method, the buckling loads are calculated and are plotted in the form of interaction curves. In the limiting cases of bending alone, axial compression alone, tor-

[1] The results reported in this paper were obtained during the course of research, sponsored by Office of Naval Research, under contract No. N6-onr-279, Task Order V.

[2] Professor of Aeronautical Engineering, New York University.
[3] Research Assistant, New York University.
[4] De la Cierva Fellow, Daniel Guggenheim School of Aeronautics, New York University.

[5] Numbers in parentheses refer to the Bibliography at the end of the paper.

Contributed by the Applied Mechanics Division and presented at the Annual Meeting, New York, N. Y., November 28–December 3, 1954, of The American Society of Mechanical Engineers.

Discussion of this paper should be addressed to the Secretary, ASME, 29 West 39th Street, New York, N. Y., and will be accepted until October 10, 1955, for publication at a later date. Discussion received after the closing date will be returned.

Note: Statements and opinions advanced in papers are to be understood as individual expressions of their authors and not those of the Society. Manuscript received by ASME Applied Mechanics Division, October 12, 1953. Paper No. 54—A-102.

sion alone, and combined bending and axial compression, the results agree with those obtained previously.

## Formulation of the Problem

By assuming isotropic core material and neglecting the bending rigidity of the faces about their own middle surfaces, the equilibrium equations for an element of a sandwich cylinder have been derived in reference (4). By neglecting terms that were regarded as small by Donnell (6), these equations can be reduced to a single equation in terms of the lateral deflection $w$ only

$$D\nabla^4 w + \left(1 - \frac{D}{C}\nabla^2\right)\left[\frac{2tE}{a^2}\frac{\partial^4 w}{\partial x^4} - \nabla^4\left(N_x\frac{\partial^2 w}{\partial x^2} + N_y\frac{\partial^2 w}{\partial y^2} + 2N_{xy}\frac{\partial^2 w}{\partial x\,\partial y}\right)\right] = 0 \quad \ldots\ldots [1]$$

This is the so-called Donnell's equation modified to include the effects of transverse shear for sandwich curved plates and shells first obtained by Stein and Mayers (7).

In the case of sandwich cylinders under combined compression, torsion, and bending loads, we have

$$\left.\begin{aligned} N_x &= -N_1 + (2Mat/I)\cos\theta \\ N_{xy} &= T/2\pi a^2, \quad N_y = 0 \end{aligned}\right\} \quad \ldots\ldots [2]$$

where $N_1$ is the force per unit length due to axial compression, $M$ is the bending moment, $I$ is the moment of inertia of the cylinder, and $T$ is the torsional moment. With such a loading, Equation [1] thus becomes

$$D\nabla^4 w + \left(1 - \frac{D}{C}\nabla^2\right)\left\{\frac{2tE}{a^2}\frac{\partial^4 w}{\partial x^4} - \nabla^4\left[\left(-N_1 + \frac{2Mat}{I}\cos\theta\right)\frac{\partial^2 w}{\partial x^2} + \frac{T}{\pi a^2}\frac{\partial^2 w}{\partial x\,\partial\theta}\right]\right\} = 0 \quad \ldots\ldots [3]$$

where $y$ is taken as $a\theta$.

## Galerkin's Method

Equation [3] may be solved by means of Galerkin's method as follows: We first assume the deflection $w$ of the cylinder after buckling in the form of a series that satisfies the boundary conditions but with undetermined parameters. For long cylinders, however, the boundary conditions at the two ends become unimportant and we may assume the deflection series without any regard for the end conditions. For a cylinder under combined axial compression and bending, $w$ may be assumed in the following form (3)

$$w = \sin\frac{m\pi x}{l}\sum_{n=0}^{\infty} A_n \cos n\theta \quad \ldots\ldots [4]$$

and for a cylinder under torsion only, the deflection after buckling is of the following form (4)

$$w = \sum_{n=1}^{\infty} B_n \sin\left(\frac{m\pi x}{l} - n\theta\right) = \sum_{n=1}^{\infty} B_n\left(\sin\frac{m\pi x}{l}\cos n\theta - \cos\frac{m\pi x}{l}\sin n\theta\right) \quad \ldots\ldots [5]$$

Guided by these expressions, we shall assume the deflection of the cylinder in the case of combined loading as follows

$$w = \sin\frac{m\pi x}{l}\sum_{n=0}^{n_1} A_n \cos n\theta + \cos\frac{m\pi x}{l}\sum_{n=1}^{n_1} B_n \sin n\theta \quad \ldots [6]$$

With $w$ expressed in a proper series, we shall next substitute this series into Equation [3]. If the Expression [6] happens to be the exact solution of Equation [3], after substitution Equation [3] will be identically equal to zero. In general, this will not be so and the resulting expression will be a function of $x$ and $\theta$ which we shall denote by $Q$. Galerkin's equations for the determination of the coefficients $A_n$ and $B_n$ are

$$\int_0^{2\pi}\int_0^{l} Q \sin\frac{m\pi x}{l}\cos n\theta\, a\,d\theta\,dx = 0 \quad \ldots\ldots [7]$$

$$\int_0^{2\pi}\int_0^{l} Q \cos\frac{m\pi x}{l}\sin n\theta\, a\,d\theta\,dx = 0 \quad \ldots\ldots [8]$$

which, when written out, become

$$\int_0^{2\pi}\int_0^{l}\left(D\nabla^4 w + F\frac{\partial^4 w}{\partial x^4} - \frac{DF}{C}\nabla^2\frac{\partial^4 w}{\partial x^4}\right)\sin\frac{m\pi x}{l}\cos n\theta\, a\,d\theta\,dx + N_1\int_0^{2\pi}\int_0^{l}\left(\nabla^4\frac{\partial^2 w}{\partial x^2} - \frac{D}{C}\nabla^6\frac{\partial^2 w}{\partial x^2}\right)\sin\frac{m\pi x}{l}\cos n\theta\, a\,d\theta\,dx - \frac{2Mat}{I}\int_0^{2\pi}\int_0^{l}\left(\nabla^4\frac{\partial^2 w}{\partial x^2} - \frac{D}{C}\nabla^6\frac{\partial^2 w}{\partial x^2}\right)\sin\frac{m\pi x}{l}\cos n\theta\cos\theta\, a\,d\theta\,dx - \frac{T}{\pi a^2}\int_0^{2\pi}\int_0^{l}\left(\nabla^4\frac{\partial^2 w}{\partial x\,\partial\theta} - \frac{D}{C}\nabla^6\frac{\partial^2 w}{\partial x\,\partial\theta}\right)\sin\frac{m\pi x}{l}\cos n\theta\, a\,d\theta\,dx = 0 \quad [9]$$

in which $F = 2tE/a^2$, and

$$\int_0^{2\pi}\int_0^{l}\left(D\nabla^4 w + F\frac{\partial^4 w}{\partial x^4} - \frac{DF}{C}\nabla^2\frac{\partial^4 w}{\partial x^4}\right)\cos\frac{m\pi x}{l}\sin n\theta\, a\,d\theta\,dx + N_1\int_0^{2\pi}\int_0^{l}\left(\nabla^4\frac{\partial^2 w}{\partial x^2} - \frac{D}{C}\nabla^6\frac{\partial^2 w}{\partial x^2}\right)\cos\frac{m\pi x}{l}\sin n\theta\, a\,d\theta\,dx - \frac{2Mat}{I}\int_0^{2\pi}\int_0^{l}\left(\nabla^4\frac{\partial^2 w}{\partial x^2} - \frac{D}{C}\nabla^6\frac{\partial^2 w}{\partial x^2}\right)\cos\frac{m\pi x}{l}\sin n\theta\cos\theta\, a\,d\theta\,dx - \frac{T}{\pi a^2}\int_0^{2\pi}\int_0^{l}\left(\nabla^4\frac{\partial^2 w}{\partial x\,\partial\theta} - \frac{D}{C}\nabla^6\frac{\partial^2 w}{\partial x\,\partial\theta}\right)\cos\frac{m\pi x}{l}\sin n\theta\, a\,d\theta\,dx = 0 \quad [10]$$

Substituting the assumed function $w$ into these equations and carrying out the integration, we obtain

$$\left[\frac{D(\lambda^2+n^2)^4}{a^3}+\frac{F\lambda^4}{a^4}+\frac{DF\lambda^4(\lambda^2+n^2)}{Ca^6}-\frac{N_1\lambda^2(\lambda^2+n^2)^2}{a^6}-\frac{N_1D\lambda^2(\lambda^2+n^2)^3}{Ca^8}\right]A_n+\left[\frac{Tn\lambda(\lambda^2+n^2)^2}{\pi a^5}+\frac{TDn\lambda(\lambda^2+n^2)^3}{\pi Ca^{10}}\right]B_n+\left[\frac{Mat\lambda^2(\lambda^2+n^2)^2}{Ia^6}+\frac{MatD\lambda^2(\lambda^2+n^2)^3}{ICa^8}\right](A_{n-1}+A_{n+1})=0 \quad [11]$$

and

$$\left[\frac{D(\lambda^2+n^2)^4}{a^3}+\frac{F\lambda^4}{a^4}+\frac{DF\lambda^4(\lambda^2+n^2)}{Ca^6}-\frac{N_1\lambda^2(\lambda^2+n^2)^2}{a^6}-\frac{N_1D\lambda^2(\lambda^2+n^2)^3}{Ca^8}\right]B_n+\left[\frac{Tn\lambda(\lambda^2+n^2)^2}{\pi a^5}+\frac{TDn\lambda(\lambda^2+n^2)^3}{\pi Ca^{10}}\right]A_n+\left[\frac{Mat\lambda^2(\lambda^2+n^2)^2}{Ia^6}+\frac{MatD\lambda^2(\lambda^2+n^2)^3}{ICa^8}\right](B_{n-1}+B_{n+1})=0 \quad [12]$$

Instead of working with these two equations, it is found convenient to combine them into the following ones. Thus, by subtracting Equation [12] from [11], we obtain

$$\left[\frac{D(\lambda^2+n^2)^4}{a^3}+\frac{F\lambda^4}{a^4}+\frac{DF\lambda^4(\lambda^2+n^2)}{Ca^6}-\frac{N_1\lambda^2(\lambda^2+n^2)^2}{a^6}-\frac{N_1D\lambda^2(\lambda^2+n^2)^3}{Ca^8}-\frac{Tn\lambda(\lambda^2+n^2)^2}{\pi a^5}-\frac{TDn\lambda(\lambda^2+n^2)^3}{\pi Ca^{10}}\right]K_n+\left[\frac{Mat\lambda^2(\lambda^2+n^2)^2}{Ia^6}+\frac{MatD\lambda^2(\lambda^2+n^2)^3}{ICa^8}\right](K_{n-1}+K_{n+1})=0 \quad [13]$$

in which $\lambda = m\pi a/l$, $K_n = A_n - B_n$, and in which $2K_0$ is to be substituted for $K_0$ at $n = 1$; $K_n = 0$ when $n > n_1$. When Equations [11] and [12] are added, we have

$$\left[\frac{D(\lambda^2+n^2)^4}{a^3}+\frac{F\lambda^4}{a^4}+\frac{DF\lambda^4(\lambda^2+n^2)}{Ca^6}-\frac{N_1\lambda^2(\lambda^2+n^2)^2}{a^6}-\frac{N_1D\lambda^2(\lambda^2+n^2)^3}{Ca^8}+\frac{Tn\lambda(\lambda^2+n^2)^2}{\pi a^5}+\frac{TDn\lambda(\lambda^2+n^2)^3}{\pi Ca^{10}}\right]K'_n+\left[\frac{Mat\lambda^2(\lambda^2+n^2)^2}{Ia^6}+\frac{MatD\lambda^2(\lambda^2+n^2)^3}{ICa^8}\right](K'_{n-1}+K'_{n+1})=0 \quad [14]$$

in which $K'_n = A_n + B_n$. Again at $n = 1$, $2K'_0$ is to be substituted for $K'_0$ and $K'_n = 0$ when $n > n_1$.

The substitution of $n$ from 0 to $n_1$ in Equations [13] and [14] results in $2n_1 + 1$ simultaneous algebraic equations for $2n_1 + 1$ unknowns. One solution to these equations is, of course, the trivial one, namely

$$K_n = K'_n = 0 \quad (n = 0, 1, 2, 3, \ldots, n_1)$$

The nontrivial solution is carried out in the following section.

## Determination of Buckling Loads

To find the nontrivial solutions of Equations [13] and [14] in their present forms is a very difficult problem. However, from the previous investigations (1, 2, 3) it was found that the minimum buckling loads occur at $\lambda = \infty$. Dividing Equations [13] and [14] by $\lambda^6$, and remembering that $n_1$ also may be very large, we shall drop all terms containing $\lambda$ to a power greater than zero in the denominator but keep terms containing the ratio $n/\lambda$. Equations [13] and [14] thus become

$$\left(1+\frac{n^2}{\lambda^2}-\frac{N_1}{C}-\frac{T}{\pi a^2C}\frac{n}{\lambda}\right)K_n+\frac{Mat}{IC}(K_{n-1}+K_{n+1})=0 \quad [15]$$

$$\left(1+\frac{n^2}{\lambda^2}-\frac{N_1}{C}+\frac{T}{\pi a^2C}\frac{n}{\lambda}\right)K'_n+\frac{Mat}{IC}(K'_{n-1}+K'_{n+1})=0 \quad [16]$$

After dividing these equations through by $Mat/IC$, we have

$$K_{n+1}+L_nK_n+K_{n-1}=0 \quad [17]$$

$$K'_{n+1}+L'_nK'_n+K'_{n-1}=0 \quad [18]$$

in which

$$L_n=\frac{IC}{Mat}\left(1+\frac{n^2}{\lambda^2}-\frac{N_1}{C}-\frac{T}{\pi a^2C}\frac{n}{\lambda}\right) \quad [19]$$

$$L'_n=\frac{IC}{Mat}\left(1+\frac{n^2}{\lambda^2}-\frac{N_1}{C}+\frac{T}{\pi a^2C}\frac{n}{\lambda}\right) \quad [20]$$

Following the examples worked out in reference (3), one may attempt to solve Equations [17] and [18] as finite-difference equations. This, however, was not found possible. The reason is that Equations [17] and [18] are now finite-difference equations with variable coefficients and the solutions of such equations are difficult mathematical problems. Instead, we shall solve the problem in the following manner:

Let us first investigate the magnitude of $n_1$. If $n_1$ is small compared to $\lambda$, then $n_1/\lambda \to 0$ as $\lambda \to \infty$ and Equations [17] and [18] reduce to the governing equations in the case of combined compression and bending. In order that the torsional load may have any effect on the buckling phenomena, $n_1$ must also be a large number so that the ratio $n_1/\lambda$ may remain finite. For any $n$ close to $n_1$, say, $n = n_1 - 1, n_1 - 2, \ldots, n_1 - q$, ($q \ll n_1$), it is obvious that such terms as $1/\lambda, 2/\lambda, \ldots, q/\lambda$ vanish as $\lambda \to \infty$. Thus, for the equations in which $n = n_1, n_1 - 1, n_1 - 2, \ldots, n_1 - q$, the following relations hold

$$L_{n_1}=L_{n_1-1}=L_{n_1-2}=\ldots=L_{n_1-q}=\frac{IC}{Mat}\left(1+\frac{n_1^2}{\lambda^2}-\frac{N_1}{C}-\frac{T}{\pi a^2C}\frac{n_1}{\lambda}\right)=L \quad [21]$$

Therefore, if in the series for $w$ we take the summation of terms from $n_1 - q$ to $n_1$, the system of equations will be as follows

$$\left.\begin{aligned} LK_{n_1}+K_{n_1-1}&=0\\ K_{n_1}+LK_{n_1-1}+K_{n_1-2}&=0\\ &\cdots\\ K_{n_1-q+1}+LK_{n_1-q}&=0\end{aligned}\right\} \quad [22]$$

and

$$\left.\begin{aligned} L'K'_{n_1}+K'_{n_1-1}&=0\\ K'_{n_1}+L'K'_{n_1-1}+K'_{n_1-2}&=0\\ &\cdots\\ K'_{n_1-q+1}+L'K'_{n_1-q}&=0\end{aligned}\right\} \quad [23]$$

where

$$L' = \frac{IC}{Mat}\left(1 + \frac{n_1^2}{\lambda^2} - \frac{N_1}{C} + \frac{T}{\pi a^2 C}\,\frac{n_1}{\lambda}\right)$$

To obtain the nontrivial solution of Equation [22] we set the determinant of the coefficients $K_n$ equal to zero, namely

$$\begin{vmatrix} L & 1 & 0 & 0 & 0 \cdots 0 & 0 \\ 1 & L & 1 & 0 & 0 \cdots 0 & 0 \\ 0 & 1 & L & 1 & 0 \cdots 0 & 0 \\ & & & \cdot & & \\ & & & \cdot & & \\ & & & \cdot & & \\ 0 & 0 & 0 & 0 & 0 \cdots 1 & L \end{vmatrix} = 0 \quad \ldots [24]$$

Equation [24] can be rewritten as

$$\left.\begin{aligned} L - \cfrac{1}{L - \cfrac{1}{L - \cdots - \cfrac{1}{L - \cfrac{1}{L - \cfrac{1}{L}}}}} = 0 \end{aligned}\right\} \quad \ldots [25]$$

By taking more and more terms in the expression for $w$, we have successively larger and larger continued fractions in Equation [25] and in each case the roots $L$ are found.

The question now arises as to which of the roots obtained in solving Equation [25] is the one which should be used in the final analysis. This is easily determinable from Relation [21], which, when rewritten, becomes

$$M = \frac{IC}{Lat}\left(1 + \frac{n_1^2}{\lambda^2} - \frac{N_1}{C} - \frac{T}{\pi a^2 C}\,\frac{n_1}{\lambda}\right) \quad \ldots [26]$$

Obviously, the lowest value of the critical bending moment $M$ occurs for the largest value of $L$; therefore, in solving Equation [25], the largest root obtained in each case is the one selected.

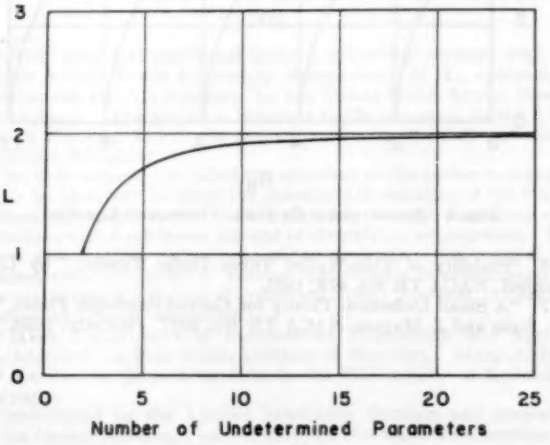


FIG. 2 RESULT OF EVALUATING $L$ BY METHOD OF SUCCESSIVE APPROXIMATIONS

It is noted, Fig. 2, that the largest root of Equation [26] approaches the value of 2.00 as larger and larger continued fractions are considered. Therefore the value $L = 2.00$ is taken as the solution. Equation [26] therefore becomes, after dividing through by $IC/Lat$

$$\frac{2Mat}{IC} = 1 + \frac{n_1^2}{\lambda^2} - \frac{N_1}{C} - \frac{T}{\pi a^2 C}\,\frac{n_1}{\lambda} \quad \ldots [27]$$

In order to find the lowest possible value of the term $2Mat/IC$, it is necessary to minimize the right-hand side of Equation [27] with respect to the variable $n_1/\lambda$. It may be pointed out that $n_1/\lambda$ actually takes on only discrete values on account of the integral character of $n_1$ and of $\lambda$ ($= m\pi a/l$). However, where $\lambda$ is very large (as it is in this case), it is possible to consider $n_1/\lambda$ as a continuous function in the minimizing process.

Having established that it is permissible to consider $n_1/\lambda$ as a continuous variable, let us minimize the right-hand side of Equation [27] by setting

$$\frac{\partial}{\partial(n_1/\lambda)}\left(1 + \frac{n_1^2}{\lambda^2} - \frac{N_1}{C} - \frac{T}{\pi a^2 C}\,\frac{n_1}{\lambda}\right) = 0 \quad \ldots [28]$$

Hence

$$\left.\begin{aligned} 2\,\frac{n_1}{\lambda} - \frac{T}{\pi a^2 C} &= 0 \\ \text{or} \qquad \frac{n_1}{\lambda} &= \frac{T}{2\pi a^2 C} \end{aligned}\right\} \quad \ldots [29]$$

Consequently, Equation [27] becomes

$$\frac{2Mat}{IC} = 1 - \frac{N_1}{C} - \left(\frac{T}{2\pi a^2 C}\right)^2 \quad \ldots [30]$$

or

$$\frac{T}{2\pi a^2 C} = \pm\sqrt{1 - \frac{N_1}{C} - \frac{2Mat}{IC}} \quad \ldots [31]$$

Exactly the same result is obtained if we solve for the nontrivial solution for Equation [23]. This indicates that for sandwich circular cylinders with weak core the cylinder will buckle when the maximum principal compressive force $N$ reaches the magnitude $hG$ or $C$ as can be seen from the following calculations:[6] Let

$$N_{\text{principal}} = -C = \frac{N_x}{2} + \sqrt{\left(\frac{N_x}{2}\right)^2 + N_{xy}^2}$$

Then

$$\left(C + \frac{N_x}{2}\right)^2 = \left(\frac{N_x}{2}\right)^2 + N_{xy}^2$$

or

$$\frac{N_{xy}}{C} = \pm\sqrt{1 + \frac{N_x}{C}} \quad \ldots [32]$$

Since

$$N_{xy} = \frac{T}{2\pi a^2} \quad \text{and} \quad N_{xx} = -N_1 - \frac{2Mat}{I}$$

Equation [32] becomes [31].

In the case where the cylinder is under axial compression alone $M = T = 0$, and Equation [31] becomes

$$\left.\begin{aligned} \pm\sqrt{1 - N_1/C} &= 0 \\ \text{or} \qquad N_1 &= C \end{aligned}\right\} \quad \ldots [33]$$

Equation [33] is exactly the one obtained in reference (1).

In the case where the cylinder is under torsional loads alone, $M = N_1 = 0$ and Equation [31] becomes

[6] The authors are indebted to Prof. P. P. Bijlaard of Cornell University who pointed out this fact.

$$\left.\begin{aligned} &\frac{T}{2\pi a^2 C} = \pm 1 \\ \text{or} \\ &N_{xy} = \pm C \end{aligned}\right\} \quad \ldots\ldots\ldots\ldots [34]$$

Equation [34] is the identical equation obtained in reference (2).

In the case where the cylinder is under bending moments alone, Equation [31] becomes

$$\left.\begin{aligned} &\pm \sqrt{1 - 2Mat/IC} = 0 \\ \text{or} \\ &\frac{2Mat}{I} = C \end{aligned}\right\} \quad \ldots\ldots\ldots\ldots [35]$$

Equation [35] is exactly the one obtained in reference (3).

If we define the stress ratios $R_C$, $R_B$, $R_T$ according to the following formulas

$$R_C = \frac{N_1}{C} = \frac{\text{critical compressive stress}}{\text{buckling stress under compression alone}}$$

$$R_B = \frac{2Mat}{IC} = \frac{\text{critical bending moment}}{\text{buckling moment under bending alone}}$$

$$R_T = \frac{T}{2\pi a^2 C} = \frac{\text{critical torsional moment}}{\text{buckling moment under torsion alone}}$$

then Equation [31] may be written as

$$R_T = \pm \sqrt{1 - (R_B + R_C)} \quad \ldots\ldots\ldots\ldots [36]$$

The interrelationship between compression, bending, and torsional stress ratios given by Equation [36] is plotted for engineering use in Figs. 3 and 4. Once any two stress ratios are specified, the buckling value of the remaining stress ratio can be determined graphically from these curves.

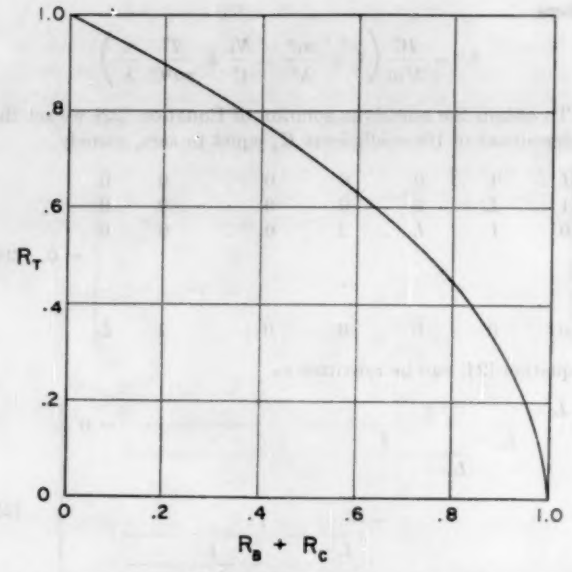


FIG. 3 INTERACTION CURVE: TORSION-STRESS RATIO VERSUS SUM OF BENDING AND COMPRESSION-STRESS RATIOS

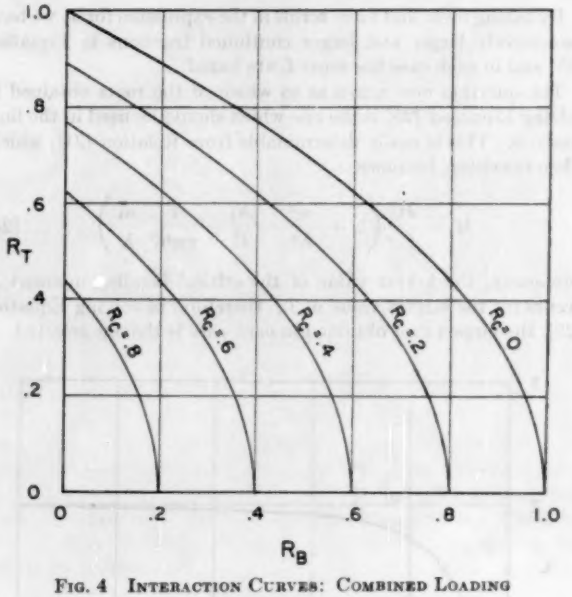


FIG. 4 INTERACTION CURVES: COMBINED LOADING

## BIBLIOGRAPHY

1 "Buckling of Sandwich Cylinders Under Axial Compression," by F. K. Teichmann, Chi-Teh Wang, and G. Gerard, *Journal of the Aeronautical Sciences*, vol. 18, 1951, pp. 398–406.

2 "Torsional Instability of a Long Sandwich Cylinder," by G. Gerard, Proceedings of First National Congress for Applied Mechanics, ASME, 1952, pp. 391–394.

3 "Buckling of Sandwich Cylinders Under Bending and Combined Bending and Axial Compression," by Chi-Teh Wang and D. P. Sullivan, *Journal of the Aeronautical Sciences*, vol. 19, 1952, pp. 468–471.

4 "Finite Deflections of Curved Sandwich Plates and Sandwich Cylinders," by F. K. Teichmann and Chi-Teh Wang, Sherman M. Fairchild Fund Paper No. FF-4, Institute of the Aeronautical Sciences, January, 1951.

5 "A Study of an Analogous Model Giving the Nonlinear Characteristics in the Buckling Theory of Sandwich Cylinders," by Chi-Teh Wang and G. V. R. Rao, *Journal of the Aeronautical Sciences*, vol. 19, 1952, p. 93.

6 "Stability of Thin-Walled Tubes Under Torsion," by L. E. Donnell, NACA TR No. 479, 1934.

7 "A Small Deflection Theory for Curved Sandwich Plates," by M. Stein and J. Mayers, NACA TN No. 2017, February, 1950.

# The Accuracy of Donnell's Equations[1]

By N. J. HOFF,[2] BROOKLYN, N. Y.

**Solutions of Donnell's equations of the small deformations of the perfectly elastic thin-walled circular cylindrical shell are compared with those obtainable from Flügge's equations. The range of the basic parameters is found within which the two solutions are approximately equal.**

## Nomenclature

The following nomenclature is used in the paper:

$a$ = radius of cylinder
$a, b, c, d$ = real quantities, defined in Equations [12]
$e$ = base of natural logarithms
$h$ = wall thickness
$i = \sqrt{(-1)}$ = imaginary unit
$m$ = integer
$n$ = real number
$p$ = complex root of characteristic equation
$q$ = radial load per unit area
$s$ = real number
$w$ = radial displacement divided by radius
$A$ = amplitude of radial deflections
$B$ = amplitude of radial load expression
$C$ = function of $n$ and $K$, defined in Equation [44]
$D = Eh^3/[12(1 - \nu^2)]$ = bending rigidity of wall of shell per unit length
$E$ = Young's modulus of elasticity
$K$ = parameter, defined in Equation [2]
$K' = K/n$
$L$ = length of shell
$M, N$ = real quantities, defined in Equation [13]
$P$ = polynomial
$Q, R$ = real quantities, defined in Equation [13]
$R$ = function of $n$, $K$, and $\nu$, defined in Equation [45]
$S, T, V, W$ = real quantities defined in Equations [25]
$\alpha, \beta, \gamma, \delta$ = real quantities assumed small as compared to unity
$\nu$ = Poisson's ratio
$\varphi$ = circumferential co-ordinate, measured in radians
$\Omega$ = real quantity defined in Equation [22]
$\partial$ = partial differential sign

## Introduction

In the past few years Donnell's equations defining the small deformations of thin-walled circular cylindrical shells have been used by a number of authors in the solution of problems of equilibrium and stability. In recent discussions at scientific meetings, objections have been raised as to the accuracy of these equations. It is the purpose of this paper to establish the accuracy of the results obtainable from Donnell's equations.

As a standard of comparison, Flügge's equations will be used. These were originally derived by Flügge (1)[3] in 1932, on the basis of Love's (2) theory first published in 1888; they can be found in such well-known textbooks as "Statik und Dynamik der Schalen" by W. Flügge (3), and "Technische Dynamik," by Biezeno and Grammel (4). The Donnell equations were published in 1933 (5). They were developed from Love's theory on the basis of order-of-magnitude considerations and are much easier to solve than the Flügge equations. They are therefore preferable in engineering applications if their accuracy is satisfactory for the purposes of engineering.

The present author and his co-workers at the Polytechnic Institute of Brooklyn made use of the Donnell equations in solving line-load and concentrated-load problems at an earlier time (6, 7, 8). The accuracy of the solution was established through comparison of typical results obtained from the Flügge and the Donnell equations (9) and (10). However, the validity of the proof was restricted to cylinders with dimensions closely resembling those of the particular cylinder investigated.

A more general analysis of the accuracy was required, and is presented here, to establish the range of the parameter values within which the results obtained from Donnell's equations do not differ appreciably from those derived from Flügge's equations. This analysis is not carried out on the basis of an evaluation of the relative magnitudes of the various terms in Flügge's equations but rather by means of a comparison of the solutions obtainable from the two sets of differential equations.

When surface loads acting upon the cylindrical shell are represented by trigonometric expressions, it is often possible to find solutions of the same form. Under these conditions the accuracy of the Donnell approximation can easily be ascertained by means of a direct comparison of the numerical factors in the two solutions.

It was shown in references (6 to 8), as well as in (11) and (12), that line loads and concentrated loads preferably can be considered as edge loads; solutions of the problem can then be obtained with the aid of the eigenfunctions of the differential equations. This procedure has the advantage that single, rather than double, summations are needed to represent the deflections and the stresses. Moreover, the convergence of the series so ob-

[1] This work was performed under a consulting contract with the Knolls Atomic Power Laboratory, Schenectady, N. Y., operated by the General Electric Company for the United States Atomic Energy Commission. The author is indebted to the company, to the AEC, and to Dr. John Zickel, the project supervisor, for their permission to publish this paper.

Dr. Eric Reissner has called the attention of the author to a recent paper by Moe (14)[3] in which the characteristic equation of the Flügge differential equations was solved explicitly through ingenious substitutions with a minimum amount of simplifying assumptions. The paper also contains comparisons of the accuracy of the roots of the characteristic equations of various approximate representations of the equilibrium conditions of cylindrical shells; however, it does not discuss the Donnell equations.

[2] Head, Department of Aeronautical Engineering and Applied Mechanics of the Polytechnic Institute of Brooklyn. Mem. ASME.

[3] Numbers in parentheses refer to the Bibliography at the end of the paper.

Contributed by the Applied Mechanics Division and presented at the Annual Meeting, New York, N. Y., November 28–December 3, 1954, of The American Society of Mechanical Engineers.

Discussion of this paper should be addressed to the Secretary, ASME, 29 West 39th Street, New York, N. Y., and will be accepted until October 10, 1955, for publication at a later date. Discussion received after the closing date will be returned.

Note: Statements and opinions advanced in papers are to be understood as individual expressions of their authors and not those of the Society. Manuscript received by ASME Applied Mechanics Division, May 20, 1954. Paper No. 54—A-105.

tained is more rapid than that of the double series of the approach first mentioned.

The accuracy of the solution by means of the eigenfunctions $e^{p\varphi}\cos nx$ and $e^{px}\cos n\varphi$ of the Donnell equations was determined by comparing the values of $p^2$ obtained from the Donnell equations with those derived by a perturbation method from the Flügge equations. As the values of $p$ define the variation of the deflections and the stresses in the co-ordinate directions and they also determine the numerical factors in the expressions obtainable for the deflections and the stresses, small differences between the $p$-values satisfying the Donnell and the Flügge equations are an indication of a satisfactory accuracy of the Donnell equations.

Naturally, the accuracy of a solution of a problem in elasticity cannot depend upon the choice of the functions representing the loads and the displacements unless singularities of an unsatisfactory nature are introduced by the choice; the second part of this statement was proved recently by Sternberg (13). Consequently, the error committed by the use of the Donnell equations must be the same whether a concentrated load is represented by one of the two types of eigenfunctions or by the double Fourier series. However, the accuracy of any one term of the solution, which in itself corresponds to a physical problem, can vary greatly from one representation of a concentrated load to another. The determination of the accuracy of any one term is the task undertaken in this paper.

## Solution by Eigenfunctions With Trigonometric Expressions in the Longitudinal Direction

In agreement with Equation [1] of references (7, 11), the first of the three Donnell equations can be written in the following nondimensional form when all external loads are absent

$$\nabla^8 w + 4K^4(\partial^4 w/\partial x^4) = 0 \quad [1]$$

where $w$ is the radial inward displacement of a point of the median surface of the shell divided by the median radius $a$, $x$ is the axial co-ordinate divided by the radius $a$, and

$$4K^4 = 12(1 - \nu^2)(a/h)^2 \quad [2]$$

and

$$\nabla^2 = (\partial^2/\partial x^2) + (\partial^2/\partial\varphi^2) \quad [3]$$

with $h$ the wall thickness of the shell and $\nu$ Poisson's ratio of the material. It was shown in reference (7) that Equation [1] and suitable boundary conditions are satisfied by the eigenfunctions

$$w = e^{p\varphi}\cos nx \quad [4]$$

where

$$n = m\pi(a/L) \quad [5]$$

and $L$ is the length of the shell and $m$ is an odd integer. Substitution of $w$ from Equation [4] into Equation [1] and solution yield the following four expressions for $p^2$

$$\left.\begin{aligned} p_1^2 &= (n^2 + nK) + inK \\ p_2^2 &= (n^2 + nK) - inK \\ p_3^2 &= (n^2 - nK) + inK \\ p_4^2 &= (n^2 - nK) - inK \end{aligned}\right\} \quad [6]$$

A more complete set of equations defining the deformations of thin cylindrical shells was derived by Flügge (1) in 1932. Kempner (9, 10) has shown that these equations can be brought into a form resembling that of the Donnell equations; when this is done, the first of the resulting three equations contains only the nondimensional radial displacement $w$ and the axial and circumferential displacements are absent from it. If $(h/a)^2$ is neglected against unity, the complete equation in $w$ can be written as

$$\nabla^8 w + 4K^4 w^{IV} + 2\nu\ddot{w}^{VI} + 6\ddot{w}^{IV} + 2(4 - \nu)\dddot{w}'' + 2(2 - \nu)\ddot{w}'' + 2\dddot{w} + w = 0 \quad [7]$$

In this equation primes and Roman numerals indicate differentiation with respect to $x$, and dots differentiation with respect to the circumferential angular co-ordinate $\varphi$. Substitution from Equation [4] yields the following quartic in $p^2$

$$(p^2 - n^2)^4 + 4n^4K^4 + 2p^8 + [1 - 2(4 - \nu)n^2]p^4 + [6n^4 - 2(2 - \nu)n^2]p^2 - 2\nu n^8 = 0 \quad [8]$$

The conditions will now be investigated under which Equations [6] can be considered as a satisfactory approximation to the solution of Equation [8]. It will be assumed that the four values of $p^2$ can be written as

$$\left.\begin{aligned} p_1^2 &= (n^2 + nK)(1 + \alpha) + inK(1 + \beta) \\ p_2^2 &= (n^2 + nK)(1 + \alpha) - inK(1 + \beta) \\ p_3^2 &= (n^2 - nK)(1 + \gamma) + inK(1 + \delta) \\ p_4^2 &= (n^2 - nK)(1 + \gamma) - inK(1 + \delta) \end{aligned}\right\} \quad [9]$$

where $\alpha$, $\beta$, $\gamma$, and $\delta$ are small as compared to unity. If Equations [9] are the solutions of Equation [8] and are correct up to second-order small quantities in $\alpha$, $\beta$, $\gamma$, and $\delta$, the polynomial $P$ defined as

$$P = (p^2 - p_1^2)(p^2 - p_2^2)(p^2 - p_3^2)(p^2 - p_4^2) \quad [10]$$

must be identical with the left-hand member of Equation [8] to the same degree of accuracy. Substitutions from Equation [9] and evaluation yield

$$\begin{aligned} P = {} & (p^2 - n^2)^4 + 4n^4K^4 - 2(a + K'b)n^2p^6 \\ & + 2[a(3 - K'^2) + 2K'b + K'^2c]n^4p^4 \\ & + 2[a(2K'^2 - 3) - K'b - 2K'^2c + 2K'^3d]n^6p^2 \\ & + 2[a(1 - K'^2 + 2K'^4) + 2K'^3b \\ & + K'^2(1 + 2K'^2)c - 2K'^3d]n^8 \end{aligned} \quad [11]$$

where

$$K' = K/n \quad [12]$$

and

$$\left.\begin{aligned} a &= \alpha + \gamma, & b &= \alpha - \gamma \\ c &= \beta + \delta, & d &= \beta - \delta \end{aligned}\right\} \quad [13]$$

The polynomials given in Equations [7] and [10] are identical if

$$\left.\begin{aligned} a + K'b &= -(1/n^2) = M \\ a(3 - K'^2) + 2K'b + K'^2c &= [1 - 2(4 - \nu)n^2]/2n^4 = N \\ a(2K'^2 - 3) - K'b - 2K'^2c + 2K'^3d &= [3n^2 - 2 + \nu]/n^4 = Q \\ a(1 - K'^2 + 2K'^4) + 2K'^3b + K'^2(1 + 2K'^2)c - 2K'^3d &= -(\nu/n^2) = R \end{aligned}\right\} \quad [14]$$

where $M$, $N$, $Q$, and $R$ are symbols introduced to obtain a more concise representation of the solution of the simultaneous equations. The solution is

$$\left.\begin{aligned} 8K'^2(1 + K')\alpha &= -M(1 - 6K'^2 - 4K'^3) + N(1 - 2K'^2) + Q + R \\ 8K'^4\beta &= -M(1 + 6K' + 6K'^2) + N(1 + 4K' + 2K'^2) + Q(1 + 2K') + R \\ 8K'^2(1 - K')\gamma &= M(1 - 6K'^2 + 4K'^3) - N(1 - 2K'^2) - Q - R \\ 8K'^4\delta &= -M(1 - 6K' + 6K'^2) + N(1 - 4K' + 2K'^2) + Q(1 - 2K') + R \end{aligned}\right\} \quad [15]$$

The derivations just presented are correct, and the Donnell equations represent a satisfactory approximation to the Flügge equations, when $\alpha$, $\beta$, $\gamma$, and $\delta$ computed from Equations [15] are small as compared to unity. However, the approximation may be satisfactory even when not all of the quantities $\alpha$, $\beta$, $\gamma$, $\delta$ turn out to be small. In particular, it is unreasonable to require $\gamma$ to be small when $n$ and $K$ are almost equal. In such a case even a large $\gamma$ is unlikely to modify $p_3^2$ and $p_4^2$ to an appreciable degree.

To cope with such a situation, it is advisable to assume the quantities $p^2$ in the form

$$\left.\begin{aligned} p_1^2 &= n^2 + nK(1+\alpha) + inK(1+\beta) \\ p_2^2 &= n^2 + nK(1+\alpha) - inK(1+\beta) \\ p_3^2 &= n^2 - nK(1+\gamma) - inK(1+\delta) \\ p_4^2 &= n^2 - nK(1+\gamma) + inK(1+\delta) \end{aligned}\right\} \quad \ldots [16]$$

The polynomial $P$ defined in Equation [10] is now

$$\begin{aligned} P = (p^2 - n^2)^4 &+ 4n^4K^4 - 2n^2p^6K'b \\ &+ n^4p^4(-2K'^2a + 6K'b + 2K'^2c) \\ &+ n^6p^2(4K'^2a - 6K'b - 4K'^2c + 4K'^3d) \\ &+ n^8[(4K'^4 - 2K'^2)a + 2K'b \\ &+ (4K'^4 + 2K'^2)c - 4K'^3d] \quad \ldots [17] \end{aligned}$$

The polynomials of Equations [8] and [17] are identical if

$$\left.\begin{aligned} K'b &= M \\ -K'^2a + 3K'b + K'^2c &= N \\ 2K'^2a - 3K'b - 2K'^2c + 2K'^3d &= Q \\ (2K'^4 - K'^2)a + K'b + (2K'^4 + K'^2)c - 2K'^3d &= R \end{aligned}\right\} \quad . [18]$$

where $M$, $N$, $Q$, and $R$ have the same values as in Equations [14]. The solution is

$$\left.\begin{aligned} 4K'^4a &= (6K'^2 - 1)M - (2K'^2 - 1)N + Q + R \\ K'b &= M \\ 4K'^4c &= -(6K'^2 + 1)M + (2K'^2 + 1)N + Q + R \\ 2K'^3d &= -3M + 2N + Q \end{aligned}\right\} \quad . . [19]$$

### Solution by Eigenfunctions With Trigonometric Expressions in Circumferential Direction

In references (11) and (12), Equation [1] was solved by assuming that

$$w = e^{px} \cos n\varphi \quad \ldots [20]$$

where $n$ is a real number. It is an integer when the cylinder is closed. The squares of the roots of the characteristic equation obtained in references (11) and (12) can be generalized to represent solutions of the more complete Equation [7]

$$\left.\begin{aligned} p_1^2 &= (n^2 - K\Omega)\,[(1+\alpha) - i(K/\Omega)\,(1+\beta)] \\ p_2^2 &= (n^2 - K\Omega)\,[(1+\alpha) + i(K/\Omega)\,(1+\beta)] \\ p_3^2 &= (n^2 + K\Omega)\,[(1+\gamma) - i(K/\Omega)\,(1+\delta)] \\ p_4^2 &= (n^2 + K\Omega)\,[(1+\gamma) + i(K/\Omega)\,(1+\delta)] \end{aligned}\right\} \quad . . [21]$$

where $$\Omega^2 = -(K^2/2) + [(K^2/2)^2 + n^4]^{1/2} \quad \ldots [22]$$

The polynomial $P$ of Equation [10] becomes

$$\begin{aligned} P = (p^2 - n^2)^4 &+ 4K^4p^4 + (-2n^2a + 2K\Omega b)p^6 \\ &+ [2(2n^4 + \Omega^4)a - 4n^2K\Omega b + 2(K^2\Omega^2 + 2K^4)c \\ &- 4n^2K\Omega(K/\Omega)^2d]p^4 - 2\Omega^2[n^2(3\Omega^2 + K^2)a + 2n^2K^2c \\ &+ K\Omega(K^2 - \Omega^2)b - 2K^3\Omega d]p^2 \\ &+ 2n^4\Omega^4[a + (K/\Omega)^2c] \quad \ldots [23] \end{aligned}$$

In the derivation of this equation use was made of the identities

$$n^4 - K^2\Omega^2 = \Omega^4 \quad \ldots [24a]$$

and

$$[1 + (K/\Omega)^2]\,[n^4 - K^2\Omega^2] = n^4 \quad \ldots [24b]$$

Substitution of the solution assumed in Equation [20] into Equation [7] yields

$$\begin{aligned} (p^2 - n^2)^4 &+ 4K^4p^4 + 2\nu p^6 - 6n^2p^4 \\ &+ 2n^2\,[(4-\nu)n^2 - 2 + \nu]p^2 + n^4(1 - 2n^2) = 0 \quad \ldots [25] \end{aligned}$$

The left-hand member of Equation [25] is identical with the polynomial $P$ of Equation [23] if

$$\left.\begin{aligned} -n^2a + K\Omega b &= S \\ (3n^4 - K^2\Omega^2)a - 2n^2K\Omega b + (n^4 + K^2\Omega^2)\,(K/\Omega)^2c & \\ - 2n^2K\Omega(K/\Omega)^2d &= T \\ -n^2(3n^4 - 2K^2\Omega^2)a + (n^4 - 2K^2\Omega^2)K\Omega b & \\ - 2n^2\Omega^4(K/\Omega)^2c + 2\Omega^4K\Omega(K/\Omega)^2d &= V \\ 2\Omega^4a + 2\Omega^4(K/\Omega)^2c &= W \end{aligned}\right\} \quad . . [26]$$

where

$$\left.\begin{aligned} S &= \nu \\ T &= -3n^2 \\ V &= n^2[(4-\nu)n^2 - 2 + \nu] \\ W &= 1 - 2n^2 \end{aligned}\right\} \quad \ldots [27]$$

and, as before, $a$, $b$, $c$, and $d$ are defined by Equations [13]. Solution of the four simultaneous equations yields

$$\begin{aligned} a = -[n^6S &+ \Omega^4T + n^2V \\ &+ (1/2)\Omega^4W]/[2K^2\Omega^2(n^4 + \Omega^4)] \quad \ldots [28a] \end{aligned}$$

$$b = (1/K\Omega)\,(S + n^2a) \quad \ldots [28b]$$

$$c = (\Omega/K)^2[(W/2\Omega^4) - a] \quad \ldots [28c]$$

$$\begin{aligned} d = (\Omega/2n^2K^3)\,[-2K^2\Omega^2a &- 2n^2S - T \\ &- (1/2)\,(n^4 + K^2\Omega^2)\,(W/\Omega^4)] \quad \ldots [28d] \end{aligned}$$

A different assumption for the solution of the Flügge equation is given below, but in it the quantities $\alpha$ to $\delta$ do not clearly represent the error.

$$\left.\begin{aligned} p_1^2 &= n^2[(1+\alpha) - i(K/\Omega)\,(1+\beta)] & \\ &\quad - K\Omega[1 - i(K/\Omega)] \\ p_2^2 &= n^2[(1+\alpha) + i(K/\Omega)\,(1+\beta)] & \\ &\quad - K\Omega[1 + i(K/\Omega)] \\ p_3^2 &= n^2[(1+\gamma) - i(K/\Omega)\,(1+\delta)] & \\ &\quad + K\Omega[1 - i(K/\Omega)] \\ p_4^2 &= n^2[(1+\gamma) + i(K/\Omega)\,(1+\delta)] & \\ &\quad + K\Omega[1 + i(K/\Omega)] \end{aligned}\right\} \quad [29]$$

The polynomial becomes

$$\begin{aligned} P = (p^2 - n^2)^4 &+ 4K^4p^4 - 2n^2ap^6 \\ &+ [6n^4a + 2n^2K\Omega b + 2n^4(K/\Omega)^2c - 2n^2K\Omega(K/\Omega)^2d]p^4 \\ &- 2\,\{n^2(3n^4 + 2K^4)a + 2n^4K\Omega(n/\Omega)^4b + 2n^2(K\Omega)^2c\}p^2 \\ &+ 2n^6\,\{n^2a + K\Omega b + n^2(K/\Omega)^2c + K\Omega(K/\Omega)^2d\} \quad \ldots [30] \end{aligned}$$

Comparison with Equation [25] yields

$$-n^2a = S$$

$$\left.\begin{aligned} 3n^2a + K\Omega b + n^2(K/\Omega)^2c - K\Omega(K/\Omega)^2d &= (T/n^2) \\ (3n^4 + 2K^4)a + 2n^2K\Omega(n/\Omega)^4b + 2(K\Omega)^2c &= -(V/n^2) \\ n^2a + K\Omega b + n^2(K/\Omega)^2c + K\Omega(K/\Omega)^2d &= (W/2n^2) \end{aligned}\right\} \quad . . [31]$$

The symbols $S$ to $W$ have the same meaning as in Equations [27]. Solution gives

$$a = -S/n^2 \quad \ldots [32a]$$

$$2(K\Omega)^2[2 + (K/\Omega)^2]b = (3n^4 + 2K^4 - 4\Omega^4)S - \Omega^4(T/n^2) - V - \Omega^4(W/2n^2) \quad [32b]$$

$$2K^4[2 + (K/\Omega)^2]c = n^2[4(n/\Omega)^4 - 2(K/n)^4 - 3]S + (n/\Omega)^4T + (V/n^2) + (n/\Omega)^4(W/2) \quad [32c]$$

$$d = [-S - (T/2n^2) + (W/4n^2)]/[K\Omega(K/\Omega)^2] \quad [32d]$$

### Solution When Eigenfunction Is Constant in $x$ or $\varphi$-Direction

When the solution is in the form

$$w = e^{px} \cos n\varphi$$

and $n = 0$, Equation [7] reduces to

$$(\partial^8 w/\partial\varphi^8) + 2(\partial^6 w/\partial\varphi^6) + (\partial^4 w/\partial\varphi^4) = 0 \quad [33]$$

which is a form of the equation defining the deformations of a circular ring. Substitution yields a characteristic equation which has a quadruple root at $p = 0$ and double roots at $p = \pm i$. Therefore the solution contains deflection functions of the form $\cos\varphi$, $\sin\varphi$, $\varphi\cos\varphi$, and $\varphi\sin\varphi$; this result cannot be deduced from the Donnell equation which in this case is simply

$$(\partial^8 w/\partial\varphi^8) = 0 \quad [34]$$

These functions are seldom used in the solution of shell problems because they are not compatible with the usual boundary conditions. It is of some interest to note that the polynomial $c_0 + c_1\varphi + c_2\varphi^2 + c_3\varphi^3$ corresponding to the quadruple root is a spurious solution; it does not satisfy the lower-order equations from which the Donnell and the Flügge-Kempner equations were derived. An exception in this regard is the constant $c_0$ to which correspond linear expressions in $u$ and $v$.

When the solution is in the form

$$w = e^{px} \cos n\varphi$$

and $n = 0$, Donnell's equation reduces to

$$(\partial^8 w/\partial x^8) + 4K^4(\partial^4 w/\partial x^4) = 0 \quad [35]$$

This equation is derived in the theory of the axially symmetric deformations of thin cylindrical shells. Substitution yields the condition

$$p^4(p^4 + 4K^4) = 0 \quad [36]$$

Hence the four values of $p^2$ are

$$\left.\begin{aligned} p_1^2 &= p_2^2 = 0 \\ p_3^2 &= i(2K^2) \\ p_4^2 &= -i(2K^2) \end{aligned}\right\} \quad [37]$$

The Flügge-Kempner equation (Equation [7]) reduces to

$$(\partial^8 w/\partial x^8) + 4K^4(\partial^4 w/\partial x^4) + 2\nu(\partial^6 w/\partial x^6) = 0 \quad [38]$$

Consequently the characteristic equation is

$$p^4(p^4 + 2\nu p^2 + 4K^4) = 0 \quad [39]$$

and the roots are

$$\left.\begin{aligned} p_1^2 &= p_2^2 = 0 \\ p_3^2 &= -\nu - i2K^2[1 - (\nu^2/8K^4)] \\ p_4^2 &= -\nu + i2K^2[1 - (\nu^2/8K^4)] \end{aligned}\right\} \quad [40]$$

As the smallest value of $K$ for which the Flügge-Kempner equation is valid is about 5 and since $\nu = 0.3$, the correction term in the imaginary part is not greater than $18 \times 10^{-6}$ which is certainly negligible. The real part is smaller than 1 per cent of the imaginary part and thus it has a negligible effect upon the values of $p$. Again, the solutions corresponding to $p_1$ and $p_2$ are spurious in the sense discussed above.

### Solution of Inhomogeneous Equations

When the load is represented by double Fourier series, the deflections also can be assumed in the same form. Comparison of the coefficients of identical trigonometric functions yields values for the unknown coefficients of the series representing deflections. This procedure is so simple and straightforward that there is little reason to make use of Donnell's equations in preference to the Flügge equations. The importance of each term also can be seen immediately when numerical values are substituted in the equations.

By way of example the case is treated here when the load $q$ per unit area is applied in the radial direction. It is represented by the expression

$$q = B \cos sx \cos n\varphi \quad [41]$$

Under these conditions the right-hand member of Equations [1] and [7] is $(a^2/D)\nabla^4 q$ rather than 0. The radial deflection $w$ can be assumed as

$$w = A \cos sx \cos n\varphi \quad [42]$$

Substitution in the left-hand member of Equation [7] and use of the expression given in Equation [41] for the load term in calculating the right-hand member result in

$$(s^2 + n^2)^4 + 4K^4s^4 - 2\nu s^6 - 6s^4n^2 - 2(4 - \nu)s^2n^4 + 2(2 - \nu)s^2n^2 - 2n^6 + n^4 = (a^2/D)(s^2 + n^2)^2(B/A) \quad [43]$$

The left-hand member of Donnell's equation is

$$C = (s^2 + n^2)^4 + 4K^4s^4 \quad [44]$$

Hence the percentage error made because of the use of Donnell's equation is

$$100\, R/(C + R)$$

where

$$R = -2\nu s^6 - 6s^4n^2 - 2(4 - \nu)s^2n^4 + 2(2 - \nu)s^2n^2 - 2n^6 + n^4 \quad [45]$$

### Numerical Results

When the deflection function is trigonometric in the axial direction, Equations [15] must be used to calculate $\alpha$, $\beta$, $\gamma$, and $\delta$ unless $K/n$ is equal to, or not too different from, unity. When this is the case, the quantities are computed from Equations [19]. In the computations three values were assumed for $K$, namely, 5, 10, and 50. When $K$ is considerably smaller than 5, the assumptions of thin-shell theory become invalid and $(h/a)^2$ cannot be neglected as compared to unity. When $K$ is greater than 50, the shell is so thin-walled that it can hardly fulfill structural requirements. The values obtained are given in Table 1.

TABLE 1 ERROR WHEN $w$ TRIGONOMETRIC IN $x$ DIRECTION

| $K$ | $n$ | $\alpha$ | $\beta$ | $\gamma$ | $\delta$ |
|---|---|---|---|---|---|
| 5 | 0.1 | −1.46 | 0.479 | 0.518 | 0.508 |
| 5 | 0.3 | −0.360 | 0.0428 | 0.303 | 0.0538 |
| 5 | 0.5 | −0.194 | 0.0085 | 0.207 | 0.0170 |
| 5 | 1.0 | −0.082 | −0.0064 | 0.127 | 0.0019 |
| 5 | 10.0 | −0.003 | 0.0167 | −0.0353 | 0.0210 |
| 10 | 0.1 | −0.617 | 0.121 | 0.381 | 0.125 |
| 10 | 0.3 | −0.174 | 0.0114 | 0.159 | 0.0128 |
| 10 | 0.5 | −0.098 | 0.0027 | 0.102 | 0.0038 |
| 10 | 1.0 | −0.045 | −0.0010 | 0.056 | $10^{-4}$ |
| 10 | 10.0 | −0.003 | 0.0067 | −0.005 | 0.0018 |
| 50 | 0.1 | −0.105 | 0.0049 | 0.0952 | 0.0049 |
| 50 | 0.3 | −0.0336 | 0.0005 | 0.0330 | 0.0005 |
| 50 | 0.5 | −0.0199 | 0.0001 | 0.0201 | 0.0001 |
| 50 | 1.0 | −0.0099 | $-2 \times 10^{-5}$ | 0.0102 | $-2 \times 10^{-5}$ |
| 50 | 10.0 | −0.0008 | $-1 \times 10^{-4}$ | 0.0013 | $-4 \times 10^{-5}$ |

TABLE 2 ERROR WHEN $w$ TRIGONOMETRIC IN $\varphi$ DIRECTION

| $K$ | $n$ | $\alpha$ | $\beta$ | $\gamma$ | $\delta$ |
|---|---|---|---|---|---|
| 5 | 1 | −0.998 | −0.498 | −0.150 | $-9.55 \times 10^{-4}$ |
| 5 | 2 | −0.400 | −0.210 | −0.0353 | $-37.2 \times 10^{-4}$ |
| 5 | 3 | −0.179 | −0.0874 | −0.0122 | $-75.0 \times 10^{-4}$ |
| 5 | 4 | −0.0991 | −0.0343 | −0.00315 | $-132 \times 10^{-4}$ |
| 5 | 10 | −0.0141 | +0.0220 | +0.00306 | $-280 \times 10^{-4}$ |
| 10 | 1 | −1.00 | −0.500 | −0.150 | $-0.600 \times 10^{-4}$ |
| 10 | 2 | −0.409 | −0.218 | −0.0374 | $-2.40 \times 10^{-4}$ |
| 10 | 3 | −0.194 | −0.104 | −0.0163 | $-5.35 \times 10^{-4}$ |
| 10 | 4 | −0.115 | −0.0580 | −0.00851 | $-9.47 \times 10^{-4}$ |
| 10 | 10 | −0.0144 | −0.00630 | $+0.483 \times 10^{-4}$ | $-33.0 \times 10^{-4}$ |
| 50 | 1 | −1.00 | −0.500 | −0.150 | $-0.0960 \times 10^{-4}$ |
| 50 | 2 | −0.409 | −0.219 | −0.0375 | $-0.384 + 10^{-4}$ |
| 50 | 3 | −0.195 | −0.105 | −0.0167 | $-0.864 \times 10^{-4}$ |
| 50 | 4 | −0.117 | −0.0608 | $-90.1 \times 10^{-4}$ | $-1.53 \times 10^{-4}$ |
| 50 | 10 | −0.0183 | −0.00994 | $-14.9 \times 10^{-4}$ | $-9.60 \times 10^{-4}$ |

The values in Table 1 were computed from Equations [15] except the ones contained in row $K = 5$, $n = 10$ and in row $K = 10$, $n = 10$. Values in the latter two rows were obtained from Equations [19].

It can be seen from the results that for comparatively thick-walled cylinders ($K = 5$) the Donnell equations are accurate enough only when $n$ is equal to, or greater than, unity; in the medium-thickness range the limiting value of $n$ is about 0.5; and for very thin-walled cylinders $n$ may be as low as 0.1. Since $n = m\pi(a/L)$, the restrictions on $n$ correspond to restrictions on the length of the cylinder. The first term of the family of deflection functions is characterized by $m = 1$. The present solution of the Donnell equations is therefore accurate enough in the case of the first term for the following limiting combinations of $K$ and $(L/a)$

| $K =$ | 5 | 10 | 50 |
|---|---|---|---|
| $(L/a) \simeq$ | 3 | 6 | 30 |

For longer cylinders than the ones listed, the Donnell solution is inaccurate for the first term of the series. When $m > 1$, the accuracy is always better than for $m = 1$.

At first sight it is disconcerting that $\beta$ and $\delta$ are larger for $n = 10$ than for $n = 1$. Nevertheless, the Donnell solution does not deteriorate with increasing $n$ as an analysis will easily demonstrate.

When $n$ is very large, one has from Equations [14]

$$\left.\begin{aligned} M &= -(1/n^2), & N &= -(4-\nu)/n^2 \\ Q &= (3/n^2), & R &= -(\nu/n^2) \end{aligned}\right\} \quad \ldots\ldots [46]$$

With the aid of these expressions, Equations [15] become

$$\left.\begin{aligned} \alpha &= (1-\nu)/4nK, & \gamma &= -(1-\nu)/4nK \\ \beta &= -(1-\nu)n/2K^2, & \delta &= (1-\nu)n/2K^2 \end{aligned}\right\} \quad [47]$$

Obviously, $\alpha$ and $\gamma$ approach zero as $n$ tends to infinity. On the other hand, $\beta$ and $\delta$ increase beyond all limits. Nevertheless, the roots of the Donnell equation represent satisfactory approximations to the roots of the Flügge equation as can be seen if the foregoing values of $\alpha$, $\beta$, $\gamma$, and $\delta$ are substituted in Equations [9]. When $n$ becomes very large one obtains

$$\left.\begin{aligned} p_1^2 &= n^2[1 - i(1-\nu)(1/2K^2)] \\ p_2^2 &= n^2[1 + i(1-\nu)(1/2K^2)] \\ p_3^2 &= n^2[1 + i(1-\nu)(1/2K^2)] \\ p_4^2 &= n^2[1 - i(1-\nu)(1/2K^2)] \end{aligned}\right\} \quad \ldots\ldots [48]$$

As in the limit the Donnell equation yields

$$p_1^2 = p_2^2 = p_3^2 = p_4^2 = n^2 \ldots\ldots [49]$$

the correction is the imaginary part of the root. The greatest value of the imaginary part is 1.4 per cent of the real part if $\nu = 0.3$ and the smallest practically allowable value of $K$ is taken as 5.

Of course the expressions obtained for $\alpha$ to $\delta$ are valid only if their numerical values are small as compared to unity. When this is not true for $\beta$ and $\delta$ at very large values of $n$, one can re-examine Equation [8]. The first two terms in this equation are also present in the characteristic equation of Donnell's equation; the other terms represent the correction to the Donnell solution. But each power of $p$ in the first two terms is multiplied by a factor which is at least $n^2$ times the factor of the same power of $p$ in the correction terms. Hence Equation [8] approaches Donnell's characteristic equation as $n$ increases beyond all limits. Thus Donnell's and Flügge's equations must yield the same results within engineering accuracy when $n$ is sufficiently large (see reference 9).

When the deflection function is trigonometric in the circumferential direction, the values of $p^2$ are calculated from Equations [28] or [32]. As in this case $n$ must be an integer when the shell is complete (closed), the computations were carried out for $n = 1$, 2, 3, 4, and 10 and for $K = 5$, 10, and 50. The results are given in Table 2.

All the values listed were computed from Equations [28]. According to the table, the influence of $K$ upon the accuracy is small. At all values of $K$ investigated the accuracy of the solution is satisfactory when $n$ is equal to or greater than 4; at $n \leq 3$ the error is too large.

When $n$ is very large, one may set in Equations [27]

$$V = (4-\nu)n^4, \qquad W = -2n^2 \ldots\ldots [50]$$

Then from Equations [28] and [12]

$$\left.\begin{aligned} \alpha &= \nu/2Kn, & \gamma &= -\nu/2Kn \\ \beta &= (1-\nu)n/2K^2, & \delta &= -(1-\nu)n/2K^2 \end{aligned}\right\} \quad \ldots [51]$$

On the other hand, Equations [27] are not valid when $\beta$ and $\delta$ exceed, say, 0.1 in absolute value. With $K = 10$ this occurs when $n > 300$. For even greater values of $n$ one can interpret the polynomial of Equation [25]. In the Donnell version the only terms are

$$(p^2 - n^2)^4 + 4K^4p^4 = 0 \ldots\ldots [52]$$

In the remaining terms of Equation [25] each power of $p$ is multiplied by a factor which is at most of the order of magnitude of $(1/n^2)$ times the factor of the corresponding term in $(p^2 - n^2)^4$. Hence all the terms not corresponding to the Donnell equations are negligibly small if $n$ is greater than 10.

When $n$ tends to infinity, the characteristic equation of Flügge approaches rapidly the characteristic equation of Donnell. Hence for all practical purposes the roots are the same when $n$ is large.

As far as the solution of the inhomogeneous equations is concerned, the example of the radial surface load distributed according to Equation [41] can be continued here. Numerical values computed are given in Table 3.

The values computed here for the error are, of course, accurate

TABLE 3 ERROR IN DOUBLE-TRIGONOMETRIC SOLUTION

| When $s = 1$ | | | When $s = 0.5$ | | |
|---|---|---|---|---|---|
| $n$ | $K$ | Error, per cent | $n$ | $K$ | Error, per cent |
| 1 | 3 | 3.5 | 1 | 5 | 1.5 |
| 1 | 5 | 0.5 | 2 | 5 | 40.8 |
| 1 | 10 | ~0 | 3 | 5 | 25.6 |
| 2 | 3 | 34.1 | 1 | 10 | 0.1 |
| 2 | 5 | 8.4 | 2 | 10 | 5.2 |
| 2 | 10 | 0.6 | 3 | 10 | 18.4 |

even when they are large. They show that the error resulting from the use of Donnell's equations in the solution of the inhomogeneous problem is large when $n$ and $K$ are small. As $s = 1$ corresponds to the first trigonometric term in the axial direction when $(L/a) = \pi$, and $s = 0.5$ to that when $(L/a) = 2\pi$, this type of solution of the Donnell equations should be used with caution when the length of the cylinder is greater than the diameter.

## Conclusions

Simple expressions have been derived for the computation of the error made when the more complete Flügge equations are replaced by the simpler Donnell equations. Computed results show that the deviation between the squares of the roots of the characteristic equations according to Donnell and Flügge is not greater than about 10 per cent for all the terms of the solution $e^{p\varphi} \cos nx$ when $K$ is greater than 5 and the length of the cylinder is less than 3 times the radius; and it is smaller than about 11 per cent for all the terms of the solution $e^{px} \cos n\varphi$ when $n$ is equal to or greater than 4.

As the form of the deflection and stress curves depends upon the roots, and the multipliers of all the deflection and stress quantities are linear functions of the roots, the solutions obtained from the Donnell equations under the conditions stated should have terms deviating only slightly from the solutions of the Flügge equations.

It follows then from these statements that the solution $e^{p\varphi} \cos nx$ is most suitable when the cylinder is short. The accuracy of solution $e^{px} \cos n\varphi$ depends little on $K$ when the cylindrical shell is complete (closed). In this solution the terms corresponding to $n < 4$ are inaccurate; they should be replaced by a solution of the Flügge equations.

In the solution of the inhomogeneous problem by means of double trigonometric series the results may be inaccurate for various values of $n$ when the length of the cylinder is considerably greater than the diameter. Since in this case the computations by means of the Flügge-Kempner equations are only slightly lengthier than those by means of the Donnell equations, use of the Donnell equations is not recommended unless the cylinder is very short.

## BIBLIOGRAPHY

1 "Die Stabilität der Kreiszylinderschale," by W. Flügge, *Ingenieur-Archiv*, vol. 3, 1932, p. 463.

2 "The Small Free Vibrations and Deformations of a Thin Elastic Shell," by A. E. H. Love, *Philosophical Transactions of the Royal Society*, London, England, series A, vol. 179, 1888, p. 491.

3 "Statik und Dynamik der Schalen," by W. Flügge, Julius Springer, Berlin, Germany, 1934, p. 118.

4 "Technische Dynamik," by C. B. Biezeno and R. Grammel, Julius Springer, Berlin, Germany, 1939, p. 469.

5 "Stability of Thin-Walled Tubes Under Torsion," by L. H. Donnell, National Advisory Committee for Aeronautics, Technical Report No. 479, Washington, D. C., 1933.

6 "Deformations and Stresses Caused in Circular Cylindrical Shells by Pipe Attachments—Part I, Summary of the Investigations," by N. J. Hoff, Joseph Kempner, S. V. Nardo, and F. V. Pohle, KAPL Report No. 921, November, 1953.

7 "Deformations and Stresses Caused in Circular Cylindrical Shells by Pipe Attachments—Part II, Line Loads Acting Along Generatrices of Circular Cylindrical Shells," by N. J. Hoff, Joseph Kempner, and F. V. Pohle, KAPL Report No. 922, June, 1952.

8 "Line Load Applied Along Generators of Thin-Walled Circular Cylindrical Shells of Finite Length," by N. J. Hoff, Joseph Kempner, and F. V. Pohle, *Quarterly of Applied Mathematics*, vol. 11, 1954, p. 411.

9 "Deformations and Stresses Caused in Circular Cylindrical Shells by Pipe Attachments—Part VI, Derivation of Generalized Donnell-Type Equations for Circular Cylindrical Shells With Application to Line Loads Along Generatrices," by Joseph Kempner, KAPL Report No. 926, June, 1953.

10 "Remarks on Donnell's Equations," by Joseph Kempner, Journal of Applied Mechanics, Trans. ASME, vol. 77, 1955, pp. 117–118.

11 "Stresses in Cylinders With Elastic Edge Support—Part II, Boundary Value Problems of the Thin-Walled Circular Cylinder," by N. J. Hoff, submitted to the Knolls Atomic Power Laboratory in January, 1953.

12 "Boundary-Value Problems of the Thin-Walled Circular Cylinder," by N. J. Hoff, Journal of Applied Mechanics, Trans. ASME, vol. 76, 1954, pp. 343–350.

13 "The Elastic Sphere Under Concentrated Loads," by E. Sternberg and F. Rosenthal, Journal of Applied Mechanics, Trans. ASME, vol. 74, 1952, p. 413.

14 "On the Theory of Cylindrical Shells; Explicit Solution of the Characteristic Equation and Discussion of the Accuracy of Various Shell Theories," by Johannes Moe, Publications of the International Association for Bridge and Structural Engineering, vol. 13, 1953, p. 283.

# Lateral Buckling of Asymmetrical Beams

By H. L. LANGHAAR,[1] URBANA, ILL.

**A simplified theory of lateral buckling of asymmetrical beams under the action of uniform bending moments and axial thrusts is developed.**

FIG. 1 represents a cross section of any flanged beam, such that the principal axes of inertia through the centroid are parallel and perpendicular to the web. Since there may be a thrust force, the neutral axis is not necessarily the centroidal axis.

It is assumed that, when buckling occurs, the lateral deflection of the web in the $z$-direction, Fig. 1, is

$$w = (C_1 + C_2 y) \sin \frac{\pi x}{L} \quad \ldots\ldots\ldots\ldots\ldots [1]$$

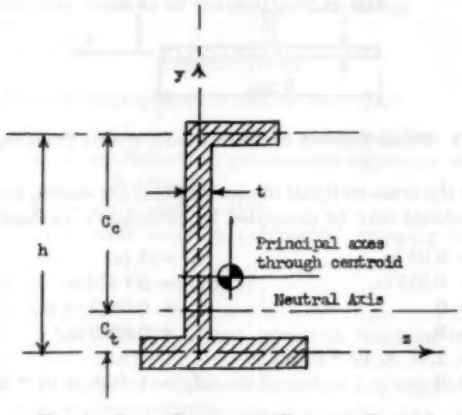


FIG. 1 CROSS SECTION OF FLANGED BEAM

in which $C_1$ and $C_2$ are constants, and $L$ is the length of the beam. This assumption implies that the ends of the beam are free to rotate about the vertical axes. End conditions other than simple support may be taken into account by regarding $L$ as a reduced length.[2]

The bending of eccentric flanges in their planes induces incremental longitudinal strains $\Delta\epsilon_c$ and $\Delta\epsilon_t$ at the upper and lower edges of the web. It is assumed that these strains are proportional to the lateral curvatures of the flanges. Consequently

$$\Delta\epsilon_c = C_3 \sin \frac{\pi x}{L}, \quad \Delta\epsilon_t = C_4 \sin \frac{\pi x}{L} \quad \ldots\ldots\ldots [2]$$

in which $C_3$ and $C_4$ are constants.

By plate theory, Equations [1] and [2] determine the strain energy of the buckled web, provided that the longitudinal strains vary linearly throughout the depth of the web. Also, Equations [1] and [2] determine the strain energy of the buckled flanges, since the flanges remain perpendicular to the web. The strain energy due to longitudinal strains in a flange must be augmented by the strain energy due to twisting. The twist of either flange is $\partial^2 w/\partial x \partial y$.

The potential energy of the external forces is $\Omega = -\int e\sigma_x \, dA$ where $\sigma_x$ is the compression stress in a fiber just before buckling, and $e$ is the contraction of the fiber. The incremental contraction $\Delta e$ that occurs at buckling consists of two parts: $\Delta e = \Delta_1 e + \Delta_2 e$ in which $\Delta_1 e$ is the contraction due to incremental strain of the fiber, and $\Delta_2 e$ is the contraction due to bowing of the fiber. $\Delta_1 e$ is irrelevant, since it contributes nothing to the second variation of the potential energy. The contraction due to bowing is

$$\Delta_2 e = {}^1/_2 \int_0^L [(\partial v/\partial x)^2 + (\partial w/\partial x)^2] dx$$

in which $v$ is the deflection in the $y$-direction. The $y$-component of deflection of a fiber of a flange results from twisting of the flange.

The total potential energy of the buckled beam is $V = U + \Omega$, in which $U$ is the strain energy. The potential energy may be represented in the form

$$V = V_0 + \delta V + (1/2)\delta^2 V + \ldots\ldots$$

in which $V_0$ is independent of $C_1$, $C_2$, $C_3$, $C_4$; $\delta V$ is a linear form in $C_1$, $C_2$, $C_3$, $C_4$; and $\delta^2 V$ is a quadratic form in these variables. By definition

$$(1/2)\delta^2 V = \sum_{i=1}^{4} \sum_{j=1}^{4} a_{ij} C_i C_j \quad \ldots\ldots\ldots\ldots [3]$$

After some integrations, one obtains

$$\left.\begin{aligned}
a_{11} &= \frac{\pi^2(I_c + I_t)}{h^2 L^2} + \frac{\pi^2 D}{EhL^2} - \epsilon_c \left[\frac{t}{2C_c} - \frac{tC_t}{hC_c} - \frac{C_t A_t}{C_c h^2} + \frac{A_c}{h^2}\right] \\
a_{22} &= \frac{\pi^2 I_c}{h^2 L^2} + \frac{J_c + J_t}{2(1+\nu)h^4} + \frac{\pi^2 D}{3EhL^2} + \frac{2(1-\nu)D}{Eh^2} - \epsilon_c \left[\frac{t}{4C_c} - \frac{C_t t}{3C_c h} + \frac{A_c}{h^2} + \frac{I_c}{h^4} - \frac{C_t I_t}{C_c h^4}\right] \\
a_{33} &= \frac{A_c}{h^2} + \frac{t}{3h}, \quad a_{44} = \frac{A_t}{h^2} + \frac{t}{3h} \\
a_{12} &= a_{21} = \frac{\pi^2 I_c}{h^2 L^2} + \frac{\pi^2 D}{2EhL^2} - \epsilon_c \left[\frac{t}{3C_c} - \frac{tC_t}{2hC_c} + \frac{A_c}{h^2}\right] \\
a_{13} &= a_{31} = a_{23} = a_{32} = \frac{\pi Q_c}{h^2 L}, \quad a_{14} = a_{41} = \frac{\pi Q_t}{h^2 L} \\
a_{24} &= a_{42} = 0, \quad a_{34} = a_{43} = \frac{t}{6h}
\end{aligned}\right\} \quad \ldots [4]$$

[1] Professor of Theoretical and Applied Mechanics, University of Illinois, Urbana, Ill. Mem. ASME.

[2] "Theory of Elastic Stability," by S. Timoshenko, McGraw-Hill Book Company, Inc., New York, N. Y., 1936, p. 245.

Contributed byt he Applied Mechanics Division and presented at the Annual Meeting, New York, N. Y., November 28–December 3, 1954, of THE AMERICAN SOCIETY OF MECHANICAL ENGINEERS.

Discussion of this paper should be addressed to the Secretary, ASME, 29 West 39th Street, New York, N. Y., and will be accepted until October 10, 1955, for publication at a later date. Discussion received after the closing date will be returned.

NOTE: Statements and opinions advanced in papers are to be understood as individual expressions of their authors and not those of the Society. Manuscript received by ASME Applied Mechanics Division, May 17, 1954. Paper No. 54—A-99.

where, besides the notations which are shown in Fig. 1

$A_c$, $A_t$ = cross-sectional areas of compression and tension flanges

$I_c$, $I_t$ = moments of inertia of cross sections of compression and tension flanges about the $y$-axis (Fig. 1)

$Q_c$, $Q_t$ = moments of area of cross sections of compression and tension flanges about the $y$-axis (positive if centroids of the flanges lie on positive side of web)

$D = \dfrac{Et^3}{12(1-\nu^2)}$ = flexural rigidity of web

$GJ_c$, $GJ_t$ = torsional stiffnesses of compression and tension flanges ($G$ is shear modulus)

$\epsilon_c$ = compression strain in compression flange at instant of buckling

The coefficients $a_{ij}$ have been rendered dimensionless by elimination of irrelevant constant factors. An apparent lack of symmetry in Equations [4] results from the fact that the bending of the tension flange is determined by $C_1$ alone, whereas both $C_1$ and $C_2$ determine the bending of the compression flange.

A necessary and sufficient condition for stability is that $\delta^2 V$ be positive definite; $\delta^2 V$ ceases to be positive definite when the determinant of the matrix $(a_{ij})$ becomes zero. Accordingly, the buckling criterion is

$$\det (a_{ij}) = 0 \qquad [5]$$

The determinant in Equation [5] is symmetrical. Only the coefficients $a_{11}$, $a_{22}$, $a_{12}$, $a_{21}$ contain $\epsilon_c$. The other coefficients $a_{ij}$ depend only on geometrical properties of the cross section and on the location of neutral axis. Accordingly, Equation [5] is a quadratic equation in $\epsilon_c$. For pure bending, one root is positive and the other is negative. The negative root corresponds to buckling with a reversed bending moment.

When the numerical values of the coefficients in the last two rows and columns of the determinant in Equation [5] are determined, the equation may be simplified by multiplying the last row by a properly chosen constant and adding the resulting row to the first row, so that $a_{14}$ is eliminated. Similarly, $a_{24}$ may be eliminated. Thus three zeros are obtained in the right-hand column. Laplace's development then reduces the determinant to the third order. By a repetition of the process, the determinant is reduced to the form, $\det (A_{ij}) = 0$, where $(A_{ij})$ is a two-rowed matrix whose terms are linear functions of $\epsilon_c$. This reduction preserves symmetry, i.e., $A_{12} = A_{21}$. Consequently, the critical compression strain $\epsilon_c$ of the compression flange is determined by

$$A_{11}A_{22} = A_{12}^2 \qquad [6]$$

If the cross section of the beam is symmetrical about the $y$-axis, Equation [6] reduces to

$$a_{11}a_{22} = a_{12}^2 \qquad [6a]$$

An implicit assumption in the theory is that the web is displaced only in the $z$-direction when buckling occurs. This assumption sometimes causes appreciable errors when there is a large thrust force, if the flanges are wide compared to the depth of the beam.

For buckling of a doubly symmetrical I-beam, the present theory agrees with Timoshenko's theory.[2, 3] For lateral buckling of a plate without flanges, it yields a critical load that is slightly higher than that given by Prandtl's theory, but the difference is less than 1 per cent if $L/h > 6$.

The main advantage of the present theory is that it is easily applied in some cases for which Timoshenko's formula is inapplicable, for example, beams with unequal flanges, tee beams, and beams with unsymmetrical cross sections. A comprehensive comparison with the more general theory of Goodier[4] is difficult.

## Example

A beam with the cross section shown in Fig. 2 is subjected to pure bending, so that the free edge of the vertical web is in compression. The length $L$ is 30 in.; Poisson's ratio is 0.30.

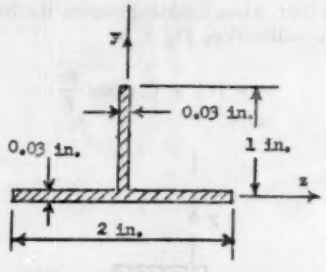


Fig. 2 Cross Section of Beam Subjected to Pure Bending

With the cross-sectional dimensions that are shown, the following constants may be computed by elementary methods:

| | |
|---|---|
| $t = 0.03$ in. | $h = 1$ in. |
| $C_c = 0.833$ in. | $C_t = 0.167$ in. |
| $A_c = 0$ | $A_t = 0.0600$ sq in. |
| $I_c = 0$ | $I_t = 0.0200$ in.$^4$ |
| $D/E = 2.47 \times 10^{-6}$ cu in. | |
| $J_c = 0$ | $J_t = 1.800 \times 10^{-6}$ in.$^4$ |

Equation [4] accordingly yields

$$a_{11} = 0.0002193$$
$$a_{22} = 0.00001038 - 0.0030\epsilon_c$$
$$a_{12} = -0.0090\epsilon_c$$

Since the $y$-axis is an axis of symmetry of the cross section, Equation [6a] may be used instead of the more general relation, Equation [6]. Consequently, only the constants $a_{11}$, $a_{22}$, $a_{12}$ are needed. Equation [6a] yields

$$219.3(10.38 - 3000\epsilon_c) = 81 \times 10^6\epsilon_c^2$$

The positive root of this equation, (which correspond to a bending moment that places the free edge of the web in compression) is $\epsilon_c = 0.00262$. This is the critical compression strain at the free edge of the web. The corresponding bending moment is $M_{cr} = 23.6 \times 10^{-6}E$ lb-in. This result agrees with that obtained by Goodier's theory.[4]

[3] "Buckling Strength of Metal Structures," by F. Bleich, McGraw-Hill Book Company, Inc., New York, N. Y., 1952.

[4] "Flexural-Torsional Buckling of Bars of Open Sections Under Bending, Eccentric Thrust, or Torsional Loads," by J. N. Goodier, Cornell University, Engineering Experiment Station Bulletin 28, 1942.

# The Root Section of a Swept Wing—A Problem of Plane Elasticity

By B. C. HOSKIN[1] and J. R. M. RADOK,[1] MELBOURNE, AUSTRALIA

**The methods of N. I. Muskhelishvili are used to obtain the stresses in an approximately square plate, subject to concentrated forces at two opposite corners, acting in the direction of the diagonal, and to certain shear-stress distributions along the sides. These shear-stress distributions have been chosen to conform approximately with those observed at the corresponding boundaries during tests on a 45-deg sweptback tube with ribs normal to the leading edge. Numerical results, involving loading parameters, are presented in the form of tables and graphs. Use of the numerical results is illustrated by application to a wing under varying degrees of torsion and bending.**

## Nomenclature

The following nomenclature is used in the paper:

$a$ = arbitrary constant in stress function $\varphi$
$a_j$ = coefficients in power-series expansion of stress function $\varphi$
$b_j$ = see Equations [14]
$c_j$ = coefficients in polynomial mapping function $\omega(\zeta)$
$f = f_1 + if_2$ = see Equations [9]
$i$ = $\sqrt{-1}$
$n$ = order of highest power in mapping function $\omega(\zeta)$
$s$ = arc co-ordinate on boundary $L$ of original region
$u, v$ = displacements
$z = x + iy$ = co-ordinate in original plane
$A$ = arbitrary constant in mapping function
$A(\zeta)$ = see Equation [19]
$A_k$ = Fourier coefficients of $A(\zeta)$; see Equation [20]
$K_j$ = see Equations [16] and [17]
$L$ = boundary of original region in $z$-plane
$P_1, P_2$ = concentrated forces per unit thickness of plate
$P_1', P_2'$ = concentrated forces
$S_0$ = uniform shear on boundary of $L$
$S$ = maximum shear on boundary of transformed region
$S_1$ = maximum shear on boundary of original region
$S_2$ = maximum shear on boundary of perfect square
$T_{xx}, T_{yy}, T_{xy}$ = stresses in original region
$X_n, Y_n$ = external stresses on $L$, in directions $Ox$, $Oy$, respectively
$2\alpha$ = length of diagonal of perfect square
$\gamma$ = unit circle
$\zeta$ = complex variable in transformed region
$\theta$ = polar angle in $\zeta$-plane
$\kappa$ = see Equations [4] and [5]
$\mu$ = shear modulus
$\nu$ = Poisson's ratio
$\sigma$ = arc co-ordinate on $\gamma$
$\varphi, \psi$ = complex stress functions
$\omega(\zeta)$ = mapping function
$\overline{\varphi(\zeta)}$, etc. = conjugate complex function to $\varphi(\zeta)$
$\breve{\varphi}(\zeta)$ = $\overline{\varphi(\bar{\zeta})}$, etc.
$\varphi'(\zeta)$ = $\dfrac{d\varphi}{d\zeta}$, etc.

## 1 Introduction

The internal structure of the swept wings of present-day, high-speed aircraft belongs, in principle, to one of two general types, depending on the orientation of the ribs. These may be either perpendicular to the leading edge ("structural ribs"—Fig. 1) or parallel to the center line of the aircraft ("aerodynamic ribs"—Fig. 2). The problem of plane elasticity, solved in this paper, is related to that presented by wings of the former type.

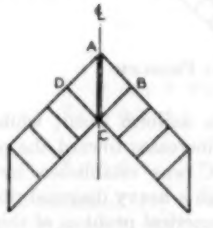


Fig. 1 "Structural" Ribs

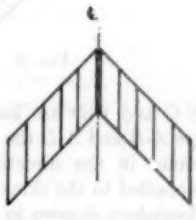

Fig. 2 "Aerodynamic" Ribs

Conventional stress analysis of wings utilizes in more or less refined manner the familiar formulas of the engineering theory of beams. Relying on Saint Venant's principle, it ignores in the first place the local effects at the fixed end of the wing. However, since normally the width-length ratio of wings is considerably larger than that assumed in beam theory, the actual stress distribution in the root section may affect a large section of the wing area. In fact, the rib at the root section of a swept wing always will be very heavy and, as a consequence, the stress distribution in the cover sheet along this line ($A$-$C$ in Fig. 1) will be nonuniform when the wing is subject to external loading. To the authors' knowledge, there exists no accurate treatment of the problem of the stresses in the root section ($A$-$B$-$C$-$D$ in Fig. 1) of such a wing.

A possible approach is to consider a root triangle ($A$-$B$-$C$ in Fig. 1) of the cover sheet and to formulate a boundary-value problem of plane elasticity for that region. Load distributions along the edges $A$-$B$ and $B$-$C$, based on experimental data or estimates obtained from shell theory applied to the outer wing, may be assumed and a displacement condition may be introduced along the root rib $A$-$C$. The most common assumption for these displace-

[1] Scientific Officer of the Structures and Materials Division, Aeronautical Research Laboratories, Department of Supply.

Contributed by the Applied Mechanics Division and presented at the Annual Meeting, New York, N. Y., November 28–December 3, 1954, of The American Society of Mechanical Engineers.

Discussion of this paper should be addressed to the Secretary, ASME, 29 West 39th Street, New York, N. Y., and will be accepted until October 10, 1955, for publication at a later date. Discussion received after the closing date will be returned.

Note: Statements and opinions advanced in papers are to be understood as individual expressions of their authors and not those of the Society. Manuscript received by ASME Applied Mechanics Division, February 23, 1954. Paper No. 54—A-97.

ments postulates a rigid rib, i.e., zero displacements. Apart from the fact that this assumption does not conform with the actual circumstances, because of the flexibility of any real rib, solution of the corresponding boundary-value problem encounters severe analytical difficulties because of the nonhomogeneous nature of the boundary conditions.

For this reason the present investigation deals with the root section, rather than with the root triangle. It presents only a partial solution in that the effect of the elastic root rib has not been included, although the displacements along the diagonal *A-C* have not been assumed beforehand. In fact, the problem solved in this paper may be conceived as referring to the top or bottom skin of the root section.

This statement will be elucidated further in the next section. It also should be noted that the boundary stresses, assumed for the numerical application to a 45-deg sweptback wing, may of course be varied; they have been chosen here to approximate to some degree those expected from shell theory as well as to ease the computations when calculating the actual stresses.

## 2 The Boundary-Value Problem

Experiments on a 45-deg swept tube with normal ribs have shown that the stresses on the boundary of the root section have the distribution shown in Fig. 3.[2] It is thus seen that the

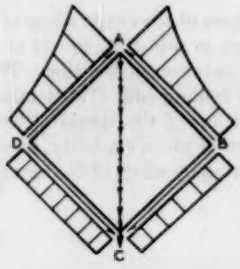


Fig. 3 Actual Problem

edges *B-C* and *C-D* are loaded in uniform shear, while along the edges *A-B* and *A-D* the shear increases toward the point *A*. Equilibrium in the direction *A-C* was established by direct stresses applied to the skins through a heavy diagonal rib.

The boundary stresses in the numerical problem of this paper are based on the foregoing results. However, the following simplifications had to be introduced in order to be able to cope with the computations with the available calculating machines and to bring the problem within the range of the theory of plane elasticity, as developed by N. I. Muskhelishvili.[3] Thus an approximately square plate has been considered for the root section; in fact, in the conformal mapping of the perfect square onto the circle, an approximate mapping function has been used which in effect implies rounding off the corners, Fig. 4. The shear stresses along the edges *B-C* and *C-D* again have been assumed constant, while those along the other two edges are of the type shown in Fig. 5. It is seen that they vary approximately linearly, increasing toward *A*, but that they decrease in a narrow region in the vicinity of *A*. This choice of stress distribution was conditioned by the desire to restrict computations, and the position of the maximum stress is closely linked with the approximate mapping function, as will become apparent later on. This digression from the actually expected stress distribution of Fig. 3 should not be

[2] "Strains and Deformations Measured Near the Root of a 45° Swept Rectangular Tube," by J. E. Wheeler and N. B. Joyce, ARL S and M Note 197, May, 1952.

[3] "Some Basic Problems of the Mathematical Theory of Elasticity," by N. I. Muskhelishvili, translated by J. R. M. Radok, P. Noordhoff, Groningen, Holland, 1953.

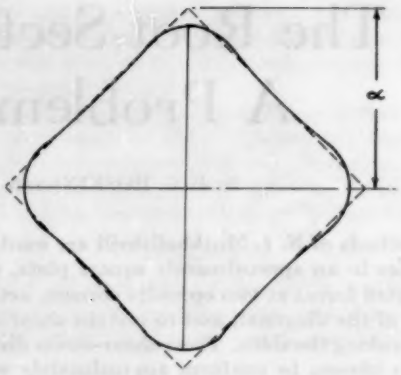


Fig. 4 Square With Rounded Corners

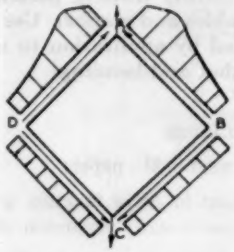


Fig. 5 Simplified Problem

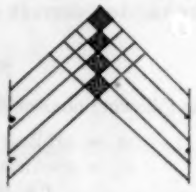

Fig. 6 Root Subsections

critical, since for other reasons the theory of elasticity would not give accurate results in the neighborhoods of the corners.

Obviously, equilibrium will be maintained in the direction *B-D* by the symmetry of the plate under consideration and of the assumed stress distribution. In the actual case, the forces maintaining equilibrium in the direction *A-C* will be introduced into the plate along the diagonal *A-C*, Fig. 3. Owing to analytical difficulties which as yet have not been resolved, these distributed forces have been replaced by two forces acting at *A* and *C*, respectively. Thus the corresponding solution may be interpreted in two ways: (*a*) It may be conceived as referring to the entire root section in which case the problem will be made definite by fixing the relative displacement of two points of the diagonal *A-C*. This will correspond to the case when the skins are attached to a given rib at those points so that the assumption of zero relative displacement will imply a rigid rib. (*b*) The solution may be conceived as referring to root subsections, say, contained between two spars or stringers and the same reasoning may be applied, Fig. 6.

Thus it is seen that the theoretical solution of this paper is restricted in the sense that the presence of the root rib does not affect the stress distribution in the skins in a manner which conforms with the actual conditions. It is hoped to consider the more complicated problem at a later stage.

One particular case of the problem under consideration is that of the square plate loaded by concentrated forces at two opposite corners, Fig. 7. This problem has been investigated by photoelastic methods,[4] and it will be shown later that the theoretical and experimental results are in good agreement.

Before solving the boundary-value problem, discussed previously, the analytical method of solution to be used will be summarized in the next section. As mentioned earlier, this method, as well as a number of others, is due to N. I. Muskhelishvili.[3] Al-

[4] "Photo Elasticity," by M. M. Frocht, John Wiley & Sons, Inc., New York, N. Y., 1941, p. 296.

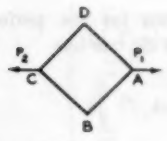


FIG. 7

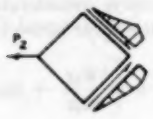


FIG. 8

FIG. 9

though these methods were published 20 years ago in the form of a monograph, they have found only limited use outside the USSR. The authors of this paper feel, therefore, that the importance of these methods, particularly with regard to aircraft stressing, has not yet been fully realized and that a number of current problems will find their solution by the application of these methods.

### 3 Mathematical Statement of Problem and Its Solution

In the work by N. I. Muskhelishvili,[3] the solution of boundary-value problems of plane elasticity is reduced to the determination of two analytic functions $\varphi$, $\psi$ of the complex variable $z$ which have to satisfy certain conditions at the boundary $L$ of the region under consideration in the $z$-plane. The displacements $u$, $v$ and the stresses $T_{xx}$, $T_{xy}$, $T_{yy}$ at the point $z$ are then given by

$$2\mu(u + iv) = \kappa\varphi(z) - z\overline{\varphi'(z)} - \overline{\psi(z)} \quad [1]$$

$$T_{xx} + T_{yy} = 2[\varphi'(z) + \overline{\varphi'(z)}] \quad [2]$$

$$T_{yy} - T_{xx} + 2iT_{xy} = 2[\bar{z}\varphi''(z) + \psi'(z)] \quad [3]$$

where

$$\kappa = 3 - 4\nu \text{ for plane strain} \quad [4]$$

$$= 3 - \frac{4\nu}{1+\nu} \text{ for generalized plane stress} \quad [5]$$

$$\left.\begin{aligned} \nu &= \text{Poisson's ratio} \\ \mu &= \text{shear modulus} \end{aligned}\right\} \quad [6]$$

$$z = x + iy, \qquad \bar{z} = x - iy \quad [7]$$

$$\varphi'(z) = \frac{d\varphi}{dz}, \text{ etc., } \varphi'(z)\,\overline{\varphi'(z)} = |\varphi'(z)|^2, \text{ etc.} \quad [8]$$

Further, the resultant force acting on a line $A$-$B$ is given by

$$f = f_1 + if_2 = i\int_A^B (X_n + iY_n)ds = [\varphi(z) + z\,\overline{\varphi'(z)} + \overline{\psi(z)}]_A^B \quad [9]$$

where $s$ is the arc co-ordinate along $A$-$B$.

The method of solution selected for the present problem is based on certain properties of analytical functions and Cauchy integrals. In particular, the evaluation of such integrals is simplified greatly if the region under consideration has a circular boundary. For this reason an essential step in the method of solution involves the conformal mapping of the region under consideration onto the unit circle by means of a regular analytical function.

Let $z = \omega(\zeta)$ be the mapping function, $\sigma$ be a point on the unit circle $\gamma$. Then,[5] the boundary condition for the functions $\varphi$, $\psi$ takes the form

$$\varphi(\sigma) + \frac{\omega(\sigma)}{\overline{\omega'(\sigma)}}\overline{\varphi'(\sigma)} + \overline{\psi(\sigma)} = f_1 + if_2 = f \quad [10]$$

where, by Equation [9], $f$ is a known function of $\sigma$.

[5] By §78 of footnote 3.

It is shown in the same footnote 5 that the functional equations for $\varphi(\zeta)$, $\psi(\zeta)$ with $\zeta$ the complex variable in the plane of the circle $\gamma$ are

$$\varphi(\zeta) = \frac{1}{2\pi i}\int_\gamma \frac{f\,d\sigma}{\sigma - \zeta} - \frac{1}{2\pi i}\int_\gamma \frac{\omega(\sigma)}{\overline{\omega'(\sigma)}}\frac{\overline{\varphi'(\sigma)}}{(\sigma - \zeta)}\,d\sigma - \bar{a} \quad [11]$$

$$\psi(\zeta) = \frac{1}{2\pi i}\int_\gamma \frac{\bar{f}\,d\sigma}{\sigma - \zeta} - \frac{1}{2\pi i}\int_\gamma \frac{\overline{\omega(\sigma)}}{\omega'(\sigma)}\frac{\varphi'(\sigma)}{\sigma - \zeta}\,d\sigma \quad [12]$$

where $\bar{a}$ is a constant which does not influence the stress distribution.

In the particular case when $\omega(\zeta)$ is a polynomial

$$z = \omega(\zeta) = c_1\zeta + c_2\zeta^2 + \ldots + c_n\zeta^n,\ c_1 \neq 0,\ c_n \neq 0 \quad [13]$$

these equations are easily solved by elementary means. In fact, one has

$$\frac{\omega(\zeta)}{\bar{\omega}'\left(\frac{1}{\zeta}\right)} = \frac{c_1\zeta + \ldots + c_n\zeta^n}{\bar{c}_1 + 2\bar{c}_2\zeta^{-1} + \ldots + n\bar{c}_n\zeta^{-n+1}} = b_n\zeta^n + \ldots + b_1\zeta + b_0 + \sum_{k=1}^{\infty} b_{-k}\zeta^{-k} \quad [14]$$

where only the $b_k$, $k \geq 0$ will be required. As $\varphi(\zeta)$ is a function, analytic inside $\gamma$, it has the power-series expansion

$$\varphi(\zeta) = a_1\zeta + \ldots + a_n\zeta^n + \ldots, \quad |\zeta| < 1 \quad [15]$$

where the $a_k$ are at present unknown. Using properties of the boundary values of Cauchy integrals,[6] it can be shown that

$$\frac{1}{2\pi i}\int_\gamma \frac{\omega(\sigma)}{\overline{\omega'(\sigma)}}\frac{\overline{\varphi'(\sigma)}}{(\sigma - \zeta)}\,d\sigma = K_0 + K_1\zeta + \ldots + K_n\zeta^n \quad [16]$$

where

$$\left.\begin{aligned} K_1 &= \bar{a}_1b_1 + 2\bar{a}_2b_2 + \ldots + n\bar{a}_nb_n \\ K_2 &= \bar{a}_1b_2 + \ldots + (n-1)\bar{a}_{n-1}b_n \\ &\ldots\ldots \\ K_n &= \bar{a}_1b_n \end{aligned}\right\} \quad [17]$$

Hence, by Equation [11]

$$\varphi(\zeta) + \bar{a} + K_0 + K_1\zeta + \ldots + K_n\zeta^n = \frac{1}{2\pi i}\int_\gamma \frac{f\,d\sigma}{\sigma - \zeta} = A(\zeta) \quad [18]$$

Developing the known function $A(\zeta)$ in a power series

$$A(\zeta) = \sum_{k=0}^{\infty} A_k\zeta^k \quad [19]$$

where obviously

$$A_k = \frac{1}{2\pi}\int_0^{2\pi} fe^{-ik\theta}\,d\theta \quad [20]$$

are the Fourier coefficients of the function $f$; substituting from Equations [15] and [19] in Equation [18] and equating coefficients of $\zeta^k$, it is found that the $a_k$ are determined by the system of equations

$$\left.\begin{aligned} a_1 + \bar{a}_1b_1 + \ldots + n\bar{a}_nb_n &= A_1 \\ a_2 + \bar{a}_1b_2 + \ldots + (n-1)\bar{a}_{n-1}b_n &= A_2 \\ &\ldots\ldots \\ \bar{a}_n + \bar{a}_1b_n &= A_n \end{aligned}\right\} \quad [21]$$

[6] Explained in part IV of footnote 3.

Having solved the System [21] for $a_k$, the function $\varphi(\zeta)$ may be written down by Equation [18]

$$\varphi(\zeta) = \sum_1^\infty A_k\zeta^k + \sum_1^n (a_k - A_k)\zeta^k + \bar{a} = A(\zeta) - \sum_1^n K_k\zeta^k + \bar{a} \quad \ldots\ldots [22]$$

Similarly, it can be shown that

$$\psi(\zeta) = \frac{1}{2\pi i}\int_\gamma \frac{\bar{f}d\sigma}{\sigma - \zeta} - \frac{\bar{\omega}\left(\frac{1}{\zeta}\right)}{\omega'(\zeta)}\varphi'(\zeta) + \sum_{k=1}^n \bar{K}_k\zeta^{-k} \quad [23]$$

The stresses and displacements can now be found from Equations [1] and [2], using the Expressions [22] and [23], where it must be noted that the derivatives in Equations [1] and [2] are with respect to the variable $z$.

It is thus seen that the following distinct stages of computation will be required for the solution of a boundary-value problem of the foregoing type, where the stresses on the boundary are known and where the region under consideration is mapped onto the unit circle by a polynomial-type mapping function $\omega(\zeta)$:

1 Find a polynomial $z = \omega(\zeta)$ mapping the region onto the unit circle.

2 Calculate the coefficients $b_k$, defined by Equation [14].

3 Determine the Fourier coefficients $A_k$, defined by Equation [20].

4 Solve the system of Equations [21] for $a_k$.

5 Write down $\varphi(\zeta)$, using Equations [22], and $\psi(\zeta)$, using Equation [23].

6 Calculate $\varphi'(\zeta)$, $\varphi''(\zeta)$, $\psi'(\zeta)$, and hence $\varphi'(z)$, $\varphi''(z)$, and $\psi'(z)$.

7 Calculate the stresses and displacements from Equations [1] and [2].

In the case where the mapping function is an infinite power series, an approximate solution may be obtained by retaining only the first few terms of the exact mapping function. It may be shown that the obtained approximate solution will be improved with increase in the number of retained terms.

## 4 Application to the Square Plate

The boundary-value problem discussed in Section 2 will now be solved by the method of Section 3. The boundary stresses are shown in Fig. 5 and it is immediately seen that the problem resolves itself into two parts which can be treated separately. The

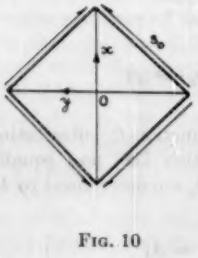


Fig. 10

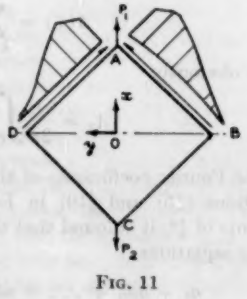


Fig. 11

first part deals with a square plate under uniform shear, Fig. 10, while the second part deals with the problem illustrated in Fig. 11.

*Square Plate Under Uniform Shear Loads.* This problem is easily solved by elementary considerations for the perfectly square plate. Denoting the shear stress by $S_0$, one has

$$\left.\begin{aligned} T_{xx} &= S_0, \quad u = \frac{S_0 x}{2\mu} + \text{const} \\ T_{yy} &= -S_0, \\ T_{xy} &= 0, \quad v = \frac{-S_0 y}{2\mu} + \text{const} \end{aligned}\right\} \quad \ldots\ldots [24]$$

*Square With Rounded Corners, Subject to Concentrated Forces and Certain Shear Loads.* Following the scheme indicated at the end of Section 3, the mapping function will be determined first. Using the Schwarz-Christoffel transformation, one finds

$$z = \omega(\zeta) = A\int_0^\zeta \frac{1}{\sqrt{1-\zeta^4}}\,d\zeta \quad \ldots\ldots [25]$$

where

$$A = \alpha\int_0^1 \frac{1}{\sqrt{1-\zeta^4}}\,d\zeta = 0.7627\alpha \quad \ldots\ldots [26]$$

$2\alpha$ = diagonal of square

The integral occurring in this transformation function is elliptic.

Expanding the root under the integral in a power series and integrating, one finds

$$z = \omega(\zeta) = A\left(\zeta + \frac{1}{10}\zeta^5 + \frac{1}{24}\zeta^9 + \frac{5}{208}\zeta^{13} + \frac{35}{2176}\zeta^{17} + \ldots\right) \quad \ldots\ldots [27]$$

Retaining only the terms given in the foregoing, one finds that the region mapped onto the unit circle by this transformation is of the form shown in Fig. 4. By increasing the number of terms the corners of the mapped regions will become sharper.

Using

$$z = \omega(\zeta) = A(\zeta + 0.1\zeta^5 + 0.0417\zeta^9 + 0.0240\zeta^{13} + 0.0161\zeta^{17}) \quad \ldots\ldots [28]$$

one finds from Equations [14]

$$\frac{\omega(\zeta)}{\bar{\omega}'\left(\frac{1}{\zeta}\right)} = b_{17}\zeta^{17} + b_{13}\zeta^{13} + \ldots + b_1\zeta + b_0 + \sum_{k=1}^\infty b_{-k}\zeta^{-k}$$

$$= 0.0161\zeta^{17} + 0.0160\zeta^{13} + 0.0277\zeta^9 + 0.0751\zeta^5 + 0.9427\zeta + \sum_1^\infty b_{-k}\zeta^{-k} \quad \ldots\ldots [29]$$

i.e., one has

$c_1 = 1$, $c_5 = 0.1$, $c_9 = 0.0417$, $c_{13} = 0.0240$, $c_{17} = 0.0161$
$b_1 = 0.9427$, $b_5 = 0.0751$, $b_9 = 0.0277$, $b_{13} = 0.0160$, $b_{17} = 0.0161$
while all other $b_k$, $k \geq 0$ are zero. It is easily seen that this last fact will simplify greatly the ensuing computations.

Next, the Fourier coefficients $A_k$ will be determined. Theoretically, if the function $f$, defined by Equation [9], is known, the $A_k$ may be calculated since the arc co-ordinate $s$ on the boundary of the original region can be expressed in terms of $\theta$ by use of the mapping function (see Appendix). However, an indirect method will be adopted here in order to restrict computations. This indirect approach implies the assumption of a function $f(\theta)$ in the transformed region, i.e., around the unit circle, and subsequent calculation of the stresses on the sides of the square. Let

$$f(\theta) = f_1 + if_2 = \begin{cases} i\left[P_1 + S(1-i)\left(\frac{\pi}{2}\theta - \frac{\theta^2}{2}\right)\right], & 0 \le \theta \le \frac{\pi}{2} \\ i\left[P_1 + S(1-i)\frac{\pi^2}{8}\right], & \frac{\pi}{2} \le \theta < \pi \\ i\left[P_1 - P_2 + S(1-i)\frac{\pi^2}{8}\right], & \pi \le \theta \le \frac{3\pi}{2} \\ i\left[P_1 - P_2 + S(1-i)\frac{\pi^2}{8} - S(1+i)\left(\frac{3\pi}{2}\theta - \frac{\theta^2}{2} - \frac{9\pi^2}{8}\right)\right], & \frac{3\pi}{2} \le \theta < 2\pi \end{cases} \quad \ldots [30]$$

where $S$ is a parameter. Since

$$f(s) = i\int_0^s (X_n + iY_n)ds$$

one has

$$X_n + iY_n = -i\frac{df(s)}{ds} = -i\frac{df(\theta)}{d\theta}\frac{d\theta}{ds} = -i\frac{df(\theta)}{d\theta}\frac{1}{|\omega'(\zeta)|} \quad \ldots [31]$$

and hence

$$(X_n + iY_n)ds = \begin{Bmatrix} P_1 \text{ at } A(\theta=0) \\ -P_2 \text{ at } C\ (\theta=\pi) \end{Bmatrix} \quad \ldots [32]$$

superimposed on which

$$X_n + iY_n = \begin{cases} S(1-i)\left(\frac{\pi}{2} - \theta\right)\frac{1}{|\omega'(\zeta)|} & \text{on } A\text{-}D \\ 0 & \text{on } D\text{-}C,\ C\text{-}B \\ -S(1+i)\left(\frac{3\pi}{2} - \theta\right)\frac{1}{|\omega'(\zeta)|} & \text{on } B\text{-}A \end{cases}$$

The stress $X_n$, along $A$-$D$, is shown in Fig. 12; the other stresses

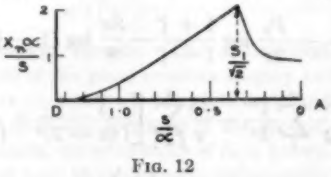


FIG. 12

vary in a similar manner. As mentioned earlier, these stresses depend to some degree on the mapping function as a result of the adopted indirect approach. It is seen from Equations [30] that for equilibrium in the direction of the real axis it is necessary that

$$P_1 - P_2 + \frac{S\pi^2}{4} = 0 \quad \ldots [33]$$

Graphical integration of the stress distribution Equation [32] on the square with rounded corners shows that

$$P_1 - P_2 + 0.84S_1\alpha = 0 \quad \ldots [34]$$

where $S_1$ is now the maximum value of the shear stress on the edge of the square. Assuming the shear stress to be distributed linearly with the maximum value $S_1$ occurring at the corner $A$ and with the total applied force equal to that obtained from the distribution, Equation [32], one finds the relation

$$S_1 = 1.19S_2 \quad \ldots [35]$$

while comparison of Equations [33] and [34] gives

$$S = 0.340S_1\alpha \quad \ldots [36]$$

By Equations [20] and [30], the Fourier coefficients $A_k$ take the form

$$A_k = \frac{1}{2\pi}\left[P_2\frac{1-(-1)^k}{k} - S\left\{\frac{\pi^2}{4k} + \frac{\pi}{k^2} - \frac{2-(-i)^k - i^k + i[(-i)^k - i^k]}{k^2}\right\}\right] \quad \ldots [37]$$

where $P_1$ has been eliminated by use of Equation [33]. The numerical values of the $A_k$ ($k = 1, 2, \ldots, 17$) are given in Table 1.

TABLE 1 NUMERICAL VALUES

| k | $A_k$ (Fourier coefficients) Equation [20] | | $a_k$ Equation [21] | | $b_k$ Equation [21] | | $f_n$ | |
|---|---|---|---|---|---|---|---|---|
| | $P_2$ | S | $P_2$ | S | $P_2$ | S | $P_2$ | S |
| 1 | 0.318310 | -0.256079 | 0.148730 | -0.108573 | 0.169580 | -0.147506 | 0.239579 | -0.424065 |
| 2 | | -0.211772 | | -0.200762 | | -0.241010 | | -0.389644 |
| 3 | 0.106103 | -0.188456 | 0.074961 | -0.136716 | 0.031148 | -0.049760 | 0.214129 | -0.369104 |
| 4 | | -0.129425 | | -0.078361 | | -0.051084 | | -0.367020 |
| 5 | 0.063662 | -0.093447 | 0.039523 | -0.065671 | 0.026139 | -0.027776 | 0.235280 | -0.326763 |
| 6 | | -0.076398 | | -0.058617 | | -0.017775 | | -0.291930 |
| 7 | 0.045473 | -0.066304 | 0.031823 | -0.044917 | 0.013650 | -0.021387 | 0.234300 | -0.337845 |
| 8 | | -0.056900 | | -0.036651 | | -0.022249 | | -0.346604 |
| 9 | 0.035368 | -0.048933 | 0.021532 | -0.035524 | 0.010836 | -0.013409 | 0.245400 | -0.317066 |
| 10 | | -0.043633 | | -0.034155 | | -0.009478 | | -0.296812 |
| 11 | 0.028937 | -0.039832 | 0.021793 | -0.028208 | 0.007144 | -0.011624 | 0.252759 | -0.346135 |
| 12 | | -0.036197 | | -0.026110 | | -0.010087 | | -0.334208 |
| 13 | 0.024485 | -0.032877 | 0.018924 | -0.025853 | 0.005561 | -0.007024 | 0.246887 | -0.308249 |
| 14 | | -0.030369 | | -0.025323 | | -0.005046 | | -0.302147 |
| 15 | 0.021221 | -0.028402 | 0.017601 | -0.021800 | 0.003620 | -0.006602 | 0.261687 | -0.367042 |
| 16 | | -0.026497 | | -0.020032 | | -0.006465 | | |
| 17 | 0.018784 | -0.024700 | 0.016329 | -0.022953 | 0.002395 | -0.001747 | | |

A study of the expression for $A_k$ and of the numerical values shows that

$$A(\zeta) = \sum_1^\infty A_k\zeta^k = \frac{P_2}{2\pi}\log\frac{1+\zeta}{1-\zeta} + \frac{S\pi}{8}\log(1-\zeta) - \frac{S}{2}\sum_1^\infty\frac{\zeta^k}{k^2} + \frac{2S}{\pi}\sum_1^\infty\left[\frac{\zeta^{4k-3}}{(4k-3)^2} + \frac{\zeta^{4k-2}}{(4k-2)^2}\right] \quad \ldots [38]$$

where the series which have not been summed are rapidly absolutely convergent for $|\zeta| < 1$.

The coefficients $a_j$ of Equation [15] are now easily determined. The corresponding system of linear Equations [21] is presented in matrix form in Table 2. Since all the coefficients are real, the $a_j$ will be real. Although there is a total of 17 simultaneous equations, these may be solved in three independent groups of 4, 5, and 8 equations because of the fact that the mapping function in-

TABLE 2 EQUATIONS [21] FOR THE DETERMINATION OF THE COEFFICIENTS $a_k$ (See Table 1)

| | $a_1$ | $a_2$ | $a_3$ | $a_4$ | $a_5$ | $a_6$ | $a_7$ | $a_8$ | $a_9$ | $a_{10}$ | $a_{11}$ | $a_{12}$ | $a_{13}$ | $a_{14}$ | $a_{15}$ | $a_{16}$ | $a_{17}$ | = |
|---|---|---|---|---|---|---|---|---|---|---|---|---|---|---|---|---|---|---|
| $a_1$ | 1·8427 | 0 | 0 | 0 | 0·0751 | 0 | 0 | 0 | 0·0277 | 0 | 0 | 0 | 0·0160 | 0 | 0 | 0 | 0·0161 | 0·318310$P_2$ |
| $a_2$ | 0 | 1 | 0 | 0 | 0 | 0 | 0 | 0 | 0 | 0 | 0 | 0 | 0 | 0 | 0 | 0 | 0 | −0·256079 |
| $a_3$ | 0 | 0 | 1·2253 | 0 | 0 | 0 | 0 | 0 | 0 | 0 | 0 | 0 | 0 | 0 | 0 | 0 | 0 | −0·241772 |
| $a_4$ | 0 | 0 | 0 | 0·1502 | 0 | 0 | 0 | 0·0554 | 0 | 0 | 0·0480 | 0 | 0·0320 | 0 | 0·0483 | 0 | 0·0322 | −0·106103$P_3$ |
| $a_5$ | 0 | 0 | 1·2253 | 0 | 0 | 0 | 0·0831 | 0 | 0 | 0·0640 | 0 | 0 | 0 | 0·0644 | 0 | 0 | 0 | −0·106456 |
| $a_6$ | 0 | 0 | 0 | 0·1502 | 0 | 0 | 0 | 0·0554 | 0 | 0 | 0·0480 | 0 | 0·0320 | 0 | 0·0483 | 0 | 0·0322 | −0·129425 |
| $a_7$ | 0 | 0 | 1·2253 | 0 | 0 | 0 | 0·0831 | 0 | 0 | 0·0640 | 0 | 0 | 0 | 0·0644 | 0 | 0 | 0 | −0·093447 |
| $a_8$ | 0 | 0 | 0 | 0·1502 | 0 | 0 | 0 | 0·0554 | 0 | 0 | 0·0480 | 0 | 0·0320 | 0 | 0·0483 | 0 | 0·0322 | −0·076302 |
| $a_9$ | 0 | 0 | 1·2253 | 0 | 0 | 0 | 0·0831 | 0 | 0 | 0·0640 | 0 | 0 | 0 | 0·0644 | 0 | 0 | 0 | −0·066304 |
| $a_{10}$ | 0 | 0 | 0 | 0·1502 | 0 | 0 | 0 | 0·0554 | 0 | 0 | 0·0480 | 0 | 0·0320 | 0 | 0·0483 | 0 | 0·0322 | −0·056003 |
| $a_{11}$ | 0 | 0 | 1·2253 | 0 | 0 | 0 | 0·0831 | 0 | 0 | 0·0640 | 0 | 0 | 0 | 0·0644 | 0 | 0 | 0 | −0·048333 |
| $a_{12}$ | 0 | 0 | 0 | 0·1502 | 0 | 0 | 0 | 0·0554 | 0 | 0 | 0·0480 | 0 | 0·0320 | 0 | 0·0483 | 0 | 0·0322 | −0·043033 |
| $a_{13}$ | 0 | 0 | 1·2253 | 0 | 0 | 0 | 0·0831 | 0 | 0 | 0·0640 | 0 | 0 | 0 | 0·0644 | 0 | 0 | 0 | −0·039832 |
| $a_{14}$ | 0 | 0 | 0 | 0·1502 | 0 | 0 | 0 | 0·0554 | 0 | 0 | 0·0480 | 0 | 0·0320 | 0 | 0·0483 | 0 | 0·0322 | −0·038167 |
| $a_{15}$ | 0 | 0 | 1·2253 | 0 | 0 | 0 | 0·0831 | 0 | 0 | 0·0640 | 0 | 0 | 0 | 0·0644 | 0 | 0 | 0 | −0·032877 |
| $a_{16}$ | 0 | 0 | 0 | 0·1502 | 0 | 0 | 0 | 0·0554 | 0 | 0 | 0·0480 | 0 | 0·0320 | 0 | 0·0483 | 0 | 0·0322 | −0·030369 |
| $a_{17}$ | 0 | 0 | 1·2253 | 0 | 0 | 0 | 0·0831 | 0 | 0 | 0·0640 | 0 | 0 | 0 | 0·0644 | 0 | 0 | 0 | −0·026402 |
| | 0 | 0 | 0 | 0·1502 | 0 | 0 | 0 | 0·0554 | 0 | 0 | 0·0480 | 0 | 0·0320 | 0 | 0·0483 | 0 | 0·0322 | −0·024747 |

volves only five of the possible terms of the seventeenth-order polynomial. These three sets of equations involve $(a_3, a_7, a_{11}, a_{15})$, $(a_1, a_5, a_9, a_{13}, a_{17})$, and $(a_2, a_4, a_6, a_8, a_{10}, a_{12}, a_{14}, a_{16})$, respectively. Using Crout's method[7] the values of the $a_j$ have been computed and are shown in Table 1.

The function $\varphi(\zeta)$ may be written down immediately. By Equations [22] one has

$$\varphi(\zeta) = A(\zeta) - \sum_1^{17} K_k \zeta^k + \bar{a}$$

$$= \frac{P_2}{2\pi} \log \frac{1+\zeta}{1-\zeta} + \frac{S\pi}{8} \log (1-\zeta) - \frac{S}{2} \sum_1^{\infty} \frac{\zeta^k}{k^2}$$

$$+ \frac{2S}{\pi} \sum_1^{\infty} \left[ \frac{\zeta^{4k-3}}{(4k-3)^2} + \frac{\zeta^{4k-2}}{(4k-2)^2} \right] - \sum_1^{17} K_k \zeta^k + \bar{a} \quad \ldots\ldots [39]$$

where the values of the $K_k = A_k - a_k$ are given in Table 1.

By Equation [23], the function $\psi(\zeta)$ is given by

$$\psi(\zeta) = \frac{1}{2\pi i} \int \frac{\bar{f} d\sigma}{\sigma - \zeta} - \frac{\bar{\omega}\left(\frac{1}{\zeta}\right)}{\omega'(\zeta)} \varphi'(\zeta) + \sum_1^{17} \frac{\overline{K}_k}{\zeta^k}. \quad [40]$$

The integral in this expression can be expressed in the same manner as the function $A(\zeta)$ to which it is closely related.
In fact

$$\frac{1}{2\pi i} \int_\gamma \frac{\bar{f} d\sigma}{\sigma - \zeta} = - \frac{P_2}{2\pi} \log \frac{1+\zeta}{1-\zeta} - \frac{S\pi}{8} \log (1-\zeta)$$

$$- \frac{S}{2} \sum_1^{\infty} \frac{\zeta^k}{k^2} - \frac{2S}{\pi} \sum_1^{\infty} \left[ \frac{\zeta^{4k-2}}{(4k-2)^2} + \frac{\zeta^{4k-1}}{(4k-1)^2} \right] \quad \ldots\ldots [41]$$

and $\psi(\zeta)$ takes the form

$$\psi(\zeta) = - \frac{P_2}{2\pi} \log \frac{1+\zeta}{1-\zeta} - \frac{S\pi}{8} \log (1-\zeta)$$

$$- \frac{S}{2} \sum_1^{\infty} \frac{\zeta^k}{k^2} - \frac{2S}{\pi} \sum_{k=1}^{\infty} \left[ \frac{\zeta^{4k-2}}{(4k-2)^2} + \frac{\zeta^{4k-1}}{(4k-1)^2} \right]$$

$$- \frac{\bar{\omega}\left(\frac{1}{\zeta}\right)}{\omega'(\zeta)} \varphi'(\zeta) + \sum_{k=1}^{17} \frac{\overline{K}_k}{\zeta^k} \quad \ldots\ldots [42]$$

where all terms are now known. It is shown in the Appendix that $\psi(\zeta)$ is regular at $\zeta = 0$ and formulas are derived for the calculation of this function for small values of $\zeta$.

The formal determination of the required derivatives of the functions $\varphi(\zeta)$ and $\psi(\zeta)$ presents no difficulties. With a view to numerical calculations, certain infinite series occurring in these derivatives again have been replaced by their sums much in the same way as this was done in the case of the function $A(\zeta)$. These derivatives are

[7] "A Short Method for Evaluating Determinants and Solving Systems of Linear Equations With Real or Complex Coefficients," by P. D. Crout, Trans. AIEE, vol. 60, 1941, p. 1235.

$$\varphi'(\zeta) = \frac{P_2}{\pi}\frac{1}{1-\zeta^2} - \frac{S\pi}{8(1-\zeta)} + \frac{S}{2\zeta}\log(1-\zeta) + \frac{2S}{\pi\zeta}\sum_{k=1}^{\infty}\left[\frac{\zeta^{4k-3}}{(4k-3)^2} + \frac{\zeta^{4k-2}}{(4k-2)^2}\right] - \sum_{k=1}^{17} kK_k\zeta^{k-1} \quad [43]$$

$$\varphi''(\zeta) = \frac{P_2}{\pi}\frac{2\zeta}{(1-\zeta^2)^2} - \frac{S\pi}{8(1-\zeta)^2} - \frac{S}{2}\left[\frac{1}{\zeta(1-\zeta)} + \frac{\log(1-\zeta)}{\zeta^2}\right] + \frac{S}{\pi\zeta^2}\left[\frac{1}{2}\log\frac{1+\zeta}{(1-\zeta)^2} + \arctan\zeta\right] - \frac{2S}{\pi\zeta^2}\sum_{k=1}^{\infty}\left[\frac{\zeta^{4k-3}}{(4k-3)^2} + \frac{\zeta^{4k-2}}{(4k-2)^2}\right] - \sum_{k=1}^{17} k(k-1)K_k\zeta^{k-2} \quad [44]$$

$$\psi'(\zeta) = -\frac{P_2}{\pi}\frac{1}{1-\zeta^2} + \frac{S\pi}{8(1-\zeta)} + \frac{S}{2\zeta}\log(1-\zeta) - \sum_{k=1}^{17}\frac{k\overline{K}_k}{\zeta^{k+1}} - \left\{\frac{\bar{\omega}\left(\frac{1}{\zeta}\right)\varphi''(\zeta)}{\omega'(\zeta)} + \frac{\varphi'(\zeta)}{[\omega'(\zeta)]^2}\left[\omega'(\zeta)\bar{\omega}'\left(\frac{1}{\zeta}\right) - \bar{\omega}\left(\frac{1}{\zeta}\right)\omega''(\zeta)\right]\right\} - \frac{2S}{\pi}\frac{1}{\zeta}\sum_{1}^{\infty}\left[\frac{\zeta^{4k-2}}{(4k-2)^2} + \frac{\zeta^{4k-1}}{(4k-1)^2}\right] \quad [45]$$

When calculating $\psi'(\zeta)$ for small values of $\zeta$, it may be preferable to use the derivative of the expression, deduced in the Appendix.

Finally, since by Equations [1] to [3] the calculation of the stresses requires the derivatives of the functions $\varphi$, $\psi$ with respect to $z$, one has to use the formulas

$$\left.\begin{aligned}\varphi'(z) &= \varphi'(\zeta)\frac{d\zeta}{dz} = \frac{\varphi'(\zeta)}{\omega'(\zeta)}\\ \varphi''(z) &= \frac{\omega'(\zeta)\varphi''(\zeta) - \varphi'(\zeta)\omega''(\zeta)}{[\omega'(\zeta)]^2}\\ \psi'(z) &= \frac{\psi'(\zeta)}{\omega'(\zeta)}\end{aligned}\right\} \quad [46]$$

*General Numerical Results.* The actual evaluation of the stresses at points of the plate involves lengthy and tedious computations. Since the stresses in the plate under uniform shear are easily obtained from the formulas of the section, Square Plate Under Shear Loads, once the value of $S_0$ is known, consideration will be restricted here to the stresses corresponding to the problem discussed in the section, Square With Rounded Corners. . . . As mentioned earlier, this problem involves two parameters $P_2$ and $S$ by means of which it can be modified to account for a number of different types of loading. For example, by putting $S = 0$, one obtains the plate stretched by two diagonal forces acting at opposite corners, Fig. 7. Putting $P_2 = 0$, one finds the solution of the plate with the assumed shear loading, balanced in the diagonal direction by a force acting at that corner of the plate about which the shear distribution is symmetrical, Fig. 9. Combining these two solutions, one can obtain the solution of the problem where the shear forces are balanced by a concentrated force acting at the corner between the two unloaded edges of the plate, Fig. 8. Finally, $P_2$ and $S$ may be given any convenient finite values.

The values of the functions $\varphi(\zeta)$, $\psi(\zeta)$ and of their derivatives have been evaluated at the following points of the diagonals of the plate

$\zeta = -0.8, -0.6, -0.4, -0.2, 0, 0.2, 0.4, 0.6, 0.8$

$\frac{z}{\alpha} = -0.64, -0.46, -0.31, -0.15, 0, 0.15, 0.31, 0.46, 0.64$

$\zeta = 0.2i, 0.4i, 0.6i, 0.8i$

$\frac{z}{\alpha} = 0.15i, 0.31i, 0.46i, 0.64i$

The values of these functions are given in Table 3 with $S$ and $P_2$ as parameters. The corresponding stress distributions along the diagonals of the square are contained in Table 4 and Figs. 13 and 14.

The displacements of points of the diagonal in the $x$-direction have been calculated using Equation [1]. They are tabulated in Table 5 and graphed in Fig. 15. The arbitrary constant, omitted in Table 3, has been chosen so that the displacements are zero at $z = 0$.

*Application to a Particular Case.* In order to demonstrate the use of the foregoing numerical results, consider the case of a 45-deg swept wing with root chord 10 ft and assume there is to be no relative displacement between the two points

$x_{1,2} = \pm 0.64\alpha = \pm 0.64 \times 60 = \pm 38.4$ in. of the center line of the root section.

By Equation [34] one has for that part of the boom load which is diffused into, for example, the top skin

$$X = \left(\sqrt{2}\,S_0\alpha + \frac{0.84}{\sqrt{2}}S_1\alpha\right)t$$

where the quantities $X$ and $S_0$ will be given the following values

| | |
|---|---|
| $X = 72{,}000$ lb, | $S_0 = 0$ |
| $X = 96{,}000$ lb, | $S_0 = 5000$ psi |
| $X = 120{,}000$ lb, | $S_0 = 10{,}000$ psi |
| $X = 144{,}000$ lb, | $S_0 = 15{,}000$ psi |

corresponding to various degrees of torsion and bending. Substituting for $X$ and $S_0$ in the foregoing formula, one finds for the maximum values $S_0 + S_1$ of the shear on the boundary of the root section in all cases

$$S_0 + S_1 = 20{,}000 \text{ psi}$$

Consider first the case, with $t = 0.1$ in.

$$X = 72{,}000 \text{ lb}, \qquad S_0 = 0, \qquad S_1 = 20{,}000 \text{ psi}$$

By Table 5 the relative displacement of the points $x_{1,2}$ is given by

$$u(x_1) - u(x_2) = \frac{1}{\mu}[2 \times 0.376P_2 - (0.036 + 0.144)\alpha S_1] = \frac{1}{\mu}(0.752P_2 - 0.180 \times 60 \times 20{,}000) = \frac{1}{\mu}(0.752P_2 - 2.16 \times 10^6)$$

Hence, for zero relative displacement of these two points, one has

$$P_2 = \frac{2.16 \times 10^6}{0.752} = 287{,}000 \text{ lb per in.}$$

TABLE 3 NUMERICAL VALUES OF STRESS FUNCTIONS AND THEIR DERIVATIVES

| $\zeta$ | $z$ | $\varphi(\zeta)$ | | $\psi(\zeta)$ | | $\varphi'(\zeta)$ | | $\varphi'(z)$ | | $\psi'(\zeta)$ | | $\psi'(z)$ | | $\varphi''(\zeta)$ | | $\varphi''(z)$ | |
|---|---|---|---|---|---|---|---|---|---|---|---|---|---|---|---|---|---|
| | | $P_2$ | $S$ | $P_2$ | $S$ | $P_2$ | $S$ | $P_2/\alpha$ | $S/\alpha$ | $P_2$ | $S$ | $P_2/\alpha$ | $S/\alpha$ | $P_2$ | $S$ | $P_2/\alpha^2$ | $S/\alpha^2$ |
| $-0.8$ | $-0.64\alpha$ | $-0.1847$ | $0.0087$ | $0.736$ | $0.2578$ | $0.5472$ | $0.0384$ | $0.5532$ | $0.0388$ | $-2.6982$ | $0.2107$ | $-2.7876$ | $0.2130$ | $-2.9363$ | $-0.0086$ | $-2.0825$ | $-0.055$ |
| $-0.6$ | $-0.46\alpha$ | $-0.1098$ | $0.0155$ | $0.4139$ | $0.2963$ | $0.2717$ | $0.0271$ | $0.3323$ | $0.0331$ | $-1.0527$ | $0.1804$ | $-1.2877$ | $0.2207$ | $-0.6373$ | $-0.0954$ | $-0.7518$ | $-0.1227$ |
| $-0.4$ | $-0.31\alpha$ | $-0.0639$ | $0.0185$ | $0.2435$ | $0.3321$ | $0.1909$ | $0.0008$ | $0.2471$ | $0.0010$ | $-0.7128$ | $0.1855$ | $-0.9225$ | $0.2401$ | $-0.2479$ | $-0.1707$ | $-0.3732$ | $-0.2859$ |
| $-0.2$ | $-0.15\alpha$ | $-0.0304$ | $0.0147$ | $0.1147$ | $0.3736$ | $0.1581$ | $-0.0426$ | $0.2071$ | $-0.0558$ | $-0.5945$ | $0.2281$ | $-0.7789$ | $0.2988$ | $-0.0985$ | $-0.2710$ | $-0.1613$ | $-0.4663$ |
| $0$ | $0$ | $0$ | $0$ | $0$ | $0.4268$ | $0.1487$ | $-0.1094$ | $0.1950$ | $-0.1434$ | $-0.5630$ | $0.3235$ | $-0.7381$ | $-0.4241$ | $0$ | $-0.4015$ | $0$ | $-0.6902$ |
| $0.2$ | $0.15\alpha$ | $0.0304$ | $-0.0291$ | $-0.1147$ | $0.5079$ | $0.1581$ | $-0.2085$ | $0.2071$ | $-0.2732$ | $-0.5945$ | $0.5087$ | $-0.7789$ | $0.6638$ | $0.0985$ | $-0.6146$ | $0.1613$ | $-1.0492$ |
| $0.4$ | $0.31\alpha$ | $0.0639$ | $-0.0873$ | $-0.2435$ | $0.6407$ | $0.1909$ | $-0.3690$ | $0.2471$ | $-0.4776$ | $-0.7128$ | $0.8627$ | $-0.9225$ | $1.1165$ | $0.2479$ | $-1.0370$ | $0.3732$ | $-1.6557$ |
| $0.6$ | $0.46\alpha$ | $0.1098$ | $-0.1876$ | $-0.4139$ | $0.8835$ | $0.2717$ | $-0.6708$ | $0.3323$ | $-0.8205$ | $-1.0527$ | $1.7010$ | $-1.2877$ | $2.0807$ | $0.6373$ | $-2.1976$ | $0.7518$ | $-2.7903$ |
| $0.8$ | $0.64\alpha$ | $0.1848$ | $0.3882$ | $-0.736$ | $1.4862$ | $0.5472$ | $-1.5267$ | $0.5532$ | $-1.5433$ | $-2.6982$ | $5.6302$ | $-2.7876$ | $5.6916$ | $2.9363$ | $-8.5610$ | $2.0625$ | $-6.1869$ |
| $0.2i$ | $0.15\alpha i$ | | $0.00791$ | | $0.4141$ | $0.1400$ | $-0.0927$ | $0.1834$ | $-0.1214$ | $-0.5348$ | $0.2815$ | $-0.7004$ | $0.3688$ | | $-0.3862$ | | $-0.6265$ |
| | | $0.0292i$ | $-0.0206i$ | $-0.1107i$ | $+0.0619i$ | | $-0.07794$ | | $-0.1021i$ | | $+0.1207i$ | | $+0.1581i$ | $0.0839i$ | $-0.1541i$ | $0.1478i$ | $-0.2671i$ |
| $0.4i$ | $0.31\alpha i$ | | $0.0303$ | | $0.3798$ | $0.1170$ | $-0.0502$ | $0.1514$ | $-0.0650$ | $-0.4651$ | $0.1735$ | $-0.6019$ | $0.2245$ | | $-0.2899$ | | $-0.4539$ |
| | | $0.0550i$ | $-0.0353i$ | $-0.2110i$ | $+0.1099i$ | | $-0.1438i$ | | $-0.1861i$ | | $+0.2102i$ | | $+0.2720i$ | $0.1406i$ | $-0.2598i$ | $0.2613i$ | $-0.4482i$ |
| $0.6i$ | $0.46\alpha i$ | | $0.0644$ | | $0.3266$ | $0.0856$ | $0.0072$ | $0.1047$ | $0.0088$ | $-0.3798$ | $0.0119$ | $-0.4846$ | $0.0148$ | | $-0.2405$ | | $-0.2149$ |
| | | $0.0754i$ | $-0.0397i$ | $-0.3008i$ | $+0.1289i$ | | $-0.1956i$ | | $-0.2392i$ | | $+0.2480i$ | | $+0.3034i$ | $0.1704i$ | $-0.3041i$ | $0.3165i$ | $-0.4496i$ |
| $0.8i$ | $0.64\alpha i$ | | $0.1088$ | | $0.2838$ | $0.0483$ | $0.0664$ | $0.0488$ | $0.0871$ | $-0.3002$ | $-0.2321$ | $-0.3035$ | $0.2348$ | | $-0.4066$ | | $0.0087$ |
| | | $0.0889i$ | $-0.0323i$ | $-0.3638i$ | $+0.1104i$ | | $-0.2528i$ | | $-0.2556i$ | | $+0.2170i$ | | $+0.2194i$ | $0.2123i$ | $-0.2675i$ | $0.2981i$ | $-0.1819i$ |

TABLE 4 STRESSES ALONG THE DIAGONALS

| $\alpha$ | $\sigma_{xx}$ | | | $\sigma_{yy}$ | | | $\tau_{xy}$ | | |
|---|---|---|---|---|---|---|---|---|---|
| | $S_0/\zeta$ | $S_0/\alpha$ | $S_1$ | $S_0/\alpha$ | $S_0/\alpha$ | $S_1$ | $S_0/\alpha$ | $S_0/\alpha$ | $S_1$ |
| $-0.6\alpha$ | 2.5012 | − .1002 | −.0341 | −.2884 | .2557 | .0869 | 0 | 0 | 0 |
| $-0.4\alpha$ | 1.6065 | − .2109 | −.0717 | −.2773 | .3433 | .1167 | 0 | 0 | 0 |
| $-0.2\alpha$ | 1.3010 | − .3267 | −.1111 | −.3126 | .3310 | .1125 | 0 | 0 | 0 |
| $-0.1\alpha$ | 1.1689 | − .1803 | −.1633 | −.3605 | .2571 | .0874 | 0 | 0 | 0 |
| 0 | 1.1281 | − .7109 | −.2417 | −.3681 | .1373 | .0467 | 0 | 0 | 0 |
| $0.1\alpha$ | 1.1689 | −1.0538 | −.3583 | −.3605 | −.0390 | −.0133 | 0 | 0 | 0 |
| $0.2\alpha$ | 1.3010 | −1.5584 | −.5299 | −.3126 | −.1760 | −.0598 | 0 | 0 | 0 |
| $0.4\alpha$ | 1.6065 | −2.4381 | −.8290 | −.2773 | −.8439 | −.2869 | 0 | 0 | 0 |
| $0.6\alpha$ | 2.5012 | −4.0188 | −1.3664 | −.2884 | −1.3547 | −.4606 | 0 | 0 | 0 |
| $0.1\alpha$ | 1.0450 | − .5725 | −.1945 | −.3114 | .0859 | .0292 | 0 | .2858 | .0836 |
| $0.3\alpha$ | .8237 | − .2637 | −.0897 | −.2181 | .0037 | .0013 | 0 | .4127 | .1403 |
| $0.4\alpha$ | .5270 | .3098 | .0713 | −.1082 | −.0785 | −.0267 | 0 | .4084 | .1368 |
| $0.6\alpha$ | .2103 | .4728 | .1606 | −.0151 | −.2040 | −.0694 | 0 | .2138 | .0727 |

TABLE 5 DISPLACEMENTS ALONG X-WISE DIAGONAL

| $\alpha$ | $S_0/\zeta$ | $S_1/\zeta$ |
|---|---|---|
| $-0.6\alpha$ | −.376 | .036 |
| $-0.4\alpha$ | −.240 | .031 |
| $-0.2\alpha$ | −.147 | .023 |
| $-0.1\alpha$ | −.072 | .016 |
| 0 | 0 | 0 |
| $0.1\alpha$ | .072 | −.016 |
| $0.2\alpha$ | .147 | −.040 |
| $0.4\alpha$ | .240 | −.077 |
| $0.6\alpha$ | .376 | −.144 |

By Equation [34]

$$P_1 = P_2 - 0.84 \times \alpha S_1 = 287{,}000 - 0.84 \times 60 \times 20{,}000 = -721{,}000 \text{ lb per in.}$$

so that for a skin thickness of 0.1 in.

$$P_2' = 28{,}700 \text{ lb}, \quad P_1' = -72{,}100 \text{ lb}$$

Next, consider the case

$$X = 96{,}000 \text{ lb}, \qquad S_0 = 5000 \text{ psi}, \qquad S_1 = 15{,}000 \text{ psi}$$

Then, by Equation [24], one has the additional displacement

$$\frac{1}{\mu} S_0 \times 0.64 \times 60 = \frac{1}{\mu} 5000 \times 38.4 = \frac{1}{\mu} 1.92 \times 10^5$$

and the condition for $P_2$ becomes

$$P_2 = \frac{0.180 \times 60 \times 15{,}000 - 1.92 \times 10^5}{0.752} = \frac{1.62 \times 10^5 - 1.92 \times 10^5}{0.752}$$

while

$$P_1 = -39{,}800 - 0.84 \times 60 \times 15{,}000 = -716{,}200 \text{ lb per in.}$$

so that for the same skin thickness

$$P_2' = -3980 \text{ lb}, \quad P_1' = -71{,}620 \text{ lb}$$

Similarly, one has for the case

$$X = 120{,}000 \text{ lb}, \quad S_0 = 10{,}000 \text{ psi}, \quad S_1 = 10{,}000 \text{ psi}$$
$$P_2 = -367{,}000 \text{ lb per in.}, \quad P_1 = -871{,}000 \text{ lb per in.}$$
$$P_2' = -36{,}700 \text{ lb}, \quad P_1' = -87{,}100 \text{ lb}$$

while the case

$$X = 144{,}000 \text{ lb}, \quad S_0 = 15{,}000 \text{ psi}, \quad S_1 = 5000 \text{ psi}$$

gives

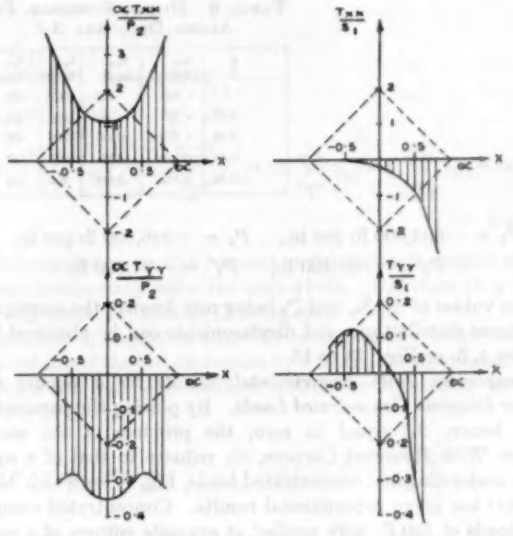

FIG. 13 STRESSES ALONG DIAGONAL IN THE $X$-DIRECTION

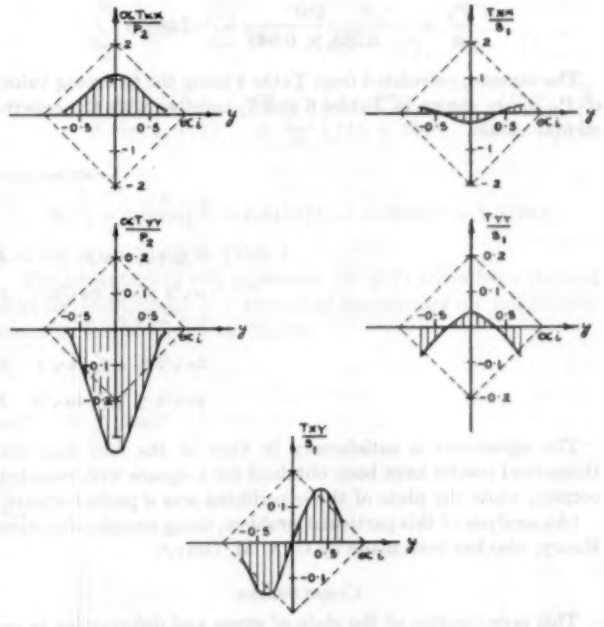

FIG. 14 STRESSES ALONG DIAGONAL IN $Y$-DIRECTION

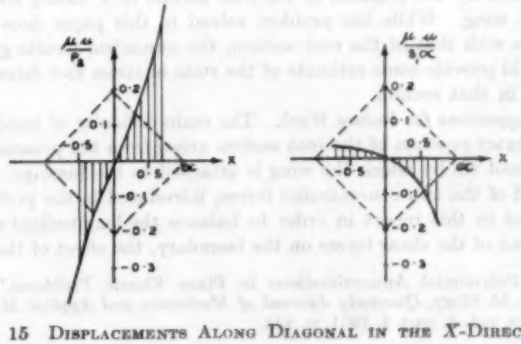

FIG. 15 DISPLACEMENTS ALONG DIAGONAL IN THE $X$-DIRECTION

TABLE 6 DIRECT STRESSES, PSI, ALONG DIAGONAL *A-C*

| $\frac{s}{\alpha}$ | $\sigma_{xx}$ (Theory) | $\sigma_{xx}$ (Expt.) | $\sigma_{yy}$ (Theory) | $\sigma_{yy}$ (Expt.) |
|---|---|---|---|---|
| 0 | - 844 | - 903 | 260 | 281 |
| 0.15 | - 878 | - 932 | 255 | 273 |
| 0.31 | - 973 | -1040 | 238 | 254 |
| 0.46 | -1202 | -1251 | 207 | 197 |
| 0.64 | -1671 | -1705 | 216 | 144 |

TABLE 7 DIRECT STRESSES, PSI, ALONG DIAGONAL *B-D*

| $\frac{s}{\alpha}$ | $\sigma_{xx}$ (Theory) | $\sigma_{xx}$ (Expt.) | $\sigma_{yy}$ (Theory) | $\sigma_{yy}$ (Expt.) |
|---|---|---|---|---|
| 0 | - 844 | - 903 | 260 | 281 |
| 0.151 | - 782 | - 836 | 233 | 261 |
| 0.311 | - 616 | - 663 | 163 | 168 |
| 0.461 | - 394 | - 417 | 81 | 89 |
| 0.611 | - 157 | - 153 | 11 | 23 |

$$P_2 = -694{,}000 \text{ lb per in.}, \quad P_1 = -946{,}000 \text{ lb per in.}$$
$$P_2' = -69{,}400 \text{ lb}, \quad P_1' = -94{,}600 \text{ lb}$$

The values of $S_1$, $S_0$, and $P_2$ being now known, the corresponding stress distributions and displacements can be obtained from Tables 4, 5, or Figs. 13 to 15.

*Comparison With Experimental Results for a Square Plate Under Diagonal Concentrated Loads.* By placing the parameter $S$ (and hence, $S_1$) equal to zero, the problem of the section, Square With Rounded Corners. . ., reduces to that of a square plate under diagonal concentrated loads, Fig. 7, for which M. M. Frocht[4] has given experimental results. Concentrated compression loads of 180 lb were applied at opposite corners of a square plate with diagonal of length 1.885 in., and thickness 0.255 in.; hence

$$\frac{P_2}{\alpha} = -\frac{180}{0.255 \times 0.943} = -748 \text{ psi}$$

The stresses, calculated from Table 4 using the foregoing value of $P_2/\alpha$, are shown in Tables 6 and 7, together with the experimental values.

| Location | | Type of load | $x$-component | $y$-component |
|---|---|---|---|---|
| $s = 0$ | $A$ | Concentrated force per unit thickness | $P_1$ | |
| $0 \le s \le \alpha\sqrt{2}$ | $A$-$D$ | Stress | $\frac{S_1}{2\alpha}\left(\alpha\sqrt{2} - s\right)$ | $-\frac{S_1}{2\alpha}\left(\alpha\sqrt{2} - s\right)$ |
| $\alpha\sqrt{2} \le s \le 2\alpha\sqrt{2}$ | $D$-$C$ | Stress | 0 | 0 |
| $s = 2\alpha\sqrt{2}$ | $C$ | Concentrated force per unit thickness | $-P_1$ | 0 |
| $2\alpha\sqrt{2} \le s \le 3\alpha\sqrt{2}$ | $C$-$B$ | Stress | 0 | 0 |
| $3\alpha\sqrt{2} \le s \le 4\alpha\sqrt{2}$ | $B$-$A$ | Stress | $\frac{S_2}{2\alpha}\left(s - 3\alpha\sqrt{2}\right)$ | $\frac{S_2}{2\alpha}\left(s - 3\alpha\sqrt{2}\right)$ |

The agreement is satisfactory in view of the fact that the theoretical results have been obtained for a square with rounded corners, while the plate of the experiment was a perfect square.

(An analysis of this particular problem, using complex-function theory, also has been made by C. A. M. Gray.[5])

## CONCLUSIONS

This investigation of the state of stress and deformation in an almost square plate with rounded corners under certain shear loading and concentrated forces at the boundary has been influenced by the problem of the root section of a 45-deg swept-back wing. While the problem solved in this paper does not agree with that of the root section, the numerical results given should provide some estimate of the state of stress and deformation in that section.

*Suggestions for Future Work.* The main difficulty of handling the exact problem of the root section arises from the presence of the root rib by which the wing is attached to the fuselage. Instead of the two concentrated forces, introduced in the problem solved in this report in order to balance the longitudinal component of the shear forces on the boundary, the effect of the rib will be equivalent to sources of such forces along the corresponding diagonal where the local magnitude of these forces will depend on the local deformation of the rib-skin combination. In principle, this problem should be solvable by the methods of N. I. Muskhelishvili,[3] and it is intended to consider it in the near future.

[5] "Polynomial Approximations in Plane Elastic Problems," by C. A. M. Gray, *Quarterly Journal of Mechanics and Applied Mathematics*, vol. 4, part 4, 1951, p. 444.

## ACKNOWLEDGMENT

The authors are indebted to Mr. S. Gee for his careful rechecking of the numerical results.

# Appendix

## DIRECT SOLUTION OF BOUNDARY-VALUE PROBLEM

Instead of the indirect approach used in the main part of this paper by which the stress distribution on the boundary in the image region was assumed, one may, of course, start from a given stress distribution on the boundary of the original region. Thus let this distribution be as follows, where $s$ is the arc co-ordinate along the sides of the perfect square with $s = 0$ corresponding to the point $A$ of Fig. 3:

This distribution is similar to that of Fig. 11 except that the shear stresses along $A$-$B$ and $A$-$D$ now vary linearly from zero at points $B$ and $D$ to a value $S_2$ at $A$. Since, by Equation [9]

$$f(s) = i\int_0^s (X_n + iY_n)ds$$

one has

$$f(s) = \begin{cases} i\left[P_1 + (1-i)S_2\left(\frac{s}{\sqrt{2}} - \frac{s^2}{4\alpha}\right)\right], & 0 \le s \le \sqrt{2}\alpha \\ i\left[P_1 + (1-i)S_2\frac{\alpha}{2}\right], & \sqrt{2}\alpha \le s < 2\sqrt{2}\alpha \\ i\left[P_1 - P_2 + (1-i)S_2\frac{\alpha}{2}\right], & 2\sqrt{2}\alpha \le s \le 3\sqrt{2}\alpha \\ i\left[P_1 - P_2 + (5+4i)S_2\alpha - S_2\frac{3}{\sqrt{2}}(1+i)s + \frac{S_2}{4\alpha}(1+i)s^2\right], & 3\sqrt{2}\alpha \le s < 4\sqrt{2}\alpha \end{cases}$$

Hence, putting $s = 4\sqrt{2}\alpha$

$$P_1 - P_2 + S_2\alpha = 0$$

is the condition of equilibrium of the external forces.

Finally, since, as is easily seen

$$s = \sqrt{2}\,y = \sqrt{2}\,(\alpha - x) = \frac{1+i}{\sqrt{2}}\,(\alpha - z) \text{ for } 0 \le s \le \sqrt{2}\alpha$$

while

$$s = 4\alpha\sqrt{2} + \frac{1-i}{\sqrt{2}}\,(z - \alpha) \text{ for } 3\sqrt{2}\alpha \le s \le 4\sqrt{2}\alpha$$

one has now the function $f(s)$ in terms of the complex variable $z$. Transforming by use of the mapping function

$$z = \omega(\zeta)$$

one finds $f(z)$ as function of $\zeta = e^{i\vartheta}$ and the Fourier coefficients $A_k$ may be determined by Equation [20].

## Regularity of $\psi(\zeta)$ at $\zeta = 0$

At first sight, the function $\psi(\zeta)$ as determined by Equation [23] may appear to be singular at $\zeta = 0$. It will now be shown that this function is regular at that point and at the same time an alternative expression will be deduced for its numerical evaluation for small values of $\zeta$.

Consider $$\frac{\bar{\omega}\left(\frac{1}{\zeta}\right)}{\omega'(\zeta)}\,\varphi'(\zeta)$$

which may be written by definition

$$\frac{\bar{\omega}\left(\frac{1}{\zeta}\right)}{\omega'(\zeta)}\,\varphi'(\zeta) = \left[\frac{\bar{b}_n}{\zeta^n} + \frac{\bar{b}_{n-1}}{\zeta^{n-1}} + \ldots + \frac{\bar{b}_1}{\zeta} + \bar{b}_0 + \frac{R(\zeta)}{\omega'(\zeta)}\right]\varphi'(\zeta)$$

where the $b_j$ are the same as in Equations [14] and $R(\zeta)$ is a polynomial. Hence

$$\frac{\bar{\omega}\left(\frac{1}{\zeta}\right)}{\omega'(\zeta)}\,\varphi'(\zeta) = \frac{R(\zeta)}{\omega'(\zeta)}\,\varphi'(\zeta) + \left(\frac{\bar{b}_n}{\zeta^n} + \ldots + \frac{\bar{b}_1}{\zeta} + \bar{b}_0\right)\left(\sum_1^n k a_k \zeta^{k-1} + \sum_{n+1}^{\infty} k a_k \zeta^{k-1}\right)$$

$$= \frac{R(\zeta)}{\omega'(\zeta)}\,\varphi'(\zeta) + \sum_{k=1}^{n}\frac{\overline{K}_k}{\zeta^k} + \sum_{k=0}^{n-2} L_k\zeta^k + \sum_1^n \frac{\bar{b}_k}{\zeta^k}\sum_{n+1}^{\infty}\zeta^n k a_k \zeta^{k-n-1} + \bar{b}_0\,\varphi'(\zeta)$$

or

$$-\frac{\bar{\omega}\left(\frac{1}{\zeta}\right)}{\omega'(\zeta)}\,\varphi'(\zeta) + \sum_1^n \frac{\overline{K}_k}{\zeta^k}$$

$$= -\frac{R(\zeta)}{\omega'(\zeta)}\,\varphi'(\zeta) - \sum_0^{n-2} L_k\zeta^k - \sum_1^n \bar{b}_k\zeta^{n-k}\sum_{n+1}^{\infty} k a_k \zeta^{k-n-1} - \bar{b}_0\varphi'(\zeta)$$

which is regular, since $\omega'(\zeta)$ cannot vanish inside the region which it maps conformally onto the unit circle. Therefore it is seen from Equation [23] that $\psi(\zeta)$ is regular.

Replacing in Equation [42] the corresponding terms on the left-hand side of the last expression by those on the right-hand side, one finds the earlier-mentioned alternative expression for the function $\psi(\zeta)$

$$\psi(\zeta) = -\frac{P_2}{2\pi}\log\frac{1+\zeta}{1-\zeta} - \frac{S\pi}{8}\log(1-\zeta) - \frac{S}{2}\sum_1^{\infty}\frac{\zeta^k}{k^2}$$

$$-\frac{2S}{\pi}\sum_1^{\infty}\left[\frac{\zeta^{4k-2}}{(4k-2)^2} + \frac{\zeta^{4k-1}}{(4k-1)^2}\right] - \frac{R(\zeta)}{\omega'(\zeta)}\,\varphi'(\zeta)$$

$$-\sum_0^{15} L_k\zeta^k - \sum_1^{17} b_j\zeta^{17-j}\left\{\frac{P_2\zeta}{\pi(1-\zeta^2)} - \frac{S\pi}{8(1-\zeta)}\right.$$

$$\left. -\frac{S}{2}\sum_1^{\infty}\frac{\zeta^{k-1}}{k+17} + \frac{2S}{\pi}\sum_0^{\infty}\left[\frac{\zeta^{4k}}{(18+4k)^2} + \frac{\zeta^{4k+2}}{(21+4k)^2}\right]\right\}$$

where

$$R(\zeta) = 0.2580\zeta^{13} + 0.3147\zeta^{11} + 0.3848\zeta^7 + 0.5126\zeta^3$$

and the $L_k$ are given in Table 1.

The advantage of this expression for $\psi(\zeta)$ arises from the fact that for small values of $\zeta$ numerical calculations are not complicated by loss of significant figures.

# Bending of Pretwisted Beams[1]

By J. ZICKEL,[2] SCHENECTADY, N. Y.

**The general theory of pretwisted beams and columns[3,4] is applied to the bending of an initially straight and uniformly pretwisted beam of doubly symmetric thin-walled section. Pretwisting brings planes of various bending stiffness into play with a resulting stiffness which in a sense averages the stiffness of the beam in its principal directions. It is shown that compared with bending of an untwisted beam in its most flexible direction a thin strip can have its deflection in the plane of bending reduced 72 per cent by an initial twist of $0.83\pi$. Simultaneously, however, lateral deflections of almost equal magnitude are induced. For pretwists above $2\pi$, the lateral deflections become practically negligible and the deflections in the plane of bending are still reduced as much as 44 per cent. With increasing initial twist, however, the pretwisted beam becomes more flexible, and for an initial twist of $6.5\pi$ it is as flexible as the untwisted beam in its most flexible direction. Beams of equal flexibility in all directions simply become more flexible with initial twist, a fact which corresponds to the observations made by Den Hartog[5] in some of his experiments.**

## General Concepts and Description of Results

IF a beam, which is very flexible when bent in one plane but quite stiff in the perpendicular plane, is loaded so that the plane of bending is the stiffer plane, it will buckle in the flexible direction. In general, the resulting deflection for such a beam, no matter what the plane of the moments, will strongly favor the flexible direction. The effect of pretwisting the beam appreciably means that there will not be a more flexible plane or a stiffer one. However, a weakening effect due to twist is introduced simultaneously. Den Hartog[5] points out the interesting fact that a pretwisted beam with equal bending stiffness in all directions shows considerably larger deflections than the same beam without the initial twist and challenges the reader to offer an explanation.

In his "Theory of Naturally Curved Rods," Love[6] describes the configuration of the rod by means of three co-ordinate systems. The same method is used for the pretwisted beam, Fig. 1. The $x_0$, $y_0$, $z_0$-system, which is the fixed co-ordinate system, locates the beam in space. The $x$, $y$, $z$-system is the system referred to the pretwisted, but unstressed, beam. At any cross section the $x$ and $y$-axes are directed along the principal axes of the cross section and the $z$-axis is tangent to the beam axis or center line.

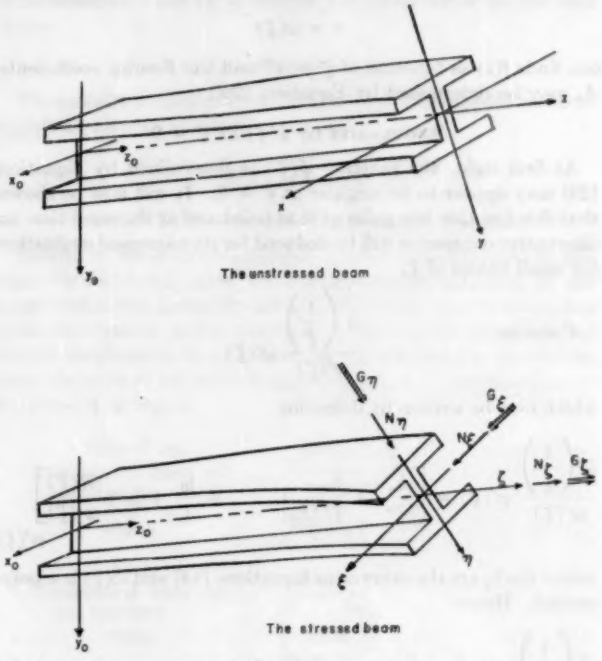


Fig. 1 Pretwisted Beam With Its Co-Ordinate Systems

Finally, the $\xi$, $\eta$, $\zeta$-system is the system of the stressed beam where $\xi$ and $\eta$ are the co-ordinates along the principal axes of any cross section and $\zeta$ is tangent to the center line $l$.

The normal stresses in the beam are considered to be in the direction of the fibers and shear stresses to be perpendicular to the fibers.[3] After linearization, the expression for the fiber stress contains five components resulting from compression, bending about each of the principal axes, warping of the cross section, and interaction of initial and additional twist. The shear stresses are those of the Saint Venant theory of torsion and those which are developed as a result of the variation of fiber stress along the length of the beam. Stress resultants are obtained by integrating the derived stresses over the cross-sectional area. The stress-couples are found by a similar integration, using appropriate moment arms. They in turn must be in equilibrium with the applied external moments. To simplify the analysis the beam is supposed initially straight, initially twisted at a uniform rate $\delta_0'$, and the pair of equal and opposite moments is assumed to act in the $y_0$, $z_0$-plane. The extension to bending moments acting in any other plane presents no difficulties.

Equations [6$a$], [6$b$], [6$c$][7] are reduced in complexity by transformation from the relative displacements $u$ and $v$ along the $\xi$, $\eta$-axes to absolute displacements $U$ and $V$ along the $x_0$, $y_0$-axes.

[7] These equations appear in the next section.

---

[1] The results presented in this paper were obtained in the course of research sponsored by the Office of Naval Research under Contract N7onr-358 with Brown University.

[2] Engineer, General Electric Company. Formerly Research Associate, Graduate Division of Applied Mathematics, Brown University.

[3] "General Theory of Pretwisted Beams and Columns," by J. Zickel, Report All-73, Graduate Division of Applied Mathematics, Brown University, June, 1952.

[4] The author is indebted to the Column Research Council and the Rhode Island Department of Public Works for sponsoring part of this work.

[5] "Advanced Strength of Materials," by J. P. Den Hartog, McGraw-Hill Book Company, Inc., New York, N. Y., 1952, p. 319.

[6] "A Treatise on the Mathematical Theory of Elasticity," by A. E. H. Love, Dover Publications, New York, N. Y., chapter 21, 1944.

Contributed by the Applied Mechanics Division and presented at the Diamond Jubilee Spring Meeting, Baltimore, Md., April 18–21, 1955, of The American Society of Mechanical Engineers.

Discussion of this paper should be addressed to the Secretary, ASME, 29 West 39th Street, New York, N. Y., and will be accepted until October 10, 1955, for publication at a later date. Discussion received after the closing date will be returned.

Note: Statements and opinions advanced in papers are to be understood as individual expressions of their authors and not those of the Society. Manuscript received by ASME Applied Mechanics Division, June 11, 1954. Paper No 55—S-2.

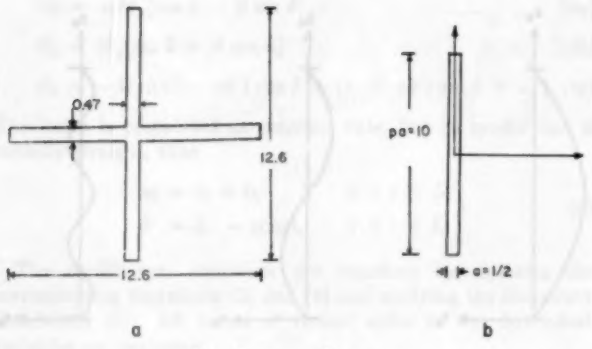


FIG. 2 CROSS SECTIONS

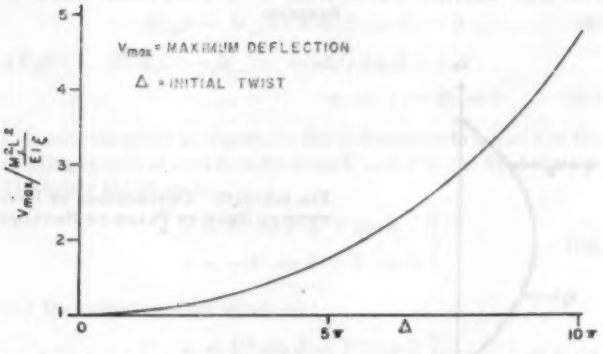


FIG. 3 RELATIVE MAXIMUM DEFLECTION OF PRETWISTED BEAM WITH CRUCIFORM SECTION

The additional twist $\beta$ remains unchanged. It is assumed that the beam is supported so that no displacements will be possible at either end and rotation is prevented at one end. The moments are assumed applied in such a manner that no warping stress exists at the ends.

A beam of cruciform section with equal moments of inertia in all directions, Fig. 2(*a*), is discussed first because it is the simplest case and yet furnishes an insight into the behavior of pretwisted beams in bending. The cruciform cross section not only has equal moments of inertia in all directions but it also has equal modified moments of inertia. The word "modified" indicates an effective value based upon considerations of the initial twist. When there is no initial twist, the modified moment of inertia is identical with the usual moment of inertia.

The twist causes an inclination of the fibers to the axis or center line which increases with the radial distance from the center line. Not only does this inclination have the effect of producing a smaller strain for a given curvature but in addition, the fiber stress is concentrated more toward the center than in the usual untwisted beam. The resisting moment is thus decreased considerably for a given curvature. At the same time, the resistance to torsion is increased with increasing pretwist.

The pretwisted beam of cruciform cross section deflects only in the plane of the applied bending moments and it does not twist any further. The deflection, which is given by Equation [12], is a function of the modified moment of inertia, just as the deflection of the untwisted beam is a function of the ordinary moment of inertia. Fig. 3 shows the ratio of the maximum deflection of the pretwisted beam and the untwisted beam, which is called the relative maximum deflection of the pretwisted beam, for a beam with the cross-sectional dimensions of Fig. 2(*a*). Although there is hardly any weakening noticeable for initial twists up to $\pi/2$, it becomes very apparent for larger pretwists. If a beam with an initial twist of $10\pi$ were perfectly elastic then it would deflect 4.7 times as much as an untwisted beam.

The cruciform section, and any cross section with a third axis of symmetry at 45 deg to the principal axes, has equal modified moments of inertia in any direction. This property permits an explicit solution for the deflection. A beam of any other doubly symmetric cross section, however, has unequal modified principal moments of inertia. As a consequence the deflections can best be obtained by successive approximations.

The greatest advantage of intial twist should be expected from a beam which has one plane far more flexible than the perpendicular plane. The example chosen for illustration is a thin strip with a ratio of principal moments of inertia of 400:1, Fig. 2(*b*).

For purposes of comparison, the maximum deflections, assuming perfect elasticity, were nondimensionalized by division by the maximum deflection that the same beam, but untwisted, would experience if it were bent in its most flexible plane. This quantity which again has been called the relative maximum deflection is shown in Fig. 4. Depending on the orientation of the beam at the end at which rotation about the beam axis is prevented, it be-

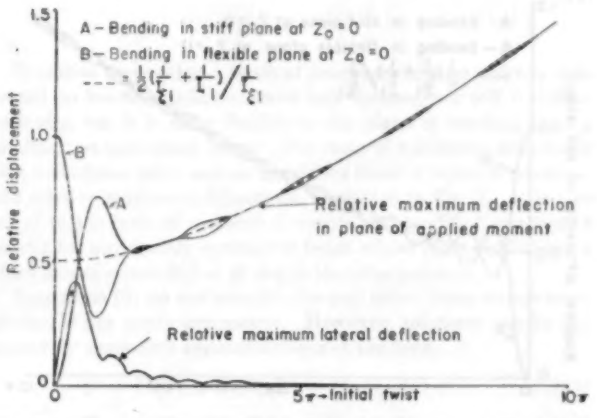


FIG. 4 RELATIVE MAXIMUM DISPLACEMENTS OF PRETWISTED BEAM IN BENDING

comes more flexible (curve A) or stiffer (curve B) for initial twists up to $0.83\pi$. For pretwists of $1.5\pi$ and greater the initial orientation becomes quite unimportant. It is, however, recognizable for pretwists which are close to being odd integer mutiples of $\pi$. Of course, for pretwists of $0.5\pi$, $1.5\pi$, $2.5\pi$, etc., the deflections are necessarily independent of the orientation. In addition to the deflection in the plane of the applied moments, there is a lateral deflection which increases for initial twists up to $0.4\pi$ and then decreases gradually; for initial twists above $2\pi$ it is extremely small.

Thus it is found that pretwisting a beam which is bent by a pair of moments can stiffen it so that it will deflect as little as 28 per cent of what the same beam, when untwisted, will deflect. However, lateral deflections are induced, which may offset any gain that has been derived. A decided advantage is obtained for initial twists between $2\pi$ and $6.5\pi$, but for higher pretwists the beam becomes more flexible than the untwisted beam. This flexibility which has been explained previously for the cruciform section is due to the inclination of the fibers which increases with radial distance from the center line. The modified moments of inertia express this effect in the form of an equivalent moment of inertia for pretwisted beams. Its reciprocal is equal to the average of the reciprocals of the principal modified moments of inertias

$$\frac{1}{I} = \frac{1}{2}\left(\frac{1}{I_{\xi_1}} + \frac{1}{I_{\eta_1}}\right) \quad \ldots\ldots [1]$$

If the smallest moment of inertia is divided by the equivalent moment of inertia of a beam, a curve is obtained which is identical with the average relative maximum deflection, Fig. 4. This curve is a close approximation to the flexibility of a pretwisted beam for initial twists of $1.5\pi$ and greater.

The flexibility of a beam in bending is frequently discussed in terms of difference of slopes at the ends. When these values for a pretwisted beam are divided by the difference of slopes for a similar, but untwisted, beam (which is bent in its most flexible plane), then the relative difference of end slopes is obtained, Fig. 5. A beam with an initial twist of $0.72\pi$ is stiffened most to a relative difference of end slopes of 0.40. In this type of comparison the flexibility of pretwisted beams is independent of orientation for initial twists which are multiples of $0.5\pi$; however, it is also nearly so for pretwists above $1.5\pi$. The average relative difference of end slopes is identical with the average relative maximum deflection, and for initial twists above $1.5\pi$ it is a good

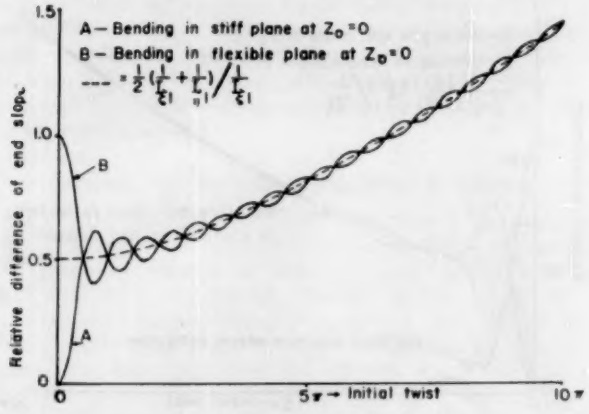


FIG. 5 RELATIVE DIFFERENCE OF END SLOPES FOR PRETWISTED BEAM IN BENDING

approximation to the actual flexibility. Except for initial twists up to $1.5\pi$, which also induce relatively large lateral deflections, the flexibility of a pretwisted beam is equal to that of an untwisted beam with a moment of inertia as given by Equation [1].

It is interesting to note the actual deflections of a pretwisted beam in bending. In the plane of bending the projection of the beam is predominantly circular, as for any beam in pure bending. Superimposed on this major deflection are curves of the form

$$V_{II} = C_2 \sin 2\Delta \quad \ldots\ldots [2a]$$

as shown in Fig. 6(*b*), though greatly magnified. Except for very small initial twist, the superimposed curve is of negligible amplitude and need not be considered.

The lateral deflections and the additional twist are of the same form but the magnitude of the twist is so small that it can be neglected. The form of the lateral deflection is shown in Fig. 6(*a*). If the initial twist is an integral multiple of $0.5\pi$, then the projection is a sine wave, such as

$$U = e_1 \sin 2\Delta \quad \ldots\ldots [2b]$$

For intermediate values of pretwist the loops are pulled out of their symmetric shape, but the general pattern of the projection is still the same.

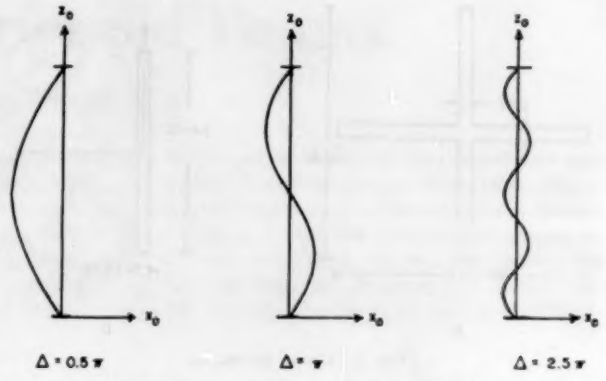


FIG. 6(*a*) LATERAL DEFLECTIONS OF A PRETWISTED BEAM IN BENDING

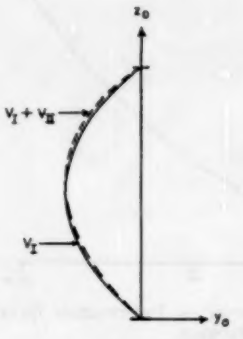


FIG. 6(*b*) (*left*) DEFLECTIONS OF PRETWISTED BEAM IN PLANE OF BENDING

## MATHEMATICAL DERIVATION

In the "General Theory of Pretwisted Beams and Columns,"[3] three equations were developed for the stress-couples of pretwisted beam-columns of doubly symmetric section. These equations are

$$\left.\begin{aligned} G_\xi = {} & (EI_{\xi_1} + 4N_\xi\bar{\eta}^4\delta'^2)c + 2N_\xi\bar{\eta}^4\delta'^2cc_0 \\ & - 4E\Phi_2\delta'^2\beta''k - 4E\Gamma_6\bar{\eta}^4\delta'^2\beta'''c_0 \\ & + E(\Gamma_6\bar{\eta}^4\delta'^4\delta'')\beta''c_0 - 2E(\Phi_2 + 2\Gamma_6\bar{\eta}^2\delta'^2\delta'')\delta'^2\beta''k_0 \\ & + 2(EI_{\xi_1}\delta'^2 + GI_{\xi_1} - 2EI_{\xi_1}\bar{\beta}^2\delta'^2 + 4G\bar{C}\,\bar{\eta}^4\delta'^2)\delta'\beta'c_0 \end{aligned}\right\} \quad [3a]$$

$$\left.\begin{aligned} G_\eta = {} & (EI_{\eta_1} + 4N_\xi\bar{\xi}^4\delta'^2)k + 2N_\xi\bar{\xi}^4\delta'^2k_0 \\ & - 4E\Phi_2\delta'^2\beta''c + 4E\Gamma_6\bar{\xi}^4\delta'^2\beta'''k_0 \\ & + E(\Gamma_6\bar{\xi}^4\delta'^4\delta'')\beta''k_0 - 2E(\Phi_2 + 2\Gamma_6\bar{\xi}^2\delta'^2\delta'')\delta'^2\beta''c_0 \\ & + (2EI_{\eta_1}\delta'^2 + GI_{\eta_1} - 2EI_{\eta_1}\bar{\beta}^2\delta'^2 + 4G\bar{C}\bar{\xi}^4\delta'^2)\delta'\beta'k_0 \end{aligned}\right\} \quad [3b]$$

$$\left.\begin{aligned} G_\zeta = {} & -E\bar{\Gamma}_1\beta''' + E\bar{\Gamma}_2\delta'\delta''\beta'' + (G\bar{C}A_1 + N_\xi\bar{\beta}^2A_2)\beta' \\ & -E\delta'(I_{\xi_1} + 2I_{\xi_1}\bar{\beta}^2\delta'^2 - I_{\xi_1}\delta'^2)(c^2 + cc_0) \\ & - E\delta'(I_{\eta_1} + 2I_{\eta_1}\bar{\beta}^2\delta'^2 - I_{\eta_1}\delta'^2)(k^2 + kk_0) + N_\xi\bar{\beta}^2\delta' \end{aligned}\right\} \quad [3c]$$

As a bending moment only is applied at the ends, the external forces

$$X = Y = Z = 0$$

and the external moments

$$M_y = M_z = 0$$

These conditions determine the stress-resultant

$$N_\zeta = 0$$

and the stress-couples

$$G_\xi = -M_x(\cos\delta - \beta\sin\delta) \quad [4a]$$

$$G_\eta = M_x(\sin\delta + \beta\cos\delta) \quad [4b]$$

$$G_\zeta = -M_x[(u' - v\delta')\cos\delta - (v' + u\delta')\sin\delta + u_0'] \quad [4c]$$

The beam is pretwisted at constant rate, but its center line is initially straight, thus

$$\left.\begin{aligned} u_0 = v_0 = 0, \quad & 0 \le l \le L \\ \delta' = \delta_0' = \text{const}, \quad & 0 \le l \le L \end{aligned}\right\} \quad [5]$$

The equilibrium equations are obtained by equating the corresponding Equations [3] and [4] and applying the Boundary Conditions [5]. All terms of second order in the dependent variables are neglected

$$EI_{\xi_1}c + M_x(\cos\delta - \beta\sin\delta) = 0 \quad [6a]$$

$$EI_{\eta_1}k - M_x(\sin\delta + \beta\cos\delta) = 0 \quad [6b]$$

$$E\bar{\Gamma}_1\beta''' - G\bar{C}A_1\beta' - M_x[(u' - v\delta_0')\cos\delta - (v' + u\delta_0')\sin\delta] = 0 \quad [6c]$$

It is advantageous to transform the displacements $u$ and $v$ in the rotating system of axes to deflections $U$ and $V$ in the fixed system. The latter are given by

$$\left.\begin{aligned} u &= U\cos\delta + V\sin\delta \\ v &= -U\sin\delta + V\cos\delta \end{aligned}\right\} \quad [7a]$$

and the curvatures are given by

$$\left.\begin{aligned} c &= U''\sin\delta - V''\cos\delta \\ k &= U''\cos\delta + V''\sin\delta \end{aligned}\right\} \quad [7b]$$

If Equations [6] are divided by their respective leading coefficients and Expressions [7a] and [7b] are substituted for the displacements and curvatures, then the equilibrium equations become

$$U''\sin\delta - V''\cos\delta - B_1\beta\sin\delta = -B_1\cos\delta \quad [8a]$$

$$U''\cos\delta + V''\sin\delta - B_2\beta\cos\delta = B_2\sin\delta \quad [8b]$$

$$\beta''' - B_3^2\beta' - B_4U' = 0 \quad [8c]$$

with

$$B_1 = M_x/EI_{\xi_1}$$
$$B_2 = M_x/EI_{\eta_1}$$
$$B_3 = \sqrt{G\bar{C}A_1/E\bar{\Gamma}_1}$$
$$B_4 = M_x/E\bar{\Gamma}_1$$

The separation of variables $U$ and $V$ in Equations [8a] and [8b] results in the following equations

$$U'' - \beta(B_6 + B_5\cos 2\delta) = B_5\sin 2\delta \quad [9a]$$

$$V'' - \beta B_5\sin 2\delta = B_6 - B_5\cos 2\delta \quad [9b]$$

Equations [8c] and [9a] can be solved for $U$ and $\beta$. Subsequently, the solution for $\beta$ can be substituted in Equation [9b], leading to a solution for $V$. To simplify the writing of the equations, the following notation is used

$$B_5 = \frac{1}{2}(B_2 - B_1) \qquad B_6 = \frac{1}{2}(B_1 + B_2)$$

For a beam of cruciform cross section these equations simplify appreciably, yet remain significant enough to give an insight into the behavior of pretwisted beams in bending. The simplification is due to the equal modified moments of inertia and the dropping out of the Wagner constant $\Gamma$. As a consequence

$$B_5 = 0 \quad B_6 = B_1 \quad \bar{\Gamma}_1 = 0$$

Thus Equations [9] and [8c] become

$$U'' - B_1\beta = 0 \quad [10a] \qquad V'' = B_1 \quad [10b]$$

$$\beta' + B_7U' = 0 \quad [10c]$$

with

$$B_7 = M_x/G\bar{C}A$$

The beam is simply supported, the moments are applied so that no warping stresses exist at the ends, and to eliminate rigid body motion, additional twisting is prevented at one end

$$\left.\begin{aligned} U &= 0 \\ V &= 0 \\ \beta &= 0 \\ \beta'' &= 0 \end{aligned}\right\} \text{ at } l = 0 \qquad \left.\begin{aligned} U &= 0 \\ V &= 0 \\ \beta'' &= 0 \end{aligned}\right\} \text{ at } l = L \quad [11]$$

Under these conditions the solutions to Equations [10] are

$$\left.\begin{aligned} V &= \frac{1}{2}R_1l(l - L) \\ U &= \beta = 0 \end{aligned}\right\} \quad [12]$$

It is thus shown that a beam of cruciform section which is subjected to bending will not twist any further, nor will it deflect laterally, but it is more flexible in the plane of bending than a similar, but untwisted, beam. The ratio of maximum deflections of a pretwisted beam and an untwisted beam of equal dimensions, the relative maximum deflections, is plotted in Fig. 3. It is also equal to the ratio of moment of inertia and modified moment of inertia for any doubly symmetric beam whose cross section has a third axis of symmetry at 45 deg to the principal axes.

Equations [9] do not simplify for any other beam whose cross section is not triply symmetric. However, solutions can be obtained by successive approximations of the form

$$U = U_I(l) + U_{II}(l, \beta_I) + U_{III}(l, \beta_{II}) + \cdots \quad [13]$$

$$V = V_I(l) + V_{II}(l,\beta_I) + V_{III}(l, \beta_{II}) + \cdots \quad [14]$$

$$\beta = \beta_I(l,U_I) + \beta_{II}(l,U_{II}) + \cdots \quad [15]$$

and application of the Boundary Conditions [11].

For the first approximation, Equations [9a] and [9b] become

$$U'' = B_5\sin 2\delta$$
$$V''_I = B_6 - B_5\cos 2\delta$$

Their solutions are

$$U_I = \frac{P_5}{4\delta_0'^2}\left(\frac{l}{L}\sin 2\Delta - \sin 2\delta\right) \quad [13a]$$

$$V_I = \frac{1}{2}B_6l(l - L) + \frac{B_5}{4\delta_0'^2}\left(\cos 2\delta - 1 - \frac{l}{L}\cos 2\Delta + \frac{l}{L}\right) \quad [14a]$$

Applying the same process to Equation [8c] results in

$$\beta_I''' - B_3^2\beta_I' = B_4U_I'$$

The first approximation to the additional twist, when $U_I'$ is substituted in the foregoing equation, becomes

$$\beta_I = B_5\left[B_3^2\sin 2\delta + \left(4\delta_0'^2\frac{\sinh B_3l}{\sinh B_3L} - 4\delta_0'^2\frac{l}{L} - B_3^2\frac{l}{L}\right)\sin 2\Delta\right] \quad [15a]$$

The first approximations to $U$ and $V$ satisfy the nonhomogeneous parts of Equations [9a] and [9b], and subsequent approximations need only satisfy the homogeneous part of these equations. For the second approximation they become

$$U_{II}'' = \beta_I(B_6 + B_5 \cos 2\delta)$$
$$V'' = \beta_I B_5 \sin 2\delta$$

The second terms of the solutions are

$$U_{II} = B_{11}l(L^2 - l^2) + \left(8B_6B_9 - \frac{B_{10}}{\delta_0'}\right)\left(\sin 2\delta - \frac{l}{L}\sin 2\Delta\right) + B_5B_9\left(\sin 4\delta - \frac{l}{L}\sin 4\Delta\right) + B_{10}l\,(\cos 2\delta - \cos 2\Delta) + B_{11}\left(\sinh B_3l - \frac{l}{L}\sinh B_3L\right) + B_{12}\left(\sinh B_3l\cos 2\delta - \frac{l}{L}\sinh B_3L\cos 2\Delta\right) + B_{14}\left(\cosh B_3l\sin 2\delta - \frac{l}{L}\cosh B_3L\sin 2\Delta\right) \quad . [13b]$$

$$V_{II} = 8B_5B_9\delta_0'^2l(L - l) + \frac{B_{10}}{\delta_0'}\left(\cos 2\delta - 1 - \frac{l}{L}\cos 2\Delta + \frac{l}{L}\right) - B_5B_9\left(\cos 4\delta - 1 - \frac{l}{L}\cos 4\Delta + \frac{l}{L}\right) + B_{10}l\,(\sin 2\delta - \sin 2\Delta) + B_{13}\left(\sinh B_3l\sin 2\delta - \frac{l}{L}\sinh B_3L\sin 2\Delta\right) - B_{14}\left(\cosh B_3l\cos 2\delta - \frac{l}{L}\cosh B_3L\cos 2\Delta\right) \quad . [14b]$$

Again applying the same process to Equation [8c] results in

$$\beta_{II}''' - B_2\beta_{II}' = B_4U_{II}$$

When Solution [13b] is substituted in the foregoing equation, then the second term of the solution for $\beta_{II}$ is of order

$$\beta_{II} = 0\left[\frac{B_4B_{11}}{4\delta_0'^2(4\delta_0'^2 + B_2^2)}\right]$$

In general, $\beta_{II}$ is negligible in comparison with $\beta_I$.

The evaluation of the integrals for the cruciform section and the thin strip of Fig. 2 have already been developed in the supplement of "Buckling of Pretwisted Columns"[8] by the author. The constants $B_9$, $B_{10}$, $B_{11}$, $B_{12}$, $B_{13}$, and $B_{14}$, which were used to simplify the expressions, are listed in that reference.[9] Figs. 3 and 4 are the curves which were obtained from Solutions [12], [13], and [14]. For very small values of initial twist per unit length, however, the Solutions [13] and [14] do not give satisfactory results. Solutions in the form of power series of twist per unit length are more appropriate for this case

$$U = \sum_{n=0}^{\infty} U_n\delta_0'^n \quad [16]$$

$$V = \sum_{n=0}^{\infty} V_n\delta_0'^n \quad [17]$$

$$\beta = \sum_{n=0}^{\infty} \beta_n\delta_0'^n \quad [18]$$

By expanding the trigonometric terms, Equations [9] and [8c] are expressed in powers of $\delta_0'$. The coefficients for Solutions [16], [17], and [18] are then obtained by equating terms of equal power in $\delta_0'$, e.g.

$$U_0 = 0 \quad [16a]$$

$$V_0 = \frac{1}{2}B_3l(l - L) \quad [17a]$$

$$\beta_0 = 0 \quad [18a]$$

$$U_1 = B_5\left[\frac{1}{B_{13}^2}\left(l - \frac{L\sin B_{13}l}{\sin B_{13}L}\right) + \frac{B_{13}^2L}{B_3^4}\,\frac{\sinh B_3l}{\sinh B_3L}\right] \quad [16b]$$

$$V_1 = 0 \quad [17b]$$

$$\beta_1 = \frac{B_5}{B_2}\left[\frac{L\sin B_{13}l}{\sin B_{13}L} + \frac{B_{13}^2L}{B_3^2}\,\frac{\sinh B_3l}{\sinh B_3L} - l\right] \quad [18b]$$

$$U_2 = 0 \quad [16c]$$

$$V_2 = B_{17}l(l^2 - L^2) + B_{15}\left[\operatorname{csch} B_3L\left(l\sinh B_3l - l\sinh B_3L + \frac{2}{B_3} - \frac{2l}{B_3L} - \frac{2}{B_3}\cosh B_3l + \frac{2l}{B_3L}\cosh B_3L\right) + \operatorname{csc} B_{13}L\left(l\sin B_{13}L - l\sin B_{13}l + \frac{2}{B_{13}} - \frac{2l}{B_{13}L} - \frac{2}{B_{13}}\cos B_{13}l + \frac{2l}{B_{13}L}\cos B_{13}L\right)\right] \quad . [17c]$$

$$\beta_2 = 0 \quad [18c]$$

The number of terms that are necessary for the desired accuracy of Solutions [16], [17], and [18] depends on the number of terms that are required in the expansion of the trigonometric functions of the initial twist.

The difference of end slopes can be obtained from Solution [14] by differentiation and integration over the length of the beam

$$\text{DES} = \int_0^L V'dl \quad [19]$$

When this difference of end slopes is divided by the difference of end slopes of an untwisted beam, then the relative difference of end slopes results (Fig. 5).

## Conclusion

Pretwisting a beam of thin-walled section has two effects. The obvious one is that flexible and stiff axes of bending are distributed continuously in many or all directions so that the properties of the beam may be almost equalized for all planes of bending. A necessary and probably undesirable accompaniment is an increase in flexibility caused by the inclination of the fibers.

## Acknowledgment

The author is indebted to Dr. D. C. Drucker, Professor of Engineering, Brown University, for his advice and criticism given during the preparation of this paper

[8] "Buckling of Pretwisted Columns," by J. Zickel, Report All-74, Graduate Division of Applied Mathematics, Brown University, Providence, R. I., June, 1952.

[9] Ibid., pp. 22–23.

# Stress Distributions in Orthotropic Strips

By H. D. CONWAY,[1] ITHACA, N. Y.

**The distribution of stress in orthotropic strips stretched by equal and opposite concentrated loads acting centrally and parallel to the longer sides is discussed. Numerical results are given for oak, the grain being, respectively, perpendicular and parallel to the longer sides of the strip.**

## Introduction

THE isotropic version of the infinite-strip problem shown diagrammatically in Fig. 1(*a*) has been discussed by Howland (1)[2] and Girkmann (2), who obtained distributions of the $\sigma_x$ stresses for the cross sections at various distances from the load. The solution for the practical problem shown in Fig. 1(*b*)

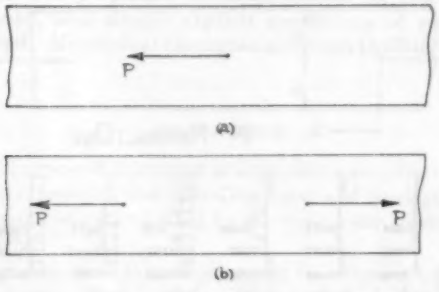


FIG. 1

is obtained by the principle of superposition, it being assumed that the distance between the forces $P$ is at least sufficiently large for a uniform tensile stress to be induced on the cross section midway between the forces. Since the load distribution is probably as far removed from being uniformly distributed as is possible, the solution throws some light on the problem of finding the shortest distance from the applied load before, by the principle of Saint Venant, the stress is constant at all points on the cross section.

The object of the present paper is to treat the corresponding orthotropic version of the problem in Fig. 1(*b*), one of the principal axes of orthotropy corresponding to the direction of the infinite sides of the strip. Green (3) has discussed the general problem of the orthotropic strip but, in so far as the author is aware, no numerical results are available on the subject.

## Analysis

Problems of the type to be considered involve the solution of the equation

$$\left(\frac{\partial^2}{\partial x^2} + \alpha_1^2 \frac{\partial^2}{\partial y^2}\right)\left(\frac{\partial^2}{\partial x^2} + \alpha_2^2 \frac{\partial^2}{\partial y^2}\right)\phi = 0 \quad \ldots\ldots [1]$$

subject to the boundary conditions, the stresses being given by the equations

$$\sigma_x = \frac{\partial^2\phi}{\partial y^2},\ \sigma_y = \frac{\partial^2\phi}{\partial x^2},\ \tau_{xy} = -\frac{\partial^2\phi}{\partial x \partial y} \quad \ldots\ldots [2]$$

The constants $\alpha_1$ and $\alpha_2$ are given by the equations

$$\alpha_1^2\alpha_2^2 = S_{11}/S_{22},\ \alpha_1^2 + \alpha_2^2 = (S_{66} + 2S_{12})/S_{22} \quad \ldots\ldots [3]$$

where the moduli are defined by the stress-strain equations

$$\left.\begin{aligned} \epsilon_x &= S_{11}\sigma_x + S_{12}\sigma_y \\ \epsilon_y &= S_{12}\sigma_x + S_{22}\sigma_y \\ \gamma_{xy} &= S_{66}\tau_{xy} \end{aligned}\right\} \quad \ldots\ldots [4]$$

it being assumed that the $x$, $y$-directions correspond to those of the principal axes of orthotropy.

The problem of a concentrated load $P$ acting at a point in an infinite plate of thickness $h$ and parallel to one of the principal axes of orthotropy is first considered. Use is made of a stress function in the Fourier integral form

$$\phi' = \int_0^\infty \frac{1}{\beta^2}(A'e^{-\beta y/\alpha_1} + B'e^{-\beta y/\alpha_2}) \sin \beta x d\beta \quad \ldots\ldots [5]$$

and the procedure is as given in a recent paper (4). Assuming initially that the direction of the load corresponds to the direction in which $S_{11}$ is measured, it is found that

$$\left.\begin{aligned} A' &= \frac{P}{2\pi h}\,\frac{\alpha_1\alpha_2^2 S_{22} - \alpha_1 S_{12}}{(\alpha_2^2 - \alpha_1^2)S_{22}} \\ B' &= \frac{-P}{2\pi h}\,\frac{\alpha_1^2\alpha_2 S_{22} - \alpha_2 S_{12}}{(\alpha_2^2 - \alpha_1^2)S_{22}} \end{aligned}\right\} \quad \ldots\ldots [6]$$

and, in particular

$$\sigma_x' = \frac{Px}{2\pi h(\alpha_2^2 - \alpha_1^2)S_{22}}\left[\frac{\alpha_1(\alpha_2^2 S_{22} - S_{12})}{\alpha_1^2 x^2 + y^2} - \frac{\alpha_2(\alpha_1^2 S_{22} - S_{12})}{\alpha_2^2 x^2 + y^2}\right] \quad \ldots\ldots [7]$$

In order to nullify the $\sigma_y$ and $\tau_{xy}$ stresses left by the foregoing stress function on the boundaries $y = \pm b$, use is made of a second stress function

$$\phi'' = \int_0^\infty \frac{1}{\beta^2}(A'' \cosh \beta y/\alpha_1 + B'' \cosh \beta y/\alpha_2) \sin \beta x d\beta \quad \ldots [8]$$

and writing

$$\sigma_y' + \sigma_y'' = 0,\quad \tau_{xy}' + \tau_{xy}'' = 0,\quad y = \pm b \quad \ldots\ldots [9]$$

we obtain

---

[1] Professor of Mechanics, Cornell University. Assoc. Mem. ASME.

[2] Numbers in parentheses refer to the Bibliography at the end of the paper.

Contributed by the Applied Mechanics Division and presented at the Diamond Jubilee Spring Meeting, Baltimore, Md., April 18–21, 1955, of THE AMERICAN SOCIETY OF MECHANICAL ENGINEERS.

Discussion of this paper should be addressed to the Secretary, ASME, 29 West 39th Street, New York, N. Y., and will be accepted until October 10, 1955, for publication at a later date. Discussion received after the closing date will be returned.

NOTE. Statements and opinions advanced in papers are to be understood as individual expressions of their authors and not those of the Society. Manuscript received by ASME Applied Mechanics Division, July 19, 1954. Paper No. 55—S-1.

$$A''\left[\frac{1}{\alpha_2}\sinh\frac{\beta b}{\alpha_2}\cosh\frac{\beta b}{\alpha_1}-\frac{1}{\alpha_1}\sinh\frac{\beta b}{\alpha_1}\cosh\frac{\beta b}{\alpha_2}\right]$$
$$=\frac{-P}{2\pi h(\alpha_2^2-\alpha_1^2)S_{22}}\left\{e^{-\beta b/\alpha_1}\left[\left(\alpha_1\alpha_2S_{22}-\frac{\alpha_1}{\alpha_2}S_{12}\right)\sinh\frac{\beta b}{\alpha_2}+(\alpha_2^2S_{22}-S_{12})\cosh\frac{\beta b}{\alpha_2}\right]-e^{-\beta b/\alpha_2}\left[(\alpha_1^2S_{22}-S_{12})\sinh\frac{\beta b}{\alpha_2}+(\alpha_1^2S_{22}-S_{12})\cosh\frac{\beta b}{\alpha_2}\right]\right\}$$

$$B''\left[\frac{1}{\alpha_2}\sinh\frac{\beta b}{\alpha_2}\cosh\frac{\beta b}{\alpha_1}-\frac{1}{\alpha_1}\sinh\frac{\beta b}{\alpha_1}\cosh\frac{\beta b}{\alpha_2}\right]$$
$$=\frac{P}{2\pi h(\alpha_2^2-\alpha_1^2)S_{22}}\left\{e^{-\beta b/\alpha_1}\left[(\alpha_2^2S_{22}-S_{12})\sinh\frac{\beta b}{\alpha_1}+(\alpha_2^2S_{22}-S_{12})\cosh\frac{\beta b}{\alpha_1}\right]-e^{-\beta b/\alpha_2}\left[\left(\alpha_1\alpha_2S_{22}-\frac{\alpha_2}{\alpha_1}S_{12}\right)\sinh\frac{\beta b}{\alpha_1}+(\alpha_1^2S_{22}-S_{12})\cosh\frac{\beta b}{\alpha_1}\right]\right\} \quad \ldots [10]$$

The $\sigma_x$ stresses in Fig. 1(*a*) are finally

$$\sigma_x=\sigma_x'+\sigma_x'' \quad \ldots [11]$$

where $\sigma_x'$ is given by Equation [7] and

$$\sigma_x''=\int_0^\infty\left(\frac{A''}{\alpha_1^2}\cosh\frac{\beta y}{\alpha_1}+\frac{B''}{\alpha_2^2}\cosh\frac{\beta y}{\alpha_2}\right)\sin\beta x d\beta \quad \ldots [12]$$

where the constants $A''$ and $B''$ are given by Equations [10]. The problem in Fig. 1(*b*) is then solved by superposition.

The evaluation of the $\sigma_x''$ stresses involves a considerable amount of labor, and was accomplished by evaluating the integrand for various values of $\beta b$ between zero and 6. The integral was then evaluated between these limits by Simpson's rule. Above $\beta b = 6$, the integrand can be written in a much simpler form which enables the integral to be evaluated in closed form between $\beta b = 6$ and infinity.

The elastic constants chosen for the numerical work were those for oak, these having been given by Hörig (5). For the case where the direction of the grain of the wood corresponds to that of the shorter sides of the strip and taking the constants $S_{11}$, $S_{22}$, $S_{12}$, and $S_{66}$ as 0.01015, 0.00172, —0.00087, and 0.0128 sq mm per kg, respectively, $\alpha_1^2$ and $\alpha_2^2$ are found from Equations [3] to be 5.321 and 1.109, respectively. The constants $\alpha_1$ and $\alpha_2$ are replaced by their reciprocals when the direction of the grain is reversed and, in addition, $S_{22}$ is replaced by $S_{11}$.

## Results

Fig. 2 shows the distributions of longitudinal stresses on cross sections at various distances from the loads, calculated by the foregoing method, the loads being, respectively, perpendicular and parallel to the grain of the wood. As previously stated, it is assumed that the distance between the forces is at least sufficiently large to allow a uniform distribution of tensile stress to be induced on the central cross section. It is observed that the variations from the average value of $P/2bh$ in the loaded portion of the strip are much greater when the load is parallel to the grain than when the load is perpendicular to the grain. In the latter case the stresses appear to become very nearly uniformly distributed in a distance from the load equal to the width of the strip. When the loads are parallel to the grain, the value of the integrand in Equation [12] varies rapidly with $\beta b$ in the region $\beta b = 0$ and when the distance $x$ from the load is large. This makes accurate estimates of the stresses difficult to obtain. However, it appears that the stresses become very nearly uniformly distributed in a distance equal to about twice the strip width.

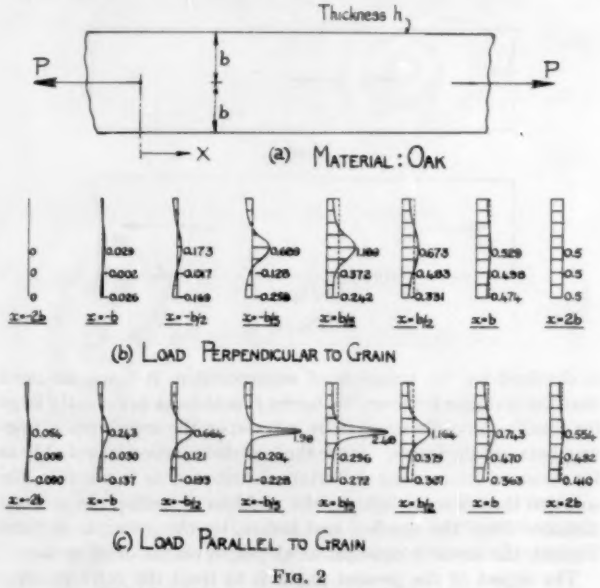


Fig. 2
(Multiply values given by $P/hb$ to obtain stresses.)

## Bibliography

1 "Stress Systems in an Infinite Strip," by R. C. J. Howland, Proceedings of the Royal Society of London, England, series A, vol. 124, 1929, p. 89.

2 "Angriff von Einzellasten in der streifenförmigen Scheibe," by K. Girkmann, *Ingenieur Archiv*, vol. 13, 1943, p. 273.

3 "Stress Systems in Aelotropic Plates—II," by A. E. Green, Proceedings of the Royal Society of London, England, series A, vol. 173, 1939, p. 173.

4 "Some Problems in Orthotropic Plane Stress," by H. D. Conway, Journal of Applied Mechanics, Trans. ASME, vol. 75, 1953, pp. 72–76.

5 "Anwendung, der Elastizitätstheorie anisotroper Körper auf Messungen an Holz," by H. Hörig, *Ingenieur Archiv*, vol. 6, 1935, p. 8.

# Vibrations of a Helicopter Rotor-Fuselage System Induced by the Main Rotor Blades in Flight[1]

By M. MORDUCHOW,[2] S. W. YUAN,[3] AND H. REISSNER,[4] BROOKLYN, N. Y.

**Based on a simplified model of the hub-fuselage structure, a theoretical analysis is made of the response of the hub and fuselage of a helicopter in flight to harmonic forces transmitted by the rotor blades to the hub both in, and normal to, the plane of rotation. The assumed structure is in the form of a plane framework with masses concentrated at the joints. Simple expressions are derived for the vibration amplitudes of the mass points as functions of the masses and natural frequencies of the hub and the fuselage. The pertinent nondimensional parameters are determined, and simple explicit conditions of resonance are derived. Numerical examples are given to illustrate the results.**

## Introduction

THE purpose of this paper is to present a simplified analysis of the response of a helicopter rotor and fuselage to harmonic forces transmitted by the main rotor blades to the hub in flight.

Although considerable work on ground vibrations of helicopters has been accomplished (for example, references 1 and 2),[5] relatively little theoretical research has been performed on the response of rotors to harmonic exciting forces in flight. The chief work, which is fairly recent, along these lines is reference (3), where an analysis is made of the response of helicopter rotors to harmonic blade-forces in the plane of rotation. The method of analysis there is based on the ground-vibration analysis of reference (1).

Since the actual helicopter-rotor structure is complicated, it is necessary, in analyzing theoretically the response of a rotor to harmonic forces, to make certain simplifying assumptions. In particular it is necessary to assume a simplified rotor and fuselage, but, nevertheless, to retain the essentials of the actual structure. For this purpose a particularly simple physical model of the hub-fuselage structure, in the form of a plane framework with masses concentrated at the joints, is assumed in the present analysis. In spite of the simplicity of such a model, it will be seen that it includes most of the essentials of the actual helicopter configuration, such as the mass and elastic characteristics of both the hub and the fuselage.

A further simplification in the present analysis is the approximating assumption that the motion of the hub-fuselage structure does not appreciably affect the forces transmitted by the rotating blades to the hub. Consequently the problem, as it is analyzed here, becomes essentially one of the forced vibrations of an elastic structure induced by given external exciting forces. A detailed theoretical analysis of the harmonic forces transmitted in flight by the rotor blades to the hub in the plane of rotation and normal to this plane has been made in reference (4). It is shown there that the net forces transmitted at the hub by balanced blades will be harmonics which are certain multiples of the rotor angular speed (cf. Equations [2*a*,*b*] and [3] which appear later). A convenient summary of such forces is also given in reference (5).

The analysis in this investigation can be considered an extension of that in reference (3) in the sense that the effect of the fuselage vibrations is now included, while forces and motions normal to, as well as in, the plane of rotation are considered. However, the structural model studied here, and consequently the analysis, is considerably different from that in reference (3), where the Lagrange equations of motion were applied to a system of $(n + 2)$ degrees of freedom (one degree of freedom per blade, in addition to two degrees of freedom of the rotor). In the present analysis, a simple application is made of D'Alembert's principle to the motion of three mass points essentially connected by springs.

## The Simplified Structure

The simplified hub-fuselage structure assumed in the present analysis is shown in Fig. 1. This may be regarded as a symmetrical plane framework with masses concentrated at the joints. The bars connecting the three joints may be assumed as free of bending vibration, so that only longitudinal vibrations occur in the bars; i.e., the bars act only in tension or compression. The mass $m_1$ at joint 1 consists primarily of the total mass of the rotor blades and of the pylon-hub-blade connections. The masses $m_2$ at joints 2 and 3 may each be considered as equal to half of the gross mass of the fuselage. Since only translational motions are thus considered, the mass of the fuselage, rather than its moment of inertia, appears here. As in the case of a helicopter in flight, the structure in Fig. 1 is assumed to be suspended freely in space by the lift on the rotor blades.

The bars *A* and *B*, between points 1 and 2, and 1 and 3, may be interpreted as representing the structure at the hub, while the bar *C* between points 2 and 3 may be regarded as representing the fuselage structure. These three bars can be treated dynamically as springs with elastic moduli $k_A$, $k_B$ $(= k_A)$ and $k_C$, respectively, where $k_A$ represents the elastic resistance of the hub and $k_C$ that

[1] This research was sponsored by the Air Force, Wright Air Development Center, Contract No. AF 18(600)-154.

[2] Associate Professor of Applied Mathematics, Polytechnic Institute of Brooklyn.

[3] Research Professor of Aeronautical Engineering, Polytechnic Institute of Brooklyn.

[4] Professor of Aerodynamics and Aerostructures, Polytechnic Institute of Brooklyn. Mem. ASME.

[5] Numbers in parentheses refer to the Bibliography at the end of the paper.

Contributed by the Applied Mechanics Division and presented at the Diamond Jubilee Spring Meeting, Baltimore, Md., April 18–21, 1955, of The American Society of Mechanical Engineers.

Discussion of this paper should be addressed to the Secretary, ASME, 29 West 39th Street, New York, N. Y., and will be accepted until October 10, 1955, for publication at a later date. Discussion received after the closing date will be returned.

Note: Statements and opinions advanced in papers are to be understood as individual expressions of their authors and not those of the Society. Manuscript received by ASME Applied Mechanics Division, August 10, 1954. Paper No. 55—S-7.

of the fuselage. If the bars are regarded as ordinary structural components of a framework, then, by Hooke's law

$$k_A = E_A S_A / l_A, \quad k_C = E_C S_C / l_C \quad \ldots\ldots [1]$$

where $E$ = modulus of elasticity of material of a bar, $S$ = cross-sectional area, and $l$ = length of a bar. It will be seen subsequently that it is more convenient to replace $k_A$ and $k_C$ by parameters proportional to the natural frequencies of the hub support and of the fuselage.

It is assumed that given external harmonic forces of the form

$$F_x = F_1 \cos \nu\Omega t \quad \ldots\ldots [2a]$$

$$F_z = F_2 \cos \nu\Omega t \quad \ldots\ldots [2b]$$

act at point 1, Fig. 1, in the $z$ and $x$-directions, respectively, where $z$ is normal to the rotor plane of rotation, and $x$ is perpendicular to $z$ and in the plane of the (simplified) structure of hub and fuselage. $F_1$ and $F_2$ are given constants, i.e., independent of time, and are considered as representing the magnitudes of the net forces transmitted by the rotor-blade system to the hub in directions normal to, and in, the plane of rotation, respectively. $\Omega$ denotes the angular speed of the rotor, while $\nu$ is a given number (integer). If the blades are balanced, and only a single harmonic is assumed to be transmitted to the hub, then, as shown in reference (4)

$$\nu = n \quad \ldots\ldots [3]$$

where $n$ is the number of rotor blades.

## Basic Dynamic Equations

The equations of motion for each mass point in Fig. 1 can be derived by applying D'Alembert's theorem of inertia forces, and assuming that each bar exerts a restoring force which acts in the direction of the longitudinal axis of the bar, and which has a magnitude proportional to the elongation and to the spring modulus $k$, of the bar. Let $u_i$ and $v_i$ denote the displacements of the mass point $i$ in the $x$ and $z$-directions, respectively, and let it be assumed that these displacements are sufficiently small so that only first-degree terms in these displacements need be taken into account. Then the elongation ($\Delta l$) of each bar will be

$$\left.\begin{aligned} (\Delta l)_A &= (u_1 - u_2)\cos\theta + (v_1 - v_2)\sin\theta \\ (\Delta l)_B &= (u_3 - u_1)\cos\theta + (v_1 - v_3)\sin\theta \\ (\Delta l)_C &= u_3 - u_2 \end{aligned}\right\} \quad \ldots\ldots [4]$$

where $\theta$ is the structural angle shown in Fig. 1.

The conditions of equilibrium of inertia, elastic, and external forces for each of the three mass points in the $x$ and $z$-directions yield, with the use of Equations [2a], [2b], and [4], the following six linear differential equations in the six unknowns $u_i(t)$, $v_i(t)$ ($i = 1, 2, 3$)

$$-m_1\ddot{u}_1 + k_A[(u_2 - 2u_1 + u_3)\cos\theta + (v_2 - v_3)\sin\theta]\cos\theta + F_1 \cos \nu\Omega t = 0 \quad [5a]$$

$$-m_1\ddot{v}_1 - k_A[(u_3 - u_2)\cos\theta + (2v_1 - v_2 - v_3)\sin\theta]\sin\theta + F_2 \cos \nu\Omega t = 0 \quad [5b]$$

$$-m_2\ddot{u}_2 + k_A[(u_1 - u_2)\cos\theta + (v_1 - v_2)\sin\theta]\cos\theta + k_C(u_3 - u_2) = 0 \quad [5c]$$

$$-m_2\ddot{v}_2 + k_A[(u_1 - u_2)\cos\theta + (v_1 - v_2)\sin\theta]\sin\theta = 0 \quad [5d]$$

$$-m_3\ddot{u}_3 + k_A[(u_1 - u_3)\cos\theta + (v_3 - v_1)\sin\theta]\cos\theta + k_C(u_2 - u_3) = 0 \quad [5e]$$

$$-m_3\ddot{v}_3 + k_A[(u_3 - u_1)\cos\theta + (v_1 - v_3)\sin\theta]\sin\theta = 0 \quad [5f]$$

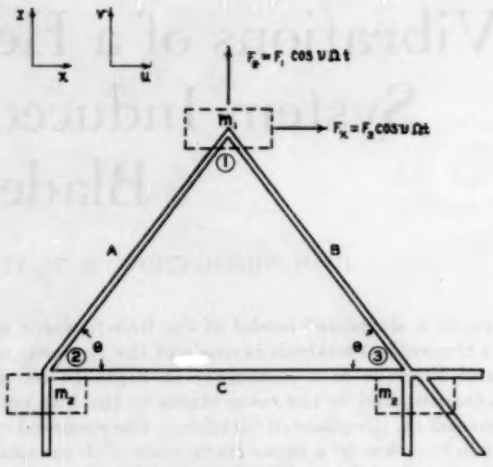


Fig. 1 Simplified Hub-Fuselage Structure

As indicated previously, the hub and fuselage structural properties can be characterized by natural frequencies instead of by the spring moduli, although the natural frequencies are determined by the spring moduli. Such natural frequencies can be obtained by first considering the motion of the hub without the motion of the fuselage. In the simplified structure of Fig. 1 this can be interpreted as letting points 2 and 3 be fixed, while only point 1 is free to move. The natural frequency thus obtained would be that of a structure composed of (massless) springs $A$ and $B$ with ends fixed in a fixed rigid bar $C$, and with a mass $m_1$ at point 1.

An expression for this natural frequency can be derived from Equations [5a] and [5b] by setting $F_1 = F_2 = u_2 = u_3 = v_2 = v_3 = 0$, and noting that the solutions of the two resulting differential equations denote simple harmonic motions with frequencies $\omega_{hu}$ and $\omega_{hv}$, respectively, given by

$$\omega_{hu}^2 = \frac{2k_A \cos^2\theta}{m_1} \quad \ldots\ldots [6a]$$

$$\omega_{hv}^2 = \frac{2k_A \sin^2\theta}{m_1} \quad \ldots\ldots [6b]$$

These frequencies can be interpreted as the natural frequencies of the hub structure for motion in, and normal to, the plane of rotation, respectively. $\omega_{hu}$ and $\omega_{hv}$ can, if desired, also be interpreted simply as reference natural frequencies *defined* by Equations [6a] and [6b]. For $\theta = 45$ deg, which is the case to be worked out in detail in the present analysis, $\omega_{hu} = \omega_{hv} = \omega_h$, say, where

$$\omega_h^2 = \frac{k_A}{m_1} \quad \ldots\ldots [7]$$

An expression for a natural frequency denoting the elastic stiffness of the fuselage (without hub) can be obtained in an analogous fashion. Here, one can consider the motion, in the $x$-direction, of the structure composed of the two masses $m_2$ connected by the (massless) spring of modulus $k_C$. The natural frequency of this system can be derived by setting $k_A = 0$ (i.e., fuselage isolated from hub) in Equations [5c] and [5e], and noting that the simple harmonic solution of these equations then has a frequency $\omega_f$ given by

$$\omega_f^2 = \frac{2k_C}{m_2} \quad \ldots\ldots [8]$$

Thus $k_C$ can be replaced by the physically more significant parameter $\omega_f$, which again may be regarded as either a reference

frequency *defined* by Equation [8], or as the natural frequency of the fuselage structure, unaffected by the hub or pylon connections.

## General Solution of Equations

To obtain the general solution of Equations [5a]–[5f], no significant loss in generality will be incurred if $\theta$ is given a specific value. Consequently, it will now be assumed, for simplicity, that $\theta = 45$ deg. Moreover, it will be convenient to give the solution separately for $F_1 = 0$, and for $F_2 = 0$, since the solution for $F_1$, $F_2 \neq 0$ simultaneously will simply be the sum of these two separate solutions.

Equations [5a]–[5f] can be solved by setting

$$\left.\begin{aligned} u_i &= e_{ist} \cos \nu\Omega t \\ v_i &= e_{ist} \cos \nu\Omega t \\ (i &= 1, 2, 3) \end{aligned}\right\} \quad \ldots\ldots [9]$$

where $e_{ist}$ and $e_{ist}$ are constants. Six linear algebraic equations in the six unknowns $e_{ist}$ and $e_{ist}$ are thus obtained. For $\theta = 45$ deg and $F_1 = 0$, the solution of these equations is found to be

$$e_{1st} = \frac{F_2}{m_1\Omega^2} \frac{1 - (MH^2/\nu^2)}{(1 + M)H^2 - \nu^2} \quad \ldots\ldots [10a]$$

$$e_{2st} = -\frac{F_2}{2m_1\Omega^2} \frac{(MH^2/\nu^2)}{(1 + M)H^2 - \nu^2} \quad \ldots\ldots [10b]$$

$$e_{3st} = e_{2st}, \quad e_{1st} = 0, \quad e_{2st} = -e_{3st} = e_{2st} \quad [10c]\text{–}[10f]$$

For $\theta = 45$ deg and $F_2 = 0$, the solution is found to be (using primes to denote the case $F_2 = 0$)

$$e_{1st}' = 0 \quad \ldots\ldots [11a]$$

$$e_{2st}' = -\frac{F_1}{2m_1\Omega^2} \frac{M}{M\left(\nu^2 - \frac{\varphi^2}{2}\right) + \left(1 - \frac{\nu^2}{H^2}\right)(\nu^2 - \varphi^2)} \quad [11b]$$

$$e_{3st}' = -e_{2st}' \quad \ldots\ldots [11c]$$

$$e_{1st}' = \frac{F_1}{m_1\Omega^2} \frac{-M\left(1 - \frac{\varphi^2}{2\nu^2}\right) + \frac{\nu^2}{H^2}\left(1 - \frac{\varphi^2}{H^2}\right)}{M\left(\nu^2 - \frac{\varphi^2}{2}\right) + \left(1 - \frac{\nu^2}{H^2}\right)(\nu^2 - \varphi^2)} \quad \ldots\ldots [11d]$$

$$e_{2st}' = -\frac{F_1}{2m_1\Omega^2} \frac{M\left(1 - \frac{\varphi^2}{\nu^2}\right)}{M\left(\nu^2 - \frac{\varphi^2}{2}\right) + \left(1 - \frac{\nu^2}{H^2}\right)(\nu^2 - \varphi^2)} \quad \ldots [11e]$$

$$e_{3st}' = e_{2st}' \quad \ldots\ldots [11f]$$

where the nondimensional parameters are defined as follows

$$\left.\begin{aligned} M &\equiv m_1/m_2 \\ H &\equiv \omega_h/\Omega \\ \varphi &\equiv \omega_f/\Omega \end{aligned}\right\} \quad \ldots\ldots [12]$$

$M$ is a mass-ratio parameter, while $H$ and $\varphi$ are elastic parameters of the hub and the fuselage structure, respectively.

Since the structure analyzed here is suspended freely in space, it follows that the three mass points can be displaced in such a manner that the entire structure moves as a rigid body. The expressions given in Equations [10a]–[10f] and [11a]–[11f], therefore, include rigid-body displacements, and denote the sum of such displacements and elastic displacements. (The subscript $t$ consequently has been used to denote "total" displacements.)

The rigid-body displacements themselves can be derived from Equations [10a]–[11f] by letting $H \to \infty$ and $\varphi \to \infty$ there; i.e., by letting the hub and fuselage become infinitely stiff. The following expressions (denoted by subscript $r$) are thus obtained for the rigid-body displacements (with $\theta = 45$ deg) for $F_1 = 0$ and for $F_2 = 0$, respectively

$$e_{1sr} = -\left(\frac{F_2}{m_1\Omega^2\nu^2}\right)\left(\frac{M}{1 + M}\right) \quad \ldots\ldots [13a]$$

$$e_{2sr} = e_{3sr} = e_{1sr}/2 \quad \ldots\ldots [13b]\text{–}[13c]$$

$$e_{1sr} = 0 \quad \ldots\ldots [13d]$$

$$e_{2sr} = -e_{3sr} = -e_{1sr}/2 \quad \ldots\ldots [13e]\text{–}[13f]$$

$$e_{1sr}' = e_{2sr}' = e_{3sr}' = 0 \quad \ldots\ldots [14a]\text{–}[14c]$$

$$e_{1sr}' = -\left(\frac{F_1}{m_1\Omega^2\nu^2}\right)\left(\frac{M}{2 + M}\right) \quad \ldots\ldots [14d]$$

$$e_{2sr}' = e_{3sr}' = e_{1sr}' \quad \ldots\ldots [14e]\text{–}[14f]$$

As a check on these expressions it can be verified from Equations [4] that if the displacement amplitudes are given by Equations [13a]–[14f], then the elongation of each bar will be zero.

The displacements which are probably of the most practical interest here are the elastic displacements, which may be denoted as $e_{is}$ and $e_{is}$ (subscripts $r$ and $t$ are omitted), and which can be defined by relations of the form

$$e_{is} = e_{ist} - e_{isr}, \text{ etc} \quad \ldots\ldots [15]$$

Substitution of Equations [10], [11], [13], and [14] into Equations [15] leads to the following expressions for the *elastic* deflections of the three mass points

$$e_{1s} = \frac{F_2}{m_1\Omega^2} \frac{1}{1 + M} \frac{1}{(1 + M)H^2 - \nu^2} \quad \ldots\ldots [16a]$$

$$e_{2s} = e_{3s} = -(M/2)e_{1s} \quad \ldots\ldots [16b]\text{–}[16c]$$

$$e_{1s} = 0, \quad e_{2s} = -e_{3s} = -(M/2)e_{1s} \quad [16d]\text{–}[16f]$$

$$e_{1s}' = 0 \quad \ldots\ldots [17a]$$

$$e_{2s}' = -\frac{F_1}{2m_1\Omega^2} \frac{M}{M\left(\nu^2 - \frac{\varphi^2}{2}\right) + \left(1 - \frac{\nu^2}{H^2}\right)(\nu^2 - \varphi^2)} \quad \ldots [17b]$$

$$e_{3s}' = -e_{2s}' \quad \ldots\ldots [17c]$$

$$e_{1s}' = \frac{F_1}{m_1\Omega^2} \frac{1}{2 + M} \frac{(2/H^2)(\nu^2 - \varphi^2) - M}{M\left(\nu^2 - \frac{\varphi^2}{2}\right) + \left(1 - \frac{\nu^2}{H^2}\right)(\nu^2 - \varphi^2)} \quad \ldots [17d]$$

$$e_{2s}' = e_{3s}' = -(M/2)e_{1s}' \quad \ldots\ldots [17e]\text{–}[17f]$$

(Unprimed quantities refer to the case $F_1 = 0$, while primed quantities correspond to $F_2 = 0$.)

If more than a single external harmonic force acts at the hub; for example, if $F_x = \sum_\nu F_{2\nu} \cos \nu\Omega t$, then Equations [16a]–[17f] remain valid for each $\nu$, with $F_2$, for example, replaced by $F_{2\nu}$, and the resulting expressions for each $\nu$ need merely be added. In the subsequent discussion, however, it will be assumed that only a single exciting harmonic force acts at the hub, and that $\nu$ can be replaced by $n$, the number of rotor blades (cf. Equation [3]).

### Resonance and Other Implications of General Solution

Equations [16*a*]-[17*f*] are particularly simple general expressions giving the response of the hub-fuselage structure to harmonic forces transmitted by the blades to the hub in flight. The terms with subscript $x$ denote vibrational motions in the rotor plane of rotation, while those with subscript $z$ denote motions normal to the plane.

It should be noted that for $F_1 = 0$, i.e., for external harmonic forces acting only in the plane of rotation, the deflections, as functions of the pertinent parameters, will be of the form

$$e = \frac{F_2}{m_1\Omega^2}\,\phi(M, H) \qquad [18a]$$

For $F_2 = 0$, i.e., for external harmonic forces acting only normal to the plane of rotation, the deflection will be of the form[6]

$$e' = \frac{F_1}{m_1\Omega^2}\,\phi'(M, H, \varphi) \qquad [18b]$$

Thus the deflections are proportional to the parameters $(F_2/m_1\Omega^2)$ or $(F_1/m_1\Omega^2)$, and are functions of the three dimensionless parameters $M$, $H$, and $\varphi$. For forces acting only in the plane of rotation, however, the deflections are seen to be independent of the fuselage frequency parameter $\varphi$.

Because of the fact that in practice $M \ll 1$, it will be found that for external harmonic forces in the plane of rotation, $e_{1x}$ ordinarily will have the largest magnitude. This means that the mass point 1, Fig. 1, corresponding to the hub-rotor blade connections, will vibrate with greater amplitude than mass points 2 and 3, corresponding to the hub-fuselage connections. This is, perhaps, to be expected, since the external harmonic forces, transmitted by the blades to the hub, are assumed to act at point 1. However, for an external harmonic force acting normal to the rotor plane of rotation, it will be seen subsequently that points 1 and 2 may vibrate with roughly equal amplitudes under certain special conditions (cf. Equations [21] and [22] which appear later).

The conditions of resonance are of particular practical importance, since they indicate the conditions which should be avoided in actual design. Resonance may be defined here as the condition under which the magnitudes of the deflections, as given by Equations [16*a*]-[17*f*], become indefinitely large. For the system analyzed here, there will be two different types of resonance conditions, namely, one for a force acting in the plane of rotation ($F_1 = 0$), and one for a force acting normal to the plane of rotation ($F_2 = 0$).

For a *force in the plane of rotation*, Equations [16*a*]-[16*f*] imply that resonance will occur when

$$(1 + M)\,H^2 - n^2 = 0 \qquad [19a]$$

Therefore the value $(H_{res})$ of $H$ for resonance is

$$H_{res} = \frac{n}{\sqrt{1 + M}} \qquad [19b]$$

Thus, resonance will occur for a "hub natural frequency" $\omega_h$ slightly less than $n\Omega$.

For a *force normal to the plane of rotation*, Equations [17*a*]-[17*f*] imply the following condition for resonance

$$M\left(n^2 - \frac{\varphi^2}{2}\right) + \left(1 - \frac{n^2}{H^2}\right)(n^2 - \varphi^2) = 0 \qquad [20a]$$

or

$$\varphi_{res}^2 = n^2\,\frac{n^2 - (1 + M)H^2}{n^2 - \left(1 + \frac{M}{2}\right)H^2} \qquad [20b]$$

Equation [20*b*] will ordinarily imply that for a given $H$, $\varphi^2 \approx n^2$ for resonance, i.e., for a given hub natural-frequency parameter $H$, resonance will occur when the "fuselage natural frequency" $\omega_f$ is approximately equal to $n\Omega$. For a given fuselage natural-frequency parameter $\varphi$, the value of $H^2$ for resonance due to an exciting force normal to the plane of rotation, according to Equation [20*a*], will be

$$H_{res}^2 = n^2\,\frac{n^2 - \varphi^2}{n^2(1 + M) - \varphi^2\left(1 + \frac{M}{2}\right)} \qquad [20c]$$

Thus, for a given $\varphi$, $H_{res} \approx n$, or $\omega_h \approx n\Omega$, for resonance. If $\varphi < n$, then $H_{res} < n$, but if $n < \varphi < \sqrt{2}\,n$, then $H_{res} > n$ (unlike the case of resonance due to an exciting force in the plane of rotation).

For a fixed *ratio* $f(\equiv \omega_f/\omega_h \equiv \varphi/H)$ of fuselage to hub natural frequency, the condition of resonance is somewhat different in nature from that (cf. Equation [20*c*]) for a fixed fuselage natural frequency. For a fixed $f$, in fact, there will, in general, be *two* values of $H$ for resonance, given according to Equation [20*a*] by

$$H_{res}^2 = n^2\,\frac{1 + M + f^2 \pm \sqrt{(f^2 - 1)^2 + M(2 + M)}}{f^2(2 + M)} \qquad [20d]$$

Equation [20*d*], with $M$ (necessarily) positive, implies that if (and only if) $0 < f < \sqrt{2}$, then one of the values of $H_{res}$ will be less than $n$, while the other will exceed $n$. Equations [20*a*]-[20*d*] are, of course, all mathematically equivalent, but indicate the different points of view discussed in the foregoing.

It may be of interest to observe the asymptotic behavior of the elastic deflections as the natural frequencies of the hub and of the fuselage become infinitely large, i.e., as the hub-fuselage structure becomes infinitely stiff. As $H \to \infty$, it follows from Equations [16*a*]-[16*f*] that $e_{1x}$ and $e_{1z} \to 0$. Moreover, as $H \to \infty$ while $f$ is fixed, and hence $\varphi \to \infty$, Equations [17*a*]-[17*f*] imply that $e_{1x}'$ and $e_{1z}' \to 0$. These results are, of course, to be anticipated on physical grounds. However, if $\varphi$ (instead of $f$) is fixed, then as $H \to \infty$, it follows from Equations [17*b*] and [17*d*] that

$$\left.\begin{aligned} (e_{2x}')_{H\to\infty} &\to -\frac{F_1}{2m_1\Omega^2}\,\frac{M}{n^2(1 + M) - \varphi^2\left(1 + \frac{M}{2}\right)} \\ (e_{1x}')_{H\to\infty} &\to \frac{2}{2 + M}\,(e_{2x}')_{H\to\infty} \end{aligned}\right\} \qquad [21]$$

Relations [21] indicate that with the fuselage natural-frequency parameter $\varphi$ fixed, the vibrations due to a harmonic force normal to the plane of rotation will approach a finite (i.e., nonzero) magnitude as the hub natural frequency becomes indefinitely large. This result can be explained by noting that in this case, since $\varphi$ is fixed, the fuselage elastic stiffness does *not* at the same time also become indefinitely large.

It may be observed from Equations [17*a*]-[17*f*] that in the special case of $\varphi = \nu\,(= n)$, i.e., $\omega_f = n\Omega$, the response of the hub-fuselage structure to a harmonic force (of frequency $n\Omega$) normal to the plane of rotation will be independent of $H$, i.e., independent of the hub stiffness. Hence resonance cannot occur in this

[6] Equation [18*b*] also could be derived by dimensional analysis.

special case for any nonvanishng value of $H$. In this case, in fact, Equations [17$b$] and [17$d$] yield

$$\left.\begin{aligned}(e_{2z}')_{\varphi=n} &= -\frac{F_1}{m_1\Omega^2 n^2}\\ (e_{1z}')_{\varphi=n} &= -\frac{F_1}{m_1\Omega^2 n^2}\left(\frac{2}{2+M}\right)\end{aligned}\right\}\quad\ldots\ldots\ [22]$$

In this case, therefore, as also in the case $H \to \infty$ with $\varphi$ fixed (cf. Equations [21]), point 2, Fig. 1, will have an amplitude of deflection slightly greater than that of point 1.

It is interesting, finally, to note that for an external harmonic force acting normal to the rotor plane of rotation, a condition exists under which the elastic vibrational motions of the hub-fuselage structure will occur only in the plane of rotation. From Equations [17$d$]–[17$f$] it is seen that this will occur when

$$2(n^2 - \varphi^2) - MH^2 = 0$$

or

$$H^2 = \frac{2}{M}(n^2 - \varphi^2)\quad\ldots\ldots\ldots\ldots\ldots\ [23]$$

When Equation [23] is satisfied, then since only $e_{2z}'$ and $e_{3z}'$ will not vanish (cf. Equations [17$a$]–[17$f$]), the forced elastic vibrations of the hub-fuselage due to a harmonic force (of frequency $n\Omega$) normal to the plane of rotation will consist only of vibrations of points 2 and 3 (fuselage-hub connections, Fig. 1) in the plane of rotation.

## Numerical Examples

To illustrate more explicitly the results of the present analysis, numerical examples will be worked out, based on the following data, which are fairly typical:

$$\begin{aligned} n &= 3 \text{ (three-bladed rotor)}\\ m_1 &= 9.30 \text{ slugs } (=300 \text{ lb})\\ \Omega &= 28 \text{ radians/sec (268 rpm)}\\ M &= 0.15\end{aligned}$$

It will be assumed, moreover, that

$$F_1 = 400 \text{ lb}, \quad F_2 = 1000 \text{ lb}$$

Since the amplitudes of the vibrations are directly proportional to $F_1$ and $F_2$, it follows that for any values of $F_1$ and $F_2$ other than those assumed in the present examples, the deflections can be obtained readily from those to be given here.

Since the largest deflections in these examples will be $|e_{1z}|$ due to the force (given by $F_2$) in the plane of rotation, and $|e_{1z}'|$ due to the force (given by $F_1$) normal to the plane of rotation, only these two quantities need be considered here in detail.

From Equation [16$a$] it follows, with the present data, that

$$e_{1z} = \frac{1.240}{H^2 - 7.81}\ \text{in.}\quad\ldots\ldots\ldots\ldots\ [24]$$

Equation [24] for $|e_{1z}|$ versus $H$ is plotted in Fig. 2. It is interesting to note that Equation [24] is quite similar, even quantitatively, to the expression for hub response derived for a 3-bladed rotor in reference (3). However, it must be observed that the essential structure (rotor and fuselage) analyzed here is different from that (rotor blades and rotor) in reference (3), although the mass parameter $M$ (= ratio of blade and pylon mass to half of the fuselage mass) here is of the same order of magnitude as the different mass parameter $\mu$(= ratio of blade mass to total hub, blade and pylon mass) of reference (3).

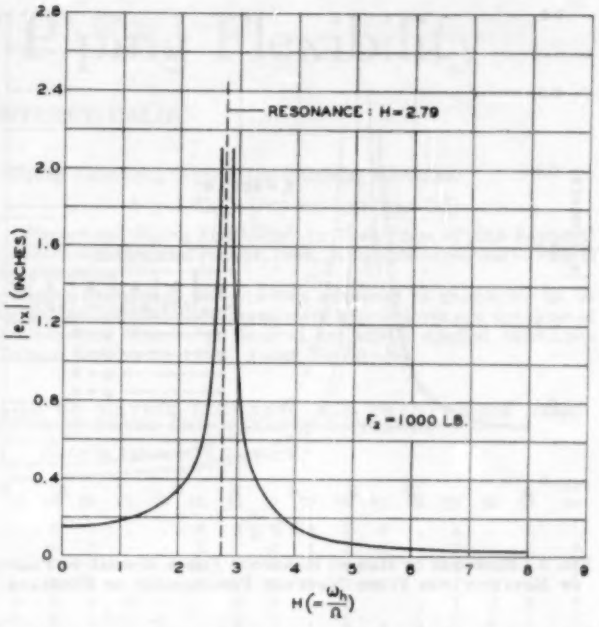


Fig. 2 Response of Hub to Harmonic Force in Plane of Rotation

For $F_2 = 0$ and $F_1 = 400$ lb, substitution of the data assumed here into Equation [17$d$] yields

$$e_{1z}' = \frac{0.305}{H^2}\,\frac{2(9-\varphi^2) - 0.15H^2}{(10.35 - 1.075\varphi^2) - \frac{9}{H^2}(9-\varphi^2)}\ \text{in.}\ldots\ [25a]$$

In terms of the fuselage-hub natural-frequency ratio $f(=\varphi/H)$, Equation [25$a$] can be written in the form

$$e_{1z}' = 0.305\,\frac{(18/H^2) - 0.15 - 2f^2}{10.35 - f^2(9 - 1.075H^2) - (81/H^2)}\ \text{in.}\ldots\ldots\ [25b]$$

Equations [25$a$] and [25$b$] for $|e_{1z}'|$ as a function of $H$ for various fixed fuselage natural frequencies (fixed $\varphi$), and as a function of $H$ for various fixed fuselage-hub natural-frequency ratios ($f$), are shown plotted in Figs. 3 and 4, respectively. The resonance conditions are also tabulated there.[7]

## Conclusions

By using a simple model to represent the helicopter hub and fuselage, an analysis has been made of the hub-fuselage response to harmonic forces transmitted in flight by the rotor blades to the hub both in, and normal to, the plane of rotation. The expressions derived for the amplitudes of the forced vibrations both in, and normal to, the plane of rotation are particularly simple, and are very convenient for calculations. The resonance conditions thus derived are also quite simple. The pertinent nondimensional parameters are the number of blades $n$, the ratio of hub natural frequency to rotor angular speed ($H = \omega_h/\Omega$), the ratio of fuselage natural frequency to rotor speed ($\varphi = \omega_f/\Omega$), and the ratio of blade and pylon mass to half of the fuselage mass ($M = m_1/m_2$). The vibration amplitudes, moreover, are proportional to ($F/m_1\Omega^2$) where $F$ denotes the amplitude of the exciting harmonic force. The vibrations due to a force in the plane of rotation are

[7] One of the choices for $f$ in Fig. 4, namely, $f = \sqrt{2M}$, was made on the basis of supposing $kc = k_A$, and comparing Equations [7] and [8].

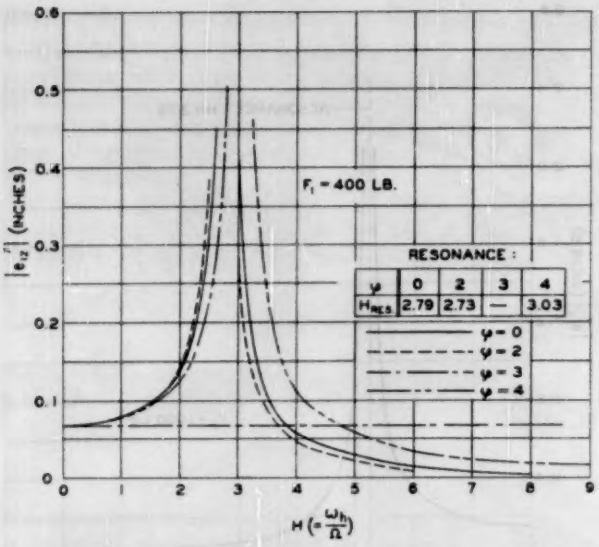


FIG. 3 RESPONSE OF HUB TO HARMONIC FORCE NORMAL TO PLANE OF ROTATION FOR FIXED NATURAL FREQUENCIES OF FUSELAGE

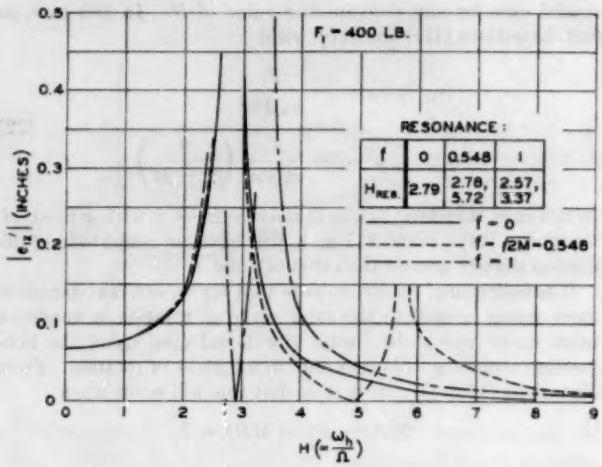


FIG. 4 RESPONSE OF HUB TO HARMONIC FORCE NORMAL TO PLANE OF ROTATION FOR FIXED RATIOS OF FUSELAGE TO HUB NATURAL FREQUENCIES

independent of the fuselage natural-frequency parameter $\varphi$

Despite the simplicity of the physical structure analyzed, and of the final analytical expressions, the results of a typical numerical example based on the present analysis agree well with those based on a considerably different, and somewhat more involved, type of analysis for the hub response (without fuselage) in the rotor plane of rotation due to exciting harmonic forces in this plane.

As an extension of the present analysis, a space-framework type of structure, instead of the plane structure treated here, can be assumed as a physical model of the hub fuselage. In this manner it would be possible to take into account the effect of the actual rotation (cf., for example, reference 4) of the harmonic force transmitted by the rotor blades to the hub in the plane of rotation.

## BIBLIOGRAPHY

1 "Theory of Mechanical Instability of Rotors," by M. L. Deutsch, AAF Report 459-1-18, January, 1943.

2 "Theory of Self-Excited Mechanical Oscillations of Hinged Rotor Blades," by R. P. Coleman, NACA Wartime Report AAR 3G29, July, 1943.

3 "The Response of Helicopter Rotors to Oscillatory Rotor Plane Drag Forces at the Blades," by O. R. Rogers and W. Oleksak, WADC Technical Report 52-270, RDO No. 455-45, September, 1952.

4 "Helicopter Blade-Forces Transmitted to the Rotor Hub in Flight" by M. Morduchow, S. W. Yuan, and K. E. Peress, WADC Technical Report 53-355, May, 1953.

5 "Aerodynamics of the Helicopter," by A. Gessow and G. C. Myers, Jr., The Macmillan Company, New York, N. Y., 1952.

# Matrix Analysis of Piping Flexibility

By J. E. BROCK,[1] MONTEREY, CALIF.

SEVERAL correspondents have pointed out the inconvenience resulting from restricting the orientation symbols in an earlier paper by the author,[2] in which the letters appear in cyclic order $x$, $y$, $z$. Accordingly, Tables 7 and 8 of that reference are here extended, as Table 7($a$) and 8($a$), to include anticyclic symbols.[3]

One should note also that the formulas for $k$ and $\beta$ in Table 4 of the earlier paper[2] are now obsolete. The ASA Report on "Piping Flexibility"[4] gives the following formulas:

$$k = 1.65h^{-1} \text{ (but not less than 1.0)}$$

[1] Professor of Mechanical Engineering, U. S. Naval Postgraduate School. Mem. ASME.

[2] "A Matrix Method for Flexibility Analysis of Piping Systems," by J. E. Brock, JOURNAL OF APPLIED MECHANICS, Trans. ASME, vol. 74, 1952, p. 501.

[3] There are a few minor changes in the manner of presenting the data. In the headings of both Tables 7($a$) and 8($a$) and in the body of Table 8($a$), the symbol $C$ has been omitted and only the subscripts are shown. Also, a symbol is included which describes the k-matrix (see bottom of p. 502 of footnote 2) for the orientation. The sequence refers to the three rows of the k-matrix. The values denote the column in which a unit value appears. The negative sign indicates negative unity. The other six elements of the k-matrix are zero.

Contributed by the Applied Mechanics Division and presented at the Diamond Jubilee Spring Meeting, Baltimore, Md., April 18–21, 1955, of THE AMERICAN SOCIETY OF MECHANICAL ENGINEERS.

Discussion of this paper should be addressed to the Secretary, ASME, 29 West 39th Street, New York, N. Y., and will be accepted until October 10, 1955, for publication at a later date. Discussion received after closing date will be returned.

[4] Report on "Piping Flexibility" by Task Force of ASA Sectional Committee B-31, dated June 21, 1954. Available on request to ASME Headquarters.

NOTE: Statements and opinions advanced in papers are to be understood as individual expressions of their authors and not those of the Society. Manuscript received by ASME Applied Mechanics Division, October 25, 1954. Paper No. 55—S-5.

TABLE 8($a$) INTERCHANGE OF MATRIX ELEMENTS FOR TWENTY-FOUR BASIC ORIENTATIONS OF BENDS AND INCLINED TANGENTS[a]

(Refer to Tables 5a, 6, 7a, and 9.)

| Case No. | Orient. Symbol | 11 | 12 | 13 | 15 | 16 | 22 | 23 | 24 | 26 | 33 | 34 | 35 | 44 | 45 | 46 | 55 | 56 | 66 | Case No. |
|---|---|---|---|---|---|---|---|---|---|---|---|---|---|---|---|---|---|---|---|---|
| 1 | +x,+y | A | B | . | . | C | D | . | . | E | F | G | H | I | J | . | K | . | L | 1 |
| 2 | +x,-y | A | -B | . | . | -C | D | . | . | E | F | -G | H | I | -J | . | K | . | L | 2 |
| 3 | -x,+y | A | -B | . | . | C | D | . | . | -E | F | G | -H | I | -J | . | K | . | L | 3 |
| 4 | -x,-y | A | B | . | . | -C | D | . | . | -E | F | -G | -H | I | J | . | K | . | L | 4 |
| 5 | +y,+z | F | . | . | G | H | A | B | C | . | D | E | . | L | . | . | I | J | K | 5 |
| 6 | +y,-z | F | . | . | -G | H | A | -B | -C | . | D | E | . | L | . | . | I | -J | K | 6 |
| 7 | -y,+z | F | . | . | G | -H | A | -B | C | . | D | -E | . | L | . | . | I | -J | K | 7 |
| 8 | -y,-z | F | . | . | -G | -H | A | B | -C | . | D | -E | . | L | . | . | I | J | K | 8 |
| 9 | +z,+x | D | . | B | E | . | F | . | H | G | A | . | C | K | . | J | L | . | I | 9 |
| 10 | +z,-x | D | . | -B | E | . | F | . | H | -G | A | . | -C | K | . | -J | L | . | I | 10 |
| 11 | -z,+x | D | . | -B | -E | . | F | . | -H | G | A | . | C | K | . | -J | L | . | I | 11 |
| 12 | -z,-x | D | . | B | -E | . | F | . | -H | -G | A | . | -C | K | . | J | L | . | I | 12 |
| 13 | +x,+z | A | . | B | -C | . | F | . | -G | -H | D | . | -E | I | . | J | L | . | K | 13 |
| 14 | +x,-z | A | . | -B | C | . | F | . | G | -H | D | . | -E | I | . | -J | L | . | K | 14 |
| 15 | -x,+z | A | . | -B | -C | . | F | . | -G | H | D | . | E | I | . | -J | L | . | K | 15 |
| 16 | -x,-z | A | . | B | C | . | F | . | G | H | D | . | E | I | . | J | L | . | K | 16 |
| 17 | +y,+x | D | B | . | . | -E | A | . | . | -C | F | -H | -G | K | J | . | I | . | L | 17 |
| 18 | +y,-x | D | -B | . | . | -E | A | . | . | C | F | -H | G | K | -J | . | I | . | L | 18 |
| 19 | -y,+x | D | -B | . | . | E | A | . | . | -C | F | E | -G | K | -J | . | I | . | L | 19 |
| 20 | -y,-x | D | B | . | . | E | A | . | . | C | F | E | G | K | J | . | I | . | L | 20 |
| 21 | +z,+y | F | . | . | -H | -G | D | B | -E | . | A | -C | . | L | . | . | K | J | I | 21 |
| 22 | +z,-y | F | . | . | -H | G | D | -B | -E | . | A | C | . | L | . | . | K | -J | I | 22 |
| 23 | -z,+y | F | . | . | H | -G | D | -B | E | . | A | -C | . | L | . | . | K | -J | I | 23 |
| 24 | -z,-y | F | . | . | H | G | D | B | E | . | A | C | . | L | . | . | K | J | I | 24 |

[a] Opposite desired case number and under symbol for desired element find letter together with algebraic sign giving desired entry. Thus $C_{14}$ in Case 8 is negative of $C$-value given in Tables 5, 6, or 9. Elements $C_{14}$, $C_{24}$, $C_{34}$, are zero.

TABLE 7($a$) INTERCHANGE OF MATRIX ELEMENTS FOR TWENTY-FOUR BASIC ORIENTATIONS[a]

| Case No. | Orient. Symbol | K Matrix | 11 | 12 | 13 | 14 | 15 | 16 | 22 | 23 | 24 | 25 | 26 | 33 | 34 | 35 | 36 | 44 | 45 | 46 | 55 | 56 | 66 | Case No. |
|---|---|---|---|---|---|---|---|---|---|---|---|---|---|---|---|---|---|---|---|---|---|---|---|---|
| 1 | +x,+y | +1,+2,+3 | 11 | 12 | 13 | 14 | 15 | 16 | 22 | 23 | 24 | 25 | 26 | 33 | 34 | 35 | 36 | 44 | 45 | 46 | 55 | 56 | 66 | 1 |
| 2 | +x,-y | +1,-2,-3 | 11 | -12 | -13 | 14 | -15 | -16 | 22 | 23 | -24 | 25 | 26 | 33 | -34 | 35 | 36 | 44 | -45 | -46 | 55 | 56 | 66 | 2 |
| 3 | -x,+y | -1,+2,-3 | 11 | -12 | 13 | 14 | -15 | 16 | 22 | -23 | -24 | 25 | -26 | 33 | 34 | -35 | 36 | 44 | -45 | 46 | 55 | -56 | 66 | 3 |
| 4 | -x,-y | -1,-2,+3 | 11 | 12 | -13 | 14 | 15 | -16 | 22 | -23 | 24 | 25 | -26 | 33 | -34 | -35 | 36 | 44 | 45 | -46 | 55 | -56 | 66 | 4 |
| 5 | +y,+z | +3,+1,+2 | 33 | 13 | 23 | 36 | 34 | 35 | 11 | 12 | 16 | 14 | 15 | 22 | 26 | 24 | 25 | 66 | 46 | 56 | 44 | 45 | 55 | 5 |
| 6 | +y,-z | -3,+1,-2 | 33 | -13 | 23 | 36 | -34 | 35 | 11 | -12 | -16 | 14 | -15 | 22 | 26 | -24 | 25 | 66 | -46 | 56 | 44 | -45 | 55 | 6 |
| 7 | -y,+z | -3,-1,+2 | 33 | 13 | -23 | 36 | 34 | -35 | 11 | -12 | 16 | 14 | -15 | 22 | -26 | -24 | 25 | 66 | 46 | -56 | 44 | -45 | 55 | 7 |
| 8 | -y,-z | +3,-1,-2 | 33 | -13 | -23 | 36 | -34 | -35 | 11 | 12 | -16 | 14 | 15 | 22 | -26 | 24 | 25 | 66 | -46 | -56 | 44 | 45 | 55 | 8 |
| 9 | +z,+x | +2,+3,+1 | 22 | 23 | 12 | 25 | 26 | 24 | 33 | 13 | 35 | 36 | 34 | 11 | 15 | 16 | 14 | 55 | 56 | 45 | 66 | 46 | 44 | 9 |
| 10 | +z,-x | -2,-3,+1 | 22 | 23 | -12 | 25 | 26 | -24 | 33 | -13 | 35 | 36 | -34 | 11 | -15 | -16 | 14 | 55 | 56 | -45 | 66 | -46 | 44 | 10 |
| 11 | -z,+x | +2,-3,-1 | 22 | -23 | -12 | 25 | -26 | -24 | 33 | 13 | -35 | 36 | 34 | 11 | -15 | 16 | 14 | 55 | -56 | -45 | 66 | 46 | 44 | 11 |
| 12 | -z,-x | -2,+3,-1 | 22 | -23 | 12 | 25 | -26 | 24 | 33 | -13 | -35 | 36 | -34 | 11 | 15 | -16 | 14 | 55 | -56 | 45 | 66 | -46 | 44 | 12 |
| 13 | +x,+z | +1,-3,+2 | 11 | -13 | 12 | 14 | -16 | 15 | 33 | -23 | -34 | 36 | -35 | 22 | 24 | -26 | 25 | 44 | -46 | 45 | 66 | -56 | 55 | 13 |
| 14 | +x,-z | +1,+3,-2 | 11 | 13 | -12 | 14 | 16 | -15 | 33 | -23 | 34 | 36 | -35 | 22 | -24 | -26 | 25 | 44 | 46 | -45 | 66 | -56 | 55 | 14 |
| 15 | -x,+z | -1,+3,+2 | 11 | -13 | -12 | 14 | -16 | -15 | 33 | 23 | -34 | 36 | 35 | 22 | -24 | 26 | 25 | 44 | -46 | -45 | 66 | 56 | 55 | 15 |
| 16 | -x,-z | -1,-3,-2 | 11 | 13 | 12 | 14 | 16 | 15 | 33 | 23 | 34 | 36 | 35 | 22 | 24 | 26 | 25 | 44 | 46 | 45 | 66 | 56 | 55 | 16 |
| 17 | +y,+x | +2,+1,-3 | 22 | 12 | -23 | 25 | 24 | -26 | 11 | -13 | 15 | 14 | -16 | 33 | -35 | -34 | 36 | 55 | 45 | -56 | 44 | -46 | 66 | 17 |
| 18 | +y,-x | -2,+1,+3 | 22 | -12 | -23 | 25 | -24 | -26 | 11 | 13 | -15 | 14 | 16 | 33 | -35 | 34 | 36 | 55 | -45 | -56 | 44 | 46 | 66 | 18 |
| 19 | -y,+x | +2,-1,+3 | 22 | -12 | 23 | 25 | -24 | 26 | 11 | -13 | -15 | 14 | -16 | 33 | 35 | -34 | 36 | 55 | -45 | 56 | 44 | -46 | 66 | 19 |
| 20 | -y,-x | -2,-1,-3 | 22 | 12 | 23 | 25 | 24 | 26 | 11 | 13 | 15 | 14 | 16 | 33 | 35 | 34 | 36 | 55 | 45 | 56 | 44 | 46 | 66 | 20 |
| 21 | +z,+y | -3,+2,+1 | 33 | -23 | -13 | 36 | -35 | -34 | 22 | 12 | -26 | 25 | 24 | 11 | -16 | 15 | 14 | 66 | -56 | -46 | 55 | 45 | 44 | 21 |
| 22 | +z,-y | +3,-2,+1 | 33 | -23 | 13 | 36 | -35 | 34 | 22 | -12 | -26 | 25 | -24 | 11 | 16 | -15 | 14 | 66 | -56 | 46 | 55 | -45 | 44 | 22 |
| 23 | -z,+y | +3,+2,-1 | 33 | 23 | -13 | 36 | 35 | -34 | 22 | -12 | 26 | 25 | -24 | 11 | -16 | -15 | 14 | 66 | 56 | -46 | 55 | -45 | 44 | 23 |
| 24 | -z,-y | -3,-2,-1 | 33 | 23 | 13 | 36 | 35 | 34 | 22 | 12 | 26 | 25 | 24 | 11 | 16 | 15 | 14 | 66 | 56 | 46 | 55 | 45 | 44 | 24 |

[a] Opposite desired case number and under symbol for desired element find symbol of corresponding element in basic Case 1 preceded by appropriate algebraic sign. Thus $C_{14}$ for Case 10 is negative of $C_{14}$ for Case 1.

TABLE 5(a) INFLUENCE COEFFICIENTS FOR BENDS
(Elements $C_{ij}$ refer to Case 1.)

| | |
|---|---|
| A | $C_{11} = kR^3[0.5(\theta_2 - \theta_1) + 0.25(\sin 2\theta_2 - \sin 2\theta_1)]/EI$ |
| B | $C_{12} = -0.25kR^3(\cos 2\theta_2 - \cos 2\theta_1)/EI$ |
| C | $C_{15} = -kR^2(\sin \theta_2 - \sin \theta_1)/EI$ |
| D | $C_{22} = kR^3[0.5(\theta_2 - \theta_1) - 0.25(\sin 2\theta_2 - \sin 2\theta_1)]/EI$ |
| E | $C_{26} = kR^2(\cos \theta_2 - \cos \theta_1)/EI$ |
| F | $C_{33} = 1.5R^3(\theta_2 - \theta_1)/EI$ |
| G | $C_{34} = 1.5R^2(\sin \theta_2 - \sin \theta_1)/EI$ |
| H | $C_{35} = -1.5R^2(\cos \theta_2 - \cos \theta_1)/EI$ |
| I | $C_{44} = R[0.5(1.5 + k)(\theta_2 - \theta_1) + 0.25(1.5 - k)(\sin 2\theta_2 - \sin 2\theta_1)]/EI$ |
| J | $C_{46} = -0.25R(1.5 - k)(\cos 2\theta_2 - \cos 2\theta_1)/EI$ |
| K | $C_{55} = R[0.5(1.5 + k)(\theta_2 - \theta_1) - 0.25(1.5 - k)(\sin 2\theta_2 - \sin 2\theta_1)]/EI$ |
| L | $C_{66} = kR(\theta_2 - \theta_1)/EI$ |

$C_{21} = C_{12}$; $C_{61} = C_{16}$; $C_{62} = C_{26}$; $C_{43} = C_{34}$; $C_{53} = C_{35}$; $C_{54} = C_{45}$.
All other $C_{ij}$ are zero.

$$i = 0.9h^{-2/3} \text{ (but not less than 1.0)}$$

the symbol $i$ (rather than $\beta$) being used for the stress-intensification factor. The formula for $h$ remains

$$h = tRr^{-2}$$

Table 5 of the author's paper[2] is here modified as Table 5(a).[5]

This corrects errors appearing in items A and D of footnote 2 (corrected in the reprints) and also modifies items I, J, and K so as to include the flexibility factor $k$ for "out-of-plane" bending as well as "in-plane" bending in accordance with Note 1 of Chart 1 of the footnote 4.

[5] Tables 6 has not been modified. The errors in items A and D of Table 5 were errors of transcription and did not affect Table 6. Obviously new coefficients in items I, J, and K, depend on the value of $k$ so that it is not convenient to modify Table 6; values for these items should be computed separately.

# Inertia Forces in Lubricating Films

By R. S. BRAND,[1] STORRS, CONN.

**The usual theory of hydrodynamic lubrication is based on the assumption that the inertia forces in the equations of motion are negligible compared to the viscous forces. This paper shows that if the Reynolds number $\rho R\omega/\mu$ is of the same order as $R/h$, then the inertia forces will be of the same order as the viscous forces.**

PROBLEMS in fluid mechanics are often classified according to the relative importance of the viscous terms and the inertia terms in the equations of motion. In lubrication problems, because of the high rates of shear, the viscous terms usually are considered to be predominant and the inertia terms are neglected. However, Fogg's experiments with parallel-surface thrust bearings (1)[2] led to speculation that centrifugal forces might be important, and Shaw and Strang (2) have developed a bearing in which the flow due to a centrifugal field is responsible for the bearing's load capacity. It is the purpose of this paper to demonstrate, by order of magnitude arguments, that inertia forces are not negligible provided a suitably defined Reynolds number is large enough.

Ladanyi (3) has considered the inertia forces arising from an acceleration of the sliding element of a bearing but neglects the inertia forces which are present even with steady flow. Shaw and Macks (4) discuss the possibility of the existence of a critical Reynolds number above which the flow in bearings is turbulent, and Wilcock conducted some remarkable experiments (5) which were interpreted as confirmation of the existence of such a critical Reynolds number. The present paper is not concerned with turbulence but merely shows that even with laminar flow the Reynolds number is a significant parameter if large enough, and that the consideration of inertia forces in a laminar oil film may explain certain high-speed phenomena not adequately accounted for by the usual hydrodynamic theory.

## Steady Flow of Incompressible Fluid

The Navier-Stokes equations for the steady flow of an incompressible fluid take the following form in cylindrical co-ordinates

$$\left.\begin{aligned} u\frac{\partial u}{\partial r}+\frac{v}{r}\frac{\partial u}{\partial \theta}+w\frac{\partial u}{\partial z}-\frac{v^2}{r}&=-\frac{1}{\rho}\frac{\partial p}{\partial r}\\ &+\frac{\mu}{\rho}\left(\frac{\partial^2 u}{\partial r^2}+\frac{1}{r}\frac{\partial u}{\partial r}+\frac{1}{r^2}\frac{\partial^2 u}{\partial \theta^2}+\frac{\partial^2 u}{\partial z^2}\right.\\ &\left.-\frac{u}{r^2}-\frac{2}{r^2}\frac{\partial v}{\partial \theta}\right)\\ u\frac{\partial v}{\partial r}+\frac{v}{r}\frac{\partial v}{\partial \theta}+w\frac{\partial v}{\partial z}+\frac{uv}{r}&=-\frac{1}{\rho r}\frac{\partial p}{\partial \theta}\\ &+\frac{\mu}{\rho}\left(\frac{\partial^2 v}{\partial r^2}+\frac{1}{r}\frac{\partial v}{\partial r}+\frac{1}{r^2}\frac{\partial^2 v}{\partial \theta^2}+\frac{\partial^2 v}{\partial z^2}\right.\\ &\left.+\frac{2}{r^2}\frac{\partial u}{\partial \theta}-\frac{v}{r^2}\right)\\ u\frac{\partial w}{\partial r}+\frac{v}{r}\frac{\partial w}{\partial \theta}+w\frac{\partial w}{\partial z}&=-\frac{1}{\rho}\frac{\partial p}{\partial z}\\ &+\frac{\mu}{\rho}\left(\frac{\partial^2 w}{\partial r^2}+\frac{1}{r}\frac{\partial w}{\partial r}+\frac{1}{r^2}\frac{\partial^2 w}{\partial \theta^2}+\frac{\partial^2 w}{\partial z^2}\right) \end{aligned}\right\} \quad \ldots [1]$$

(continued)

where $u$, $v$, $w$ are the velocity components in the $r$, $\theta$, $z$-directions, respectively, $p$ is the pressure, $\rho$ the density, and $\mu$ the viscosity.

Consider a thrust bearing with the runner in the $r$, $\theta$-plane and the axis of rotation coinciding with the $z$-axis. Let $R$ be the radius of the runner, $\omega$ its angular velocity, and $h$ the mean thickness of the lubricant film measured in the $z$-direction. $R \gg h$.

We nondimensionalize the equations by the following substitutions

$$\left.\begin{aligned} r&=r'R & u&=u'R\omega & p&=p'\rho R^2\omega^2\\ z&=z'h & v&=v'R\omega & &\\ & & w&=w'h\omega & & \end{aligned}\right\} \quad \ldots [2]$$

The first two of Equations [1] are then

$$\left.\begin{aligned} u'\frac{\partial u'}{\partial r'}+\frac{v'}{r'}\frac{\partial u'}{\partial \theta}+w'\frac{\partial u'}{\partial z'}-\frac{v'^2}{r'}&=-\frac{\partial p'}{\partial r'}\\ &+\frac{\mu}{\rho R^2\omega}\left(\frac{\partial^2 u'}{\partial r'^2}+\frac{1}{r'}\frac{\partial u'}{\partial r'}+\frac{1}{r'^2}\frac{\partial^2 u'}{\partial \theta^2}\right.\\ &\left.+\frac{R^2}{h^2}\frac{\partial^2 u'}{\partial z'^2}-\frac{u'}{r'^2}-\frac{2}{r'^2}\frac{\partial v'}{\partial \theta}\right)\\ u'\frac{\partial v'}{\partial r'}+\frac{v'}{r'}\frac{\partial v'}{\partial \theta}+w'\frac{\partial v'}{\partial z'}+\frac{u'v'}{r'}&=-\frac{1}{r'}\frac{\partial p'}{\partial \theta}\\ &+\frac{\mu}{\rho R^2\omega}\left(\frac{\partial^2 v'}{\partial r'^2}+\frac{1}{r'}\frac{\partial v'}{\partial r'}+\frac{1}{r'^2}\frac{\partial^2 v'}{\partial \theta^2}\right.\\ &\left.+\frac{R^2}{h^2}\frac{\partial^2 v'}{\partial z'^2}+\frac{2}{r'^2}\frac{\partial u'}{\partial \theta}-\frac{v'}{r'^2}\right) \end{aligned}\right\} \quad \ldots [3]$$

By choosing $h$ instead of $R$ as the length parameter in nondimensionalizing $z$ and $w$, we have made $u'$, $v'$, $w'$, and their first and second derivatives all of order of magnitude one. The relative magnitudes of the terms in Equations [3] are thus given by the constant coefficients, the variables being all of order one. Since $R^2/h^2$ is a very large number, a good approximation to Equations [3] is

$$\left.\begin{aligned} u'\frac{\partial u'}{\partial r'}+\frac{v'}{r'}\frac{\partial u'}{\partial \theta}+w'\frac{\partial u'}{\partial z'}-\frac{v'^2}{r'}&=-\frac{\partial p'}{\partial r'}\\ &+\frac{\mu}{\rho\omega h^2}\frac{\partial^2 u'}{\partial z'^2} \end{aligned}\right\} \quad \ldots [4]$$

---

[1] Associate Professor of Mechanical Engineering, University of Connecticut. Assoc. Mem. ASME.

[2] Numbers in parentheses refer to the Bibliography at the end of the paper.

Contributed by the Applied Mechanics Division and presented at the Diamond Jubilee Semi-Annual Meeting, Boston, Mass., June 19–23, 1955, of The American Society of Mechanical Engineers.

Discussion of this paper should be addressed to the Secretary, ASME, 29 West 39th Street, New York, N. Y., and will be accepted until October 10, 1955, for publication at a later date. Discussion received after the closing date will be returned.

Note: Statements and opinions advanced in papers are to be understood as individual expressions of their authors and not those of the Society. Manuscript received by ASME Applied Mechanics Division, June 28, 1954. Paper No. 55—SA-1.

$$\mu' \frac{\partial v'}{\partial r'} + \frac{v'}{r'} \frac{\partial v'}{\partial \theta} + w' \frac{\partial v'}{\partial z'} + \frac{u'v'}{r'} = -\frac{1}{r'} \frac{\partial p'}{\partial \theta} + \frac{\mu}{\rho \omega h^2} \frac{\partial^2 v'}{\partial z'^2} \quad \left.\begin{array}{r}\\ \\ \\ \end{array}\right\} \ldots [4] \text{ (continued)}$$

## Conclusion

We are investigating the conditions under which the inertia terms (the left sides of Equations [4]) are of the same order of magnitude as the remaining viscous terms. Since the inertia terms are of order one, for them to be significant $\mu/\rho\omega h^2$ also must be of order one, or

$$\rho \frac{R\omega h}{\mu} \approx \frac{R}{h}$$

$\rho R\omega h/\mu$ may be thought of as the Reynolds number for the problem, as $R\omega$ is the characteristic velocity and $h$ measures the width of the flow passage.

While a thrust bearing has been envisioned in the foregoing analysis, a similar conclusion is reached for a journal bearing. For the inertia forces to be of the same order as the viscous forces in a journal bearing

$$\rho \frac{R\omega c}{\mu} \approx \frac{R}{c}$$

where $R$ is the shaft radius and $c$ is the radial clearance.

Substitution of a few typical values shows that while very high velocities are required to make the Reynolds number of the same order as $R/h$, these velocities are not outside the operating range of some bearings.

## BIBLIOGRAPHY

(1) "Film Lubrication of Parallel Thrust Surfaces," by A. Fogg. Proceedings of The Institution of Mechanical Engineers, London, England, vol. 155, 1946, pp. 49–67.

(2) "The Hydrosphere—A New Hydrodynamic Bearing," by M. C. Shaw and C. D. Strang, Jr., Journal of Applied Mechanics, Trans. ASME, vol. 70, 1948, pp. 137–145.

(3) "Effects of Temporal Tangential Bearing Acceleration on Performance Characteristics of Slider and Journal Bearings," by D. Ladanyi, NACA Technical Note 1730, October, 1948.

(4) "Analysis and Lubrication of Bearings," by M. C. Shaw and E. F. Macks, McGraw-Hill Book Co., New York, N. Y., 1949, p. 356.

(5) "Turbulence in High-Speed Journal Bearings," by D. F. Wilcock, Trans. ASME, vol. 72, 1950, pp. 825–834.

# Nutation of a Free Gyro Subjected to an Impulse

By B. T. PLYMALE[1] and R. GOODSTEIN,[1] SEATTLE, WASH.

**It is the purpose of this paper to call attention to a particular gyro motion which has been observed and studied in our laboratories. The phenomenon is of extreme practical importance for all instruments which use a gyro as a space-stable element, and no published usable information has been found concerning it. A description and explanation of the motion will be presented. An Appendix contains the basic equations for the system and the results of approximate solutions.**

## Description

CONSIDER a gyro of the type shown in Fig. 1. The wheel and gimbals are balanced, the bearings have negligible friction, and windage is negligible. Hence no external torques are acting on the system, and the wheel and gimbal assembly maintains a fixed position in space. Now, if either the inner or outer gimbal is struck sharply with a hammer, imparting an impulse to the system, a wobbly motion of the wheel occurs which, in the absence of dissipative torques, would persist indefinitely. This motion is referred to as "nutation." It is observed that for small angular displacements the motions of the inner and outer gimbal are approximately sinusoidal. However, closer examination and testing reveal that when the inner and outer gimbals are not initially perpendicular, the inner gimbal will oscillate about a fixed center position but the outer gimbal will exhibit oscillations accompanied by a steadily increasing angular displacement of the "center" position of the oscillations. It is this average angular rate accompanying the outer gimbal oscillations which can lead to loss of reference in a free-gyro instrument.

## Explanation

A physical explanation of the phenomenon will be presented. The configuration of the gyro can be specified by the three angles $\psi$, $\theta$, and $\varphi$ shown in Fig. 1. $\psi$ is the angular position of the wheel relative to the inner gimbal, $\theta$ is the angular position of the inner gimbal relative to the outer gimbal, and $\varphi$ is the angular position of the outer gimbal relative to inertial space, with the positive directions as shown. For some initial angle $\theta_0$ between 0 and 90 deg, suppose an impulse is applied to the inner gimbal so that in an infinitesimal time interval, the inner gimbal acquires a positive angular velocity $\dot{\theta}_0$. The basic gyro wheel relation[2] $\vec{\tau} = \vec{\omega} \times \vec{H}$, where $\vec{\tau}$ is a torque applied to the wheel, $\vec{H}$ is the angular momentum, and $\vec{\omega}$ is the angular velocity of the $H$-vector, indicates that a torque must be acting on the wheel and inner gimbal in the negative direction along the outer gimbal axis. Since no external torque is acting, this torque is the "inertial torque" associated with an angular acceleration of the outer gimbal. This results in a positive angular velocity $\dot{\varphi}$ of the outer gimbal, which initially was at rest. Now this angular velocity must be accompanied by a torque along the inner gimbal axis in the positive direction, which can come only from an inertial torque and a decrease in angular velocity $\dot{\theta}$ of the inner gimbal. As the motion progresses, $\dot{\varphi}$ will increase to a maximum and $\dot{\theta}$ will decrease to 0 as dictated by the conservation of energy. Then $\dot{\theta}$ will reverse and $\dot{\varphi}$ will decrease, and oscillatory motion of the gimbal angles will be observed, with a 90-deg phase difference between $\dot{\theta}$ and $\dot{\varphi}$.

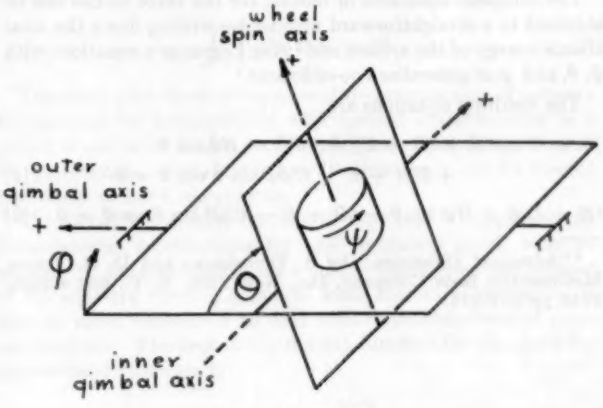


Fig. 1 Free Gyro

Further consideration of the phase relationships and the gyro wheel equation $\vec{\tau} = \vec{\omega} \times \vec{H}$ reveals why a net angular displacement of the outer gimbal occurs for each cycle of the oscillation. For angular velocities $\dot{\varphi}$ the torque along the inner gimbal axis, $\tau_i$, is related to $\dot{\varphi}$ by $\tau_i = \dot{\varphi} H \sin\theta$. For the half cycle of each period during which $\dot{\varphi}$ is positive, the inner gimbal angle is greater than the initial inner gimbal angle, and for the half cycle for which $\dot{\varphi}$ is negative, the inner gimbal angle is less than the initial inner gimbal angle. Hence, during the half cycle for which $\dot{\varphi}$ is positive, the values of $\theta$ and $\sin\theta$ are greater than the values for the other half cycle. For the same range of values $\tau_i$ for each half cycle, and for constant $H$, $|\dot{\varphi}|$ during the half cycle in which it is negative will be greater than during the half cycle in which it is positive, and thus an average angular displacement in the negative $\varphi$-direction will occur for each cycle of the motion.

In other words, the inner gimbal inertial torques are more effective in producing outer gimbal motion when the inner gimbal is close to gimbal lock ($\theta = 0$) than at the other extreme of its motion. The inner gimbal will not accrue an angular displacement per cycle since the maximum outer gimbal inertial torque for each half cycle of the motion occurs when the inner gimbal is at $\theta = \theta_0$.

---

[1] Research Engineer, Boeing Airplane Company.

[2] "An Introduction to the Study of Gyroscopic Instruments," by W. R. Weems, Department of Aeronautical Engineering, Massachusetts Institute of Technology, Cambridge, Mass., 1948, pp. 8-25 to 8-29.

Contributed by the Applied Mechanics Division and presented at the Diamond Jubilee Semi-Annual Meeting, Boston, Mass., June 19–23, 1955, of The American Society of Mechanical Engineers.

Discussion of this paper should be addressed to the Secretary, ASME, 29 West 39th Street, New York, N. Y., and will be accepted until October 10, 1955, for publication at a later date. Discussion received after the closing date will be returned.

Note: Statements and opinions advanced in papers are to be understood as individual expressions of their authors and not those of the Society. Manuscript received by ASME Applied Mechanics Division, July 26, 1954. Paper No. 55—SA-3.

# Appendix

The following nomenclature is used in an analytical treatment of this problem:

$\varphi$ = angular position of outer gimbal
$\theta$ = angular position of inner gimbal relative to outer gimbal
$\psi$ = angular position of wheel relative to inner gimbal
$\theta_0$ = initial inner gimbal angle
$\dot{\theta}_0$ = initial angular velocity imparted to inner gimbal by an impulse
$\zeta_0$ = amplitude of inner gimbal oscillations
$\omega_n$ = natural frequency of system
$\bar{\dot{\varphi}}$ = average angular rate term for outer gimbal velocity
$A$ = moment of inertia of wheel about its spin axis
$B$ = moment of inertia of wheel about an axis perpendicular to spin axis
$C$ = moment of inertia of inner gimbal about spin axis
$D$ = moment of inertia of inner gimbal about inner gimbal axis
$E$ = moment of inertia of inner gimbal about an axis perpendicular to spin and inner gimbal axes
$F$ = moment of inertia of outer gimbal about outer gimbal axis
$I_o = F + C\cos^2\theta_0 + (B + E)\sin^2\theta_0$
$I_i = B + D$
$t$ = time

The complete equations of motion for the three bodies can be obtained in a straightforward manner by writing down the total kinetic energy of the system and using Lagrange's equations with $\psi$, $\theta$, and $\varphi$ as generalized co-ordinates.[3]

The resulting equations are

$$[F + C\cos^2\theta + (B + E)\sin^2\theta]\ddot{\varphi} - H\dot{\theta}\sin\theta + 2(B + E - C)\dot{\theta}\dot{\varphi}\sin\theta\cos\theta = 0 \quad [1]$$

$$(B + D)\ddot{\theta} + H\dot{\varphi}\sin\theta - (B + E - C)\dot{\varphi}^2\sin\theta\cos\theta = 0 \quad [2]$$

$$A(\dot{\psi} + \dot{\varphi}\cos\theta) = H \quad [3]$$

where $H$ = const = angular momentum of wheel about spin axis.

Two approximation methods of solution were used. One method attempted to keep track of the mechanics involved, and the other used a classical, well-established perturbation[4] method at the expense of any physical significance. Both methods yielded the following significant results:

$$\omega_n = \frac{H\sin\theta_0}{\sqrt{I_o I_i}} \quad [4]$$

= frequency at which system oscillates

$$\zeta_0 = \frac{\dot{\theta}_0}{\omega_n} \quad [5]$$

= amplitude of inner gimbal motion

$$\bar{\dot{\varphi}} = -\frac{H\zeta_0^2\cos\theta_0}{2I_o}\left(\frac{F + C}{I_o}\right) \quad [6]$$

= average angular rate of outer gimbal

The accuracy of the results degenerates rapidly as $\theta_0$ approaches 0, and the results are for small amplitude motion ($\zeta_0 \ll 1$).

The third terms on the left side of the basic Equations [1] and [2] are coriolis and centrifugal torques, respectively. The mechanics of the motion described in the main section of the paper deal with the first two terms of Equations [1] and [2], since the coriolis and centrifugal torques are small. However, the centrifugal torque contributes to the average rate, since the time integral of the torque over each cycle is not zero, and Equation [6] includes its effect.

Equation [6] indicates that there will be no average rate of the outer gimbal if the gimbals are initially perpendicular or if the inertia of the gimbals is negligible.

[3] "Advanced Dynamics," by S. Timoshenko and D. H. Young, McGraw-Hill Book Company, Inc., New York, N. Y., first edition, 1948, pp. 212–214.

[4] "Introduction to Non-Linear Mechanics," by N. Minorsky, Edwards Brothers, Inc., Ann Arbor, Mich., 1947, pp. 149–153.

# Shortcomings of Present Methods of Measuring and Simulating Vibration Environments

By C. T. MORROW[1] and R. B. MUCHMORE,[2] LOS ANGELES, CALIF.

**This paper concerns itself with the problem of measuring a vibration environment to be encountered by a delicate instrument or electronic device in the field and of attempting to simulate the vibration in laboratory test as a check on the reliability of the design.**

FIELD vibration is usually either random in time or of a fixed frequency nature. Until recently, the vibrations applied in laboratory test have been fixed frequencies applied at resonances, or single-frequency sweeps. In general, it is not possible to simulate one type of vibration by another, except in special cases, or to express measured data of one type in the language of another without loss of accuracy. For example, it is not valid to analyze random vibration in terms of number of $g$ versus frequency. When the vibration to be encountered is random, the vibration applied in test for proof of design should likewise be random, and single-frequency sweeps should be used only for proof of workmanship with a specification based on the design limits of the item. Random vibration can be applied through the use of an electronically driven vibrator. A procedure for analyzing a random vibration and deriving a specification is presented.

## Nature of a Continuous Spectrum

Most of the vibration encountered by military equipment, and in particular the internal components of guided missiles, is random with time rather than periodic and has a frequency spectrum which is continuous rather than discrete. In short, no randomly fluctuating vibration can be expressed as a discrete spectral line, even if it is accentuated by structural resonance. When random vibration is analyzed by a conventional wave analyzer, the indicating meter will fluctuate; as the analyzer is tuned it will become evident that the vibration is distributed rather than concentrated at particular frequencies. Thus random vibration may readily be distinguished from periodic and its spectrum is called "continuous."

Vibration data are usually summarized in terms of spectra. A correct procedure for describing the continuous spectrum will be presented after a brief discussion of statistics.

## Probability Distributions for Random Vibration

It will be assumed that the instantaneous accelerations in any frequency band have a normal or Gaussian probability distribution about zero as a mean, illustrated in Fig. 1, and given by the formula

$$p(a)da = \frac{1}{\sqrt{2\pi}\sigma} \epsilon^{\frac{-a^2}{2\sigma^2}} da \quad \ldots\ldots [1]$$

where $a$ is a given instantaneous acceleration, $p(a)da$ is the probability that $a$ lies in the interval between $a$ and $a + da$, and $\sigma$ can be shown to be the rms acceleration and is known as the standard deviation. In short

$$\int_{-\infty}^{\infty} a^2 p(a)da = \sigma^2 \quad \ldots\ldots [2]$$

Transient vibrations of occasional occurrence and of severity too extreme for compatibility with normal characteristics in a record of one hr or longer, i.e., which form a class too infrequent to approximate normality in one hr time, say, can be treated separately as shock phenomena.

The probability density function of Equation [1] applies to the instantaneous accelerations for any frequency band, wide or narrow. If the disturbance has a narrow band, however, because of the selective filtering action of some structural resonance, it may be more convenient to deal with the distribution of peak accelerations. The probability density function for the peaks for narrow-band vibration is

$$p(a_p)da_p = \frac{a_p}{\sigma^2} \epsilon^{\frac{-a_p^2}{2\sigma^2}} da_p \quad \ldots\ldots [3]$$

where the $a_p$ are the peaks of the instantaneous accelerations and $\sigma$ is the rms instantaneous acceleration as in Equations [1] and [2]. This is known as a Rayleigh distribution and is also illustrated in Fig. 1.

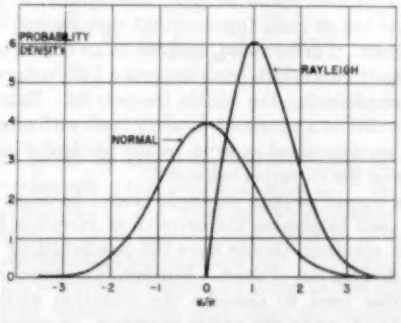


Fig. 1 Comparison of the Normal Distribution for Instantaneous Acceleration and Rayleigh Distribution for Peaks

Fig. 2 is a plot of the fraction of instantaneous accelerations and the fraction of peaks that exceed a given multiple of $\sigma$. There is,

---

[1] Member of Technical Staff, The Ramo-Wooldridge Corporation; formerly, Research Physicist, Hughes Research and Development Laboratories, Hughes Aircraft Company, Culver City, Calif.

[2] Senior Member of Technical Staff, The Ramo-Wooldridge Corporation; formerly Senior Member of the Technical Staff, Hughes Aircraft Company.

Contributed by the Applied Mechanics Division and presented at the Diamond Jubilee Semi-Annual Meeting, Boston, Mass., June 19–23, 1955, of The American Society of Mechanical Engineers.

Discussion of this paper should be addressed to the Secretary, ASME, 29 West 39th Street, New York, N. Y., and will be accepted until October 10, 1955, for publication at a later date. Discussion received after the closing date will be returned.

Note: Statements and opinions advanced in papers are to be understood as individual expressions of their authors and not those of the Society. Manuscript received by ASME Applied Mechanics Division, January 5, 1954. Paper No. 55—SA-2.

theoretically, a finite probability of exceeding any given acceleration.

There are special situations in which the instantaneous accelerations will not be precisely normal, but will have a modified distribution which is simply related to normality. For example,

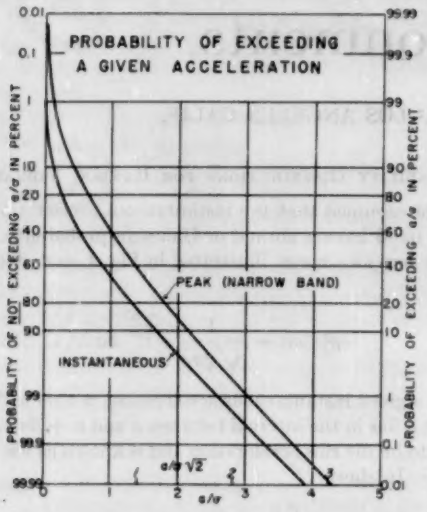


FIG. 2 PROBABILITY OF EXCEEDING A GIVEN ACCELERATION

the distribution would not be normal if a vibration mount bottomed frequently under vibration. This example is an undesirable situation and, hopefully, an uncommon one. It will not be treated in this paper. Likewise, the more subtle effects produced on the distribution by nonlinearity due to friction damping will not be considered here.

## UNITS FOR MEASUREMENT AND ANALYSIS OF RANDOM VIBRATION

By now, a large body of vibration data has been collected in the literature which, however, most of us look upon as being controversial to some degree. From the point of view of this paper, it is found that there has been little effort to distinguish between continuous spectra and discrete spectra. The attempt is usually made to "measure the number of $g$ at each frequency," and the bandwidth of the analyzing equipment is not usually recorded, nor is it even stated whether the bandwidth was constant with frequency. Yet, in regions where the continuous spectrum has no extreme hills or valleys, the number of $g$ indicated will be proportional to the square root of the bandwidth of the wave analyzer. This also would be true, incidentally, if the spectra were discrete but so close together that they cannot be resolved by the analyzer. Furthermore, analysis on an octave basis rather than a constant bandwidth basis imparts a 3 db/octave tilt to the spectrum, emphasizing the higher frequencies. Random-vibration data quoted on a $g$ versus frequency basis with no reference to bandwidth are dependent as much on the particular instrumentation used as on the vibration measured.

The data should be on a per-cycle basis. In other words, the quantities used to express the severity of vibration in different parts of the spectrum should have the bandwidth of the instrumentation divided out of them. Further, it is necessary that any single number used to describe the vibration within a given frequency band, or in the entire spectrum, be obtainable by a root-mean-square operation from a plot of the spectrum.

Let us first consider the latter problem of a single number to express the vibration in a specified band or in the entire spectrum. Fig. 3 shows a time plot of random acceleration for an entire

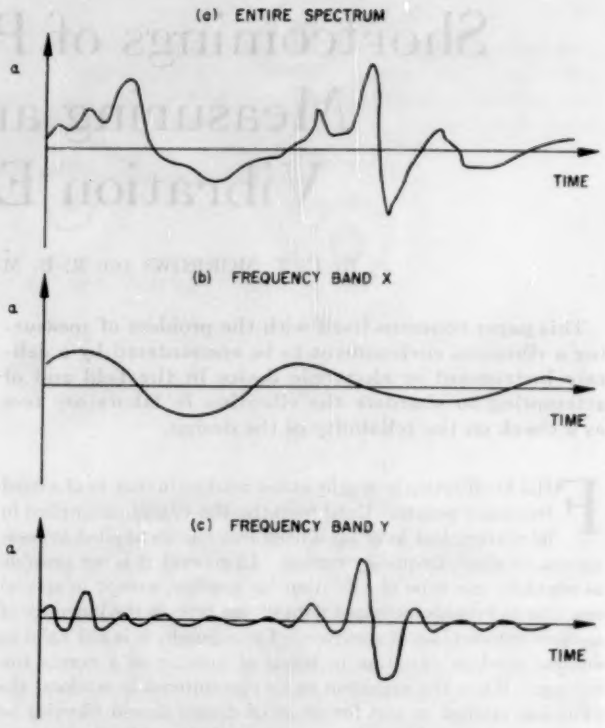


FIG. 3 ACCELERATION—TIME PLOTS

spectrum and for each of two smaller and nonoverlapping frequency bands.

Now, what single number for each of these should be picked to typify the corresponding acceleration? Clearly, the peak acceleration for each time record is not appropriate. Voltmeters designed to read peak for a recurrent sine wave do not necessarily read peak for a varying complex wave. Furthermore, the peaks in band $X$ and band $Y$ do not necessarily occur at the same time or in the same direction, are not directly additive, and cannot be combined in any simple way to assist in predicting the peak for the complete spectrum. Finally, if we observe long enough, theoretically we can observe any peak acceleration we choose.

The average of the absolute values would be less open to criticism, but is not optimum to deal with statistically.

Three considerations favor the root mean square of the instantaneous accelerations: (1) The rms value is by definition the standard deviation of the instantaneous accelerations about zero as a mean, and lends itself conveniently to statistical analysis; (2) rms values for two or more random collections, even though they are in different frequency bands, generally may be combined as the square root of the sum of the squares; (3) the rms value is the time-honored standard measure of a-c voltage in electrical circuitry.

There remains the problem to determine what quantity should be plotted against frequency to describe a spectral distribution. This should be simply related to the rms acceleration in any frequency band. More specifically, if $W(f)$ is the function plotted against frequency, it should be possible to calculate the rms acceleration $\sigma$ between any two frequencies $f_1$ and $f_2$ by a simple operation based on the requirement that the rms value for an entire frequency band be the square root of the sum of the mean-square values for all bands within. This is satisfied if we define

$$W(f) = \lim_{\Delta f \to 0} \frac{\sigma^2_{\Delta f}}{\Delta f} \quad \ldots\ldots\ldots\ldots\ldots\ldots [4]$$

where $\sigma^2_{\Delta f}$ is the mean square acceleration in the rectangular bandwidth $\Delta f$, for it follows that

$$\sigma = \operatorname{Lim}_{\Delta f \to 0} \sqrt{\sum A^2_{\Delta f}} = \operatorname{Lim}_{\Delta f \to 0} \sqrt{\sum \frac{A^2_{\Delta f}}{\Delta f} \Delta f}$$

$$= \sqrt{\int_{f_1}^{f_2} W(f) df} \quad \ldots\ldots [5]$$

In short, the root-mean-square acceleration is the square root of the area under the curve between $f_1$ and $f_2$.

The function $W(f)$ will be called the mean-square acceleration per cycle or the mean-square acceleration density. It follows that the mean-square density in $g^2$/cps is the most convenient means of describing the frequency distribution of a continuous spectrum.

Let $I(f)$ be the meter or oscilloscope indication in $g$ of a wave-analyzer device which is to be used for the analysis of a normally distributed random vibration. If $I(f)$ is obtained as the square root of the time average of the squared acceleration, i.e., if $I(f)$ is an rms indication such as would be obtained from a slow-acting hot-wire or thermocouple meter, the mean-square density is given by

$$W(f) = \frac{I^2(f)}{A} \quad \ldots\ldots [6]$$

where $A$ is the area under the square of the selectivity curve normalized to unity at the center frequency and can be obtained graphically or in special cases may be obtained by formulas which are given below.

If $I(f)$ is obtained as the time average of the absolute value of the instantaneous accelerations, such as is approximated by filtering the output of a full-wave average-value rectifier, the mean-square density is given by

$$W(f) = \frac{\pi I^2(f)}{2A} \quad \ldots\ldots [7]$$

If the bandwidth $B$ is small by comparison with an octave, the signal applied to the detector is a sine wave of slowly varying phase and amplitude, and the peaks are in a Rayleigh distribution. If, then, $I(f)$ is obtained as the time average of the peak acceleration, by averaging the output of a full-wave peak rectifier whose internal cutoff frequency remains not appreciably less than half the band width, the mean-square density is given by

$$W(f) = \frac{2I^2(f)}{\pi A} \quad \ldots\ldots [8]$$

For a detector which functions according to either of the last two situations, but is calibrated in terms of single-frequency root-mean-square signal, Formulas [7] and [8] reduce to

$$W(f) = \frac{4I^2(f)}{\pi A} \quad \ldots\ldots [9]$$

Note that the case of a peak rectifier of long internal time constant has not been calculated. The result would depend on the characteristics of the rectifier tube and its d-c load. A formula for a particular instrument of this type can be obtained by calibration with a random signal of known rms value for a frequency band in the region of the frequency to which the analyzer is tuned.

In case the analyzer has a selectivity curve approximating that of a single resonant circuit, the area is given by

$$A_1 = \frac{\pi B_1}{2} \quad \ldots\ldots [10]$$

More generally, if the analyzer has a selectivity curve approximating that of $n$ resonant circuits of identical $Q$, cascaded without interaction, the area is given by

$$A_n = \frac{(2n-3)(2n-5)\ldots(1)\pi B_n}{2^n(n-1)!\sqrt{2^{\frac{1}{n}}-1}} \quad \ldots\ldots [11]$$

For such a system of $n$ resonant circuits, the bandwidth for which the responses are down a factor, $r$ has the following ratio to the bandwidth between the half-power points

$$R = \frac{\sqrt{r^{\frac{2}{n}}-1}}{\sqrt{2^{\frac{1}{n}}-1}} \quad \ldots\ldots [12]$$

This expression may be used to determine the number of resonant circuits that best approximate the selective filter of a wave analyzer.

Alternately, a particular analyzer can be given an over-all calibration for effects of both rectifier and selective circuit by applying a random signal whose rms value over a definite frequency band has been measured using a thermocouple meter or other square-law meter.

For a distribution other than normal, the use of rms and $g^2$/cps is still valid although not a complete description. The formulas in the foregoing for interpretation of the wave-analyzer indications are still accurate approximations. The distribution changes its shape as different bands are combined; the tendency is for narrow-band vibration to be accurately normal even when a complete spectrum has noticeable discrepancies. Vibration damage to structures ordinarily occurs at resonances. The vibration in the resonant members tends to be normal, due to restricted bandwidth, even when the entire applied spectrum is not. Thus the proposed use of mean-square density will be adequate for specifications except when the deviation from normality in the entire spectrum is extreme, or when the structures to be tested are highly damped.

A test for normality on a wide or narrow-band basis is to count the number of instants the acceleration time plot passes through various chosen accelerations. For a narrow band, it is sufficient to count the number of peaks above each chosen value, which is a similar operation and leads to a curve which is Gaussian in shape. The theoretical population, including both positive and negative peaks, is obtained by integrating the Rayleigh distribution from $a_p$ to infinity

$$\int_{a_p}^{\infty} \frac{a_p}{\sigma^2} \epsilon^{-\frac{a_p^2}{2\sigma^2}} da_p = \int_{a_p/2\sigma^2}^{\infty} \epsilon^{-\frac{a_p^2}{2\sigma^2}} d\frac{a_p}{2\sigma^2}$$

$$= \epsilon^{-\frac{a_p^2}{2\sigma^2}} \quad \ldots\ldots [13]$$

The exact shape of selectivity curve chosen for the wave analyzer is relatively unimportant so long as it is taken into account in calculating the mean-square-acceleration density. The bandwidth should be narrow (comparable to or smaller than that of the resonances in the structure that transmitted the vibration) to provide resolving power and detail in the analysis.

Some special considerations arise when the analysis is to be carried out on an acceleration-time signal which is recorded on a short length of tape. Recirculating a loop of tape makes the signal under analysis artificially periodic at the frequency of recirculation. The special effects arising from this will not be considered here except to say that the loop of tape should be long

enough so that several of the harmonics of the recirculation frequency will lie within the bandwidth of the analyzer.

In some analyses it may be found convenient to play back a magnetic tape at a higher speed than it was recorded. This would, for example, permit analysis down to lower frequencies. It must be remembered in doing this that the effective bandwidth to be used in the formulas given in the foregoing is inversely proportional to the speed at which the tape is reproduced.

The indicating device of the wave analyzer, in general, should have a time constant of a second or more. Otherwise there will be insufficient averaging carried out in one sweep to give a reproducible result; several sweeps would have to be carried out and averaged in an appropriate manner. The rate of sweep of the analyzer must be correspondingly slow so that the analyzer will not lose the resolving power inherent in its selectivity curve.

## Application of Continuous Spectra in Tests

The use of continuous spectra in vibration test requires the application of complex waves and necessitates, consequently, the use of a vibrator driven by an electronic, hydraulic, or other device capable of handling a complex-wave shape. In short, it ordinarily requires a voice coil-actuated vibrator and also an amplifier of sufficient output over the frequency range of interest to operate the system. In particular, two general methods are possible in applying continuous spectra. One is to play into the system a recording or mixture of recordings of vibration that actually occurred in transportation or in use. The other method is to use as a source an electronic-noise generator, i.e., a "white-noise" generator, and filter the output in accordance with a specification derived from vibration measurements. Facilities for applying complex waves to vibration tables should be made generally available as soon as possible.

It is suggested that "white-vibration" specifications be derived from measured data by drawing a simple curve through the highest peaks in the $g^2$/cps plot, or by multiplying this by any necessary further margin of safety.

## Simulation by Line Spectra

It has been customary until recently to do all vibration testing in terms of discrete spectra, and in particular, single-frequency sweeps. Apparatus for this is available in common use and is simpler than that described in the foregoing for the application of white noise. It is clear that this technique is entirely valid, even though perhaps not preferable, for proof of workmanship as the specifications for such a purpose can be derived appropriately from the severity that a particular design with an acceptable standard of workmanship can stand. It is desirable to go further, however, and explore the validity of the single-frequency technique for proof of design in type testing, based on specifications derived from the tactical conditions.

Inspection of the problem shows that a single-frequency line which is equivalent in any degree to the original spectrum can be derived only for the immediate region of a resonance. A further complication of the problem of equivalence is that the degree of equivalence will depend on the particular type of failure expected whether it is simple malfunction, wear, or fatigue. To avoid dealing for the moment with this last complication, we will speak of a reference spectral line rather than an equivalent spectral line. The reference spectral line is defined as the number of single-frequency $g$ applied which would result in the same rms acceleration at a particular mass in the resonant system under test.

To explore the utility of this limited concept of equivalence, a reference spectral line can be computed for a simple resonant system consisting of a mass attached to a vibrator by a spring and a dashpot, and excited by a white-noise spectrum of constant mean-square density. The method of calculation is to evaluate the integral of the product of the mean square $g$ per cycle and the square of the transmission curve of the resonant system, take the square root, and divide by the transmission of the resonant system at resonance so as to obtain the number of $g$ at the vibrator platform. The detailed calculation is carried out in the Appendix. The result is

$$A_{ref} \cong \sqrt{\pi W(f_0) B} \quad [14]$$

where $A_{ref}$ is the peak acceleration of the reference sine wave in $g$, $W(f_0)$ is the mean-square density at the resonant frequency $f_0$, and $B$ is the bandwidth of the simple resonance as defined in the Appendix.

It will be seen, then, that the reference spectral line, in number of $g$, is proportional to the square root of the bandwidth of the resonance of the system under test. It can be said immediately, then, that even this limited degree of equivalence cannot be obtained in general until something is known of the dynamics of the system under test. Note further that the method of arriving at the reference spectral line implies that it would not be swept through the frequency range covered by a vibration specification but rather left to excite the corresponding particular resonance for the entire duration of the specified test. For a sweep there is an additional problem of juggling the number of $g$ applied and the rate of sweep. It may be concluded that there is no mathematically valid way of arriving at a conventional single-frequency sweep that is equivalent to a continuous spectrum. Any specification with this objective must be considered arbitrary and in the area of engineering judgment and calculated risk, except, perhaps, for a few cases of simple malfunction.

For those cases of malfunction in which it may be worth while, the concept of reference spectra may be carried one step further to consider the case of a system of several degrees of freedom. The spectrum may be divided into bands corresponding to the region of each resonance, and a separate reference acceleration for each calculated for any mass in the system. If two resonances are extremely close together it may be more useful to combine these and compute for them a single reference acceleration. Comparison of a reference acceleration with the probability distribution of the peaks, as given in Fig. 1, will reveal something of the probability of malfunction.

## Conclusions

In conclusion, data on vibration that is continuously distributed in frequency should be recorded in units which are appropriate to continuous spectra. Single-frequency tests may then be specified if necessary, in an arbitrary manner for proof of design, through the use of engineering judgment, but these should not be interpreted as valid descriptions of what happens under tactical conditions. It has been shown that the possibility of obtaining valid single-frequency equivalence is quite restricted. Furthermore, a single-frequency reference spectral line, as defined in this paper, is not meaningful if much chattering or other nonlinear effects occur. Under these conditions, the applied continuous spectrum tends to concentrate itself not only at structural resonances, but also at multiples and combinations of them.

To avoid unacceptable complexity in deriving specifications from vibration data, some arbitrariness is inevitable, even if a single-frequency sweep is not to be used to prove out design. It is desirable to weight the arbitrariness in such a way that the specification conditions are in no way less severe than those shown by the data. For tests to be performed on not more than a few units, it is commendable to increase the severity further beyond the tactical mean by a reasonable factor to include a margin of safety against variation of tactical conditions

or workmanship from missile to missile, in short, to guarantee a significant reliability with respect to the tactical environment. Thus design-approval-test specifications do not have the same objective as descriptions of the tactical environment and the two should be kept distinct.

## REFERENCES

For further information on characteristics of random noise or vibration refer to the following:


1 "Threshold Signals, Radiation Laboratory Series No. 24," by J. L. Lawson and G. E. Uhlenbeck, McGraw-Hill Book Company, Inc., New York, N. Y., 1950.

2 "Mathematical Analysis of Random Noise," by S. O. Rice, *Bell System Technical Journal*, vol. 23, 1944, p. 282; vol. 25, 1945, p. 46.

3 "Aspects of the Turbulence Problem," by H. W. Liepmann, *Journal of Applied Mathematics and Physics*, vol. 3, 1952, p. 321.

4 "Homogeneous Turbulence," by G. K. Batchelor, Cambridge University Press, Cambridge, England, 1953.

5 "Acoustic Measurements," Beranek, John Wiley & Sons, Inc., New York, N. Y., 1949, chapters 10 and 11.


# Appendix

In this Appendix a solution for the acceleration of a mass in a simple one-degree-of-freedom resonant system will be found for both a sinusoidal applied acceleration and a random acceleration having a flat spectrum. The conditions for equivalence, in the sense that rms accelerations are made equal, will then be found. This defines the reference spectral line as discussed in the text.

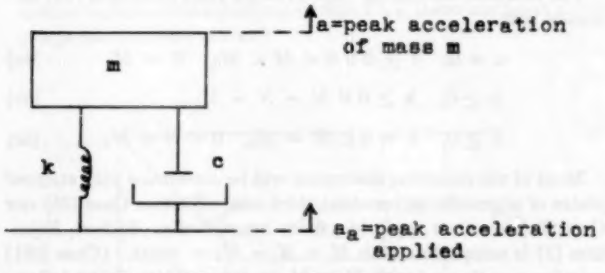


FIG. 4 MECHANICAL SYSTEM CONSIDERED

The mechanical system considered is shown in Fig. 4 in which $m$ = mass, $k$ = spring constant, and $c$ = damping coefficient. For sinusoidal accelerations

$$ma + c\frac{a - a_a}{j\omega} - k\frac{a - a_a}{\omega^2} = 0 \quad [15]$$

Hence

$$a = a_a \frac{\frac{c}{j\omega} - \frac{k}{\omega^2}}{m + \frac{c}{j\omega} - \frac{k}{\omega^2}} = a_a \frac{j\omega\frac{c}{k} + 1}{1 + j\omega\frac{c}{k} - \frac{\omega^2 m}{k}} \quad [16]$$

Let $$\omega_0 = \sqrt{\frac{k}{m}} \quad [17]$$

and the damping ratio $$\zeta = \frac{c\omega_0}{2k} \quad [18]$$

The latter is the ratio of the damping coefficient to that of critical damping.

Then

$$\left.\begin{aligned} a &= a_a \frac{\frac{2j\zeta\omega}{\omega_0} + 1}{1 - \frac{\omega^2}{\omega_0^2} + j\frac{2\zeta\omega}{\omega_0}} \\ &\cong \frac{a_a}{1 - \frac{\omega^2}{\omega_0^2} + j\frac{2\zeta\omega}{\omega_0}} \end{aligned}\right\} \quad [19]$$

The last expression holds for small damping, which condition will be assumed hereafter.

At $\omega = \omega_0$ one has

$$a = -\frac{ja_a}{2\zeta} \quad [20]$$

With a flat spectrum of acceleration applied, the mean-square acceleration of $m$ is

$$\left.\begin{aligned} \sigma_m^2 &= \int_0^\infty \frac{W}{\left|1 + \frac{2j\zeta\omega}{\omega_0} - \frac{\omega^2}{\omega_0^2}\right|^2} df \\ &= \frac{W\omega_0}{8\zeta} \end{aligned}\right\} \quad [21]$$

Here $W$ is the mean-square density and is taken as independent of frequency.

Now, to find the peak value in $g$ of the reference sine wave which produces the same root-mean-square acceleration of $m$ as does the continuous spectrum, set

$$\sigma_m^2 = \frac{a_{mp}^2}{2} \quad [22]$$

From Equations [21], [22], and [20]

$$\frac{W\omega_0}{8\zeta} = \frac{a_{mp}^2}{2} = \frac{a_{ref}^2}{8} \quad [23]$$

This yields a reference peak acceleration in $g$ of

$$a_{ref} = \sqrt{W\omega_0\zeta} \quad [24]$$

It can easily be shown from Equation [19] that the shift in frequency needed to reduce the response to $1/\sqrt{2}$ times that at resonance is

$$\Delta f = \zeta f_0 = \frac{1}{2}B \quad [25]$$

where $f_0$ is the resonant frequency and $B$ as defined by this equation is called the bandwidth. Thus Equation [24] can be written

$$a_{ref} = \sqrt{\pi WB} \quad [26]$$

If the applied spectral density is not constant everywhere but does not vary too rapidly in the vicinity of $\omega_0$, Equation [26] can be written approximately as

$$a_{ref} \cong \sqrt{\pi W(f_0)B} \quad [27]$$

# Limits of Economy of Material in Plates[1]

By H. G. HOPKINS[2] AND W. PRAGER,[3] PROVIDENCE, R. I.

**The paper is concerned with the limits of economy of material in a simply supported circular plate under a uniformly distributed transverse load. The plate material is supposed to be plastic-rigid and to obey Tresca's yield condition and the associated flow rule. The criterion of failure adopted is that used in limit analysis. It is shown that the plate of uniform thickness has a weight efficiency of about 82 per cent. Stepped plates of segmentwise constant thickness are discussed, and the plate of continuously varying thickness is treated as the limiting case obtained by letting the number of steps go to infinity.**

## Introduction

THE limits of economy of material in structures have not yet been investigated in a systematic and comprehensive manner. Structures that have been discussed from this point of view include trusses (1, 2),[4] beams and frames (3, 4, 5), reinforced stressed-skin panels (6), and shells (7). The present paper is concerned with the limits of economy of material in a simply supported circular plate of varying thickness under a uniformly distributed transverse load. The plate material is supposed to be plastic-rigid and to obey Tresca's yield condition and the associated flow rule. The criterion of failure adopted in this paper is that used in limit analysis (8).

As Hill (9) has pointed out, this concept of failure is most readily explained for a structure consisting of rigid-plastic elements. For a given type of loading of slowly increasing intensity, the yield point of such a structure is defined as the load intensity at which deformation first becomes possible. For most practical purposes the structure can be considered to be on the verge of failing when the yield point is reached. It should be noted that the stresses may attain the yield limit locally long before the yield point of the structure is reached, but plastic deformations in such a local plastic region are inhibited by the adjacent rigid material. This inhibiting effect vanishes only at the yield point of the structure when the spreading plastic region reaches a critical size or shape.

## Fundamental Relations

In the spirit of the theory of thin plates, the following analysis treats the plate as a two-dimensional continuum. On account of the rotational symmetry of loading and support, the state of stress at the yield point and the incipient plastic deformation are specified when the radial bending moment $M$, the circumferential bending moment $N$, and the rate of deflection $w$ are known as functions of $r$. The bending moments must satisfy the equation of equilibrium

$$(rM)' - N = -\frac{1}{2}pr^2 \quad [1]$$

where $p$ is the uniformly distributed transverse load, and the prime denotes differentiation with respect to $r$. In terms of the rate of deflection $w(r)$, the radial and circumferential rates of curvature $\kappa$ and $\lambda$, respectively, are defined by

$$\kappa = -w', \quad \lambda = -w'/r \quad [2]$$

For the considered conditions of loading and support the bending moments $M$ and $N$ are found to be non-negative. Tresca's yield condition for the plate (10) then requires that at least one of the bending moments $M$ and $N$ equals the fully plastic bending moment $M_0 = \sigma_0 h^2$, where $\sigma_0$ is the yield stress in simple tension (or compression), and $2h$ denotes the thickness of the plate. Note that $M_0$ may vary with $r$ since the plate is not assumed to have uniform thickness.

The flow rule associated with Tresca's yield condition (10) demands that

$$\kappa = 0, \quad \lambda \geq 0 \text{ if } 0 < M < M_0, \quad N = M_0 \quad [3a]$$

$$\kappa \geq 0, \quad \lambda \geq 0 \text{ if } M = N = M_0 \quad [3b]$$

$$\kappa \geq 0, \quad \lambda = 0 \text{ if } M = M_0, \quad 0 < N < M_0 \quad [3c]$$

Most of the following discussion will be concerned with stepped plates of segmentwise constant thickness. Neither Case [3b] nor Case [3c] can then apply to a finite interval of $r$. Indeed, Equation [1] is compatible with $M = N = M_0 = \text{const.}$ (Case [3b]) only for $p = 0$; and with $M = M_0 = \text{const.}$ (Case [3c]) it follows from Equation [1] that $N = M_0 + (1/2)pr^2 > M_0$, which is in contradiction to the condition that $N < M_0$ for this case.

## Stepped Plate

Consider a simply supported circular plate of radius $R$ subjected to a uniformly distributed transverse load $p$. In accordance with the rotational symmetry of loading and support, the plate thickness will be assumed to depend on $r$ only; specifically, it will be assumed to be constant in each of the intervals bounded by $0 = r_0 < r_1 < \ldots < r_n = R$. In the $k$th interval, $r_{k-1} < r < r_k$, let the plate thickness be denoted by $2h_k$, the radial and circumferential bending moments by $M_k(r)$ and $N_k(r)$, and the fully plastic bending moment by $M_{0k}$.

It has been shown at the end of the preceding section that only Case [3a] is admissible for any finite interval of $r$ in which the plate thickness has a constant value. For the $k$th interval considered in the foregoing, there are therefore only the following possibilities: Either Case [3c] applies throughout the entire interval or the interval consists of subintervals to each of which Case [3a] applies with $M_k = M_{0k}$ on the boundary between adjacent subintervals. The latter possibility, however, is ruled out by the following argument: With $N_k(r) = M_{0k}$, integration of Equation [1] yields

$$M_k(r) = M_{0k} - \frac{1}{6}pr^2 + \frac{c_k}{r} \quad [4]$$

---

[1] The results presented in this paper were obtained in the course of research sponsored by the Ballistic Research Laboratories of Aberdeen Proving Ground under Contract DA-19-020-ORD-798. The authors are indebted to the Authorities of the Ballistic Research Laboratories for the permission to publish the paper.

[2] Visiting Professor of Applied Mathematics, Brown University.

[3] Professor of Applied Mechanics, Brown University. Mem. ASME.

[4] Numbers in parentheses refer to the Bibliography at the end of the paper.

Presented at the National Conference of the Applied Mechanics Division, Troy, N. Y., June 16–18, 1955, of THE AMERICAN SOCIETY OF MECHANICAL ENGINEERS.

Discussion of this paper should be addressed to the Secretary, ASME, 29 West 39th Street, New York, N. Y., and will be accepted until October 10, 1955, for publication at a later date. Discussion received after the closing date will be returned.

NOTE: Statements and opinions advanced in papers are to be understood as individual expressions of their authors and not those of the Society. Manuscript received by ASME Applied Mechanics Division, June 1, 1954. Paper No. 55—APM-2.

where $c_k$ is a constant of integration. If $M_k(\rho) = M_{0k}$ for some radius $\rho$ satisfying $r_{k-1} < \rho < r_k$, then $c_k = (1/6)p\rho^2$ and

$$M_k(r) = M_{0k} + \frac{1}{6}\,p\rho^2\left(\frac{\rho}{r} - \frac{r^2}{\rho^2}\right) \quad [5]$$

For $r < \rho$ this gives $M_k(r) > M_{0k}$ in contradiction to the condition that Case [3a] prevails on both sides of the circle $r = \rho$. It follows that $M_k(r)$ assumes the value $M_{0k}$ only for $r = r_{k-1}$ or not at all.

As regards the rate of deflection $w$, necessarily continuous, it follows from the first of Equations [2] and Case [3a] that $w$ is linear or segmentwise linear in $r$. In the latter case the circles where the derivative $w'$ has a discontinuity are hinge circles; the radial bending moment must equal the fully plastic bending moment at such hinge circles. It has just been proved, therefore, that hinge circles can occur only at the inner boundaries of the annuli of constant thickness.

Under a given type of loading a given structure usually fails in a well-defined way. A minimum weight structure, however, is capable of failing in any one of a number of different ways. In the present case the nature of the competing failure modes follows immediately from the fact that $w$ must be linear or segmentwise linear with hinge circles at the inner boundaries of the annuli of constant thickness. For any failure mode the rate at which the load does work must equal the rate at which mechanical energy is dissipated in plastic flow. For a given critical load $p$, this energy balance is expressed by an equation that is linear in the fully plastic bending moments $M_{01}, \ldots, M_{0n}$. Since there can be at most $n$ independent equations of this kind, there can be at most $n$ independent failure modes.[5]

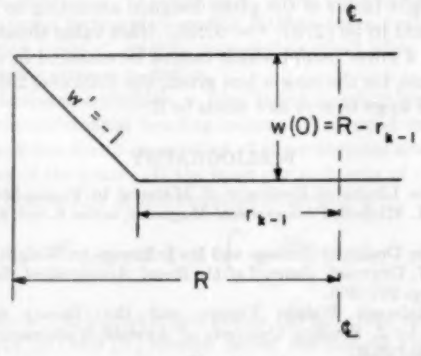


FIG. 1

Fig. 1 shows a possible failure mode. The corresponding energy balance is obtained as follows. As the annulus $r_{k-1} < r < R$ is bent into a cone, mechanical energy is dissipated at the rate

$$D_1 = 2\pi \int_{r_{k-1}}^{R} N\lambda r\, dr \quad [6]$$

With $\lambda r = -w' = 1$ and $N$ equal to the fully plastic bending moment in each annulus, Equation [6] yields

$$D_1 = 2\pi[(r_k - r_{k-1})M_{0k} + (r_{k+1} - r_k)M_{0k+1} + \ldots + (R - r_{n-1})M_{0n}] \quad [7]$$

The rate $D_2$ at which mechanical energy is dissipated along the hinge circle $r = r_{k-1}$ is obtained by considering this hinge circle as the limiting case of a narrow annulus across which $w'$ changes rapidly but in a continuous manner. When $D_2$ is evaluated as the limit of the integral

$$\int 2\pi(M\kappa + N\lambda)r\, dr$$

extended over this annulus, the following result is obtained

$$D_2 = 2\pi r_{k-1}M_{0k} \quad [8]$$

Finally, the rate of work of the uniformly distributed load $p$ is found to be

$$W = 2\pi p \int_0^R wr\, dr = \frac{\pi p}{3}(R^3 - r_{k-1}^3) \quad [9]$$

The energy balance is therefore expressed by

$$r_kM_{0k} + (r_{k+1} - r_k)M_{0k+1} + \ldots + (R - r_{n-1})M_{0n} = \frac{p}{6}(R^3 - r_{k-1}^3) \quad [10]$$

Equations of this form can be written for $k = 1, 2, \ldots, n-1$. For $k = n$, the energy balance is expressed by

$$R\,M_{0n} = \frac{p}{6}(R^3 - r_{n-1}^3) \quad [11]$$

When the critical load intensity and the radii $r_1, \ldots, r_n = R$ are given, Equation [11] yields $M_{0n}$ and hence the thickness $2h_n$ of the outermost annulus. Equation [10] written for $k = n-1$ then yields $M_{0n-1}$ and hence $h_{n-1}$, and so on.

The preceding analysis is based on assumed failure modes. Before these can be accepted it must be shown that they are associated with statically correct bending moments that satisfy the yield condition. The equilibrium of the plate requires that the radial bending moment is continuous across any hinge circle. In the annulus $r_{k-1} \le r \le r_k$ the radial bending moment $M_k$ therefore varies according to Equation [4] so as to assume the values $M_{0k}$ and $M_{0k+1}$ for $r_{k-1}$ and $r_k$ respectively. When $c_k$ is eliminated from the equations satisfying these boundary conditions, the following relation is obtained

$$r_kM_{0k} - r_kM_{0k+1} = \frac{p}{6}(r_k^3 - r_{k-1}^3) \quad [12]$$

If the corresponding equations for $k+1, \ldots, n$ are added to Equation [12], then Equation [10] is obtained. The failure modes considered are therefore associated with statically correct bending-moment distributions.

For a plate with constant thickness, $n = 1$ and, of course, $r_0 = 0$. Equation [11] then furnishes $M_{01} = pR^2/6$ in agreement with the results found in an earlier paper (10). The weight of this plate of constant thickness is

$$G_1 = 2\gamma\pi R^2h = 2\gamma\pi R^2(M_{01}/\sigma_0)^{1/2} = \gamma\pi R^3\left(\frac{2p}{3\sigma_0}\right)^{1/2} \quad [13]$$

where $\gamma$ is the specific weight of the plate material. For an arbitrary plate, the weight will be written in the form

$$G = \alpha\gamma\pi R^3\left(\frac{2p}{3\sigma_0}\right)^{1/2} \quad [14]$$

and the coefficient $\alpha$ will be called the weight factor; it compares the weight of the considered plate to that of a plate of uniform thickness capable of carrying the same load $p$.

For a plate with a single step, Fig. 2 shows the variation of $h_2/h_1$ with $r_1/R$, and Fig. 3 shows the variation of the weight factor $\alpha$ with $r_1/R$. It is seen that the lightest plate of this type is obtained

[5] This argument is due to Cox and Smith (6).

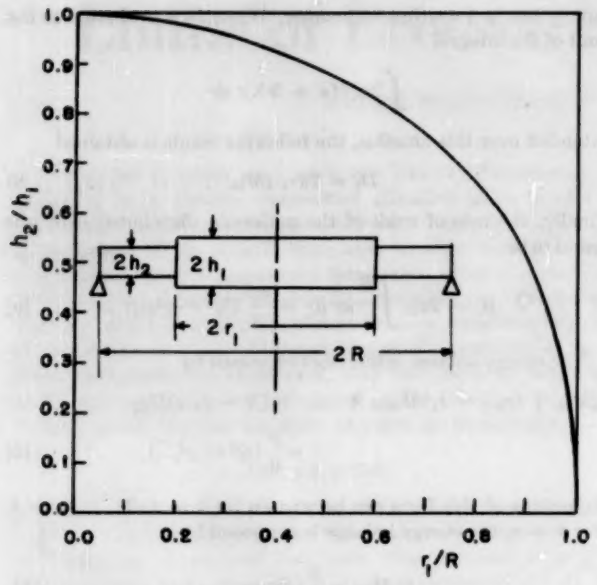


FIG. 2

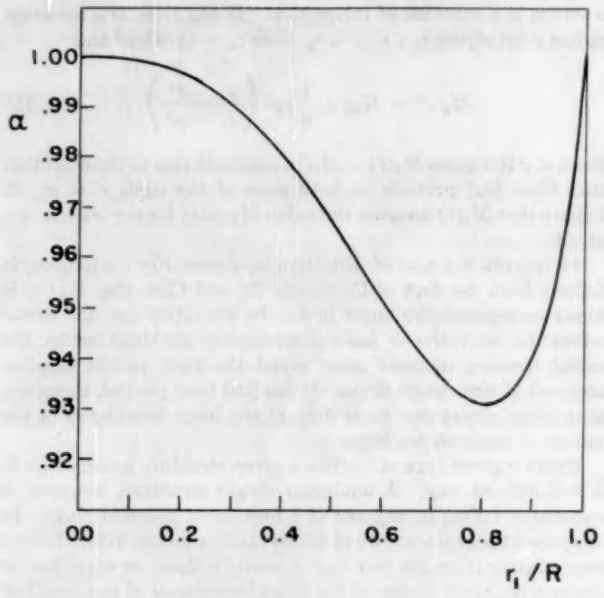


FIG. 3

when $r_1/R$ is about 0.8 and that the weight of this plate is about 7 per cent less than that of an equally strong plate of constant thickness.

For regularly stepped plates ($r_k = kR/n$), Table 1 shows the weight factors $\alpha$ as well as thickness factors $\beta_k$ defined by

$$h_k = \beta_k R(p/6\sigma_0)^{1/2} \quad [15]$$

As the number of steps increases indefinitely, the weight factor is found to tend toward 0.816.

TABLE 1 WEIGHT AND THICKNESS FACTORS FOR REGULARLY STEPPED PLATES

| $n$ | $\alpha$ | $\beta_1$ | $\beta_2$ | $\beta_3$ | $\beta_4$ | $\beta_5$ |
|---|---|---|---|---|---|---|
| 1 | 1.000 | 1 | ... | ... | ... | ... |
| 2 | 0.967 | 1.061 | 0.935 | ... | ... | ... |
| 3 | 0.938 | 1.097 | 1.045 | 0.839 | ... | ... |
| 4 | 0.917 | 1.120 | 1.092 | 0.987 | 0.760 | ... |
| 5 | 0.901 | 1.135 | 1.117 | 1.052 | 0.924 | 0.699 |

## PLATE OF CONTINUOUSLY VARYING THICKNESS

The plate of continuously varying thickness can be treated as the limiting case of a regularly stepped plate when the number of steps increases indefinitely. It follows from this point of view that the minimum weight plate of continuously varying thickness must be capable of developing a hinge circle anywhere. This means that for any value of $r$ between 0 and $R$, the bending moments $M$ and $N$ must equal the fully plastic bending moment $M_0(r)$ corresponding to the plate thickness $2h(r)$ at this radius. When

$$M(r) = N(r) = M_0(r) = \sigma_0 h^2(r) \quad [16]$$

is substituted into the equation of equilibrium [1], integration under the boundary condition $M(R) = 0$ yields

$$M(r) = N(r) = \frac{pR^2}{4}\left(1 - \frac{r^2}{R^2}\right) = \sigma_0 h^2(r) \quad [17]$$

or

$$h(r) = \frac{R}{2}\left(\frac{p}{\sigma_0}\right)^{1/2}\left(1 - \frac{r^2}{R^2}\right)^{1/2} \quad [18]$$

Since the present analysis considers only the bending strength of the plate, the relation $h(R) = 0$ is a necessary consequence of the edge condition $M(R) = 0$. Actually, the value of $h(R)$ is determined not by a required bending strength but by the shear strength necessary to transmit the shear force $pR/2$ per unit length of the circumference of the plate.

The weight factor of the plate designed according to Equation [18] is found to be $(2/3)^{1/2} \approx 0.816$. This value should be considered as a lower bound which cannot be attained in actual design because, for the reason just given, the thickness $2h(r)$ cannot be allowed to go to zero as $r$ tends to $R$.

## BIBLIOGRAPHY

1 "The Limits of Economy of Material in Frame-Structures," by A. G. M. Michell, *Philosophical Magazine*, series 6, vol. 8, 1904, pp. 589–597.

2 "The Design of Trusses and Its Influence on Weight and Stiffness," by J. Drymael, *Journal of the Royal Aeronautical Society*, vol. 46, 1942, pp. 297–308.

3 "Minimum Weight Design and the Theory of Plastic Collapse," by J. Foulkes, *Quarterly of Applied Mathematics*, vol. 10, 1953, pp. 347–358.

4 "Minimum Weight Design of Structural Frames," by J. Foulkes, Proceedings of the Royal Society of London, England, series A, vol. 223, 1954, pp. 482–494.

5 "Plastic Design of Plane Frames for Minimum Weight," by J. Heyman, *Structural Engineer*, vol. 31, 1953, pp. 125–129.

6 "Structures of Minimum Weight," by H. L. Cox and H. E. Smith, Aeronautical Research Committee (Great Britain) Reports and Memoranda No. 1923, His Majesty's Stationery Office, London, England, 1943.

7 "Weight-Strength Analysis of Aircraft Structures," by F. R. Shanley, McGraw-Hill Book Company Inc., New York, N. Y., 1952.

8 "Theory of Perfectly Plastic Solids," by W. Prager and P. G. Hodge, Jr., John Wiley & Sons Inc., New York, N. Y., 1951.

9 "On the State of Stress in a Plastic-Rigid Body at the Yield Point," by R. Hill, *Philosophical Magazine*, Series 7, vol. 42, 1951, pp. 868–875.

10 "The Load Carrying Capacities of Circular Plates," by H. G. Hopkins and W. Prager, *Journal of the Mechanics and Physics of Solids*, vol. 2, 1953, pp. 1–13.

# The Permanent Deflection of a Plastic Plate Under Blast Loading[1]

By A. J. WANG,[2] CHICAGO, ILL.

**This paper is concerned with a simply supported circular plastic plate that is exposed to a strong blast. Equations of deformation are developed.**

IN DETERMINING the deflection of the plate in this problem, it is assumed that the blast imparts instantaneously the transverse velocity $u_0$ to the entire plate and that thereafter the plate is free from transverse loads. The plate is supposed to have uniform thickness and to consist of a perfectly plastic-rigid material that obeys Tresca's yield condition and the associated flow rule [see, for instance, Prager (1)[3]]. A general theory of circular plastic plates under static or dynamic loading has been given by Hopkins and Prager (2, 3) but the present problem has not been discussed by these authors. The same problem with built-in support is solved in a separate paper by Hopkins and the author (4).

## Equation of Dynamic Equilibrium

*Yield Condition and Flow Rule.* Let $r$, $\varphi$, $z$ be cylindrical coordinates, the origin being at the center of the undeformed middle surface of the plate, and the $z$-axis pointing vertically downward. Because of rotational symmetry, the shearing stresses $\tau_{r\varphi}$ and $\tau_{\varphi z}$ vanish identically. Furthermore, if the plate thickness $2h$ is small compared to the plate radius $R$, then the normal stress $\sigma_z$ and shearing stress $\tau_{rz}$ may be regarded as small when compared to the bending stresses $\sigma_r$ and $\sigma_\varphi$.

The transverse deflection $w$, the radial bending moment $M$, and the circumferential bending moment $N$ depend only on the radius $r$ and the time $t$ on account of the rotational symmetry of the motion of the plate. If the mass per unit area of the middle surface is denoted by $\mu$, the equation of motion is

$$\frac{\partial}{\partial r}(rM) = N + \int_0^r \mu \frac{\partial^2 w}{\partial t^2} r\,dr \quad \ldots\ldots [1]$$

In the theory of Hopkins and Prager (2) the plate is treated as rigid if both $|M|$ and $|N|$ remain below the critical value $M_0 = \sigma_0 h^2$, where $\sigma_0$ is the yield stress in simple tension or compression and $2h$ denotes the thickness of the plate. Moreover, when $N = M_0$ while $0 < M < M_0$, the rate of radial curvature

$$\kappa = -\partial^2 w/\partial r^2 \partial t \quad \ldots\ldots [2]$$

vanishes and the rate of circumferential curvature

$$\lambda = -(1/r)\partial^2 w/\partial r \partial t \quad \ldots\ldots [3]$$

cannot be negative. When $M = N = M_0$, on the other hand, the only restriction on $\kappa$ and $\lambda$ is that these rates of curvature cannot be negative.

*Solution.* For the present problem, the plate cannot deform without becoming plastic at the center. By rotational symmetry, we thus have $M = N = M_0$ at the center. At the simply supported edge $r = R$ we must have $M = 0$.

Let us consider the following velocity field

$$\left.\begin{aligned} \partial w/\partial t &= u_0 \text{ for } 0 \le r \le \rho(t) \\ &= u_0 \frac{R - r}{R - \rho(t)} \text{ for } \rho(t) \le r \le R \end{aligned}\right\} \quad \ldots [4]$$

where $\rho(t)$ is a function of time. The central circular region $0 \le r \le \rho(t)$ moves with the uniform velocity $u_0$ and the rates of curvature in this region vanish. For the surrounding annulus $\rho(t) \le r \le R$, the rate of radial curvature $\kappa$ vanishes, while the rate of circumferential curvature is positive. Thus the assumed velocity distribution is compatible with the assumption that $M = N = M_0$ in the central circular region, while $N = M_0$, $0 < M < M_0$ in the surrounding annulus. Moreover, $M = N = M_0$ and $\partial w/\partial t = u_0$ satisfy the equation of motion, Equation [1]. There remains then the question whether $\rho(t)$ can be made to vary with time in such a manner that substitution of $N = M_0$ and the acceleration obtained from [4] into [1] results in a differential equation for $M(r, t)$ that has a solution satisfying the following conditions for $t > 0$

$$\left.\begin{aligned} M(\rho, t) &= M_0, \qquad M(R, t) = 0 \\ 0 < M(r, t) &< M_0 \text{ for } 0 < \rho(t) < r < R \end{aligned}\right\} \quad \ldots\ldots [5]$$

Elementary though somewhat lengthy analysis leads to the following cubic for $\rho(t)$

$$\left(\frac{\rho}{R}\right)^3 - \left(\frac{\rho}{R}\right)^2 - \frac{\rho}{R} = \frac{12M_0}{\mu u_0 R^2} t - 1 \quad \ldots\ldots [6]$$

Here, the initial condition $\rho(0) = R$ has been used in accordance with the assumption that the entire plate is to have the velocity $u_0$ at $t = 0$.

Equation [6] shows that $\rho = 0$ at the instant

$$t_1 = \frac{\mu u_0 R^2}{12 M_0} \quad \ldots\ldots [7]$$

Let us determine the deflection at this instant. From Equation [6] we readily find the instant $t(r)$ at which $\rho$ equals a given $r$. The velocity of a particle at a fixed radius $r$ is given by the first line of Equation [4] for $t < t(r)$ and by the second line for $t > t(r)$. Thus integration yields the deflection

---

[1] The results presented in this paper were obtained in the course of research conducted under Contract DA-19-020-ORD-798 between Ballistic Research Laboratories, Aberdeen Proving Ground, and Brown University. The author is indebted to the Authorities of Ballistic Research Laboratories for permission to publish this paper.

[2] Formerly, Division of Applied Mathematics, Brown University, Providence, R. I. At present, Assistant Professor, Department of Mechanics, Illinois Institute of Technology.

[3] Numbers in parentheses refer to the Bibliography at the end of the paper.

Presented at the National Conference of the Applied Mechanics Division, Troy, N. Y., June 16–18, 1955, of The American Society of Mechanical Engineers.

Discussion of this paper should be addressed to the Secretary, ASME, 29 West 39th Street, New York, N. Y., and will be accepted until October 10, 1955, for publication at a later date. Discussion received after the closing date will be returned.

Note: Statements and opinions advanced in papers are to be understood as individual expressions of their authors and not those of the Society. Manuscript received by ASME Applied Mechanics Division, April 20, 1954. Paper No. 55—APM-1.

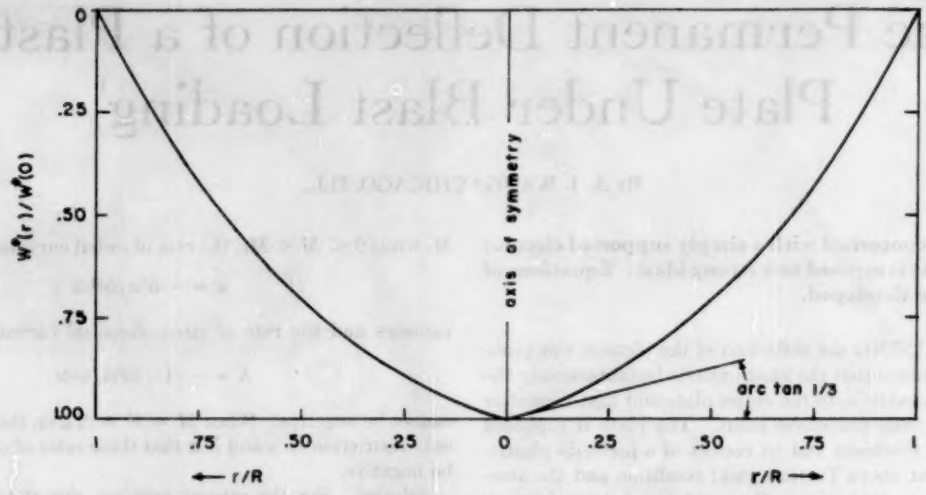


FIG. 1 DIMENSIONLESS RATIO $w^*(r)/w^*(0)$ AS FUNCTION OF $r/R$

$$w(r, t_1) = u_0\left(1 - \frac{r}{R}\right)\int_{t(r)}^{t_1}\frac{dt}{1 - \rho/R} + u_0 t(r) \quad [8]$$

One finds

$$w(r, t_1) = u_0 t_1\left[1 - \frac{1}{2}\left(\frac{r}{R}\right)^2 - \frac{1}{2}\left(\frac{r}{R}\right)^3\right] \quad [9]$$

For $t > t_1$ the preceding analysis is no longer valid. Let us assume that

$$w(r, t) = W(t)\left(1 - \frac{r}{R}\right) + w(r, t_1) \text{ for } t > t_1 \quad [10]$$

Since the rate of radial curvature $\kappa$ computed from Equation [10] vanishes while the rate of circumferential curvature $\lambda$ is positive, the motion Equation [10] is compatible with the assumption that $N = M_0$ while $0 < M < M_0$ for $0 < \rho < R$. Substituting $N = M_0$ and the acceleration obtained from Equation [10] into the equation of motion, Equation[1], we find that the resulting differential equation for $M$ has a solution satisfying the boundary conditions $M(0, t) = M_0$, $M(R, t) = 0$ if

$$\frac{d^2W}{dt^2} = -\frac{u_0}{t_1} \quad [11]$$

This differential equation must be integrated under the initial conditions

$$t = t_1\colon\ \partial W/\partial t = u_0,\ \ W = 0 \quad [12]$$

For $t > t_1$ we therefore have

$$w(r, t) = w(r, t_1) - \left(1 - \frac{r}{R}\right)\left[\frac{u_0}{2t_1}t^2 - 2u_0 t + \frac{3}{2}u_0 t_1\right] \quad [13]$$

We see from this equation that the entire plate comes to rest at $t = 2t_1$. The permanent deflection $w^*$ of the plate at this instant is given by

$$w^* = \frac{\mu u_0^2 R^2}{24 M_0}\left[3 - \frac{r}{R} - \left(\frac{r}{R}\right)^2 - \left(\frac{r}{R}\right)^3\right] \quad [14]$$

Fig. 1 shows the dimensionless ratio $w^*(r)/w^*(0)$ as function of $r/R$.

## BIBLIOGRAPHY

1 "On the Use of Singular Yield Conditions and Associated Flow Rules," by W. Prager, JOURNAL OF APPLIED MECHANICS, Trans., ASME, vol. 75, 1953, pp. 317–320.

2 "The Load Carrying Capacities of Circular Plates," by H. G. Hopkins and W. Prager, *Journal of the Mechanics and Physics of Solids*, vol. 2, 1953, pp. 1–13.

3 "On the Dynamics of Plastic Circular Plates," by H. G. Hopkins and W. Prager, *Zeitschrift für Angewandte Mathematik und Physik*, July, 1954, vol. 5, pp. 317–330.

4 "On the Plastic Deformation of Built-in Circular Plates Under Impulsive Load," by A. J. Wang and H. G. Hopkins, *Journal of the Mechanics and Physics of Solids*, vol. 3, 1954, pp. 22–37.

# The Extended Theory of the Viscous Vibration Damper

By F. M. LEWIS,[1] CAMBRIDGE, MASS.

**The paper extends the theory of the Viscous Vibration Damper either tuned or untuned to multimass systems and shows how an optimum damper can be designed for any installation. Special formulas are derived for the two mass plus damper systems.**

## Introduction

THE THEORY of the viscous vibration damper, tuned or untuned, has so far been developed only in application to a single-degree-of-freedom system. The majority of engine applications are of many degrees of freedom, and some of these depart so far, even in approximation, from a single-degree-of-freedom system, that the theory gives but little clue to the optimum damper characteristics.

A common type of installation, for example, consists of a multicrank engine, a flywheel, and a driven generator. In many cases, the important mode of vibration will approximate to the vibration of a two-mass system, engine plus flywheel constituting one mass, and the generator the other. It may be advantageous to fit a damper to the generator end of such an arrangement. The solution of this case is obviously remote from that for the single-degree-of-freedom-plus-damper system, and a damper designed to reduce the amplitude of the criticals in the engine shaft would be entirely inadequate to reduce the criticals between flywheel and generator.

The extended-damper theory is based on a general theorem which we will call the "Fixed-Point Theorem," which is proved in Appendix 1. It may be stated as follows:

Let there be a linear multimass system of inertia constants $m_1$, $m_2$, ..... etc.[2]

On some of these masses there act exciting forces (or torques) $F_1$, $F_2$, etc., and these forces are phased either zero or 180 deg.

One of the springs is paralleled by a dashpot of constant $b$, and there is no other damping in the system.

Then, if the resonance curve for the force in any spring, or the displacement of any mass, is plotted, there exists a series of points[3] where the amplitude of this force or displacement is independent of the damping constant $b$. These points are called the "fixed points."

This theorem has long been known in application to a single-degree-of-freedom system, plus damper. The fixed points are at the intersections of the resonance curves for the system with $b = 0$, i.e., the damper free; and $b = \infty$, i.e., the damper locked; the amplitude being plotted only positive.

In application to the damping of torsional vibration in engines two cases are to be considered. These are the untuned or Lanchester type damper, with only viscous damping connecting the damper flywheel to the system, and the tuned type where the viscous damping is paralleled by a spring. But it should be noted that other arrangements are possible—for example, a damper flywheel connected to a case by viscous damping, with the case connected to the engine by a spring. Also, in a general sense, any elastic element in the drive, such as an elastic coupling, which is paralleled by dashpot action, constitutes a damper.

The constructive details of dampers may take many forms and are outside the scope of this paper. We note that the original form of the Lanchester damper which utilized Coulomb friction with the slippage of dry surfaces has been largely superseded by the viscous-friction types using either engine oil or silicone fluids as the viscous medium.

## The Untuned Damper

We first consider the untuned damper. An engine system, of $n$ masses (damper excluded), which is free to rotate in space, i.e., the springs $k_1$, $k_2$, etc., are zero, will have $n - 1$ natural frequencies. The resonance curves of the locked and the unlocked damper will have $2n - 2$ intersections, all of which are fixed points with respect to the damping constant $b$. The general nature of these curves for a system of 4 masses, plus damper, is shown in Fig. 1. The six fixed points are encircled.

In an engine application one of these fixed points will be of predominant importance, say it is 4. Then for the chosen damper size, the amplitude at fixed point 4 is the smallest which can be obtained. The optimum damping constant is that which will pass the resonance curve through point 4 with a zero slope.

The procedure for calculating damper characteristics is as follows:

Choose a tentative damper size. The torque in a particular shaft section is of predominant interest. Plot the resonance curve of this torque in the vicinity of the resonant peak of primary interest for the conditions of damper locked and damper free. The intersection gives the minimum amplitude which can be obtained and the position of the resonance peak with damper. If this amplitude is too large it is necessary to use a larger damper or make other changes. The damper size being fixed, the optimum damper constant can be found as follows:

Take a value of $\omega^2$ slightly lower than that of the fixed point and with $b$ as an algebraic unknown calculate the amplitude. Equating this amplitude to that at the fixed point, $b$ can be solved for.

Another such calculation is made with a value of $\omega^2$ equidistant to the right of the fixed point. The mean of the two values of $b$ thus obtained will be very close to the optimum value, as close, in fact, as is necessary for any practical application.

---

[1] Professor of Marine Engineering, Massachusetts Institute of Technology. Mem. ASME.

[2] $m = w/g$ for linear motions lb, sec$^2$/in.
$= J/g$ for torsional motions lb in., sec$^2$.
Each mass is connected to a rigid frame by a spring of constant $k_1$, $k_2$, etc. ($k$ may be zero), and they are interconnected by springs $k_{12}$, $k_{13}$, $k_{23}$, etc.

[3] Note reference of Carter (1),[4] Neugebauer (2), Hahnkamm (3), Den Hartog (4). This property was also observed by O'Connor (5) in the case of a particular multimass engine system.

[4] Numbers in parentheses refer to the Bibliography at the end of the paper.

Presented at the National Conference of the Applied Mechanics Division, Troy, N. Y., June 16–18, 1955, of The American Society of Mechanical Engineers.

Discussion of this paper should be addressed to the Secretary, ASME, 29 West 39th Street, New York, N. Y., and will be accepted until October 10, 1955, for publication at a later date. Discussion received after the closing date will be returned.

Note: Statements and opinions advanced in papers are to be understood as individual expressions of their authors and not those of the Society. Manuscript received by ASME Applied Mechanics Division, March 26, 1954. Paper No. 55—APM-3.

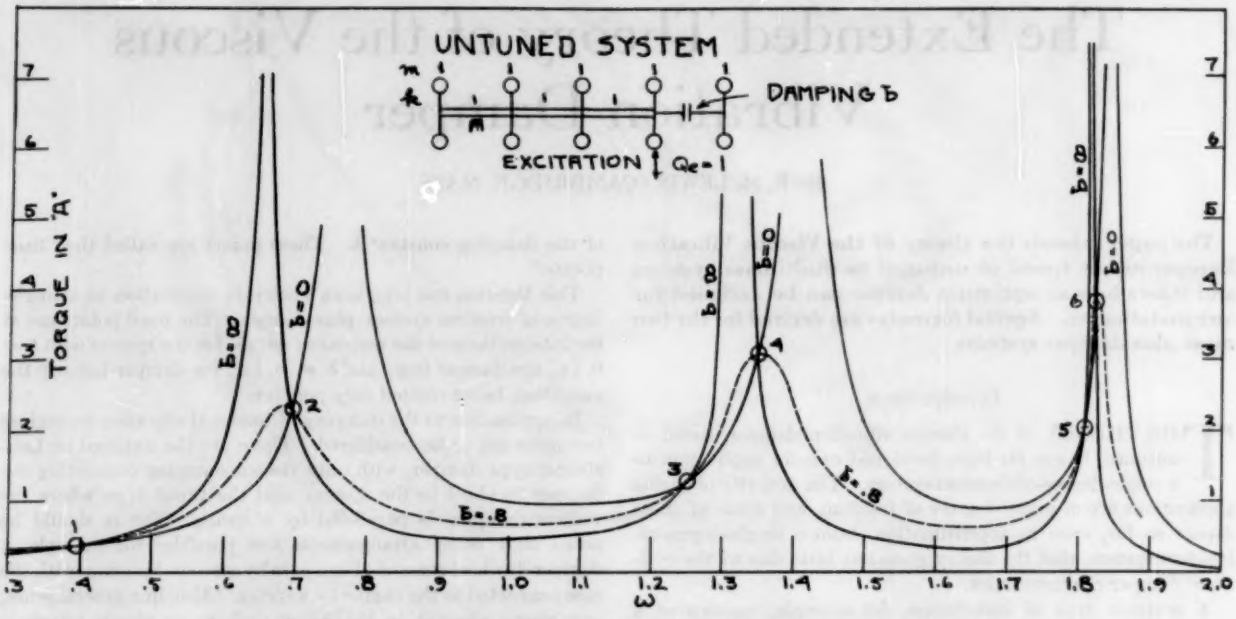


FIG. 1 RESONANCE CURVES FOR UNTUNED SYSTEM OF FOUR MASSES PLUS DAMPER

The calculation is made according to the well-known "sequence" or Holzer method of calculation with complex algebra. In this an inertia reaction is $m\omega^2\theta_n$, a spring torque is $-k(\theta_n - \theta_{n-1})$ and a damping torque is $-jb\omega\theta_n$. A spring paralleled by a dashpot is equivalent to a spring of constant $k + jb\omega$. The computation for a free or locked damper or for a finite damping constant is identical up to the point of attachment of the damper mass. Therefore it is advantageous to start the computation at the end of the system remote from the damper, and to plot curves of torque and amplitude versus $\omega$ at the point of attachment of the damper. With $\theta$ the unknown amplitude at the starting end, the torque and amplitude at the point of attachment of the damper are of the form

$$\theta_d = c_1 + c_2\theta$$
$$Q_d = c_3 + c_4\theta$$

and curves are needed for $c_1$, $c_2$, $c_3$, $c_4$. Starting with these curves the effect of various damper sizes and damping constants can be investigated readily, without the necessity of repeating the full calculation for each change.

Restrictions in the fixed-point theorem would appear to make this procedure invalid if there is any damping in the system other than that in the damper, and for minor criticals in which the exciting torques are out of phase. These points offer no great difficulties. In general, damping in the system will be small compared to that in the damper and its effect will be to reduce the amplitude below that computed for the damper alone. For minor criticals a close approximation to an optimum damper can be obtained by placing at No. 1 crank an exciting torque $Q_e\Sigma\beta$ where $\Sigma\beta$ is the vector sum of the relative amplitudes of vibration of the cranks in the particular mode under consideration, made in accordance with the usual procedure for amplitude calculations. This same approximation can be made also for major criticals, where the exciting torques are in phase, with but little loss of accuracy, and the calculations are considerably shortened thereby.

### THE TUNED OR SPRING-CONNECTED DAMPER

For the damper with a spring-connected damper mass applied to an engine system of $n$ masses there are $2n - 2$ fixed points. These lie at the intersections of the resonance curves with the damper damping constant zero and infinity (locked damper). Fig. 2 illustrates the general nature of these curves for a 4-mass system, plus damper, with the excitation applied to mass 4 and the relative amplitude $\theta_{12}$ plotted. Both the damping constant $b$ and the spring constant $k$ are subject to adjustment, and the endeavor will be to so adjust them that the amplitude in the vicinity of the resonant peak which is of predominant interest is minimized. This is a matter of trial for which no fixed rules can be given. The position of and amplitude at the fixed points are altered by adjusting the spring constant $k$. An optimum value of $k$ is that which will minimize the amplitude at the fixed points of interest and this may be, as in the case of the single-degree-of-freedom system, when two adjacent fixed points have equal amplitudes.

In the system of Fig. 2, note that $k$ is optimum as regards points 5 and 6 but not as regards 3 and 4. To equalize 3 and 4 would have required a slightly lower $k$ but then the amplitude at 5, 6, would have been larger. With $k$ suitably adjusted, $b$ can be found by the method previously outlined so as to hold the amplitude to the approximate value at the fixed points. In the example shown in Fig. 2, $b$ was determined so as to give zero slope at fixed point 3.

It will be noted that this damper is quite ineffective for the lowest peak. To reduce this would require a much smaller spring constant in the damper.

Some engine arrangements can be approximated by a system of two spring-connected masses. In Appendix 2 formulas are devised for four special cases of this arrangement for the tuned and untuned (Lanchester) damper and for the excitation applied at the same end and on the remote end to the damper. These derivations are lengthy and only the salient steps are given. The previously known solutions for a single-degree-of-freedom system plus damper are special cases of these more general solutions.

### BIBLIOGRAPHY

1 "Torsional Vibration in Engines—Effects of Fitting a Damper, etc.," by B. C. Carter, British Aeronautical Research Committee, Technical Reports, 1926–1927 (R. & M. 1053, February, 1926), pp. 731–767.

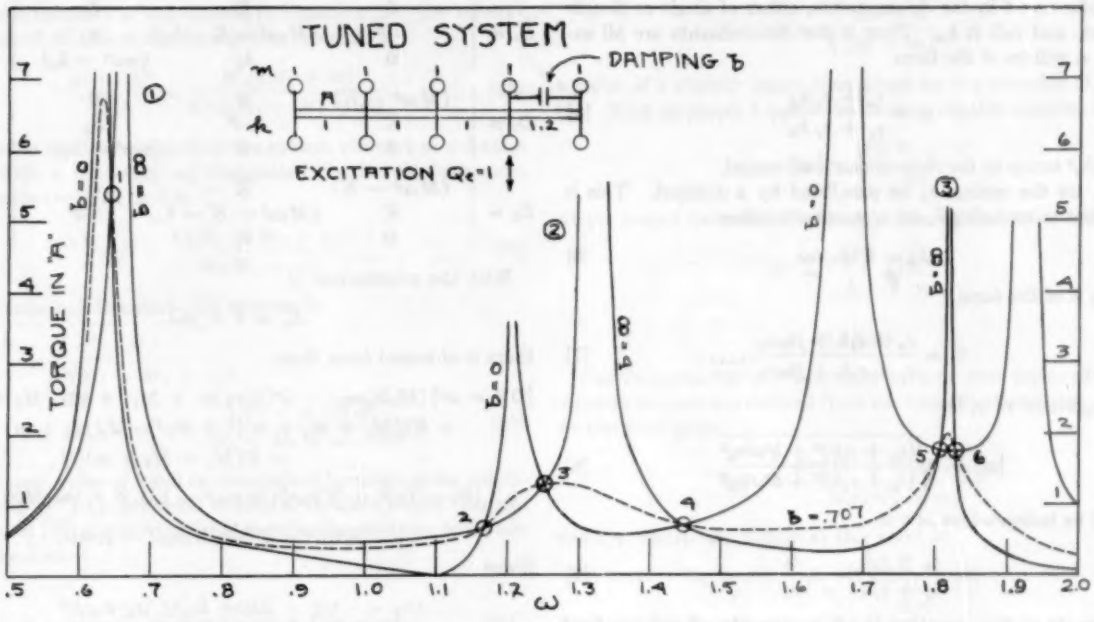


FIG. 2 RESONANCE CURVES FOR TUNED SYSTEM OF FOUR MASSES

2 "Schwingungsdämpfung bei endlicher Dämpferträgheit, etc.," by F. Neugebauer, *Technische Mechanik und Thermodynamik*, vol. 1, 1930, pp. 137–147, 184–197.

3 "Erzwungene Schingungen reibungsgekoppelter Schwingungssysteme," by E. Hahnkamm, *Zeitschrift für Angewandte Mathematik und Mechanik*, vol. 13, 1933, pp. 183–202.

4 "Mechanical Vibrations," by J. P. Den Hartog, McGraw-Hill Book Company, Inc., New York, N. Y., third edition, 1947.

5 "The Viscous Torsional Vibration Damper," by B. E. O'Connor, Society of Automotive Engineers, Quarterly Transactions, vol. 1, 1947, pp. 87–97.

6 "A Note on the Damped Vibration Absorber," by J. E. Brock, JOURNAL OF APPLIED MECHANICS, Trans. ASME, vol. 68, 1946. p. A-284.

# Appendix 1

## THE FIXED-POINT THEOREM

A system of masses $m_1$, $m_2$, etc., are connected to a rigid frame by springs $k_1$, $k_2$, etc., and interconnected by springs $k_{12}$, $k_{13}$, etc. Fig. 3 represents such a system for three masses. In the ordinary torsional system only the springs $k_{12}$, $k_{23}$, $k_{34}$, etc., are present. Simple harmonic forces $F_1$, $F_2$ etc., act on the masses. Considering all forces and motions as rotating vectors whose horizontal projection is equal to the actual motion, the force equations for

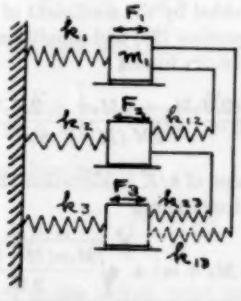


FIG. 3 SYSTEM FOR THREE MASSES

$m_1$, $m_2$ etc., are

$$\left.\begin{aligned}
&\begin{bmatrix} m_1\omega^2 - k_1 \\ -k_{12} - k_{13} \ldots \end{bmatrix} x_1 + k_{12}x_2 + k_{13}x_3 + \text{etc.} = -F_1 \\
&k_{12}x_1 + \begin{bmatrix} m_2\omega^2 - k_2 \\ -k_{12} - k_{23} \ldots \end{bmatrix} x_2 + k_{23}x_3 + \text{etc.} = -F_2 \\
&k_{13}x_1 + k_{23}x_2 + \begin{bmatrix} m_3\omega^2 - k_3 \\ -k_{13} - k_{23} \ldots \end{bmatrix} x_3 + \text{etc.} = -F_3 \\
&\ldots\ldots \quad \ldots\ldots \quad \ldots\ldots \quad = \ldots\ldots
\end{aligned}\right\} \ldots [1]$$

Solving for $x_1$ by determinants, there is obtained

$$x_1 = D_1/D \ldots\ldots\ldots\ldots\ldots\ldots [2]$$

where

$$D = \begin{vmatrix} \begin{bmatrix} m_1\omega^2 - k_1 \\ -k_{12} - k_{13} \ldots \end{bmatrix}, & k_{12}, & k_{13} & \ldots \\ k_{12}, & \begin{bmatrix} m_2\omega^2 - k_2 - k_{12} \\ -k_{23} \ldots \end{bmatrix}, & k_{23} & \ldots \\ k_{13}, & k_{23}, & \begin{bmatrix} m_3\omega^2 - k_3 \\ -k_{13} - k_{23} \ldots \end{bmatrix} & \ldots \\ \ldots & \ldots & \ldots & \ldots \end{vmatrix} \ldots [3]$$

and

$$D_1 = \begin{vmatrix} -F_1, & k_{12}, & k_{13} & \ldots \\ -F_2, & \begin{bmatrix} m_2\omega^2 - k_2 - k_{12} \\ -k_{23} \ldots \end{bmatrix}, & k_{23} & \ldots \\ -F_3, & k_{23}, & \begin{bmatrix} m_3\omega^2 - k_3 \\ -k_{13} - k_{23} \ldots \end{bmatrix} & \ldots \\ \ldots & \ldots & \ldots & \ldots \end{vmatrix} \ldots [4]$$

Consider any $k$ in the determinants, either of single or double subscript, and call it $k_d$. Then if the determinants are all expanded $x_1$ will be of the form

$$x_1 = \frac{c_a + c_b k_d}{c_e + c_f k_d} \quad [5]$$

for the $k_d^2$ terms in the determinants all cancel.

Now, let the spring $k_d$ be paralleled by a dashpot. This is equivalent to replacing $k_d$ by a complex number

$$k_d = k + jb\omega \quad [6]$$

Then $x_1$ is of the form

$$x_1 = \frac{c_a + c_b k + jb\omega c_b}{c_e + c_f k + jb\omega c_f} \quad [7]$$

The amplitude[5] of $x_1$ is

$$|x_1| = \sqrt{\frac{(c_a + c_b k)^2 + b^2\omega^2 c_b^2}{(c_e + c_f k)^2 + b^2\omega^2 c_f^2}} \quad [8]$$

$|x_1|$ will be independent of $b$ if

$$\frac{c_a + c_b k}{c_e + c_f k} = \pm \frac{c_b}{c_f} \quad [9]$$

The roots of this equation in $\omega^2$, necessarily all real, are fixed points for $|x_1|$.

For $x_2$ there can be written

$$x_2 = D_2/D \quad [10]$$

and for the relative motion

$$x_1 - x_2 = (D_1 - D_2)/D \quad [11]$$

$x_1 - x_2$ is of the same form as Equation [7] and therefore has fixed points with amplitude independent of $b$.

Since $x_1$ and $x_2$ can represent any two masses the theorem is true for all masses or all relative motions.

If the $F$-forces are not in phase or if there is other than a single spring paralleled by damping, an equation of the form of Equation [7] cannot be written, and fixed points do not exist. The procedure in such cases has been discussed earlier in the text.

In the derivative $F$ has been assumed constant, but obviously the proof holds if the $F$-forces are proportional to $\omega^2$ or are any other function of $\omega$, provided only that they are in zero or 180-deg phase.

# Appendix 2

## CASE 1

Consider a 2-mass system plus tuned damper, excitation applied to the damper end, Fig. 4.

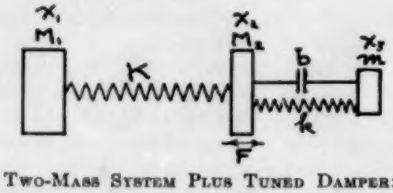


FIG. 4 TWO-MASS SYSTEM PLUS TUNED DAMPER: CASE 1

By Appendix 1 the motion determinants are

$$D = \begin{vmatrix} (M_1\omega^2 - K) & K & 0 \\ K & (M_2\omega^2 - K - k_d) & k_d \\ 0 & k_d & (m\omega^2 - k_d) \end{vmatrix} \quad [12]$$

[5] Amplitude: here defined as length of the rotating vector.

$$D_1 = \begin{vmatrix} 0 & K & 0 \\ -F & (M_2\omega^2 - K - k_d) & k_d \\ 0 & k_d & (m\omega^2 - k_d) \end{vmatrix} \quad [13]$$

$$D_2 = \begin{vmatrix} (M_1\omega^2 - K) & 0 & 0 \\ K & -F & k_d \\ 0 & 0 & (m\omega^2 - k_d) \end{vmatrix} \quad [14]$$

$$D_3 = \begin{vmatrix} (M_1\omega^2 - K) & K & 0 \\ K & (M_2\omega^2 - K - k_d) & -F \\ 0 & k_d & 0 \end{vmatrix} \quad [15]$$

With the substitution of

$$k_d = k + jb\omega \quad [16]$$

there is obtained from these

$$|D|^2 = \omega^4\{[M_1M_2m\omega^4 - \omega^2\langle Km(M_1 + M_2) + kM_1(M_2 + m)\rangle + Kk(M_1 + M_2 + m)]^2 + b^2\omega^2[\omega^2M_1(M_2 + m) - K(M_1 + M_2 + m)]^2\} \quad [17]$$

$$|D_1 - D_2|^2 = |F|^2\omega^4\{(M_1m\omega^2 - kM_1)^2 + b^2\omega^2M_1^2\} \quad [18]$$

$$|D_2 - D_3|^2 = |F|^2\omega^4(M_1m\omega^2 - Km)^2 \quad [19]$$

Since

$$|x_1 - x_2|^2 = \frac{|D_1 - D_2|^2}{|D|^2} = \frac{c_1 + c_2b^2}{c_3 + c_4b^2} \quad [20]$$

The relative motion $|(x_1 - x_2)|$ is independent of $b$ if

$$\frac{c_1}{c_2} = \pm \frac{c_3}{c_4} \quad [21]$$

and then the relative amplitude at the fixed points is given by

$$|x_1 - x_2|^2 = \frac{c_2}{c_4} \quad [22]$$

Equation [21] reduces to the equation of the fixed points

$$\omega^4[2M_1M_2m + M_1m^2] - \omega^2[2kM_1M_2 + 2kM_1m + 2KM_1m + 2KM_2m + Km^2] + 2Kk[M_1 + M_2 + m] = 0 \quad [23]$$

and Equation [22] gives

$$\frac{|x_1 - x_2|}{|F|} = \pm \frac{M_1}{\omega^2_{a,b}M_1(M_2 + m) - K(M_1 + M_2 + m)} \quad [24]$$

Taking + for $\omega_a^2$ and — for $\omega_b^2$ and equating the amplitudes, there results

$$(\omega_a^2 + \omega_b^2)M_1(M_2 + m) - 2K(M_1 + M_2 + m) = 0 \quad [25]$$

But $\omega_a^2 + \omega_b^2$ is equal to the coefficient in brackets of the $\omega^2$ term of Equation [23] divided by the coefficient of the $\omega^4$ term. Substituting this in Equation [25] and simplifying, there is obtained the condition of optimum tuning

$$\frac{k}{K} = \frac{m(2M_1M_2 + 3M_2m + 2M_2^2 + m^2)}{2M_1(M_2 + m)^2} \quad [26]$$

Substituting this value of $k/K$ in Equation [23], there is obtained the equation of the fixed points

$$\omega^2_{a,b} = K\left\{\frac{(M_1 + M_2 + m) \pm \sqrt{\frac{M_1m(M_1 + M_2 + m)}{2M_2 + m}}}{M_1(M_2 + m)}\right\} \quad [27]$$

With these values of $\omega^2$ substituted in Equation [24] the relative amplitude of $M_1$, $M_2$ at the fixed points is obtained

$$\frac{|x_1 - x_2|^2}{|F|^2} = \frac{M_1(2M_2 + m)}{K^2m(M_1 + M_2 + m)} \quad [28]$$

If $M_2$ and $m$ are locked together the system vibrates as a 2-mass system with a frequency $\omega_L$ designated the locked frequency, which lies between $\omega_a$ and $\omega_b$

$$\omega_L^2 = \frac{K(M_1 + M_2 + m)}{M_1(M_2 + m)} \quad [29]$$

At this frequency Equation [22] reduces to

$$\frac{|x_1 - x_2|^2}{|F^2|} = \frac{M_1^2}{K^2(M_1 + M_2 + m)^2} + \frac{(M_2 + m)^2M_1b^2}{(M_1 + M_2 + m)m^4K^2} \quad [30]$$

The optimum value of $b$ will be determined by making the amplitude at the locked point equal to that at the fixed points. Equating [28] and [30] and solving for $b^2$ there is obtained the optimum damping constant

$$b^2 = \frac{Km^2(2M_1M_2 + 3M_2m + 2M_2^2 + m^2)}{(M_2 + m)^2(M_1 + M_2 + m)} \quad [31]$$

With optimum $k$ from Equation [26] and optimum $b$ from Equation [31] substituted in the relation

$$|x_2 - x_3| = \frac{|D_2 - D_3|}{|D|} \quad [32]$$

there is obtained the relative damper amplitude at the locked point

$$|x_2 - x_3| = \frac{|F|M_1(M_2 + m)}{Km(M_1 + M_2 + m)} \quad [33]$$

Numerical calculations show that for the ordinary proportions of damper mass to main masses the maximum relative amplitude of $M_1$ and $M_2$ and the relative damper amplitude will exceed the amplitudes at the fixed point, given by Equations [28] and [33], respectively, by only a few per cent. For a precise calculation of the maximum Equations [30] and [32] can be plotted:

## CASE 1(a)

The formulas for the single mass plus damper system are obtained from the foregoing by writing $M_1 = \infty$, $M_2 = M$. We note the results.

The optimum tuning is given by

$$\frac{k}{K} = \frac{mM}{(m + M)^2}$$

With this value of $k$ the fixed points are located at

$$\omega^2_{a,b} = \frac{K}{M + m}\left[1 \pm \frac{m}{\sqrt{m^2 + 2Mm}}\right]$$

and the amplitude at these points is

$$|x_F| = \frac{|F|}{K}\sqrt{\frac{m + 2M}{m}}$$

For equal amplitudes at the locked point and the fixed points there is obtained

$$b = \sqrt{\frac{2m^2MK}{(M + m)^2}}$$

a value of $b$ slightly larger than given by the criterion of Brock (6). With optimum $k$ and $b$ the damper relative amplitude is

$$|x_1 - x_3| = \frac{|F|(M + m)}{km}$$

At the locked frequency the energy absorbed per cycle will be

$$W = \frac{\pi|F|^2}{K}\sqrt{\frac{2M}{m}}$$

## CASE 2

The formulas for the two-mass system plus untuned (Lanchester) damper are derived from the foregoing by setting $k = 0$. At the fixed point

$$\omega_F^2 = \frac{K(2M_1 + 2M_2 + m)}{M_1(2M_2 + m)}$$

and the relative amplitude at this point is

$$|x_1 - x_2| = \frac{|F|(2M_2 + m)}{Km}$$

The optimum damping constant is determined from the condition

$$\frac{d}{d(\omega^2)}\frac{|D_1 - D_2|^2}{|D|^2} = 0 \quad \text{at} \quad \omega = \omega_F$$

which leads to

$$b^2 = \frac{KM_2m^2(2M_1 + 2M_2 + m)}{M_1(M_2 + m)(2M_2 + m)}$$

### CASE 2(a)

Single degree of freedom plus untuned damper. With $M_1 = \infty$, $M_2 = M$ in Case 2, the formulas reduce to

$$\omega_F^2 = \frac{2K}{2M + m}$$

$$|x_1| = \frac{F(2M + m)}{Km}$$

$$b^2 = \frac{2Mm^2K}{(M + m)(2M + m)}$$

a result derived independently by Carter, Neugebauer, and Brock (1, 2, 6).

## CASE 3

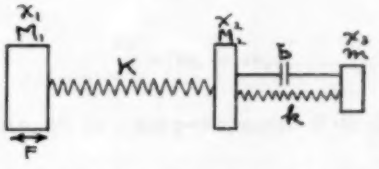


FIG. 5 TWO-MASS SYSTEM PLUS TUNED DAMPER; CASE 3

Fig. 5, two-mass system plus tuned damper—excitation applied at the end remote from the damper.

The derivation is similar to that for Case 1, and we merely note the results.

The fixed points are located at

$$\omega^2_{a,b} = \frac{K(M_1 + M_2 + m)}{M_1(M_2 + m)} \pm \frac{K\sqrt{2M_1M_2m(M_1 + M_2 + m)}}{2M_1M_2(M_2 + m)}$$

at which the relative amplitude is

$$|x_1 - x_2| = \frac{|F|}{K}\sqrt{\frac{2M_2(M_2 + m)^2}{M_1m(M_1 + M_2 + m)}}$$

The optimum tuning is given by

$$\frac{k}{K} = \frac{m(2M_1M_2 + 2M_2^2 + 2M_2m - M_1m)}{2M_1(M_2 + m)^2}$$

and the optimum damping

$$b^2 = \frac{K(8M_1M_2 + 8M_2^2 + 8M_2m - M_1m)m^2}{4(M_2 + m)^2(M_1 + M_2 + m)}$$

At the locked point the damper relative amplitude is

$$|x_2 - x_3| = \frac{|F|(M_2 + m)^2}{Km(M_1 + M_2 + m)}$$

## CASE 4

Fig. 5, untuned damper, exciting force at the end removed from the damper.

The fixed point is given by

$$\omega_F^2 = \frac{K(2M_1M_2 + 2M_2^2 + 2M_2m + M_1m)}{2M_1M_2(M_2 + m)}$$

and the amplitude at this is

$$|x_1 - x_2| = \frac{2|F|M_2(M_2 + m)}{KM_1m}$$

The optimum damping is given by

$$b^2 = \frac{KM_2m^2[2M_1M_2 + 2M_2^2 + 2M_2m + M_1m]}{2M_1(M_2 + m)^3}$$

For the untuned damper, in the preceding derivation, as well as in the more general case, the "optimum" damping has been defined as that which passes the resonance curve through the fixed point of interest with a zero slope.

For the tuned damper the optimum tuning has been defined as that which gives equal amplitudes at the fixed points, and the optimum damping as that which gives equal amplitudes at the locked point and the fixed points. This definition of optimum damping has been adopted because of the relative simplicity of the analysis. It gives a damping constant and a maximum amplitude differing slightly from that of Brock (6), who defines it as the mean of the values which give a zero slope at each of the fixed points.

None of these definitions produces a true minimum for the amplitude. The determination of this has so far proved prohibitively difficult. The amplitudes produced by the foregoing optimum values are so close to the true minimum values that the discrepancy is of no importance.

# An Approximate Nonuniform Bending Theory and Its Application to the Swept-Plate Problem[1]

By H. J. PLASS, JR.,[2] AUSTIN, TEXAS

**Differential equations and boundary conditions are derived, by means of the calculus of variations, for cylindrical bars in nonuniform bending. The resulting equations are used, together with similar nonuniform torsion equations, to obtain deflections and stresses in swept cantilever plates of uniform rectangular cross section. Comparisons are made with experimental results for plates with four different sweep angles. The theory predicts deflections quite close to those found experimentally. Stresses computed from the equations, however, are not in as close agreement. It is also noticed that the theory is less accurate for large sweep angles than for small ones.**

## 1 Introduction

BECAUSE of certain aerodynamic advantages, modern high-speed aircraft have been equipped with swept-back wings. Analysis of the deformation of such structures under given loads is very difficult unless certain simplifying assumptions are made. Recent studies on this problem have been carried out at the California Institute of Technology[3] in which the swept wing is idealized as a flat homogeneous isotropic plate having the same plan form as the wing. In this study, both theoretical and experimental values were obtained for the deflection under various kinds of static loading. The theoretical phase of the study is based on plate theory and predicts values of deflection which are consistently too large.

In this paper the assumption is made that the wing can be idealized as a homogeneous isotropic prismatic bar having the same cross section as the wing. The advantage of treating the problem in this fashion is that cross sections other than rectangular can be handled with ease. As parameters which describe the deformation of the idealized wing, we select the slope of he axis, the angle of twist, and the chordwise curvature of sections perpendicular to the axis of the bar. The conditions assumed for the end corresponding to the root of the wing are those which most closely approximate a fixed end. Details about these boundary conditions occur later in the paper. Now we mention only that they are conditions on the rate of twist, the axial curvature, and chordwise curvature at the origin. Such conditions cause the torsion and bending of the bar to be nonuniform.

A suitable approximate theory of nonuniform torsion has been developed by Goodier.[4] Certain important results of this theory will be presented in Section 2 of this paper. What remains to be developed is an approximate theory of nonuniform bending, in which the change in shape of the cross section due to Poisson's ratio is considered. The details of nonuniform bending are presented in Section 3. In Section 4 the results of the two theories are combined in the analysis of a skew cantilever cylinder of rectangular cross section. An approximation of a similar nature has been given by Reissner and Stein;[5] however, theirs uses plate theory as a basis. Computations are made for one particular model of a skew cylinder subjected to a twisting torque at its end. Comparisons are then made with the experimental results obtained by the group at California Institute of Technology for this model. In some instances, good agreement is obtained, and in others, especially for the cases of high sweep angles, the agreement is poor (see Figs. 5 and 6).

## 2 Nonuniform Torsion

The classical Saint-Venant solution for the problem of uniform torsion of prismatic bars demands that the cross sections, originally plane, become warped after the application of the twisting torque. Each cross section suffers the same amount of warping. In the co-ordinate system of Fig. 1 the displacements in the $x$, $y$, and $z$-directions are respectively

$$\left.\begin{aligned} u &= -\alpha yz \\ v &= \alpha xz \\ w &= \alpha\phi(x, y) \end{aligned}\right\} \quad \ldots\ldots\ldots\ldots\ldots\ldots [1]$$

where $\phi$ is the warping function, which is dependent upon the shape of the cross section. It satisfies Laplace's equation

$$\frac{\partial^2\phi}{\partial x^2} + \frac{\partial^2\phi}{\partial y^2} = 0 \text{ in } R \quad \ldots\ldots\ldots\ldots\ldots [2a]$$

and on the boundary $L$, the normal derivative satisfies the condition

$$\frac{d\phi}{dn} = yn_x - xn_y \quad \ldots\ldots\ldots\ldots\ldots [2b]$$

where $n_x$ and $n_y$ are the $x$ and $y$-components of the unit outward normal.

---

[1] The results of this paper were obtained in the course of research sponsored by the Navy Bureau of Ordnance under Contract NOrd-9195 with The University of Texas.

[2] Associate Professor of Engineering Mechanics and Research Engineer, Defense Research Laboratory, The University of Texas.

[3] Series of reports entitled: "Theoretical and Experimental Effect of Sweep Upon the Stress and Deflection Distribution in Aircraft Wings of High Solidity," AF Technical Report No. 5761; experimental results referred to are given in Part 3 of the series.

Presented at the National Conference of the Applied Mechanics Division, Troy, N. Y., June 16–18, 1955, of The American Society of Mechanical Engineers.

Discussion of this paper should be addressed to the Secretary, ASME, 29 West 39th Street, New York, N. Y., and will be accepted until October 10, 1955, for publication at a later date. Discussion received after the closing date will be returned.

Note: Statements and opinions advanced in papers are to be understood as individual expressions of their authors and not those of the Society. Manuscript received by ASME Applied Mechanics Division, March 2, 1954. Paper No. 55—APM-6.

[4] "The Buckling of Compressed Bars by Torsion and Flexure," by J. N. Goodier, Cornell University Engineering Experiment Station, Bulletin No. 27, December, 1941. Goodier's work is a generalisation of Timoshenko's nonuniform torsion equation for I-beams. See "Collected Papers," by S. P. Timoshenko, McGraw-Hill Book Company, Inc., New York, N. Y., 1954.

[5] "Torsion and Transverse Bending of Cantilever Plates," by E. Reissner and M. L. Stein, NACA TN 2369, 1951.

If the conditions of the Saint-Venant problem are altered by requiring that one end, say, $z = 0$, be fastened to a rigid base so that it cannot warp, then the twist rate is no longer a constant. This is most readily demonstrated by means of the theorem of

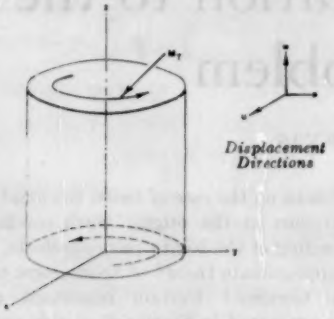


FIG. 1 TWISTED CYLINDER

minimum potential energy. Goodier[4] has published the details of the method, and hence only the important features are repeated here for the benefit of future reference. It is assumed that the displacements are given by the following equations

$$\left.\begin{aligned} u &= -\Omega y \\ v &= \Omega x \\ w &= \Omega' \phi(x, y) \end{aligned}\right\} \quad \ldots\ldots\ldots\ldots\ldots [3]$$

where $\Omega$ is the angle of twist of the cross section in radians, and is considered to be a function of $z$ only. The prime indicates differentiation with respect to $z$. The potential energy of the twisted bar acted on by a torque $M_T$ is given by

$$V_T = \frac{GC}{2}\int_0^l (\Omega')^2 dz + \frac{E\Gamma}{2}\int_0^l (\Omega'')^2 dz - M_T\Omega(l) \ldots [4]$$

where

$G$ = shear modulus
$E$ = elastic modulus

$$C = \text{torsion constant} = \iint_R \left(x^2 + y^2 + x\frac{\partial\phi}{\partial y} - y\frac{\partial\phi}{\partial x}\right) dx\, dy$$

$$\Gamma = \text{torsion-bending constant} = \iint_R [\phi(x, y)]^2\, dx\, dy$$

In this expression, the first term represents the strain energy of torsional shear strains, and the second term represents the strain energy of axial strains caused by restraint of warping of the cross sections. The theorem of minimum potential energy states that of all possible sets of displacement functions which might be used to describe the shape of the twisted bar, the true set is the one which minimizes the potential energy. Our assumed displacements, as given in Equations [3], certainly are not of general enough form to include all possibilities. We can at best get only an approximation by choosing $\Omega$ such that $V_T$ is minimized. This approximation is sufficiently good for most engineering applications. When the calculus of variations is applied to Equation [4] we obtain the following differential equation and boundary condition for $\Omega$

$$GC\Omega' - E\Gamma\Omega''' = M_T \ldots\ldots\ldots\ldots\ldots [5]$$

$$\Omega''(l) = 0 \ldots\ldots\ldots\ldots\ldots [6]$$

It is assumed that at $z = 0$ we satisfy the geometric conditions

$$\Omega(0) = 0 \ldots\ldots\ldots\ldots\ldots [7a]$$

$$\Omega'(0) = 0 \ldots\ldots\ldots\ldots\ldots [7b]$$

The solution to Equation [5] subject to the Boundary Conditions [6] and [7b] is

$$\Omega' = \frac{M_T}{GC}\left[1 + \tanh ql \sinh qz - \cosh qz\right] \ldots\ldots [8]$$

where $q = \sqrt{(GC)/(E\Gamma)}$. For very long cylinders, we can consider $\tanh ql = 1$, and $\Omega'$ can be written

$$\Omega' = \frac{M_T}{GC}\left[1 - e^{-qz}\right] \ldots\ldots\ldots\ldots [9]$$

It is seen from Equation [9] that as $z$ gets larger, the value of $\Omega'$ approaches the constant value $M_T/(GC)$, the value for uniform Saint-Venant torsion.

## 3 NONUNIFORM BENDING

When a prismatic bar is loaded by pure bending couples in a principal plane of its cross section, the centroidal axis of the bar is bent into a circular arc, and the shape of the cross section is changed due to the effect of Poisson's ratio. The section change is such that straight lines in the section perpendicular to the plane of the bending are curved in the opposite sense to the axial curvature. This phenomenon is known as anticlastic curvature.

In the event that this anticlastic curvature is prevented, say, at one end, it is reasonable to assume that the axial curvature will not be constant near that end. It is the purpose of this section of the paper to construct an approximate theory for this type of bending.

For cylinders in uniform torsion, the angle of twist is a linear function of the axial co-ordinate. The approximate nonuniform torsion theory is an extension of the uniform torsion theory with the added assumption that strain energy over and above that due to torsional stresses arises from variation of warping along the axis. As a parallel to the development for torsion, we start here with a bending problem, whose exact solution is known, in which the axial curvature $\Lambda'$, as shown in Fig. 2, is a linear function of the axial co-ordinate $z$. This problem is the terminal load flexure problem. The complete solution in the form used in this paper can be found in Sokolnikoff's book.[5] The solution for this problem predicts a warping of cross sections proportional to the rate of change with respect to $z$ of the axial curvature. The corresponding relation in the uniform torsion theory is the proportionality between warping and twist per unit length, as given by the expression for $w$ in Equation [3]. From the solution in Sokolnikoff's book, we have the displacements in the $x$, $y$, $z$-directions, respectively, given by

$$\left.\begin{aligned} u &= -\alpha zy + \frac{W}{EI}\left[\frac{\nu}{2}(l - z)(x^2 - y^2) - \frac{z^3}{6} + \frac{l}{2}z^2\right] \\ v &= \alpha zx + \frac{W}{EI}\nu(l - z)\,xy \\ w &= \alpha\phi(x, y) - \frac{W}{EI}\left[\Phi(x, y) + xy^2 + \left(lz - \frac{z^2}{2}\right)x\right] \end{aligned}\right\} \ldots [10]$$

where

$W$ = terminal load
$I$ = moment of inertia of section about $y$-axis
$\nu$ = Poisson's ratio
$\Phi(x, y)$ = flexure warping function

[4] "Mathematical Theory of Elasticity," by I. S. Sokolnikoff, McGraw-Hill Book Company, Inc., New York, N. Y., 1946, p. 122.

It is assumed in deriving Equations [10] that the $x$ and $y$-axes are principal axes through the centroid of the section. The terms containing $\alpha$ are torsional displacements which vary in size as the position of application of $W$ is changed. If $W$ is applied at the shear center, then $\alpha$ will be zero. For sections symmetric about

FIG. 2 CYLINDER IN TERMINAL LOAD FLEXURE

the $x$-axis, the position of $W$ for no torsion will be along the $x$-axis. Now, making use of the fact that the bending moment at any section is given by $M_B = W(l - z)$, and that $M_B/EI = \Lambda'$, we rewrite Equations [10] as follows

$$\left.\begin{aligned} u &= -\Omega y + \int_0^z \Lambda dz + \frac{\nu}{2}\Lambda'(x^2 - y^2) \\ v &= \Omega x + \nu\Lambda xy \\ w &= \Omega'\phi(x, y) - \Lambda x + \Lambda''[\Phi(x, y) + xy^2] \end{aligned}\right\} \quad \ldots\ldots [11]$$

To simplify the discussion, we now assume $W$ so applied that the torsional displacements vanish. Then we get

$$\left.\begin{aligned} u &= \int_0^z \Lambda dz + \frac{\nu}{2}\Lambda''(x^2 - y^2) \\ v &= \nu\Lambda' xy \\ w &= -\Lambda x + \Lambda''[\Phi(x, y) + xy^2] \end{aligned}\right\} \quad \ldots\ldots [12]$$

The first term in the expression for $w$ in Equations [12] is the axial displacement which we get from elementary beam theory, in which plane sections are assumed to remain plane. The second term represents the out-of-plane warping associated with varying curvature.

One of the conclusions to be drawn from Equations [12] is that the transverse curvature, equal to $\partial^2 u/\partial y^2$, is equal to $-\nu\Lambda'$, $\Lambda'$ being the axial curvature. It is not reasonable to assume that this relation holds in the case of nonuniform bending. It is more probable that the axial and transverse curvatures have no simple relationship connecting them. To take account of this possibility we modify Equations [12] so that a new variable $K$, the transverse curvature, appears together with $\Lambda$. Consider the displacement $u$ or $x = 0$. From Equations [12] we have

$$(u)_{x=0} = \int_0^z \Lambda dz - \nu\Lambda' \frac{y^2}{2} \quad \ldots\ldots [13]$$

We shall replace $\nu\Lambda'$ in the second term of Equation [13] by $K$. The actual manner in which $K$ varies with $z$ will be found later by means of the theorem of minimum potential energy. The assumption is now made that in those terms representing variations of displacement in the transverse direction, $\nu\Lambda'$ is always replaced by $K$. With this assumption, we can easily modify the first two displacement relations of Equations [12]. We obtain for $u$ and $v$ the following

$$\left.\begin{aligned} u &= \int_0^z \Lambda dz - K\frac{y^2}{2} + \nu\Lambda'\frac{x^2}{2} \\ v &= Kxy \end{aligned}\right\} \quad \ldots\ldots [14]$$

Before we can modify, in like manner, the deflection $w$, the structure of the flexure warping function $\Phi(x, y)$ must be examined. Since the paper is primarily concerned with applications to wing-like structures, we limit our attention to the approximate form of $\Phi(x, y)$ for sections whose width in the $y$-direction greatly exceeds the thickness in the $x$-direction. The function $\Phi(x, y)$ must be a harmonic function subject to the boundary condition on $C$

$$\frac{d\Phi}{dn} = -\left[\frac{\nu}{2}x^2 + \left(1 - \frac{\nu}{2}\right)y^2\right] n_x - (2 + \nu)xy\, n_y$$

(footnote 6, page 229). For our case, that is, the very thin section, $d\Phi/dn$ is approximately equal to $\partial\Phi/\partial x$, except near the ends of the section. Then $\partial\Phi/\partial x$ on the boundary is approximately

$$\frac{\partial\Phi}{\partial x} \doteq -\left[\frac{\nu}{2}x^2 + \left(1 - \frac{\nu}{2}\right)y^2\right] \text{ on } L \quad \ldots\ldots [15]$$

Consider the harmonic function

$$\Phi = A(x^3 - 3xy^2) + Bx \quad \ldots\ldots [16]$$

On differentiating, we obtain

$$\frac{\partial\Phi}{\partial x} = 3A(x^2 - y^2) + B \quad \ldots\ldots [17]$$

Thus, at $x = \pm a$, the upper and lower surfaces

$$\frac{\partial\Phi}{\partial x} = 3A(a^2 - y^2) + B \quad \ldots\ldots [18]$$

Then, on comparing Equation [15] with Equation [18], we obtain

$$3Aa^2 + B = -\frac{\nu}{2}a^2$$

$$3A = \left(1 - \frac{\nu}{2}\right)$$

$$B = -\frac{\nu a^2}{2} - 3Aa^2 = -\frac{\nu a^2}{2} - a^2 + \frac{\nu a^2}{2} = -a^2$$

$$A = \frac{1}{3}\left(1 - \frac{\nu}{2}\right)$$

Thus we have approximately

$$\Phi \doteq \frac{1}{3}\left(1 - \frac{\nu}{2}\right)(x^3 - 3xy^2) - a^2x \quad \ldots\ldots [19]$$

Then from Equations [12] and [19] we have for $w$ the following

$$w = -\Lambda x + \Lambda''\left[\frac{\nu}{2}xy^2 + \frac{1}{3}\left(1 - \frac{\nu}{2}\right)x^3 - a^2x\right] \quad \ldots [20]$$

On using our assumed modification, that of replacing $\nu\Lambda'$ by $K$ whenever variations with $y$ occur, we have for all three deformations (see Equation [14])

$$\left.\begin{aligned} u &= \int_0^z \Lambda dz - K\frac{y^2}{2} + \nu\Lambda'\frac{x^2}{2} \\ v &= Kxy \\ w &= -\Lambda x + \frac{1}{2}K'xy^2 + \Lambda''\left[\frac{1}{3}\left(1 - \frac{\nu}{2}\right)x^3 - a^2x\right] \end{aligned}\right\} \quad \ldots [21]$$

The last terms in the expressions for $u$ and $w$ in Equations [21] represent the shear deformation due to the transverse shear load $W$. These deformations will be ignored in what is to follow, as is done in elementary beam theory. When we drop these terms, we have

$$\left.\begin{aligned} u &= \int_0^z \Lambda dz - K\frac{y^2}{2} \\ v &= Kxy \\ w &= -\Lambda x + \frac{1}{2}K'xy^2 \end{aligned}\right\} \quad \ldots\ldots\ldots\ldots [22]$$

It will be assumed now that the deflections of all thin cylinders are given by Equations [22]. The method of finding the values of $\Lambda$ and $K$ at various cross sections is discussed below.

Consider the strain energy of a bent cylinder, whose deflections are those of Equations [22]. We use the usual relations connecting strains with displacements, and Hooke's law for a homogeneous isotropic material and obtain the stresses

$$\left.\begin{aligned} \sigma_x &= \tau_{zx} = \tau_{xy} = 0 \\ \sigma_y &= \frac{E}{1-\nu^2}\left(K - \nu\Lambda' x + \frac{1}{2}K''xy^2\right) \\ \sigma_z &= \frac{E}{1-\nu^2}\left(\nu Kx - \Lambda' x + \frac{1}{2}K''xy^2\right) \\ \tau_{zy} &= 2GK'xy \end{aligned}\right\} \quad \ldots\ldots [23]$$

The strain energy is given by

$$U_B = \frac{1}{2}\iiint [\sigma_y\epsilon_y + \sigma_z\epsilon_z + \tau_{zy}\gamma_{zy}]\, dx\, dy\, dz$$

On substitution of stresses and strains into this expression, we obtain

$$U_B = \frac{EI}{2(1-\nu^2)}\int_0^l [K^2 - 2\nu K\Lambda' + (\Lambda')^2]dz + \frac{E\Gamma}{2(1-\nu^2)}\int_0^l [\nu KK'' - \Lambda'K'' + 2(1-\nu)(K')^2]dz + \frac{EH_B}{2(1-\nu^2)}\int_0^l (K'')^2 dz \ldots [24]$$

The constant $\Gamma$ has been defined following Equation [4]. An examination of the structure of the warping function $\phi(x, y)$ shows that for thin sections $\phi(x, y) \doteq xy$ + small additional corrections. Thus $\Gamma \doteq \iint_R x^2y^2\, dx\, dy$ in the foregoing. The constant $H_B$ is defined as

$$H_B = \frac{1}{4}\iint_R x^2y^4\, dx\, dy$$

The potential energy of the strained bar together with its loads is as follows

$$V_B = U_B - \iint_R dM_B\left[\Lambda(l) - K'(l)\frac{y^2}{2}\right] \ldots\ldots [25]$$

where $U_B$ is given by Equation [24] and $dM_B$ is the portion of the bending moment acting over an element of length $dy$. The bracketed expression is simply the angle of rotation of this element about the $y$-axis.

Assuming

$$\sigma_z = -\frac{M_B}{I}x, \text{ and } w(l) = -[\Lambda(l) - \tfrac{1}{2}K'(l)y^2]\, x$$

we get

$$V_B = U_B - M_B\Lambda(l) + M_B\frac{\Gamma}{2I}K'(l) \ldots\ldots [26]$$

For equilibrium, the variation of $V_B$ must be zero. Treating $\Lambda'$ and $K$ as independent, we have

$$\delta V_B = \frac{EI}{1-\nu^2}\int_0^l [K\delta K - \nu(K\delta\Lambda' + \Lambda'\delta K) + \Lambda'\delta\Lambda']\, dz + \frac{G\Gamma}{1-\nu}\int_0^l [\nu(K\delta K'' + K''\delta K) - (\Lambda'\delta K'' + K''\delta\Lambda') + 4(1-\nu)K'\delta K']\, dz + \frac{EH_B}{1-\nu^2}\int_0^l K''\delta K''\, dz - M_B\left[\int_0^l \delta\Lambda'\, dz - \frac{\Gamma}{2I}\int_0^l \delta K''dz\right] = 0$$

Upon integration by parts in the foregoing, we obtain

$$\int_0^l \left[\frac{EI}{1-\nu^2}(-\nu K + \Lambda') - \frac{G\Gamma}{1-\nu}K'' - M_B\right]\delta\Lambda'\, dz + \int_0^l \left\{\frac{EI}{1-\nu^2}(K - \nu\Lambda') + \frac{G\Gamma}{1-\nu}[(-4 + 6\nu)K'' - \Lambda''' + \frac{2GH_B}{1-\nu}K^{iv}\right\}\delta K\, dz + \left\{\left[\frac{G\Gamma}{1-\nu}(\nu K - \Lambda') + \frac{2GH_B}{1-\nu}K'' + \frac{M_B\Gamma}{2I}\right]\delta K'\right\}_0^l + \left\{\left[4G\Gamma K' - \frac{G\Gamma}{1-\nu}(\nu K' - \Lambda'') - \frac{2GH_B}{1-\nu}K'''\right]\delta K\right\}_0^l = 0 \quad \ldots. [27]$$

The integrands both vanish identically because of the arbitrariness of $\delta\Lambda'$ and $\delta K$. Thus we obtain a pair of simultaneous linear differential equations in $\Lambda'$ and $K$, which can be reduced to the following

$$\left.\begin{aligned} EIK - 4GIK'' + \frac{G}{1-\nu}\left(2H_B - \frac{\Gamma^2}{2I}\right)K^{iv} &= \nu M_B \\ \Lambda'' &= \frac{M_B(1-\nu^2)}{EI} + \nu K + \frac{\Gamma}{2I}K'' \end{aligned}\right\} \ldots [28]$$

The boundary conditions are of two types, the geometric and the natural. The geometric conditions are those specified for $u$, $\Lambda$, $\Lambda'$, $K$, and $K'$. The actual specification of the values of these quantities will be given later. In our problem they can be specified only at $z = 0$, and having been once selected, it is assumed that their variations are zero in the variational theorem. The natural boundary conditions are those resulting from setting equal to zero the last two bracketed expressions in Equation [27] for $z = l$. The results are

$$K''(l) = 0$$

$$4G\Gamma K'(l) - \frac{G\Gamma}{1-\nu}[\nu K'(l) - \Lambda''(l)] - \frac{2GH_B}{1-\nu}K'''(l) = 0 \ldots [29]$$

We must then solve for $K$ from the first of Equations [28] with two geometric boundary conditions at $z = 0$ and the two natural boundary conditions, Equations [29]. The terms involving derivatives of $\Lambda$ can be related to $K$ through the second of Equations [28].

It is known that when a cylinder whose cross section is thin compared to its width is subject to bending, the anticlastic curvature is considerably different from the simple parabolic shape which is predicted by linear elasticity theory. To discuss this effect in detail we require a nonlinear theory, that is, one which takes account of the fact that changes in shape of the body are significant in determining the stresses. Such a theory is given by Ashwell.[7] For very wide cylinders, the section shape is not curved uniformly, but is quite flat except near the ends. Because of the flatness, transverse stresses are present, and the moment-axial curvature relation is

$$M_B = \frac{EI}{1-\nu^2}\Lambda'$$

instead of $EI\Lambda'$.

To include this effect in our theory, we shall change $I$ to $I/(1-\nu^2)$ in Equations [28]. No change occurs in the boundary conditions. We then have

$$\left.\begin{aligned} \frac{EI}{1-\nu^2}K - 4G\Omega K'' + \frac{G}{1-\nu}\left[2H_B - \frac{\Gamma^2(1-\nu^2)}{2I}\right]K^{IV} &= \nu M_B \\ \Lambda' = \frac{M_B(1-\nu^2)^2}{EI} + \nu K + \frac{\Gamma(1-\nu^2)}{2I}K'' & \end{aligned}\right\} \quad [30]$$

In the calculations of deflection for the specimens considered in this paper, Equations [30] are used instead of Equations [28].

## 4 Nonuniform Torsion and Bending of Skew Cylinders

As an application of the foregoing theory, we consider a skew cylinder, Fig. 3, of slant length $l$, and swept angle $\beta$. One end of the cylinder is assumed to be clamped, the other subject to bending and twisting moments $\bar{M}_B$ and $\bar{M}_T$. From statics, we can show that the bending and twisting moments on section $R$, i.e. $z =$ constant, are given by

$$\left.\begin{aligned} M_B &= \bar{M}_T \sin\beta + \bar{M}_B \cos\beta \\ M_T &= \bar{M}_T \cos\beta - \bar{M}_B \sin\beta \end{aligned}\right\} \quad [31]$$

We shall assume that the differential equations governing the deflection are Equations [5] and [30]. Some remarks must be made concerning the boundary conditions at the two ends of the skew cylinder. At the fixed end we shall assume that the deflection of the origin is zero, that the angle of twist $\Omega$ is zero at the origin. Next, we assume that the deflection of the point $P$ in Fig. 3 is zero also. In addition to these conditions, we also assume that the curvature in the direction of $OP$, and the twist rate at the origin are zero. If we let $u_0$ be the symbol for the deflection of the middle plane of the cylinder in the $x$-direction, the conditions on deflection and twist are

$$\left.\begin{aligned} u_0(-b,\, b\tan\beta) &= 0 \\ \Omega(0) &= 0 \end{aligned}\right\} \quad [32]$$

The conditions on curvature and rate of twist are

$$\left.\begin{aligned} K(0)\cos^2\beta - 2\Omega'(0)\sin\beta\cos\beta - \Lambda'(0)\sin^2\beta &= 0 \\ \Omega'(0)(\cos^2\beta - \sin^2\beta) + [\Lambda'(0) + K(0)]\sin\beta\cos\beta &= 0 \end{aligned}\right\} \quad [33]$$

The manner in which the conditions for the loaded end are specified will now be discussed. The assumption is made here that the deformations of the cylinder are the same, whether the moments are applied as shown in Fig. 3, or are applied on a section $z = l$ perpendicular to the axis, as long as the resultant

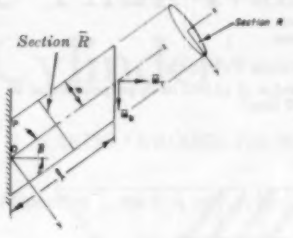


Fig. 3 Cantilever Skew Cylinder Loaded in Torsion and Bending

moment is the same; that is, the resultant moment, and not the surface on which it is applied, is considered of primary importance. Thus the conditions at $z = l$ are the same as in an unswept cylinder, and we have the boundary conditions

$$\left.\begin{aligned} \Omega'(l) &= 0 \\ K'(l) &= 0 \\ K'(l) + \frac{1}{1-\nu}\left[\frac{1-\nu^2}{8I} - \frac{H_B}{2\Gamma}\right]K'''(l) &= 0 \end{aligned}\right\} \quad [34]$$

## 5 Comparison With Experiment

The theory of Section 4, together with the stress formulas of Equation [23], was applied to a series of specific cases for which experimental data are available.[8] Only the results of computations are shown in this paper. Fig. 4 shows the model for which comparisons are made. Figs. 5($a$, $b$, $c$, $d$) show the comparison between theory and experiment for lines of equal deflection; and Figs. 6($a$, $b$, $c$, $d$) show the comparison for stresses. A glance at these figures tells us immediately that the largest discrepancies in both deflection and stress occur in the vicinity of the fixed end. This is not surprising since the theory is not flexible enough to fit the conditions of a truly fixed end. The results are quite satisfactory for points not close to the fixed end.

It should be mentioned that agreement between the theory presented in this paper and the experimental results selected constitutes primarily a check on the nonuniform bending theory, since the torsion-bending constant $\Gamma$ is very small for narrow rectangular sections.

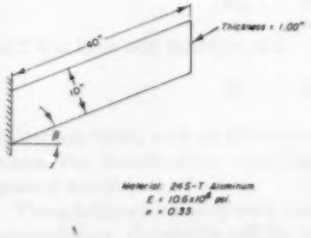


Fig. 4 Model Used in Experiments

[7] "The Anticlastic Curvature of Rectangular Beams and Plates," by D. G. Ashwell, *Journal of the Royal Aeronautical Society*, vol. 54, 1950, p. 708.

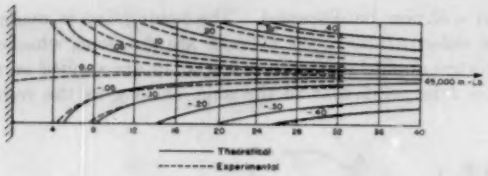


FIG. 5(a) DEFLECTION PATTERN
(Loaded at tip with torsional moment vector of 45,000 in-lb perpendicular to tip; $\beta$ = 0 deg.)

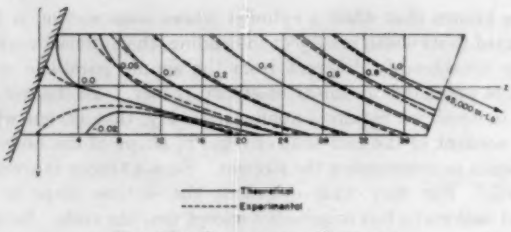


FIG. 5(b) DEFLECTION PATTERN
(Loaded at tip with torsional moment vector of 45,000 in-lb perpendicular to tip; $\beta$ = 20 deg.)

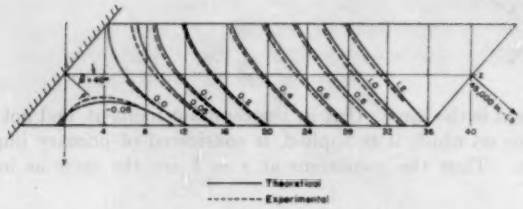


FIG. 5(c) DEFLECTION PATTERN
(Loaded at tip with torsional moment vector of 45,000 in-lb perpendicular to tip; $\beta$ = 40 deg.)

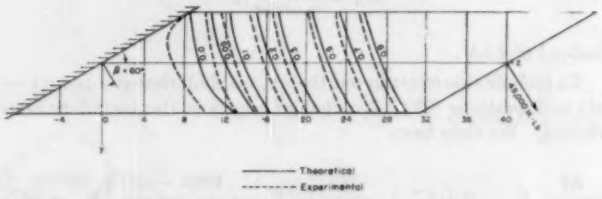


FIG. 5(d) DEFLECTION PATTERN
(Loaded at tip with torsional moment vector of 45,000 in-lb perpendicular to tip; $\beta$ = 60 deg.)

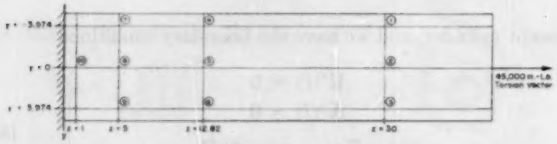


Principal Stresses (psi)

| Point | 1 | | 2 | | 3 | | 4 | | 5 | |
|---|---|---|---|---|---|---|---|---|---|---|
| Theoretical | +13500 | -13500 | +13800 | -13800 | +13800 | -13800 | +13440 | -13440 | +13440 | -13440 |
| Experimental | +11700 | -10900 | +11800 | -12400 | +10000 | -10600 | +10900 | -11100 | +11800 | -12000 |

| Point | 6 | | 7 | | 8 | | 9 | | 10 | |
|---|---|---|---|---|---|---|---|---|---|---|
| Theoretical | +13440 | -13440 | +11886 | -11886 | +11886 | -11886 | +11886 | -11886 | +4672 | -4672 |
| Experimental | +11800 | -10300 | +9600 | -11500 | +11300 | -11200 | +11900 | -9300 | +6200 | -6200 |

FIG. 6(a) PRINCIPAL STRESSES, $\beta$ = 0 DEG

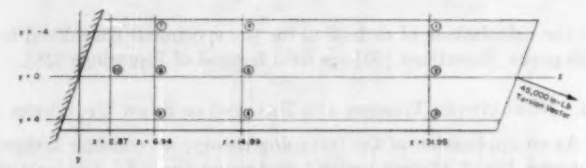


Principal Stresses (psi)

| Point | 1 | | 2 | | 3 | | 4 | | 5 | |
|---|---|---|---|---|---|---|---|---|---|---|
| Theoretical | +9219 | -17449 | +9219 | -17449 | +9219 | -17449 | +9130 | -17449 | +9185 | -17428 |
| Experimental | +8800 | -17000 | +9400 | -18400 | +9400 | -17200 | +9000 | -17100 | +9000 | -16000 |

| Point | 6 | | 7 | | 8 | | 9 | | 10 | |
|---|---|---|---|---|---|---|---|---|---|---|
| Theoretical | +9219 | -17449 | +9219 | -17449 | +7829 | -18009 | +7858 | -18009 | +4350 | -13500 |
| Experimental | +9000 | -18900 | +8400 | -18000 | +9000 | -18900 | +8800 | -18100 | +7500 | -12900 |

FIG. 6(b) PRINCIPAL STRESSES, $\beta$ = 20 DEG

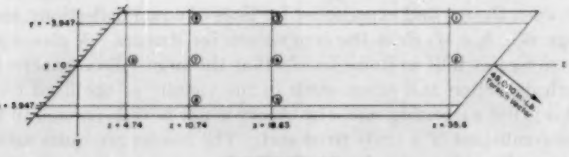


Principal Stresses (psi)

| Point | 1 | | 2 | | 3 | | 4 | |
|---|---|---|---|---|---|---|---|---|
| Theoretical | +849 | -20686 | +9179 | -20640 | +908 | -20634 | +589 | -20632 |
| Experimental | +4900 | -20500 | +6700 | -23500 | +500 | -20100 | +5200 | -21800 |

| Point | 5 | | 6 | | 7 | | 8 | |
|---|---|---|---|---|---|---|---|---|
| Theoretical | +1147 | -20687 | +6175 | -20459 | +4721 | -20579 | +4023 | -21179 |
| Experimental | +5200 | -21800 | +4900 | -21900 | +5400 | -20700 | +4800 | -19300 |

| Point | 9 | |
|---|---|---|
| Theoretical | +3380 | -17824 |
| Experimental | +4900 | -14100 |

FIG. 6(c) PRINCIPAL STRESSES, $\beta$ = 40 DEG

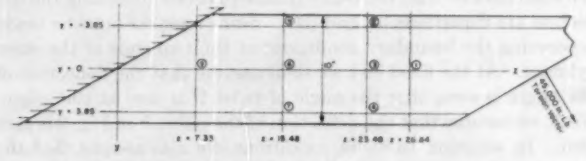


Principal Stresses (psi)

| Point | 1 | | 2 | | 3 | | 4 | |
|---|---|---|---|---|---|---|---|---|
| Theoretical | +1093 | -22917 | +1976 | -22944 | +2197 | -22953 | +1976 | -22944 |
| Experimental | +2700 | -24500 | +2300 | -23000 | +2300 | -24000 | +2300 | -23200 |

| Point | 5 | | 6 | | 7 | | 8 | |
|---|---|---|---|---|---|---|---|---|
| Theoretical | +1093 | -22917 | +1771 | -22725 | +1825 | -23089 | -914 | -21816 |
| Experimental | +2200 | -23800 | +2700 | -23800 | +2100 | -22800 | -2800 | -15200 |

FIG. 6(d) PRINCIPAL STRESSES, $\beta$ = 60 DEG

# Simplified Formulas for Boundary-Value Problems of the Thin-Walled Circular Cylinder[1]

By FREDERICK V. POHLE[2] AND S. V. NARDO,[3] BROOKLYN, N. Y.

**N. J. Hoff[4] has presented formulas which can be used in the solution of boundary-value problems of circular cylinders. The purpose of this note is to express these results in exact simplified form; a more detailed investigation appears elsewhere.[5] The notation will be that of Hoff,[4] unless otherwise stated.**

THE quantities $\sigma_x, \sigma_\varphi, \tau_{x\varphi}, M_x, M_\varphi, M_{x\varphi}, Q_x, Q_\varphi, Q_{\varphi\,\text{eff}}, Q_{x\,\text{eff}}$ are known in terms of the displacements and their derivatives, by Equations [8–12].[4] The displacements are given by Equations [13 *a*, *b*, *c*][4] and the complex constants $B$ and $C$ are known in terms of the real constant $A$ by Equations [14],[15].[4] The essential property of these coefficients $B$, $C$, is that the numerators are polynomials in $p$ and the denominators are solely of the form $(p^2 - n^2)^2$.

Let

$$p_1 = -\alpha_1 + i\beta_1;\ p_2 = -\alpha_2 + i\beta_2 \quad \ldots\ldots [1]$$

to distinguish the $p$-values in Equations [30],[40], respectively, by Hoff[4]; $p_1$ and $p_2$ are the distinct roots of Equation [17*a*][4]; that is

$$p_1^2 + p_2^2 = 2n^2 + 2iK^2 \quad \ldots\ldots [2]$$

and

$$p_1^2 p_2^2 = n^4 \quad \ldots\ldots [3]$$

Also, one has

$$\left.\begin{aligned} p_1^2 - n^2 &= -(1+i)Kp_1 \\ p_2^2 - n^2 &= (1+i)Kp_2 \end{aligned}\right\} \quad \ldots\ldots [4]$$

Equations [4] follow from Equations [39*b*], [17*b*],[4] respectively. If the two sides of the equations in Equations [4] are subtracted, respectively, then $p_1$ and $p_2$ are linearly related as follows

$$p_1 - p_2 = -(1+i)K \quad \ldots\ldots [5]$$

Squaring both sides of Equation [5] and comparing the result with Equation [2] one gets

$$p_1 p_2 = n^2 \quad \ldots\ldots [6]$$

Equations [4] show that any positive integral power of $p$ ($= p_1, p_2$) can be expressed as a linear function of $p$. The only form of any denominator containing $p$ is $(p^2 - n^2)^2$ and this expression can always be replaced by $2iK^2p^2$ by Equation [17*a*].[4] Since $p_1^2 = n^4/p_1^2$, $p_2^2 = n^4/p_1^2$ by Equation [3], the expression $1/(p_1^2 - n^2)^2$, say, can be written as $p_2^2/2iK^2$; thus the denominator expression in $p_1$ has been transferred into a numerator expression in $p_2$. Since the remaining numerator terms also may be written solely in terms of $p_2$ by Equation [5], the resulting expression is again a polynomial in $p_2$, which can be reduced to a linear expression in $p_1$ (or $p_2$). The result is that all coefficients in the Hoff formulas[4] can be written in terms of linear combinations of $\alpha_1, \alpha_2, \beta_1, \beta_2$, alone.

## Application of Procedure

The systematic application of the procedure just outlined leads to the results listed in Tables 1 and 2. The constants $H_1, \ldots H_8$ have been used in place of $A_1, \ldots A_8$ of Hoff.[4] The relations between them are

$$\left.\begin{aligned} A_n &= (-1)^{n+1}(1/2)(H_n + H_{n+4});\ (n = 1, \ldots 4) \\ A_n &= (-1)^{n+1}(1/2)(H_{n-4} - H_n);\ (n = 5, \ldots 8) \end{aligned}\right\} \quad \ldots [7]$$

To indicate the use of the tables, a typical term of, say, $M_x/[(D/a)\cos n\varphi]$ in Table 1 will be listed. The coefficient of $H_1$ is

$$\cosh(\alpha_1 x)\cos(\beta_1 x)[-(1-\nu)n^2 - K(\alpha_1 + \beta_1)] + \sinh(\alpha_1 x)\sin(\beta_1 x)\,[-(\alpha_1 + \beta_1)K]$$

The coefficients of $H_2 \ldots H_8$ are determined in a similar manner.

If the cylinder extends from $x = 0$ to $x = \infty$, then

$$H_n = H_{n+4};\ (n = 1, \ldots 4) \quad \ldots\ldots [8]$$

and all results can be simplified. If $w$ is an even function of $x$

$$H_5, \ldots H_8 = 0 \quad \ldots\ldots [9]$$

and if $w$ is an odd function of $x$

$$H_1, \ldots H_4 = 0 \quad \ldots\ldots [10]$$

In certain cases, such as that corresponding to simply supported edges, the simultaneous equations can be solved explicitly in general terms.

The solutions for $n = 0$ were omitted in the earlier paper.[4] For completeness, the results will be listed here. To avoid confusion with the cases $n > 1$, the constants will be denoted by $G_1 \ldots G_8$. The results are

---

[1] This work was performed under a consulting contract with the Knolls Atomic Power Laboratory, Schenectady, N. Y., operated by the General Electric Company for the United States Atomic Energy Commission. The authors are indebted to the company, to the AEC, to Dr. John Zickel, and to Mr. Daniel R. Miller, the project supervisor, for their permission to publish this paper.

[2] Assistant Professor of Applied Mechanics, Polytechnic Institute of Brooklyn.

[3] Associate Professor of Aeronautical Engineering, Polytechnic Institute of Brooklyn.

[4] "Boundary-Value Problems of the Thin-Walled Circular Cylinder," by N. J. Hoff, JOURNAL OF APPLIED MECHANICS, Trans. ASME, vol. 76, 1954, pp. 343–350.

[5] "Stresses in Cylinders With Elastic Edge Support. Part III, Simplification of Equations," by F. V. Pohle and S. V. Nardo. To appear as a KAPL report.

Presented at the National Conference of the Applied Mechanics Division, Troy, N. Y., June 16–18, 1955, of THE AMERICAN SOCIETY OF MECANICAL ENGINEERS.

Discussion of this paper should be addressed to the Secretary, ASME, 29 West 39th Street, New York, N. Y., and will be accepted until October 10, 1955, for publication at a later date. Discussion received after the closing date will be returned.

NOTE: Statements and opinions advanced in papers are to be understood as individual expressions of their authors and not those of the Society. Manuscript received by ASME Applied Mechanics Division, September 14, 1954. Paper No. 55—APM-9.

TABLE 1 RESULTS FOR FINITE CYLINDER; $n \geq 1$

| Column 1 | Column 2 | Column 3 | Column 4 | Column 5 |
|---|---|---|---|---|
| $w/\cos n\varphi$ | 1 | 0 | 1 | 0 |
| $2nK^3v/\sin n\varphi$ | $(-\alpha_2 + \beta_2)K$ | $(1+\nu)n^2 + K(\alpha_2 + \beta_2)$ | $(\alpha_1 - \beta_1)K$ | $(1+\nu)n^2 - K(\alpha_1 + \beta_1)$ |
| $2K^2\sigma_x/En^2 \cos n\varphi$ | 0 | $-1$ | 0 | $-1$ |
| $2K^2\sigma_\varphi/E \cos n\varphi$ | $(-\alpha_2 + \beta_2)K$ | $n^2 + K(\alpha_2 + \beta_2)$ | $(\alpha_2 - \beta_2)K$ | $n^2 - K(\alpha_2 + \beta_2)$ |
| $M_x/[(D/a) \cos n\varphi]$ | $-(1-\nu)n^2 - K(\alpha_2 + \beta_2)$ | $(-\alpha_2 + \beta_2)K$ | $-(1-\nu)n^2 + K(\alpha_2 + \beta_2)$ | $(\alpha_2 - \beta_2)K$ |
| $M_\varphi/[(D/a) \cos n\varphi]$ | $(1-\nu)n^2 - \nu K(\alpha_2 + \beta_2)$ | $-\nu K(\alpha_2 - \beta_2)$ | $(1-\nu)n^2 + \nu K(\alpha_2 + \beta_2)$ | $\nu K(\alpha_2 - \beta_2)$ |
| $Q_\varphi/[(D/a^2)Kn \sin n\varphi]$ | $\alpha_2 + \beta_2$ | $\alpha_2 - \beta_2$ | $-\alpha_2 - \beta_2$ | $-\alpha_2 + \beta_2$ |
| $Q_{\varphi\,\mathrm{eff}}/[(D/a^2)n \sin n\varphi]$ | $(1-\nu)n^2 + (2-\nu)K(\alpha_2 + \beta_2)$ | $(2-\nu)K(\alpha_2 - \beta_2)$ | $(1-\nu)n^2 - (2-\nu)K(\alpha_2 + \beta_2)$ | $-(2-\nu)K(\alpha_2 - \beta_2)$ |
| $\cosh \alpha_1 x \cos \beta_1 x$ | $H_1$ | $-H_2$ | ... | ... |
| $\sinh \alpha_1 x \sin \beta_1 x$ | $H_2$ | $H_1$ | ... | ... |
| $\cosh \alpha_2 x \cos \beta_2 x$ | ... | ... | $H_3$ | $-H_4$ |
| $\sinh \alpha_2 x \sin \beta_2 x$ | ... | ... | $H_4$ | $H_3$ |
| $\cosh \alpha_1 x \sin \beta_1 x$ | $-H_3$ | $-H_4$ | ... | ... |
| $\sinh \alpha_1 x \cos \beta_1 x$ | $-H_4$ | $H_3$ | ... | ... |
| $\cosh \alpha_2 x \sin \beta_2 x$ | ... | .... | $-H_5$ | $-H_7$ |
| $\sinh \alpha_2 x \cos \beta_2 x$ | ... | ... | $-H_7$ | $H_5$ |

TABLE 2 RESULTS FOR FINITE CYLINDER; $n \geq 1$

| | | | | |
|---|---|---|---|---|
| $w_{,x}/\cos n\varphi$ | $-\alpha_1$ | $\beta_1$ | $-\alpha_2$ | $\beta_2$ |
| $2K^3u/\cos n\varphi$ | $(1+\nu)\beta_2 - \nu K$ | $(1+\nu)\alpha_2 + \nu K$ | $(1+\nu)\beta_1 + \nu K$ | $(1+\nu)\alpha_1 - \nu K$ |
| $2K^3\tau_{x\varphi}/En \sin n\varphi$ | $-\beta_1$ | $-\alpha_1$ | $-\beta_2$ | $-\alpha_2$ |
| $M_{x\varphi}/[(1-\nu)(D/a)n \sin n\varphi]$ | $\alpha_1$ | $-\beta_1$ | $\alpha_2$ | $-\beta_2$ |
| $Q_x/[(D/a^2)K \cos n\phi]$ | $n^2 + 2K\beta_1$ | $n^2 + 2K\alpha_1$ | $-n^2 + 2K\beta_2$ | $-n^2 + 2K\alpha_2$ |
| $Q_{x\,\mathrm{eff}}/[(D/a^2) \cos n\phi]$ | $Kn^2 - (1-\nu)n^2\alpha_1 + 2K^2\beta_1$ | $Kn^2 + 2K^2\alpha_1 + (1-\nu)n^2\beta_1$ | $-Kn^2 - (1-\nu)n^2\alpha_2 + 2K^2\beta_2$ | $-Kn^2 + 2K^2\alpha_2 + (1-\nu)n^2\beta_2$ |
| $\cosh \alpha_1 x \sin \beta_1 x$ | $-H_2$ | $-H_1$ | ... | ... |
| $\sinh \alpha_1 x \cos \beta_1 x$ | $-H_1$ | $H_2$ | ... | ... |
| $\cosh \alpha_2 x \sin \beta_2 x$ | ... | ... | $-H_4$ | $-H_3$ |
| $\sinh \alpha_2 x \cos \beta_2 x$ | ... | ... | $-H_3$ | $H_4$ |
| $\cosh \alpha_1 x \cos \beta_1 x$ | $H_3$ | $-H_4$ | ... | ... |
| $\sinh \alpha_1 x \sin \beta_1 x$ | $H_4$ | $H_3$ | ... | ... |
| $\cosh \alpha_2 x \cos \beta_2 x$ | ... | ... | $H_7$ | $-H_5$ |
| $\sinh \alpha_2 x \sin \beta_2 x$ | ... | ... | $H_5$ | $H_7$ |

$$w = G_1 \cosh(Kx)\cos(Kx) + G_2 \sinh(Kx)\sin(Kx) + G_3\nu/(1-\nu^2) + G_5 \sinh(Kx)\cos(Kx) + G_6 \cosh(Kx)\sin(Kx) \quad [11]$$

$$w_{,x} = [(G_5 + G_6)K]\cosh(Kx)\cos(Kx) + [(-G_5 + G_6)K]\sinh(Kx)\sin(Kx) + [(G_1 + G_2)K]\sinh(Kx)\cos(Kx) + [(-G_1 + G_2)K]\cosh(Kx)\sin(Kx) \quad [12]$$

$$u = (\nu/2K)(G_5 - G_6)\cosh(Kx)\cos(Kx) + (\nu/2K)(G_5 + G_6)\sinh(Kx)\sin(Kx) + (\nu/2K)(G_1 - G_2)\sinh(Kx)\cos(Kx) + [(\nu/2K)(G_1 + G_2)\cosh(Kx)\sin(Kx)] + G_3 + [G_3/(1-\nu^2)]x \quad [13]$$

$$v = G_4 + G_7 x \quad [14]$$

$$\sigma_x = [E/(1-\nu^2)]G_3 \quad [15]$$

$$\sigma_\varphi = -E[G_1 \cosh(Kx)\cos(Kx) + G_2 \sinh(Kx)\sin(Kx) + G_5 \sinh(Kx)\cos(Kx) + G_6 \cosh(Kx)\sin(Kx)] \quad [16]$$

$$\tau_{x\varphi} = [E/2(1+\nu)]G_7 \quad [17]$$

$$M_x = -(D/a^2)(2K^2)[-G_1 \sinh(Kx)\sin(Kx) + G_2 \cosh(Kx)\cos(Kx) - G_5 \cosh(Kx)\sin(Kx) + G_6 \sinh(Kx)\cos(Kx)] \quad [18]$$

$$M_\varphi = \nu M_x \quad [19]$$

$$M_{x\varphi} = 0 \quad [20]$$

$$Q_x = (D/a^2)(2K^2)[(G_5 + G_6)\sinh(Kx)\sin(Kx) + (G_5 - G_6)\cosh(Kx)\cos(Kx) + (G_1 + G_2)\cosh(Kx)\sin(Kx) + (G_1 - G_2)\sinh(Kx)\cos(Kx)] \quad [21]$$

$$Q_\varphi = 0 \quad [22]$$

$$Q_{x\,\mathrm{eff}} = Q_x \quad [23]$$

$$Q_{\varphi\,\mathrm{eff}} = 0 \quad [24]$$

# Forced Vibrations of a Body on an Infinite Elastic Solid

By R. N. ARNOLD,[1] G. N. BYCROFT,[2] and G. B. WARBURTON[3]

**The paper considers the forced vibration of a rigid body resting on a homogeneous elastic medium of infinite surface area and constant depth which may be finite or infinite. Four modes of vibration for a body with a circular base are investigated; (*a*) vertical translation, (*b*) torsion, (*c*) horizontal translation, (*d*) rocking. For a semi-infinite medium the amplitude response can be obtained for any mass in terms of known constants of the system and two fundamental functions $f_1$ and $f_2$, whicl depend only on the exciting frequency and the properties of the medium. Close approximations to these functions have been evaluated for each mode. Experiments on an elastic model are described, the results of which are in good agreement with theoretical prediction. The behavior of a stratum of infinite area is more complex since functions $f_1$ and $f_2$ also depend on stratum depth. These functions have been evaluated for the torsional mode only, experimental results being given for the other modes.**

## Nomenclature

The following nomenclature is used in the paper:

$a = kr$

$a_0 = kr_0$ = frequency factor

$A$ = amplitude of vibration

$B$, $C$, $F$ = functions of $s$, $\eta$, and $\delta$

$b = \dfrac{m_0}{\rho r_0^3}$ = mass ratio (translational modes)

$b' = \dfrac{I_0}{\rho r_0^5}$ = inertia ratio (rotational modes)

$E$ = Young's modulus

$f_1$, $f_2$ = functions of $a_0$ and $\nu$

$f_{1a}$, $f_{1p}$ = limits of $f_1$

$f_{2a}$, $f_{2p}$ = limits of $f_2$

$h = \left(\dfrac{\rho}{\lambda + 2\mu}\right)^{1/2} p$

$I_0$ = relevant moment of inertia of mass $m_0$

$k = \left(\dfrac{\rho}{\mu}\right)^{1/2} p$

$m_0$ = mass resting on surface of medium

$M$ = amplitude of exciting couple

$n$ = integer

$p$ = circular frequency of force (or couple) applied to plate

$P$ = amplitude of exciting force

$r$ = radial distance from center of plate

$r_0$ = radius of plate

$R = \dfrac{\delta}{r_0}$

$s$ = dimensionless variable used for integration

$t$ = time

$u$, $v$, $w$ = displacements of plate in radial, tangential, and vertical directions

$z$ = vertical distance from surface of medium

$\alpha = (k^2 s^2 - h^2)^{1/2}$

$\beta = (k^2 s^2 - k^2)^{1/2}$

$\Delta$ = dilatation

$\delta$ = depth of stratum

$\epsilon$ = constant

$\eta = \dfrac{h}{k} = \left(\dfrac{\mu}{\lambda + 2\mu}\right)^{1/2} = \left[\dfrac{1 - 2\nu}{2(1 - \nu)}\right]^{1/2}$

$\theta$ = angular co-ordinate

$\lambda = \dfrac{E\nu}{(1 + \nu)(1 - 2\nu)}$ = Lamé's elastic constant

$\mu$ = modulus of rigidity

$\nu$ = Poisson's ratio

$\rho$ = density of medium

$\sigma_z$ = normal stress parallel to $Z$-axis

$\tau_{zr}$, $\tau_{z\theta}$ = shear stresses in plane perpendicular to $Z$-axis and in radial and tangential directions, respectively

$\phi$ = angular displacement about horizontal axis

$\psi$ = angular displacement about vertical axis

$\omega_\theta$, $\omega_r$, $\omega_z$ = components of rotation

## Introduction

The paper considers the forced vibrations of a mass with a rigid circular base resting on (*a*) a semi-infinite homogeneous elastic medium, (*b*) a homogeneous elastic stratum of infinite area and constant depth $\delta$ supported by an infinite rigid foundation, Fig. 1. The response of the mass to harmonic forces or couples is obtained for four modes of vibration. The applied forces and couples are $P_z \sin pt$, $M_z \sin pt$, $P_x \sin pt$, and $M_y \sin pt$ and the corresponding

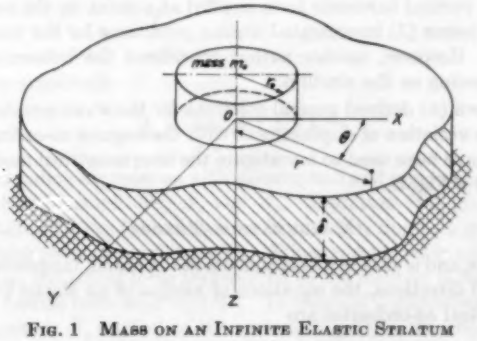


Fig. 1 Mass on an Infinite Elastic Stratum

[1] Regius Professor of Engineering, University of Edinburgh, Edinburgh, Scotland.

[2] National Research Scholar of the Department of Scientific and Industrial Research, Wellington, New Zealand.

[3] Lecturer, Department of Engineering, University of Edinburgh, Edinburgh, Scotland.

Presented at the National Conference of the Applied Mechanics Division, Troy, N. Y., June 16–18, 1955, of The American Society of Mechanical Engineers.

Discussion of this paper should be addressed to the Secretary, ASME, 29 West 39th Street, New York, N. Y., and will be accepted until October 10, 1955, for publication at a later date. Discussion received after the closing date will be returned.

Note: Statements and opinions advanced in papers are to be understood as individual expressions of their authors and not those of the Society. Manuscript received by ASME Applied Mechanics Division, August 16, 1954. Paper No. 55—APM-10.

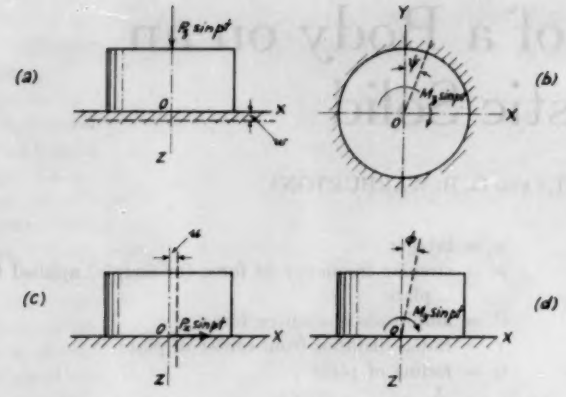


FIG. 2 MODES OF VIBRATION OF MASS ON SEMI-INFINITE ELASTIC MEDIUM

displacements of the mass $w$, $\psi$, $u$, and $\phi$, Fig. 2. These modes are referred to as ($a$) vertical translation, ($b$) torsion, ($c$) horizontal translation, and ($d$) rocking. In ($c$) and ($d$) the motion is constrained to be translation along $OX$ and rotation about $OY$, respectively, although owing to the position of the center of gravity of the mass both motions normally exist together.

Vibrations of a machine foundation resting on the ground may be excited in any of these modes by unbalanced forces. However, this practical problem has added complexity, since the ground cannot be considered as an elastic medium and the base of a foundation will not, in general, be circular. Nevertheless, the problem investigated here is an essential preliminary to a complete solution of the effects of ground vibration.

For a semi-infinite elastic medium the modes, vertical translation and torsion, have been investigated analytically by previous workers, but experimental work seems to have been confined to nonlinear media, such as ground. Lamb (1)[4] studied the propagation of waves in elastic solids and derived the solution for the dynamic displacement caused by a vertical harmonic force applied at a point on the surface of a semi-infinite medium. Reissner (2) considered the vertical motion of a rigid mass of circular base resting on a semi-infinite medium, when subjected to a periodic vertical force, and obtained an approximate solution by assuming uniform pressure distribution between the mass and the medium. He also gave an approximate solution (3) for the torsional mode and with Sagoci (4) derived the exact solution for this mode by using a system of oblate spheroidal co-ordinates.

For a stratum Marguerre (5) derived displacements resulting from a vertical harmonic force applied at a point on the surface, and Reissner (3) investigated similar conditions for the torsional mode. However, neither author considered the influence of a mass resting on the stratum.

Sezawa (6) derived general solutions for the wave equations to include variation of displacement with the angular co-ordinate $\theta$; these have been used to investigate the unsymmetrical modes ($c$) and ($d$) of Fig. 2.

## MATHEMATICAL THEORY

If $u$, $v$, and $w$ are the displacements in the radial, tangential, and vertical directions, the equations of motion of an elastic body in cylindrical co-ordinates are

$$(\lambda + 2\mu)\frac{\partial \Delta}{\partial r} - \frac{2\mu}{r}\frac{\partial \omega_z}{\partial \theta} + 2\mu\frac{\partial \omega_\theta}{\partial z} = \rho\frac{\partial^2 u}{\partial t^2} \quad \ldots\ldots [1]$$

$$(\lambda + 2\mu)\frac{1}{r}\frac{\partial \Delta}{\partial \theta} - 2\mu\frac{\partial \omega_r}{\partial z} + 2\mu\frac{\partial \omega_z}{\partial r} = \rho\frac{\partial^2 v}{\partial t^2} \quad \ldots\ldots [2]$$

$$(\lambda + 2\mu)\frac{\partial \Delta}{\partial z} - \frac{2\mu}{r}\frac{\partial}{\partial r}(r\omega_\theta) + \frac{2\mu}{r}\frac{\partial \omega_r}{\partial \theta} = \rho\frac{\partial^2 w}{\partial t^2} \quad \ldots\ldots [3]$$

where the dilatation

$$\Delta = \frac{1}{r}\frac{\partial}{\partial r}(ru) + \frac{1}{r}\frac{\partial v}{\partial \theta} + \frac{\partial w}{\partial z}$$

the rotations

$$\omega_\theta = \frac{1}{2}\left(\frac{\partial u}{\partial z} - \frac{\partial w}{\partial r}\right), \quad \omega_r = \frac{1}{2}\left(\frac{1}{r}\frac{\partial w}{\partial \theta} - \frac{\partial v}{\partial z}\right)$$

and

$$\omega_z = \frac{1}{2r}\left[\frac{\partial}{\partial r}(rv) - \frac{\partial u}{\partial \theta}\right]$$

and $\lambda$ and $\mu$ are Lamé's elastic constants.

Particular solutions of Equations [1] to [3] have been derived (6) as

$$u = u_1 + u_2 + u_3, \quad v = v_1 + v_2 + v_3, \quad w = w_1 + w_2 \ldots [4]$$

where

$$u_1 = -B_n\frac{k}{h^2}\frac{\partial}{\partial r}[J_n(krs)]\, e^{-\alpha z + ipt}\cos n\theta$$

$$v_1 = B_n\frac{nk}{h^2}\frac{1}{r}J_n(krs)\, e^{-\alpha z + ip}\sin n\theta$$

$$w_1 = B_n\frac{\alpha k}{h^2}J_n(krs)\, e^{-\alpha z + ipt}\cos n\theta$$

$$u_2 = -C_n\frac{\beta}{k^2}\frac{\partial}{\partial r}[J_n(krs)]\, e^{-\beta z + ipt}\cos n\theta$$

$$v_2 = C_n\frac{\beta n}{k^2}\frac{1}{r}J_n(krs)\, e^{-\beta z + ipt}\sin n\theta$$

$$w_2 = C_n s^2 J_n(krs)\, e^{-\beta z + ipt}\cos n\theta$$

$$u_3 = \frac{F_n}{s^2}\frac{1}{kr}J_n(krs)\, e^{-\beta z + ipt}\frac{\partial}{\partial \theta}\sin(n\theta + \epsilon)$$

$$v_3 = -\frac{F_n}{ks^2}\frac{\partial}{\partial r}[J_n(krs)]\, e^{-\beta z + ipt}\sin(n\theta + \epsilon)$$

$$h^2 = \frac{\rho p^2}{\lambda + 2\mu}, \quad k^2 = \frac{\rho p^2}{\mu}, \quad \text{and} \quad \alpha^2 + h^2 = \beta^2 + k^2 = k^2 s^2$$

The normal stress in the $Z$-direction and the components of shear stress in planes perpendicular to the $Z$-axis are given in terms of displacement by

$$\left.\begin{aligned} \sigma_z &= \lambda\Delta + 2\mu\frac{\partial w}{\partial z} \\ \tau_{zr} &= \mu\left(\frac{\partial u}{\partial z} + \frac{\partial w}{\partial r}\right) \\ \tau_{z\theta} &= \mu\left(\frac{1}{r}\frac{\partial w}{\partial \theta} + \frac{\partial v}{\partial z}\right) \end{aligned}\right\} \quad \ldots\ldots [5]$$

In the problem to be considered a mass with a rigid circular base rests on the surface of the medium, Fig. 1. A periodic disturbing force or couple is applied to the mass and is distributed in some manner over this circular area. Thus the boundary con-

[4] Numbers in parentheses refer to the Bibliography at the end of the paper.

ditions are (*a*) zero stress at the free surface for $r > r_0$, (*b*) constant amplitude of linear or angular displacement of surface (depending on mode) for $r \leq r_0$, (*c*) no reflection of elastic waves from boundaries situated at infinity. These conditions are difficult to satisfy, as the stress distribution under the mass during vibration is unknown. In the following analysis this distribution is assumed to be the same as that produced by the corresponding static force or couple. By applying this distribution to the vibrating surface of the medium, it is found that the surface does not remain plane for $r \leq r_0$ and thus condition (*b*) is violated. However, two limiting displacements corresponding to $r = 0$ and $r = r_0$ may be obtained. Moreover, analysis reveals that it is possible to obtain a weighted average displacement by integrating over the circular area and that the true displacement lies between this average value and that obtained for $r = r_0$. This method will now be applied to the four modes of vibration.

### Vertical Translation for Semi-Infinite Medium

For this mode the relevant expressions for symmetrical displacement are obtained from Equation [4], if $n = 0$ and $F_n = 0$. For forced vibration the solution is generalized by integrating with respect to $s$ from 0 to $\infty$; the normal displacement and stress components at any point on the surface of the medium ($z = 0$) are, in terms of the nondimensional quantities $s$, $\eta$ ($= h/k$), and $a$ ($= kr$)

$$w = \mathrm{Re}\left[e^{ipt}\int_0^\infty \left\{B\frac{(s^2-\eta^2)^{1/2}}{\eta^2} + Cs^2\right\} J_0(as)ds\right] \quad [6]$$

$$\sigma_z = \mathrm{Re}\left[\mu k e^{ipt}\int_0^\infty \left\{B\frac{(1-2s^2)}{\eta^2} - 2Cs^2(s^2-1)^{1/2}\right\} J_0(as)ds\right] \quad [7]$$

$$\tau_{zr} = \mathrm{Re}\left[\mu k e^{ipt}\int_0^\infty \left\{-B\frac{2s(s^2-\eta^2)^{1/2}}{\eta^2} + Cs(1-2s^2)\right\} J_1(as)ds\right] \quad [8]$$

where Re signifies that the real part of the complex expression is taken.

The shear stress $\tau_{zr}$ is equated to zero over the whole surface of the medium, giving a relation between $B$ and $C$. This assumes that there is no friction between the base and the medium. The distribution of direct stress is taken to be that of the analogous static case given by Timoshenko (7); thus for a periodic disturbing force $P_z e^{ipt}$ the direct stress

$$\sigma_z = \frac{P_z e^{ipt}}{2\pi r_0(r_0^2 - r^2)^{1/2}} \text{ for } r \leq r_0 \quad [9]$$

$$= 0 \qquad \text{for } r > r_0$$

Expanding Equation [9] by the Fourier-Bessel integral and equating the result to Equation [7] gives an integral for the displacement $w$ at radius $r$. If this integral is analyzed by contour integration, it is found that an additional term must be added if the complete solution is to contain only diverging waves and satisfy the boundary condition at infinity. (This term corresponds to free waves in the medium.) The complete expression for the displacement is

$$w = \mathrm{Re}\left[\frac{P_z e^{ipt}}{8\mu\pi r_0}\int_0^\infty \frac{(s^2-\eta^2)^{1/2}\sin a_0 s\, J_0(as)ds}{G(s)} - \frac{P_z e^{ipt} i(s_1^2-\eta^2)^{1/2}\sin a_0 s_1\, J_0(as_1)}{8\mu r_0 G'(s_1)}\right] \quad [10]$$

where the Cauchy principal value of the integral is understood

$$G(s) = \left(s^2 - \frac{1}{2}\right)^2 - s^2(s^2-1)^{1/2}(s^2-\eta^2)^{1/2}$$

$s_1$ is the real root of $G(s) = 0$, the condition for the existence of free waves

$$G'(s_1) = \left[\frac{dG(s)}{ds}\right]_{s=s_1}$$

and the nondimensional frequency factor $a_0 = pr_0(\mu/\rho)^{1/2}$.

The corresponding expression of Reissner (2), who assumed a uniform stress between the circular base and the medium, is obtained by substituting $J_1(a_0 s)$ and $J_1(a_0 s_1)$ for sin $(a_0 s)$ and sin $(a_0 s_1)$, respectively, in Equation [10]. In Reissner's equation for $w$ the sign of the free-wave term is given as positive; this error affects his computed values of amplitude.

The weighted average value of the dynamic displacement (denoted by subscript $a$ throughout the paper) is given by

$$w_a = \int_0^{r_0} \frac{wr\,dr}{r_0(r_0^2-r^2)^{1/2}} \quad [11]$$

It is a mean displacement over the circular area, the displacement at any radius $r$ being weighted by a factor proportional to the assumed stress at that radius.

After substituting from Equation [10], this average displacement becomes

$$w_a = \mathrm{Re}\left[\frac{P_z e^{ipt}}{8\mu\pi r_0}\int_0^\infty \frac{(s^2-\eta^2)^{1/2}\sin^2 a_0 s\, ds}{a_0 s\, G(s)} - \frac{P_z e^{ipt} i(s_1^2-\eta^2)^{1/2}\sin^2 a_0 s_1}{8\mu r_0 a_0 s_1\, G'(s_1)}\right] \quad [12]$$

and can be expressed in the form

$$w_a = \mathrm{Re}\left[\frac{P_z e^{ipt}}{\mu r_0}\{f_{1a}(a_0,\nu) + if_{2a}(a_0,\nu)\}\right]$$

Functions $f_{1a}$ and $f_{2a}$ are real functions of the frequency factor $a_0$ and Poisson's ratio $\nu$ and correspond to the real and imaginary parts of the integral and free-wave term of Equation [12]. If the corresponding unknown functions giving the true displacement of the rigid base are $f_1$ and $f_2$ and if the functions giving the peripheral displacement (obtained by substituting $r = r_0$ or $a = a_0$ in Equation [10]) are $f_{1p}$ and $f_{2p}$, then

$$f_{1a} > f_1 > f_{1p} \text{ and } f_{2a} > f_2 > f_{2p}$$

Taking the real parts, the true displacement

$$w = \frac{P_z}{\mu r_0}(f_1 \cos pt - f_2 \sin pt) \quad [13]$$

and the amplitude

$$A = \frac{P_z}{\mu r_0}(f_1^2 + f_2^2)^{1/2} \quad [14]$$

Corresponding expressions with subscripts $a$ and $p$ give the limiting values of amplitude, $A_a$ and $A_p$. Equation [14] gives the amplitude of a rigid massless base of radius $r_0$ due to a periodic disturbing force of magnitude $P_z$. When a mass $m_0$ is added to this base, the actual force transmitted to the medium is modified by the inertia force $m_0(d^2w)/(dt^2)$. In terms of a disturbing force of magnitude $P_z$ applied to the system, Fig. 2(*a*), the amplitude of the mass is given by Reissner (2) as

$$A = \frac{P_z}{\mu r_0}\left[\frac{f_1^2 + f_2^2}{(1 + ba_0^2 f_1)^2 + (ba_0^2 f_2)^2}\right]^{1/2} \quad [15]$$

where $b = m_0/\rho r_0^3$.

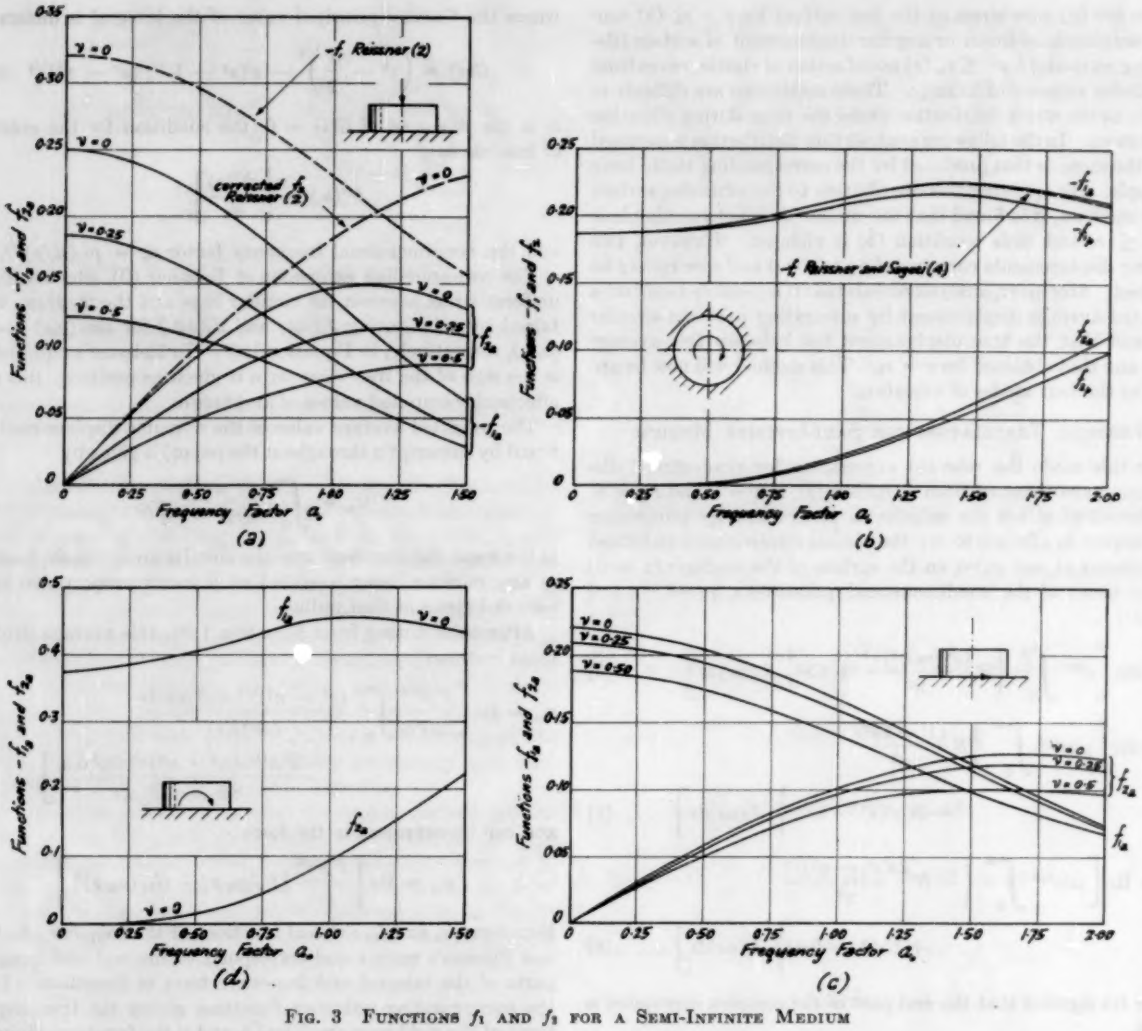


FIG. 3 FUNCTIONS $f_1$ AND $f_2$ FOR A SEMI-INFINITE MEDIUM

It is found that $f_{1a}$, $f_{1p}$, and $f_{2a}$, $f_{2p}$ give close limits for the true values of the functions $f_1$, $f_2$ for the frequency factor $a_0$ in the range 0 to 1.5. In Fig. 3($a$) values of $f_{1a}$ and $f_{2a}$ are plotted against $a_0$ for three values of Poisson's ratio. The broken lines show the values of $f_1$ and $f_2$ obtained by Reissner (2) for $\nu = 0$. (The error previously mentioned only affects his values for $f_2$ and these have been corrected.) Response curves for this mode with $\nu = 0$ for various values of $b$ are given in Fig. 4($a$); they are plotted non-dimensionally as amplitude factor $A\mu r_0/P_z$ against frequency factor $a_0$. The experimental results plotted in this diagram will be discussed later. A curve obtained from Reissner's results has been added for comparison.

### MODES OF SEMI-INFINITE MEDIUM AND STRATUM

For the translational modes the linear displacement is shown to be the real part of

$$\left[\frac{Pe^{ipt}}{\mu r_0}(f_1 + if_2)\right]$$

and similarly for the rotational modes the angular displacement is the real part of

$$\left[\frac{Me^{ipt}}{\mu r_0^3}(f_1 + if_2)\right]$$

The functions $f_1$ and $f_2$ have a different form for each mode. For the semi-infinite medium they are functions of $a_0$ and $\nu$ (except in the torsional mode when they are independent of $\nu$); for the stratum $f_1$ and $f_2$ are also functions of the depth factor $R = \delta/r_0$.

For all modes limiting values of the functions $f_1$ and $f_2$ can be found, but, in general, only the average values $f_{1a}$ and $f_{2a}$ have been evaluated. Equation [15] can be used to find the amplitude of the plate with the addition of mass $m_0$ for all the translational modes; the corresponding expression for the amplitude of a rotational mode ($\psi$ or $\phi$), when a disturbing torque $Me^{ipt}$ is applied to a mass having a relevant moment of inertia $I_0$, is

$$A = \frac{M}{\mu r_0^3}\left[\frac{f_1^2 + f_2^2}{(1 + b'a_0^2 f_1)^2 + (b'a_0^2 f_2)^2}\right]^{1/2} \quad \ldots\ldots [16]$$

where $b' = I_0/(\rho r_0^5)$.

The method of obtaining $f_1$ and $f_2$ is similar for all modes and only the basic equations required to derive these functions will be given for the remainder.

### TORSIONAL MODE FOR SEMI-INFINITE MEDIUM

The only component of displacement is $v$ obtained from Equations [4] by putting $B = C = 0$, $\epsilon = -\pi/2$, and $n = 0$, which

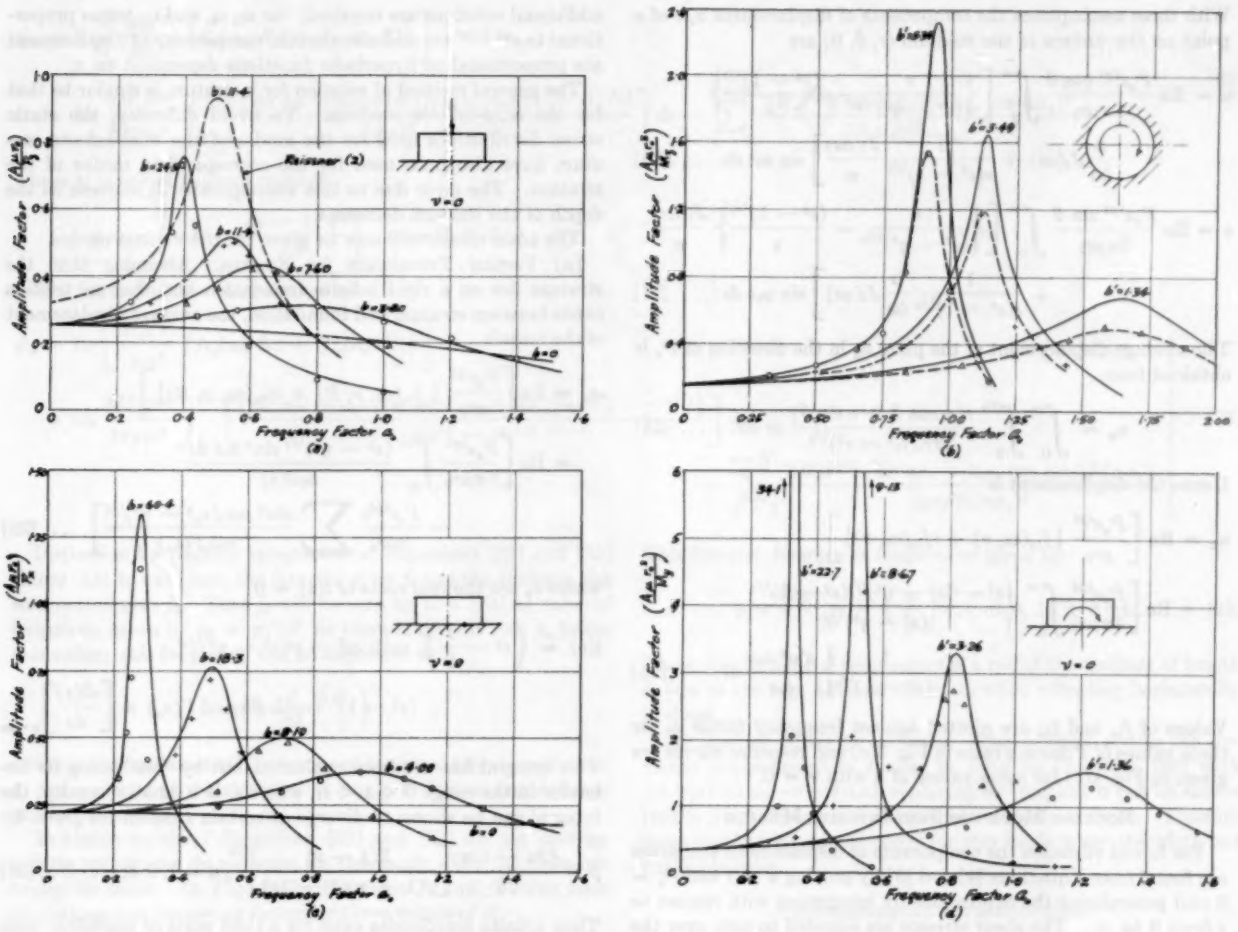


FIG. 4 AMPLITUDE AND FREQUENCY RESPONSE FOR A SEMI-INFINITE MEDIUM

satisfies the condition of symmetry. For forced vibration the tangential displacement at any point on the surface is

$$v = \mathrm{Re}\left[ -e^{ipt} \int_0^\infty \frac{F}{s} J_1(as) ds \right] \quad \ldots\ldots\ldots [17]$$

The shear-stress distribution due to a periodic disturbing torque $M_z e^{ipt}$ is assumed to be

$$\tau_{z\theta} = \frac{3M_z e^{ipt} r}{4\pi r_0^3 (r_0^2 - r^2)^{1/2}} \text{ for } r \leq r_0 \quad \ldots\ldots\ldots [18]$$

$$= 0 \qquad \text{for } r > r_0$$

With this assumption the average dynamic rotation is

$$\psi_a = \mathrm{Re}\left[ \frac{M_z e^{ipt}}{\mu r_0^3} \{ f_{1a}(a_0) + i f_{2a}(a_0) \} \right]$$

$$= \mathrm{Re}\left[ \frac{9M_z e^{ipt}}{8\mu\pi r_0^3} \int_0^\infty \left\{ \frac{\sin a_0 s - a_0 s \cos a_0 s}{a_0 s (s^2 - 1)^{1/2}} \right\} \left\{ \frac{\sin a_0 s - a_0 s \cos a_0 s}{(a_0 s)^2} \right\} ds \right] \quad \ldots\ldots [19]$$

The corresponding expression for $\psi_p$ is obtained by substituting

$$\frac{2}{3} J_1(a_0 s) \text{ for } \left\{ \frac{\sin a_0 s - a_0 s \cos a_0 s}{(a_0 s)^2} \right\}$$

in Equation [19].

The functions $f_{1a}$, $f_{2a}$, $f_{1p}$, and $f_{2p}$ have been plotted against frequency factor $a_0$ in Fig. 3(*b*). The broken line on the diagram shows the exact values of $f_1$ found by Reissner and Sagoci (4); those of $f_2$ are coincident with $f_{2a}$ found from Equation [19]. The agreement between values obtained by exact theory and by the averaging procedure suggested that it was only necessary to compute $f_{1a}$ and $f_{2a}$ for the other modes. Using Equation [16] response curves have been plotted for three values of $b'$ in Fig. 4(*b*).

### HORIZONTAL TRANSLATION FOR SEMI-INFINITE MEDIUM

The relevant expressions for the components of stress and displacement at any point on the surface are obtained by putting $n = 1$, $\epsilon = 0$, and $z = 0$ in Equations [4] and integrating with respect to $s$ from 0 to $\infty$. In order to obtain an approximate solution it is assumed that $w$ is zero over the whole surface, that

$$\frac{2B(s^2 - \eta^2)^{1/2}}{\eta^2} + C(2s^2 - 1) = -\frac{(s^2 - 1)^{1/2} F}{s^2} \quad \ldots [20]$$

and that the shear-stress distribution due to a horizontal disturbing force, $P_x e^{ipt}$ is

$$\tau_{zr} = \frac{P_x e^{ipt} \cos\theta}{2\pi r_0 (r_0^2 - r^2)^{1/2}} \text{ for } r \leq r_0, \quad \tau_{zr} = 0 \text{ for } r > r_0 \ldots [21]$$

$$\tau_{z\theta} = \frac{P_x e^{ipt} \sin\theta}{2\pi r_0 (r_0^2 - r^2)^{1/2}} \text{ for } r \leq r_0, \quad \tau_{z\theta} = 0 \text{ for } r > r_0 \ldots [22]$$

With these assumptions the components of displacement $u$, $v$ of a point on the surface of the medium $(r, \theta, 0)$ are

$$u = \mathrm{Re}\,\frac{P_x e^{ipt}\cos\theta}{2\pi\mu r_0}\int_0^\infty \left[\left\{\frac{s}{(s^2-\eta^2)^{1/2}} - \frac{(s^2-1)^{1/2}}{s}\right\} \frac{\partial}{\partial a} J_1(as) + \frac{1}{s(s^2-1)^{1/2}}\frac{J_1(as)}{a}\right] \sin a_0 s\, ds \quad \ldots\ldots [23]$$

$$v = \mathrm{Re}\,\frac{P_x e^{ipt}\sin\theta}{2\pi\mu r_0}\int_0^\infty \left[\left\{\frac{s}{(s^2-\eta^2)^{1/2}} - \frac{(s^2-1)^{1/2}}{s}\right\} \frac{J_1(as)}{a} + \frac{1}{s(s^2-1)^{1/2}}\frac{\partial}{\partial a} J_1(as)\right] \sin a_0 s\, ds \quad \ldots\ldots [24]$$

The average displacement of the plate $u_a$ in the direction of $P_x$ is obtained from

$$u_a = \int_0^{r_0}\int_0^{2\pi} \frac{r(u\cos\theta + v\sin\theta)}{2\pi r_0 (r_0^2 - r^2)^{1/2}}\, dr\, d\theta \quad \ldots\ldots [25]$$

Hence the displacement is

$$u_a = \mathrm{Re}\left[\frac{P_x e^{ipt}}{\mu r_0}\{f_{1a}(a_0, \nu) + i f_{2a}(a_0, \nu)\}\right] = \mathrm{Re}\left[\frac{P_x e^{ipt}}{4\pi\mu r_0}\int_0^\infty \left\{\frac{s^2 - (s^2-\eta^2)^{1/2}(s^2-1)^{1/2}}{(s^2-\eta^2)^{1/2}} + \frac{1}{(s^2-1)^{1/2}}\right\} \frac{\sin^2 a_0 s}{a_0 s}\, ds \quad \ldots\ldots [26]$$

Values of $f_{1a}$ and $f_{2a}$ are plotted against frequency factor $a_0$ for three values of Poisson's ratio in Fig. 3(*c*) and response curves are given in Fig. 4(*c*) for some values of $b$ with $\nu = 0$.

### Rocking Mode for Semi-Infinite Medium

For forced vibration the components of displacement and stress are found from Equations [4] and [5] by putting $n = 1$ and $F_n = 0$ and generalizing the expressions by integrating with respect to $s$ from 0 to $\infty$. The shear stresses are equated to zero over the whole surface and the following expression is assumed for the direct stress at $(r, \theta, 0)$ due to a disturbing torque $M_y e^{ipt}$

$$\sigma_z = \frac{3M_y e^{ipt} r\cos\theta}{2\pi r_0^3 (r_0^2 - r^2)^{1/2}} \quad \text{for } r \le r_0 \quad \ldots\ldots [27]$$
$$= 0 \text{ for } r > r_0$$

Hence the average angular displacement of the mass is

$$\phi_a = \mathrm{Re}\left[\frac{M_y e^{ipt}}{\mu r_0^3}\{f_{1a}(a_0, \nu) + i f_{2a}(a_0, \nu)\}\right] = \mathrm{Re}\left[\frac{9M_y e^{ipt}}{16\pi\mu r_0^3}\int_0^\infty \frac{(s^2-\eta^2)^{1/2}(\sin a_0 s - a_0 s\cos a_0 s)^2\, ds}{(a_0 s)^3\, G(s)} - \frac{9M_y e^{ipt} i(s_1^2-\eta^2)^{1/2}(\sin a_0 s_1 - a_0 s_1\cos a_0 s_1)^2}{16\mu r_0^3 (a_0 s_1)^3\, G'(s_1)}\right] \quad \ldots\ldots [28]$$

The functions $f_{1a}$ and $f_{2a}$ are plotted against frequency factor $a_0$ for $\nu = 0$ in Fig. 3(*d*) and response curves are given for some values of $b$ in Fig. 4(*d*).

### Stratum of Infinite Area on a Rigid Base

The Solutions [4] to the wave equations apply only to a semi-infinite medium. For the various modes of a mass on a stratum additional solutions are required; for $u_1$, $v_1$, and $w_1$ terms proportional to $e^{as+ipt}$ are added so that the components of displacement are proportional to hyperbolic functions dependent on $z$.

The general method of solution for a stratum is similar to that for the semi-infinite medium. To avoid difficulty, the static stress distributions used for the modes of the semi-infinite medium have also been used for the corresponding modes of the stratum. The error due to this assumption will increase as the depth of the stratum decreases.

The main results will now be given for the various modes.

(*a*) *Vertical Translation for Stratum.* Assuming that the stratum lies on a rigid infinite foundation and that no friction exists between stratum and foundation, the average displacement of the mass is

$$w_a = \mathrm{Re}\left[\frac{P_z e^{ipt}}{\mu r_0}\{f_{1a}(a_0, \nu, R) + i f_{2a}(a_0, \nu, R)\}\right] = \mathrm{Re}\left[\frac{P_z e^{ipt}}{8\pi\mu r_0}\int_0^\infty \frac{(s^2-\eta^2)^{1/2}\sin^2 a_0 s\, ds}{a_0 s\, l(s)} - \frac{P_z e^{ipt} i}{8\mu r_0}\sum \frac{\sin^2 a_0 s_n (s_n^2-\eta^2)^{1/2}}{a_0 s_n\, l'(s_n)}\right] \quad \ldots\ldots [29]$$

where $s_n$ are the real roots of $l(s) = 0$

$$l(s) = \left(s^2 - \frac{1}{2}\right)^2 \coth\alpha\delta - s^2(s^2-\eta^2)^{1/2}(s^2-1)^{1/2}\coth\beta\delta \text{ and } l'(s_n) = \left[\frac{dl(s)}{ds}\right]_{s=s_n}$$

This integral has not been evaluated but by considering its behavior in the range $0 < s < \epsilon_1$, where $\epsilon_1$ is a small quantity, the integral can be shown to diverge at certain frequencies given by

$$p = \frac{(2n-1)\pi}{2\delta}\left[\frac{E(1-\nu)}{\rho(1+\nu)(1-2\nu)}\right]^{1/2}, n = 1, 2, 3, \text{etc.} \quad \ldots\ldots [30]$$

Thus infinite amplitudes exist for a rigid plate of negligible mass at the natural frequencies of longitudinal vibration of a rod of length $\delta$, free at the top, fixed at the base, and laterally constrained.

If it is assumed that the stratum is fastened to the rigid foundation, it is found that the frequencies at which these infinite amplitudes occur are unchanged.

(*b*) *Torsional Mode for Stratum.* For forced vibration the tangential displacement at any point can be written in the form

$$v = \mathrm{Re}\, e^{ipt}\int_0^\infty [B\cos\{kz(1-s^2)^{1/2}\} + C\sin\{kz(1-s^2)^{1/2}\}]J_1(as)ds \quad \ldots [31]$$

Assuming that the stratum is fixed to the rigid foundation (i.e., $v = 0$ at $z = \delta$) and that the shear stress on the surface is given by Equation [18], the average dynamic rotation of the plate due to a disturbing torque $M_z e^{ipt}$ is

$$\left.\begin{aligned}\psi_a &= \mathrm{Re}\left[\frac{M_s e^{ipt}}{\mu r_0^3}\left\{f_{1a}(a_0, R) + if_{2a}(a_0, R)\right\}\right] \\ &= \mathrm{Re}\,\frac{9M_s e^{ipt}}{8\pi\mu r_0^3}\int_0^\infty \left[\frac{(\sin a_0 s - a_0 s\cos a_0 s)^2 \tan\left\{a_0 R(1-s^2)^{1/2}\right\}}{(a_0 s)^3(1-s^2)^{1/2}}\right] ds - \sum_{n=1}^{n=N} \frac{9M_s e^{ipt} i(\sin a_0 s_n - a_0 s_n \cos a_0 s_n)^2}{8\mu r_0^3 R(a_0 s_n)^4}\end{aligned}\right\} \quad [32]$$

where $s_n$ is one of the real roots of

$$a_0 s_n = \left[a_0^2 - \frac{(2n-1)^2\pi^2}{4R^2}\right]^{1/2},\ n = 1, 2, 3 \ldots, N.$$

The lower limit for the rotation is

$$\left.\begin{aligned}\psi_p &= \mathrm{Re}\left[\frac{M_s e^{ipt}}{\mu r_0^3}\left\{f_{1p}(a_0, R) + if_{2p}(a_0, R)\right\}\right] \\ &= \mathrm{Re}\,\frac{3M_s e^{ipt}}{4\pi\mu r_0^3}\int_0^\infty \left[\frac{(\sin a_0 s - a_0 s\cos a_0 s)J_1(a_0 s)\tan\left\{a_0 R(1-s^2)^{1/2}\right\}}{a_0 s(1-s^2)^{1/2}}\right] ds \\ &\quad - \sum_{n=1}^{n=N} \frac{3M_s e^{ipt} i(\sin a_0 s_n - a_0 s_n \cos a_0 s_n)J_1(a_0 s_n)}{4\mu r_0^3 R(a_0 s_n)^2}\end{aligned}\right\} \quad [33]$$

Inspection by contour integration of Equations [32] and [33] shows that in each case the integral gives $f_1$ and the terms in the summation give $f_2$. Thus $f_2$ will be zero up to a critical value of frequency given by $a_0 = \pi/2R$, as there is no real root $s_n$ below this value; this frequency can be expressed as

$$p = \frac{\pi}{2\delta}\left(\frac{\mu}{\rho}\right)^{1/2}$$

which is the fundamental frequency of torsional vibration of a rod of the material of the stratum, of length $\delta$, free at one end and fixed at the other.

As the integrals of Equations [32] and [33] do not diverge, infinite amplitudes do not exist for this mode when the plate has negligible mass. In Fig. 5 the functions $f_1$ and $f_2$ have been plotted against frequency factor for three values of $R$.

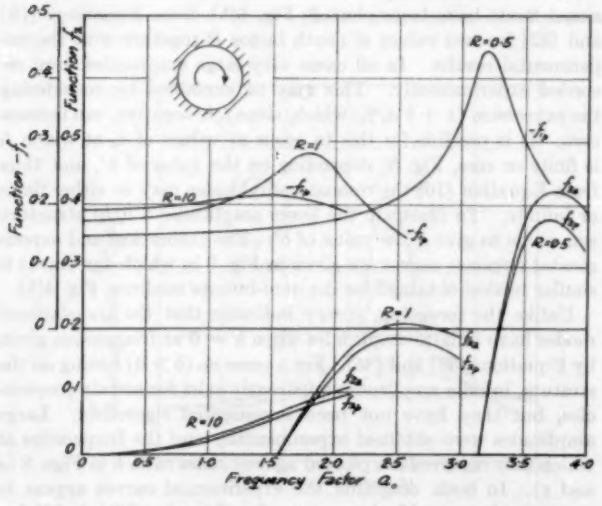


FIG. 5 FUNCTIONS $f_1$ AND $f_2$ FOR AN INFINITE STRATUM

(*c*) *Horizontal Translation for Stratum.* For forced vibration the expression for the dynamic displacement at a point on the surface of the stratum contains terms of the form

$$\int_0^\infty \frac{\sin a_0 s \tanh\left[k\delta(s^2-1)^{1/2}\right]J_1(as)}{as\,(s^2-1)^{1/2}}\,ds \quad [34]$$

This integral diverges at frequencies given by

$$p = \frac{(2n-1)\pi}{2\delta}\left(\frac{\mu}{\rho}\right)^{1/2},\quad n = 1, 2, 3, \text{ etc.} \quad [35]$$

These are the natural frequencies of a rod of the medium of length $\delta$, free at the top, fixed at the base, when vibrating horizontally in shear.

(*d*) *Rocking Mode for Stratum.* The integral giving the dynamic displacement is similar in form to Equation [29] with $[(1/a_0 s)\sin a_0 s - \cos a_0 s]^2$ replacing $\sin^2 a_0 s$, but it can be shown that it is not divergent for any value of stratum depth. Thus infinite amplitudes do not occur for this mode when the plate has negligible mass.

## EXPERIMENTAL INVESTIGATIONS

(*a*) *Elastic Medium.* In geometrically similar systems with the same density ratios of mass to medium, $b$ remains constant, and for the terms within the square root (Equation [15]) to be identical, functions $f_1$ and $f_2$ must be the same for both systems. Since these are functions of $a_0$ and $\nu$, two systems of different materials having the same Poisson's ratio will behave in a similar manner, when the disturbing frequencies have the relation

$$\frac{p_1}{p_2} = \frac{r_{02}}{r_{01}}\left(\frac{\rho_2\mu_1}{\rho_1\mu_2}\right)^{1/2} \quad [36]$$

Provided a medium can be obtained with the required value of $\nu$ it is thus possible to find $f_1$ and $f_2$ by experiment.

Theoretically the elastic model should have an infinite area, but a finite model can be used provided reflections from the edges are eliminated. Twelve sheets of foam rubber, 3 ft square and each approximately 1 in. thick, were sufficient to represent the semi-infinite medium, as the damping in the rubber eliminated random reflections but was small enough to allow the experimental results to be compared with those for the theoretical undamped medium. Disks of base radius 0.375 to 2.25 in. were attached to the surface of the rubber. Two varieties of foam rubber were used, one for the stratum and the other for the semi-infinite case. The physical constants of these are given in Table 1.

TABLE 1 PHYSICAL CONSTANTS FOR FOAM RUBBER

| | $E$, psi | $\mu$, psi | $\nu$ | $\rho$, pci |
|---|---|---|---|---|
| Stratum case | 9.96 | 4.98 | ≈0 | 0.00505 |
| Semi-infinite case | 17.3 | 8.65 | ≈0 | 0.00520 |

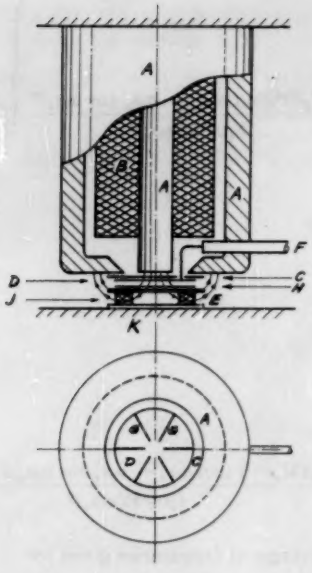


A, Steel magnetic circuit
B, Direct-current field coil
C, Bakelite insulating washer
D, Copper pickup plate
E, Direct-current field
F, Cable to pickup plate
G, Slots to minimize eddy currents
H, Earthed pickup plate
J, Exciting coil
K, Foam rubber

FIG. 6 DETAILS OF EXCITING AND PICKUP ASSEMBLY

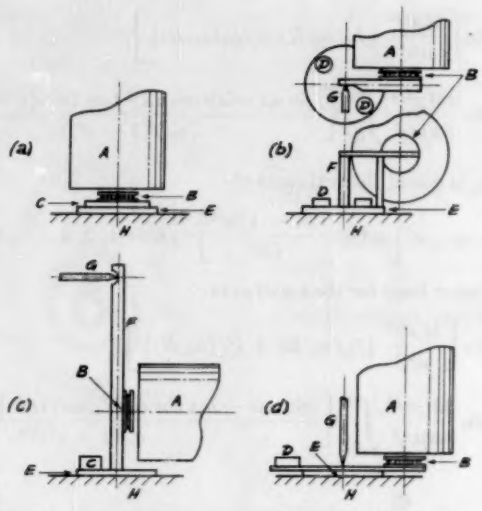


A, Field and pickup plate
B, Exciting coil
C, Additional mass
D, Additional inertia
E, Base of radius $r_0$
F, Fiber structure
G, Knife-edge
H, Foam rubber

FIG. 7 EXPERIMENTAL ARRANGEMENTS FOR EXCITING THE MODES OF VIBRATION

(*b*) *Measuring Equipment.* Applied force, frequency of excitation, and vibration amplitude of the mass were measured. The force was produced by the interaction of a d-c electromagnet *A*, Fig. 6, and a small coil *J*, which formed part of the mass and through which an alternating current was passed. Displacements were measured by change of capacitance; in order to record force and amplitude at the same location, the magnetic exciter and capacity pickup (*D*, *H*) were located in the same head. Provided the gap between the plates *D* and *H* was large compared with the movement, the response was linear.

Fig. 7 illustrates the methods adopted to insure the correct displacement of the mass in the four modes of vibration, the same magnetic and pickup head being used for all modes. Thus in Fig. 7(*a*) the mass $m_0$ consists of a small bakelite disk *E*, which was sufficiently thick to be considered rigid, the thin brass disk *C* and the exciting coil *B*. In the other modes the required force or couple was obtained by means of knife-edges *G*, Figs. 7 (*b*), (*c*), and (*d*).

## COMPARISON OF THEORETICAL AND EXPERIMENTAL RESULTS

(*a*) *Semi-Infinite Medium.* The experimental points, Fig. 4, have been added to the theoretical amplitude-frequency curves for the four modes. For the translational modes (*a*) and (*c*) there is close agreement between the theoretical and experimental results, but for the rotational modes the experimental points lie below the theoretical curves, especially at frequencies close to resonance. From Equation [15] and the form of functions $f_1$ and $f_2$, Fig. 3, it can be seen that the amplitude has a maximum close to the value of $a_0$ that makes $(1 + ba_0^3 f_1)$ equal to zero. Moreover, this maximum amplitude is approximately proportional to $1/f_2$. The function $f_2$ is a measure of the rate at which energy is dissipated and for the theoretical undamped medium all energy is propagated outward. However, in the experimental system additional energy is lost because of damping within the medium. Now it can be shown that the predominant effect of introducing damping into the analysis is to provide a small increase in $f_2$; thus the experimental damping will affect the rotational modes more than the translational modes, because smaller values of $f_2$ are, in general, associated with the former.

Comparison of Equation [15] with Fig. 3 also shows that as $b$ (or $b'$) increases the resonant amplitudes increase and occur at decreasing values of $a_0$, as shown for each mode in Fig. 4. The theoretical response curves for $b = 0$ (corresponding to a rigid plate of negligible mass) show a drooping characteristic for all modes.

(*b*) *Stratum on a Rigid Base.* Theoretical curves for the torsional mode have been plotted, Fig. 8(*b*), from Equations [15] and [32] for two values of depth factor $R$ together with the experimental results. In all cases very large amplitudes were recorded experimentally. This may be explained by considering the expression $(1 + b'a_0^3 f_1)$ which, since $f_1$ is negative, can become zero. It is possible for this to occur at values of $a_0$ at which $f_2$ is finite or zero, Fig. 5, depending on the value of $b'$, and thus from Equation [16] the resonant amplitudes may be either finite or infinite. To illustrate the lower amplitudes a light structure was made to give a low value of $b'$. The theoretical and experimental response curves are given in Fig. 9 in which agreement is similar to that obtained for the semi-infinite medium, Fig. 4(*b*).

Unlike the foregoing, theory indicates that the translational modes have infinite amplitudes when $b = 0$ at frequencies given by Equations [30] and [35]. For a mass $m_0$ ($b > 0$) resting on the stratum, infinite amplitudes apparently exist for certain frequencies, but they have not been investigated rigorously. Large amplitudes were obtained experimentally and the frequencies at which they occurred are plotted against mass ratio $b$ in Figs. 8 (*a* and *c*). In both diagrams the experimental curves appear to converge to a specific frequency when $b = 0$. In (*a*) this frequency is approximately 220 cycles per sec (cps). Theoretically the fundamental frequency for $b = 0$ and $\delta = 1.05$ in. is 207 cps from Equation [30]. In (*c*) the corresponding experimental frequency is approximately 155 cps which may be compared with the theoretical value of 146 cps obtained from Equation [35].

In Fig. 8(*d*) experimental response curves are given for three values of $b'$ for the rocking mode. Analytically this mode

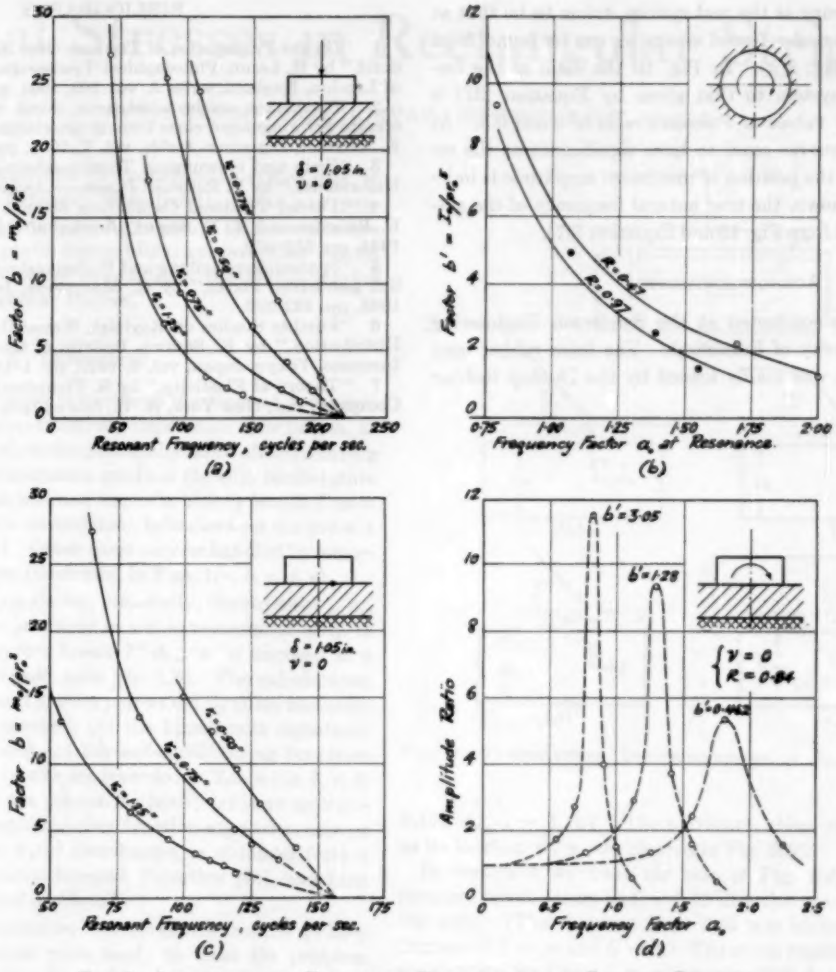


FIG. 8 AMPLITUDE AND FREQUENCY RESPONSE FOR AN INFINITE STRATUM

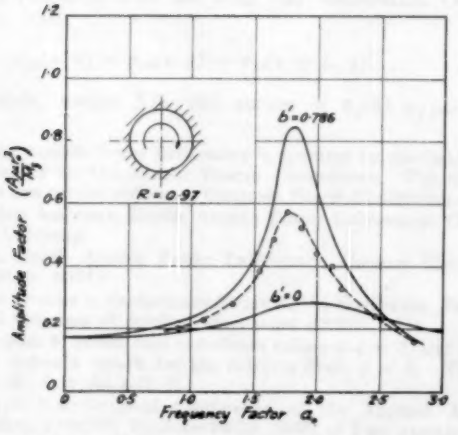


FIG. 9 AMPLITUDE-FREQUENCY RESPONSE FOR AN INFINITE STRATUM

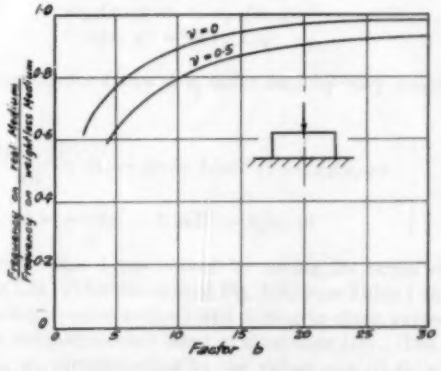


FIG. 10 COMPARISON OF FREQUENCY OF MASS ON A REAL MEDIUM WITH THAT ON A WEIGHTLESS MEDIUM

behaves in a manner similar to that of torsion. This is shown by the decrease in maximum amplitude as $b'$ decreases.

### RELATION TO SIMPLE SPRING-MASS SYSTEM

When a vertical static load is applied through a rigid base of radius $r_0$ to a semi-infinite medium, the static stiffness of the system is $(2r_0E)/(1 - \nu^2)$. If the mass of the medium is neglected, the natural frequency of the resulting simple spring-mass system is

$$\frac{1}{2\pi}\left[\frac{2r_0E}{(1-\nu^2)m_0}\right]^{1/2} \quad \ldots\ldots\ldots\ldots\ldots\ldots [37]$$

The natural frequency of the real system, taken to be that at maximum amplitude under forced vibration, can be found from Equation [15] and Fig. 3(*a*). In Fig. 10 the ratio of the frequency of the real system to that given by Equation [37] is plotted against $b$ for values of Poisson's ratio of 0 and 0.5. At low values of $b$ the curves cease to have significance as the response is so flat that the position of maximum amplitude is indeterminate. If $\nu$ is known, the true natural frequency of the system can be computed from Fig. 10 and Equation [37].

## Acknowledgments

This research was conducted at the Sanderson Engineering Laboratories, University of Edinburgh. The foam rubber used in the investigations was kindly loaned by the Dunlop Rubber Company.

## BIBLIOGRAPHY

1 "On the Propagation of Tremors Over the Surface of an Elastic Solid," by H. Lamb, Philosophical Transactions of the Royal Society of London, England, series A, vol. 203, 1904, pp. 1–42.

2 "Stationäre, axialsymmetrische, durch eine schüttelnde Masse erregte Schwingungen eines homogenen elastischen Halbraumes," by E. Reissner, *Ingenieur-Archiv*, vol. 7, 1936, pp. 381–396.

3 "Freie und erzwungene Torsionsschwingungen des elastischen Halbraumes," by E. Reissner, *Ingenieur-Archiv*, vol. 8, 1937, p. 229.

4 "Forced Torsional Oscillations of an Elastic Half-Space," by E. Reissner and H. F. Sagoci, *Journal of Applied Physics*, vol. 15, 1944, pp. 652–662.

5 "Spannungsverteilung und Wellenausbreitung in der kontinuierlich gestützten Platte," by K. Marguerre, *Ingenieur-Archiv*, vol. 4, 1933, pp. 332–353.

6 "Further Studies on Rayleigh Waves Having Some Azimuthal Distribution," by K. Sezawa, Bulletin of the Earthquake Research Institute, Tokyo, Japan, vol. 6, 1929, pp. 1–18.

7 "Theory of Elasticity," by S. Timoshenko, McGraw-Hill Book Company, Inc., New York, N. Y., first edition, 1934, p. 338.

# Thermal Stresses in Rectangular Strips—II[1]

By J. S. BORN[2] and G. HORVAY,[3] SCHENECTADY, N. Y.

**Stresses and deformations in rectangular strips due to various longitudinal temperature distributions are presented in formulas, tables, and graphs. The results are important for slabs, plate assemblies, rectangular ducts, tube-sheet ligaments; they apply, in a more qualitative fashion, also to cylindrical bodies.**

## 1 Discussion

THE purpose of the paper is to extend the theory,[4] developed for the (vertical) step-function temperature distribution, illustrated in Fig. 1(*a*), to the practically more often recurring cases of a break in the temperature gradient (briefly, temperature break) as in Fig. 1(*b*), an inclined step of arbitrary length $L$ as in Fig. 1(*c*) (idealized by the dashed line), behavior near the end of a strip as in Figs. 1(*d* and *e*). Other cases may be handled by superpositions of the basic cases illustrated in Figs. 1(*a, b, c, d, e*).

In Figs. 2(*a, b, c, d, e*) are shown, pictorially, the stresses $\sigma_x$, $\sigma_y$, $\tau$ and displacements, $u$, $v$ produced in a thin rectangular strip of width $2b$ when a temperature break $T'$ deg/in. is imposed at a cross section far from the ends, as in Fig. 1(*b*). The calculations, carried out in Sections 2 and 3, were performed by three methods: (*a*) the Fourier integral method, (*b*) the biharmonic eigenfunction-expansion method, and (*c*) the self-equilibrating function-expansion method. The results are recorded in Table 1(*a, b, c, d, e*). Methods (*a*) and (*b*) are precise methods; (*c*) is an approximate method. The self-equilibrating function expansion uses as starting point the precise $\delta_x(y)$ distribution as obtained from a numerically evaluated Fourier integral, Equation [9*a*], and then solves the problem as an end problem.[5]

In Section 4 we superimpose the foregoing results (where available, the precise values were used) to treat the problem of the inclined-step, Fig. 1(*c*), for various lengths, $L$, of the step. For instance, if subscript $b$ refers to the Fig. 1(*b*) temperature distribution, subscript $c$ to the Fig. 1(*c*) distribution (with $T/L = T'$), then

$$\sigma_{xc}(x, y) = \sigma_{xb}(x, y) - \sigma_{xb}(x + L, y) \quad \ldots\ldots [1]$$

Fig. 3(*a*) plots, versus $L/b$, the curves of $\delta_x(0)$, $\sigma_{x\,max} = \delta_x(b)$, $\sigma_{y\,max} = \delta_y(0)$. The maximum shear stress $\tau_{max}$ as well as its location $x_\tau$, $y_\tau$ are plotted in Fig. 3(*b*).

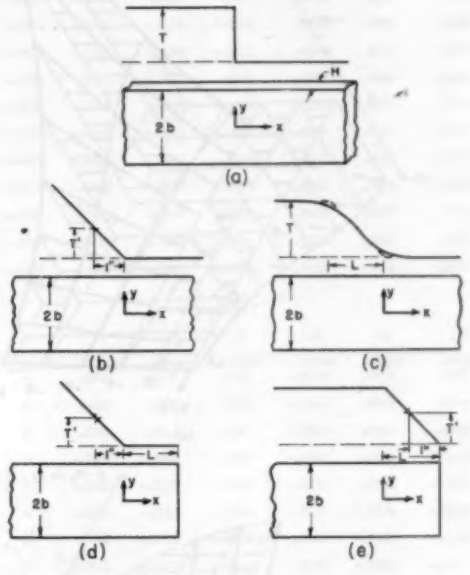


Fig. 1 Temperature Discontinuities in Rectangular Strip

In Section 5 we treat the case of Fig. 1(*d*), where a temperature break occurs at $L = 0.4b$ distance away from an end of the strip. (The distance $L = 0.4b$ was chosen as a judicious average of $L = \infty$ and $L = 0$.) The stress results, except for sign, are identical for Cases *d*, *e*; using subscripts *d*, *e*, we may write

$$\left.\begin{aligned} \sigma_{x.e}(x, y) &= -\sigma_{x.d}(x, y) \\ \sigma_{y.e}(x, y) &= -\sigma_{y.d}(x, y) \\ \tau_e(x, y) &= -\tau_d(x, y) \end{aligned}\right\} \quad \ldots\ldots [2a]$$

The displacements for Cases *d*, *e*, differ only by very simple expressions

$$\left.\begin{aligned} u_e(x, y) &= \frac{3y^2 - b^2}{6b}\,[1 - (x - L)\alpha T']^2 - u_d(x, y) \\ v_e(x, y) &= -y(x - L)\alpha T' - v_d(x, y) \end{aligned}\right\} \quad \ldots [2b]$$

The problem of Case *d* was solved by taking the stress values $\sigma_x(0.4b, y)$, $\tau(0.4b, y)$ for the case of Fig. 1(*b*) from Table 1 (in the self-equilibrating approximation) and fitting to these values, by least squares, the polynomials listed in Equations [18]. The Airy functions $\varphi_\sigma$, $\varphi_\tau$ corresponding to the values $-\sigma_x(0.4b, y)$, $-\tau(0.4b, y)$ are next expanded into self-equilibrating functions in Equations [20]. Superposition of the effect of the compensating edge stresses $\widehat{\varphi}_{\sigma,yy}$, $\widehat{\varphi}_{\tau,xy}$ on the Fig. 1(*b*) stress condition eliminates the unwanted stresses along edge $x = L$ and leads to Fig. 4. (The arc above $\varphi$ is used to refer to the boundary values at the right edge.) One finds that the largest stress for Case *d*, $L/b = 0.4$, is

$$\sigma_{x\,max} = \sigma_x(-0.03b, b) = -0.234S \quad \ldots\ldots [3a]$$

$$S = E\alpha T'b \quad \ldots\ldots [3b]$$

---

[1] The Knolls Atomic Power Laboratory is operated by the General Electric Company for the Atomic Energy Commission. The work reported here was carried out under Contract No. W-31-109 Eng.-52.

[2] Engineering Assistant, Knolls Atomic Power Laboratory, General Electric Company.

[3] Engineer, Knolls Atomic Power Laboratory, General Electric Company. Mem. ASME.

[4] "Thermal Stresses in Rectangular Strips, I," by G. Horvay, Proc. 2nd National Congress of Applied Mechanics, ASME, 1954.

[5] As in reference 4, we use bars to indicate values at $x = 0$, and the circumflex to indicate values for the extreme fiber, $y = b$. Thus $\bar{\sigma}_x(y) \equiv \sigma_x(0, y)$, $\hat{\sigma}_x(x) \equiv \sigma_x(x, b)$.

Presented at the National Conference of the Applied Mechanics Division, Troy, N. Y., June 16–18, 1955, of The American Society of Mechanical Engineers.

Discussion of this paper should be addressed to the Secretary, ASME, 29 West 39th Street, New York, N. Y., and will be accepted until October 10, 1955, for publication at a later date. Discussion received after the closing date will be returned.

Note: Statements and opinions advanced in papers are to be understood as individual expressions of their authors and not those of the Society. Manuscript received by ASME Applied Mechanics Division, May 7, 1954. Paper No. 55—APM-4.

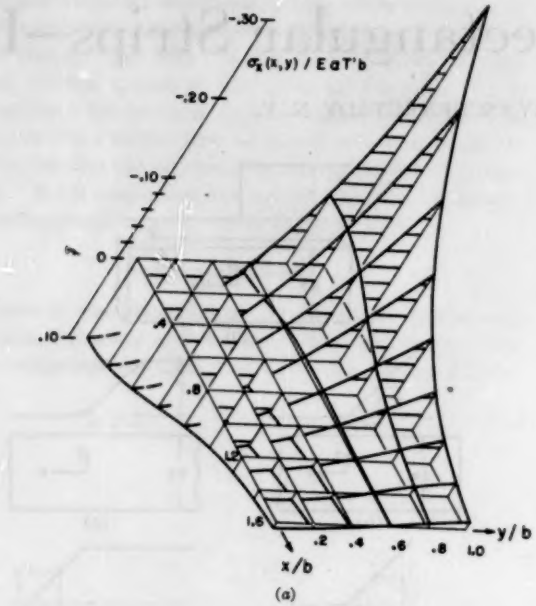


(a)

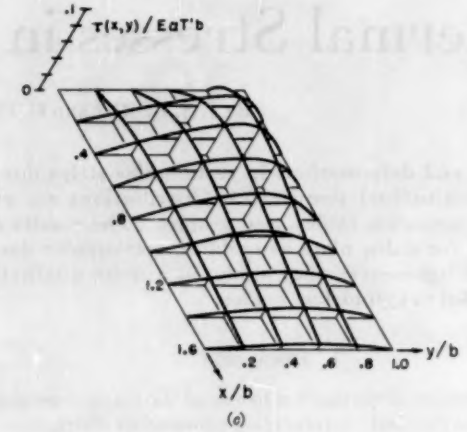


(c)

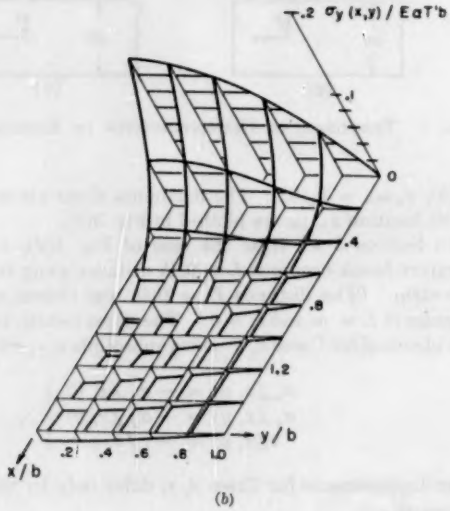


(b)

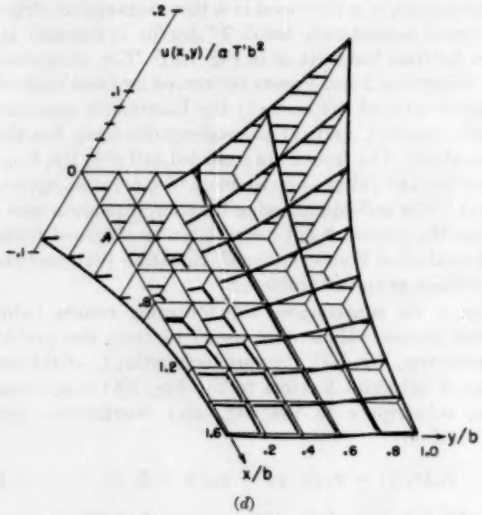


(d)

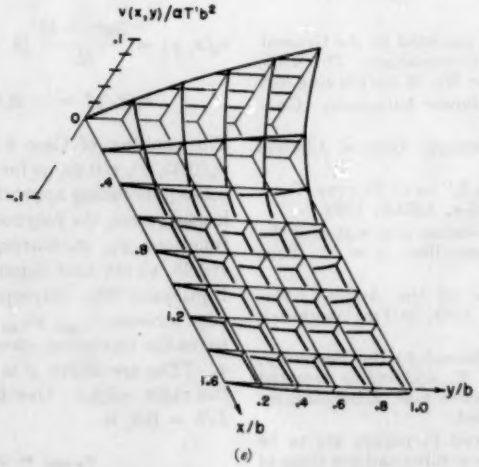


(e)

FIG. 2 STRESSES AND DISPLACEMENTS IN RECTANGULAR STRIP CAUSED BY BREAK IN TEMPERATURE GRADIENT FAR FROM THE ENDS

TABLE 1 STRESSES AND DEFORMATIONS DUE TO A TEMPERATURE BREAK

(a) $\sigma_x/E\alpha T'b$

| x/b \ y/b | 0 | .2 | .4 | .6 | .8 | .9 | .95 | 1.0 |
|---|---|---|---|---|---|---|---|---|
| 0 | .0980* | .0895 * | .0621* | .0096* | -.0860* | -.1670* | -.2265 * | -.3277* |
| 0 | .1029# | .0814# | .0566# | .0015# | -.0766# | -.1637# | -.2343# | -.3208# |
| 0 | .0967 | .0906 | .0638 | .0068 | -.0843 | -.1649 | -.2291 | -.3213 |
| .1 | | | | | | | | -.2808* |
| .1 | .0961 | .0888 | .0617 | .0065 | -.0858 | -.1632 | -.2197 | -.2958 |
| .2 | | | | | | | | -.2375* |
| .2 | .0927 | .0845 | .0572 | .0044 | -.0850 | -.1583 | -.1999 | -.2561 |
| .4 | | | | | | | | -.1661* |
| .4 | .0805# | .0720# | .0451# | -.0036# | -.0776# | -.1222# | -.1444# | -.1660# |
| .4 | .0798 | .0707 | .0454 | -.0004 | -.0734 | -.1237 | -.1533 | -.1864 |
| .6 | .0608 | .0540 | .0334 | -.0026 | -.0565 | -.0912 | -.1108 | -.1320 |
| .8 | .0471# | .0408# | .0217# | -.0083# | -.0435 # | -.0597# | -.0665 # | -.0723# |
| .8 | .0435 | .0385 | .0232 | -.0028 | -.0402 | -.0636 | -.0765 | -.0903 |
| 1.0 | .0292 | .0258 | .0154 | -.0022 | -.0270 | -.0422 | -.0505 | -.0593 |
| 1.2 | .0186 | .0163 | .0097 | -.0015 | -.0171 | -.0266 | -.0318 | -.0372 |
| 1.4 | .0111 | .0098 | .0058 | -.0009 | -.0102 | -.0158 | -.0189 | -.0221 |
| 1.6 | .0080# | .0065 # | .0025 # | -.0027# | -.0066# | -.0071# | -.0073# | -.0069# |
| 1.6 | .0062 | .0054 | .0032 | -.0005 | -.0057 | -.0088 | -.0105 | -.0123 |
| 1.8 | .0031 | .0027 | .0016 | -.0002 | -.0028 | -.0044 | -.0052 | -.0061 |
| 2.0 | .0013 | .0011 | .0007 | -.0001 | -.0012 | -.0018 | -.0022 | -.0026 |

(b) $\sigma_y/E\alpha T'b$

| x/b \ y/b | 0 | .2 | .4 | .6 | .8 | .9 | .95 | 1.0 |
|---|---|---|---|---|---|---|---|---|
| 0 | .1105* | .1355* | .1203* | .0939* | .0547* | .0295 * | .0153* | 0* |
| 0 | .1379 | .1376 | .1217 | .0859 | .0494 | .0287 | .0079 | 0 |
| .1 | .0965 | .0905 | .0743 | .0492 | .0175 | .0048 | .0012 | 0 |
| .2 | .0597 | .0546 | .0416 | .0239 | .0054 | .0004 | -.0001 | 0 |
| .4 | .0095 | .0077 | .0033 | -.0010 | -.0022 | -.0011 | -.0004 | 0 |
| .6 | -.0154 | -.0149 | -.0131 | -.0094 | -.0038 | -.0012 | -.0003 | 0 |
| .8 | -.0242 | -.0226 | -.0181 | -.0113 | -.0039 | -.0011 | -.0003 | 0 |
| 1.0 | -.0244 | -.0226 | -.0176 | -.0105 | -.0034 | -.0010 | -.0003 | 0 |
| 1.2 | -.0208 | -.0192 | -.0148 | -.0087 | -.0028 | -.0008 | -.0002 | 0 |
| 1.4 | -.0160 | -.0148 | -.0113 | -.0066 | -.0021 | -.0006 | -.0002 | 0 |
| 1.6 | -.0116 | -.0106 | -.0082 | -.0047 | -.0015 | -.0004 | -.0001 | 0 |
| 1.8 | -.0079 | -.0073 | -.0056 | -.0032 | -.0010 | -.0003 | -.0001 | 0 |
| 2.0 | -.0052 | -.0047 | -.0036 | -.0021 | -.0007 | -.0002 | -.0000 | 0 |

(c) $\tau/E\alpha T'b$

| x/b \ y/b | 0 | .2 | .4 | .6 | .8 | .9 | .95 | 1.0 |
|---|---|---|---|---|---|---|---|---|
| 0 | 0 | 0 | 0 | 0 | 0 | 0 | 0 | 0 |
| .1 | 0 | .0147 | .0120 | .0169 | .0190 | .0181 | .0131 | 0 |
| .2 | 0 | .0101 | .0211 | .0292 | .0300 | .0234 | .0150 | 0 |
| .4 | 0 | .0167 | .0312 | .0399 | .0352 | .0232 | .0133 | 0 |
| .6 | 0 | .0177 | .0319 | .0385 | .0312 | .0194 | .0108 | 0 |
| .8 | 0 | .0154 | .0274 | .0320 | .0249 | .0151 | .0082 | 0 |
| 1.0 | 0 | .0120 | .0211 | .0244 | .0185 | .0111 | .0060 | 0 |
| 1.2 | 0 | .0086 | .0151 | .0174 | .0131 | .0078 | .0042 | 0 |
| 1.4 | 0 | .0058 | .0102 | .0117 | .0088 | .0052 | .0028 | 0 |
| 1.6 | 0 | .0037 | .0065 | .0075 | .0056 | .0033 | .0018 | 0 |
| 1.8 | 0 | .0023 | .0039 | .0045 | .0034 | .0020 | .0011 | 0 |
| 2.0 | 0 | .0013 | .0022 | .0025 | .0019 | .0011 | .0006 | 0 |

(d) $u/b^2\alpha T'$

| x/b \ y/b | 0 | .2 | .4 | .6 | .8 | .9 | .95 | 1.0 |
|---|---|---|---|---|---|---|---|---|
| 0 | -.0833* | -.0733* | -.0633* | .0067* | .0767* | .1192* | .1429* | .1667* |
| 0 | -.0784 | -.0705 | -.0653 | .0006 | .0720 | .1225 | .1542 | .1920 |
| .1 | -.0723 | -.0649 | -.0619 | -.0007 | .0626 | .1057 | .1315 | .1609 |
| .2 | -.0651 | -.0584 | -.0376 | -.0012 | .0537 | .0897 | .1105 | .1333 |
| .4 | -.0498 | -.0445 | -.0285 | -.0014 | .0376 | .0618 | .0752 | .0893 |
| .6 | -.0355 | -.0317 | -.0203 | -.0014 | .0248 | .0405 | .0489 | .0577 |
| .8 | -.0239 | -.0213 | -.0137 | -.0013 | .0154 | .0251 | .0303 | .0357 |
| 1.0 | -.0152 | -.0135 | -.0088 | -.0012 | .0089 | .0147 | .0178 | .0209 |
| 1.2 | -.0091 | -.0081 | -.0053 | -.0009 | .0048 | .0080 | .0097 | .0114 |
| 1.4 | -.0051 | -.0045 | -.0030 | -.0007 | .0022 | .0039 | .0047 | .0055 |
| 1.6 | -.0025 | -.0023 | -.0016 | -.0005 | .0008 | .0015 | .0018 | .0022 |
| 1.8 | -.0011 | -.0010 | -.0007 | -.0003 | .0001 | .0002 | .0003 | .0004 |
| 2.0 | -.0003 | -.0003 | -.0002 | -.0002 | -.0003 | -.0004 | -.0004 | -.0005 |

(e) $w/b^2\alpha T'$

| x/b \ y/b | 0 | .2 | .4 | .6 | .8 | .9 | .95 | 1.0 |
|---|---|---|---|---|---|---|---|---|
| 0 | 0* | .0280* | .0431* | .0522* | .0789* | .0866* | .0908* | .0960* |
| 0 | 0 | .0219 | .0435 | .0621 | .0778 | .0852 | .0888 | .0931 |
| .1 | 0 | .0133 | .0253 | .0356 | .0444 | .0491 | .0521 | .0559 |
| .2 | 0 | .0062 | .0115 | .0162 | .0212 | .0250 | .0276 | .0310 |
| .4 | 0 | -.0028 | -.0052 | -.0065 | -.0068 | -.0071 | -.0080 | .0085 |
| .6 | 0 | -.0066 | -.0121 | -.0154 | -.0150 | -.0131 | -.0116 | -.0098 |
| .8 | 0 | -.0072 | -.0133 | -.0169 | -.0172 | -.0159 | -.0149 | -.0136 |
| 1.0 | 0 | -.0064 | -.0118 | -.0150 | -.0156 | -.0147 | -.0141 | -.0133 |
| 1.2 | 0 | -.0051 | -.0093 | -.0120 | -.0126 | -.0121 | -.0117 | -.0111 |
| 1.4 | 0 | -.0038 | -.0069 | -.0088 | -.0094 | -.0091 | -.0089 | -.0086 |
| 1.6 | 0 | -.0026 | -.0048 | -.0062 | -.0066 | -.0065 | -.0063 | -.0062 |
| 1.8 | 0 | -.0017 | -.0031 | -.0041 | -.0044 | -.0043 | -.0043 | -.0042 |
| 2.0 | 0 | -.0011 | -.0020 | -.0025 | -.0028 | -.0028 | -.0027 | -.0027 |

NOTE: Star denotes value obtained by numerical evaluation of Fourier integral; sign # denotes value obtained by four-term biharmonic eigenfunction expansion; unmarked values refer to results obtained by four-term self-equilibrating function expansion.

as compared with

$$\sigma_{x\,\max} = \sigma_x(0, b) = -0.328S \quad \ldots\ldots\ldots\ldots [3c]$$

for Case *b*. It is somewhat surprising to see that the nearness of the temperature break to the free edge does not effect a greater than 30 per cent reduction in the maximum stress. When $L/b \to 0$ all stresses become zero.

The foregoing results apply to the conditions of plane stress (the strip is very thin; its thickness $H \ll b$). For the case of plane strain ($H \gg b$, subscript II) the stress values are obtained in terms of the former ones (subscript I) by the formulas

$$\sigma_{II} = \frac{\sigma_I}{1-\mu}, \quad \tau_{II} = \frac{\tau_I}{1-\mu} \quad \ldots\ldots\ldots\ldots [4a]$$

i.e., simply by multiplying the results of Tables 1(*a*, *b*, *c*) by

$$k = 1/(1-\mu) = 1.43 \qquad (\text{for } \mu = 0.3)$$

The conversion of the displacements is somewhat more complicated. As well known, the displacements $u_I$, $v_I$ should first be recalculated for an effective Poisson ratio of

$$\nu = \frac{\mu}{1-\mu} = 0.43$$

and then must be multiplied by $1 + \mu$ to give $u_{II}$, $v_{II}$. If we ignore the slight change that arises in the displacements $u_I$, $v_I$ through a change of the Poisson ratio from 0.3 to 0.43 (compare in this respect Figs. 5 and 6 of footnote 6 which deals with a somewhat similar situation[7]), then we may use the simpler, though not quite accurate, formulas

$$u_{II} = (1+\mu)u_I, \; v_{II} = (1+\mu)v_I \quad \ldots\ldots\ldots [4b]$$

[6] "Transient Thermal Stresses in Circular Disks and Cylinders," by G. Horvay, Trans. ASME, vol. 76, 1954, pp. 127–135.

[7] Note the misprint in Equation [39] of footnote 6. Instead of $(k + 33)$ write $(k + 3)$.

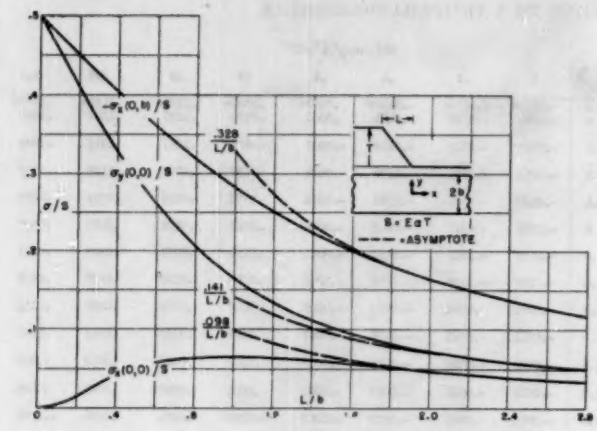


(a)

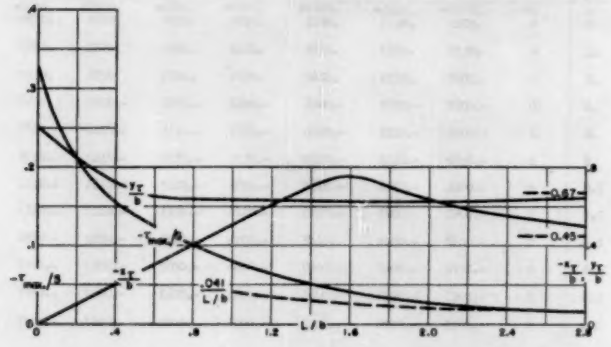


(b)

FIG. 3 STRESSES IN RECTANGULAR STRIP DUE TO INCLINED TEMPERATURE STEP

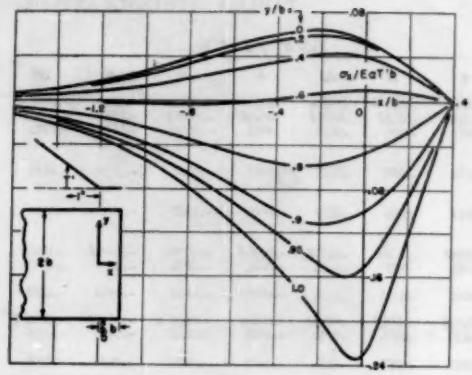


(a)

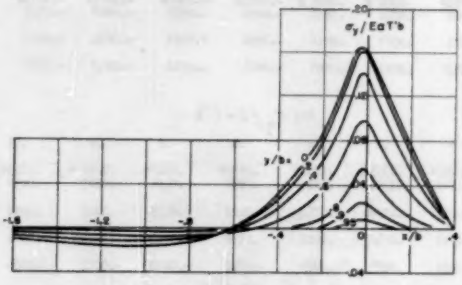


(b)

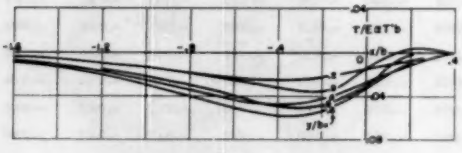


(c)

FIG. 4 STRESSES IN RECTANGULAR STRIP WHEN TEMPERATURE BREAK OCCURS NEAR FREE END

The paper is concluded by an Appendix which provides convenient formulas for least-square approximation of even and odd functions.

## 2 THE FOURIER INTEGRAL EXPRESSIONS OF STRESSES AND DEFORMATIONS CORRESPONDING TO A TEMPERATURE BREAK

The stresses and deformations for a step-function temperature distribution were given for $x \geq 0$ in [I.5].[8] We now apply the superposition principle: If the effect of the temperature step $T = -1$, applied at $x = 0$, is $F(x)$ at location $x$, then the effect of the gradient $-T'$ deg per in. (terminating at $x = 0$) is

$$G(x) = T' \int_x^\infty F(x)dx \quad \ldots\ldots [5]$$

By integrating the Expressions [I.5] in the foregoing fashion we arrive at the results for the temperature break $T'$

$$\left.\begin{aligned}
\sigma_x(x, y)/E\alpha T' &= \frac{2}{\pi}\int_0^\infty [(A + 2B)\cosh \lambda y + B\lambda y \sinh \lambda y]\frac{\cos \lambda x}{\lambda^2}\,d\lambda \\
\sigma_y(x, y)/E\alpha T' &= \frac{2}{\pi}\int_0^\infty \left[\frac{1}{2} - A\cosh \lambda y - B\lambda y \sinh \lambda y\right]\frac{\cos \lambda x}{\lambda^2}\,d\lambda \\
\tau(x, y)/E\alpha T' &= \frac{2}{\pi}\int_0^\infty [(A + B)\sinh \lambda y + B\lambda y \cosh \lambda y]\frac{\sin \lambda x}{\lambda^2}\,d\lambda \\
u(x, y)/\alpha T' &= \frac{3y^2 - 1}{12} + \frac{2}{\pi}\int_0^\infty \left[-\frac{\mu}{2} + \{(1 + \mu)A + 2B\}\cosh \lambda y + (1 + \mu)B\lambda y \sinh \lambda y\right]\frac{\sin \lambda x}{\lambda^3}\,d\lambda \\
v(x, y)/\alpha T' &= \frac{2}{\pi}\int_0^\infty \left[\frac{\lambda y}{2} - \{(1 + \mu)A - (1 - \mu)B\}\sinh \lambda y - (1 + \mu)B\lambda y \cosh \lambda y\right]\frac{\cos \lambda x}{\lambda^3}\,d\lambda
\end{aligned}\right\} \quad \ldots [6]$$

[8] We use "I" to refer to equations in footnote 4. In the present and the next section we shall assume, for simplicity of writing, that the semiwidth $b$ of the strip is unity.

where $A = \dfrac{\lambda \cosh \lambda + \sinh \lambda}{2\lambda + \sinh 2\lambda}$, $B = \dfrac{-\sinh \lambda}{2\lambda + \sinh 2\lambda}$ ....[7]

In the displacement expressions we have chosen the point ($\infty$, 0) as fixed point and the $x$-axis as fixed axis. The stresses and displacements for negative $x$ are obtained from Equations [6] in the following form:

For $x = -X < 0$

$$\left.\begin{aligned} \sigma_x(x, y) &= \sigma_x(X, y) \\ \sigma_y(x, y) &= \sigma_y(X, y) \\ \tau(x, y) &= -\tau(X, y) \\ u(x, y) &= \frac{3y^2 - 1}{6}(1 - x\alpha T')^2 \alpha T' - u(X, y) \\ v(x, y) &= -yx\alpha T' + v(X, y) \end{aligned}\right\} \quad \ldots [8]$$

One verifies, as in footnote 4, that Equations [6] and [8] satisfy all boundary conditions of the problem.

For the $x = 0$ cross section, Equations [6] lead to the particularly important results

$$\bar{\sigma}_x(y)/E\alpha T' \simeq 0.09665 - 0.12722y^2 - 0.64847y^4 + 1.13632y^6 - 0.78332y^8 \ldots [9a]$$

$$\bar{\tau}(y)/E\alpha T' = 0 \ldots [9b]$$

$$\bar{u}(y)/\alpha T' = \frac{3y^2 - 1}{12} \ldots [9c]$$

$$\bar{v}(y)/\alpha T' \simeq 0.10844y + 0.00241y^3 - 0.05258y^5 + 0.03859y^7 - 0.00083y^9 \ldots [9d]$$

The Expressions [9a], [9d] of $\bar{\sigma}_x$, $\bar{v}$ were obtained by fitting, by least squares, 8th and 9th-degree polynomials, respectively, to the values derived from Formulas [6] for $x = 0$, by numerical integration at the ordinates $y = 0$, 0.2, 0.4, 0.6, 0.8, 0.9, 0.95, 1.0. (The pertinent formulas for least-square fitting are listed in the Appendix.[9]) As expected, the temperature break of Fig. 1($b$) gives rise at $x = 0$ to a precisely parabolic displacement $\bar{u}(y)$ which is independent of $\mu$, and which has a curvature one half of that developed at $x = -\infty$.

When the strip width is $2b$ rather than 2, then all the foregoing results apply provided one makes the replacements

$$x \to x/b, \quad y \to y/b, \quad T' \to bT', \quad u \to u/b, \quad v \to v/b \ldots [10]$$

## 3 Evaluation of Stresses and Displacements

### ($a$) *Numerical Integration*

This is performed in the same manner as in footnote 4. The values obtained in this fashion are indicated in Table 1 by a star.

### ($b$) *Biharmonic Eigenfunction Expansion*

A few values of $\sigma_x(x, y)$, noted by $\sharp$ in Table 1, were obtained by expanding the Airy function of the problem (we denote it by $\mathfrak{S}_2$) into biharmonic eigenfunctions

$$\left.\begin{aligned} \mathfrak{S}_2(x, y) &= E\alpha T' \Re \sum \frac{\sin^2 z_n}{\cos^2 z_n} \frac{\Phi_n(x, y)}{z_n} \quad (x \geq 0) \\ \Phi_n(x, y) &= \frac{e^{-z_n x}}{z_n^2}(\cos z_n y - y \cot z_n \sin z_n y) \end{aligned}\right\} \ldots [11]$$

and taking

$$\sigma_x = \mathfrak{S}_{2,yy} \ldots [12]$$

(In the numerical calculations we retained four terms of the series.) In Formula [11] the summation is carried out over the roots

$$z_n = \alpha_n + i\beta_n \ldots [13a]$$

of

$$\sin 2z + 2z = 0 \ldots [13b]$$

which have positive real and imaginary parts. ($\Re$ = real part.) The function $\mathfrak{S}_2$ is obtained from Equation [I.23$a$] by taking

$$\mathfrak{S}_2(x, y) = (T'/T) \int_x^\infty \mathfrak{IC}_1(\xi, y) d\xi \quad (x \geq 0) \ldots [14]$$

[With future applications in mind we replaced the general symbol $\Phi(x, y)$ of Equation [I.23$a$] by the specific symbol $\mathfrak{IC}_1$ as representing the stress function of the temperature step of Fig. 1($a$).]

### ($c$) *Self-Equilibrating Function Expansion*

By double integration of the $x = 0$ boundary values [9$a$] of $\sigma_x$ we find that the boundary value of the Airy function is

$$\bar{\mathfrak{S}}_2(y)/E\alpha T' = \int_{-1}^{y} d\eta \int_0^\eta \bar{\sigma}_x(\eta) d\eta / E\alpha T' \ldots [15]$$

$$\simeq -0.027695 + 0.048324y^2 - 0.010601y^4 - 0.021616y^6 + 0.020291y^8 - 0.008704y^{10}$$

and therefore the expansion of $\mathfrak{S}_2(x, y)$ into self-equilibrating functions is

$$\begin{aligned} \mathfrak{S}_2(x, y)/E\alpha T' &\simeq \Sigma < \bar{\mathfrak{S}}_2/E\alpha T', f_k > f_k g_k \\ &\simeq -0.025544 f_2 g_2 - 0.000751 f_4 g_4 - 0.000068 f_6 g_6 - 0.000030 f_8 g_8 \ldots [16] \\ &\equiv \Sigma c_k f_k g_k \end{aligned}$$

Stresses and deformations have now the approximate expressions

$$\left.\begin{aligned} \sigma_x &= \mathfrak{S}_{2,yy}, \ \sigma_y = \mathfrak{S}_{2,xx}, \ \tau = -\mathfrak{S}_{2,xy} \\ u(x, y)/\alpha T' &= \Sigma c_k (f_k'' \bar{g}_k - \mu f_k g_k') \\ v(x, y)/\alpha T' &= \Sigma c_k (\bar{f}_k g_k'' - \mu f_k' g_k) \end{aligned}\right\} \ldots [17]$$

and their numerical values are listed in Table 1 without markings. (The values of the functions $f_k''(y), \ldots, g_k(x)$ are tabulated in footnote 10.)

## 4 Inclined Step-Temperature Distribution

The stress maxima and the $x$, $y$ location of the maximum shear stress are shown in Figs. 3($a$, $b$).

## 5 Temperature Break Near End of a Strip

Let the break occur a distance $L = 0.4b$ from the end. If there were no free end then the stresses $\sigma_x$ and $\tau$ developed at $x = 0.4b$ would have the values ($\eta = y/b$)

$$\left.\begin{aligned} \sigma_x(0.4b, y)/E\alpha T'b &= 0.07869 - 0.19715\eta^3 - 0.06684\eta^4 + 0.01646\eta^6 - 0.01759\eta^8 \\ \tau(0.4b, y)/E\alpha T'b &= 0.08589\eta - 0.04614\eta^3 - 0.01283\eta^5 - 0.02701\eta^7 + 0.00010\eta^9 \end{aligned}\right\} \ldots [18]$$

These are (8th and 9th degree) least-square fits to the "self-equilibrating function" values listed in Table 1.

We eliminate the Stresses [18] by applying compensating tractions

[9] Equations [9] and [18] were determined by direct solution of the relevant equation systems prior to establishment of the general Equations [24]. Because of the different rounding errors involved in the two approaches, Equations [22$a$], [24$a$] reproduce $\bar{\sigma}_x$ of Equation [9$a$] only to 0.0003 accuracy. Similar discrepancies exist also between the other equations.

[10] "Tables of Self-Equilibrating Functions," by G. Horvay and J. S. Born, *Journal of Mathematics and Physics*, in press.

$$\left.\begin{aligned}\widehat{\varphi}_{\sigma,yy} &= \varphi_{\sigma,yy}(0, y) = -\sigma_x(0.4b, y)\\ -\widehat{\varphi}_{\tau,xy} &= -\varphi_{\tau,xy}(0, y) = -\tau(0.4b, y)\end{aligned}\right\} \quad \ldots\ldots [19]$$

at the edge of the strip. The corresponding stress functions are found to be

$$\left.\begin{aligned}\varphi_\sigma/E\alpha T'b &= -0.01892f_2g_2 - 0.00023f_4g_4 - 0.00000f_6g_6\\ \varphi_\tau/E\alpha T'b &= 0.02414f_3h_2 + 0.00104f_5h_4 + 0.00006f_6h_6\end{aligned}\right\} \quad [20]$$

By superposing the stresses derived from Equations [20] on those listed in Table 1, we obtain the stress distribution in the strip, as shown in Figs. 4(*a*, *b*, *c*).

# Appendix

## Least-Square Polynomial Approximation to a Function

Because of the frequent need in problems of the present type for least-square approximation of functions $f(y)$, whose values are given at $y_i \geq 0\ (i = 1, 2, \ldots, l)$, (*a*) by an even polynomial

$$F(y) = a_0 + a_2y^2 + a_4y^4 + \ldots + a_ny^n \ldots\ldots [21a]$$

or (*b*) by an odd polynomial

$$F(y) = a_1y + a_3y^3 + a_5y^5 + \ldots + a_ny^n \ldots\ldots [21b]$$

we list the results when $y_i = 0, 0.2, 0.4, 0.6, 0.8, 0.9, 0.95, 1.0$. One can show that

$$\left.\begin{aligned}\{a_0, a_2, a_4, a_6, a_8\} &= \mathfrak{A}_8\{w_0, w_2, w_4, w_6, w_8\}\\ \{a_1, a_3, a_5, a_7, a_9\} &= \mathfrak{A}_9\{w_1, w_2, w_3, w_7, w_9\}\end{aligned}\right\} \quad [22a, b]$$

where $\{\ \}$ stands for a column matrix

$$w_k = \sum_{i=1}^{l} y_i^k f(y_i) \ldots\ldots [23]$$

and[11]

[11] The matrices $\mathfrak{A}_8, \mathfrak{A}_9$ were determined on a CPC using an eight-digit floating decimal system. In Equations [24] we show the results (with one exception) to seven digits.

$$\mathfrak{A}_8 = \begin{Vmatrix} 0.734606 & -9.919031 & 35.685346 & -47.121862 & 20.668231\\ -9.919031 & 303.341831 & -1349.166211 & 1964.616102 & -911.652436\\ 35.685346 & -1349.166211 & 6543.404490 & -9990.819026 & 4779.057527\\ -47.121862 & 1964.616102 & -9990.819026 & 15690.624313 & -7652.649474\\ 20.668231 & -911.652436 & 4779.057527 & -7652.649474 & 3785.428061 \end{Vmatrix} \quad \ldots [24a]$$

$$\mathfrak{A}_9 = \begin{Vmatrix} 42.20873 & -400.51456 & 1183.07299 & -1379.16051 & 554.96930\\ -400.51456 & 4540.63376 & -14646.12026 & 17989.56980 & -7493.48673\\ 1183.07299 & -14646.12026 & 49769.03887 & -63221.20028 & 26959 05179\\ -1379.16051 & 17989.56980 & -63221.20028 & 82140.47596 & -35598.94620\\ 554.96930 & -7493.48673 & 26959.05179 & -35598.94520 & 15614.13765 \end{Vmatrix} \quad \ldots [24b]$$

# On the Kinematic Path of Semi-Trailers

By G. A. G. FAZEKAS,[1] BROOKLYN, N. Y.

**A trailer having a rigid axle does not quite follow the path of its tractor. The author describes the basic geometry and kinematics involved. The subject matter is arranged under headings (*a*) transient trailer path in turn, (*b*) design criterion, and (*c*) transient trailer path when straightening out.**

## Introduction

IT is well known that a trailer having a rigid axle does not quite follow the path of its tractor. Difference in tracking between the two is usually measured by making the tractor execute a sudden turn of constant radius $R_0$, whereupon the trailer follows some such path as sketched in Fig. 1. For design purposes the trailer path has been characterized hitherto by two parameters; (1) the "cut-in" $c_0$, and (2) the "transition angle" $\phi_0$, the meaning of which will be self-evident from Fig. 1.

Of these two parameters the value of $c_0$ can be found readily from geometry alone, and with the nomenclature as in Fig. 1, we have

$$c_0 = R_0(1 - \sec \alpha \sin \theta_0)$$

$$\text{or } \frac{c_0}{R_0} = 1 - \sqrt{1 - \frac{L^2}{R_0^2}\left(1 - \frac{a^2}{L^2}\right)} \quad \ldots\ldots [1]$$

$\phi_0$ on the other hand, seems to have been determined experimentally so far.[2]

Some reflection will show of course that in a sharp turn (just when the cut-in has to be watched) the transition angle may amount to several hundred degrees. In a much more usual 90-deg turn therefore, the corresponding cut-in $c^*$ is not as bad as $c_0$. In the circumstances it may be of some interest to elucidate the relevant kinematics with a view to obtaining some design charts for $\phi_0$ as well as $c^*$. This is the primary reason for and purpose of these notes.

An examination of Equation [1] suggests that ($c_0 = 0$) if ($a = L$), which circumstance seems to have induced the belief that trailers so designed have perfect tracking, that is ($\phi_0 = 0$). It will be shown also that this view is quite fallacious. Whereas such a design is undoubtedly beneficial in some ways, neither $c$, nor $c^*$ vanishes, but merely appears on the side opposite to the one shown in Fig. 1.

Apart from the behavior of a trailer when proceeding in a turn, its characteristic on straightening out is of considerable import too, particularly for considering criteria of dynamic stability. A brief discussion of the relevant kinematics will be also included.

These notes are thus confined to basic geometry from which one should expect some—though very little—deviation on account of tire elasticity and slip, camber of the road, and so on. That such secondary effects induce very little error will be demonstrated by comparing calculated and experimentally found values of $\phi_0$.

The following subject matter is arranged under three main headings; namely (*a*) transient trailer path in a turn, (*b*) design criteria, and (*c*) transient trailer path when straightening out. For (*a*) and (*b*) it will be assumed—as is the convention—that the tractor executes a sudden circular turn after having proceeded previously in a straight line. For (*c*) it will be supposed that the tractor travels in a straight line.

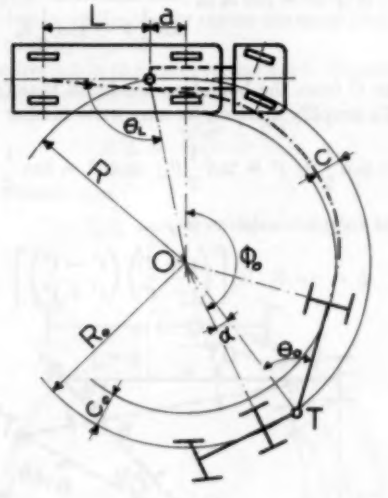


Fig. 1

## Trailer Path in a Turn

Whatever the overhang $a$, fundamentally, our case can be reduced to a fixed crank-arm $R$ towing the trailer around. Accordingly, consider the trailer in a position as sketched in Fig. 2, with its tow pin $T$ rotating around $O$ from $T'$ to $T''$, during an infinitesimally small time. The trailer itself is then bound to turn around centro $I'$, which moves to $I''$ after a turn $d\phi$. (Any trailer path can be reconstructed graphically in this manner.)

From the geometry of the layout and, in particular, from $\Delta PST'$ it follows that

$$d\psi + \theta + (\pi - d\phi - \theta - d\theta) = \pi \text{ or } d\psi - d\theta = d\phi \quad \ldots\ldots [2]$$

A second relationship is obtained from observing rotation about $I'$, whence

$$R d\phi = L \sec \theta \, d\psi \quad \ldots\ldots [3]$$

A combination of Equations [2] and [3], viz.

$$d\theta = \left(\frac{R}{L} \cos \theta - 1\right) d\phi \quad \ldots\ldots [4]$$

---

[1] Associate Professor of Mechanical Engineering, Polytechnic Institute of Brooklyn.

[2] "Trailers and Semi-Trailers," by A. Marenbon, Proceedings of The Institution of Mechanical Engineers, Automotive Division, part 4, 1951–1952, pp. 158–167.

Presented at the National Conference of the Applied Mechanics Division, Troy, N. Y., June 16–18, 1955, of The American Society of Mechanical Engineers.

Discussion of this paper should be addressed to the Secretary, ASME, 29 West 39th Street, New York, N. Y., and will be accepted until October 10, 1955, for publication at a later date. Discussion received after the closing date will be returned.

Note: Statements and opinions advanced in papers are to be understood as individual expressions of their authors and not those of the Society. Manuscript received by ASME Applied Mechanics Division, July 6, 1954. Paper No. 55—APM-11.

is then the equation of the path in a quasi-polar form. On integrating it, with $(R/L = \sec\theta_0)$, which follows from Fig. 1

$$\phi + C = \int \frac{d\theta}{\sec\theta_0 \cos\theta - 1} \quad \ldots\ldots [5]$$

where $C$ is a constant of integration. The foregoing integral can be transformed readily to

$$\phi + C = 2\int \frac{\sec^2\frac{\theta}{2}\cdot d\left(\frac{\theta}{2}\right)}{(\sec\theta_0 - 1) - (\sec\theta_0 + 1)\tan^2\frac{\theta}{2}} \quad \ldots [6]$$

which is of standard form. After some manipulations we obtain thus ultimately

$$\phi + C = \cot\theta_0 \ln \frac{\tan\frac{1}{2}\theta + \tan\frac{1}{2}\theta_0}{\tan\frac{1}{2}\theta - \tan\frac{1}{2}\theta_0} \quad \ldots\ldots [7]$$

We obtain $C$ from the boundary condition that $(\theta = \theta_i)$ for $(\phi = 0)$. To simplify matters, we may write further

$$t = \tan\frac{1}{2}\theta;\ t' = \tan\frac{1}{2}\theta_i;\ \text{and}\ t'' = \tan\frac{1}{2}\theta_0 \ldots\ldots [8]$$

and then the complete solution is

$$\phi = \cot\theta_0 \cdot \ln\left[\left(\frac{t + t''}{t - t''}\right)\left(\frac{t' - t''}{t' + t''}\right)\right] \quad \ldots\ldots [9]$$

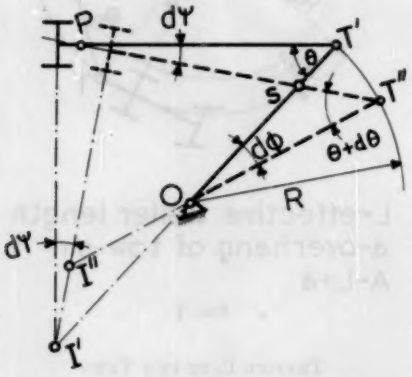


FIG. 2

To obtain the cut-in $c$ for $\phi$, with reference to Fig. 2 we have

$$c = R_0 - \sqrt{R^2 + L^2 - 2RL\cos\theta} \quad \ldots\ldots [10]$$

With $(L/R = \cos\theta_0)$, Equation [10] may be put into a more convenient form

$$c/R_0 = 1 - \sec\sqrt{1 + \cos^2\theta_0 - 2\cos\theta_0\cos\theta} \quad \ldots [11]$$

Equations [9] and [11] define thus the transient trailer path, but only if the tractor executes a truly circular turn. For other tractor paths the problem can be readily solved graphically, as intimated before with reference to Fig. 2.

## DESIGN DATA

An examination of Equation [9] shows at once that for $(\theta = \theta_0)$, i.e., for $(t = t'')$, we have $(\phi = \infty)$, so that the trailer path is of asymptotic character. Its convergence is governed by two parameters, $\theta_i$ and $\theta_0$, which in turn depend on $(L/R_0)$ and $(a/L)$, respectively. Since in most current designs $(a/L = 0)$, we will confine our investigation to this case. We have then $(t' = 1)$ and $(R = R_0)$.

Next we may inquire what is the transition angle or its equivalent; to what extent is cut-in really effective; and what improvement does accrue from an $(a = L)$ design?

*Transition Angle.* Since the trailer path is asymptotic, strictly, there is no such thing as a "transition angle." On the other hand, at or beyond some value of $\phi$ the trailer path will be a circle for all practical purposes, and this value of $\phi$ may well be termed as the transition angle, but one should add to what degree of convergence. Marenbon's experimentally obtained values of $\phi_0$ should be interpreted in this light which, partially at least, explains their scatter.

In the circumstances, perhaps it may be justified to define $\phi_0$ as that value of $\phi$, when $(c_0 - c)/R_0 = e$ does not exceed a certain small quantity, say, 5 per cent. This predicates therefore that

$$e + \sqrt{1 - \cos^2\theta_0} = \sqrt{1 + \cos^2\theta_0 - 2\cos\theta_0\cos\theta} \quad \ldots [12]$$

On squaring this expression, and neglecting $e^2$, one obtains

$$\cos\theta \sim \cos\theta_0 - e\tan\theta_0 \quad \ldots\ldots [13]$$

To obtain $\phi$ corresponding to $\theta$, the evaluation may be easier if it be supposed that $\theta$ differs from $\theta_0$ only by some small angle $\delta$, i.e., $(\theta = \theta_0 + \delta)$. On account of $\delta$ being small, we may then write

$$\cos\theta \sim \cos\theta_0 - \delta\sin\theta_0 \quad \ldots\ldots [14]$$

On comparing Equations [13] and [14] we find that

$$\delta \sim e\sec\theta_0 \quad \ldots\ldots [15]$$

so that

$$\tan\frac{1}{2}\theta = \tan\frac{1}{2}(\theta_0 + \delta) \approx t'' + \frac{1}{2}(1 + t''^2)\delta \ldots [16]$$

which one obtains on writing $\delta \sim \tan\delta$, and through subsequent expansion of the binomial $(1 - t''\delta/2)^{-1}$ to the first order of small quantities. A substitution of it into Equation [9] results therefore with $(t' = 1)$ in

$$\phi_0 \approx \cot\theta_0 \cdot \ln\left[\left(1 + \frac{4t''/\delta}{1 + t''^2}\right)\left(\frac{1 - t''}{1 + t''}\right)\right] \ldots [17]$$

This expression is plotted in Fig. 3 for $e = 1/2$ per cent and for $e = 5$ per cent, together with Marenbon's experimental data. In Marenbon's experiments it was probably the distance $(R - c)$, which is equivalent to $(c_0 - c)$, that served as the primary measurement; measuring accuracy was perhaps substantially constant. As a result of it, $e$ was less and $\phi_0$ more for a sharp turn, and vice versa, which would explain some of the scatter. Considering this factor, agreement with the 1/2 per cent curve is close enough to accept both theory and accuracy of measurements as mutually proved.

Next, we may pose the question whether $\phi_0$ could or should serve as a yardstick for design. A glance at Fig. 3 shows that in a sharp turn—just when $c_0$ is of paramount importance—it will be reached only after several hundred degrees turn, even on the 5 per cent curve. Although such turns are by no means impossible, to say the least, they are rather infrequent. It would seem therefore that for practical purposes one cannot glean a great deal of information from $\phi_0$ alone, which after all merely indicates when, say, 95 per cent of $c_0$ is reached, but does not indicate directly how much $c$ is in the far more frequent 90-deg turn.

*Effective Cut-In.* The trailer path being asymptotic, the maximum cut-in $c_0$ is never quite reached. Considering further

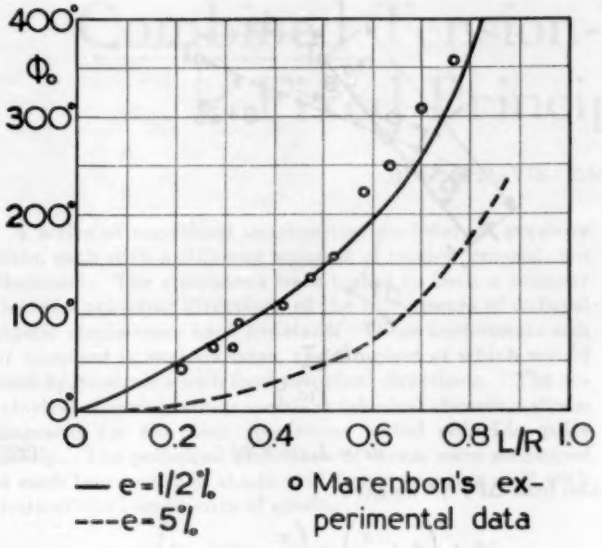


FIG. 3

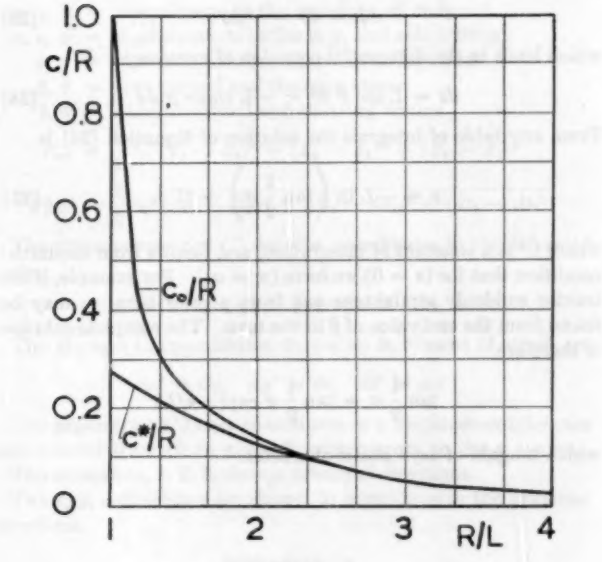


FIG. 4

that very few roads have a sharp turn exceeding 90 deg, the amount of cut-in for a 90-deg turn, $c^*$, seems to the author an apposite direct scale to judge maneuverability.

To obtain $c^*$, in Equation [9] we set ($\phi = \pi/2$), and solve for the corresponding value of ($\theta = \theta^*$)

$$\tan\frac{1}{2}\theta^* = t^*\left[\frac{2}{\frac{1+t^*}{1-t^*}\exp\left(\frac{1}{2}\pi\tan\theta_0\right)-1}+1\right] \quad [18]$$

which on substitution into Equation [11] yields $c^*$. It is plotted in Fig. 4 against the "relative turning radius" ($R/L$), together with $c_0$, for the case of zero overhang ($a = 0$). As may be seen, for ($R/L < 2$) the difference between $c_0$ and $c^*$ is appreciable indeed and may easily be in the order of 2:1.

*The a = L Design.* This rather simple construction has the lure that ($c_0 = 0$) which induced some engineers to base on it the steering mechanism of some semi and many full trailers, for which "perfect tracking" is then claimed.[3] To disprove this statement, it suffices to remember that $\theta$ must needs change from $\theta_i$ to $\theta_0$, and that the change being gradual, the transition path is ipso facto no circle!

The explanation of this somewhat mysterious zero cut-in ($c_0 = 0$) lies in the fact that our imaginary crank arm $R$ is no longer equal to, but is appreciably longer than, $R_0$, to wit

$$R = \sqrt{R_0^2 + a^2} = \sqrt{R_0^2 + L^2} \quad [19]$$

from Fig. 1. In the circumstances, and with respect to $R$, we have similar cut-in as before, the difference being that here ($\theta_i > \pi/2$) which increases $\phi_0$! With respect to $R_0$, however, we no longer have a cut-in, but a "cut-out."

To make a fair assessment of the ($a = L$) design, let it be supposed that the distance $A$ between truck and trailer axle is to remain fixed, and we wish to study the effect of tow-pin location when ($a = 0$) and when ($a = A/2 = L$). Let us further suppose that in both instances the tractor makes the same turn, defined on the ($a = 0$) basis by ($R_0/A$).

If now the tow pin is to be moved rearward, the relative sharpness of the selfsame turn will be

$$R/L = \frac{\sqrt{a^2 + R_0^2}}{A - a}$$

i.e., for the present case

$$R/L = \sqrt{1 + R_0^2/L^2} \quad [20]$$

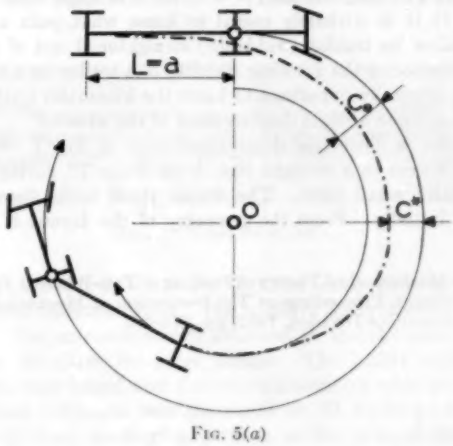


FIG. 5(a)

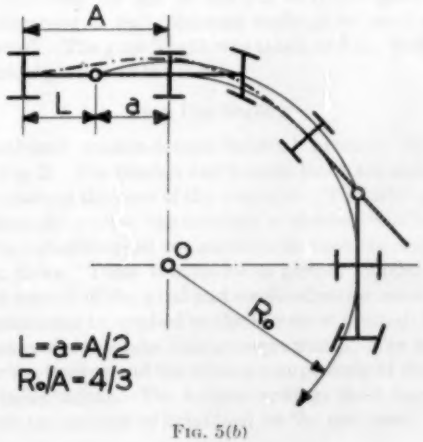


FIG. 5(b)

from Fig. 1. It also follows that

$$\theta_i = \frac{1}{2}\pi + \alpha = \frac{1}{2}\pi + \sin^{-1}(a/R_0) \quad [21]$$

Equation [20] shows clearly that as $a$ is increased, the relative curvature $(R/L)$ increases too, and hence the diminished trend to deviate. The adverse effect of increased $\theta_i$ fails to offset the benefit gained.

To illustrate matters, Figs. 5(*a*) and 5(*b*) show an $(R_0/A = 4/3)$ turn for $(a = 0)$ and for $(a = L)$. As may be seen, the latter tracks better, but tends to bulge out on the wrong side, where part of the trailer may stick out and cause just as much or more obstruction than its poorer tracking relative. The true field of the $(a = L)$ design seems to be thus confined to full trailers, where no such obstruction is liable to occur, Fig. 6.

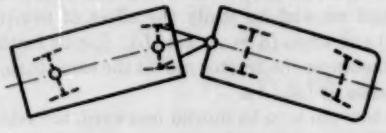

Full Trailer with Symmetrically Steered Rear Axle.

FIG. 6

### TRAILER PATH ON STRAIGHTENING OUT

The straightening-out path of a trailer is of importance in two cases: (1) It is obviously useful to know what path a trailer follows after its tractor (suddenly) straightened out of a turn. (2) In considering the dynamic stability of a trailer (or a castered wheel) it is equally important to know the kinematic trailer path consequent upon a slight displacement of the wheels.[3]

This case is illustrated diagrammatically in Fig. 7 where the tow pin moves in a straight line, from $T'$ to $T''$ during an infinitesimally small time. The trailer itself turns then about centro $I$ initially. From the geometry of the layout it follows that

[3] "The Mathematical Theory of Snaking of Two-Wheeled Trailers," by D. Williams, Proceedings of The Institution of Mechanical Engineers, Automotive Division, 1952, pp. 175–187.

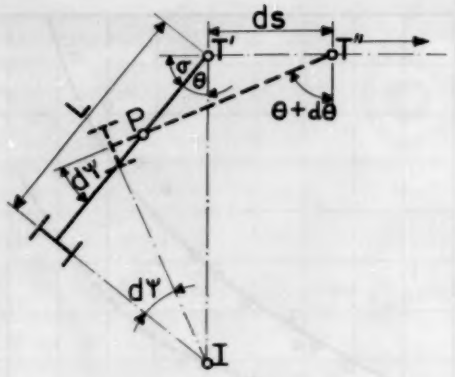


FIG. 7

$$ds = L \sec\theta \, d\psi \quad [22]$$

Also from $\Delta PT'T''$ we have

$$d\psi + \left(\theta + \frac{\pi}{2}\right) + \left(\frac{\pi}{2} - \theta - d\theta\right) = \pi$$

or

$$d\psi = d\theta = -d\sigma \quad [23]$$

which leads to the differential equation of movement

$$ds = L \sec\theta \, d\theta = -L \operatorname{cosec}\sigma \, d\sigma \quad [24]$$

From any table of integrals the solution of Equation [24] is

$$s = -L \ln\left(\tan\frac{1}{2}\sigma\right) + C' \quad [25]$$

where $C'$ is a constant of integration, and follows from the initial condition that for $(s = 0)$ we have $(\sigma = \sigma_0)$. For example, if the tractor suddenly straightens out from a prior turn, $\sigma_0$ may be found from the end value of $\theta$ in the turn. The complete solution is therefore

$$\tan\frac{1}{2}\sigma = \tan\frac{1}{2}\sigma \exp(-s/L)$$

which is again of asymptotic character.

# Combined Tension-Torsion Tests With Fixed Principal Directions

By E. A. DAVIS,[1] EAST PITTSBURGH, PA.

**A series of combined tension-torsion-internal pressure tests, each with a different amount of torsion present, are discussed. The specimens were tested in such a manner that the principal directions of the increments of natural plastic strain were kept constant. These increments can be summed in various ways, the simplest of which would yield finite strains with fixed principal directions. The octahedral shearing-stress versus octahedral shearing-strain diagrams for the four specimens tested coincide quite closely. The principal directions of stress were measured at each increment of strain and found to agree well with those of the increments of strain.**

## Nomenclature

The following nomenclature is used in the paper:

$x, y, z$ = co-ordinates in the undeformed body
$u, v, w$ = displacements in the $x$, $y$, and $z$-directions
$\sigma, \tau$ = conventional normal and shearing stress
$\bar{\sigma}, \bar{\tau}$ = true normal and shearing stress
$\bar{\epsilon}, \bar{\gamma}$ = natural normal and shearing strains

$$\bar{\tau}_{oct} = \frac{1}{3}\sqrt{(\bar{\sigma}_1 - \bar{\sigma}_2)^2 + (\bar{\sigma}_2 - \bar{\sigma}_3)^2 + (\bar{\sigma}_3 - \bar{\sigma}_1)^2}$$

$$d\bar{\gamma}_{oct} = \frac{2}{3}\sqrt{(d\bar{\epsilon}_1 - d\bar{\epsilon}_2)^2 + (d\bar{\epsilon}_2 - d\bar{\epsilon}_3)^2 + (d\bar{\epsilon}_3 - d\bar{\epsilon}_1)^2}$$

The prime superscript ($'$) denotes co-ordinates in the deformed body.

$$x' = x + u,\ y' = y + v,\ z' = z + w$$

The changes in co-ordinates during an increment of strain are

$$dx' = du,\quad dy' = dv,\quad dz' = dw$$

The superscript ($^\circ$) on a co-ordinate or a displacement denotes axes rotated through an angle $\theta'$ with respect to the $x$, $y$-axes.

The subscripts, 1, 2, 3, denote principal directions.

The $x$, $y$, $z$-directions are chosen to coincide with the principal directions.

## Introduction

Any finite plastic strain is made up of a summation of increments of strain, and since plastic deformation is an irreversible process the path over which the summation is made will be important. Previous tests, including some by the author[2] have indicated that when tubular specimens are deformed by combined axial tension and internal pressure the octahedral shearing-stress versus octahedral shearing-strain curves coincide for tests where the ratios of the principal stresses remain constant. In those tests the principal directions of both stress and strain remain fixed in space and fixed in the material.

In the present series of tests an attempt was made to deform the specimens in such a manner that the principal directions of the increments of strain would be fixed in space. Since the tests contain a component of torsion the fibers of material once in the principal directions will rotate out of these directions during the next increment of strain. If the increments associated with a fixed direction are integrated the resulting finite strains can be considered as having fixed principal directions. The principal strains described in this paper have been integrated in this manner.

## Material and Specimens

The material used in this investigation was a 1020 steel with a composition quite similar to the material used in the tests described elsewhere.[2] The test blanks were cut from a cold-drawn rod and were heated to 930 C and allowed to cool in a small furnace.

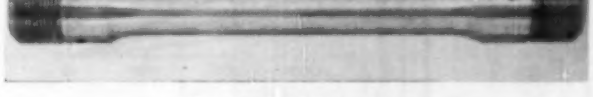

Fig. 1 Test Specimen

The specimen is shown in Fig. 1. The inside diameter is 1 in. and the wall thickness $^1/_{16}$ in. The length of the cylindrical section is 6 in. The extensometer is attached to the shoulders of the specimen to allow for large strains. The inside surfaces of the tubes were honed and the external surfaces were polished.

The wall thickness was measured at 20 positions and the average of these readings was taken as the original thickness. The wall thickness was not as uniform as might have been desired. Differences in wall-thickness readings as great as 3 mils were observed. The gage length was taken as 6 in., the length of the cylindrical portion of the tube.

## Test Equipment

The combined tension-torsion-internal pressure machine is shown in Fig. 2. The tension and torsion loads are measured by spring members at the base of the machine. The driving mechanism at the upper part of the machine is characterized by the insertion of a variable-speed transmission in both the tension and the torsion drive. These transmissions permit independent and continuous control of the axial and torsional strain rates. An internal pressure can be applied to the specimen through the lower grip by means of a separate high-pressure pump. The measuring devices for the tension and the torsion components of the load are not quite independent. The torque readings must be corrected according to the amount of axial load on the specimen.

---

[1] Advisory Engineer, Westinghouse Research Laboratories. Mem. ASME.

[2] "Yielding and Fracture of Medium Carbon Steel Under Combined Stress," by E. A. Davis, Journal of Applied Mechanics, Trans. ASME, vol. 67, 1945, p. A-13.

Presented at the National Conference of the Applied Mechanics Division, Troy, N. Y., June 16–18, 1955, of The American Society of Mechanical Engineers.

Discussion of this paper should be addressed to the Secretary, ASME, 29 West 39th Street, New York, N. Y., and will be accepted until October 10, 1955, for publication at a later date. Discussion received after the closing date will be returned.

Note: Statements and opinions advanced in papers are to be understood as individual expressions of their authors and not those of the Society. Manuscript received by ASME Applied Mechanics Division, July 9, 1954. Paper No. 55—APM-8.

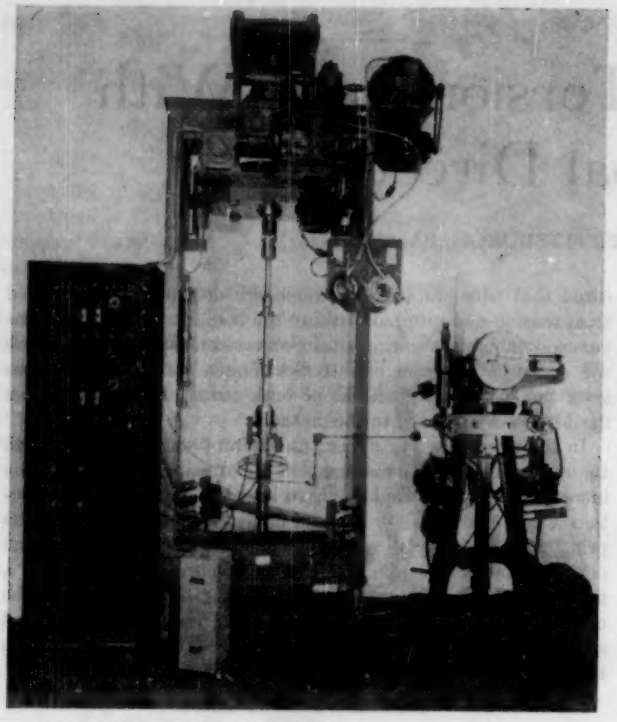

FIG. 2 (*above*) COMBINED TENSION-TORSION-INTERNAL PRESSURE MACHINE

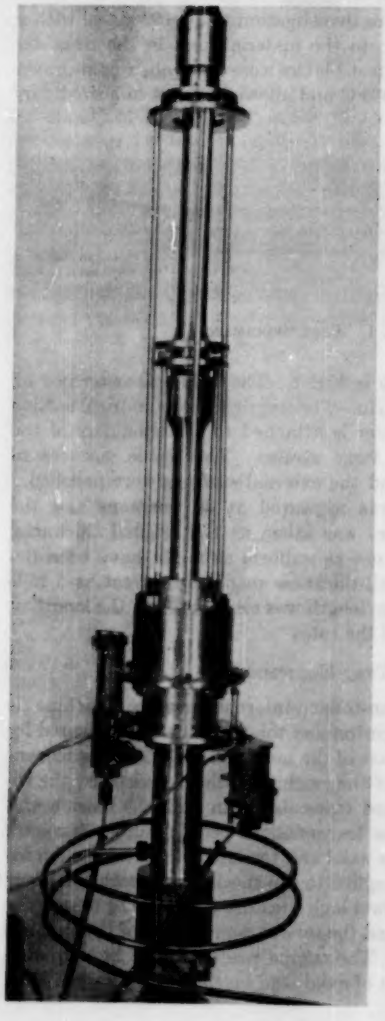

FIG. 3 (*left*) EXTENSOMETER FOR MEASURING AXIAL EXTENSION AND ANGLE OF TWIST

The axial extension and the angle of twist are measured independently by the extensometer shown in Fig. 3.

### TEST PROGRAM AND PROCEDURE

In order to understand the tests used in this investigation it is necessary to describe the increments of finite strain and the manner in which the increments are to be integrated. A state of homogeneous natural strain, which is the condition desired in a test specimen, will be obtained if the increments in the displacements are linear functions of the co-ordinates of the strained body.[1] For the two-dimensional case these can be written

$$\left.\begin{aligned} du &= da_{11}x' + da_{12}y' \\ dv &= da_{21}x' + da_{22}y' \end{aligned}\right\} \quad \ldots\ldots\ldots\ldots [1]$$

The increments of finite natural strain then have definitions quite similar in form to those for infinitesimal strain

$$\left.\begin{aligned} d\bar{\epsilon}_x &= \frac{\partial(du)}{\partial x'} = da_{11} \\ d\bar{\epsilon}_y &= \frac{\partial(dv)}{\partial y'} = da_{22} \\ d\bar{\gamma}_{xy} &= \frac{\partial(du)}{\partial y'} + \frac{\partial(dv)}{\partial x'} = da_{12} + da_{21} \end{aligned}\right\} \quad \ldots\ldots\ldots [2]$$

These increments of strain can be represented by a Mohr circle diagram and the increments of strain in any direction can be obtained from the following equations

$$d\bar{\epsilon} = \frac{d\bar{\epsilon}_1 + d\bar{\epsilon}_2}{2} + \frac{d\bar{\epsilon}_1 - d\bar{\epsilon}_2}{2} \cos 2\theta' \quad \ldots\ldots\ldots [3]$$

$$\frac{d\bar{\gamma}}{2} = \frac{d\bar{\epsilon}_1 - d\bar{\epsilon}_2}{2} \sin 2\theta' \quad \ldots\ldots\ldots\ldots [4]$$

These equations are similar to those for infinitesimal strain except that the angle $\theta'$ is measured in the deformed body. This angle will be a function of the original angle $\theta$ and the strain up to the instant the increment is taken.

In the present series of tests the specimen is a thin-walled tube. The stretching and twisting of such a tube can be visualized as the stretching and shearing of a thin plate. If the tube is subjected to the correct amount of internal pressure the mean diameter of the tube will not decrease as the specimen is stretched in the axial direction. The deformation of such a tube can be visualized as the stretching and shearing of a plate which reduces in thickness but not in width. If $x^\circ$ is the axial direction, $y^\circ$ the tangential direction, and $z^\circ$ the radial direction in the tube, the increments of deformation for combined tension and torsion with no reduction in mean diameter are

$$\left.\begin{aligned} du^\circ &= dA_{11}x^{\circ\prime} \\ dv^\circ &= dA_{21}x^{\circ\prime} \\ dw^\circ &= dA_{31}z^{\circ\prime} \end{aligned}\right\} \quad \ldots\ldots\ldots\ldots [5]$$

---

[1] For a complete description of finite strains, the reader is referred to the following:

"Theory of Flow and Fracture of Solids," by A. Nadai, McGraw-Hill Book Company, Inc., New York, N. Y., second edition, vol. 1, 1950.

"The Mathematical Theory of Plasticity," by R. Hill, Clarendon Press, Oxford, England, 1950.

"Theory of Perfectly Plastic Solids," by W. Prager and P. G. Hodge, John Wiley & Sons, Inc., New York, N. Y., 1950.

"Finite Deformation of an Elastic Solid," by F. D. Murnaghan, John Wiley & Sons, Inc., New York, N. Y., 1951.

Survey accounts of the problem of plastic stress-strain relations can be found in the following:

"Stress-Strain Relations in the Plastic Range—A Survey of Theory and Experiment," by D. C. Drucker, ONR Report A1151, Graduate Division of Applied Mathematics, Brown University, Providence, R. I., 1950.

"Plastic Behavior of Engineering Materials," Part 3, by M. C. Steele, C. K. Liu, and J. O. Smith, University of Illinois, Wright Air Development Center TR 52-89, June, 1953.

This rectangular system of co-ordinates is used to avoid the complexity of polar co-ordinates which would be necessary if the specimen were a solid cylinder or a heavy-walled tube.

For incompressible material the increments of strain in three orthogonal directions must be zero

$$dA_{11} + dA_{22} + dA_{33} = 0 \quad \ldots\ldots\ldots\ldots\ldots [6]$$

In the present series the strain in the tangential direction is zero

$$\frac{\partial(dv^\circ)}{\partial y^{\circ\prime}} = dA_{33} = 0$$

so that the increment of strain in the radial direction

$$d\bar{\epsilon}_{z^\circ} = \frac{\partial(dw^\circ)}{\partial z^{\circ\prime}} = dA_{33}$$

must be the negative equivalent of the increment of strain in the axial direction

$$d\bar{\epsilon}_{x^\circ} = \frac{\partial(du^\circ)}{\partial x^{\circ\prime}} = dA_{11}$$

The coefficient $dA_{21}$ is a measure of the amount of twisting or shearing of the specimen, and the relative size of it will be instrumental in determining the principal directions. If the $x$, $y$, and $z$-directions are taken as the principal directions, and if the principal directions of the increments of strain are defined as those directions where the increment of shearing strain is zero, then for the present tests the $x^\circ$ and the $z$-direction will coincide and the $x$, $y$ axes will be located at an angle $\theta'$ to the $x^\circ y^\circ$-axes. The increments in the displacements in the principal directions will be given by Equations [1] with the condition that the increment in shearing strain be zero

$$da_{12} + da_{21} = 0 \quad \ldots\ldots\ldots\ldots\ldots [7]$$

The standard equations for rotation of axes can be used to establish relationships between the known $dA$'s of Equations [5] and the unknown $da$'s of Equation [1]. Equation [7] can then be used to show that for the present series of tests the principal direction of the increments of strain will be given by

$$\tan 2\theta' = \frac{dA_{21}}{dA_{11}} \quad \ldots\ldots\ldots\ldots\ldots [8]$$

It will be noted that the principal directions of the increments of strain will remain fixed if the ratio on the right side of Equation [8] is a constant $K_{21}$

$$dA_{21} = K_{21} dA_{11} \quad \ldots\ldots\ldots\ldots\ldots [9]$$

In this paper only tests in which Equation [9] holds are discussed. Tension-torsion tests in which the principal directions do not remain constant could be run and analyzed by making $dA_{21}$ a controlled function of $dA_{11}$. The integration of the increments obtained in such a manner, however, would have to be defined carefully and possibly a new interpretation of principal directions of finite strain would be necessary.

In this investigation the summation of the increments has been made by keeping the angle $\theta'$ constant. The differentials of Equations [3] and [4] can then be integrated directly. This type of summation can be illustrated by considering the maximum shearing-strain increments in a thin strip in pure tension. In the plane of the strip the increment of shearing strain would be a maximum at 45 deg to the pulling direction, $\theta' = 45$ deg. The maximum shearing strain obtained by summing these maximum increments would be a finite strain which would truly be related to the maximum shearing stress. Every increment of strain would have been colinear with the maximum shearing stress. Such a strain, however, does not follow a particular fiber of the material. At each increment new and different fibers rotate into the direction under consideration.

With increments of strain defined as in Equations [1] and [2] it is not difficult to describe the strains, but it may not always be possible to integrate the displacements. For the increments as indicated in Equations [5], however, the displacements can be determined readily. Since $du^\circ = dx^{\circ\prime}$, etc., the displacements in the axial, tangential, and radial directions will be

$$\left.\begin{aligned} u^\circ &= x^{\circ\prime}(1 - e^{-A_{11}}) = x^\circ(e^{A_{11}} - 1) \\ v^\circ &= K_{21}x^{\circ\prime}(1 - e^{-A_{11}}) = K_{21}x^\circ(e^{A_{11}} - 1) \\ w^\circ &= z^{\circ\prime}(1 - e^{A_{11}}) = z^\circ(e^{-A_{11}} - 1) \end{aligned}\right\} \ldots\ldots [10]$$

These equations show that the displacement in the $y^\circ$-direction is proportional to that in the $x^\circ$-direction and hence the strain or displacement pattern for any desired value of $K_{21}$ can be laid out as a straight-line plot of axial extensometer readings versus angle-of-twist indicator readings. Paths for $\theta'$ equal to 20, 30, and 35 deg are shown as solid lines in Fig. 4. The pattern for running the tests then is to follow as closely as possible these straight lines. The points plotted in Fig. 4 indicate the actual extensometer readings and show how well the desired paths were followed.

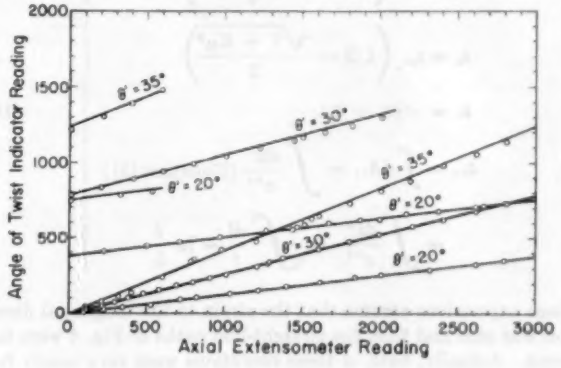


FIG. 4 DESIRED PATHS OF STRAINING

The test for $\theta' = 0$ was a combined tension-internal pressure test with the pressure adjusted so that there would be no reduction in the mean diameter of the tube. For an isotropic material the strain in the circumferential direction should be zero if the tangential stress is one half of the axial stress. For the test at $\theta' = 0$ the ratio of the conventional stresses $\sigma_{y^\circ}/\sigma_{x^\circ} = 1/2$ was maintained, and the mean diameter remained essentially constant. For the tests where there was some twisting present it was found that this ratio $\sigma_{y^\circ}/\sigma_{x^\circ}$ had to be maintained a little below 0.5 in order not to have an increase in mean diameter. This is due to the fact that the tangential stress increases more rapidly than the axial stress if the mean diameter does not increase while the wall thickness decreases.

The Mohr circles for the desired increments of strain for the four tests, $\theta' = 0$, 20, 30, and 35 deg are shown in Fig. 5. In so far as the distribution of increments of strain is concerned the test at $\theta' = 0$ corresponds to a state of pure shear. The test at $\theta' = 35$ deg corresponds very nearly to a state of simple tension.

In the process of running the tests the machine was stopped at the end of each increment of strain so that readings of load, torque, pressure, axial extension, and angle of twist could be made. The outside diameter of the tube was measured periodically and the relative magnitude of the pressure was adjusted so that the mean diameter would not vary.

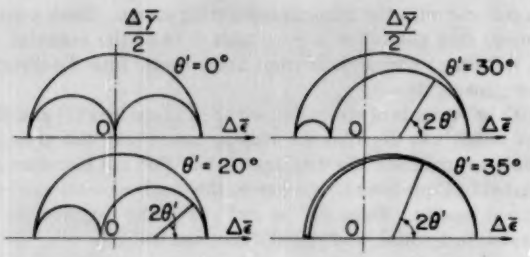


FIG. 5 DESIRED MOHR'S CIRCLES FOR INCREMENTS OF STRAIN

The usual assumption of constancy of volume was used in calculating the mean diameter and the wall thickness from which the tangential and radial strains and the true normal and shearing stresses were determined. For the purpose of calculating the octahedral shearing stress the radial stress was taken as one half the internal pressure.

The octahedral shearing strain plotted in Figs. 6 and 7 was calculated from the principal strains which in turn were obtained from the following expressions

$$\left.\begin{aligned}
\bar{\epsilon}_1 &= \bar{\epsilon}_{z_0}\left(1/2 + \frac{\sqrt{1+K_{21}^2}}{2}\right)\\
\bar{\epsilon}_2 &= \bar{\epsilon}_{z_0}\left(1/2 - \frac{\sqrt{1+K_{21}^2}}{2}\right)\\
\bar{\epsilon}_3 &= -(\bar{\epsilon}_1 + \bar{\epsilon}_2)\\
\bar{\epsilon}_{z_0} &= \int dA_{11} = \int \frac{du^\circ}{x^{\circ\prime}} \text{ (Equation [5])}\\
&= \int \frac{dx^{\circ\prime}}{x^{\circ\prime}} = \int_{l_0}^{l} \frac{dl}{l} = \ln\frac{l}{l_0}
\end{aligned}\right\} \quad \ldots\ldots [11]$$

These expressions assume that the strain in the tangential direction was zero and that the straight-line paths of Fig. 4 were followed. Actually, both of these conditions were very nearly fulfilled and the octahedral strain computed by this means is probably a better measure of the actual working of the material than a summation of the increments of octahedral strain would produce.

## DISCUSSION OF TEST RESULTS

The octahedral shearing-stress versus octahedral shearing-strain diagrams are shown in Fig. 6. The curve is drawn to fit the results of the test at $\theta' = 0$. The diagrams are plotted only to $\bar{\gamma} = 0.21$. The reason for this is that one of the tests was discontinued at this strain. To save the extensometer from damage the tests were not run to fracture. One specimen, however, failed prematurely in the fillet after a gage length strain of $\bar{\gamma}_{oct} = 0.268$. Those specimens tested beyond $\bar{\gamma}_{oct} = 0.21$ agreed about as well at the larger strains as in the region shown in Fig. 6. The stress-strain curves in Fig. 6 agree quite well with each other, and if Fig. 6 is compared with Fig. 21 of the previous reference[3] it will be seen that the agreement among the present tests is as good as it was in the series of tests where no torsion was present.

It may be argued that the present tests are not different from the former tests since they have been described as tests with fixed principal directions. However, it must be remembered that the present tests will or will not have fixed principal directions depending upon the manner in which the increments are defined and integrated. The curves in Fig. 6 do not give a picture of the amount of torsion that was applied to the specimen. To emphasize the difference in loading and straining in the present series the

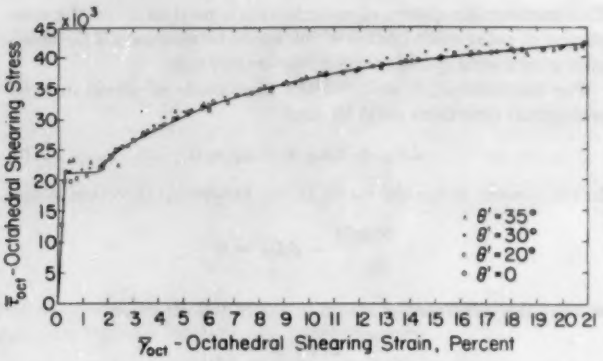


FIG. 6 STRESS-STRAIN DIAGRAMS FOR TENSION-TORSION TESTS

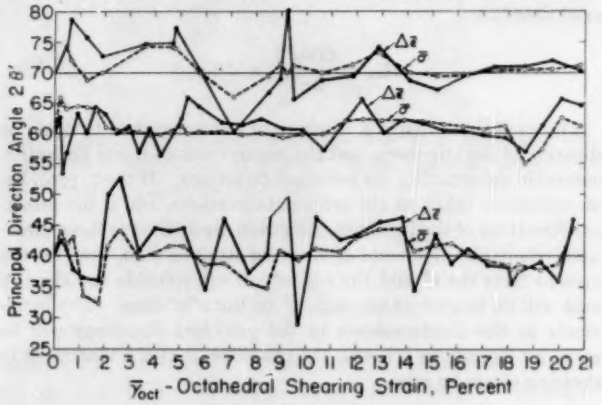


FIG. 7 PRINCIPAL DIRECTIONS OF STRESS AND INCREMENTS OF STRAIN

stresses and strains for the last points plotted in Fig. 6 are given in Table 1.

Although there seems to be good agreement among the curves in Fig. 6, and although it appears from Fig. 4 that the desired path of straining was followed quite closely, the agreement does not appear to be so good when the increments themselves are studied. The principal directions of stress and of the increments of strain are plotted against the octahedral shearing strain in Fig. 7. The dashed lines indicate the principal directions of the stress at the end of the increment. The solid lines indicate the principal directions of the increments of strain.

The roughness of the curves in Fig. 7 gives some measure of the

TABLE 1 CALCULATED DATA FOR LAST POINTS PLOTTED IN FIG. 6

| Principal direction | $\theta'$ | 0° | 20° | 30° | 35° |
|---|---|---|---|---|---|
| Axial stress | $\bar{\sigma}_{z_0}$ | 100500 | 89500 | 74500 | 59500 |
| Tangential stress | $\bar{\sigma}_{y_0}$ | 50640 | 46900 | 37300 | 29000 |
| Radial stress, $-p/2$ | $\bar{\sigma}_{x_0}$ | −2700 | −2520 | −2050 | −1670 |
| Torsional stress | $\bar{\tau}_{z_0 y_0}$ | 0 | 21000 | 34000 | 41090 |
| Principal stresses | $\bar{\sigma}_1$ | 100500 | 98150 | 94700 | 87800 |
| | $\bar{\sigma}_2$ | 50640 | 38250 | 17100 | 600 |
| | $\bar{\sigma}_3$ | −2700 | −2520 | −2050 | −1670 |
| Octahedral shearing stress | $\bar{\tau}_{oct}$ | 42200 | 41300 | 41700 | 41600 |
| Axial strain | $\bar{\epsilon}_{z_0}$ | 0.1266 | 0.1164 | 0.0941 | 0.0661 |
| Tangential strain | $\bar{\epsilon}_{y_0}$ | 0.0030 | 0.0068 | 0.0061 | 0.0029 |
| Radial strain | $\bar{\epsilon}_{x_0}$ | −0.1296 | −0.1232 | −0.1002 | −0.0690 |
| Unit angle of twist | $\alpha$ | 0 | 0.171 | 0.294 | 0.329 |
| Torsional strain | $\bar{\gamma}_{z_0 y_0}$ | 0 | 0.0915 | 0.1570 | 0.1755 |
| Octahedral shearing strain | $\bar{\gamma}_{oct}$ | 0.2090 | 0.2055 | 0.2080 | 0.2082 |

difficulty of straining a specimen according to a definite strain pattern. Trying to follow the strain paths of Fig. 4 is somewhat like trying to roll a sphere along a ridge. A small correction in the axial strain rate, made necessary by a lagging of the strain in that direction, would cause a large increase in the axial load and a corresponding decrease in the torque. This apparently unstable equilibrium was mostly responsible for the violent fluctuations of the curves in Fig. 7. It should be noted in Fig. 7, however, that the principal direction of the stress is usually a little nearer to the desired direction than that of the increments of strain. If the strain increments could have been directed exactly as planned it appears safe to conclude that the principal directions of stress would have coincided. This, then, is experimental evidence of the much-used assumption that the principal directions of the stress and of the increments of strain coincide.

The large fluctuations in the principal directions of the increments of strain are not so much indications that the principal direction of the total amount of strain is in error as they are indications of how rapidly corrections were being made to bring the actual strain path back to the desired path. Actually, the $\Delta\bar{\epsilon}$ curves in Fig. 7 would have been more jagged if the corrections to the strain rates had not been made in a gradual manner.

The diagrams in Fig. 5 show that the present series cover a full range of shear stresses. Tests with larger components of torsion could be run by using higher ratios of pressure to axial load. In such tests, however, the mean diameter would increase and the major principal stress direction would be more nearly in the circumferential direction than in the axial direction as was the case in the present tests. The natural anisotropy of the material would probably be noted if such tests were to be compared with the present tests.

## Conclusions

Based on the test results described in this paper the following conclusions can be made:

1 If combined tension-torsion tests are run in such a way that the principal directions of the increments of natural strain remain fixed, finite strains with fixed principal directions can be obtained by summation of the increments associated with a fixed direction.

2 For combined tension-torsion tests with fixed principal directions the octahedral shearing stress is a unique function of the octahedral shearing strain.

3 If a specimen is strained so that the principal directions of the increments of natural strain are kept constant, the principal directions of the stress will coincide with those of the increments of strain and also with the principal directions of the summation of the increments.

# Experiments Concerning the Yield Surface and the Assumption of Linearity in the Plastic Stress-Strain Relations[1]

By P. M. NAGHDI,[2] J. C. ROWLEY,[3] AND C. W. BEADLE,[4] ANN ARBOR, MICH.

**Combined tension and torsion experiments for six tubular 24S-T4 aluminum-alloy specimens with considerable initial anisotropy are reported. In all cases the results reveal the existence of corners on the yield loci of the material.**

## Introduction—General Background

In a recent paper,[5] experimental results on combined tension and torsion of tubular specimens made of aluminum alloy which possessed an appreciable initial anisotropy were reported. In these tests, the variable loading path was such that tension was followed by torsion and permitted the determination of the initial shear modulus $G_i$ when twist began. The modulus $G_t$, for all ratios of the increment of axial stress to the increment of shearing stress ($d\sigma_{33}/d\sigma_{23}$) during loading, was found to be considerably less than the elastic shear modulus $G_0$, except when unloading had actually taken place. Furthermore, it was repeatedly observed that plastic strains were produced for some negative values of ($d\sigma_{33}/d\sigma_{23}$) or $\left(\frac{d\sigma_{zz}}{d\tau_{\theta z}}\right)$.

These results motivated further experimental investigation on the character of the yield loci and possibly the validity of the assumption of linearity of the increment of the plastic strains in the increment of the stresses (hereafter referred to as the assumption of linearity). We recall that in the expression for the increment of the plastic-strain tensor $d\epsilon_{ij}^{p}$ in terms of a plastic potential $f$, namely

$$d\epsilon_{ij}^{p} = H \frac{\partial f}{\partial \sigma_{ij}} df$$

the existence of a smooth loading surface (which has a continuous turning tangent) is implied and furthermore it is usually assumed that $d\epsilon_{ij}^{p}$ is linear in $d\sigma_{ij}$.

Let us consider an initially smooth yield locus $f_1$ as shown in Fig. 1. Since the plastic-strain increment vector is normal to the loading surface,[6] then if the additional stress increments to produce $f_2$ and subsequently $f_3$ are small, the plastic-strain increments should be a smooth function of any of the monotonically increasing variables along the stress path. Thus, even if the subsequent loading surfaces were to distort appreciably, the existence of a smooth surface would predict that the increment of the plastic-strain vector $\vec{d\epsilon^{p}}$ would at most rotate independently of the wide excursions of the direction of the increment of the stress vector $\vec{d\sigma}$. As pointed out by Drucker and Stokton,[6,7,8] it may be emphasized that this is independent of the assumption of linearity.

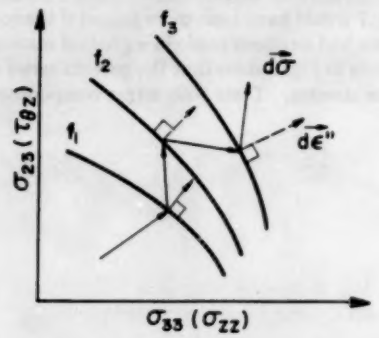


Fig. 1 Relation of Stress and Plastic-Strain-Increment Vectors to Subsequent Smooth Yield Loci

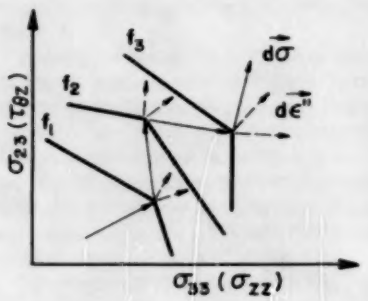


Fig. 2 Relation of Stress and Plastic-Strain-Increment Vectors to Subsequent Yield Loci Exhibiting Corners

---

[1] The results presented in this paper were obtained in the course of research sponsored by the Office of Ordnance Research under Contract DA-20-018-ORD-12099, with the University of Michigan.

[2] Professor of Engineering Mechanics, University of Michigan. Assoc. Mem. ASME.

[3] Research Assistant, Department of Engineering Mechanics, University of Michigan.

[4] Research Assistant, Department of Engineering Mechanics, University of Michigan. Assoc. Mem. ASME.

[5] "An Experimental Study of Biaxial Stress-Strain Relations in Plasticity," by P. M. Naghdi and J. C. Rowley, *Journal of the Mechanics and Physics of Solids*, vol. 3, no. 1, October, 1954, pp. 63–80.

Presented at the National Conference of the Applied Mechanics Division, Troy, N. Y., June 16–18, 1955, of The American Society of Mechanical Engineers.

Discussion of this paper should be addressed to the Secretary, ASME, 29 West 39th Street, New York, N. Y., and will be accepted until October 10, 1955, for publication at a later date. Discussion received after the closing date will be returned.

Note: Statements and opinions advanced in papers are to be understood as individual expressions of their authors and not those of the Society. Manuscript received by ASME Applied Mechanics Division, April 29, 1954. Paper No. 55—APM-5.

[6] "A More Fundamental Approach to Plastic Stress-Strain Relations," by D. C. Drucker, Proceedings of the First U. S. National Congress of Applied Mechanics, 1951, pp. 487–491; also "The Theory of the Plastic Distortion of a Polycrystalline Aggregate Under Combined Stresses," and "A Theoretical Derivation of the Plastic Properties of a Polycrystalline Face-Centered Metal," by J. F. W. Bishop and R. Hill, *Philosophical Magazine*, vol. 42, 1951, pp. 414 and 1298.

[7] "Instrumentation and Fundamental Experiments in Plasticity," by D. C. Drucker and F. D. Stokton, to appear in the Proceedings of the Society of Experimental Stress Analysis; also, ONR Technical Report No. 68, Brown University, Providence, R. I., 1952.

[8] "Experimental Evidence of Non-Linearity in Plastic Stress-Strain Relations," by F. D. Stokton, ONR Technical Report No. 88, Brown University, 1953.

If, on the other hand, in producing the subsequent surfaces $f_2$ and $f_3$, the direction of $\overrightarrow{de^p}$ depends on the direction of $\overrightarrow{d\sigma}$, then the existence of a corner or vertex on the loading surface is possible. Alternatively, since at a corner a unique normal vector is not defined, the direction of the plastic-strain-increment vector is restricted only to the directions included between the normals to the surface at adjacent points, Fig. 2; thus the dependence of $\overrightarrow{de^p}$ on $\overrightarrow{d\sigma}$ is possible.

This paper contains experimental results on the evidence of the existence of corners on the yield loci and the possible invalidity of the assumption of linearity of the increment of the plastic strains in the increment of the stresses for an aluminum alloy (24S-T4) which possessed considerable initial anisotropy. Although the experiments were performed on 14 tubular specimens, to conserve space, the results for only six specimens are reported here. (The character of the test data for the other eight is essentially the same as those described.) In all cases the loading program in combined tension and torsion was such that small additional "increments" of stress were applied to an already existing plastic state.

## Specimens and Equipment

The thin-walled specimens were made of 24S-T4 aluminum alloy which possessed considerable initial anisotropy.[9] All specimens used had the nominal dimensions of 0.75 in. ID and 0.075 in. thickness, some of which were work-hardened previously. To indicate the history of each specimen prior to the present investigation, it might be helpful to mention that the tubular specimens numbered 50 and 52 (Figs. 4 and 5) were employed in the previous experiment[5]; all other specimens, however, were virgin.

The testing machine, the extensometer, the recording instruments, and the associated equipment used in this experiment, together with the accuracies of the resulting measurements, have been described in detail elsewhere[5] and will not be repeated here.

## Experimental Results

The experiments conducted were such that the specimens were subjected to an initial tension and torsion (well into the plastic range), followed by increments of tension and torsion. The approximate character of these stress paths is shown in Fig. 3. The

[9] See fig. 4 of reference 5.

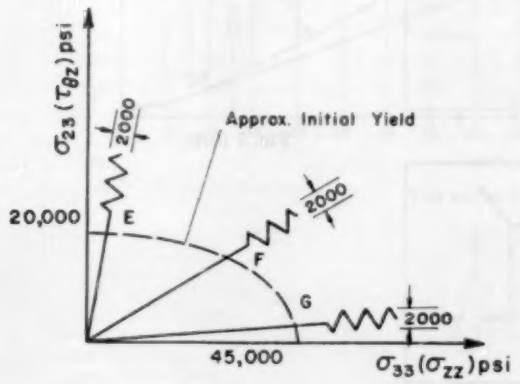


Fig. 3

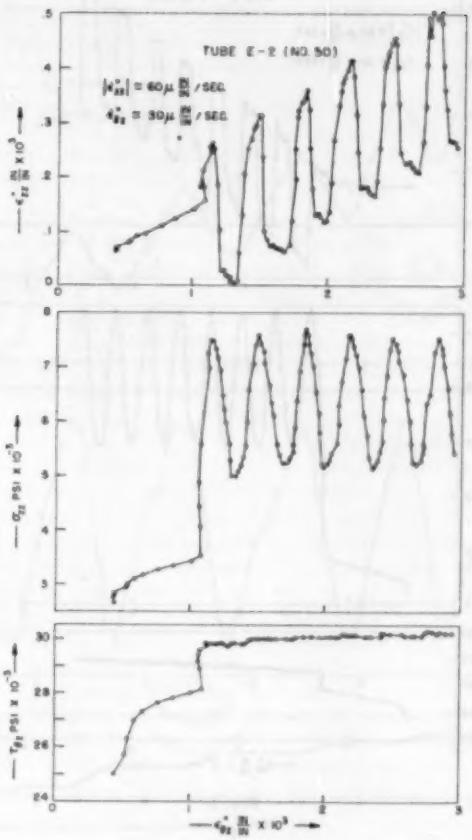
TUBE E-2 (NO. 50)
$|\dot{\epsilon}^p_{zz}|$ = 40μ in/in/sec
$\dot{\epsilon}^p_{\theta z}$ = 30μ in/in/sec
$\epsilon^p_{zz}$ x 10$^{-3}$
$\sigma_{zz}$ PSI x 10$^{-3}$
$\tau_{\theta z}$ PSI x 10$^{-3}$
$\epsilon^p_{\theta z}$ in/in x 10$^{-3}$

Fig. 4

test results for the six tubular specimens are shown in Figs. 4 to 9, inclusive. The test data have been arranged into three groups designated by E, F, and G, according to the region of the stress space, as indicated in Fig. 3. The data for each specimen are presented by three curves showing the variations of the axial and shearing stress, and one of the plastic strains, all plotted versus the other plastic strain (monotonically increasing for that test).

The approximate strain rates for each test also are indicated in Figs. 4 to 9. To emphasize the clarity and convenience of the experimental measurements afforded by the continuous recording of all variables, a facsimile of one of the oscillograph films is reproduced in Fig. 10.

We shall now discuss some of the important features of the experimental results with reference to Figs. 4 to 9. First, we note that for all specimens, $\epsilon_{\theta z}{}^p$ (or $\epsilon_{zz}{}^p$) appears to be uniformly increasing with time, even for small decreasing increments of the shearing stress $\tau_{\theta z}$ (or normal stress $\sigma_{zz}$).[10] This can be seen from Fig. 11 which is a magnified portion of the data of the specimen F-3, Fig. 7. Furthermore, it is clearly seen that there is a strong correlation between the direction of both stress and strain-increment vectors for all three groups of specimens. Specifically, let us consider the details of this correlation for group E specimens, Figs. 4 and 5. The characters of both $\epsilon_{zz}{}^p$ and $\sigma_{\theta z}$ versus $\epsilon_{\theta z}{}^p$

[10] $\epsilon_{\theta z}$ is computed as component of a tensor, ie., $\epsilon_{\theta z} = {}^1/_2\,\gamma_{\theta z}$, $\gamma_{\theta z}$ being the shearing strain in engineering notation.

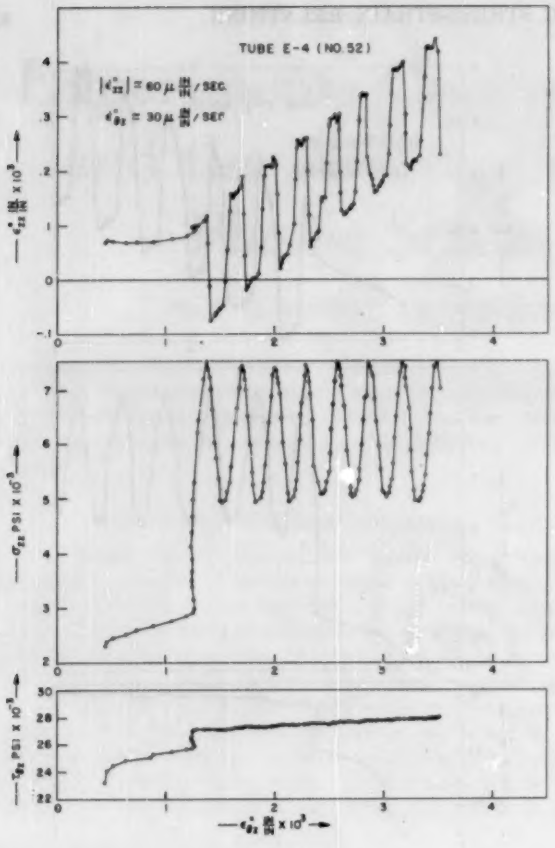
TUBE E-4 (NO. 52)
$|\dot{\epsilon}^*_{zz}| = 60\mu \frac{IN}{IN}$/SEC.
$\dot{\epsilon}^*_{\theta z} = 30\mu \frac{IN}{IN}$/SEC.
$-\dot{\epsilon}^*_{zz} \frac{IN}{IN} \times 10^3$
$-\sigma_{zz}$ PSI $\times 10^3$
$-\tau_{\theta z}$ PSI $\times 10^3$
$-\epsilon^*_{\theta z} \frac{IN}{IN} \times 10^3$

FIG. 5

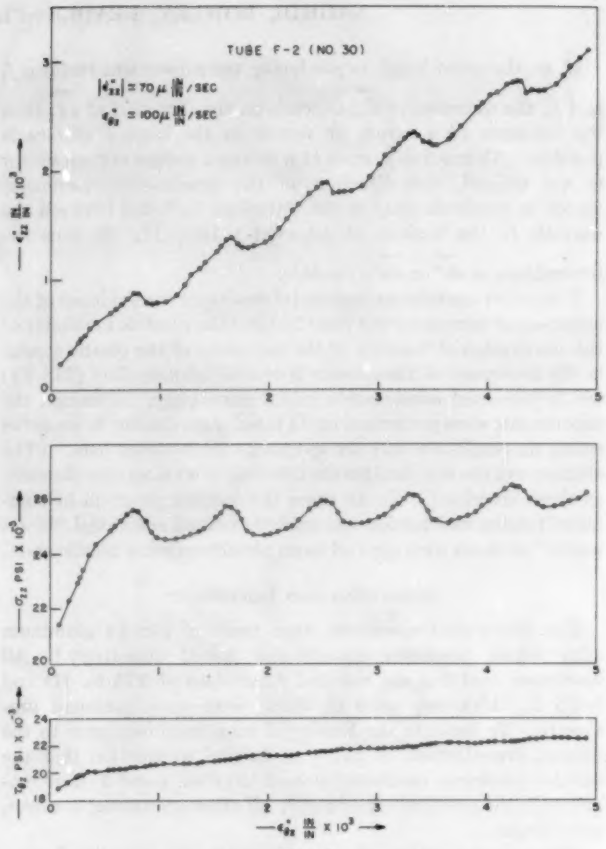
TUBE F-2 (NO. 30)
$|\dot{\epsilon}^*_{zz}| = 70\mu \frac{IN}{IN}$/SEC.
$\dot{\epsilon}^*_{\theta z} = 100\mu \frac{IN}{IN}$/SEC.
$-\dot{\epsilon}^*_{zz} \frac{IN}{IN} \times 10^3$
$-\sigma_{zz}$ PSI $\times 10^3$
$-\tau_{\theta z}$ PSI $\times 10^3$
$-\epsilon^*_{\theta z} \frac{IN}{IN} \times 10^3$

FIG. 6

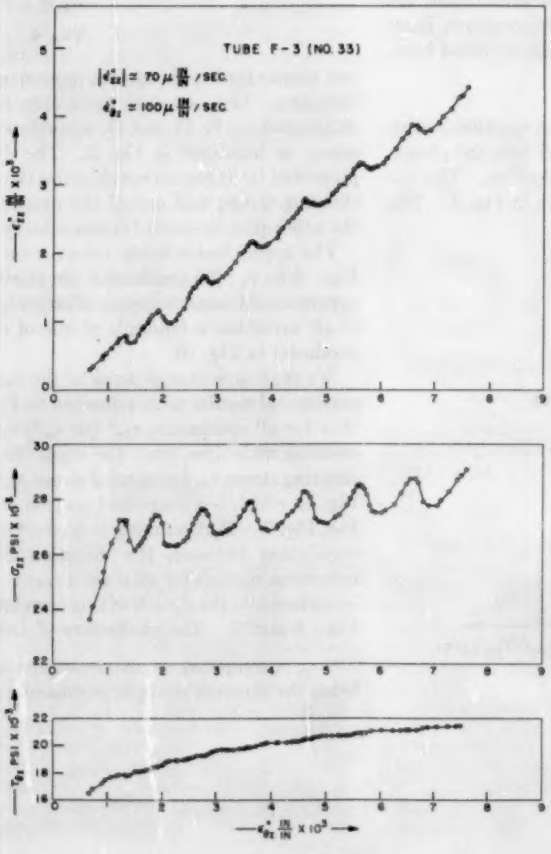
TUBE F-3 (NO. 33)
$|\dot{\epsilon}^*_{zz}| = 70\mu \frac{IN}{IN}$/SEC.
$\dot{\epsilon}^*_{\theta z} = 100\mu \frac{IN}{IN}$/SEC.
$-\dot{\epsilon}^*_{zz} \frac{IN}{IN} \times 10^3$
$-\sigma_{zz}$ PSI $\times 10^3$
$-\tau_{\theta z}$ PSI $\times 10^3$
$-\epsilon^*_{\theta z} \frac{IN}{IN} \times 10^3$

FIG. 7 (*left*)

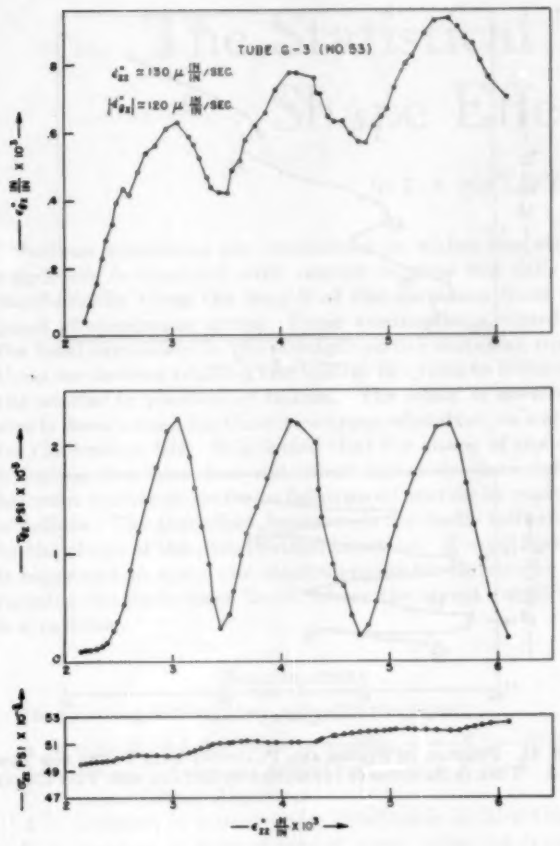


FIG. 8

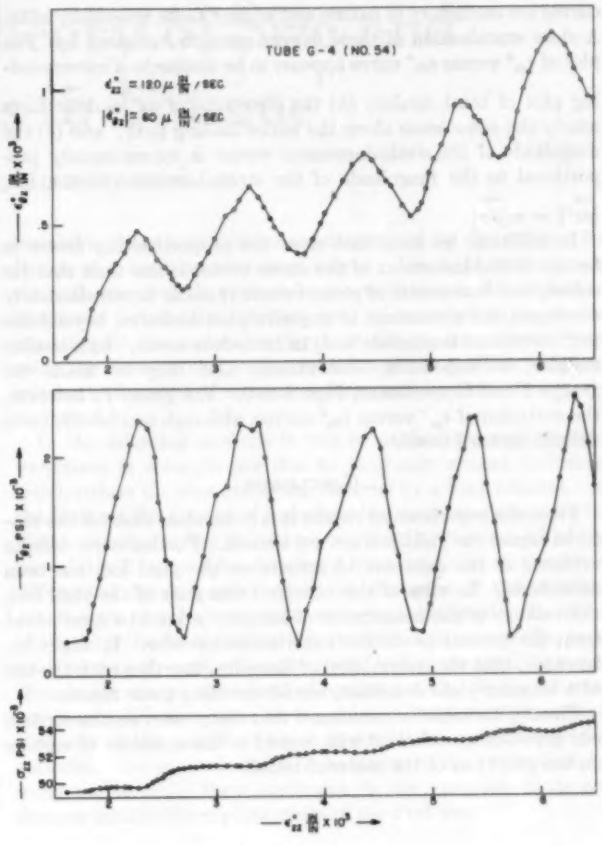


FIG. 9

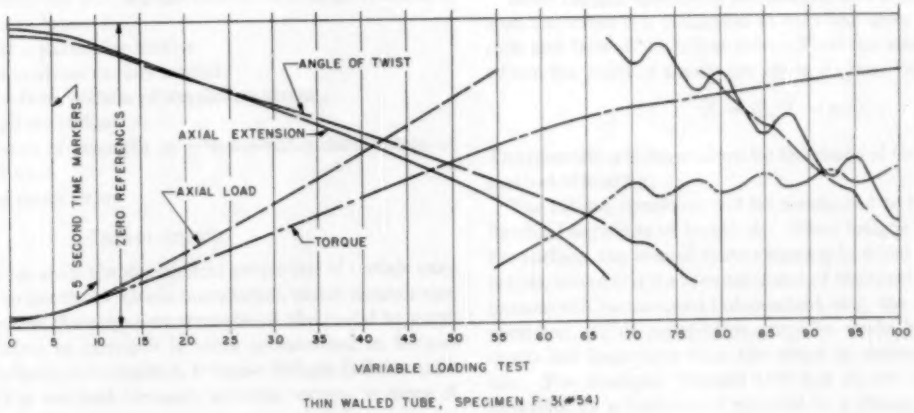


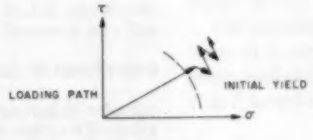


FIG. 10

curves are oscillatory in nature and appear to be essentially alike. A close examination of these curves seem to indicate: (*a*) The plot of $\epsilon_{zz}^{p}$ versus $\epsilon_{\theta z}^{p}$ curve appears to be similar to a corresponding plot of total strains; (*b*) the directions of $\overrightarrow{d\epsilon^p}$ and $\overrightarrow{d\sigma}$ have nearly the same sense along the entire loading path; and (*c*) the magnitude of the strain-increment vector is approximately proportional to the magnitude of the stress-increment vector, i.e., $|\overrightarrow{d\epsilon^p}| = m|\overrightarrow{d\sigma}|$.

In addition, we note that since the proportionality factor $m$ for the initial increment of the stress vector is less than that for subsequent increments of stress (where it seems to remain nearly constant), the occurrence of negative plastic strains, beyond the first increment is possible and, in fact, does occur. In a similar manner, corresponding observations also may be made for groups F and G specimens, Figs. 6 to 9. For group F, however, the variation of $\epsilon_{zz}^{p}$ versus $\epsilon_{\theta z}^{p}$ curves, although oscillatory, has a definite upward trend.

## Conclusion

From the experimental results it is quite clear that for the material tested the yield loci are not smooth. Furthermore, definite evidence of the existence of corners on the yield loci has been established. In view of this observed character of the yield loci, the validity of the assumption of linearity cannot be ascertained from the present or similar experimental results. It might be, however, that the assumption of linearity, together with the use of a singular yield condition, would correlate these results.

Finally, it should be mentioned that the present results confirm our previous speculation[5] with regard to the existence of corners on the yield loci of the material tested.

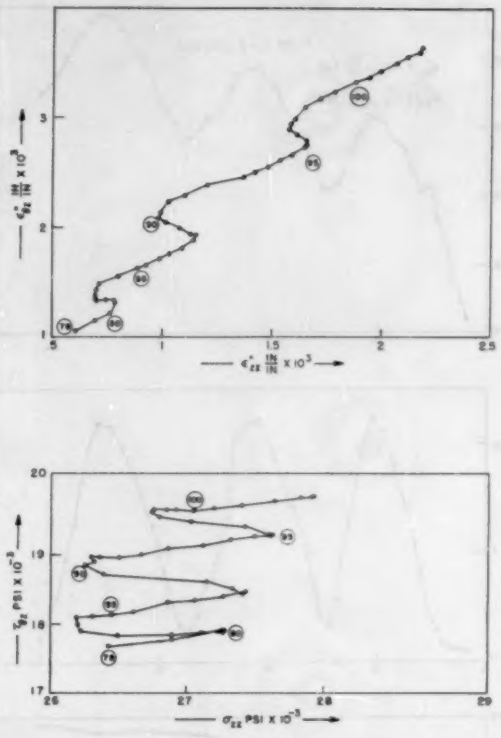


Fig. 11 Portion of Stress and Plastic-Strain Paths for Tube F-3. Time in Seconds Is Indicated to Relate the Two Curves

# The Statistical Theory of Size and Shape Effects in Fatigue[1]

By F. A. McCLINTOCK,[2] CAMBRIDGE, MASS.

**Fatigue specimens are considered in which the stress amplitude is constant with respect to time but falls off parabolically along the length of the specimen from the point of maximum stress. From assumptions regarding the local variability in the strength of the material, equations are derived relating the scatter in cycles to failure to the scatter in position of failure. The effect of specimen size is determined for these two types of scatter, as well as for the average life. It is found that the shape of the distribution function does not affect seriously the relation between scatter in cycles to failure and scatter in position of failure. The size effect, however, is markedly influenced by the shape of the distribution function. A modification is suggested to make the results applicable to tests to determine the endurance limit, where the stress amplitude is a variable.**

## Nomenclature

The following nomenclature is used in the paper:

- $a$ = constant relating stress to position, $a = (S_m - S)/S_m z^2$
- $b$ = strength of segment defined by $b = S + K \log N$
- $C$ = circumference of specimen
- $k$ = exponent in extreme-value distribution of third kind
- $K$ = negative of slope of plot of stress versus log (cycles)
- $N$ = number of cycles to failure
- $p(b)$ = probability per unit surface area of finding an element of strength below $b$
- $S$ = stress at a particular section
- $S_m$ = maximum stress on any section
- $z$ = distance from section of maximum stress
- $\sigma$ = standard deviation
- $\omega$ = lower limit of strength in extreme-value distribution of third kind
- $\bar{\ }$ denotes mean value

## Introduction

On a microscopic scale the mechanical properties of metals vary from one point to another. Grain boundaries, phase boundaries, and inclusions cause the apparent strength of the metal to vary. This local variation in strength is more pronounced in fatigue testing than in plastic deformation, because fatigue failures arise from failure of the weakest element, whereas, except in cases of instability, plastic properties are determined by the average behavior of a large number of elements. The local variations in strength manifest themselves in the variation in life of fatigue specimens tested at a constant level of repeated stress, in the variation of the endurance limit or the rupture stress found using the Prot method, in the variation of the position of failure relative to the point of maximum stress, and to some extent in the size effect.

In the following analysis it will be at first assumed that the variations in strength are due to randomly spaced inclusions which reduce the strength of the material by a fixed amount. In the limit, as the density of inclusions increases, and when the inclusions cause varying reductions in strength, the strength of the material will be considered to vary from one point to another a differential distance away as if the strengths of the different points were samples from some statistical distribution function. These hypotheses regarding the statistical nature of the local variations in strength will be developed to find the resulting variations in life at a constant level of repeated stress, the variation in position of failure relative to the point of maximum stress, and that part of the size effect which is due to the variability of the material. An approximate interpretation of the results will be suggested to make them applicable to the variation in the endurance limit or the rupture stress of the Prot test.

## Assumptions

Most fatigue specimens are shaped and loaded in such a way that the stress is a maximum at only one cross section of a specimen and falls off on either side. Thus the stress $S$ at a distance $z$ from the point of maximum stress $S_m$ may be approximated by

$$S = S_m(1 - az^2) \quad [1]$$

The quantity $a$ is determined by the shape of the specimen and the method of loading.

The fatigue specimen will be considered to be made up of differential segments of length $dz$. Since fatigue failures initiate at the surface, the area of these elements in which failure may occur is $C\,dz$, where $C$ is the circumference of the specimen. The circumference will be assumed independent of $z$, the distance along the specimen. This assumption may be made because the size is much less important than the stress in determining the fatigue life. For example, Caxaud (1)[3] has shown that changing the diameter by a factor of 4 resulted in a change in strength by a factor of only 1.2.

For moderate ranges of stress it is reasonable to assume that there is a semilogarithmic relation between the stress on any given segment $S$ and the number of cycles to failure of the segment $C\,dz$ if tested alone, $N_{C\,dz}$; that is

$$S + K \log N_{C\,dz} = b \quad [2]$$

The parameter $K$, corresponding to the negative of the slope of a plot of $S$ versus $\log N_{C\,dz}$ will be assumed constant, but the quantity $b$, which is constant for any one segment, will vary from

---

[1] This research was supported by the United States Air Force, through the Office of Scientific Research of the Air Research and Development Command.

[2] Assistant Professor of Mechanical Engineering, Massachusetts Institute of Technology. Assoc. Mem. ASME.

Presented at the National Conference of the Applied Mechanics Division, Troy, N. Y., June 16–18, 1955, of The American Society of Mechanical Engineers.

Discussion of this paper should be addressed to the Secretary, ASME, 29 West 39th Street, New York, N. Y., and will be accepted until October 10, 1955, for publication at a later date. Discussion received after the closing date will be returned.

Note: Statements and opinions advanced in papers are to be understood as individual expressions of their authors and not those of the Society. Manuscript received by ASME Applied Mechanics Division, December 9, 1954. Paper No. 55—APM-25.

[3] Numbers in parentheses refer to the Bibliography at the end of the paper.

one segment to another as a consequence of their variations in strength.

Finally, the probabilities of failure in the various segments will be assumed independent of each other. This is satisfied if failure is defined as the production of a crack of size small compared to the usual scatter in position of failure. Since the scatter in position of failure is of the order of the specimen thickness, and since cracks of even one-tenth the thickness of the specimen will grow to failure in a relatively small number of cycles, the following analysis should be valid even if the number of cycles to failure is considered to be the number of cycles to complete fracture.

### Flaws With Fixed Reduction in Strength

Suppose that the strength of a specimen is constant except for the presence of randomly distributed flaws which reduce the strength by an amount $r$. Failure will occur at the flaw nearest the center of the specimen if that flaw reduces the strength by more than the difference in stress between the center and the section containing the flaw. Thus failure can occur at a flaw whenever

$$r > S_m - S_m(1 - az^2) \quad \text{or} \quad z < \sqrt{r/aS_m}$$

Let the probability of finding a flaw in a segment of area $C\Delta z$ be $pC\Delta z$. Then the probability of not finding a flaw in any of the $2|z|/\Delta z$ segments between $-z$ and $+z$ is $(1 - pC\Delta z)^{2|z|\Delta z}$. In the limit as $\Delta z$ goes to zero this becomes $e^{-2pC|z|}$. Thus the probability of no failure within $z$ and failure between $z$ and $z + dz$ is

$$f(z)dz = e^{-2pC|z|}pC\,dz \quad \ldots\ldots [3]$$

The fraction of specimens which fail at a flaw will be

$$\int_{-\sqrt{r/aS_m}}^{\sqrt{r/aS_m}} f(z)dz = 1 - e^{-2pC\sqrt{r/aS_m}} \quad \ldots\ldots [4]$$

The remaining specimens will fail at the center. The life of a specimen failing at $z$ is found from

$$S_m(1 - az^2) + K \log N = b - r \quad \ldots\ldots [5]$$

The distribution of the logarithm of cycles to failure is found by changing the variable from $z$ to $K \log N$

$$(K \log N) = f(z)dz/dK \log N$$

$$= \frac{e^{-2pC\sqrt{(b-r-S_m-K\log N)/S_m a}}\, pCdK \log N}{2S_m a\sqrt{(b - r - S_m - K \log N)/S_m a}} \quad \ldots\ldots [6]$$

The resulting bivariate distribution function is sketched in Fig. 1. On the right is the marginal distribution of log (cycles). This latter distribution has peaks of infinite density at its lower and upper limits. Since experimental data (2) indicate a single, finite

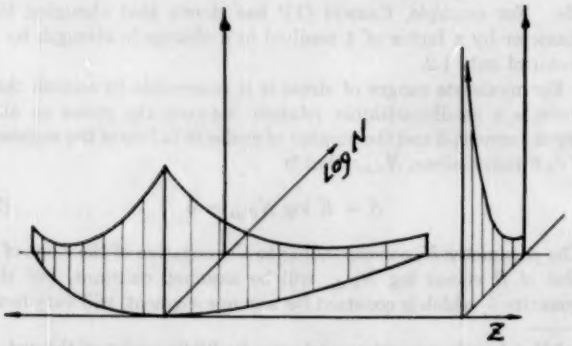


Fig. 1 Distribution of Cycles and Position of Failure for Flaws of Constant Severity

mode, one cannot consider a specimen to be of constant strength except for inclusions of fixed magnitude which are not present in all specimens.

### Flaws With Varying Reductions in Strength

The strength of a segment is the value of $S + K \log N$ at which failure occurs. Let the probability of finding a strength of $S + K \log N$ or less in a segment of area $C\,dz$ be $p(S + K \log N)\,C\,dz$. Then the probability that a segment would fail before $N$-cycles if tested alone at a stress $S$ is also

$$P_{C\,dz \text{ would fail before } N} = p(S + K \log N)C\,dz$$

The probability that a segment will fail between the cycles corresponding to $K \log N$ and $K \log N + d(K \log N)$ if tested alone at a stress $S$ is

$$p'(S + K \log N)\,C\,dz\,dK \log N$$

The probability that it would not fail before $N$-cycles if tested alone at the stress $S$ is

$$P_{C\,dz \text{ would not fail before } N} = 1 - p(S + K \log N)C\,dz$$

Since segments of differential size are being considered, this can also be expressed as

$$P_{C\,dz \text{ would not fail before } N} = \exp\,[-p(S + K \log N)C\,dz]$$

Now the failure of the complete specimen occurs when the first segment fails. For this to happen at $N$ cycles one of the segments must fail at $N$ cycles and none of the other segments can have failed sooner. Assuming independence of the probabilities of nonfailure of each of the segments, the probability of nonfailure of all of the other segments is the product of the probabilities of the nonfailure of each. Since each of the probabilities of nonfailure is in exponential form, the product can be expressed as the exponential of a sum, or in the limit as the exponential of an integral

$$P_{\text{specimen does not fail before } N} = \exp\,[-\int p(S + K \log N)C\,dz] \quad \ldots\ldots [7]$$

A similar expression has been obtained by Fowler (3).

Thus the probability of failure of the specimen in the segment $C\,dz$ between the number of cycles corresponding to $K \log N$ and $K \log N + d(K \log N)$ is

$$f dz\,dK \log N = \exp\,[\int -p(S + K \log N)C\,dz]\, p'(S + K \log N)C\,dz\,dK \log N \quad \ldots\ldots [8]$$

Introducing Equation [1] to relate the stresses to the positions of the segments, one obtains

$$f dz\,dK \log N = \exp\,[\int -p\{S_m(1 - az^2) + K \log N\}C\,dz]\, p'\{S_m(1 - az^2) + K \log N\}\,C\,dz\,dK \log N \quad \ldots\ldots [9]$$

The choice of the function $p(S + K \log N)$ should be based on the ease of developing Equation [9] as well as on agreement with expected behavior. If there is a limiting strength below which all segments will fail, the value of $p$ must become infinite at that point in order for the probability of not failing below that strength, given by Equation [7], to vanish. In order to simulate a material having an upper limit to its strength of $b$, $p$ was chosen to vary as the reciprocal, the logarithm of the reciprocal, the cotangent, and the cosecant of $(b - S - K \log N)$. It was not found possible to evaluate the desired means and standard deviations explicitly in any of these cases.

Turning to functions giving no definite upper limit to the strength, two which can be integrated to give explicit answers are

$$p = p_1 e^{a[S_m - S_m a z^2 + K \log N]} \quad \ldots\ldots [10]$$

and

$$p = p_2 (S_m - S_m a z^2 + K \log N - \omega)^k \quad \ldots\ldots [11]$$

The first of these applies to all values of $S_m - S_m a z^2 + K \log N$, the second only to those greater than $\omega$. The substitutions $p_1 = e^{-a\omega}$ and $p_2 = 1/(v_1 - \omega)^k$ put these functions into the form of asymptotic extreme-value distributions of the first and third kind as given by Gumbel (4). The asymptotic extreme-value distribution of the first kind is that which would be obtained if the specimen were considered to be made up of an indefinitely large number of segments having strength normally distributed. The asymptotic extreme-value distribution of the third kind is that which would be obtained if the strengths of the segments followed a distribution function having a definite lower limit to the possible strengths. It is only necessary to study the distribution of the third kind since, as Kendall[4] points out, when the lower limit of the strength goes to zero and the exponent $k$ goes to infinity, this distribution approaches that of the first kind as a limit.

It is desired to find the mean logarithm of the cyles to failure $\overline{\log N}$, the standard deviation of the logarithm of cycles to failure $\sigma_{\log N}$, the standard deviation of the position of failure $\sigma_z$, and a correlation coefficient $r$. These are found from the distribution function $f$, given by Equation [9], as follows

$$K \overline{\log N} = \int_{-\infty}^{\infty} K \log N \int_{-\infty}^{\infty} f \, dz \, dK \log N \quad \ldots\ldots [12]$$

$$K\sigma_{\log N} = \sqrt{\int_{-\infty}^{\infty} (K \log N)^2 \int_{-\infty}^{\infty} f \, dz \, dK \log N - (K \overline{\log N})^2} \quad \ldots\ldots [13]$$

and since by symmetry the mean position of failure is at $z = 0$

$$\sigma_z = \sqrt{\int_{-\infty}^{\infty} z^2 \int_{-\infty}^{\infty} f dK \log N \, dz} \quad \ldots\ldots [14]$$

Judging from the example already worked out, the correlation between the logarithm of life and position of failure is likely to be quadratic. Therefore the correlation coefficient will be based on the square of the position of failure

$$r = \frac{1}{K\sigma_{\log N}\sigma_{z^2}} \int_{-\infty}^{\infty} (K \log N - K \overline{\log N}) \int_{-\infty}^{\infty} (z^2 - \bar{z}^2) dz \, dK \log N \quad \ldots\ldots [15]$$

### Extreme-Value Distribution of the Third (Limited) Kind

For convenience define

$$\left.\begin{aligned} v &\equiv p_2^{1/k}(S_m + K \log N - \omega) \\ &\text{and} \\ \zeta &\equiv p_2^{1/2k} S_m^{1/2} a^{1/2} z \equiv \sqrt{\beta S_m a}\, z \end{aligned}\right\} \quad \ldots\ldots [16]$$

The integral appearing in Equation [7] is evaluated by a change of variable to $\xi = \zeta^2/v$ in order to apply Dwight[5]

$$\int_{-\sqrt{v}}^{\sqrt{v}} \frac{(v - \zeta^2)^k C \, d\zeta}{\sqrt{\beta S_m a}} = \frac{C v^{k+1/2}}{\sqrt{\beta S_m a}} \frac{\sqrt{\pi}\,\Gamma(k+1)}{\Gamma(k+3/2)}$$

The factor $p'$ is obtained by differentiating Equation [11]

$$p' = \beta k (v - \zeta^2)^{k-1}$$

Thus the frequency distribution function of $v$ and $\zeta$, corresponding to life and position of failure is

$$f \, d\zeta dv = \frac{e^{-\frac{C v^{k+1/2}}{\sqrt{\beta S_m a}} \frac{\sqrt{\pi}\,\Gamma(k+1)}{\Gamma(k+3/2)}} k (v - \zeta^2)^{k-1} C d\zeta dv}{\sqrt{\beta S_m a}} \quad \ldots [17]$$

The marginal distribution of $v$ is found by again changing the variable $\zeta$ to $\zeta^2/v \equiv \xi$ and obtaining the integral from Dwight[5]

$$\int_{-\sqrt{v}}^{\sqrt{v}} f d\zeta = e^{-\frac{C v^{k+1/2} \sqrt{\pi}\Gamma(k+1)}{\sqrt{\beta S_m a}\,\Gamma(k+3/2)}} \frac{v^{k-1/2} k C \sqrt{\pi}\,\Gamma(k)}{\sqrt{\beta S_m a}\,\Gamma(k+1/2)} \quad \ldots\ldots [18]$$

Note that, if the stress had been constant throughout an element of length $z$, the distribution would have been

$$e^{-v^k C z} k C z v^{k-1}$$

Thus the variation of stress along the length of the specimen changes the shape of the distribution of life by decreasing the exponent $k$ by $1/2$.

The mean value of the logarithm of life is found by a change of variable and with the aid of the gamma function

$$K\overline{\log N} = \omega - S_m + \frac{\Gamma\left\{1 + \frac{2}{(2k+1)}\right\}}{p_2^{1/k}} \left[\frac{\sqrt{p_2^{1/k} S_m a}\,\Gamma(k+3/2)}{C\sqrt{\pi}\,\Gamma(k+1)}\right]^{2/(2k+1)} \quad \ldots\ldots [19]$$

Similarly, the standard deviation of the logarithm of the life is

$$K\sigma_{\log N} = \left[\frac{\sqrt{p_2^{1/k} S_m a}\,\Gamma(k+3/2)}{C\sqrt{\pi}\,\Gamma(k+1)}\right]^{2/(2k+1)} \left(\frac{1}{p_2^{1/k}}\right) \sqrt{\Gamma\left(1 + \frac{4}{2k+1}\right) - \Gamma^2\left(1 + \frac{2}{2k+1}\right)} \quad \ldots\ldots [20]$$

The standard deviation of position of failure is found by first integrating with respect to $\zeta$ and then with respect to $v$, again expressing the results in terms of the gamma function

$$\sigma_z = \sqrt{\frac{1}{p_2^{1/k} S_m a (2k+1)} \left[\frac{\sqrt{p_2^{1/k} S_m a}\,\Gamma(k+3/2)}{C\sqrt{\pi}\,\Gamma(k+1)}\right]^{2/(2k+1)} \Gamma\left(1 + \frac{2}{2k+1}\right)} \quad \ldots\ldots [21]$$

The correlation coefficient is found after similar, but lengthier, computations to be

$$r = \sqrt{\frac{\Gamma\left(1 + \frac{4}{2k+1}\right) - \Gamma^2\left(1 + \frac{2}{2k+1}\right)}{[3(2k+1)/(2k+3)]\,\Gamma\left(1 + \frac{4}{2k+1}\right) - \Gamma^2\left(1 + \frac{2}{2k+1}\right)}} \quad \ldots\ldots [22]$$

[4] Reference (5), p. 222.

[5] Reference (6), 855.1.

The scatter in cycles to failure and the scatter in position of failure are shown by Equations [20] and [21] to be related as follows

$$K\sigma_{\log N} = S_m a \sigma_s^2 (2k+1) \sqrt{\frac{\Gamma\left(1+\frac{4}{2k+1}\right)}{\Gamma^2\left(1+\frac{2}{2k+1}\right)} - 1} \quad \ldots [23]$$

For specimens of two different sizes with the same concentration of flaws per unit area, $p$

$$\frac{\overline{\log N_1} - \overline{\log N_2}}{\sigma_{\log N1}} = \frac{\Gamma\left(1+\frac{2}{(2k+1)}\right)}{\sqrt{\Gamma[1+4/(2k+1)] - \Gamma^2[1+z/(2k+1)]}} \left[\left(\frac{\sqrt{a_1}}{C_1}\right)^{2/(2k+1)} - \left(\frac{\sqrt{a_2}}{C_2}\right)^{2/(2k+1)}\right] \quad \ldots [24]$$

$$\frac{\sigma_{\log N1}}{\sigma_{\log N2}} = \left[\frac{a_1 C_2^2}{C_1^2 a_2}\right]^{1/(2k+1)} \quad \ldots [25]$$

and

$$\frac{\sigma_{s1}}{\sigma_{s2}} = \sqrt{\frac{a_2}{a_1}\left[\frac{a_1 C_2^2}{C_1^2 a_2}\right]^{1/(2k+1)}} \quad \ldots [26]$$

In the limit as $k \to 0$, the results obtained approach those found from Equations [3] and [6], considering the strength of segments without flaws to be infinite so that all specimens fail at inclusions with the same strength. As mentioned previously, as $k \to \infty$ the extreme-value distribution of the first kind is approached. The question arises as to how an appropriate value of $k$ may be determined from experimental data.

As the parameter $k$ increases, the lower limit of the distribution of lives gets farther and farther below the mean. This relation is given by

$$\frac{\overline{\log N} - \log N_{\min}}{\sigma_{\log N}} = \frac{\Gamma\left(1+\frac{2}{2k+1}\right)}{\sqrt{\Gamma\left(1+\frac{4}{2k+1}\right) - \Gamma^2\left(1+\frac{2}{2k+1}\right)}} \quad \ldots [27]$$

and is plotted in Fig. 2. But this relation is not too useful for estimating $k$, since one is never quite sure he has observed the lowest possible life.

A second means of estimating $k$ might be from the skewness of the distribution of log (cycles), defined in terms of the second and third moments of the distribution about the mean, $\mu_2$ and $\mu_3$

$$\alpha_3 = \frac{\mu_3}{\mu_2^{3/2}} = \frac{\Gamma\left(1+\frac{6}{2k+1}\right) - 3\Gamma\left(1+\frac{4}{2k+1}\right)\Gamma\left(1+\frac{2}{2k+1}\right) + 2\Gamma^3\left(1+\frac{2}{2k+1}\right)}{\left[\Gamma\left(1+\frac{4}{2k+1}\right) - \Gamma^2\left(1+\frac{2}{2k+1}\right)\right]^{3/2}} \quad \ldots [28]$$

This function is plotted in Fig. 3.

In order to know how accurately $k$ may be determined using this relation, one must have some idea of the variability of the estimate of the third moment. From Kendall[6] it follows that the standard deviation of the estimate of the skewness is about $2.5/\sqrt{n}$ for $k = 3$ and increases to $8/\sqrt{n}$ as $k \to \infty$ and to $200/\sqrt{n}$ as $k \to 0$. Thus if a sample of even as large as 100 were taken and found to have zero skewness, on an approximate 95 per cent confidence basis, one could only conclude that $k$ lay between $1\frac{1}{2}$ and 10. If the skewness turned out to be —1.0, one could say almost nothing at all about the value of $k$.

[6] Reference (5), pp. 50 and 224.

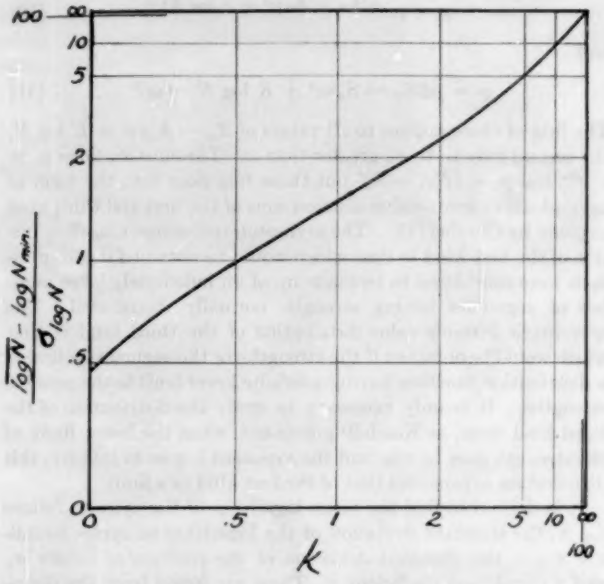


FIG. 2 LEAST VALUE OF LIFE, $N_{\min.}$, AS A FUNCTION OF EXPONENT $k$

A third possible method of evaluating $k$ would be by deducing it from the correlation between cycles to failure and position of failure. The relation between $r$ and $k$, given by Equation [22], is shown in Fig. 3. For values of the correlation coefficient of 0.2 or less, which are those of primary interest, the standard deviation of the estimate of the correlation coefficient may be very roughly approximated by $1/\sqrt{n}$ where $n$ is the number of observations.[7] Thus even 100 observations yield an estimate of the correlation coefficient which is only good to $\pm 0.2$ (95 per cent confidence), and hence useless for estimating $k$.

A final method for evaluating $k$ might be through the dependence on it of the relation between scatter in cycles to failure and scatter in position of failure, Equation [23]. This relation is plotted in Fig. 3. There is little dependence on $k$. Considering the width of the confidence intervals obtained in estimating the standard deviations, this method is hopeless for deciding what value of $k$ corresponds to the data. On the other hand, it appears that the ratio $K\sigma_{\log N}/S_m a \sigma_s^2$ is nearly constant, and may be assumed to be 2.0 to 2.6 regardless of the shape of the distribution function. Further evidence for this is presented by the results obtained assuming a finite number of segments with strengths normally distributed. In that case the ratio $K\sigma_{\log N}/S_m a \sigma_s^2$ was found by numerical integration to be 2.2 (7).

## THE SIZE EFFECT

With the shape of the distribution function, as indicated by the exponent $k$, so difficult to determine, one would hope that the choice of $k$ would be unimportant. Such is not the case, for the effect of size on the statistics is influenced by $k$. Equations [24] to [26] giving mean log (cycles) and standard deviations of log (cycles) and position of failure are plotted as functions of $k$ in Figs. 3 and 4 for geometrically similar specimens with a length ratio $L_2/L_1$ of 10. Perhaps a very carefully planned and executed test

[7] Reference (5), pp. 211 and 245.

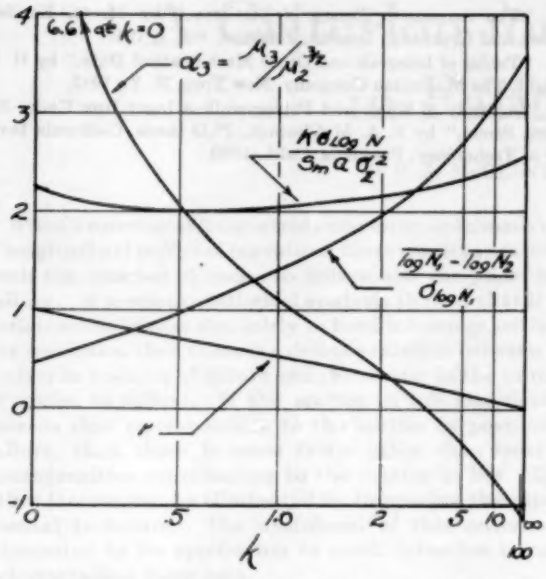


FIG. 3 SKEWNESS $\alpha_3$, CORRELATION COEFFICIENT $r$, RELATION OF SCATTER IN POSITION TO SCATTER IN LIFE, AND EFFECT OF SIZE ON MEAN LIFE AS FUNCTIONS OF EXPONENT $k$

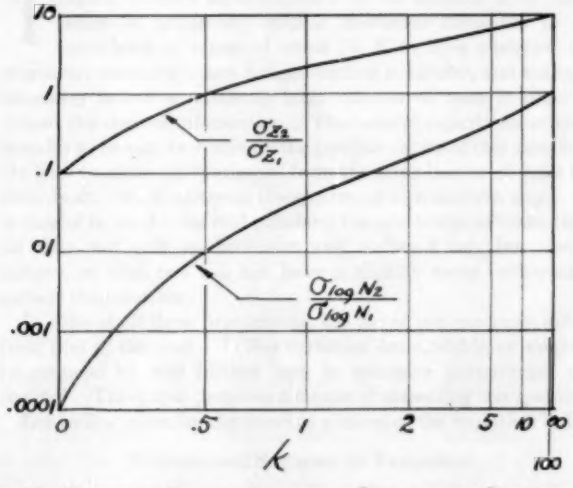


FIG. 4 EFFECT OF SIZE ON SCATTER IN LIFE AND ON SCATTER IN POSITION AS FUNCTIONS OF EXPONENT $k$

program will enable one to determine the shape of the distribution function from these relations. In the meantime these equations and figures can only be counted on to give the order of magnitude of that part of the size effect which is due to the variability of the material.

## ENDURANCE LIMIT AND PROT METHOD

In tests designed to determine the endurance limit the stress at failure is itself a variable. For an extreme-value distribution of the third kind, the joint distribution of stress at failure and position of failure is given by

$$f\,dz\,dS_m = e^{-\int p_3(S_m - S_m a z^2 - \omega)^k C\,dz}\, k p_2 (s_m - s_m a z^2 - \omega)^{k-1} C\,dz\,dS_m \quad \ldots\ldots [29]$$

Attempts to find means and standard deviations for this distribution function were unsuccessful, since the maximum stress in the specimen, $S_m$, is now a variable and is combined more closely with $z$ than was $\log N$. But a simplification is possible if the quantity $S_m - S_m a z^2$ is rewritten as

$$S_m - S_m a z^2 = \bar{S}_m - \bar{S}_m a z^2 - (S_m - \bar{S}_m) a z^2$$

for the stress difference between the point $z$ and the point of maximum stress is small compared to the maximum stress. Also, the difference between the maximum stress for one specimen and the average of the maximum stresses for all specimens is small compared to the maximum stress. Thus the third term in the foregoing expression is of smaller order of magnitude than the second and may be neglected to a first approximation. With this approximation the means and standard deviations can be evaluated, giving for the mean of the maximum stresses in specimens at failure

$$\bar{S}_m = \omega + \frac{\Gamma\left(1 + \frac{2}{2k+1}\right)}{p_2^{1/k}} \left[ \frac{\sqrt{p_2^{1/k}\,\bar{S}_m a}\;\Gamma(k + 3/2)}{C\sqrt{\pi}\;\Gamma(k+1)} \right]^{\frac{2}{2k+1}} \quad \ldots\ldots [30]$$

Equations [20] and [21] are as before with the substitution of $\bar{S}_m$ for $S_m$ and $\sigma_{S_m}$ for $\sigma_{K \log N}$.[8]

The accuracy of this approximation can be checked in the special case for which $\omega = 0$, so that the statistics of the distribution function can be evaluated explicitly. The approximation should be good only where the ratio $\sigma_{S_m}/\bar{S}_m$ is small, say, less than 0.10. It turns out that

$$\frac{\sigma_{S_m}}{\bar{S}_m} = \sqrt{\frac{\Gamma\left(1 + \frac{2}{k}\right) - \Gamma^2\left(1 + \frac{1}{k}\right)}{\Gamma^2\left(1 + \frac{1}{k}\right)}} \quad \ldots\ldots [31]$$

Correspondingly, $k$ should be greater than about 12.5. The statistics of primary interest are tabulated for $k = 12$, $L_2/L_1 = 10$ in the following

| | Approximate | Exact |
|---|---|---|
| $r$ | 0.070 | 0 |
| $\sigma_{S_m}/\bar{S}_m a \sigma_z^2$ | 2.438 | 2.434 |
| $(\bar{S}_{m1} - \bar{S}_{m2})/\sigma_{S_{m1}}$ | 3.181 | 3.165 |
| $\sigma_{S_{m2}}/\sigma_{S_{m1}}$ | 0.702 | 0.692 |
| $\sigma_{z2}/\sigma_{z1}$ | 8.38 | 8.32 |

In this case, at least, the approximation is as accurate as would be expected.

## CONCLUSION

The size effect in fatigue testing is due to many factors, one of which is the inherent variability of the material. The importance of this factor depends on the shape of the statistical distribution function describing the variability. Since the statistics determined from tests on one size of specimen are insensitive to the shape of the distribution function, a careful experimental study of specimens of different sizes will be required to determine how much of the size effect is due to variability in the material and how much to other factors.

## BIBLIOGRAPHY

1 "Fatigue of Metals," by R. Casaud, Chapman & Hall, London, England, 1953, p. 159.

[8] In conventional tests to determine the endurance limit, a truncated distribution is observed. Equation [28] for the standard deviation of position of failure will not apply if the correlation between life and position of failure is important.

2 "Symposium on Statistical Aspects of Fatigue," ASTM Special Technical Publication No. 121, 1951.

3 "On Fatigue Failure Under Triaxial Static and Fluctuating Stresses and a Statistical Explanation of the Size Effect," by F. H. Fowler, Trans. ASME, vol. 67, 1945, pp. 213–216.

4 "Statistical Theory of Extreme Values and Some Practical Applications," by E. J. Gumbel, National Bureau of Standards, Applied Mathematics Series No. 33 1954.

5 "The Advanced Theory of Statistics," by M. G. Kendall, Griffen and Company, London, England, vol. 1, 1947.

6 "Tables of Integrals and Other Mathematical Data," by H. B. Dwight, The Macmillan Company, New York, N. Y., 1947.

7 "A Study of Single and Polycrystalline Ingot Iron Under Repeated Stress," by F. A. McClintock, PhD thesis, California Institute of Technology, Pasadena, Calif., 1950.

# A Criterion for Minimum Scatter in Fatigue Testing[1]

By F. A. McCLINTOCK,[2] CAMBRIDGE, MASS.

**When a number of fatigue tests are run on specimens with a longitudinal radius of curvature, there results a scatter in both the number of cycles to failure and the position of failure. A previous statistical analysis showed that if the variations in life are due solely to local inhomogeneities in the specimen, then there is a definite relation between the scatter in position of failure and the scatter in the number of cycles to failure. If the scatter in life significantly exceeds that corresponding to the scatter in position of failure, then there is some factor other than local inhomogeneities contributing to the scatter in life. Such other factors can be eliminated by improving the experimental technique. The usefulness of this criterion is illustrated by its application to crack detection tests on polycrystalline ingot iron.**

## Introduction

THERE is often wide variation in the number of cycles to failure of apparently similar specimens subjected to the same level of repeated stress (1, 2).[3] This variation obscures the results of many fatigue-testing programs, and makes it necessary to run a relatively large number of tests in order to obtain the desired information. The careful experimenter tries, in so far as he can, to eliminate the possible causes of this variation. He tries to make his specimens from the same bar or at least the same heat. He heat-treats the specimens in a uniform way. He is careful in machining and polishing the specimens to make them all alike, not only in dimension and surface finish, but also in history, so that one will not have a slightly more cold-worked surface than another.

In spite of all these precautions, the life of one specimen differs from that of the next. Is this variation unavoidable or might it be reduced by still further care in specimen preparation and testing? This paper proposes a means of answering this question.

Let us first examine the possible sources of the variation in life.

## Microscopic Sources of Variation

Metals are not truly homogeneous. The boundaries between the various crystals are sources of stress concentration arising from the dependence of the stiffness of a crystal on its orientation. Should these grain boundaries all be favorable in a given specimen, the life at a given nominal stress would be longer. There are crystals of different phases present. There are inclusions of nonmetallics, which are weak and also are sources of stress concentration. All these factors vary within a tiny region of the order of 0.01 in., and there is little that the experimenter can do to insure that these factors will affect all his specimens in the same way. Another factor that varies within a small region may be the surface preparation. A series of fine scratches can produce local variations in strength and hence in the life of the specimen at a given stress.

## Long-Range Sources of Variation

There are factors which affect the life of one specimen relative to another without necessarily causing a variation in strength within one specimen. Any factor connected with specimen preparation may fall in this category. It is very difficult to insure that all specimens have been heat-treated alike. If the specimens are heat-treated all at the same time, it is difficult to assure that temperatures and cooling rates are the same throughout a furnace or a tempering bath. If the specimens are heat-treated at different times, they can be placed at the same points in the furnace or tempering baths, but then the variations in furnace temperature from time to time may cause trouble. In mechanical preparation, the sharpness of the tool and the patience of the polisher will wax and wane. In testing the specimen in the machine, errors in measuring the diameter and setting the load may affect the stress of the specimen and hence the life at what was thought to be one stress. All of these factors affect different specimens differently, but they can be brought under control by better and better experimental techniques.

Metallurgical factors are more difficult to control. The longest-range ones can be eliminated by selecting all the specimens from one bar. But even between one end and the other of this bar, there may be differences due to variations in rolling temperatures, cooling rate, or nearness of one end to an insufficiently cropped end of an ingot. These factors may be detected by noting whether specimens from one end or the other tend to fail earlier.

## Intermediate Sources of Variation

It is conceivable that there are some medium-range factors which vary over a distance of the order of the specimen length. For example, if a specimen is heat-treated after machining, one part of the specimen may receive a different heat-treatment from another part because of uneven temperatures or differences in cooling rates. Occasional scratches will reduce the strength wherever they may happen to fall. There may be a tendency for the quality of machining to vary along the length of the specimen.

Another possibility is the presence of stringers of inclusions whose length is of the order of magnitude of the length of the specimen. Such inclusions have very little effect on the life of the specimen when they are parallel to a uniaxial stress. The unimportance of these stringers is due to the fact that they occupy so little of the area of the specimen and cause less stress concentration than a spherical inclusion having the same diameter as the stringer. Hence we shall ignore any metallurgical

---

[1] Completion of this research was supported by the United States Air Force, through the Office of Scientific Research of the Air Research and Development Command.

[2] Assistant Professor of Mechanical Engineering, Massachusetts Institute of Technology. Assoc. Mem. ASME.

[3] Numbers in parentheses refer to the Bibliography at the end of the paper.

Presented at the National Conference of the Applied Mechanics Division, Troy, N. Y., June 16–18, 1955, of THE AMERICAN SOCIETY OF MECHANICAL ENGINEERS.

Discussion of this paper should be addressed to the Secretary, ASME, 29 West 39th Street, New York, N. Y., and will be accepted until October 10, 1955, for publication at a later date. Discussion received after the closing date will be returned.

NOTE: Statements and opinions advanced in papers are to be understood as individual expressions of their authors and not those of the Society. Manuscript received by ASME Applied Mechanics Division, December 9, 1954. Paper No. 55—APM-26.

factors which are constant within a microscopic region, but vary over the length of the specimen.

The factors affecting the scatter in life of fatigue specimens can now be tabulated according to the possibility of eliminating them and the size of the region over which they vary (Table 1).

TABLE 1 FACTORS AFFECTING SCATTER IN LIFE OF FATIGUE SPECIMENS

| Factor | Varies within a microscopic region | Constant within a microscopic region but varies over the length of a specimen | Constant within one specimen but varies from one specimen to another |
|---|---|---|---|
| *Factors which cannot be eliminated* | | | |
| Stress concentration at grain boundaries | × | — | — |
| Stress concentration at inclusions | × | — | — |
| Strength variations due to grain orientations | × | — | — |
| Strength variations due to various phases | × | — | — |
| *Factors whose influence can be eliminated or reduced* | | | |
| Composition | — | — | × |
| Heat-treatment: | | | |
| Variations within a specimen | — | × | — |
| Variations from one specimen to another | — | — | × |
| Prior mechanical history | — | — | × |
| Machining and polishing: | | | |
| Fine scratches and feedmarks | × | — | — |
| Uneven machining and polishing | — | × | — |
| Gradually increasing tool dullness | — | — | × |
| Loading in fatigue machine | — | — | × |

Study of the table shows that if the experimenter has achieved the goal of eliminating the influence of all those variables whose influence can be eliminated, then the only remaining source of variation will be in factors which vary within a microscopic region. The converse is not quite true. If the only variation remaining is due to factors which vary within a specimen, it still may be that the scatter could be yet further reduced by improvement of heat-treatment and machining and polishing techniques. However, these factors can be detected and controlled. Heat-treatment can be uniform if a large furnace and slow cooling rates are used. If the machining is done with a sharp-nosed tool and a fine uniform feed, and if the polishing is observed to be of metallographic quality, these effects are minimized. We therefore conclude that there is practically a one-to-one correspondence between the size of the region over which factors vary and the possibility of eliminating those factors. This conclusion means that if we can estimate in some way what scatter in life is due to factors which vary over a microscopic region, then it should be possible to eliminate any scatter in life above this amount.

These local variations manifest themselves in the scatter in position of failure in specimens in which the stress varies along the length, reaching a maximum at one point only. Local variations in strength can cause this variation in position of failure because sometimes the point of highest stress in a specimen will come at a point of the material which is of higher than average strength. If a sufficiently weaker point of the material is nearby, the specimen may then fail at the weaker point, even though the stress is slightly lower. Furthermore, local variations in strength within a specimen are the only cause of a variation in position of failure, for if the material were perfectly uniform, the specimen would always fail at the point of highest stress. There would then be no variation in position of failure.

In a previous paper (3), the statistical theory of the relation between the scatter in cycles to failure and the scatter in position of failure has been developed to yield the following result. Let the variation of the stress $S$, with distance $z$, from the point of maximum stress be related to the maximum stress by an equation of the form

$$S = S_m(1 - az^2) \quad [1]$$

The constant $a$ depends on the shape, size, and method of loading of the fatigue specimen. Then if $K$ denotes the negative of the slope of the plot of stress versus the logarithm of the number of cycles to failure, if $\sigma_{\log N}$ denotes the standard deviation of logarithm of the number of cycles to failure, and if $\sigma_z$ denotes the standard deviation of the position to failure

$$K\sigma_{\log N}/2.3S_m\, a\, \sigma_z^2 = 1 \quad [2]$$

The numerical factor 2.3 is not strictly a constant for all shapes of frequency-distribution functions, but varies between limits of 2.0 and 2.56, thus lying within about 10 per cent of 2.3.

## Application to Data

In studying a given set of data, it is desired to determine whether or not the variation in cycles to failure is small enough to conform to Equation [2]. But from a sample of finite size only estimates of the standard deviations, and not their exact values, are known. If $\hat{\sigma}$ denotes the estimate of a standard deviation, Equation [2] may be rewritten

$$\frac{K\hat{\sigma}_{\log N}}{2.3S_m\, a\, \hat{\sigma}_z^2} \Big/ \left(\frac{\hat{\sigma}_{\log N}}{\sigma_{\log N}} \frac{\sigma_z^2}{\hat{\sigma}_z^2}\right) = 1 \quad [3]$$

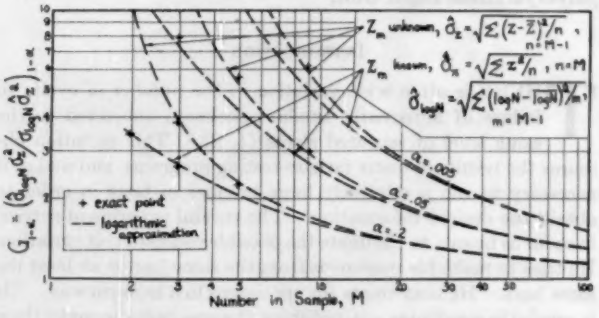


FIG. 1 UPPER LIMIT OF RATIO OF STANDARD DEVIATION TO AN INDEPENDENT VARIANCE FOR NORMAL DISTRIBUTIONS

Values of the factor $a$ are given in Table 2. Approximate confidence limits for the denominator are derived in the Appendix and are presented in Fig. 1. If the numerator divided by the largest reasonable value of the denominator is greater than unity, then there is more scatter in the cycles to failure than that due to local variations alone. Improved specimen preparation and testing technique should be sought. The importance of minimizing scatter should not be overlooked. Since the limits for the estimate of the mean vary roughly as the standard deviation over the square root of the number of specimens tested, halving the standard deviation by improved technique will give the same information with only one fourth as many specimens.

## Example of Application of Method

Tests were run on ingot iron which was being used for tests on single crystals which have been described elsewhere (4). Blanks were annealed in lots of 25 at 1700 F for $\frac{1}{2}$ hr and then furnace-cooled at an initial cooling rate of about 450 deg F per hr, giving an ASTM grain size of $3\frac{1}{2}$. The specimens were machined to the standard Moore-type test section, 0.3 in. diam with $9\frac{7}{8}$ in. radius of curvature in the longitudinal direction. The specimens were then polished, the last operation being a longitudinal polish with wet 320-grit Aloxite paper.

The rotary-bending fatigue machine used in these tests has been described previously (5). The weights were isolated by soft springs and the machine was run at 800 rpm. It was set to stop as soon as the bearing deflection had increased by about $\frac{1}{32}$ in. A

TABLE 2 TERM $a$ FOR FATIGUE SPECIMENS OF VARIOUS SHAPES

$z_m$ = co-ordinate of maximum stress

| | | |
|---|---|---|
| 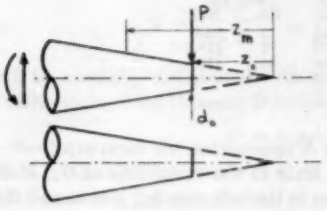 | $Z_m = 3Z_o/2$ | $a = 4/3Z_o^2$ |
| 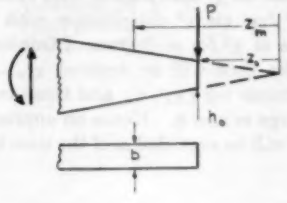 | $Z_m = 2Z_o$ | $a = 1/4Z_o^2$ |
| 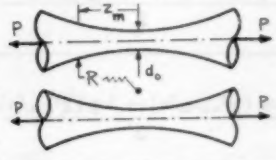 | $Z_m = 0$ | $a = 2/d_oR$ |
| 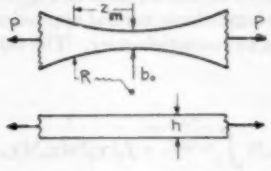 | $Z_m = 0$ | $a = 1/b_oR$ |
| 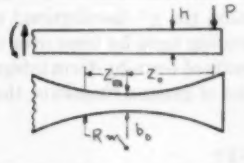 | $Z_m = \frac{b_oR}{2Z_o} - \frac{b_o^2R^2}{8Z_o^3} + \cdots$ | $a = 1/b_oR - 1/4Z_o^2 + \cdots$ |
| 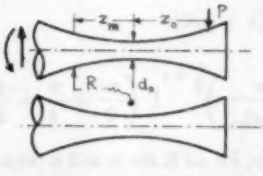 | $Z_m = \frac{d_oR}{6Z_o} - \frac{5d_o^2R^2}{216Z_o^3}$ | $a = 3/d_oR + 1/4Z_o^2 + \cdots$ |
| 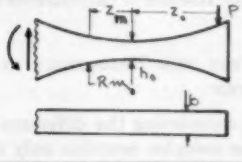 | $Z_m = \frac{h_oR}{4Z_o} - \frac{3h_o^2R^2}{64Z_o^3} + \cdots$ | $a = 3/h_oR + 1/8Z_o^2 + \cdots$ |
| 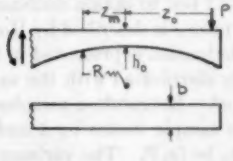 | $Z_m = \frac{h_oR}{2Z_o} - \frac{3h_o^2R^2}{16Z_o^3} + \cdots$ | $a = 1/b_oR + 1/8Z_o^2 + \cdots$ |

few tests indicated that only another 2 or 3 per cent of life would be required for complete failure.

The cycles to failure for the specimens described are listed as Group 1 in Table 3. For bars V, VI, VIII, and IX, $\delta_s$ with known $z_m$ was 0.044 in. and $\delta_{\log_{10} N}$ was 0.142. From Fig. 1, $G_{0.95} = 2.4$. The slope $K$ was found from reference (6) to be 5500 psi/$\log_{10} N$. Hence the ratio of Equation [3] was greater than 2.7 (95 per cent confidence), showing much more scatter in life than there should have been.

It was thought that differences in specimen preparation were responsible, and so the technique was improved. The final procedure adopted was to machine and polish the specimens, reanneal them in a hydrogen atmosphere in a tube furnace, cool at 100 deg F per hr, and finally repolish. The slower cooling rate markedly reduced the cycles to failure, as was shown by other tests with various surface preparations as well as by the results listed in Table 3 as Group 2. Unfortunately, there were only four specimens available by the time that this procedure had been worked out. But even so, following the method of Hald,[4] one may conclude that the standard deviation of the logarithm of the cycles to failure was reduced by a factor of 2 to 55 (98 per cent) to 0.0055 to 0.054 (98 per cent). This reduction in scatter would not have been obtained without the stimulus of the statistical analysis described. Further, the reduction in scatter permitted drawing conclusions from a minimum of data, as shown in the following.

## Cycles to Crack Formation

In the program of which this study was a part it was necessary to stop for a microscopic examination. Since stopping the test might affect the cycles to failure, the expected life of the specimen must be predicted on the basis of similar specimens run continuously to failure. Student's $t$ test for the difference of the means of two samples is modified in the Appendix for the case in which one of the samples contains only one item. From the data of Group 2, a further specimen given the same treatment would fail after 101,000 to 127,000 cycles (98 per cent confidence). Three such specimens were run for 60,000, 30,000, and 15,000 cycles, respectively. On microscopic examination at ×400, the first two were found to be cracked, but not the third. Even assuming that the second specimen would have a relatively short life and the third a relatively long one, we may conclude that the specimens showed cracks at ×400 after 12 to 34 per cent of their lives.

The presence of fatigue cracks this early is of importance for both technical and scientific reasons. Yet more emphasis should be placed on methods of crack detection as a means of preventing fatigue failures in service. Furthermore, the early formation of cracks decreases the hope of any practical form of preventive maintenance, such as reheat-treatment, for the process would have to be carried out so early and so often as to be prohibitively expensive. The scientific implication of the early presence of cracks is that any quantitative theory of fatigue will have to consider two different phenomena, i.e., the formation of cracks of the size of a grain or less, and the growth of these cracks to failure. Neither of these phenomena can be considered of negligible importance in determining cycles to failure at a given stress.

## Conclusion

A statistical analysis resulted in the method for detecting extraneous effects in fatigue tests on Moore-type specimens which is summarized in Equation [3], Fig. 1, and Table 2.

When applied to tests on ingot iron, the method stimulated the

[4] Reference (7), p. 381.

TABLE 3 ROTARY-BENDING TESTS ON POLYCRYSTALLINE INGOT IRON

| Group No. | Description of preparation | Kilocycles to failure at ±27000 psi — Bar V No. | Bar V Kc | Bar VI No. | Bar VI Kc | Bar VII No. | Bar VII Kc | Bar VIII No. | Bar VIII Kc | Bar IX No. | Bar IX Kc |
|---|---|---|---|---|---|---|---|---|---|---|---|
| 1 | Anneal, furnace cool, machine | 5 | 250 | 5 | 364 | 6 | 259 | 1 | 338 | 1 | 233 |
| | | 11 | 425 | 9 | 877 | 14 | 124 | 9 | 360 | 7 | 318 |
| | | 17 | 385 | 21 | 389 | 16 | 366 | 15 | 288 | 15 | 270 |
| 2 | Machine, anneal with slow cooling | 15 | 116 | 7 | 114 | 4 | 111 | — | — | — | — |
| | | — | — | — | — | 8 | 110 | — | — | — | — |

development of an experimental technique which reduced the scatter in cycles to failure to a few per cent.

Using a magnification of ×400, cracks were observed after 30,000 cycles but not after 15,000 cycles, in specimens whose life very probably would have been between 101,000 and 127,000 cycles.

### Acknowledgments

This work was part of a PhD thesis carried out in the Dynamics Laboratory of the California Institute of Technology under the supervision of Prof. D. E. Hudson, whom the author thanks for advice and encouragement throughout the program. He also wishes to thank Profs. D. S. Clark, P. E. Duwez, and G. W. Housner, who freely contributed their time to discuss problems which arose.

The author is grateful to the Institute for financial assistance. A generous fellowship awarded by the Shell Oil Company in 1947-1948 is also deeply appreciated.

### BIBLIOGRAPHY

1 "Review of the Fatigue of Materials Field," by R. E. Peterson, *Applied Mechanics Reviews*, vol. 5, January, 1952, p. 1.

2 "Statistical Design of Fatigue Experiments," by W. Weibull, Journal of Applied Mechanics, Trans. ASME, vol. 74, 1952, pp. 109–113.

3 "The Statistical Theory of Size and Shape Effects in Fatigue," by F. A. McClintock, published in this issue, pp. 421–426.

4 "Fatigue Tests on Single Crystals of Ingot Iron," by F. A. McClintock, Proceedings 1st National Congress of Applied Mechanics, June, 1951, The American Society of Mechanical Engineers 1952, pp. 653–659.

5 "A Sulphur Print for the Study of Crack Growth in the Corrosion Fatigue of Metals," by R. C. Brumfield, Proceedings of the ASTM, vol. 45, 1945, p. 544.

6 "An Investigation of the Fatigue of Metals," by H. F. Moore and J. B. Kommers, University of Illinois Engineering Experiment Station Bulletin No. 124, 1921.

7 "Statistical Theory With Engineering Applications," by A. Hald, John Wiley & Sons, Inc., New York, N. Y., 1952.

8 "Introduction to Mathematical Statistics," by P. G. Hoel, John Wiley & Sons, Inc., New York, N. Y., 1947.

# Appendix

### Derivation of Approximate Confidence Limits

The distributions of $\log N$ and $z$ will be assumed normal and independent of each other in order to get an approximate upper confidence limit for the ratio

$$\left(\frac{\hat{\sigma}_{\log N}/\sigma_{\log N}}{\hat{\sigma}_z^2/\sigma_z^2}\right) = G$$

The assumptions of independence and normality of $z$ hold as the exponent $k$ of Equation [6], reference (3), approaches $\infty$, and while the distribution of $\log N$ approaches the form $\exp(-e^y - y)$, it contributes relatively little to the variability of $G$. If the number of degrees of freedom in the estimate $\hat{\sigma}_{\log N}$ is $m$ and that in $\hat{\sigma}_z$ is $n$, then $m\hat{\sigma}^2_{\log N}/\sigma^2_{\log N}$ has an $\chi^2$ distribution with $m$ degrees of freedom and $n\hat{\sigma}_z^2/\sigma_z^2$ has an $\chi^2$ distribution with $n$ degrees of freedom. The value of $\chi^2$ for $m$ degrees of freedom which will be exceeded $\alpha$ of the time will be denoted $\chi^2_{m,1-\alpha}$. Now $\log G$ is $\frac{1}{2}\log(\chi_m^2/m)$ minus $\log(\chi_n^2/n)$, and these two terms are roughly normal for large $m$ and $n$. Hence an approximation to the value of $G$ which will be exceeded $\alpha$ of the time is

$$\log G_{1-\alpha} = \frac{\frac{1}{2}\log(\chi^2_{m,1-\alpha}/m) + \frac{1}{2}\log(\chi^2_{n,\alpha}/m)}{2} - \frac{\log(\chi^2_{n,1-\alpha}/n) + \log(\chi^2_{n,\alpha}/n)}{2}$$
$$+ \sqrt{\left[\frac{\frac{1}{2}\log(\chi^2_{m,1-\alpha}/m) - \frac{1}{2}\log(\chi^2_{m,\alpha}/m)}{2}\right]^2 + \left[\frac{\log(\chi^2_{n,1-\alpha}/n) - \log(\chi^2_{n,\alpha}/n)}{2}\right]^2}$$

The resulting values of $G$ are plotted as dashed lines in Fig. 1.

For small values of $m$ and $n$ the logarithmic normal approximation to the $\chi^2$ distribution may not be too satisfactory. The value of $G_{1-\alpha}$ is given exactly by

$$\alpha = \int_{G_{1-\alpha}}^{\infty} f(G)dG = \int_0^{\infty} f_m(\chi_m^2)\int_0^{\frac{n\chi_m}{\sqrt{m}G_{1-\alpha}}} f_n(\chi_n^2)d\chi_n^2 d\chi_m^2$$

When this is evaluated by introducing the $\chi^2$ distribution,[5] expanding that of $\chi_n^2$ in a series, integrating term by term over the finite interval, and expressing the results of term-by-term integration over the infinite interval in terms of gamma functions, there results

$$\alpha = \frac{1}{\Gamma\left(\frac{m}{2}\right)\Gamma\left(\frac{n}{2}\right)}\sum_{s=0}^{\infty}\frac{(-1)^s}{2^{\frac{n}{2}+s}(s+n/2)s!}\left(\frac{n}{\sqrt{m}G_{1-\alpha}}\right)^{\frac{n}{2}+s}\Gamma\left(\frac{m}{2}+\frac{n}{4}+\frac{s}{2}\right)$$

This series converges, albeit slowly, for all finite $m$ and $n$ because of the ratio $\Gamma(m/2 + n/4 + s/2)/s!$. Results of calculations are shown by crosses in Fig. 1.

### Modification of Student's $t$ Test for Prediction of a Single Item

This estimation can be made by considering the difference of two sample means when one of the samples contains only one item. The method of using Student's $t$ test to obtain confidence limits for the difference between two means is described by Hoel.[6] The desired modification of Hoel's derivation is presented in the following. Let $x$ and $y$ be normally distributed with the same mean $m$ and with the same variance $\sigma^2$. Let random samples of size $n_x$ and 1 be taken. Denote the sample means by $\bar{x}$ and $\bar{y}$. Let the variance of the sample of $n_x$ be $(s_x)^2$. The variance of

[5] Reference (7), p. 255.

[6] Reference (8), pp. 145–147.

the individual will, of course, be zero. Thus it follows from theorem 4[7] that

$$u = \frac{(\bar{x} - \bar{y})}{\sigma_{\bar{x}} - \bar{y}} = \frac{(\bar{x} - \bar{y})}{\sigma\sqrt{1/n_x + 1}}$$

will be normally distributed with zero mean and unit variance. Furthermore, from theorem 2[8] it follows that

$$v^2 = n_x s_x^2/\sigma^2$$

has a $\chi^2$ distribution with $\nu = n_x - 1$ degrees of freedom. Then it follows from theorem 4[9] that

$$t = \frac{(\bar{x} - \bar{y})}{s_x}\sqrt{\frac{n_x - 1}{n_x + 1}}$$

will have Student's $t$ distribution with $n_x - 1$ degrees of freedom. For a desired confidence level, $t$ can be found from tables such as Hoel gives.[10] Then the confidence limits for $\bar{y}$, which is the value of the individual, are

$$\bar{x} - ts_x\sqrt{n_x + 1}/\sqrt{n_x - 1} \leq \bar{y} \leq \bar{x} + ts_x\sqrt{n_x + 1}/\sqrt{n_x - 1}$$

[7] Reference (8), p. 71.
[8] Ibid., p. 138.
[9] Ibid., p. 142.
[10] Reference (8), p. 248.

# Brief Notes*

**On the recommendations of the Executive Committee of the ASME Applied Mechanics Division, it has been decided to initiate a section devoted to brief notes on technical matters in mechanics. These notes must not be longer than 750 words (about 2½ double-spaced typewritten pages, including figures) and will be subject to the usual review procedure prior to publication. After approval such notes will be published in the next issue of the Journal. The notes should be submitted to the Secretary of the ASME Applied Mechanics Division.**

## Critical Time in Creep Buckling

By J. A. H. HULT,[1] STOCKHOLM, SWEDEN

AN expression for the critical time in creep buckling of columns, i.e., the time duration necessary to cause infinite deflection, has been given by N. J. Hoff[2] considering a hinged-hinged column with an idealized I-section. Hoff's result was later generalized by F. K. G. Odqvist[3] so as to include also the effect of nonrecoverable primary creep.[4] In both these cases elastic deformation during the buckling process was neglected compared to creep deformation. This note considers the influence of elastic deformation on the critical time as deduced by Hoff and Odqvist.

The strain-rate equation to be used

$$\frac{d\epsilon}{dt} = \frac{1}{E}\frac{d\sigma}{dt} + k_0\sigma^{n_0-1}\frac{d\sigma}{dt} + k\sigma^n \quad \ldots\ldots [1]$$

differs from Odqvist's through the addition of the term $(1/E)\cdot(d\sigma/dt)$, which accounts for elastic deformation. This term, of course, will be retained at all material points throughout the buckling process. Using the same assumptions and notations as Hoff and Odqvist except for the creep relation, which is now taken in the form of Equation [1], one obtains for the column deflection the equation

$$\frac{\partial^3 w}{\partial t \partial \xi^2} + \frac{P}{P_E}\frac{\partial w}{\partial t} + \Lambda(1+w)^{n_0-1}\frac{\partial w}{\partial t} + \Pi[(1+w)^n - (1-w)^n] = 0 \quad \ldots\ldots [2]$$

where $P_E$ is the Euler load of the column. When $P_E = \infty$, this equation reduces to the one given by Odqvist. The case previously treated, $n_0 = 2$, $n = 3$, yields after integration

$$\frac{3\Pi}{2}t = \frac{1-\Lambda-P/P_E}{8}\log\frac{a^2(4+a_0^2)}{a_0^2(4+a^2)} - \frac{4\Lambda}{3\pi}\tan^{-1}\frac{2(a-a_0)}{4+aa_0} \quad \ldots\ldots [3]$$

the initial condition being $t = 0$, $a = a_0$, where $a_0$ is the initial maximum deflection of the column. Letting here $a$ tend towards infinity one obtains a finite critical buckling time $t_{cr}$

$$\frac{3\Pi}{2}t_{cr} = \frac{1-\Lambda-P/P_E}{8}\log\frac{4+a_0^2}{a_0^2} - \frac{4\Lambda}{3\pi}\tan^{-1}\frac{2}{a_0} \quad \ldots\ldots [4]$$

Equation [4] shows that the effect of elastic deformation as well as of primary creep is to shorten the critical buckling time.

Putting in Equation [4] $t_{cr} = 0$ one obtains a condition for instantaneous buckling; viz.

$$\overline{P}/P_E = 1 - \overline{\Lambda}\left[1 + \frac{32}{3\pi}\frac{\tan^{-1}2/a_0}{\log(4+a_0^2)/a_0^2}\right] \quad \ldots\ldots [5]$$

where $\overline{P}$ is the load necessary to cause instantaneous buckling, and

$$\overline{\Lambda} = 2k_0(L/\pi h)^2(\overline{P}/A)^2 \quad \ldots\ldots [6]$$

is the corresponding value of $\Lambda$. Equation [5] describes some well-known features of column buckling:

1 $k_0 = 0$ (no primary creep) yields $\overline{P} = P_E$ for all values of $a_0$; i.e., the elastic buckling load is independent of the initial curvature of the column.

2 $a_0$ vanishingly small yields $\overline{P} = P_E(1-\overline{\Lambda})$; i.e., the buckling load is lowered by the nonelastic strain.

3 $a_0$ not vanishingly small yields $\overline{P} < P_E(1-\overline{\Lambda})$; i.e., in the nonelastic region the buckling load depends on the initial curvature, the buckling load being lower in the case of great initial curvature.

## A Note on Plastic Torsion

By J. H. HUTH,[1] SANTA MONICA, CALIF.

### Introduction

THE uniform torsion of noncircular rods may be formulated according to Nadai's (deformation) theory as follows[2]

$$\frac{\partial}{\partial x}\left(\frac{1}{G}\frac{\partial\psi}{\partial x}\right) + \frac{\partial}{\partial y}\left(\frac{1}{G}\frac{\partial\psi}{\partial y}\right) = -2\theta \quad \ldots\ldots [1]$$

where $\tau_{xz} = \partial\psi/\partial y$, $\tau_{yz} = -\partial\psi/\partial x$, and $\psi$ vanishes on the boundary of a cross section. ($\theta$ is the angle of twist per unit length; $x$ and $y$ Cartesian co-ordinates in the rod cross section; $G$ the secant shear modulus; $\tau_{xz}$, $\tau_{yz}$ shearing-stress components.)

For the special case of Laning's stress-strain relation, Prager also gives a formulation[2] corresponding to the plastic-flow theory. The pertinent equation is

$$\frac{\partial}{\partial x}\left[A\frac{\partial}{\partial\theta}\left(\frac{1}{A}\frac{\partial\psi}{\partial x}\right)\right] + \frac{\partial}{\partial y}\left[A\frac{\partial}{\partial\theta}\left(\frac{1}{A}\frac{\partial\psi}{\partial y}\right)\right] = -2G_0 \quad \ldots\ldots [2]$$

---

[1] Research Assistant, Royal Institute of Technology.

[2] "Buckling and Stability," by N. J. Hoff, *Journal of the Royal Aeronautical Society*, vol. 58, January, 1954, p. 3.

[3] "Influence of Primary Creep on Column Buckling," by F. K. G. Odqvist, JOURNAL OF APPLIED MECHANICS, Trans. ASME, vol. 76, 1954, p. 295.

[4] The strain-rate equation used by Odqvist takes account of primary creep through a term, which, for constant stress, gives no contribution to the strain rate but only to the total creep strain (*Applied Mechanics Reviews*, feature article Dec., 1954, by F. K. G. Odqvist).

* Discussion of papers in Brief Notes should be addressed to the Secretary, ASME, 29 West 39th Street, New York, N. Y., and will be accepted until October 10, 1955, for publication at a later date. Discussion received after the closing date will be returned.

NOTE: Statements and opinions advanced in papers are to be understood as individual expressions of their authors and not those of the Society. Manuscript received by ASME Applied Mechanics Division, November 15, 1954.

[1] Engineer, Missiles Division, The Rand Corporation. Mem. ASME.

[2] "An Introduction to the Mathematical Theory of Plasticity," by W. Prager, *Journal of Applied Physics*, vol. 18, 1947, pp. 375–383.

Manuscript received by ASME Applied Mechanics Division, March 14, 1955.

where

$$\ln A = -\int_0^\tau \frac{1}{2}\left(\frac{G_0}{G^*} - 1\right)\frac{d\tau}{\tau}$$

and $\psi$ satisfies the same boundary conditions as in the deformation theory. ($G_0$ is the elastic shear modulus; $G^*$ the tangent shear modulus.)

The purpose of this note will be to illustrate numerical methods of handling Equations [1] and [2], and to compare the results for one particular example.

## Analysis

The numerical treatments will be illustrated for a rod of square cross section and made of chrome-nickel steel, full hard. The axial stress-strain curve for this material has been given by Ramburg and Osgood.[3] A shearing stress-strain curve can be prepared from their data by using Shanley's[4] theory of plasticity. The resulting curve is shown in Fig. 1.

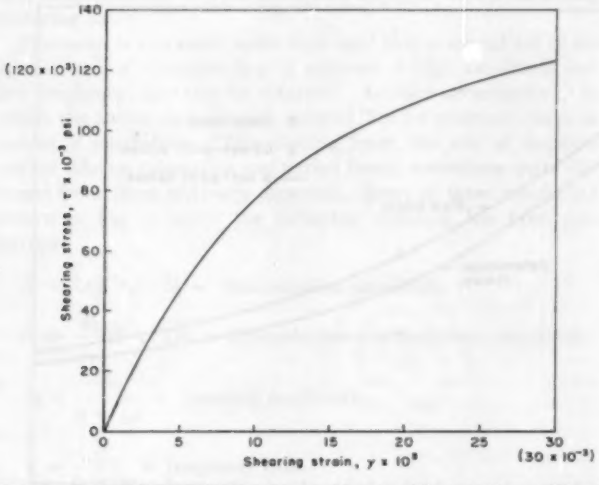


Fig. 1 Stress-Strain Diagram for Chrome-Nickel Steel (Full Hard) in Shear

Analytically, the stress-strain relationship may be expressed as

$$\gamma = \frac{\tau}{G_0}\left(1 + \beta\left(\frac{\tau}{G_0}\right)^n\right) \quad \ldots\ldots\ldots\ldots [3]$$

where

$$G_0 = 9.45 \times 10^6 \text{ psi}$$
$$\beta = 2.1 \times 10^7$$
$$n = 3.83$$

Since

$$\tau = \sqrt{\left(\frac{\partial\psi}{\partial x}\right)^2 + \left(\frac{\partial\psi}{\partial y}\right)^2}$$

the secant shear modulus $G = \tau/\gamma$ satisfies

$$\frac{1}{G} = \frac{1}{G_0}\left[1 + \frac{\beta}{G_0^n}\left\{\left(\frac{\partial\psi}{\partial x}\right)^2 + \left(\frac{\partial\psi}{\partial y}\right)^2\right\}^{\frac{n}{2}}\right] \quad \ldots\ldots [4]$$

and the tangent shear modulus $G^* = d\tau/d\gamma$ is given by

$$\frac{1}{G^*} = \frac{1}{G_0}\left[1 + \beta(n+1)\left(\frac{\tau}{G_0}\right)^n\right] \quad \ldots\ldots\ldots [5]$$

Equations [4] and [5] combine with Equations [1] and [2], respectively, to determine $\psi$.

Actually, the solutions were carried out for a nine-point square net as shown in Fig. 2.

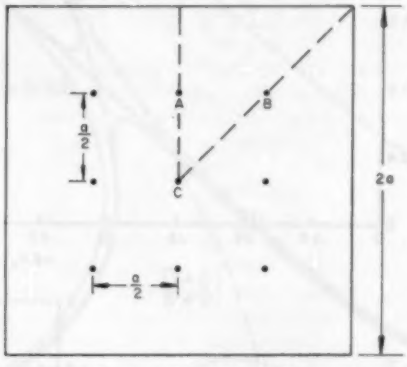


Fig. 2 Nine-Point Net

Replacing derivatives by their simplest centered finite-difference approximations

$$\left(\text{at point } B,\ \frac{\partial\psi}{\partial x} \cong \frac{\psi_A}{a},\ \frac{\partial^2\psi}{\partial x^2} \cong \frac{4[\psi_A - 2\psi_B]}{a^2}\right)$$

leads from Equation [2] to a set of three simultaneous linear algebraic equations for $\partial\psi/\partial\theta$ at points $A$, $B$, and $C$. The coefficients depend on $\psi$ and its space derivatives, and in the first step were calculated from the known elastic solution[5] (assumed to hold for $aG_0\theta = 1.06 \times 10^4$). Once $(\partial\psi/\partial\theta)$ has been determined then a small twist $\Delta\theta$ is imposed, new $\psi$ values calculated, and the process repeated.

This procedure was carried out in 50 steps to an $aG_0\theta$ of $47 \times 10^4$. The convergence was then checked by halving the interval $\theta$ and repeating the process.

Equation [1] was solved by an iteration procedure for each given value of $\theta$. At each trial the coefficients of the second derivatives

$$\left(\frac{\partial^2\psi}{\partial x^2},\ \frac{\partial^2\psi}{\partial y^2},\ \text{and}\ \frac{\partial^2\psi}{\partial x\partial y}\right)$$

were computed from the previous results and then treated as constants in determining new $\psi$ values.

The final results are given in Table 1 for one specific case, along with elastic results for comparison.

TABLE 1 ELASTIC PLASTIC COMPARISON

| | | Plastic | |
|---|---|---|---|
| Elastic | $aG_0\theta = 22.4 \times 10^4$ | Deformation theory | Flow theory |
| $\psi_A$ | $9.85 \times 10^4 a$ | $5.91 \times 10^4 a$ | $5.96 \times 10^4 a$ |
| $\psi_B$ | $7.73 \times 10^4 a$ | $4.78 \times 10^4 a$ | $4.85 \times 10^4 a$ |
| $\psi_C$ | $12.60 \times 10^4 a$ | $8.71 \times 10^4 a$ | $8.75 \times 10^4 a$ |

Once $\psi$ has been determined at each net point, then twice the volume under the surface will yield the magnitude of the applied moment. Volumes were calculated from a polynomial passing through the nine interior points and twelve boundary points.

[3] "Description of Stress-Strain Curves by Three Parameters," by W. Ramburg and W. Osgood, NACA TN No. 902, July, 1943.

[4] "An Engineering Theory of Plasticity," by F. Shanley, unpublished notes, University of California, Los Angeles, Calif.

[5] "Net-Point Methods in Solid and Fluid Mechanics," by J. Huth, PhD dissertation, Stanford University, Stanford, Calif., June, 1950.

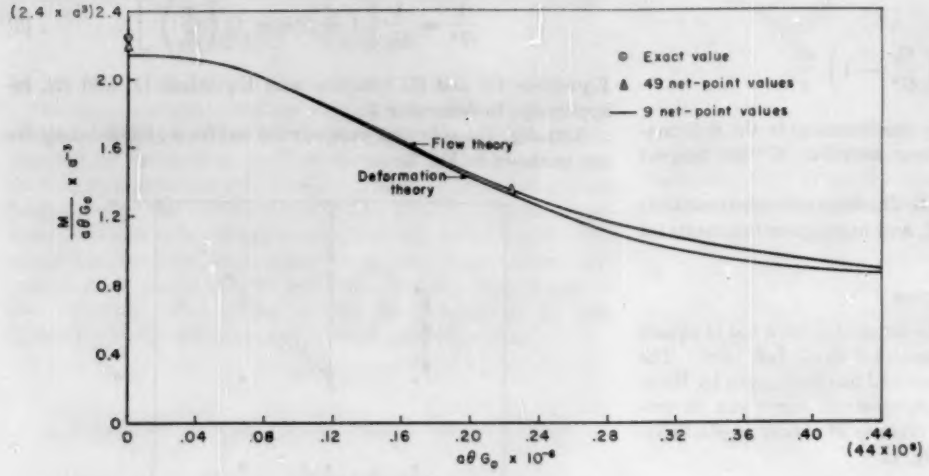


FIG. 3 EFFECTIVE TORSIONAL RIGIDITY AS A FUNCTION OF ANGLE OF TWIST

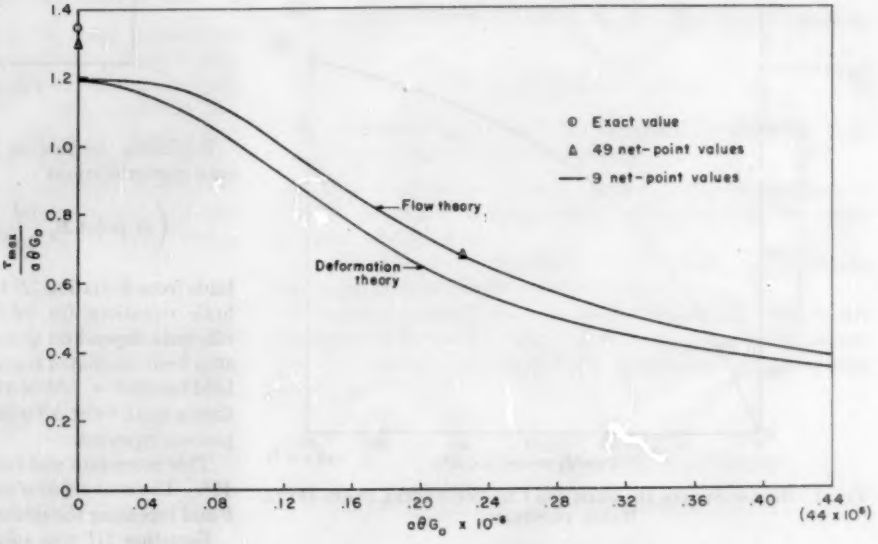


FIG. 4 MAXIMUM SHEARING STRESS AS A FUNCTION OF ANGLE OF TWIST

The maximum shearing stress occurs on the boundary at the center of each side, and follows from the normal slope of $\psi$ at that point.

### RESULTS AND CONCLUSIONS

Results are shown in Figs. 3 and 4. As $aG_0\theta$ approaches zero, $M/aG_0\theta$ of course approaches the purely elastic torsional rigidity of the bar. The curves in both figures actually terminate at the elastic nine net-point values.[5] In addition, 49 point values are given, together with "exact" elastic results.[6]

The plastic (deformation) case was also treated with the finer net for $aG_0\theta = 22.4 \times 10^4$. Results appear in Figs. 3 and 4. The indication is that the net accuracy is roughly the same as in the elastic case.

Although the coefficients in Equation [1] are quite sensitive to small changes in $\psi$, the convergence of the iteration solution does not require excessive numerical work. The forty-nine net-point case required a relaxation solution for each iteration, but still proved to be tractable.

However, the stepwise integration of Equation [2] was found to be more adaptable to punch-card techniques than the aforementioned iteration procedure.

[6] "Theory of Elasticity," by S. Timoshenko, McGraw-Hill Book Company, Inc., New York, N. Y., 1934, p. 249.

For a circular rod the deformation and flow theories would give identical results. The difference is still only slight for the case treated—in fact, less than the expected net-point error.

# Response Curves for a System With Softening Restoring Force

BY H. N. ABRAMSON,[1] COLLEGE STATION, TEXAS

**The purpose of this note is to present, and discuss briefly, calculated response curves for the nonlinear system titled. Several features of the response curves peculiar to this type of system, not previously discussed in the literature, are pointed out.**

SYSTEMS which possess a softening characteristic appear quite frequently; the motion of a pendulum and the hunting of synchronous motors under oscillating loads are two such examples. The analysis of these systems leads to a differential equation of the type

[1] Associate Professor of Aeronautical Engineering, The Agricultural and Mechanical College of Texas. Assoc. Mem. ASME.

Manuscript received by ASME Applied Mechanics Division, May 21, 1954.

$$E \equiv a\ddot{x} + b\dot{x} + c(x - \beta^2 x^3) - P \cos \Omega t = 0 \ldots\ldots [1]$$

which is known as Duffing's equation. Terms $a$, $b$, $c$, and $\beta^2$ are positive constants, $x$ is the displacement in question (measured from a static equilibrium position), and $P$ and $\Omega$ are the amplitude and frequency of a harmonic exciting force. We shall concern ourselves only with the periodic solutions of Equation [1] which have the same period as the exciting force.

It has become customary to describe the motion of simple vibratory systems by means of "response curves," in which amplitude is plotted as a function of exciting frequency. Such curves may be constructed readily when a solution of the differential equation is available. Although there is no known exact solution of Equation [1], several approximate solutions are known and have been discussed to a considerable extent.[2–4] The response curves are ordinarily shown as having the same appearance as in the linear case except that they are "swept over" toward the region of low exciting frequency. In this form it is easy to discuss the possibility of jump phenomena and to indicate regions of unstable motion in a manner similar to what is done for a system with a hardening restoring force.

However, it was noted some time ago[5] that a second set of response curves, corresponding to motions of high amplitude and low frequency, also may be obtained. Another investigation,[4] in which the author participated, showed that for a certain range of values of magnitude of the exciting force, the sets of response curves take on interesting and varied forms, sometimes quite different from those generally expected. Some of these results are shown in Fig. 1 where the following notation has been employed:

$$\bar{A} = A\beta \sqrt{3/4} = \text{dimensionless amplitude}$$

$$\bar{s} = \frac{P}{c} \beta \sqrt{3/4} = \text{dimensionless exciting-force amplitude}$$

$$D = \frac{b}{2\sqrt{ac}} = \text{damping coefficient}$$

$$\eta = \frac{\Omega}{\sqrt{c/a}} = \text{frequency ratio}$$

The computations which resulted in these curves were carried out by a method attributed to Ritz.[4] Briefly, a solution of the form

$$x = A \cos (\tau - \epsilon), \quad \tau = \Omega t \ldots\ldots\ldots\ldots [2]$$

is assumed, and the unknown amplitude and phase are determined from the algebraic equations obtained from the conditions

$$\int_0^{2\pi} E \cos \tau \, d\tau = 0, \quad \int_0^{2\pi} E \sin \tau \, d\tau = 0 \ldots\ldots [3]$$

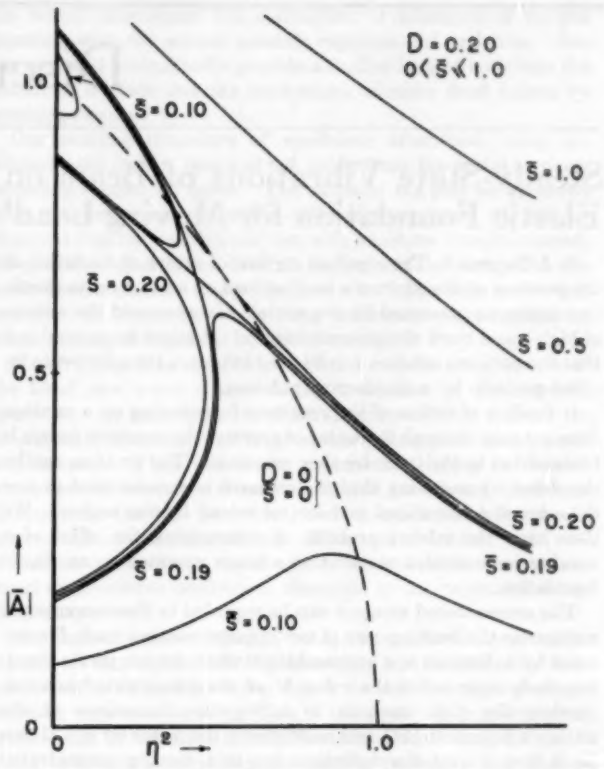


FIG. 1 RESPONSE CURVES FOR SYSTEM WITH SOFTENING RESTORING FORCE

In Fig. 1 it is seen that for small values of the exciting force ($s \leq 0.190$), a double set of response curves is obtained; one set corresponds to what might be called customary results, while the other corresponds to motions of large amplitude and low frequency. On the other hand, for large values of exciting force (e.g., $\bar{s} = 0.50$), only one set of curves is obtained, and these are similar in form to response curves obtained for the undamped system; i.e., there is no rounding off of the curves to form peaks, but instead the curves extend to the vertical axis at $\eta = 0$.

For a narrow range of exciting force, $0.190 < s \leq 0.200$, the curves take on various forms as a transition from the first type of curve just described to the second type is accomplished. Two such transition forms are shown in Fig. 1, one being for $\bar{s} = 0.200$ and the other for $\bar{s} = 0.192$. It does not seem that these results have been reported previously.

The physical significance and interpretation of these results are as yet inadequately understood. Questions concerning jump phenomena, stability, and the effects of subharmonics on the motion are plentiful and deserve elucidation. Also, experimental confirmation or denial of the existence of the transition-type curves and of those of the double set of curves corresponding to large amplitude low-frequency motions is lacking.

It should be pointed out that these results may not give an adequate description of motions with $\bar{A} \geq \sqrt{3/4}$; this is so because in this range the displacement $x$ is greater than $1/\beta$ and hence the restoring force becomes negative. However, most of the region of interest in the figure presented here lies below this value.

---

[2] "Nonlinear Vibrations," by J. J. Stoker, Interscience Publishers, New York, N. Y., 1950, pp. 213–218, chapter IV.

[3] "Forced Vibration of Systems With Non-Linear Restoring Force," by Dana Young, Proceedings of the First Midwestern Conference on Solid Mechanics, University of Illinois, Urbana, Ill., 1953, pp. 164–169.

[4] "Nonlinear Vibration Problems Treated by the Averaging Method of W. Ritz," by K. Klotter, Technical Report 17, Part II (Contract N6-onr-251-2), Stanford University, June, 1951. Also, Proceedings of the First U. S. National Congress of Applied Mechanics, THE AMERICAN SOCIETY OF MECHANICAL ENGINEERS, New York, N. Y., 1952, pp. 125–131.

[5] "Steady Oscillations of Systems With Nonlinear and Unsymmetrical Elasticity," by M. Rauscher, JOURNAL OF APPLIED MECHANICS, Trans. ASME, vol. 60, 1938, p. A-169.

# Discussion

## Steady-State Vibrations of Beam on Elastic Foundation for Moving Load[1]

H. J. Barten.[2] The excellent method of attack and solution of the problem of the effect of a moving load on a beam on an elastic foundation as presented by the author has advanced the science of high-speed track design considerably. It might be pointed out that the author's solution can be used to obtain the solution to an allied problem by a simple manipulation.

If the line of action of the resultant force acting on a carriage does not pass through its center of gravity, the resulting couple is transmitted to the track by shoe reactions. The problem can be simplified by assuming that the moment is concentrated as was done for the direct-load problem as solved by the author. We thus have the related problem of determining the effect of a moving concentrated moment on a beam mounted on an elastic foundation.

The concentrated moment can be regarded in the conventional manner as the limiting case of two opposed vertical loads $P$ separated by a distance $a$, $a$ approaching 0 while the couple $Pa$ simultaneously approaches the value $M_0$ of the concentrated moment. Analytically, this amounts to taking the derivatives of the author's Equation [14] and multiplying the value by $a$. If this procedure is used the deflection due to a moving concentrated moment becomes, for the undamped case, using the author's Equations [14$a$] and [14$b$] as follows

$$x < 0, \quad \beta = 0, \quad \theta < 1 \ldots\ldots\ldots\ldots\ldots\ldots [1]$$

$$y = -\frac{M_0\lambda^2}{k(1-\theta^4)^{1/2}}\, e^{(1-\theta^2)^{1/2}\lambda x} \sin (1+\theta^2)^{1/2}\lambda x \ldots [1a]$$

$$x > 0, \quad \beta = 0, \quad \theta < 1 \ldots\ldots\ldots\ldots\ldots\ldots [2]$$

$$y = -\frac{M_0\lambda^2}{k(1-\theta^4)^{1/2}}\, e^{-(1-\theta^2)^{1/2}\lambda x} \sin (1+\theta^2)^{1/2}\lambda x \ldots [2a]$$

$$x < 0, \quad \beta = 0, \quad \theta > 1 \ldots\ldots\ldots\ldots\ldots\ldots [3]$$

$$y = -\frac{M_0\lambda^2}{k(\theta^4-1)^{1/2}} \cos [(\theta^2+1)^{1/2} - (\theta^2-1)^{1/2}]\lambda x. \quad [3a]$$

$$x > 0, \quad \beta = 0, \quad \theta > 1 \ldots\ldots\ldots\ldots\ldots\ldots [4]$$

$$y = -\frac{M_0\lambda^2}{k(\theta^4-1)^{1/2}} \cos [(\theta^2+1)^{1/2} + (\theta^2-1)^{1/2}]\lambda x. \quad [4a]$$

An examination of these relations shows that the effect of a concentrated moment, moving on an undamped beam, mounted on an elastic foundation, is just the opposite to that for the concentrated load; i.e., at velocities below critical the deflection under the load is zero while above critical the deflection under the load is finite. Wave-length characteristics are identical, however; i.e., at supercritical velocity the length of the wave train behind the load increases with the velocity ratio while the length of the wave ahead of the load decreases.

Deflection and moment magnification factors for the damped and undamped conditions can be referred to the maximum static deflection and moment due to a concentrated moment[3]

$$y_{\text{static}} = \frac{1}{2}\sqrt{2}\, e^{-\frac{\pi}{4}} \frac{M_0\lambda^2}{k}$$

$$M_{\text{static}} = \frac{M_0}{2}$$

### Author's Closure

The author wishes to thank Mr. Barten for his excellent discussion. With the two fundamental cases of concentrated load and moment available it is, of course, relatively simple to develop the practical cases of loading by integration.

A paper, somewhat similar to the present one, has recently come to the author's attention: "Inleidend Onderzoek Naar Het Dynamisch Gedrag Van Spoorstaven" by A. D. DePater, thesis, Uitgeverij Waltman, Delft, Netherlands, 1948.

## Fretting Corrosion of Mild Steel in Air and in Nitrogen[1]

F. T. Barwell.[2] The authors have carried out a large number of experiments employing a great number of variables, yet the method of measuring the weight loss of the specimens used by them may not in all circumstances be a true indication of the extent of the fretting damage incurred by the specimens. During fretting, particularly under conditions under which oxides are formed, firm compacts of debris material lodge themselves in the pits which are formed in the surface. The authors do not make it clear whether the loss of weight measured included only the loose debris which could be removed easily from the surface of the specimens or also the highly compacted debris firmly attached to the specimens. If the former was the case, then the loss in weight would not be a true measure of the fretting damage. Work carried out by Wright in the Mechanical Engineering Research Laboratory paid considerable attention to this point. Some of the methods developed for estimating the amount of damage to the surfaces have been described recently.[3]

Another factor which appears to be of significance is the shape of the corrosive pits formed under different conditions. We have found that in air at high relative humidity the pits are shallow, while at low relative humidity they have considerable depth. From a practical point of view this is of great importance, since the latter would be expected to affect the fatigue strength of materials to a greater extent than the former. It would be interesting to learn whether or not the experience of the authors agrees with the M.E.R.L. findings regarding the shape of the corrosion pits.

---

[1] By J. T. Kenney, Jr., published in the December, 1954, issue of the Journal of Applied Mechanics, Trans. ASME, vol. 76, pp. 359–364.

[2] Technical Chief, Chicago Midway Laboratories Field Group, Eglin Air Force Base, Fla.

[3] " Beams on Elastic Foundation," by M. Hetényi, University of Michigan Press, Ann Arbor, Mich., 1946.

[1] By I-Ming Feng and H. H. Uhlig, published in the December, 1954, issue of the Journal of Applied Mechanics, Trans. ASME, vol. 76, pp. 395–400.

[2] Lubrication and Wear Division, Mechanical Engineering Research Laboratory, Thorntonhall, Glasgow, Scotland.

[3] "An Investigation of Fretting Corrosion," by K. H. R. Wright, Proceedings of The Institution of Mechanical Engineers, vol. 1B, 1952–1953, pp. 556–574.

Experiments by Wright have also shown that the time-displacement pattern has a considerable influence on the amount of damage. The elasticity of the systems to which the rubbing surfaces are attached and the friction between the surfaces can greatly modify the displacement fed into the apparatus. High elasticity and high friction are capable of transforming a sinusoidal-input displacement into a square-waved displacement-time curve and this damage, associated with the latter, is very much greater than with the former.

Finally, it may be of interest to mention that the measurement of contact resistance between fretting surfaces has been found by us to be a useful means of throwing light on the mechanism of fretting corrosion. We found that during the fretting of steel in dry air the contact resistance rose after a comparatively small number of oscillations to several meg-ohms and that the admittance of moist air, even with only 50 relative humidity, somewhat reduces the contact resistance. This indicates that, soon after starting, the fretting surfaces are separated by a weakly conducting layer of oxide debris and that, even at relatively low humidities, condensation of water vapor on the oxide debris may occur.

DOUGLAS GODFREY.[4] The quantitative data presented are useful in understanding the later stages of fretting. Inasmuch as the surfaces of the metal specimens were (runs in nitrogen excepted) completely separated by compacted $Fe_2O_3$, the effect of the different variables on weight loss possibly may be a result of changes in the physical properties of $Fe_2O_3$.

Two minor points might be considered differently.

The definition of fretting should include the thought of reciprocation at low amplitude.

The writer believes it is incorrect to use weight loss as a criterion of fretting damage produced in an inert atmosphere. Under these conditions a great deal of surface damage, as a result of "cold welding" and transfer of metal, should occur. This damage would not necessarily be revealed by weighing specimens before and after test. Would the authors describe the surfaces as found after the test?

### AUTHORS' CLOSURE

In answer to Mr. Barwell's comments: In corrosion testing of metals, weight loss of test specimens may not be the only criterion of damage one should apply when factors such as pitting or cracking also enter. But weight loss, nevertheless, is the most satisfactory quantitative measure for the majority of corrosion tests, even when some forms of pitting may accompany uniform loss of metal, as it does when metals are exposed, for example, to the atmosphere, to water, or to the soil. Therefore most corrosion data, as used practically, are reported in the form of weight-loss.

Quantitative fretting damage similarly is conveniently reported as weight loss. Our weight-loss data have confirmed, for example, several qualitative impressions by others of factors such as load, slip, and temperature, as gained from practical observations of fretting damage of metal structures and of machinery, showing that weight loss is not a misleading criterion. In addition, our data have clarified the importance of frequency and humidity, which were not among the factors recognized by qualitative tests.

It would be well worth while to measure extent of pitting as well as weight loss under test conditions where pitting varies from one set of variables to another, a procedure that we would want to follow in any longer time tests, and which we would recommend to others working in this field. Parallel with this, we would recommend the correlation of incidence of fatigue cracking with the several possible experimental variables. Doing so would undoubtedly provide a further insight both into the extent of damage and the mechanism whereby final failure by cracking results.

Our pickling procedure of specimens after test, using inhibited acid pickle, removed *all* oxide from the metal surface, including compacted oxide. The shape of the pits we observed after pickling is shown in Fig. 2(*b*) of the paper. It will be observed that for conditions of test with which we were concerned, the pits were distributed over the faying surfaces except for the outer and inner rims where the load may have been somewhat less than in the center. No large differences were noticed in shape and depth of pits as humidity varied.

We also found, as did Wright, that a certain perturbation of the ideal sine wave occurs during oscillation of the moving specimen with respect to the fixed specimen. This showed up in our oscillographic records of strain gages used to measure displacement. They were more pronounced during the initial run-in period when metal rubbed against metal, and tended to disappear as the test proceeded, and as oxide filled the space between the two metal surfaces. These perturbations were not of sufficient magnitude to alter the approach to mechanism based on sine-wave oscillations described in the paper following the present one.

Mr. Barwell's observations of change in conductivity of oxide exposed to varying humidity is interesting and confirms that the oxide itself is altered by water vapor, in addition to any effect moisture may have on the surface of the steel. It is well known in corrosion investigations that iron oxides tend to absorb and retain moisture, accelerating the rusting process. But in the fretting process the action of moisture is to reduce damage, and, therefore, it appears that moisture may, among other effects, reduce the abrasive action of the oxide in addition to acting as a possible lubricant.

In answer to Mr. Godfrey: His comments that physical properties of ferric oxide may be altered have been touched upon in the foregoing discussion on effect of moisture. There appears to be no doubt that the oxide plays an important part in the observed damage, but we are not inclined to the opinion that several variables of the tests affect the oxide alone to the exclusion of the metal surface.

Our reported data include, of course, both the initial and later stages of fretting, with the exception that the very late stages leading to fatigue or corrosion-fatigue cracking were not included. To observe the latter damage, so important from a practical standpoint, we would have found it necessary to continue our test periods for much longer times than we felt were justified at this stage of our knowledge. The fatigue aspect of fretting damage, however, deserves serious attention.

The facts indicate that a suitable definition of fretting action or fretting damage apparently does not require the inclusion of reciprocal motion. For example, in the Amsler wear machine used by M. Fink and by others to study fretting action, the motion is one of continuous slip of one surface over another, and the debris consists of both chemical reaction products and metallic particles.

Weight loss as a criterion of fretting damage has already been discussed in the foregoing, and whether one should use it or not when a metal is fretted in nitrogen depends entirely on the objective of the test. In the study of mechanism, with which we were concerned, weight loss proved to be a useful measure of damage.

The appearance of our test specimens was as follows: After test, the fretted surfaces consisted of compacted iron oxides, reddish brown in color, and outwardly relatively smooth. After

[4] Lewis Flight Propulsion Laboratory, National Advisory Committee for Aeronautics, Cleveland, Ohio.

pickling to remove such oxides, the metal surface was very rough, more or less pitted, and looked like the test specimen shown in Fig. 2(*b*). The pickle, as mentioned in the paper, was inhibited to prevent any appreciable attack of the metal itself. The extent of pitting was much less or absent in the case of a specimen fretted in nitrogen.

# Critical Examination of Procedures Used in Britain and United States to Determine Creep Stresses for Design of Power Plant for Long Life at High Temperature[1]

ERNEST L. ROBINSON.[2] It is very desirable to have the comparisons between British and American practice with respect to the use of materials at high temperature. However, a first reading of the paper suggests that we may be dealing at too long range for the most effective assistance to each other. With practice and standards subject to steady change and progressive improvement on both sides of the ocean, it is hard to be sure that each of us is not worried about the other's last year's out-moded procedure. In the case of specific activities, it would be good if we could find the means to send regular and official visitors both ways more often than has been done in the past.

In criticizing American design practices, the author quotes a statement from October, 1951, *Mechanical Engineering*, adopted by the Power Piping Section of the Code for Pressure Piping. This statement is a partial extract from a similar statement in August, 1951, *Mechanical Engineering*, which was itself an abbreviated résumé of the basis used by the Subcommittee on Stress Allowances of the ASME Boiler Code Committee. The complete statements of these rules for choice of stresses will be found for unfired pressure vessels in Appendix P of the 1950 Unfired Pressure Vessel Code, published in September, 1949, and as more recently revised in the 1952 Unfired Pressure Vessel Code, published March 15, 1953, and for Power Boilers, Section A-150 of the Power Boiler Code, published June 15, 1953. A comparison of these statements with the similar statements published in November, 1949, *Mechanical Engineering*, shows how ideas about essential requirements change from year to year in a particular and limited field of design.

Certainly, American practices in the design of jet engines, piston engines, superchargers, gas turbines, and steam turbines differ widely both among themselves and from the practical requirements of steam-generating equipment or high-temperature piping. It is the writer's impression that, in the United States, we make much use of the long-time rupture test such as described in part by Procedure 3, and that greater emphasis is attached to this test in jet-engine design and a lesser emphasis in the case of the design of steam generators whereas long-time rupture testing in Britain is largely confined to acceptance testing. It seems to me that British practice could well make wider use of this manner of testing for design guidance.

Twenty years ago, the author advocated "trading time and temperature" and his voice has not been unheard in the United States. He does not refer to the Larson-Miller parametric analysis which does just what he advocates, namely, run a short test at over temperature for long-time guidance. The Larson-Miller analysis was presented in November, 1951, and published in ASME Transactions for July, 1952. Although the Larson-Miller algebra differs from the Bailey algebra, the consequent outcome is similar to a high degree and, as far as my limited understanding goes, both analyses recognize the use of certain fundamental concepts of physical chemistry.

The author notes that pipe stresses are likely to be somewhat less than the published figures to put in the wall-thickness formula. In other words, American practice entrusts a part of its safety to the application of its formula rather than its choice of working stresses. Personally, the writer would prefer a somewhat more realistic formula together with a somewhat lower working-stress table. However, a new wall-thickness formula recently adopted for boilers and piping has done much to improve this situation. This was presented by W. R. Burrows, R. Michel, and A. W. Rankin in a paper entitled "A Wall Thickness Formula for High-Pressure High-Temperature Piping," Trans. ASME, vol. 76, 1954, pp. 427–444.

C. R. SODERBERG.[3] The author addresses himself to one of the most fundamental of the many questions concerning the application of creep data to engineering design. This is the question of whether or not the material in the course of the test alters its character, so that at the end of the test it may in fact have changed into another material. He gives this phenomenon the name "thermal-action effect" and presents a great many worthwhile points on how this effect may be taken into account. He is particularly concerned about the fact that this effect may render dangerous certain routine measures of straight-line interpolation.

The author has performed a valuable service in thus embodying his vast knowledge and experience on the subject in a few simple formulas. Exactness is not claimed for these expressions and it is perhaps somewhat unfair to criticize their approximate nature. Not the least valuable of his conclusions is his emphasis on Procedure 4, in which the dilemma of thermal-action effect is partly overcome by trading temperature for time, a procedure which also has come into vogue in the United States.

The phenomenological problem involves expressing the behavior of a substance under stress through the variables (using the author's notations) $f$, $\dot{x}$, $x$, $t$, and $\theta$. Assuming that the temperature is kept constant, he postulates a relationship between the other four variables by his Equation [3]. It is, of course, implied that this equation is based upon experience, and undoubtedly many tests could be cited in its support. Actually, however, this equation postulates a relationship which is much more rigid than that which is generally encountered in nature.

The loosest type of relationship which can be assumed is an equation connecting the differentials of these four variables. The writer has previously[4] used the following form for this relationship

$$df = \phi d\dot{x} + \psi dx - \varphi dt \quad \ldots\ldots\ldots\ldots\ldots\ldots [1]$$

The functions $\phi$, $\psi$, and $\varphi$ have been given the names "viscosity," "strain-hardening," and "annealing." A relation such as the author proposes in his Equation [3] assumes that these quantities are "properties" of the substance, depending upon the variables in a specified manner and not on the previous history. The criteria of the existence of these properties may be reduced to the question of whether $df$ is an exact differential or not. The

[1] By R. W. Bailey, published in the December, 1954, issue of the JOURNAL OF APPLIED MECHANICS, Trans. ASME, vol. 76, pp. 309–322.

[2] Structural Engineer, Turbine Division, General Electric Company, Schenectady, N. Y. Fellow ASME.

[3] Dean of the School of Engineering, Massachusetts Institute of Technology, Cambridge, Mass.; also Professor of Mechanical Engineering. Fellow ASME.

[4] "Plastic Flow and Creep in Polycrystalline Materials," by C. R. Soderberg, Proceedings of the Fifth International Congress of Applied Mechanics, 1938.

mathematicians undoubtedly have much more sophisticated ways of expressing the important aspects of the situation.

Equation [3] of the paper may in fact be written in the differential form

$$n\frac{df}{f} = \frac{d\dot{x}}{\dot{x}} + p\frac{dx}{x} - q\frac{dt}{t} \quad [2]$$

from which certain conclusions could be drawn concerning these properties, once their existence was assumed.

The situation might be described as follows: The materials exhibit certain patterns of behavior, which may or may not be possible of characterization through properties. The tests available permit us to view this complex potential of behavior through certain narrow slits as it were. The test information contains only loose and possibly disconnected fragments of the behavior pattern, and it is usually fruitless to extrapolate from one mode of test to another. An example is the question of whether or not tests at constant stress and temperature (creep tests) really contain the information necessary to predict the behavior when the total strain is held constant and the stress permitted to vary (relaxation). In so far as the writer is aware, this question still must be answered in the negative for most of our materials.

All attempts which have been made to determine these properties in the plastic state of metals at elevated temperatures have so far met with failure. We are thus forced to conclude that the type of properties implied in Equation [1] of this discussion does not generally exist for metals at elevated temperatures. Relationships of the form of Equation [3] of the paper can thus have only the nature of extremely rough approximates. Conclusions based upon such uncertain premises should be viewed with caution. This remark is made without any wish to detract from the author's contribution, but rather to emphasize the need for more exact tests which would put these relationships in a clearer light.

It seems pertinent to observe that the most insidious aspects of temperature and environment relate to the phenomena of embrittlement, leading to the possibility of brittle fracture. It is the writer's impression that this class of thermal effects is not usually reflected in the plastic-deformation pattern. The validity of the author's conclusions on the creep-to-rupture test is certainly dependent upon an assumption, not yet proved, of a relationship between deformation and fracture.

His conclusions on allowable stress are disconcerting but would appear more realistic, at least in the writer's opinion, if they related more directly to the risk of fracture. Does our experience with high-temperature machinery, in so far as deformation is concerned, really justify the author's gloomy forebodings?

### Author's Closure

The author agrees with Mr. E. L. Robinson regarding the unfortunate time lag between the appearance of a paper in one of our countries and current practice in the other country when it concerns a subject which is undergoing continual development of knowledge, principles, or testing technique. Also, he agrees that more frequent contacts between interested individuals of the two countries, as suggested by Mr. Robinson, would be a desirable measure to overcome the delay. This would bring benefit in both countries.

Most will also agree with Mr. Robinson on the need for discrimination in the choice of method or procedure according to the nature of the part and service concerned. Accordingly, it is reasonable to use stress-rupture tests in connection with design of jet-engine parts where usually the total life is not high and virtually within the range of practical test periods. This, however, is not the case with a steam-power plant where even the longest test periods would rarely occupy more than, say, one fifteenth of the life period, e.g., 10,000 hr, when the expected life would be 150,000 hr. It is the possible thermal-action effect of this unexplored very long life which presents uncertainties which require examination and representation for a procedure to be adequate and acceptable for the case of very long life, especially at the higher temperatures.

The Larson-Miller analysis does not do this, but really rules out thermal-action effect in changing the material by regarding $A$ in the relation $1/t = Ae^{-Q/RT}$ as constant. If thermal action changes the material, $A$ is not a constant but is a function of temperature $T$ and time $t$. The parameter advanced by its authors has no more significance than that it implies that the material is not changed by the thermal action encountered in the testing, and the magnitude of the quantity $C$ found for a series of test results represents no more than an average of undefined character. Then, to take an average value of $C$ for some different materials of 20, still further destroys any possibility of reliability for the case it sets out to serve, i.e., to avoid testing of very long duration of a specific material.

In the paper an empirical form was adopted for representing thermal-action effect, Figs. 1 and 2, by a suitable choice of an index $q$. The paper shows the influence of this in explaining the character of the log $f$, log $t$ diagram, Fig. 9, for stress-rupture tests. According to the paper if there were no thermal-action effect, no change in slope would be expected in Fig. 9.

Dean Soderberg quite rightly points to the approximate character of relations which from time to time are proposed to represent the phenomenon of creep, including the derived relations of the paper. That such relations must be approximate is, of course, because in the first place it has not been found possible to represent comprehensively the phenomenon of creep as exhibited by the characteristic strain-time curve for simple tension except by treating it in stages and between limits, or as viewed through "certain narrow slits" in Dean Soderberg's words. But keeping these limitations in mind, and because as a rule the acceptable magnitudes of strain are not large in practice, the approximate character of most relations, direct or derived, especially for a specific material defined by actual test data, is serviceable for design purposes.

The author does not consider that our experience with high-temperature machinery, as gained so far, would justify gloomy forebodings—or incidentally was he aware of having them—for the reason that design standards on the whole have been conservative and also that there is very little long-time experience at the highest temperatures now in vogue, where the expected full life of plant may be as much as 150,000 hr, or, say, 20 to 25 years. It is because of this comparatively untried and untested circumstance that importance is attached to understanding and taking into account the influence of thermal-action effect so that the probable behavior of the material in its later life may be assessed.

## Remarks on Donnell's Equations[1]

Abdon Rubio.[2] The problem of determining the stresses and displacements of a cylinder under various types of semiconcentrated actions is an important and complicated one. The author has presented a very interesting comparison between the well-known Donnell equations and the much more complete shell

[1] By Joseph Kempner, published in the March, 1955, issue of the Journal of Applied Mechanics, Trans. ASME, vol. 77, pp. 117–118.

[2] Structural Improvements Engineer, Large Steam Turbine-Generator Department, General Electric Company, Schenectady, N. Y.

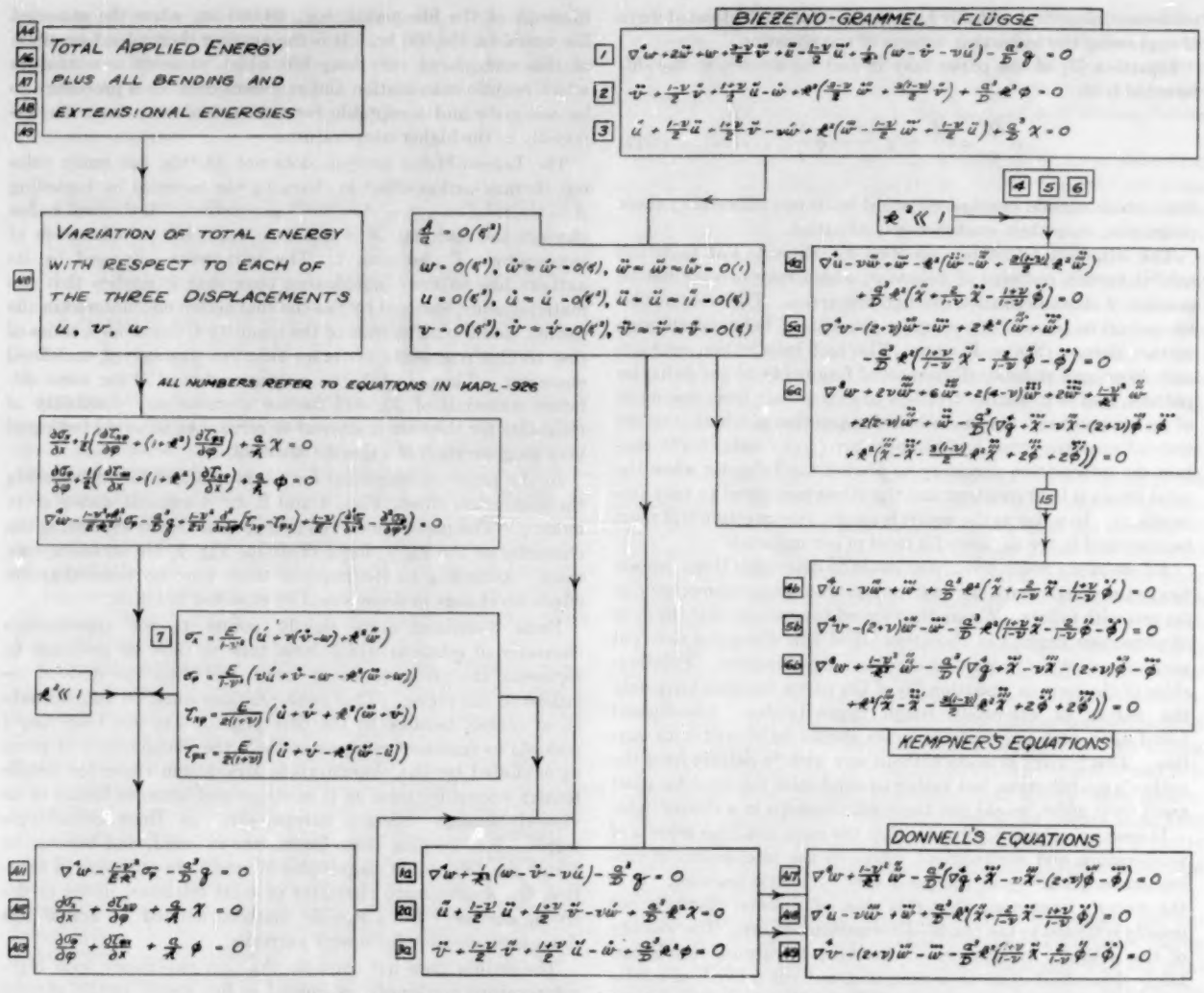
BIEZENO-GRAMMEL FLÜGGE
TOTAL APPLIED ENERGY PLUS ALL BENDING AND EXTENSIONAL ENERGIES
VARIATION OF TOTAL ENERGY WITH RESPECT TO EACH OF THE THREE DISPLACEMENTS u, v, w
ALL NUMBERS REFER TO EQUATIONS IN KAPL-926
KEMPNER'S EQUATIONS
DONNELL'S EQUATIONS

FIG. 1 COMPARISON BETWEEN TWO SETS OF SHELL EQUATIONS

equations found in the texts by either Flügge, or Biezeno and Grammel. However, the author was not able, in this short paper, to include many of the manipulations and arguments necessary for the development of the various equations. The writer wishes to present, in a block diagram, Fig. 1, herewith, two basic origins of shell equations. In this way note may be taken of where Donnell's order-of-magnitude argument takes place and just where differences, if any, exist between the two sets of displacement equations. The notation used is identical to that of the paper being discussed.

The writer has borrowed heavily from the author's KAPL-926 report. Indeed, all the numbers attached to the equations in the block diagram refer to that report, though some of them also appear in the paper.

It should be noted in the energy derivation that in order to arrive at the equilibrium Equations [A11], [A12], [A13] it was necessary to assume that $k^2 \ll 1$. There also could be considerable question as to how the

$$\frac{\partial^2 \sigma_x}{\partial x^2} - \frac{\partial^2 \sigma_\varphi}{\partial \varphi^2}$$

term disappears from Equation [A11]. This is undoubtedly the place where the terms which will be noted missing in Donnell's equations were dropped.

The order-of-magnitude argument of Donnell and the stress-displacement relationships may then be used to arrive finally at the Donnell equations. An alternative method of obtaining exactly the same equations is shown on the diagram starting with Flügge's equations. The author also begins with Flügge's equations and, by a clever method of differentiating and recombining, is able to produce an eighth-order linear partial differential equation in only one displacement (radial). Once the solution to this equation is obtained, it is relatively simple to determine the other displacements.

Equations [4], [5], and [6] on the block diagram correspond to Equations [14], [15], and [16], in the paper. If the assumption of $k^2 \ll 1$ that he suggested is used, the result is Equations [4a], [5a], and [6a]. Furthermore, Donnell's order-of-magnitude argument may be applied to these equations which results in Equations [4b], [5b], and [6b]. Note should be taken of the correspondence between these equations and Donnell's equations. Since the same arguments and assumptions are made in both derivations, exactly the same result should appear. They do not correspond because the sequence of imposing the assumptions is different.

The author expresses satisfaction at the correspondence he received between calculations from his equations and Donnell's equations. The writer believes that this satisfaction is not warranted from the results presented, since all the calculations were made at the middle of the line load on the generatrix, as far as possible away from the load discontinuity. It would be quite gratifying if the author also were able to show agreement between the two sets of equations at points of load discontinuity. In addition, it should be noted that the author only claims correspondence when all surface and body forces are zero. In this case it can be seen that Equations [A17], [A18], [A19] and [4*b*], [5*b*], [6*b*] are identical.

In closing, the author should be commended on the significant work he has done in this field and on his efforts to spread an understanding of shell problems.

LU TING.[3] In a previous paper, Hoff, Kempner, and Pohle[4] questioned the accuracy of Odqvist's work,[5] which was based upon Schorer's equation,[6] and resolved Odqvist's problem by using Donnell's equation,[7] which was derived to study the problem of stability. In the present paper, a numerical example was worked out to compare the results from the solutions in the previous paper with those from the solution of the exact equation.[8] Using the same data, the writer obtained the corresponding results from Odqvist's simple explicit solution[9] and inserted them into Table 2 of the present paper. The comparison is given in Table 1, herewith.

TABLE 1 COMPARISON OF FOURIER COMPONENTS OF DISPLACEMENT AND CIRCUMFERENTIAL MOMENT RESULTANT AT $z = 0$, $\psi = 0$

| | $(w_m/P^*) \cdot 10^4$ | | | $M_{\varphi m}/P^*$ | | |
|---|---|---|---|---|---|---|
| $m$ | From solution of "exact Eqs." [14–16] | From solution of "Donnell Eqs." [8–10] | From Odqvist solution | From solution of "exact Eqs." [14–16] | From solution of "Donnell Eqs." [8–10] | From Odqvist solution |
| 1 | 0.112 | 0.104 | 0.101 | 0.501 | 0.0497 | 0.0499 |
| 3 | 0.0219 | 0.0214 | 0.0193 | 0.0332 | 0.0282 | 0.0286 |
| 5 | 0.0107 | 0.0106 | 0.0088 | 0.0213 | 0.0213 | 0.0218 |
| 7 | 0.0068 | 0.0067 | 0.0052 | 0.0174 | 0.0174 | 0.0179 |
| 9 | 0.0047 | 0.0047 | 0.0034 | 0.0147 | 0.0147 | 0.0153 |
| 11 | 0.0035 | 0.0034 | 0.0024 | 0.0126 | 0.0126 | 0.0132 |
| Sum | 0.160 | 0.151 | 0.140 | 0.1443 | 0.1439 | 0.1467 |

It is evident that Odqvist's solution is quite satisfactory for the leading terms in this example where $a/h = 56$ and will be more accurate for larger values of $a/h$.

Based upon numerical results the author concluded "for short cylinders loaded over small regions of their surface the simple Donnell's equations are quite adequate . . .." The phrase "for short cylinders," which implies a limitation on the ratio of $L/a$ only, should be replaced by "for cylinders with $L/a \ll [3(1-\nu^2)a^2/h^2]^{1/4}$." Furthermore, the boundary conditions of the cylinders should have been prescribed. For example, the simple Donnell's equations[7] are not adequate for cylinders with free ends.

YI-YUAN YU.[9] While the author and his co-workers have recently made extensive and successful use of the Donnell equations, the writer would like to take the opportunity to report that a corresponding set of dynamic equations has been derived in a forthcoming paper[10] in a somewhat modified manner as Donnell derived the static equations. The usual set of equations of motion for thin cylindrical shells such as that given by Flügge[11] may also be arranged to appear in an analogous form. Terms involving $q$, $X$, and $\Phi$ in the author's Equations [8] to [10] and [14] to [16] are replaced by terms including the time $t$ as an independent variable in these dynamic equations.

### AUTHOR'S CLOSURE

The author wishes to express his appreciation to Mr. Rubio, Mr. Ting, and Professor Yu for their comments.

Mr. Rubio's interest in the stresses at the load discontinuity (only a distance $\delta/L = 1/40$ from the station considered) is understandable. Good agreement can be expected in a neighborhood even more immediate to the discontinuity than that considered.

Mr. Ting points out that Odqvist's solution for $w$ and $M_\varphi$ is quite adequate for the example presented. One certainly should use this solution when confident of its applicability. The condition, $L/a \ll [3(1-\nu^2)a^2/h^2]^{1/4}$, suggested for defining short cylinders is much too strict. In the present example this criterion would state $4 \ll 9.6$, which is certainly not true. Furthermore, if applied to Equation [8], it would require the omission of the second term on the left-hand side and hence, neglect of the entire "shell effect" therein. As far as boundary conditions are concerned, it was stated in the text that the shell was simply supported, the defining relations being given in footnote (4).

# Gravitational Stresses in a Circular Ring Resting on Concentrated Support[1]

H. MARCUS.[2] The author presents an interesting application of Muschelisvili's method based on complex variables. He does not mention other methods used for similar problems in two-dimensional elasticity.

It seems worth while to remember that simple and elegant solutions of the same type of equations have been obtained in the theory of circular plates by using stress functions[3] such as

$$F = \sum_n \left[ \left( A_n + \frac{r^2}{r_0^2} B_n \right) \cos(r, n) + \left( C_n + \frac{r^2}{r_0^2} D_n \right) \sin(r, n) \right] \cos n\Phi, \quad n = 1, 2, 3, \ldots$$

where

$$\cos(r, n) = \frac{r^n + r^{-n}}{2}, \qquad \sin(r, n) = \frac{r^n - r^{-n}}{2}$$

$r$ and $\Phi$ being cylindrical co-ordinates.

---

[3] Special Design Engineer, Foster Wheeler Corporation, New York, N. Y.

[4] "Line Load Applied Along Generators of Thin-Walled Cylinders," by N. J. Hoff, J. Kempner, and F. V. Pohle, *Quarterly of Applied Mathematics*, vol. 11, January, 1954, p. 411.

[5] "Action of Forces and Moments Symmetrically Distributed Along a Generatrix of a Thin Cylindrical Shell," by F. K. G. Odqvist, *Journal of Applied Mechanics*, Trans. ASME, vol. 68, 1946, p. A-106.

[6] "Line Load Action on Thin Cylindrical Shells," by H. Schorer, ASCE, vol. 61, 1935, pp. 281–316.

[7] "Stability of Thin-Walled Tubes Under Torsion," by L. H. Donnell, NACA TR 479, 1933.

[8] "Statik und Dynamik der Schalen," by W. Flügge, Julius Springer, Berlin, Germany, 1934, p. 115.

[9] Associate Professor of Mechanical Engineering, Syracuse University, Syracuse, N. Y. Assoc. Mem. ASME.

[10] "Free Vibrations of Thin Cylindrical Shells Having Finite Lengths With Freely Supported and Clamped Edges," by Yi-Yuan Yu, to be published in the JOURNAL OF APPLIED MECHANICS.

[11] Footnote (8), p. 229.

[1] By Yi-Yuan Yu, published in the March, 1955, issue of the JOURNAL OF APPLIED MECHANICS, Trans. ASME, vol. 77, pp. 103–106.

[2] Consultant, Mechanics Division, Naval Research Laboratory, Washington, D. C.

[3] "Die Theorie elastischer Gewebe und ihre Anwendung auf die Berechnung biegsamer Platten," by H. Marcus, second edition, 1932 (Library of Julius Springer, Berlin), and "Die elastischer Platten," by A. Nadai, 1925 (Library of Julius Springer, Berlin).

The stresses acting on any cylindrical surface can be expressed in terms of the constants $A_n$, $B_n$, $C_n$, $D_n$, and in the form of Fourier series.

If two loading or support conditions are prescribed also in the form of such series for the internal boundary $r = r_i$ and the external boundary $r = r_e$, we obtain for each value of $n$ four easily solved equations for the constants $A_n$, $B_n$, $C_n$, $D_n$.

This method is very useful for the analysis of the stresses produced in a large body by forces applied on the periphery of a cylindrical cavity.

F. E. NAGEL.[4] The dimensional parameters in Fig. 2 of the paper require clarification. One may take $W$ to be capital denoting the weight of the ring rather than weight density of material and $\tau$ the stress multiplied by the axial ring thickness to obtain a nondimensional parameter $\pi R\tau/W$. The rate of decay of the high stresses at the singularity near $\theta = -90$ deg, $\rho = 1$ is of interest and makes numerical evaluation at sections like $\theta = -80$ deg desirable. A comparison of the method presented with the elementary analysis of narrow rings, having a statically indeterminate tangential load and moment at $\theta = 90$ deg will furnish the engineer with a guide for the necessity of the much more involved, though rigorous analysis of the author. It may be expected that outside of the mathematical singularity which cannot be realized in practice, the simplified analysis is quite sufficient for $1/2 < \rho_0 < 1$ in many engineering applications, while, of course, for $\rho_0 \to 1$ the difference between the two methods vanishes altogether.

### AUTHOR'S CLOSURE

The author wishes to thank Dr. Marcus and Mr. Nagel for their interest in the paper.

The two well-known references mentioned by Dr. Marcus are not now available to the author. It is presumed that the form of the stress function given by Dr. Marcus refers to the general solution of the biharmonic equation in polar co-ordinates, which includes both cosine and sine terms and in which the terms corresponding to $n = 1$ are somewhat different from others. This general solution may be found in Timoshenko's book,[5] in which is also mentioned its application to the problem of a circular ring compressed by two equal and opposite forces acting along a diameter. There are two axes of symmetry in Timoshenko's problem (compared with one axis of symmetry in the problem in this paper), and the resultant force on each of the two boundaries vanishes; the problem is therefore simpler. Nevertheless, its solution[6] also appears in a series form, and a large number of terms is needed to calculate the stresses accurately. It is doubtful that the problem considered in this paper can be solved any simpler by means of the general solution in polar co-ordinates.

In solving problems related to a circular plate or a large body with a cylindrical cavity, as mentioned by Dr. Marcus, the complex variable method is almost invariably simpler and more elegant than the other methods. Its simplicity may be seen by comparing Symond's series solution[7] of the problem of a large plate containing an elliptical hole loaded by two concentrated forces with the closed-form solution of the same problem obtained by Green[8] using the complex-variable method. The elegance of the complex-variable method was indicated clearly by Morkovin[9] who applied the method to Greenspan's problem[10] of a uniformly loaded plate weakened by a small hole; the latter author had solved the problem in an extremely laborious way. The various problems related to the circular plate, including the mixed-boundary value problem, have also been solved by means of the complex-variable method in an elegant and systematic manner.[11]

Regarding Fig. 2, there appears to be a misunderstanding on the part of Mr. Nagel. None of the parameters in the figure is dimensional, and the letter $W$ is capital, as may also be seen from Table 2, according to which the curves were plotted.

The problem considered in this paper was also solved by Van den Broek[12] using the elementary energy method. For comparison purposes, the normal stress $\tau_{\theta\theta}$ in the same example in which $\rho_0 = 1/2$ has been computed according to Van den Broek's elementary solution. The results are listed in Table 1 and compared with those obtained according to the exact solution in this paper. Needless to say, the elementary solution does not indicate any normal stess $\tau_{\rho\rho}$ in the radial direction; and, according to it, only an average value of the shearing stress $\tau_{\rho\theta}$ can be computed at each cross section of the ring.

TABLE 1

| Section | $\rho$ | $\tau_{\theta\theta}\pi R/W$ (elementary solution) | $\tau_{\theta\theta}\pi R/W$ (exact solution) | Per cent difference |
|---|---|---|---|---|
| $\theta = +90°$ | 0.5 | +5.000 | +6.118 | 18.3 |
| | 1.0 | −4.000 | −2.911 | 37.4 |
| $\theta = +45°$ | 0.5 | +0.618 | +0.494 | 25.1 |
| | 1.0 | −1.020 | −0.587 | 73.8 |
| $\theta = 0°$ | 0.5 | −6.710 | −8.896 | 24.6 |
| | 1.0 | +3.568 | +2.929 | 21.8 |
| $\theta = -45°$ | 0.5 | −4.828 | −6.326 | 23.7 |
| | 1.0 | +0.788 | +0.572 | 27.4 |
| $\theta = -90°$ | 0.5 | +15.000 | +14.912 | 8.4 |
| | 1.0 | −14.000 | $-\infty$ | $\infty$ |

# Experimental and Theoretical Study of Transverse Vibrations of a Tube Containing Flowing Fluid[1]

G. W. HOUSNER.[2] The beam equation containing a mixed space-time derivative offers some difficulties for the mixed derivative connotes a coupling between the modes of vibration. This paper shows how a power-series solution can be evaluated and it points out the precautions necessary to obtain a satisfactorily accurate solution. The experimental work described by the author gives a check on the theory. As the author points out, the influence of the flowing fluid on the vibrations of the tube are

[4] Aircraft Gas Turbine Division, General Electric Company, Cincinnati, Ohio. Mem. ASME.

[5] "Theory of Elasticity," by S. Timoshenko and J. N. Goodier, McGraw-Hill Book Company, Inc., New York, N. Y., second edition, 1951, pp. 116–122.

[6] "On the Distribution of Stresses in a Circular Ring Compressed by Two Forces Acting Along a Diameter," by S. Timoshenko, *Philosophical Magazine*, vol. 44, 1922, pp. 1014–1019.

[7] "Concentrated Force Problems in Plane Strain, Plane Stress, and Transverse Bending of Plates," by P. S. Symonds, JOURNAL OF APPLIED MECHANICS, Trans. ASME, vol. 68, 1946, pp. A-191–A-195.

[8] "A Concentrated Force Problem of Plane Strain or Plane Stress," by A. E. Green, JOURNAL OF APPLIED MECHANICS, Trans. ASME, vol. 69, 1947, p. A-246.

[9] "Effect of a Small Hole on the Stresses in a Uniformly Loaded Plate," by V. Morkovin, *Quarterly of Applied Mathematics*, vol. 2, 1944, pp. 350–352.

[10] "Effect of a Small Hole on the Stresses in a Uniformly Loaded Plate," by M. Greenspan, *Quarterly of Applied Mathematics*, vol. 2, 1944, pp. 60–71.

[11] "Some Basic Problems of the Mathematical Theory of Elasticity," by N. I. Muschelisvili, translated by J. R. M. Radok, P. Noordhoff Ltd., Groningen, Holland, 1953.

[12] "Elastic Energy Theory," by J. A. Van den Broek, John Wiley & Sons, Inc., New York, N. Y., second edition, 1942, pp. 108–117.

[1] By R. H. Long, Jr., published in the March, 1955, issue of the JOURNAL OF APPLIED MECHANICS, Trans. ASME, vol. 77, pp. 65–68.

[2] California Institute of Technology, Pasadena, Calif.

small for proportions usually encountered in practice; however, the extensions of the problem can have practical applications.

The beam-bending vibrations, considered by the author, may be designated as the first class of coupled fluid-structure flexural vibrations, and the second class would be the coupled fluid-structure flexural vibrations of the wall of the container; that is, where the axis of the tube remains straight while the wall oscillates with plate-like vibrations. The influence of the fluid is much greater for such vibrations, particularly for tubes or pipes of large radius. In certain practical problems it has been found that pressure fluctuations in the fluid would excite severe vibrations of the pipe wall. Similar problems are encountered with the skin of aircraft. We are now in a trend toward higher velocities, larger structures, thinner and more closely designed sections, etc., and it can be expected that problems of coupled fluid-structure vibrations will be encountered more often in the future.

# Influence Coefficients for Hemispherical Shells With Small Openings at the Vertex[1]

W. R. Burrows,[2] R. L. Graves,[3] P. G. Stevens.[4] The author's innovational approach to the problem has significantly influenced, during the past year, the course of our work for the Design Division of the Pressure Vessel Research Committee. Following the author's lead, we have extended his investigations of the constant-thickness spherical head to include studies of two other approximate solutions which, like his Methods I and II, are even now suitable for use by engineers; and which, moreover, exhibit exceptional possibilities of further simplification owing to the exponential-trigonometric character possessed by all four in common.

Our preliminary findings concerning the accuracy of these four approximations have been obtained by a comparison of their solution results with PVRC's accurate first and second solution results.[5] The PVRC accurate method is similar in form to that of the author's Method III(b). Solution results have been calculated with it at Whiting for every 5 deg of arc for a constant-thickness hemispherical head with a diameter-thickness ratio of 30 (Memorandum D54-2, Stevens, January 15, 1954, May 20, 1954).

Specifically, the four solutions under study are, in the author's notation:

1 The Geckeler approximation, the author's Method 1

$$Q_\phi = \text{Exp}\,[\pm(1+i)\rho(\phi-\phi_b)]$$

2 The asymptotic approximation

$$Q_\phi = (J/J_b)[(1 \pm F_1) - i(\pm F_1 - G_1)](\text{Solution 1})$$

3 The Bessel approximation, the author's Method II

$$Q_\phi = \frac{B}{K^{er_1}(2^{0.5}\rho\phi)} + i\,\frac{B}{K^{ei_1}(2^{0.5}\rho\phi)}$$

4 The Langer approximation (Graves)

$$Q_\phi = [(\phi \csc \phi)/(\phi_b \csc \phi_b)](\text{Solution 3})$$

The solutions are those for the second-order system. In these solutions $\phi_b$ is the angle from the center to some reference or boundary point $b$. The Geckeler approximation is exactly the same as the author's Equation [6] or [8]. The asymptotic approximation is PVRC's development of the method of Prof. F. B. Hildebrand in a form consisting of Solution 1 with two corrective coefficients. The Bessel approximation is expressed in Kelvin functions. The Langer approximation is Solution 3 with one corrective coefficient.

Now all of these solutions (1 to 4) become unity in value at a point $b$, either in the form shown or after multiplication by a suitable constant. Hence, if they differ among themselves or from the accurate solution, it will be their $\phi$-derivatives that do so. This then is our method of comparison.

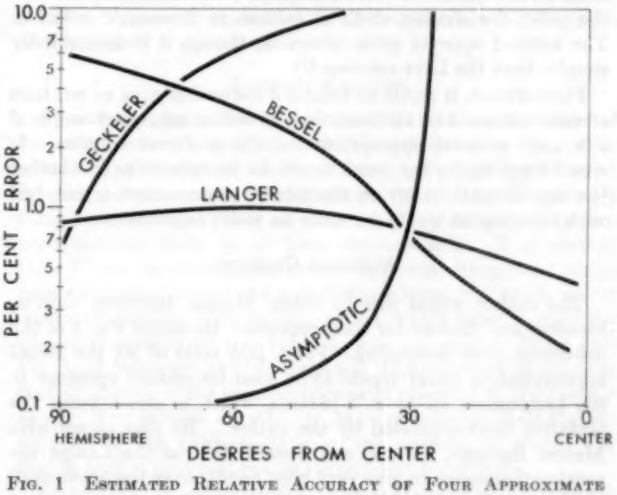


Fig. 1 Estimated Relative Accuracy of Four Approximate Solutions of a Constant-Thickness Spherical Head With Diameter-Thickness Ratio of 30

The results shown in Fig. 1 illustrate our present findings. The Geckeler approximation seems satisfactory for relatively thin, complete hemispheres, while the asymptotic approximation appears satisfactory for relatively thick, complete spherical segments approximating hemispheres. The Bessel approximation appears satisfactory at and near central holes in relatively thin, incomplete spherical segments, while the Langer approximation seems satisfactory at all points on relatively thick complete or incomplete spherical segments including hemispheres.

The possibility of synthesizing these four solutions probably is unusually good, and we are now engaged, when time is available, in this effort. It is reasonable to believe that our similar work on the constant-thickness conical head will now serve as a guide (Memorandum D53-7, April 15, 1953; Graves, March 23, 1953).

G. Horvay.[6] There are two trends in engineering analysis, both of them vital for furthering our understanding of the behavior of engineering structures. One is toward more precise analysis, employing a more accurate physical picture, and utilizing more precise differential equations; the other trend aims at simplifying the existing approaches. Shell theory provides excellent examples for the parallel progress in both directions. The

---

[1] By G. D. Galletly, published in the March, 1955, issue of the Journal of Applied Mechanics, Trans. ASME, vol. 77, pp. 20–24.

[2] Chief Engineer, Special Services Division, Standard Oil Company (Indiana), Whiting, Ind.

[3] Project Mathematician, Engineering Research Department, Standard Oil Company (Indiana).

[4] Assistant Head Engineer, Special Services Division, Standard Oil Company (Indiana).

[5] "The Basic Elastic Theory of Vessel Heads Under Internal Pressure," by G. W. Watts and W. R. Burrows, Journal of Applied Mechanics, Trans. ASME, vol. 71, 1949, Table 3.

[6] Engineer, General Electric Company, Knolls Atomic Power Laboratory, Schenectady N. Y. Mem. ASME. The Knolls Atomic Power Laboratory is operated by the General Electric Company for the Atomic Energy Commission.

search for simplifications which greatly reduce the calculational labor of existing rigorous solutions, without sacrificing their salient features, has been pursued relentlessly for 40 years. The author's numerical comparison of various approximation methods (I Geckeler, II Esslinger[7]) with results of the laborious (but essentially precise) Love theory provides the engineer with a valuable yardstick for the selection of an adequate analytical approach, when his problem is similar to Galletly's.[8]

Pending the establishment of further yardsticks (which are highly desired) the writer would like to see the list of methods compared by the author extended, so as to include also Hildebrand's asymptotic method[9] which constitutes a somewhat improved Geckeler approach without involving more labor, Hetenyi's asymptotic method[10] which is appreciably better but also more laborious, and Naghdi's recent solution,[11] which, though asymptotic, may be regarded, for thin shells, as practically precise through the entire range of the variable $\varphi$, including $\varphi = 0$. (In contrast to Hetenyi's solution, Naghdi's solution remains finite at the pole; for shallow shells it reduces to Reissner's[7] solution. The method appears quite laborious, though it is undoubtedly simpler than the Love solution.[12])

Furthermore, it would be helpful if the author gave an estimate of the time spent on each solution, as well as suggested ranges of $a/h$ and $\varphi_0$ most appropriate for the preferred solution. It would be probably too much to ask for an opinion as to whether the approximations err on the side of conservatism or not, but such information would certainly be much appreciated.

### Author's Closure

The author would like to thank Messrs. Burrows, Graves, Stevens, and Horvay for their remarks. He found Fig. 1 of the discussion most interesting. For a $D/h$ ratio of 30, the Bessel approximation would appear to be good for central openings in the hemisphere up to $\pi/3$ radians, which is about twice the tentative limit suggested by the author. He also agrees with Messrs. Burrows, Graves, and Stevens that as the Langer approximation seems to give very good results over the whole shell surface, it warrants further investigation.

Unfortunately, the author has not had time to compute the influence coefficients by the methods of Professors Hetenyi and Naghdi-de Silva, as suggested by Dr. Horvay, although such a comparison would be worth while. However, about two years ago, Messrs. Burrows and Graves computed them using their own asymptotic development of Professor Hildebrand's solution and sent them to the author in a private communication. The author has also computed the influence coefficients utilizing the approximate method outlined on pp. 163–168 of Hetenyi's book, "Beams on Elastic Foundation." The results of these calculations are tabulated in Table 1 together with those obtained using Love's exact method (Method III($b$) in the paper).

TABLE 1 VALUES OF INFLUENCE COEFFICIENTS OBTAINED BY DIFFERENT METHODS

| Method | Unit moments at the edge $\phi = \phi_0$ | | Unit forces at the edge $\phi = \phi_0$ | |
|---|---|---|---|---|
| | Ehu | EhV | Ehu | EhV |
| Love | 47.64 | 36.24 | 164.66 | 47.71 |
| Burrows-Graves Asymptotic | 46.72 | 35.92 | 162.77 | 46.73 |
| Hetenyi Approximate | 42.79 | 31.72 | 145.56 | 42.82 |

It can be seen that the Burrows-Graves asymptotic solution gives values which deviate from Love's by only 2 per cent, while the approximate method of Hetenyi gives errors up to 13 per cent. It is also interesting to note that the asymptotic method gives slightly smaller errors for the influence coefficients than does the Bessel approximation (see Table I in the paper, Method II). As the semiangle of the opening was only $10^1/_2$ degrees for the shell investigated, reference to Fig. 1 of this discussion might tend to indicate that the Bessel approximation should be better than the asymptotic. (Fig. 1 is actually for a $2a/h$ ratio of 30, while the shell investigated had a $2a/h$ ratio of 181.) As this is not the case, further investigation of the relative merits of the Bessel and asymptotic methods for varying $a/h$ ratios seems desirable.

With regard to the time spent on the various solutions, the following are approximate estimates:

Geckeler.....15 minutes
Esslinger (Bessel).....2–3 hours
Love.....1 month

The author has not investigated various $a/h$ ratios and $\phi_0$'s. Some work of this nature is, however, currently being done by the PVRC. When this is completed, it will be possible to answer Dr. Horvay's query regarding which method is the most preferable in any given case.

[7] Esslinger's work was preceded by E. Reissner's "Stresses and Small Displacements of Shallow Spherical Shells," I and II, *Journal of Mathematical Physics*, pp. 80–85 and 279–300, 1946.

[8] I.e., the engineer is able, in such a case, to pick out the method which gives him an adequately accurate solution with least expenditure of labor.

[9] "On Asymptotic Integration in Shell Theory," by F. B. Hildebrand, Proc. Symposia in Applied Math., vol. 3, McGraw-Hill Book Company, New York, N. Y., 1950. The paper, "Analysis of Short Tapered Axisymmetrical Shells," by G. Horvay, C. Linkous, J. S. Born, submitted to the Journal of Applied Mechanics, contains a convenient rearrangement of Hildebrand's formulas into a form which, it is believed, will appeal to the stress analyst.

[10] "Spherical Shells Subject to Axial Symmetrical Bending," by M. Hetenyi, Pub. Intern. Assoc. Bridge Struct. Eng., vol. 5, 173, 1938. The paper is discussed at length in Timoshenko's "Plates and Shells," McGraw-Hill Book Company, Inc., 1940, p. 473.

[11] "On Elastic Ellipsoidal Shells of Revolution," by P. M. Naghdi and C. N. de Silva, Proceedings of the Second National Congress of Applied Mechanics, ASME, 1954.

[12] For an exposition of the mathematical ideas involved in Naghdi's method, see the Section on the WKBJ approximation (as extended by Langer) in the book "Methods of Theoretical Physics," by P. M. Morse and H. Feshbach, McGraw-Hill Book Company, Inc., 1953, pp. 1092–1106.

## Membrane and Bending Analysis of Axisymmetrically Loaded Axisymmetrical Shells[1]

H. Marcus.[2] The authors made a very valuable contribution to the design of axisymmetric shells by their methodic presentation of practical formulas for computing stress and strain in membranelike shells and also for the analysis of the effects of a moment $M$ and a shear force $H$ applied along a circular edge.

The determination of specific values of $M$ and $H$ for given load and boundary conditions has not yet been shown in this paper. The writer hopes that the authors will give attention to the following considerations:

($a$) It would not be quite logical to compute displacements and rotations due to the external loads as if the shell would be a membrane and then to combine these strains with those which are produced by the edge forces in a shell capable of withstanding bending and shear.

[1] By G. Horvay and I. M. Clausen, published in the March, 1955, issue of the Journal of Applied Mechanics, Trans. ASME, vol. 77, pp. 25–30.

[2] Consultant, Mechanics Division, Naval Research Laboratory, Washington, D. C.

(*b*) The forces acting on a circular edge are composed of a normal force $N$, a transverse force $T$, and a couple $M$. It appears more or less arbitrary to assume that the resultant of $N$ and $T$ must be a horizontal force $H$.

R. J. Roark.[3] The writer will comment especially on the formulas for edge-load analysis given in Table 2 of the paper. These are applicable to the calculation of stresses at the junction of parts, a problem that arises in the design of pressure vessels, elevated tanks, domes, high-speed flanged rotors, and many other structural and machine elements. In some cases such discontinuity stresses are not especially important and may safely be permitted to go into the plastic range, but when there is a possibility of brittle fracture or fatigue, or when even a slight plastic strain is not permissible, it becomes necessary to compute such stresses as accurately as possible.

Since Geckeler's formulas, even as modified by Hetenyi, are admittedly approximate, some engineers have expressed misgivings as to the reliability of stress calculations based upon them. Experimental verification requires tests either on the actual structure in question or on a model that must be fairly large because of the local character of the strains to be measured. In either case the experimental work is likely to be expensive and time-consuming, and for that reason relevant published data are rather meager. Any information bearing on the question is therefore of value, and a description of two examples of stress calculation carried out by the writer by means of the Geckeler-Hetenyi formulas, and checked by strain measurements made on the actual structures, may be of interest.

The first example was afforded by a cast-iron drier drum of the type used in paper manufacturing; the drum had a diameter of 12 ft, a thickness of 2 in., and had bolted, slightly dished heads $3^1/_4$ in. thick. An experimental model, full size except for length, had failed during a hydrostatic test by brittle fracture near the ends, and a second model had been constructed and tested with strain gages placed at all points of high stress, especially near the junction of the cylinder and head.

This test made available an excellent opportunity to compare calculated with measured stresses. The agreement was reasonably good, and the calculations also gave results consistent with the recorded failure of the first model.

This problem was complicated by the fact that there were three elements involved—the cylindrical shell, the head, and the shell flange, and solution had to be effected by using equations of strain compatibility as between these three parts. A further difficulty was presented by the fact that the head had an angle of opening $\phi$ of only about 20 deg, which is less than the formulas contemplate.

For such nearly flat heads it is a question whether flat-plate formulas or shell formulas are more appropriate. In this instance the best results were obtained by considering the head to have the "flexibility" of a flat plate and the "expansivity" of a spherical shell, using these terms as they are defined by the authors. (In passing, it may be remarked that there is need for further study of the problem of the almost flat shell.)

The second example was afforded by a welded-steel penstock junction in which the conventional wye was replaced by a sphere, into which the main penstock led and from which the two laterals diverged. The sphere was 12 ft diam and $3^{11}/_{16}$ in. thick; the main pipe was 11 ft diam and $3^{11}/_{16}$ in. thick, and the laterals were 7 ft 9 in. diam and $3^7/_{16}$ in. thick. (The thicknesses were determined by the availability of material rather than by stress considerations.)

[3] University of Wisconsin, Madison, Wis.

The complete assemblage was tested, with strain gages at all critical points, and the measured stresses were found to be in good agreement with the calculated stresses.

Here also the problem was complicated by the presence of a third element, since a heavy reinforcing ring had to be provided at the junction of each pipe with the sphere. All the parts in this structure had relatively thick walls, and the fact that good results were obtained by calculation indicates that the formulas can be used without gross error for $R/h$ ratios as small as 20.

Without wishing to appear unduly critical on a minor point, the writer feels constrained to comment adversely on some of the notation used in this paper. It is reasonable to expect every symbol used to satisfy two requirements: (*a*) It should be familiar, so that anyone can recognize and name it; (*b*) it should be easily written so as to be unmistakably identifiable. The lower case chi and the capital letters in Fraktur fail on both counts. Finally, would it not be better to have as reference (1) the third edition, 1954, and should not reference (2) be Timoshenko's "Theory of Plates and Shells," rather than his "Strength of Materials?"

## Authors' Closure

At a shell edge three actions must be considered, those of horizontal force $H$, vertical force $V$, and moment $M$; correspondingly, there result three motions, horizontal displacement $\delta$, vertical displacement $\nabla$, and angular rotation $\chi$. However, it must be remembered that any one of $H$, $V$, $M$ gives rise (for noncylindrical shells) to all three displacements. The vertical force $V$ may be decomposed into a horizontal component which causes edge-load action and a meridional force, $N_x$, which causes membrane action. This decomposition, which must precede the edge-load analysis of our Table 2, was the central theme (see Fig. 4) of reference (6) "Stresses and Deformations of Flanged Shells;" therefore the argument was not repeated in the present paper. The authors are glad Dr. Marcus re-emphasized the importance of this preliminary step, the omission of which will usually lead to incorrect results for noncylindrical shells.

Hildebrand, in reference (4) of the paper "On Asymptotic Integration in Shell Theory," gives a valuable discussion of the limitations of present theory as caused by separation of the shell problem into a membrane problem and an edge-load problem. The authors are indebted to Professor Roark for furnishing experimental evidence that the Geckeler-Hetenyi formulas are, nevertheless, quite reliable, and for pointing out that assignment to shallow shells the "expansivity" of a flat spherical cap, the "flexibility" of a flat plate, gives good approximate results. The flat shell is undoubtedly a very important configuration. Recent references on this important subject are listed in the discussion of the paper, "Influence Coefficients for Hemispherical Shells With Small Openings at the Vertex," by G. D. Galletly.[4] This discussion is published in this issue, p. 443.

Professor Roark's comments regarding the authors' unconventional notation are appreciated. As an explanation, not an excuse, they wish to point to their (hitherto unsuccessful) search for a notation which will not conflict with notation employed in other branches of stress analysis.

In conclusion the authors wish to express their appreciation to Professors N. J. Hoff and E. Reissner for calling their attention to an important misprint in the paper. The slope $\chi$ of Table 1, Item 1*c*, should read

$$\chi = (\epsilon_x - \epsilon_\theta R/R_x) \cot \varphi - d(R\epsilon_\theta)/dx$$

[4] Journal of Applied Mechanics, Trans. ASME, vol. 77, 1955, pp. 20-24.

# Book Reviews

## Aerodynamics and Jet Propulsion

PHYSICAL MEASUREMENTS IN GAS DYNAMICS AND COMBUSTION. Edited by R. W. Ladenburg, B. Lewis, R. N. Pease, and H. S. Taylor. Vol. IX of "High Speed Aerodynamics and Jet Propulsion." Princeton University Press, Princeton, N. J., 1954. Cloth, 6 × 9½ in., 594 pp., 24 pages of plates, over 100 line drawings, $12.50.

REVIEWED BY RICHARD E. KRONAUER[1]

THIS book, nine in the projected twelve-volume series in High Speed Aerodynamics and Jet Propulsion, is divided into two parts. The first 343 pages under the editorship of the late Professor Landenburg are devoted to measurements in gas dynamics and the remaining 224 pages under the editorship of Dr. Lewis, Professor Pease, and Dean Taylor are concerned with measurements in combustion. Like the other books in the series, it is an assemblage of the work of a number of contributors (22, in this case). The contributors have been actively concerned with the problems of instrumentation and they write with authority. The material is of a uniformly high quality.

The scope of the first part (gas-dynamics measurements) has been limited in keeping with the series title "High-Speed Aerodynamics." With few exceptions, the experimental techniques discussed are aimed at investigations in high-speed wind tunnels and shock tubes. The basic instruments of wind-tunnel research are covered in considerable detail: optical methods (shadow, schlieren, and interferometer) which give fluid density, flow geometry, and (with suitable devices) the Mach number; the impact tube and its behavior throughout the exceptional range of conditions which may be encountered; temperature probes; and the hot-wire anemometer for turbulence studies. Added to this is less widely used instrumentation: afterglow, spectral absorption, and x-ray absorption for low-density measurements; ion tracing, particle tracing, and electrical discharge for velocity measurements; light reflection for shock-front measurements; light absorption and scattering for condensation study. The analog methods of the water table and electrolytic tank round out the presentation.

Since there is no introduction or summary which pictures the problem of gas-dynamics measurements as a whole, the uninitiated reader may have some difficulty in placing the several techniques in perspective. Then, too, the experimenter who is confronted with a flow which is strongly three-dimensional or a situation which precludes optical observation, will find his problem somewhat beyond the scope of this book. The sensing of stream direction and "static" pressure at an interior point of the flow are not dealt with, either in their conventional steady instrumentation or in the less conventional nonsteady forms.

The second part (combustion measurements) is directed principally at the measurement of high-stream temperatures, burning velocity, and fluid composition. That is, the emphasis is on the determination of the structure of the flame front rather than on any associated aerodynamics (including turbulence). The techniques for temperature measurement include radiation methods, thermocouples and hot-wire thermometers, pneumatic and acoustic methods. Burning velocity measurements from both stationary and moving flames are discussed and a large table of recent determinations is thoughtfully included. For composition measurement, sections on spectroscopy and mass spectroscopy are included, but not so a discussion of the problems connected with sampling the combustion field. A section on flame photography is also provided.

Low-pressure investigations have proved extremely valuable in examining the combustion process because the reaction zone thickens with decreasing pressure. A special section is devoted to these techniques, to the kind of results they produce, and to a discussion of the related theories of flame propagation. This last may seem out of place in the book devoted generally to the physical measurements per se, but in this instance it provides a useful service, for the entire section gives the reader the viewpoint of the experimenter from the concept of the investigation through the evaluation of the findings. The complexity of the combustion process and the severe demands placed on measuring apparatus gives the unified viewpoint a special significance in the experimental project.

This book is clearly not a textbook in aerodynamic instrumentation. It is a reference book, but a selective one. Within its intended scope, it is both detailed and stimulating. The bibliographies are thorough and illustrations plentiful. That more topics could not be covered is regrettable, but this fact serves to point up the near impossibility of putting a comprehensive survey between two covers. The present work is rich in ideas and critical evaluation, which makes it both entertaining and rewarding to read from beginning to end.

[1] Assistant Professor of Mechanical Engineering, Harvard University, Cambridge, Mass.

## High-Speed Flow

LINEARIZED THEORY OF STEADY HIGH SPEED FLOW. By G. N. Ward. Cambridge Monographs on Mechanics and Applied Mathematics. Cambridge University Press, New York, N. Y., 1955. Cloth, 5½ × 8½ in., xv and 243 pp., figs., appendixes, bibliography, $6.

REVIEWED BY MAX A. HEASLET[2]

AN indication of the rapid burgeoning of high-speed aerodynamic theory is to be found in the bibliography provided in Professor Ward's book. Approximately 200 titles of research papers are listed and of this number only 12 were published prior to World War II. The basic concepts have long been known, of course, and, in fact, the linearized portion of the theory, with which this book is principally concerned, can be based on the assumptions of first-order acoustic theory. Engineering demands for information, however, have brought about a considerable development of new techniques, a large number of particular solutions, and have spurred the reinvestigation of concepts applicable to the particular problems encountered in the design of high-speed aircraft. The synthesis of the resulting research is a challenging task that is here carried to completion by a man who played a prominant role in the development of the original work.

The present book is the third in the series of Cambridge Monographs on Mechanics and Applied Mathematics. The term monograph is appropriate and differentiates the style from what might be expected in a classroom text. Professor Ward has provided us with a systematic presentation of the general linearized theory of high-speed flow along with a discussion of mathematical methods available for the solution of the boundary-value problems that arise in practice. Vectorial notation is used consistently

[2] Ames Aeronautical Laboratory, National Advisory Committee for Aeronautics, Moffett Field, Calif.

and the resultant conciseness contrasts with the detailed algebra one so often encounters.

The book is divided into three parts. The first of these, entitled "General Theory," has four chapters in which the equations of motion are established, the general solutions in subsonic and supersonic flow are developed, and boundary conditions, uniqueness, and flow-reversal theorems are discussed. The second part, entitled "Special Methods," has four chapters in which subsonic and supersonic wing theory is treated in detail, along with a chapter on conical fields in supersonic flow and a special chapter devoted to the application of operational methods in supersonic flow. In the third part, slender-body theory in both the subsonic and supersonic regimes is treated.

Beginners in aerodynamics may not feel here the lively sense of a physical world to be studied and understood, as in the writings of a Prandtl or a Munk. The book does, however, convey well the spirit and trend of modern work and professional investigators will want to have ready access to it.

## Particle Size and Distribution

THE PHYSICS OF PARTICLE SIZE ANALYSIS. British Journal of Applied Physics, Supplement No. 3, October 15, 1954. The Institute of Physics, London, S.W. 1., England. Price 35s.

REVIEWED BY A. ALI KHEIRALLA[3]

THIS is a collection of 33 papers presented at a conference on the physics of particle-size analysis held at the University of Nottingham, April 6–9, 1954. There were eight sessions of which the first two were devoted to nine papers on the relative motion of particles and fluids, including both molecular phenomena and problems of size separation. The third session treated scattering and absorption of light by particles and the fourth session dealt with particle shape factors. The next three sessions consisted of 13 papers on the counting and sizing of particles, including visual and photoelectronic methods. The final session was devoted to five miscellaneous papers.

The publication should be of interest to all who are concerned with airborne dust clouds, particle distributions in lubricants and fuels, filtration, elutriators, and particle counting and sizing machines.

## Metal Cutting

FORMAZIONE DEL TRUCIOLO METALLICO. By F. Alberto Isnardi. Published by Ulrico Hoepli, Milan, Italy, second edition, 1955. 7 × 9¾ in., xvi and 269 pp., 249 ill., 11 tables, Lire 2600.

REVIEWED BY MILTON C. SHAW[4]

THIS book, which treats the question of chip formation in considerable detail, is divided into five parts. The first part has to do with the geometry of tools for turning, threading, boring, and cutoff. The principal tool angles are clearly defined in terms of the European and American systems of nomenclature, and useful relationships between these two systems are presented.

In the second part, the literature of chip formation is reviewed in considerable detail, starting with the work of Thime in 1877. Many of the more important papers appearing in the British, German, French, American, and Italian literature are discussed. A wide variety of topics is considered here, including plastic flow during chip formation, tool temperatures, tool wear, and cutting-fluid action.

In the third part the author presents results of his own research on continuous chip formation. The process studied is a two-dimensional one and the text is illustrated by many extremely clear photographs. The question of chip control and the path taken by the free-flowing chip is treated in considerable detail, both analytically and experimentally.

The formation of chips under discontinuous and segmental conditions, using a vibrating three-dimensional tool, is treated in the fourth part.

Nonmetallic turning experience of the author is treated in the fifth and final part of the book.

While this book which is concerned with the rather limited question of chip formation may not be of general interest to the engineer in the workshop, it should be of considerable value as a reference work for those engaged in metal-cutting research.

## Gas Turbines

GAS TURBINES FOR AIRCRAFT. By Ivan H. Driggs and Otis E. Lancaster. The Ronald Press Company, New York, N. Y., 1955. Cloth, 6 × 9 in., xv and 349 pp., illus. and charts, $10.

REVIEWED BY W. H. KRASE[5]

THIS new contribution to the literature on gas turbines covers with some exceptions the same material as a number of other books on the subject. A general discussion of engine types is followed by a chapter on thermodynamics. Cycle-analysis methods for a variety of engine arrangements are given, and pertinent compressible-flow relations are derived. Chapters on compressor, turbine, and combustion-system design follow. A method for computing the off-design performance of a turbine engine is given, and a general discussion of engine weight is included. Control problems are discussed from the standpoint of engine performance. An elaborate system for airplane-performance analysis is given. A chapter on historical development concludes the book. Tables and curves for standard atmosphere, gas properties, oblique shocks, and certain engine corrections are included.

Specific new material not otherwise generally available is given on the following subjects:

1 A particular engine-performance-computation system, which involves use of polytropic efficiencies rather than the conventional adiabatic efficiencies. While this system is good for limited use, the reviewer's opinion is that it will not be adopted generally, principally because it does not directly yield detailed data on conditions in the engine, and because it does not lend itself readily to systems of general type.

2 Empirical these for engine-weight estimation are given, and it is indicated that these data will vary markedly as design improvements are made.

3 Control problems are well discussed from the standpoint of performance.

4 An elaborate airplane-performance-calculation system using transparent overlays. This system does permit compressibility corrections in subsonic region, but does not seem applicable in the supersonic region.

5 Radial equilibrium requirements in turbomachinery design are recognized and briefly described.

A book of such broad coverage cannot discuss completely all of the subjects considered in the available length, and this one can hardly be called a comprehensive reference volume. References to other literature are rather scanty. A more complete

[3] Lessells and Associates, Inc., Boston, Mass.

[4] Professor of Mechanical Engineering, Massachusetts Institute of Technology, Cambridge, Mass. Mem. ASME

[5] Preliminary Design Section, Aircraft Gas Turbine Division, General Electric Company, Evendale, Ohio.

treatment would be desirable on supersonic-inlet and jet-nozzle design and off-design performance, the basis for the use of nondimensional parameters, compressor and turbine off-design characteristics, and performance analysis of dual rotor and other more complicated engine arrangements. Treatment in such detail of the particular computation systems described for engine and airplane performance seems unwarranted.

## Physics

FUNDAMENTAL FORMULAS OF PHYSICS. Edited by Donald H. Menzel. Prentice-Hall, Inc., New York, N. Y., 1955. Cloth, 5½ × 8½ in., xxxv and 765 pp., illus., index, $10.

REVIEWED BY A. ALI KHEIRALLA[6]

THIS is at once a handbook of methods and formulas and a summary of the main results of the principal subdivisions of theoretical physics and its borderline fields. It may be compared in some respects to E. Madelung's "Die Mathematischen Hilfsmittel des Physikers" although it contains many results not given in that work.

Topics covered include classical mechanics, fluid dynamics, thermodynamics, kinetic theory, electromagnetic theory, acoustics, optics, solid-state physics, and physical chemistry. Altogether there are 31 chapters. A summary of basic mathematical formulas, methods, and definitions carefully selected by Prof. Philip Franklin of M.I.T., provides a self-contained reference for the rest of the book.

It should find widespread use among research engineers, physicists, and applied mathematicians and is especially recommended for the libraries of research organizations.

## Mathematics for Engineers

ADVANCED MATHEMATICS FOR ENGINEERS. By H. W. Reddick and F. H. Miller. Third edition prepared by F. H. Miller. John Wiley & Sons, Inc., New York, N. Y., 1955; Chapman & Hall, Ltd., London, England, 1955. Cloth, 5½ × 8½ in., xiv and 548 pp., 131 figs., $6.50.

REVIEWED BY JOHN W. CELL[7]

PROF. F. H. Miller of The Cooper Union School of Engineering prepared the third edition of this much-used text. He has included some new material such as (1) a discussion of Legendre functions and their applications; (2) a brief treatment of numerical methods for the solution of ordinary and partial differential equations; and (3) a discussion of Laplace transforms and their applications. The problem lists have undergone extensive changes involving both replacements in those requiring numerical calculations and addition of new problems especially with the new material.

The first edition in 1938 was a marked success as one answer to the important problem of the selection of material beyond calculus for a year of mathematics for engineering students. The second edition in 1947, and now the third edition, include an excellent selection of material. Moreover, this year of study can, in this reviewer's opinion, serve adequately as the basis of required further study in mathematics by those engineering students in graduate programs.

With respect to the new material, the chapter on Operational Calculus is unnecessarily long, for the Heaviside $p$ and $Q\Delta\ p^{-1}$ notation are retained intact; the chapter is followed by two new articles on the Laplace transform. The addition of numerical methods for the solution of ordinary and partial differential equations is timely both because the student should be made aware of the existence of many such techniques and because of the now accepted use of digital and analog computers for such problems. Thus the introduction of the concept of changing a partial differential equation to a partial difference equation is fundamental in computer ideology.

## Feedback Control Systems

FEEDBACK CONTROL SYSTEMS. By Gilbert Howard Fett. Prentice-Hall, Inc., New York, N. Y., 1954. Cloth, 5½ × 8½ in., illus., ix and 361 pp., $10.

REVIEWED BY ROBERT R. JOHNSON[8]

THE author states, "this book is intended to serve the needs of the advanced engineering student and the practising engineer..." This statement is a good evaluation of the work. Although slanted heavily toward the electrical engineer, the basic concepts of control systems are presented in an unusually clear manner which will be of great value in all control fields. Particular care has been taken in presenting the details which bother the worker who is not an expert in the field. Specifically, the details of the block diagram, the difference between controller and servo, and the method of handling disturbances on the output or demand side have been carefully and clearly explained with supporting examples.

The first two chapters give an introduction to control devices, and the components of a feedback control system. The third chapter deals with the steady-state and transient solutions using the differential-equation methods, and includes, in addition to the common Routh-Hurwitz criterion for real coefficients, the Bilharz-Frank determinant for complex coefficients. The next three chapters deal with the various stability criteria including an extensive analysis and synthesis of complex control systems. In addition to the Nyquist diagram, a clear presentation of the inverse G function plot, and root-locus diagram are shown with several numerical examples.

The final chapter deals with nonlinear cases, and includes phase-plane, describing function, and perturbation methods of analysis. Examples are given for each of these cases. Again, of particular importance is the author's care in pointing out limitations and applicability of the various methods.

An extensive bibliography is included at the end of each chapter as well as several tables of logarithmic, polar, $G$ locus, $G^{-1}$ locus, and $M$ locus plots for different types of control and transfer functions.

[6] Lessells and Associates, Inc., Boston, Mass.

[7] Professor of Mathematics, University of North Carolina, Raleigh, N. C.

[8] Instructor, Department of Mechanical Engineering, University of Minnesota, Minneapolis, Minn. Assoc. Mem. ASME.

## Third U. S. National Congress of Applied Mechanics
### Preliminary Announcement

The Third U. S. National Congress of Applied Mechanics will be held at Brown University, Providence, Rhode Island, during June 11–14, 1958. It is hoped that the scheduling of conflicting meetings can be avoided by this early announcement of the date chosen for the Congress. Further announcements concerning the preparation of papers will be made as the Congress draws nearer.

Inquiries regarding the Congress should be addressed to one of the following members of the Organizing Committee at Brown University, Providence, R. I.:

Professor D. C. Drucker, *Secretary*
Professor E. H. Lee, *Treasurer*
Professor W. Prager, *Chairman*

$9.00
to members
and
subscribers

a uniquely collection of data, calculations, procedures, and
advice for attacking problems associated with

DYNAMICS VIBRATION WAVE MOTION
SHELLS PLATES ELASTIC INSTABILITY STRUCTURES
VISCOELASTICITY FLOW FAILURE BEHAVIOR OF MATERIALS
FLUID FLOW AERODYNAMICS HEAT TRANSFER

is provided through ninety-five technical papers, each of which constitutes
, four general lectures; hundreds of tables, diagrams, and equations;
keyed to nearly all the articles.

825-page volume of this you obtain for an unequaled amount of reference
viewpoints of recognized authorities in the field, and information on
and on the use of new analytical tools and procedures.

*Send for a copy today—you will be glad you did.*

SOCIETY OF MECHANICAL ENGINEERS, 29 W. 39th St., New York 18, N. Y.